Restore Lagoon Inflow Research (Phase 2)
Project Summary






PREPARED FOR

Florida Department of Education
325 W Gaines Street
Tallahassee, FL 32399

PREPARED BY

Jesse Blanchard, Jeff Eble, Austin Fox, Kevin B. Johnson, Ralph Turnigan, Robert J. Weaver, and Gary A. Zarillo
Florida Institute of Technology
150 West University Boulevard
Melbourne, FL 32091

Matthew Shelton and Marcy Frick
Tetra Tech, Inc.
11 Riverside Drive, Suite 204
Cocoa, FL 32922

September 2021

Table of Contents

List of Tables

List of Figures

Acknowledgements

The Restore Lagoon Inflow Research team thanks Governor Ron DeSantis; the Florida legislature especially Representative Randy Fine, Representative Thad Altman, and Senator Debbie Mayfield; and the Florida Department of Education for their roles in advancing Florida's water health and research. A special acknowledgement of Dr. Jeff Eble's contributions to the coordination of this report. In addition, we thank Dr. T. Dwayne McCay, Mr. Frank Kinney, and Mr. Robert Salonen for supporting Restore Lagoon Inflow Research project communications with all stakeholders.

We would like to thank the following regulatory agencies and organizations that we consulted on Phase 2 of the project:

- Applied Ecology, Inc.
- Brevard County Board of County Commissioners
- Brevard County Natural Resources Management Department
- Canaveral Port Authority
- Florida Department of Environmental Protection
- Florida Fish and Wildlife Conservation Commission Melbourne Fisheries Lab
- Harbor Branch Oceanographic Institute
- Herndon Solutions Group
- Indian River County Board of County Commissioners
- Indian River Lagoon National Estuary Program and IRL Council
- Marine Resources Council
- National Aeronautics and Space Administration (NASA) Kennedy Space Center
- St. Johns River Water Management District
- University of Central Florida Genomics and Bioinformatics Cluster
- U.S. Army Corps of Engineers

The views, statements, findings, conclusions, and recommendations expressed herein are those of the authors and do not necessarily reflect the views of the State of Florida or any of its sub-agencies.

The photographs on the cover were provided by the Florida Tech Principal Investigators on this project.

List of Acronyms

ADCIRC	Advanced Circulation
ADCP	Acoustic Doppler Current Profiler
ANOVA	Analyses of Variance
BACI	Before-After-Control-Impact
BRL	Banana River Lagoon
BRN	Banana River North
BRS	Banana River South
°C	Degrees Celsius
Chl-a	Chlorophyll-a
cm	Centimeter
CMS	Coastal Modeling System
COI	Cytochrome Oxidase Subunit I
DIN	Dissolved Inorganic Nitrogen
DNA	Deoxyribonucleic Acid
DO	Dissolved Oxygen
DON	Dissolved Organic Nitrogen
DOP	Dissolved Organic Phosphorus
eDNA	Environmental Deoxyribonucleic Acid
EFDC	Environmental Fluid Dynamics Code
FDEP	Florida Department of Environmental Protection
FIM	Fisheries Independent Monitoring
Florida Tech	Florida Institute of Technology
FWC	Florida Fish and Wildlife Conservation Commission
FWRI	Fish and Wildlife Research Institute
HAB	Harmful Algal Bloom
HEM3D	Hydrodynamic and Eutrophication Three-Dimensional
IRL	Indian River Lagoon
kg/m^3	Kilograms Per Cubic Meter
km	Kilometer
KSC	Kennedy Space Center
L	Liter
m	Meter
m^2	Square Meter
m^3/sec	Cubic Meters Per Second
mg/L	Milligrams Per Liter

mg/L/hr	Milligrams Per Liter Per Hour
mL	Milliliter
MWI	Moving Water Industries
N	Nitrogen
NASA	National Aeronautics and Space Administration
NAVD88	North American Vertical Datum of 1988
NH_4	Ammonium
NMDS	Non-Metric Multidimensional Scaling
NOAA	National Oceanic and Atmospheric Administration
NOx	Nitrate + Nitrite
ODOT	Oregon Department of Transportation
P	Phosphorus
PCR	Polymerase Chain Reaction
PERMANOVA	Permutational Multivariate ANOVA
PO_4	Orthophosphate
PSU	Practical Salinity Unit
rRNA	Ribosomal Ribonucleic Acid
SCUBA	Self-Contained Underwater Breathing Apparatus
SiO_2	Silica
SJRWMD	St. Johns River Water Management District
SOD	Sediment Oxygen Demand
SoI	Species of Interest
SRP	Soluble Reactive Phosphorus
SWIL	Spatial Watershed Iterative Loading
TDN	Total Dissolved Nitrogen
TDP	Total Dissolved Phosphorus
TN	Total Nitrogen
TP	Total Phosphorus
µg/L	Micrograms Per Liter
µm	Micrometer
µM	Micromolar
µmoles/m^2/hr	Micromoles Per Square Meter Per Hour
USACE	U.S. Army Corps of Engineers
YSI	Yellow Springs Instruments

Executive Summary

Over 50 years of impacts from a growing human population have taken a tragic toll on the Indian River Lagoon (IRL) system. Excessive nutrients and all forms of pollution from human activity flow overland and through groundwater to the lagoon. The seagrasses, clams, and oysters are nearly gone, displaced by nutrient laden muck, polluted water, and algal blooms. With the loss of the majority of seagrasses, manatees are dying in record numbers as they are unable to find food. Fish populations that survived the 2011 superbloom now struggle to adjust to rapidly changing conditions. Algae that once unnoticeably cycled through the seasons in clear water now cloud the water, as blooms of one dominant species quickly die out only to be replaced by the next dominant species in an unbalanced, sometimes hypoxic or anoxic, high nutrient (eutrophic) system.

Water circulation in the lagoon is restricted on all sides, increasing risk of eutrophication and ecosystem collapse. Previous federal development activity supporting space and defense projects cut off the finger flows of Banana Creek, eliminating the northern connection of the Banana River Lagoon (BRL) to IRL. To the east, natural episodic connections between the coastal ocean and IRL system have been lost with the hardened development of the barrier islands, while the benefits of water circulation through the five maintained inlets are limited by the many causeways that restrict flow north and south. To the west, polluted water which once largely drained to the St. Johns River now flows to the IRL system.

Deliberate and timely restoration of lagoon hydrology can improve water quality and help restore the rapidly deteriorating lagoon ecosystem. Elected officials; local, state, and federal government agencies; and stakeholders in the IRL region are exploring a variety of approaches to help restore the lagoon. The Restore Lagoon Inflow Research project will help determine the viability of a permanent ocean inflow system as a potential additional tool to stabilize and restore the lagoon.

With funding from the Florida Legislature in fiscal year 2020, the Florida Institute of Technology (Florida Tech) completed Phase 1 of a multi-phase research project to explore water quality improvement within the IRL system by enhancing ocean inflows. This first phase gathered baseline data and conducted modeling and experiments on water quality, biological parameters, and hydrologic conditions at candidate locations for a temporary ocean inflow system. The Florida Legislature authorized funding for Phase 2 in fiscal year 2021, which built upon the lessons learned from Phase 1, and focused on planning for construction and implementation of a small-scale, temporary ocean inflow system and the studies required to evaluate its effectiveness. The efforts in Phase 2 included site selection, agency and stakeholder engagement, conceptual engineering and optimization, pre-permitting briefings, expanded ecosystem modeling, and baseline data collection. The Phase 1 and Phase 2 results, when combined with findings from the temporary inflow pilot system, will allow for an informed determination of the feasibility and impacts of a potential permanent ocean inflow system.

A multi-disciplined team of research professionals, supported by community partners, Florida Tech staff, students, and engineering professionals from Tetra Tech, Inc., was assembled to provide expertise in:

- Modeling and Engineering – Dr. Gary Zarillo, Dr. Robert Weaver, and Tetra Tech
- Geochemistry – Dr. Austin Fox
- Biology – Dr. Kevin Johnson, Dr. Ralph Turingan, Dr. Jeff Eble, and Dr. Jesse Blanchard

Project Overview

The multi-phased Restore Lagoon Inflow Research project is envisioned to include the baseline monitoring, design, permitting, implementation, and modeling of a system providing temporary ocean inflow to IRL to help determine the viability of a permanent ocean inflow system. By improving understanding and management of the IRL system, the study results will also help to address several actions in the IRL National Estuary Program Comprehensive Conservation and Management Plan, including specifically addressing action Connected Waters-5 which calls for a pilot project to assess the benefits and risks of enhanced ocean exchange with the lagoon.

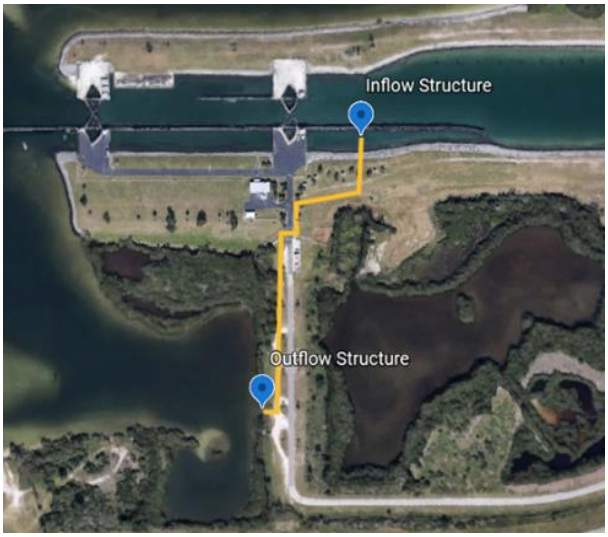

Figure ES-1. Map of the proposed inflow pilot system site and pipeline

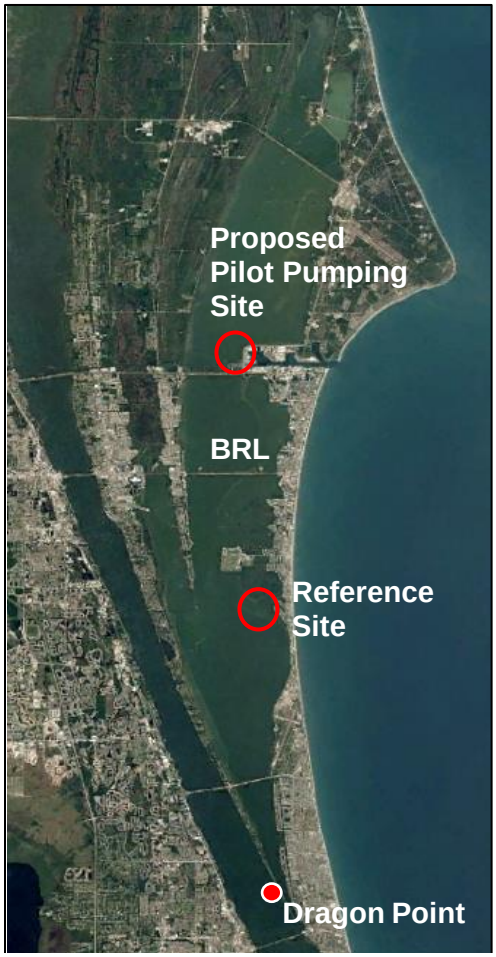

Figure ES-2. Map showing BRL proposed pilot and reference site

For future phases to complete the project, the pilot system design developed in Phase 2 will be revised to include changes discussed in the pre-application meetings with the agencies and feedback from local stakeholders, and will be used to obtain the necessary permits. The project bid documents will then be created, the request for proposals drafted and sent out for bidding, and an award made for construction of the temporary inflow pilot system. The temporary inflow pump system will be constructed in accordance with the U.S. Army Corps of Engineers and Environmental Resource Permit requirements.

The temporary inflow pump system is proposed to be operated for one year in parallel with continued focused research, monitoring, and modeling. This approach allows for data to be collected on changes due to small-scale ocean inflow at the study site compared to a reference site outside the influence of pumping, to directly assess impacts on focal biological communities and to validate dissolved oxygen (DO), nutrient, and chlorophyll-a (Chl-a) model predictions. The temporary pump system established for the project will be decommissioned at the end of the research period, with the piping and pump removed from the site. The results of the full Restore Lagoon Inflow Research project will be summarized to provide information and analysis to stakeholders and decision-makers on the viability of a permanent ocean inflow system.

Proposed Inflow Site

Based on data collected during Phase 1 and discussions with agencies and stakeholders, Phase 2 identified the northern BRL as the most feasible and cost-effective location of a temporary inflow research site. BRL is a sub-basin of IRL that lies between Cape Canaveral and Merritt Island and extends from the National Aeronautics and Space Administration (NASA) Kennedy Space Center (KSC) to Dragon Point. It is poorly flushed with no direct connection to the ocean, which results in long water residence times and increased vulnerability to nutrient accumulation.

The proposed temporary inflow system would extract water from the ocean side of the Canaveral Lock system and discharge to BRL via the cove to the west of Avocet Lagoon (**Figure ES-1**). A pump station is proposed that pumps a relatively small volume of 0.5 cubic meters per second of seawater through a pipe system above ground to the lagoon. The cove configuration will restrict flow movement from the outfall location and provide a concentration gradient to evaluate changes on water quality, geochemistry, and biology. A reference site in the central BRL was proposed (**Figure ES-2**), which was identified through model evaluation and field sampling as comparable to the proposed inflow site and outside the influence of the pilot system. The proposed pilot system configuration was selected to preserve the reference site while minimizing cost and impacts to existing infrastructure, public access, and natural resources.

Data Collection and Modeling

Florida Tech adapted the project approach based on data collected while addressing concerns/questions from stakeholders. Internal project meetings and stakeholder meetings were focused on providing the lowest cost and least invasive approach to implement the temporary inflow pilot system, without sacrificing the validity and quality of the pilot research project.

An IRL Environmental Fluid Dynamics Code model was updated to provide numerical predictions of hydrodynamics, flushing rate, water quality, and phytoplankton concentration with and without enhanced inflow. Model boundary conditions used data from St. Johns River Water Management District and Harbor Branch Oceanographic Institute IRL Observation Network, with watershed inputs from the Spatial Watershed Iterative Loading model developed by Applied Ecology and internal nutrient loading and groundwater inflow predictions compiled by Florida Tech.

Figure ES-3. Collecting water samples from a benthic chamber

Acoustic Doppler Current Profiler units were deployed in BRL near the Barge Canal, Dragon Point, and Sykes Creek to improve modeling of current directions and velocities. Data on temperature, salinity, and nutrients were also collected with a focus on the proposed temporary inflow pilot system site, reference site, and Port Canaveral. Uptake and release (fluxes) of nutrients from sediments and water column were evaluated in the field and using laboratory bench tests of IRL sediments in simulated inflow conditions (**Figure ES-3**) with the goal of investigating inflow potential to promote natural nutrient removal through improved bottom water circulation, lower water temperature, and higher and more stable DO concentrations.

In addition, biological data collection efforts for seagrass, drift algae, phytoplankton and harmful algae, benthic infauna, fish community, and environmental deoxyribonucleic acid (eDNA) continued from Phase 1. These data improve understanding of the BRL ecosystem, providing biological baselines for comparison to conditions with the proposed temporary inflow pilot system in place to identify effects of enhanced inflow to key species, communities, and habitats.

Highlighted Key Findings

Stabilizing DO and reducing water temperature can improve natural nutrient removal.
Under low oxygen conditions (hypoxia), sediments were found to be a source of dissolved nutrients to overlying water. Inflow is predicted to stabilize DO concentrations and mitigate occurrences of hypoxia, which would improve binding of orthophosphate by sediments, reduce total nitrogen (TN), and promote nutrient ratios that are less favorable for harmful algal bloom (HAB) species. Predicted lower temperatures resulting from just the temporary small-scale inflow system are estimated to prevent 1.6 metric tons of TN and 0.7 metric tons of total phosphorus (TP) from entering the lagoon, with an estimated value of $9 million per year based on the current average costs for lagoon TN and TP removal.

Net nutrient reduction is predicted as a result of enhanced inflow.
Models and field data suggest that measurable impacts of inflow will be limited to the northern compartments of the IRL system. This is supported in water quality projections for Sebastian Inlet, which indicate increased water discharge but no detectable change in nutrient concentrations. Higher inlet water exchange rates with inflow are predicted to increase nutrient loads to the coastal ocean at Sebastian Inlet by less than 1%. However, when factoring in the predicted nutrient reduction from the increased DO concentrations and lower water temperatures, a net reduction of nutrient loading is anticipated with enhanced inflow.

Water quality determines fish distribution and local population size.
Significant responses were shown to increased inflow by ecologically and recreationally valuable fishes. Many fishes are highly mobile and will adjust habitat use in response to water quality conditions. Model projections suggest the local populations of five of eight species of interest would increase and three species would decrease with enhanced inflow. Significant positive and negative associations between local fish population size and Chl-a concentrations were detected and include a strong decline in nearly all species of interest following the 2011 “superbloom.” Complimentary assessment of fish eDNA detection patterns support tracking of biodiversity loss or recovery over time against an established fixed baseline. eDNA detection patterns highlighted the negative impacts of frequent HAB outbreaks on BRL fish diversity, and presence of species rich and taxonomically diverse fish communities at sites buffered against eutrophication impacts.

Biological baseline allows tracking system response to inflow.
Phase 2 monitoring of planktonic communities identified 62 diatom, 16 dinoflagellate, and dozens of other algal species present in the pilot project area. In a healthy system, these species cycle nutrients without excessive algal blooms. In the current high nutrient IRL system, populations of one species dominate for a period, die off, sink to the bottom, increase biological oxygen demand in the sediments, and promote future HAB outbreaks. Concurrent benthic community monitoring identified 105 infauna species (species living in the sediments) at the study sites, showing that there is an opportunity for restoration of natural nutrient removal.

Low pumping volumes provide a cost-effective and low impact research design.
A natural cove a short distance from ocean water was selected to confine inflows and allow development of measurable concentration gradients in water quality parameters at relatively low pumping volumes. This design significantly reduces project installation and operation costs and potential negative impacts, while also preserving a similar reference site outside the influence of pilot pumping to test predicted impacts of inflow on lagoon water quality, nutrient removal, and biology using scientifically sound methods.

1 Introduction and Study Background

1.1 Introduction

The Indian River Lagoon (IRL) is a shallow bar-built estuary that extends 250 kilometers (km) along the central east coast of subtropical Florida, ranging in width from less than 1 km to approximately 9 km (Sigua et al., 2000). IRL is poorly flushed across most of its length, with limited exchange with the ocean occurring through six engineered inlets (from north to south): Ponce de Leon, Port Canaveral, Sebastian, Fort Pierce, St. Lucie, and Jupiter (**Figure 1**). The inlets are directly connected to the ocean except for the Port Canaveral Inlet, which is separated from the lagoon by a lock system. The northern portion of IRL is micro tidal and tidal flushing between sub-basins is negligible (Saberi and Weaver, 2016; Zarillo, 2015). Flushing in IRL is further limited by the presence of causeways connecting the mainland to the barrier islands.

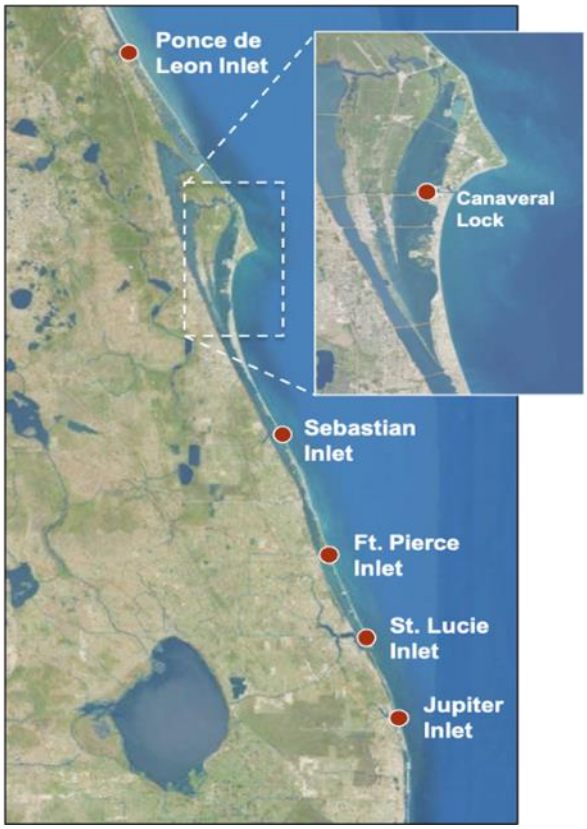

Figure 1. Location of IRL inlets

Historically, and prior to the development of human infrastructure, the IRL system was episodically connected to the coastal ocean through storm produced cuts, over washes, and persistent tidal inlets that migrated alongshore under the net southward wave produced drift of littoral sediments (Zarillo et al., 2013). Cartographic and topographic evidence indicate these features were a re-occurring presence and include evidence of overlapping storm-induced inlet cuts in the Banana River Lagoon (BRL) north of Patrick Air Force Base (Almasi,1985; Stauble, 1988; Brech, 2004). This process, over geological time, resulted in a system of wash over platforms and tidal inlet flood shoals upon which extensive human infrastructure has been built on the barrier islands bounding the east side of IRL (Stauble et al., 1988; Zarillo et al., 2013). Correspondingly, historical development of coastal Florida resulted in a major expansion of the IRL watershed from Brevard County to Martin County due to construction of the canal system and associated water control

structures bringing water formerly destined for the St. Johns River to IRL. Over this same period, existing natural and engineered tidal inlets were stabilized by jetty construction coupled with shore protection projects, which involve repeated beach restoration projects that can have a 50-year planning horizon. This resulted in the prevention of natural tidal inlet migration, episodic storm cuts, and barrier over wash events that reduced the potential for nutrient loading by providing exchanges between the coastal ocean and IRL.

Eutrophication of coastal marine ecosystems has become increasingly common due to enhanced nutrient loading from adjacent watersheds (Brady et al., 2013; Diaz and Rosenberg, 2008). In eutrophic systems, harmful algal bloom (HAB) events contribute to occurrences of hypoxia and anoxia, where even short events can promote loss of ecosystem services including coupled nitrification-denitrification that removes nitrogen (N) from the system as inert N gas and sequestration of phosphorus (P) into sediments. As the eutrophic state progresses, sediment mineralization becomes an important source of nutrients and can sustain eutrophication through the dry season (Cowan and Boynton, 1996; DiDonato et al., 2006; Seitzinger, 1988; Kemp et al., 1990). Extended periods of eutrophication can destabilize the trophic state of an estuary and lead to a shift from seagrass-dominated ecosystems to degraded, algae-dominated systems (DiDonato et al., 2006).

Several decades of increasing anthropogenic impacts have resulted in the lagoon being at risk of ecosystem collapse (Adams et al., 2019). IRL experienced a dramatic shift from a system where benthic aquatic vegetation was expanding to one dominated by planktonic microalgae following an unprecedented algal bloom in 2011 (now referred to as the “superbloom”). The post-2011 IRL is characterized by intense, recurring, and long-lasting algal blooms; widespread loss of seagrasses; and episodic wildlife mortality events. Ongoing blooms of picocyanobacteria, nanoplanktonic chlorophyte, and *Aureoumbra lagunensis* appear to be the “new normal” for the central and northern IRL (IRL National Estuary Program, 2020). As a result of declining water quality, the IRL system lost 58% seagrass habitat from 2009 to 2019 (Morris et al., 2021), which contributed to an increase in marine mammal mortality. The latest Florida Fish and Wildlife Conservation Commission (FWC) data documents 929 manatee deaths in Florida as of August 27, 2021, with deaths more than doubling the five-year average for manatee mortality due in part to IRL seagrass losses and manatee malnourishment and starvation (FWC, 2021).

A multifaceted approach to IRL restoration is underway by multiple state and local government and non-governmental organizations. The Restore Lagoon Inflow Research project seeks to evaluate the efficacy of enhancing ocean inflow to the lagoon as a potential tool for stabilizing and restoring the lagoon ecosystem. This project was inspired by the understanding that restricted circulation is a critical issue, particularly in northern IRL (Smith, 1993; Bilskie at al., 2019). Destin Harbor, Florida, successfully installed a pumping system in 1992 to mitigate a similar issue. Enhanced circulation projects in India (Ghosh et al., 2006), Netherlands (Wijnhoven et al., 2010), New Zealand (Schallenberg et al., 2010), China (Li et al., 2013), Australia (Humphries and Robinson, 1995), Denmark (Peterson, et al., 2008), and Portugal (Lillebo et al., 2005) highlight interest in this approach to combat eutrophication. St. Johns River Water Management District (SJRWMD) initiated a feasibility study for enhanced inflow in 2017 near Port Canaveral, and the Restore Lagoon Inflow Research project evaluated those lessons learned. With improvements to site selection, costs, and potential impacts to infrastructure and lagoon biology, the Restore Lagoon Inflow Research project was designed to directly evaluate the feasibility of enhanced ocean inflow with development of a small-scale, temporary inflow system.

1.2 Study Area

BRL is a sub-basin of IRL that lies between Cape Canaveral and Merritt Island and extends from the National Aeronautics and Space Administration (NASA) Kennedy Space Center (KSC) to Dragon Point. BRL is poorly flushed with no direct connection to the ocean, which leads to some of the longest residence times in the IRL system. According to the Florida Department of Environmental Protection (FDEP), it takes approximately two years for water to flush in BRL (FDEP, 2013). The BRL northern section was historically connected to IRL by Banana Creek, which was a series of finger-like channels that were almost completely filled in during the development of NASA KSC. Banana Creek was also periodically connected to the Atlantic Ocean at Pepper Haulover, which was an intermittent storm cut just east of where Launch Complex 39A stands today (U.S. Army Corps of Engineers [USACE], 1882). Prior to development of the barrier island, each IRL basin was subjected to episodic over washing and breaching of the barrier island by storms, as evidenced by numerous relict tidal inlet shoals and expansive wash over sediment fans (Brech, 2004). This historical inflow would bring in ocean water and enhance circulation in the estuary.

Impacts from declining water quality and increasingly frequent HABs are not evenly distributed across IRL, and the northern IRL and BRL appear to be particularly vulnerable (Badylak and Phlips, 2004; Phlips et al., 2011). Since 2011, large and persistent algal blooms resulted in an unprecedented decline in water clarity, which negatively impacted seagrass growth and distribution (**Figure 2;** Scheidt, 2021a). In BRL, seagrass percent cover dropped drastically from 35% in 2011 to less than 2% in 2012. Additional bloom events, which started in late fall 2015 and persisted into late spring and summer 2016, had a further negative impact. By 2019, seagrasses were absent across most of the region. The previously extensive seagrass beds in BRL provided good forage habitat and safe harbor for Florida Manatee (*Trichechus manatus latirostris*; Provancha and Provancha, 1988; Provancha and Hall, 1991; Lefebvre et al., 2016; Scheidt, 2021b). The catastrophic loss of the once stable manatee seagrass forage in BRL has led to mass starvation events and populations declining to historically low numbers (**Figure 2**). Long-term persistence of manatees in BRL is only possible with restoration of ecosystem integrity and recovery of seagrass foraging habitats (Scheidt, 2021b).

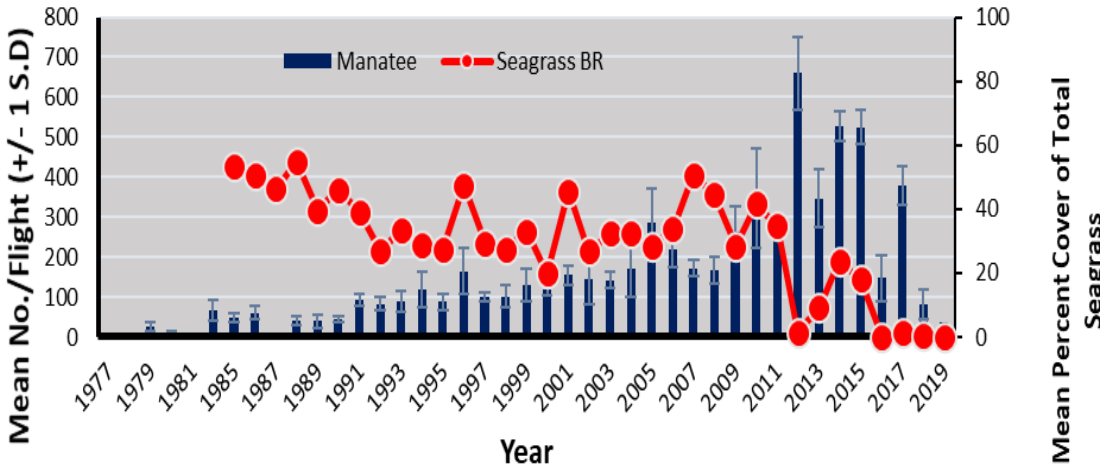

Figure 2. Mean number of manatees (blue bars) per flight from summer aerial surveys and annual mean seagrass percent cover for BRL transects (red line; used with permission from Scheidt, 2021b)

Phase 2 of the Restore Lagoon Inflow Research study built on the Phase I efforts to evaluate possible impacts of enhanced circulation in BRL with an emphasis at two primary locations: (1) north BRL considered as a likely inflow study site (centered near 28.407, -80.638), and (2) central BRL evaluated as a reference site where any impacts of inflow would be minimized due to geomorphological conditions that limit circulation (centered near 28.287, -80.6100) (**Figure 3**). A natural cove adjacent to Port Canaveral was selected to confine inflow, so that pumping rates for the pilot study could be minimized to reduce installation costs and impacts to the greater IRL system, while still creating water quality concentration gradients that can be monitored and evaluated for their potential to improve ecosystem functions. Furthermore, this approach uses a reference site that was selected based upon model evaluations to identify a location with limited circulation associated with proposed pilot pumping volumes, as well as a comparison of water depth and bottom type similar to the proposed inflow site. The reference site allows for correlation and comparison of data to better evaluate changes strictly due to pumping within the highly variable IRL system.

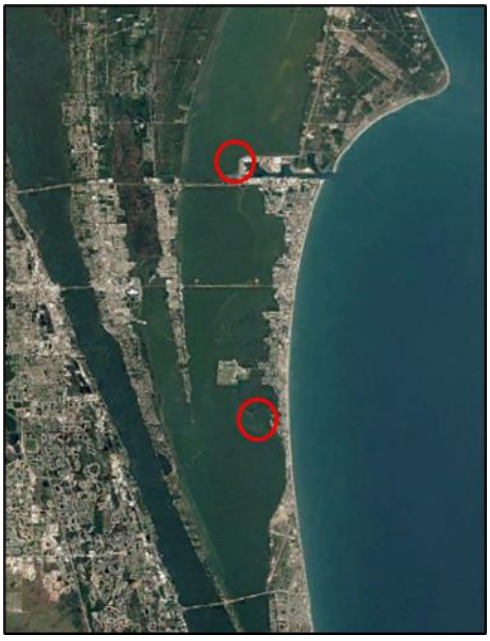

Figure 3. Proposed pilot inflow site in north BRL and reference site in central BRL

1.3 Support for Lagoon Efforts

The Restore Lagoon Inflow Research project builds upon and complements ongoing efforts to better understand the IRL system and identify effective restoration measures. The results will help to determine whether enhanced ocean inflow could be a tool to address declining water quality and ecosystem degradation. In addition, this project is gathering data to help directly address two vital signs and four actions from the IRL National Estuary Program Comprehensive Conservation and Management Plan (2020). The Connected Waters and Watersheds and Hydrology and Hydrodynamics vital signs include the following actions that the study will help to inform:

- Connected Waters-5: Better understand the physical, chemical, and biological implications, benefits, risks, and expected outcomes of enhancing oceanic exchange and develop a pilot project, as appropriate.
- Hydrology-1: Support advancements in hydrological model development, verification, and application.

- Hydrology-2: Apply the best available models to better evaluate connectivity between IRL sub-basins.
- Hydrology-3: Continue evaluation of options to enhance water flow through engineering solutions that have well defined water quality and ecological outcomes.

The engineering design for the Restore Lagoon Inflow Research project builds upon past work by SJRWMD who contracted with CDM Smith, in association with Taylor Engineering, to identify potential locations where enhanced circulation projects would be beneficial. The first phase (CDM Smith et al., 2014) involved a literature review and geographic information system desktop analysis, which identified ten locations for future evaluation. Based on a screening matrix, the top ranked project from this evaluation was a culvert at Port Canaveral (CDM Smith et al., 2015). The third phase developed the conceptual design for a culvert and temporary pump at Port Canaveral at State Road 401 (CDM Smith et al., 2017). As part of the Restore Lagoon Inflow Research project engineering, the exact intake and inflow structures were modified from the proposed design in CDM Smith et al. (2017) to minimize the impact to channel banks and overlying infrastructure. Modifications were also made to provide an outfall location with natural restrictions to allow for a significantly reduced pumping volume that would still facilitate study of inflow impacts at a smaller scale. This approach greatly reduces the cost and wider reaching impacts of inflow on IRL until a more complete assessment of inflow is evaluated using the pilot system data.

1.4 Coordination

As part of Phase 2, Florida Institute of Technology (Florida Tech) and Tetra Tech consulted with key stakeholders and agencies to gather feedback on study design, develop details for the pilot project, and work through complex permitting concerns and needs. The team closely coordinated with USACE to negotiate the use of USACE lands for the pilot project. Input on project development and permitting was provided by the Canaveral Port Authority, FDEP, FWC, Brevard County Board of County Commissioners, Brevard County Natural Resources Management Department, Indian River County Board of County Commissioners, IRL National Estuary Program, Marine Resources Council, NASA KSC, SJRWMD, University of Central Florida, State Representative Thad Altman, State Representative Randy Fine, and State Senator Debbie Mayfield. From these discussions, the project team identified lessons learned from previous projects and the most cost-effective approach to investigating the impact of enhanced inflow on the IRL system.

2 Key Findings

In Phase 2, Florida Tech continued to explore solutions for improving water quality in the lagoon with initiation of a pilot project to investigate the impacts of restoring periodic historical ocean inflows. Phase 2 further developed baseline data and modeling on existing water quality, biological parameters, and hydrologic conditions at the proposed pilot system location. The modeling and engineering proceeded in parallel with biological and water quality monitoring. The results of the full Restore Lagoon Inflow Research project will provide information and analysis to the lead agency and appropriate decision-makers to help determine the viability of a full-scale, permanent ocean inflow system. The key findings from the project to date are summarized below.

Task 1 Modeling and Engineering Key Findings:

- A small-scale pilot structure capable of pumping 0.5 cubic meters per second (m^3/sec) was designed with an estimated cost of $551,000 to construct, $50,000 to operate for one year, and $112,000 to decommission once the pilot project has ended.
- Water levels throughout IRL naturally fluctuate as much as 0.76 meters (m) (2.5 feet) between annual high and low water periods. The Environmental Fluid Dynamics (EFDC) model projects a 1 to 7 centimeters (cm) increase in BRL water level with inflows greater than 1 m^3/sec.
- Model projections indicate at an inflow rate of 2.5 m^3/sec and higher, dissolved oxygen (DO) concentrations would increase in the BRL northern compartment while total nitrogen (TN), total phosphorus (TP), and chlorophyll-a (Chl-a) concentrations would decrease.
- Circulation models and multi-year current profiles indicate seasonally reversing flow direction in BRL and northern IRL may limit the measurable impacts of inflow to the IRL northern compartments.
- Water quality projections for Sebastian Inlet predict higher inlet water exchange rates with 5 m^3/sec inflow, but no detectable change in inlet nutrient concentration.

Task 2 Geochemistry Key Findings:

- Inflow of seawater would bring cooler, saltier, denser water into the lagoon, which is predicted to promote circulation in bottom water, lower water temperature, and raise and stabilize DO concentrations at the sediment-water interface.
- Lower rates of organic matter mineralization and lower N:P ratios in Port Canaveral would, when mixed with lagoon water, help to increase rates of nutrient removal while promoting lower N:P ratios that are less favorable to some HAB species.
- The estimated amount of nutrients removed via changes to benthic fluxes with inflow is expected to be greater than the projected amount of nutrients that would be discharged to the coastal ocean with increased water discharge rates.
- Increased inlet water discharge with pilot inflow of 0.5 m^3/sec is predicted to produce a maximum net discharge of 1.5 metric tons of N and 0.4 metric tons of P per year into the coastal ocean, increasing current nutrient discharge rates by less than 1%.
- Lower water temperatures estimated to result from pilot inflow (0.5 m^3/sec) were calculated to prevent 1.6 metric tons of N and 0.7 metric tons of P from entering the lagoon each year, which translates into an estimated savings of $9 million per year based on the current estimated costs for lagoon N and P removal (Tetra Tech, 2021; $384 per pound of TN and $4,650 per pound of TP).
- Under hypoxic conditions, sandy sediments were a source of dissolved orthophosphate (PO_4) to overlying water. Inflow is predicted to stabilize DO concentrations, mitigating occurrences of hypoxia and promoting sorption of PO_4 in sediments while also promoting

preferential fluxes of nitrate rather than ammonium (NH_4) that are less favorable for HAB species.
- A newly established network of bottom water DO sensors showed that concentrations of DO in bottom water, where it has the greatest impact on benthic nutrient cycling, were often lower and more frequently hypoxic than concentrations measured at mid depths, where most monitoring currently occurs.

Task 3 Biology Key Findings:

- Fish abundance models with a demonstrated 90% accuracy were developed to quantify fish responses to changes in salinity, DO, and temperature in space and time.
- Model projections for BRL suggest local abundances of five of eight species of interest would increase and three species would decrease in response to increased ocean inflow, as species adjust habitat use in response to water quality conditions.
- Significant positive and negative associations between fish abundances and Chl-a concentrations were detected in BRL, with a strong decline in nearly all species of interest following the 2011 “superbloom.”
- Telemetry data provided by NASA KSC revealed significant differences in species site fidelity and habitat use, including the valuable Red Drum and Spotted Seatrout, establishing the baseline for direct assessment of species response to pilot inflow.
- One full seasonal cycle of environmental deoxyribonucleic acid (eDNA) baseline data collection was used to establish three approaches to investigate inflow impacts based eDNA detection patterns.
- Similar fish communities were detected at the inflow and reference sites, setting the foundation for before-after-control-impact tests.
- Fish diversity based on eDNA detections increased from north to south, with the lowest diversity occurring in BRL.
- Comparison of eDNA-based estimates of taxonomic distinctness measures against a fixed baseline highlight the impact of frequent HABs on fish diversity in BRL and the presence of taxonomically diverse fish communities at sites buffered against eutrophication impacts.
- A total of 105 infaunal species were confirmed present at the study sites. Seven polychaetes, 4 amphipods, 1 ostracod, 1 sipunculan, 1 phoronid, 2 gastropods, and 3 bivalves were abundantly present at both locations throughout all seasons and years.
- A total of 62 diatom, 16 dinoflagellate, and a dozen other algal species were confirmed phytoplankton at both study sites. Of these, 8 diatoms and 2 dinoflagellates were present at both locations during most seasons and years.
- Benthic and planktonic species detected in BRL are predominately euryhaline and experience natural water quality fluctuations that exceed changes projected for the inflow pilot study.
- Principle components analyses indicates sediment conditions (percent organic content, percent silt-clay content, percent water content) and bottom water DO determine benthic species occurrence.
- Seagrass *Halodule wrightii* and rooted macroalgae *Caulerpa prolifera* were documented in the project area, but were rare reflecting a significant decline from historic abundances.

Additional details on these key findings are presented in **Section 4**, which is a summary of the reports prepared by the Florida Tech Principal Investigators. The Task 1 Modeling and Engineering report was prepared by Dr. Gary Zarillo and Dr. Robert Weaver, and the full report is provided as Appendix A. The Task 2 Geochemistry report was prepared by Dr. Austin Fox, and the full report is provided as Appendix B. The Task 3 Biology report was prepared by Dr. Kevin

Johnson, Dr. Ralph Turingan, Dr. Jeff Eble, and Dr. Jesse Blanchard, and the full report is provided as Appendix C.

3 Recommendations and Next Steps

The multi-phased, full research project is envisioned to include the baseline monitoring, design, permitting, implementation, and investigation of a system providing temporary ocean inflow to IRL. The results of the full Restore Lagoon Inflow Research project will provide information and analysis to the lead agency and appropriate decision-makers to help determine the viability of a full-scale, permanent ocean inflow system.

3.1 Recommendations

Phase 1 provided essential baseline monitoring and ecosystem modeling for the project. The project team carefully evaluated the parameters required to assess the effectiveness, environmental effects, and limitations of an inflow system. Phase 2 continued to build on these critical datasets that are valuable for the inflow project, as well as the research community and management agencies addressing related questions in IRL and nearshore Atlantic Ocean. The project team adapted the project approach based on data collected while addressing additional concerns/questions from stakeholders. Internal project meetings and stakeholder meetings were focused on providing the lowest cost and least invasive approach to implement the temporary inflow pilot system, without sacrificing the validity and quality of the science produced by the project. Future phases include final design of the temporary inflow pilot system, permitting, and preparation of bid specifications, as well as the construction of the temporary inflow pilot system, system operation and maintenance, and a final report of the research project findings.

As part of the proposed future project phases, the current temporary inflow pilot system design from Phase 2 would be developed to a 90% design. The 90% design will include the changes discussed in the pre-application meetings with USACE, FDEP, and SJRWMD, as well as incorporate pertinent feedback from stakeholders. The 90% design will include the construction drawings for the temporary inflow pilot pumping system, draft technical and environmental specifications, contingency plan, and opinion of the probable cost of construction. The 90% design will be coordinated with the permitting agencies to obtain the necessary permits. This involves holding additional pre-application meetings, drafting and submitting permit applications, and responding to requests for additional information. The permits include USACE or FDEP Section 404, USACE Section 408, and Florida Environmental Resource Permit. Based on the feedback from the permitting agencies, the 100% design will be prepared.

The project bid documents will then be created, the request for proposals will be drafted and sent out for bidding, and an award will be made for construction of the temporary inflow pilot system. The pilot system will then be constructed in accordance with USACE permit requirements. The temporary inflow pilot system is proposed to be operated for one year in parallel with continued research monitoring and modeling. This approach allows for data to be collected on changes due to small scale ocean inflow at the study site compared to the reference site, directly assessing impacts on focal biological communities and to validate DO, nutrient, and Chl-a predictions. The temporary pump system established for the project will be decommissioned at the end of the research period with the pipe and pump removed from the site. The results of the full Restore Lagoon Inflow Research project will be summarized to provide information and analysis to stakeholders and decision-makers on the viability of a full-scale, permanent ocean inflow system.

3.2 Next Steps

As part of the proposed subsequent phases of the full Restore Lagoon Inflow Research project, specific next steps for each project task are summarized below.

3.2.1 Modeling and Engineering (Task 1)

3.2.1.1 Inflow Design

The engineering team will continue to work with Tetra Tech to address any requests for additional information or modifications to the design as part of the permitting process. Future work includes preparing and submitting the permit application, which is estimated to take between six months to more than a year, depending on the discussions with the agencies. Once permitted, construction of the pilot system could happen relatively quickly, and it could be possible to start pumping water within the year.

The engineering team will also continue to evaluate options for a permanent inflow structure, if deemed feasible from the pilot system results. At scales greater than those proposed for the pilot system, a pump system may be inefficient so alternative passive mechanisms allowing tidal exchange will be investigated. To provide better evidence for the benefits of such large-scale exchange, manuscripts developed during Phase 2 will be completed and submitted for publication in a peer-reviewed journal.

3.2.1.2 Water Level, Salinity, Temperature, and Circulation Monitoring

The long-term water level, salinity and temperature stations will continue to operate. The stations were surveyed last year to North American Vertical Datum of 1988 (NAVD88) vertical datum. The team will continue to adjust the historical data to this new datum, and all new data cataloged will be converted to the NAVD88 datum. Data will continue to be offloaded and instruments serviced on a quarterly schedule. Work will continue to validate and evaluate the conductivity and salinity data, as salinity has the greatest uncertainty. The sensor array will provide valuable data on the performance of the pilot inflow system, which will guide collocating real-time sensors to measure salinity and temperature in the experimental and reference sites. The Acoustic Doppler Current Profiler (ADCP) deployments carried out in the latter part of Phase 1 and continued through Phase 2 improved understanding of IRL and BRL circulation patterns. These deployments should continue to establish a multi-year record of IRL circulation patterns and capture interannual variations in estuarine circulation linked to the large sea level oscillations in the coastal ocean that have been observed at multiyear time scales. The ongoing monitoring effort combined with the planned enhancements will allow an additional level of confidence in model predictions in BRL by providing for further model validation within the pilot project period.

3.2.1.3 Modeling

New data collected by the project team combined with long-term monitoring conducted by Ocean Research and Conservation Association and Harbor Branch Oceanographic Institute will be used to calibrate and validate two-dimensional circulation models such as Advanced Circulation (ADCIRC). The timeline to complete the ADCIRC modeling and validation using in-situ data would be one year, which would involve collection of updated data, system modeling using the latest published model framework, and final results analysis. The resulting data and models will help to better understand the natural flushing cycles that occur between late summer and winter in IRL.

The EFDC/Hydrodynamic and Eutrophication Three-Dimensional (HEM3D) model produced results that document the potential benefits of enhanced flows into BRL. The next step will be to improve the coupling between the watershed Spatial Watershed Iterative Loading (SWIL) model and in-estuary EFDC model. Refinements of the SWIL model include TN and TP components

that will be used to improve the already well calibrated EFDC model. This will require an estimated 12-month effort. Model predictions of Chl-a and the potential to predict HAB outbreaks are also encouraging and will be improved by further adjustments to the model rates and coefficients. The effort to predict HAB conditions is enhanced by the ADCP survey of circulation dynamics and EFDC model tracer studies. Variations in water quality and HAB occurrence will be investigated in the next phase. Continued effort is required to quantify water quality inputs through the tidal inlets that connect the coastal ocean to the IRL system. This will require continued search for nearshore coastal ocean water quality data, including evidence of HAB triggers that may be associated with Gulf Stream dynamics. Along with continued monitoring and further calibration of ongoing models, this effort should extend over a 12-month period in the next phase.

3.2.2 Geochemistry (Task 2)

This project has greatly improved our understanding of nutrient cycling in the IRL system, especially in sandy sediment and water column. These data are useful not only to modeling possible impacts of inflow, but for HAB and generalized nutrient load modeling, especially to help evaluate changes to temperature and rainfall associated with changing climatic patterns. The lagoon is dynamic and, with this temporally limited dataset, it is not possible to isolate natural, seasonal patterns from event scale occurrences. This would be more feasible in the near future (1–2 years) if data collection were to continue. Data to date have demonstrated the importance of processes in sandy sediments and on particles, and have yielded wide ranges of values for these critical processes. Additional data collection is needed to explain seasonal versus event-scale variability and improve statistical power of trends identified to date, improving confidence in extrapolated models. Due to the importance of bottom water DO towards cycling of both N and P and because this is the only continuous dataset for bottom water DO to date, long-term support is needed for this network of quality controlled bottom water sensors. These collective datasets are tools that will help managers select restoration projects based on potential to restore the natural cycling of N or P to make efficient use of taxpayer dollars. To continue the specific study of inflow, the next step is to investigate changes in oxygen and nutrient cycling in direct mixtures of lagoon water and seawater over time. This next step requires one year and reflects the large fraction of overall nutrient cycling that occurs in the water column and non-conservative changes when particles are mixed. This information would also validate nutrient loading models developed during Phase 2. These next steps would take place before and concurrently with the proposed pilot inflow project. Data to date support a limited test of inflow as part of a multifaceted approach to lagoon restoration.

3.2.3 Biology (Task 3)

3.2.3.1 Fish Community Modeling

In the next phase, Phase 2 abundance projections would be updated using the most current predictions for salinity, DO, and temperature under alternative pumping scenarios. This timeline would be less than three months, once finalized water quality data are available from the inflow system. The second goal would be to build on Phase 1 and 2 modelling efforts with development of mechanistic models to quantify the cause-effect responses of fish abundance, movement, and habitat use to specific change in salinity, DO, and temperature. This would require continuing the relationship with NASA KSC and Herndon Solutions Group biologists to study fish movement in in response to inflow via acoustic telemetry. This work would begin a few months before, continue during, and extend for at least six months after pilot pumping occurs. The partnership with KSC biologists leverages state and federal funding through integration with the IRL Florida Atlantic Coast Telemetry array. As part of these efforts, support would be provided for Fish and Wildlife Research Institute's (FWRI) Fisheries Independent Monitoring (FIM) team to increase sampling frequency and BRL data availability. Data collection for this effort would begin before pilot

construction, continue through the pilot pumping, and extend for a minimum of six months after the temporary inflow pilot pumping finishes to observe the pumping effects and collect sufficient data to create mechanistic models. Building the mechanistic models is time and resource intensive, but model infrastructure can be built concurrently with field data collection, which would then be integrated into the mechanistic model to produce final projections of species and community response to inflow.

3.2.3.2 eDNA

Baseline eDNA sample analyses initiated in Phase 1 and completed in Phase 2 improved understanding of biodiversity patterns in the lagoon and confirmed the utility of the three approaches initiated to investigate system response to enhanced inflow. To fully leverage eDNA data, we propose enhancement of existing eDNA baselines and post-pumping eDNA sampling and data analysis in the next phase as a compliment to fish modeling and direct assessment of experimental inflow impacts on key groups. The eDNA goals for the next phase are broken down into core deliverables: (1) final metazoan and crustacean marker testing and application to newly collected and archived samples (1 year); (2) process and analyze samples collected in July during Phase 2 (2 months); (3) post pumping sampling, sample processing, and analysis (6 months); and (4) final analyses and assessment of inflow impacts on lagoon biodiversity. eDNA deliverables can be completed concurrently in a period of one year that would extend six months past completion of the pilot inflow system pumping.

3.2.3.3 Benthic Fauna, Seagrasses, and Phytoplankton

Detailed assessment of important planktonic and benthic communities during Phases 1 and 2, taken together with existing datasets from project partners and long-term biological monitoring programs led by SJRWMD and NASA KSC, underscore the high variability of targeted communities, and need for improved restoration efforts to ensure the stability and recovery of the lagoon ecosystem. These findings demonstrate the importance of investigating impacts on the ecosystem and key species through construction of a temporary inflow pilot system to predict the benefits and potential negative impacts of a larger project. To address the naturally high seasonal and inter-annual variability of lagoon communities, an additional year of pre-inflow monitoring during the permitting process is recommended. To investigate inflow-driven environmental shifts, monitoring community response during and for up to one year after implementation of the temporary inflow pilot system is required. This will allow for data collected during and after completion of the pilot project to be compared to multi-year pre-inflow baseline data, where much of the seasonal variation can be accounted for to better reveal inflow effects. With these data, a final assessment of the effects of inflow on key benthic and planktonic communities will be conducted to allow stakeholders and elected representatives to evaluate enhanced inflow as a lagoon conservation and restoration tool.

4 Task Summaries

4.1 Modeling and Engineering (Task 1)

The objectives of the modeling and engineering task were to:

- Conduct numerical model predictions of hydrodynamics, flushing rate, and water quality with and without enhanced inflow using EFDC and HEM3D models at a two-year scale.
- Conduct salinity, water temperature, and water level predictions over a minimum of a two-year time scale with and without enhanced inflow.
- Support the Biological Monitoring Team (Task 3) and other project teams with model produced environmental data.
- Setup and run a coastal processes model to provide predictions of sediment transport, shoaling, and currents within Port Canaveral with and without enhanced inflows.
- Collect flow and water level data supporting model verification at verification Dragon Point, Sykes Creek, and Barge Canal.
- Build an archive of model data to support permit activities.
- Advance the design of a temporary inflow structure.
- Prepare for permitting of a temporary pumping station, transporting seawater from the ocean into BRL.

4.1.1 Approach

The Phase 2 project approach included a combination of numerical modeling and continued data collection to quantify the influence of enhanced inflows on flushing rates and water quality in the north BRL, assuming pumping produced inflows from the west compartment of Port Canaveral. The overall approach was designed to meet permit requirements governed by federal and state regulations. The permitting process was initiated based on the final site and design determination.

The engineering team, including graduate and undergraduate student interns, assimilated research results from all project tasks to address questions and concerns from the permitting agencies and stakeholders. During the agency pre-application meetings, issues were discussed and a determination of permitting requirements established. Appropriate design modifications were made based on the input from stakeholders. Working with the support of experts from Tetra Tech, the structure design developed by Florida Tech to the 20% level during Phase 1 was advanced to the greater than 60% design level during Phase 2. The location and scope of the pilot was finalized, and the final pilot design was presented to agencies and stakeholders.

The modeling approach included continued assessment of flushing rates using the EFDC environmental modeling platform. This model code was successfully applied in Phase 1 to assess and compare pumping and water control structure scenarios for BRL and central IRL. In Phase 2, the model predictions were extended to include calculation of water quality constituents using the water quality module contained within the EFDC modeling platform. The model computational grid area extends from Ponce de Leon Inlet north of the Mosquito Lagoon into the IRL compartments to Fort Pierce Inlet. This multi-parameter finite difference model represents estuarine flow and material transport in three dimensions and has been extensively applied to shallow estuarine environments in Florida and other coastal states.

The EFDC model was coupled with the water quality model, HEM3D, which represents the four algae species in carbon units. The three organic carbon variables play an equivalent role to biochemical oxygen demand. Organic carbon, N, and phosphorous (P) are represented by up to

three reactive sub-classes: refractory particulate, labile particulate, and labile dissolved. To produce useful predictions for BRL and IRL, water quality boundary conditions were applied. Watershed-based and tributary-based nutrient loads were specified along with measured and assumed nutrient flux rates from benthic sediments.

Additional updates to the modeling scheme to produce water quality model boundary conditions include watershed inputs from the SWIL model and groundwater inflow predictions compiled by Florida Tech (Dr. Pandit and his team). Under the Restore Lagoon Inflow Research project, the SWIL model was updated to produce predictions of nutrient loads though the end of June 2020. By extending EFDC modeling to include water quality predictions, Dr. Pandit and his team updated the groundwater inflow predictions to include nutrient concentrations. This, in combination with the other nutrient boundary conditions, provided a more complete representation of the IRL nutrient budget and facilitated sensitivity tests based on the proposed enhanced inflows to BRL.

An additional modeling approach was conducted to evaluate potential impacts within the Port Canaveral basin from pumping water from west compartment into BRL. The enhanced flows were evaluated for effects on the Port's circulation and potential for altering sedimentation rates. The model predictions were performed using the USACE Coastal Modeling System (CMS) that was used to assess enhanced inflows in earlier studies (Zarillo, 2015 and 2018). The previous studies did not include sediment transport calculations, which were added to the updated application. Model simulations included a full set of boundary conditions consisting of water level time series, wind forcing, and wave forcing. CMS-Flow produced predictions of water level and circulation and was coupled with the CMS-Wave model to provide wave forcing and wave-current interaction, which are important for the sediment transport regime at the Port Canaveral entrance.

The modeling effort was supported by continued water quality and hydrodynamic sampling in BRL. These data were crucial in supporting Phase 2 to identify a location and design for the pilot project. The modeling team continued collection of current velocity and water level data at key locations in BRL. The water level and flow data were applied to verify performance of the hydrodynamic model. New sensors were also deployed in the inflow basin. A transect of four instruments was deployed in the cove out into BRL just south of the Canaveral Locks. These four stations measured salinity, temperature, and water depth.

4.1.2 Results

4.1.2.1 Inflow Design

A pipe and pump system with a flow rate of 0.5 m^3/sec was chosen for the pilot project due to its feasibility and practicality of construction and operation. The system can be used as a temporary structure to study the physical, chemical, and biological effects of introducing ocean water into IRL or as a permanent structure, if the inflow proves beneficial. The system is easy to control, and the pipe can be blocked off at any time.

The pump intake would be located east of the State Road 401 bridge and west of the Canaveral Locks. An optimal path for the pipeline was identified with discharge into BRL in a semi-enclosed basin just south of the locks. The design for pilot pumping is based on past work funded by SJRWMD and produced by CDM Smith (2014, 2015, and 2017) and modified to meet the flow rate needs of this project. The intake structure was modified from the design in CDM Smith (2017) to minimize the impact to the channel banks, and the outfall structure is similar to CDM Smith (2017) but modified for the new location.

The inflow structure will be located inside Canaveral Inlet, directly behind the fendering wall that protects the lock system and will protect the structure during storm events (**Figure 4**). The inflow structure will consist of the pump intake in a vertical orientation and a 90-degree bend so the pipeline will run parallel to the water surface until it contacts the ground. The intake will be surrounded by a cage structure to ensure manatees, fish, and other marine animals are not pulled into the pipe or harmed from the intake propellers. The intake and pipe portion over water will be supported by pairs of piles evenly spaced along the pipeline so that the pipeline does not exceed its maximum deflection. The electric drive unit of the pump will be placed on land near the pipeline on top of a skid frame.

The outflow structure will be placed on the west side of Mullet Road so the fresh ocean water will feed directly into BRL, enabling it to flush BRL and IRL (**Figure 4**). The pipe will run over land and will cross Mullet Road inside of the USACE property. Once across the road, the pipeline will continue west-southwest to the shrub line, and then cross the fence heading south on the west side of the access road. To minimize impact to the existing mangroves, the pipeline outfall will use the existing access points to BRL that have been cleared (**Figure 4**).

Figure 4. Location of inflow and outflow structures inside Port Canaveral (Google, 2021)

4.1.2.1.1 Pipeline and Pump

The most feasible pipe diameter was determined to be 20 inches (0.51 m), due to the required hydraulic and shaft power. All pipe diameters evaluated had a similar pump efficiency at the pilot flow rate. Key factors included height constraints for designing a vehicle ramp, as well as annual cost savings by using an axial flow pump compared to a mixed flow pump. Most of the pipe's path from the inflow structure to the outflow structure is uninhabited land with very few disruptions; however, the pipe must cross an access road to reach the outflow basin. To protect the pipe, the pipe will be laid across the road inside of USACE property, just south of the Lock. **Figure 5** shows where the pipe will cross the access road with an arrow pointing to the location of the crossing.

Figure 5. Location of pipe road crossing (Google, 2021)

Since the pipe will be above ground, a ramp must be added so traffic is able to get inside USACE property. Due to construction on the locks, trucks may need access to this road. Therefore, the design vehicle chosen for the ramp design is an intermediate semitrailer WB-40. The maximum weight of the semitrailer is 80,000 pounds (36,287 kilograms) with a fully loaded trailer and the maximum axle load for a tandem axle is 34,000 pounds (15,422 kilograms) (Harwood et al., 2003).

Manufacturing companies, such as Bluff Manufacturing, make crossover ramps out of heavy-duty steel to protect pipes and allow heavy equipment to pass over the obstacle. Bluff Manufacturing crossover ramps can accommodate equipment up to 160,000 pounds (72,575 kilograms) (Bluff Manufacturing, 2021). The Crossover Ramp Worksheet with site-specific dimensions was sent to Bluff Manufacturing to receive a quote for the production and freight of a ramp that fits the project location. **Figure 6** shows a top view of the location and ramp placement.

The inflow structure was designed based on the Moving Water Industries (MWI) Pumps Hydraflo™ model HAC316 pump specifications and dimensions. The standard vertical Hydraflo™ pump will be submerged and placed in an inflow cage while the electric drive unit will be located on land (MWI Pumps, 2020). The MWI Pumps Hydraflo™ model HAC316 will be installed with a vertical orientation.

4.1.2.1.2 Inflow Structure

A top view of the proposed inflow structure location is displayed in **Figure 7**. A minimum intake clearance was calculated to ensure particles of fine sediment will not be pulled into the pump intake. To protect wildlife, such as manatees and fish, and to protect the pump from human impacts, the pump will be surrounded by a cage structure with grated screens on the side. The cage will be placed on the seabed and the pipe and intake pump will be lowered vertically inside of the cage. For the protection of manatees, the maximum grating space will be 8 inches (0.20 m) apart (Comprehensive Everglades Restoration Plan, 2006). For the protection of small fish, the grating should be 1 inch by 4 inches (0.03 m by 0.10 m) (U.S. Fish and Wildlife Service, 2019). Therefore, the grating that will be used on the caged inflow structure will be 1 inch by 4 inches (0.03 m by 0.10 m) galvanized steel grating.

Figure 6. AutoCAD drawing of ramp structure top view

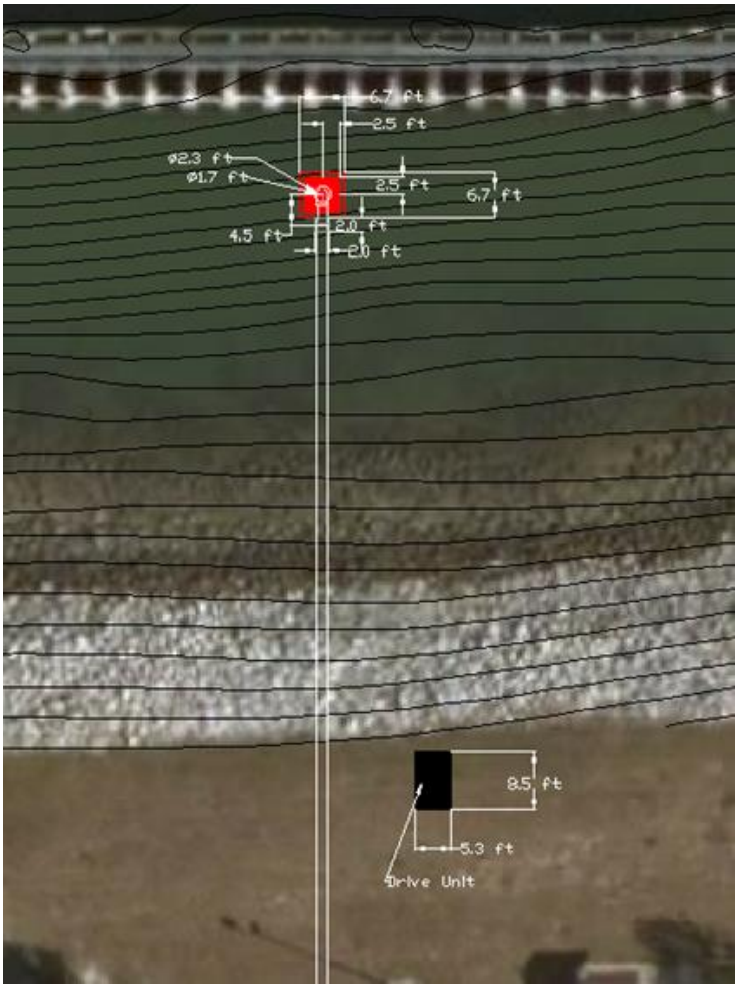

Figure 7. AutoCAD drawing of inflow structure top view

4.1.2.1.3 Outflow Structure

The outflow structure was designed based on the Hydraulics Manual from the Oregon Department of Transportation (ODOT). An energy dissipator is needed at the pipe outlet so that the bank is protected from erosion as the water flows out of the pipe and into BRL. The design of the outflow structure for the pipe and pump system uses riprap pads and riprap lined basins. Riprap pad dissipators allow the flowing water to cross over riprap before it enters the waterbody, causing a considerable decrease in hydraulic energy from the flow (ODOT, 2014). Riprap lined basins are often used for projects where fish passage is desired, flow depths and velocities exceed acceptable values for a riprap pad, and the pool is not a safety hazard to the public (ODOT, 2014).

The dimensions of the riprap pad were calculated to be 6.67 feet in length, 8.35 feet in width, and 2.3 feet in thickness (2.03 m by 2.55 m by 0.70 m). The riprap pad toe must extend past mean lower low water (a distance of 37.7 feet [11.5 m]) to prevent erosion (ODOT, 2014). Under the riprap, a geotextile, non-woven filter fabric will be placed on the foundation. A 2-inch (0.05 m) sand layer is also needed on top of the filter fabric to protect it from ripping when coming into contact with the riprap rocks. A top view of the outflow structure location is shown in **Figure 8**.

Figure 8. AutoCAD drawing of outflow structure top view

4.1.2.1.4 Cost Analysis

The pipe and pump system cost analysis included construction, annual costs for one year, and decommissioning. The overall cost for these items was estimated to be $711,245.32.

The costs to construct each component of the system were estimated. A 30% contractor mobilization and overhead cost was added to the total price, as well as a 40% contingency for miscellaneous site work and uncertainties. The total construction cost is $551,084.33 (**Table 1**). The annual cost included operational costs for electricity to run the pump for 24 hours a day for one year, and maintenance costs for the pump and pipeline. A 40% contingency was added for increased electricity costs and unexpected maintenance costs. The total annual cost is $47,578.63 (**Table 2**). The decommissioning costs at the end of the project's lifespan included the removal of the system components. A 30% contractor mobilization and overhead cost was

added to the total price, as well as a 40% contingency for miscellaneous site work and uncertainties. The total decommissioning cost is $112,582.37 (**Table 3**).

Table 1. Projected construction cost for pipe and pump system

Structure	Total Cost
Pipeline	$93,635.00
Pump	$149,092.00
Ramp	$49,806.00
Inflow	$31,196.25
Outflow	$438.00
Subtotal	$324,167.25
Contractor Mobilization, Overhead, and Profit (30%)	$97,250.18
Contingency (40%)	$129,666.90
Total	***$551,084.33***

Table 2. Projected annual cost for pipe and pump system (U.S. Department of Energy, 2001; ElectricRate, 2020)

Item	Number	Units	Per Unit Cost	Total Cost
Electricity	287423	Kilowatt Hours	$0.1165	$33,484.73
Routine Maintenance	1	EA	$500.00	$500.00
Subtotal				$33,984.73
Contingency (40%)				$13,593.89
Total				***$47,578.63***

Table 3. Projected decommissioning cost for pipe and pump system (RSMeans, 2021; Kaiser, 2017; CDM Smith, 2017)

Item	Number	Units	Per Unit Cost	Total Cost
Riprap Removal	10	Tons	$33.25	$332.50
Pile Removal - Equipment and Labor	1	EA	$10,250.00	$10,250.00
Pile Removal - Labor for Crew	12	Hours	$800.00	$9,600.00
Pipeline Removal (On Ground)	850	Feet	$11.40	$9,691.29
Pipeline Removal (Over Water)	150	Feet	$57.01	$8,551.14
Safety Signs	5	Days	$2,000.00	$10,000.00
Diver, Boat, Misc.	5	Days	$3,560.00	$17,800.00
Subtotal				$66,224.92
Contractor Mobilization, Overhead, and Profit (30%)				$19,867.48
Contingency (40%)				$26,489.97
Total				***$112,582.37***

4.1.2.2 Monitoring Data

4.1.2.2.1 Long-term Water Levels

Three existing stations were upgraded with a real-time data collection and reporting system. In April 2021, student researchers installed the new instruments at Kars Park on Merritt Island (closest to the inflow site), Lansing Island in Indian Harbour Beach, and Riverside Park in Sebastian (**Figure 9**). The live readout of water level, temperature, and pressure plots from these locations can be viewed at https://dashboard.hobolink.com/public/11961/Dashboard%2003-31-2021-04-15-2021%2020:39:32.

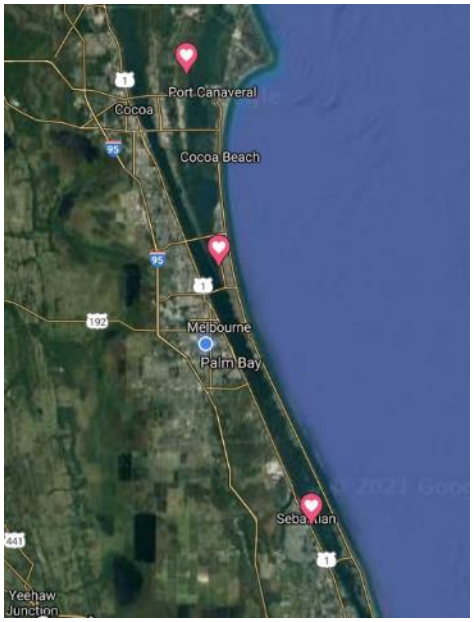

Figure 9. Location of long-term water level gauges

The long-term water level data show very small water level fluctuations in the northern BRL (closest to the study site), on the order of a few cm. Larger water level fluctuations are driven by meteorological disturbances. On a longer time scale, the water levels vary on a seasonal basis, with higher water levels in late fall and lower water levels in the summer, as seen in the 2.5-year record from November 2014 to June 2017 (**Figure 10**).

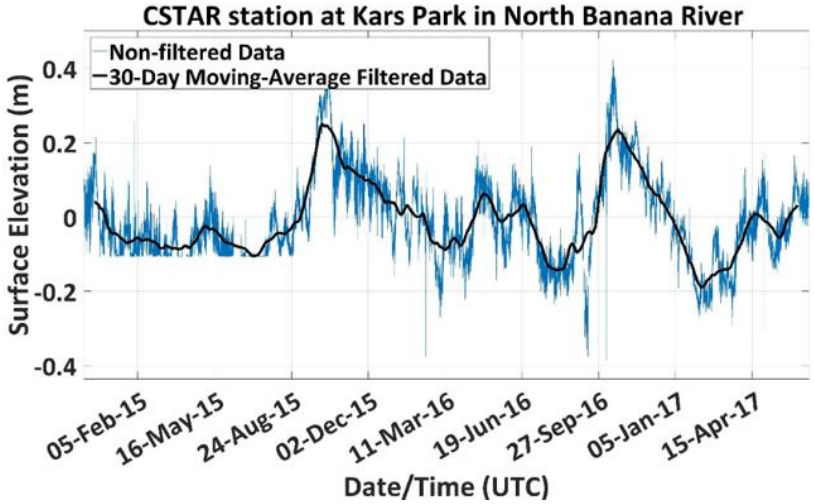

Figure 10. Long-term water level record for northern BRL station at Kars Park

4.1.2.2.2 Salinity, Temperature, and Depth

During Phase 2, four new instrument stations were deployed to monitor mean water level fluctuations, salinity, and land temperature along a transect within the inflow project site (**Figure 11**). Stations 1, 2, and 3 contain a conductivity-temperature sensor and pressure transducer. Station 4 only contains conductivity-temperature sensors (**Figure 11**). It was originally deployed with a single bottom-mounted conductivity-temperature sensor and another sensor was deployed on the date of the first data retrieval to monitor the difference between bottom and surface values.

Figure 11. Locations of the four salinity and depth instrument stations in the project area

Station 1 is located deep into the cove, just seaward of where the outfall will be located. The conductivity-temperature probe data showed highly varying salinity over the duration of deployment (upper and middle plots in **Figure 12**). The temperature data are more continuous and capture the gradual warming of BRL into the summer months (bottom plot in **Figure 12**). The salinity values appear to have been impacted by biofouling partway through the dataset. The pressure readings for station 1 were more accurate and dependable. The pressure data were converted into water level (depth), and ranged from 1.25 to 1.75 m. The water level fluctuations are mostly dependent on atmospheric disturbances as BRL is a wind dominated system.

Station 2 had similar issues with conductivity, which translated to the calculated salinity. The temperature data are in agreement with the temperature sensor on the pressure instrument. Both recorded the increasing temperature in summer (**Figure 13**). Station 2 recorded daily water level variation on the order of cm, and monthly fluctuations on the order of tens of cm. This is consistent with the measurements recorded across BRL at the long-term water level station at Kars Park.

Station 3 was found to be missing when the team was on deployment 7. It is thought that the buoy line was most likely cut by a passing boat and was dragged away by the current, or that the keel from a larger vessel moored nearby impacted the instrument, dragging it through the soft sediment bottom and burying it in the muck. Data for this station are only available May 28, 2021.

Station 4 has bottom- (**Figure 15**) and surface-mounted (**Figure 16**) conductivity-temperature sensors. The primary purpose was to study the mixing between the surface and bottom layers. The salinity from the surface mounted gauge was higher than the bottom mounted gauge, which could be due to groundwater seepage. This suggests that the water is not completely mixed and there is something causing a change in salinity between the surface and seafloor.

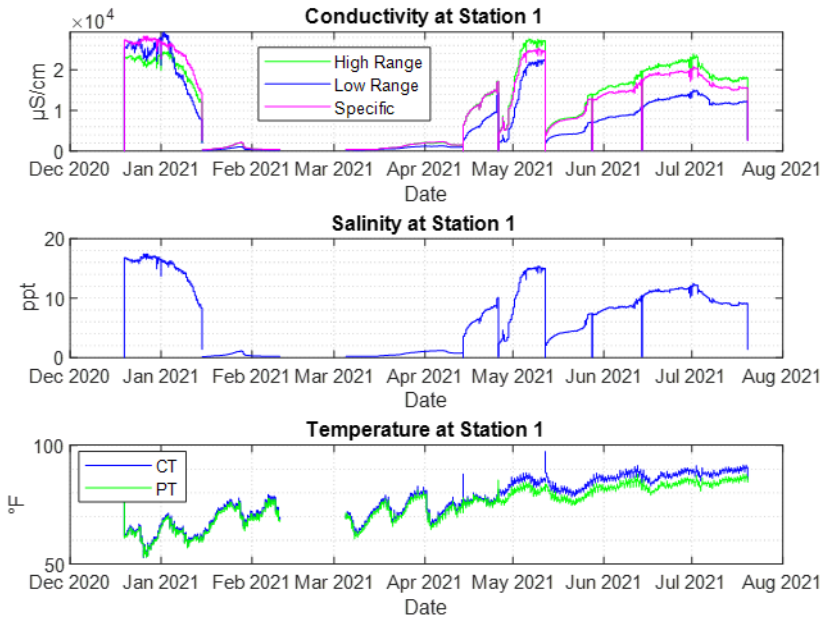

Figure 12. Station 1 data with recorded conductivity (top) converted to salinity (middle), and temperature (bottom) from the pressure (green) and conductivity sensors (blue)

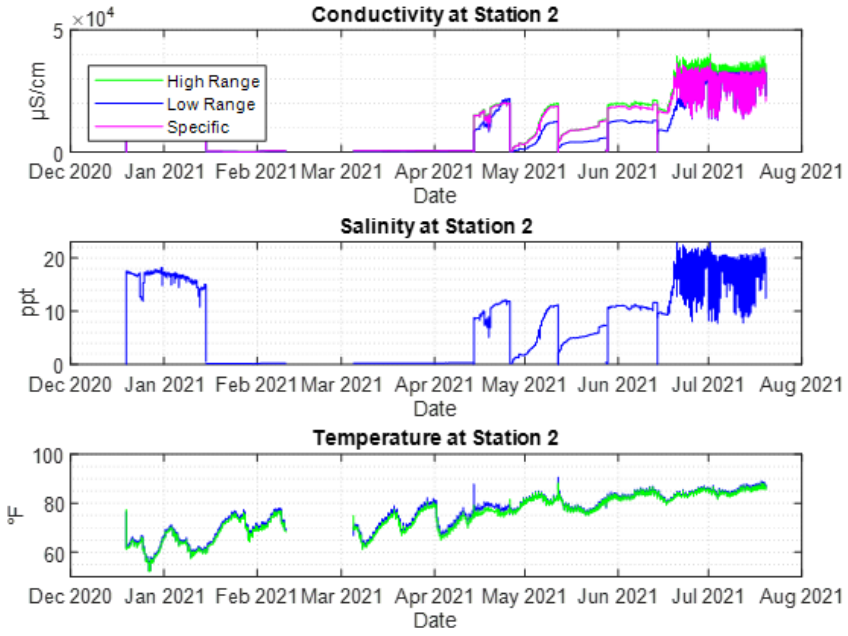

Figure 13. Station 2 data with recorded conductivity (top) converted to salinity (middle) and temperature (bottom) from the pressure (green) and conductivity sensors (blue)

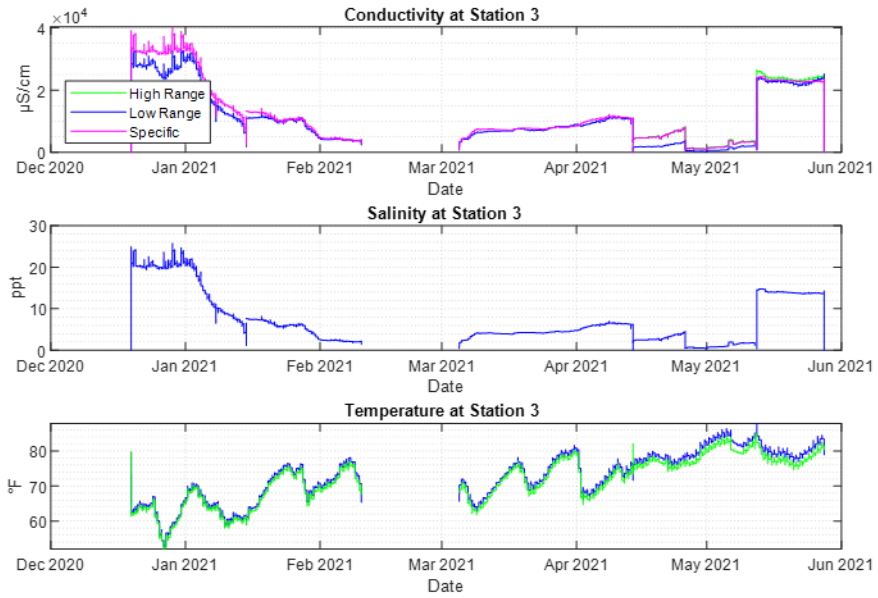

Figure 14. Station 3 data with recorded conductivity (top) converted to salinity (middle) and temperature (bottom) from the pressure (green) and conductivity sensors (blue)

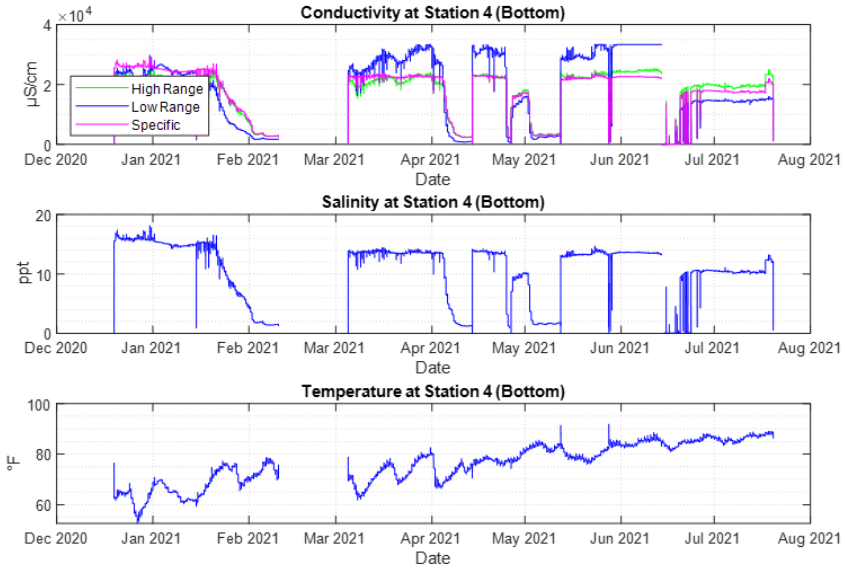

Figure 15. Bottom mounted conductivity/temperature sensor at station 4

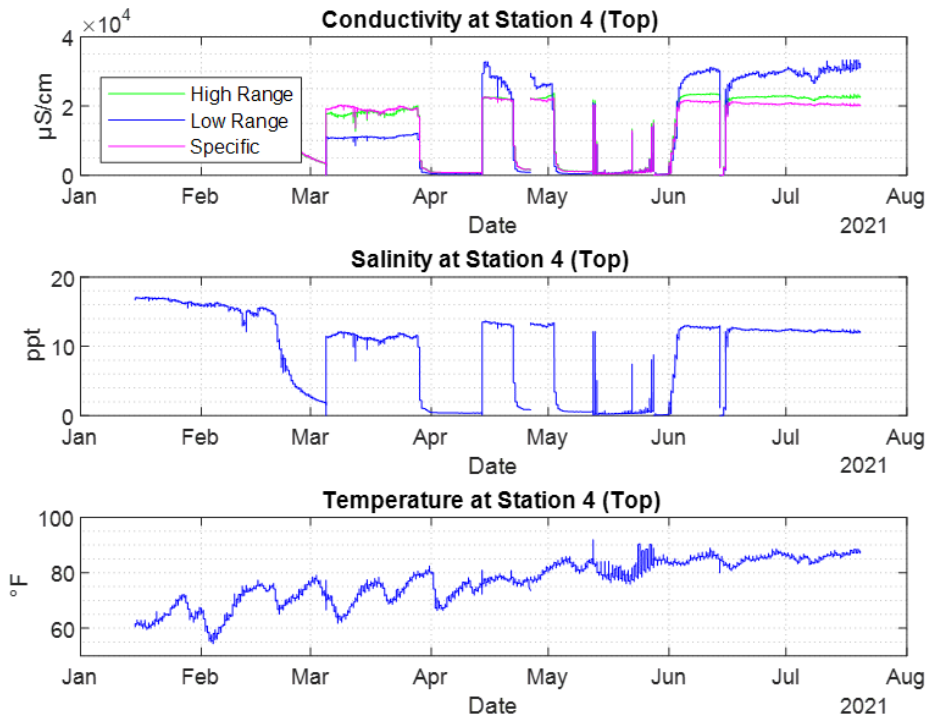

Figure 16. Surface/top mounted conductivity/temperature at station 4

4.1.2.2.3 ADCP Units

In early 2020, three ADCPs were deployed to record current velocities and directions. The ADCPs were placed at three locations: (1) Dragon Point, located at the southern tip of BRL; (2) Barge Canal, which runs east-to-west connecting BRL to IRL; and (3) Sykes Creek, which bisects Merritt Island and has inflow from IRL and freshwater sources (**Figure 17**).

The ADCPs maintain a blanking distance, or minimum distance to first cell of measurement in the water column, and record ten cells or "bins" meaning individual depth interval of averaged current speed and direction. Quality control of the data entails rejection of any bin higher than the recorded water level. While it is possible to use the binned plots, it is more helpful to average the velocities across the water column. To maximize the utility of the data, the velocities were averaged for every bin in the water column for each record. However, due to some large data gaps, this skews data by adding weight to the bins that pass quality control and thus must be treated with caution. A 24-hour moving average was also calculated and plotted.

The direction of the currents were also subject to quality control, and their display via rose-plot is weighted based on the corresponding bin velocity and then averaged to better illustrate the direction of flow. The two-month break (April and May 2020) in recording to retrofit additional memory into the ADCP deployed at Sykes Creek is seen in **Figure 18**. There is a large spike in current velocities in October and November 2020, which is as-yet inexplicable. The gap present in March and April 2021 is due to data recorded at the noise floor of the unit, which seems to be correlated with excess biofouling but could have been compounded by a lack of battery capacity. The currents at Sykes Creek flow predominantly south (**Figure 19**). This does not vary with season and only a proportion of directionality changes with the tides. A possible reason for this is the inflow from both ends of the Barge Canal and inflow from the northern extent Sykes Creek.

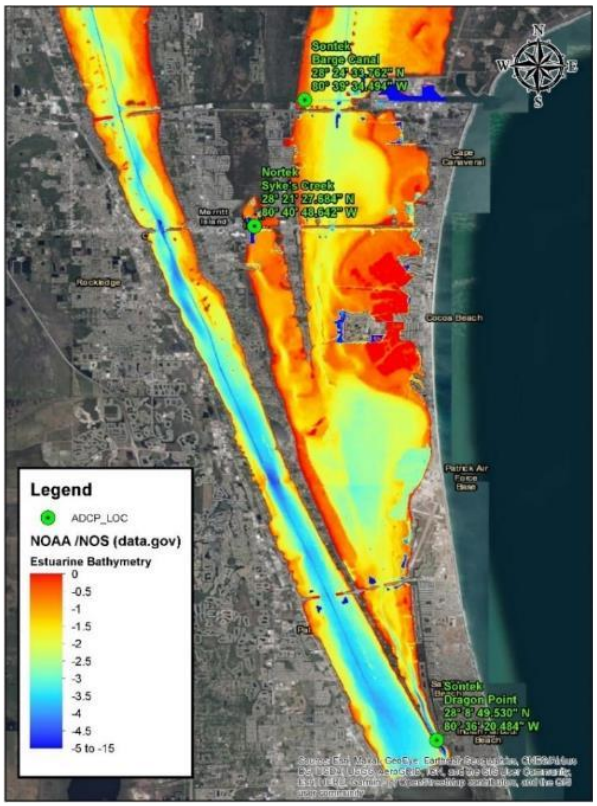

Figure 17. ADCP deployment locations and approximate bathymetry

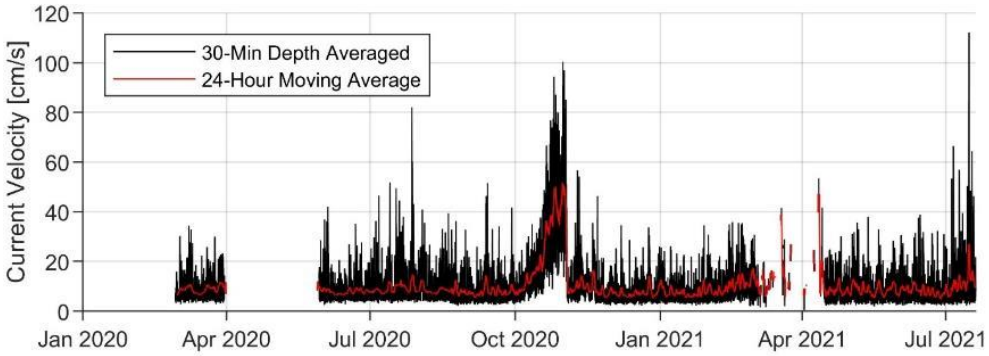

Figure 18. Time series of depth-averaged current velocities at Sykes Creek

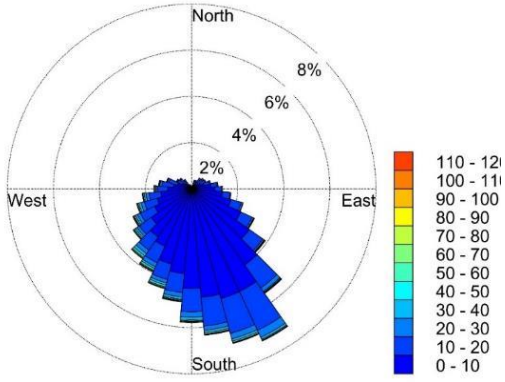

Figure 19. Rose plot of current direction at Sykes Creek

For Barge Canal, nearer the surface of the water column, more consistent data could be collected due to quality. This is likely due to the higher transmissibility of lower-frequency signals in fluid. To mitigate issues of the depth-averaged velocities being skewed toward the higher rate of transport as indicated in **Figure 20**, the increase in current velocities during October and November 2020 seem to disappear and the increase in velocities experienced from February through April 2021 remain. There seems to be a similar condition in the previous year. The direction of currents at Barge Canal, as shown in **Figure 21**, oscillate from east to west with some proportion flowing south. No significant proportion of these currents flow to the north. Between October 2020 and February 2021, these data suffered from poor quality in all but one bin, potentially weighting the current velocities in that range slightly higher.

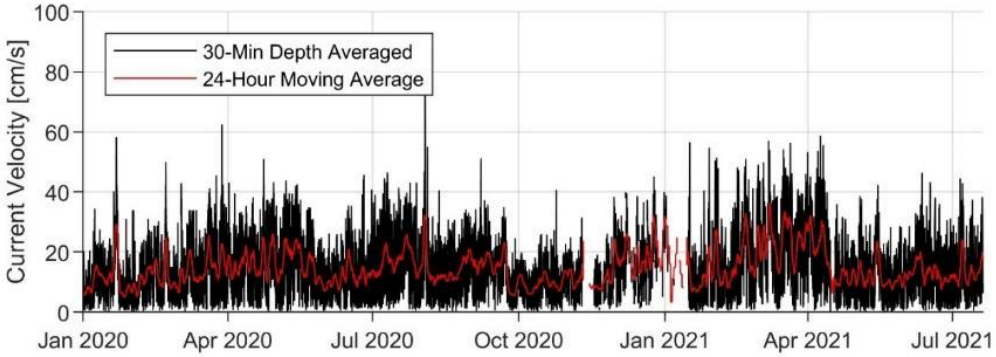

Figure 20. Time series of surface current velocities at Barge Canal

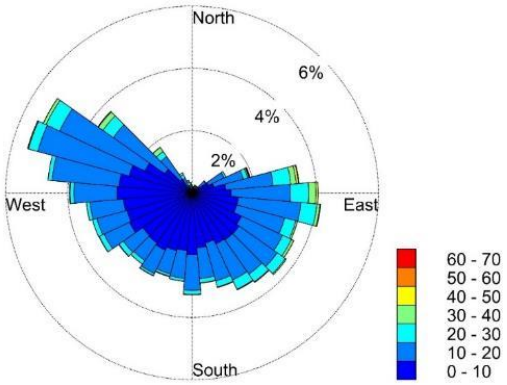

Figure 21. Rose plot of current direction at Barge Canal

The data for Dragon Point, as shown in **Figure 22**, are also marked by inconsistent quality during the October and November 2020 timeframe, and the moving average does not indicate any significant oscillation or trend. The direction of the currents at Dragon Point, as shown in **Figure 23**, are from southeast to northwest, which is expected because the channel in which it is located goes in the same directions.

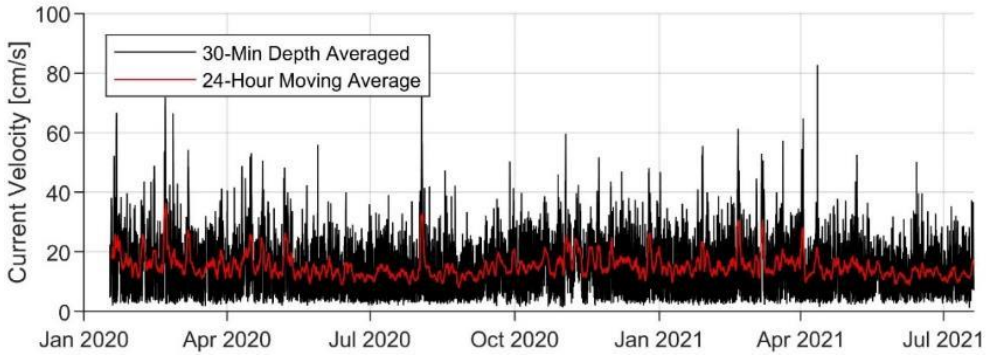

Figure 22. Time series of depth-averaged current velocities at Dragon Point

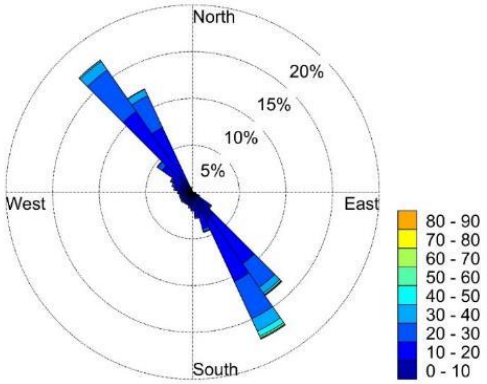

Figure 23. Rose plot of current direction at Dragon Point

The hydrostatic pressure is reported in decibars, which is approximately equal to one m of depth per decibar. These time series have been demeaned to better show correlation and a trend of increased water level is apparent between September and November 2020 (**Figure 24**).

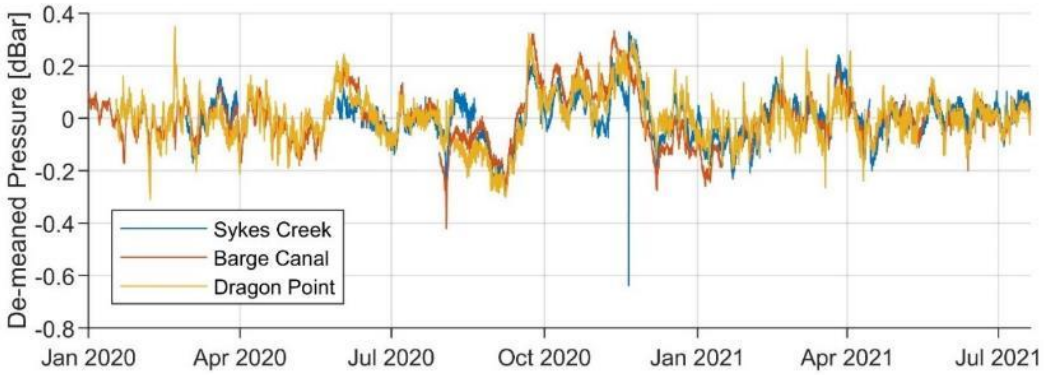

Figure 24. Combined demeaned pressure time series

The temperature of the water at each location varies predictably and seasonally with seemingly higher variation in late winter to early spring (**Figure 25**). Daily variation is greater at Sykes Creek and Barge Canal than at Dragon Point due to the depth of the units, Dragon Point being the deepest, but the pattern of oscillation in temperature looks the same at each unit.

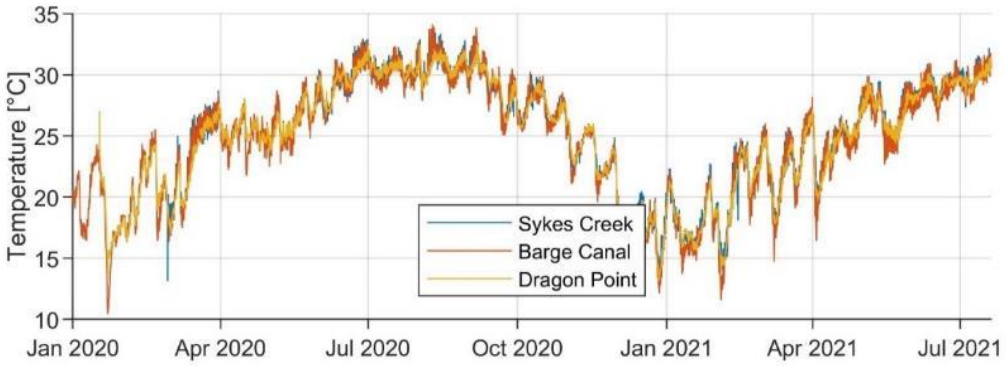

Figure 25. Temperature time series

These data were analyzed to find relationships between the data collected and environmental factors, such as water level and wind. Trident Pier at Cape Canaveral is the primary source of data and is sourced from the National Oceanic and Atmospheric Administration (NOAA) National Data Buoy Center (TRDF1). It is also useful to compare transport through the Florida Current to draw conclusions about the contributors to overall water level. These data were sourced from NOAA's Atlantic Oceanographic and Meteorological Laboratory's Western Boundary Time Series.

There is very little tidally influenced water level fluctuation in BRL. This is because the fluid flux at its boundaries are relatively constrained. One might assume that the water level at the Atlantic Ocean would have little effect, considering the locks at the Port restrict any flux and the next inlet is 35.4 km south of the southern opening to BRL and another 30 km north to the Barge Canal. However, a long-term relationship is seen when the water level in BRL is compared to the flux in the Gulf Stream (**Figure 26**). As shown in **Figure 26**, the water levels recorded at the three ADCPs and Trident Pier's 24-hour moving average of water levels track well. In **Figure 27**, the inverse relationship between Florida Current transport and BRL water levels is apparent.

The inverse relationship between Gulf Stream flux and water level is also apparent in the water level data from Trident Pier subject to a 24-hour moving average as shown in **Figure 28**.

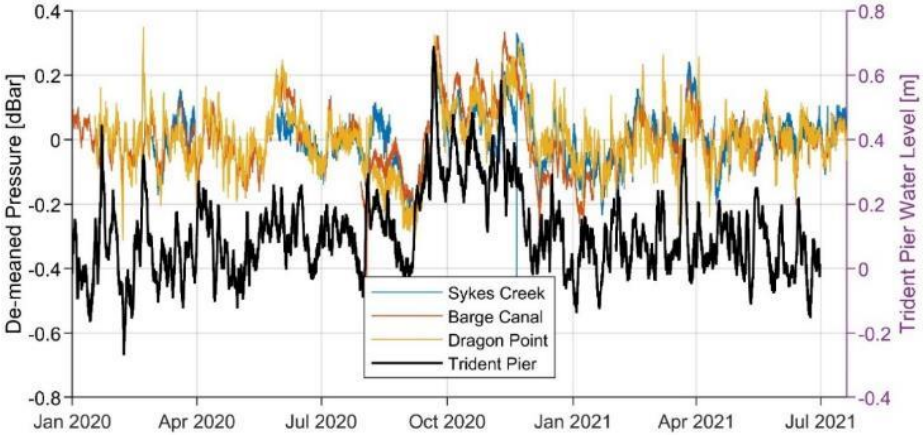

Figure 26. Water levels at ADCPs and Trident Pier

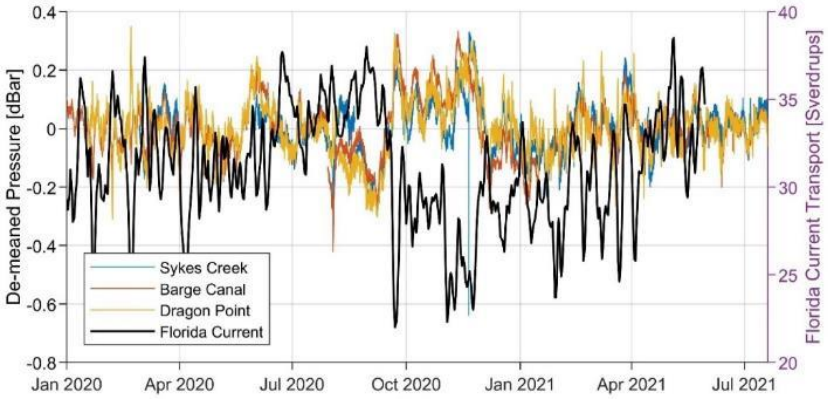

Figure 27. BRL water levels and Gulf Stream flux

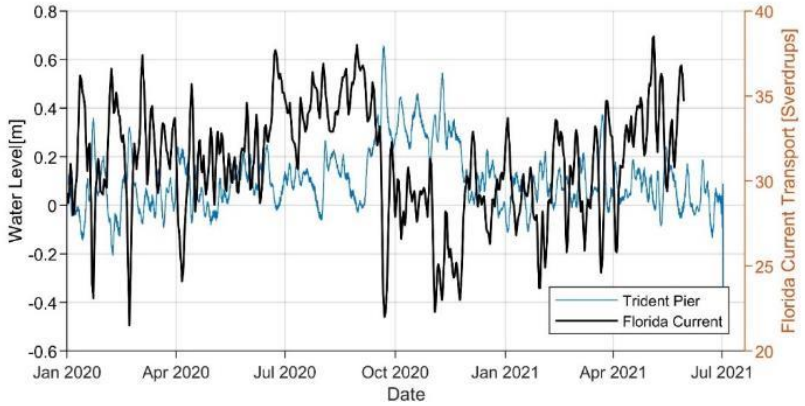

Figure 28. Trident Pier water levels and Gulf Stream flux

The flow in BRL in this northern compartment, which is essentially a restricted basin, was thought to be primarily driven by the wind, but these data suggest that coastal sea level and to a limited extent tides influence the direction of the current at Dragon Point.

Based on the ADCP pressure data, the tides have a small effect on the water levels in BRL but are distinguishable in the frequency spectrum. The pressure data were filtered by subtracting a moving average of 12.5 hours from the time series, which was then subject to a moving average of 6.5 hours to remove high frequency oscillations to better resolve the tidal influence in the time series. **Figure 29** clearly indicates tidal influence at the predictable diurnal and semi-diurnal tides.

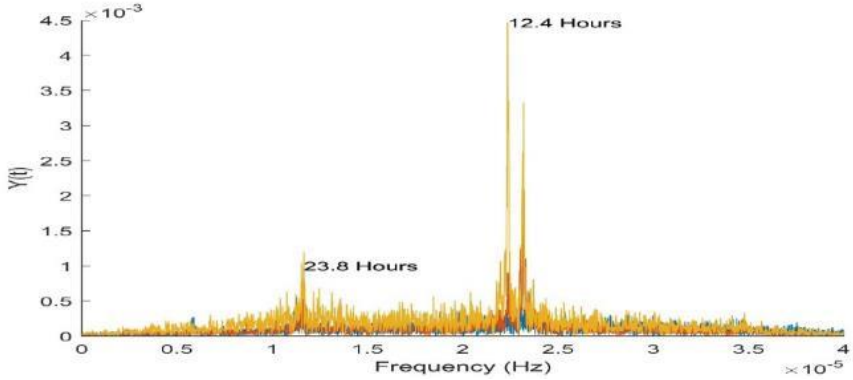

Figure 29. Frequency spectrum of water levels at 3 ADCP locations

To better resolve the flow patterns for BRL, it is also helpful to filter the directional data with a 6.5 hour moving average. This helps clarify the directional trends and allows for better interpretation (**Figure 30** and **Figure 31**).

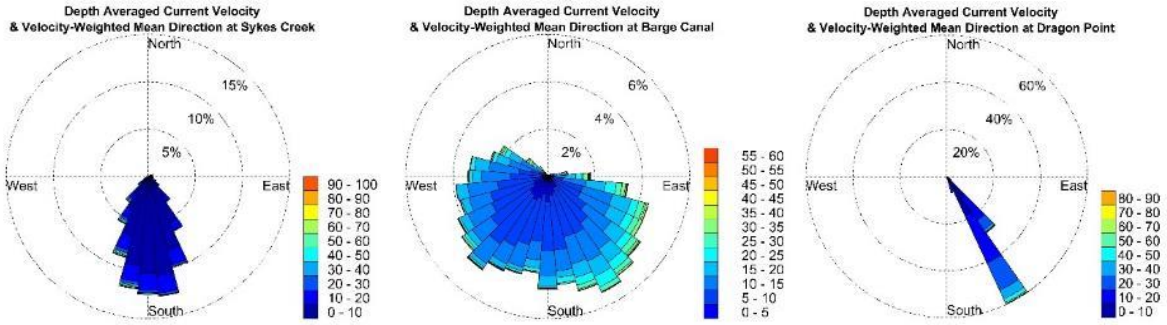

Figure 30. Filtered directional rose plots during south flow

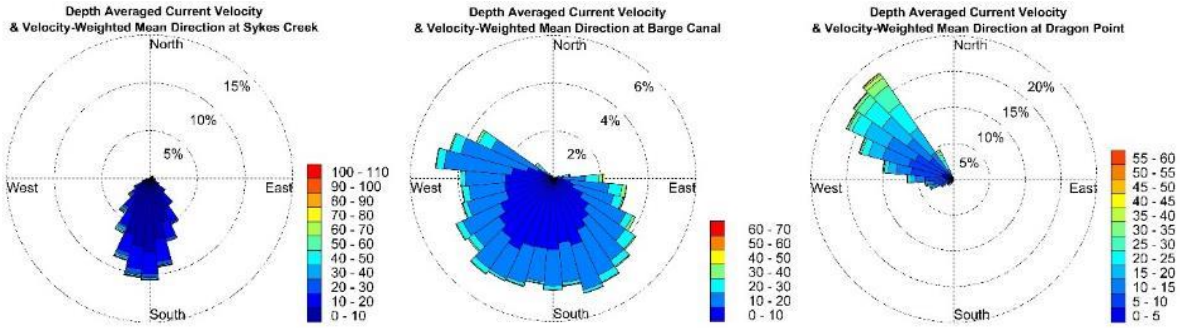

Figure 31. Filtered directional rose plots during north flow

Sykes Creek never reverses flow to the north and the flows around the Barge Canal ADCP are ambiguous, but there is a visible east-west oscillation in these rose plots. During a northward flow, water masses pass Dragon Point into BRL. By the time this flow pattern reaches the Barge Canal, there is likely hydraulic pressure from both ends as the influx from Dragon Point begins to be influenced by lower water levels of the coastal ocean. This results in variable currents in the Barge Canal station and, instead of circulating into IRL, the water is forced into Sykes Creek and reintroduced into BRL. Flows at Barge Canal are also potentially impacted by the isolation caused by State Roads 520 and 528 through IRL and BRL. **Figure 32** shows both the south (left) and north (right) current directions exemplifying a time varying reversing circulation pattern.

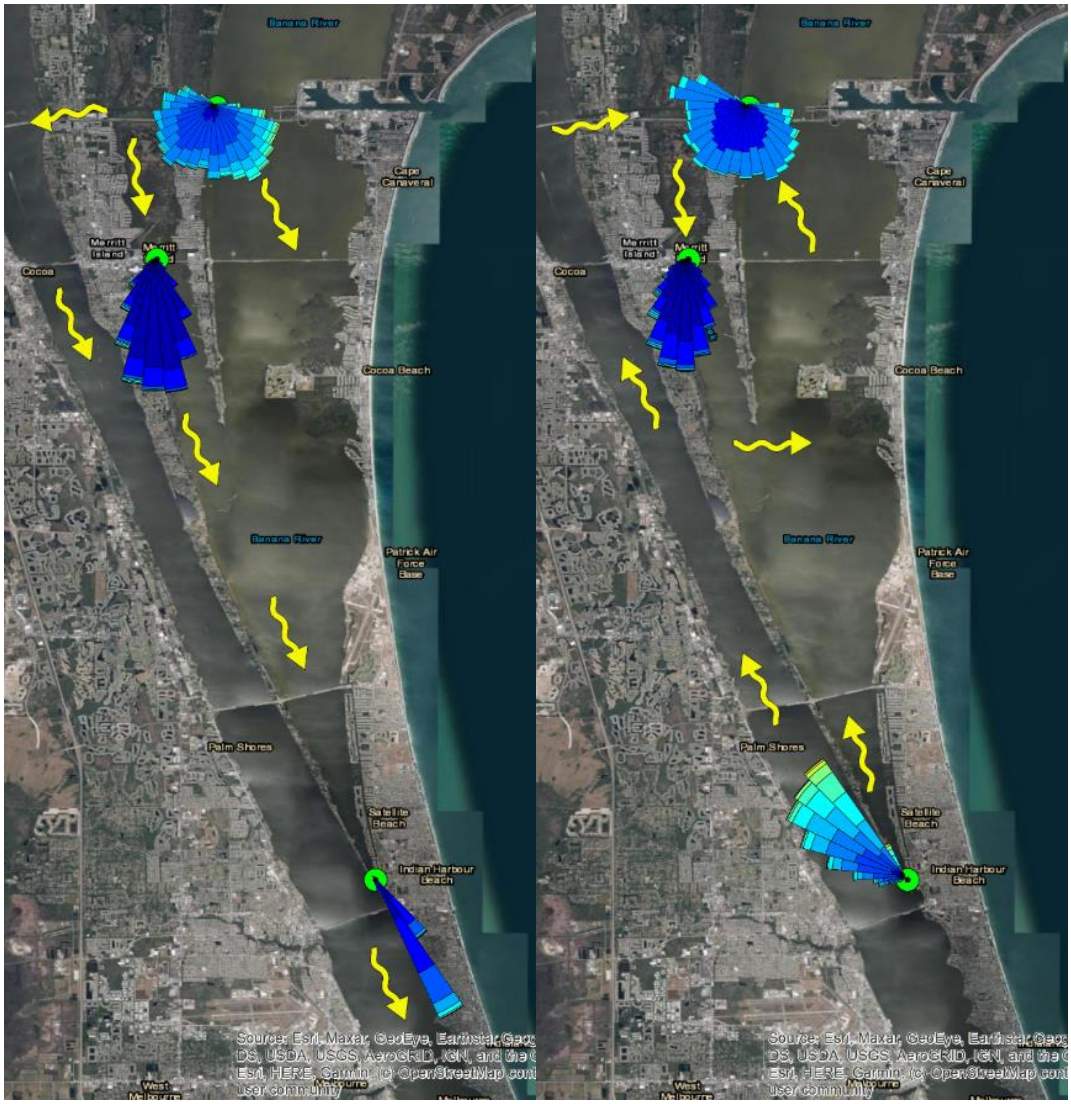

Figure 32. South and north directed current patterns

4.1.2.3 Modeling

Table 4 lists the model runs that were used to assess the potential benefits of enhanced inflows to BRL though the west end of the Port Canaveral basin. Five model cases were run including the exiting condition, in which no additional inflows were set, and inflows 1 m^3/sec, 2.5 m^3/sec, 5 m^3/sec, and 10 m^3/sec. The 1 m^3/sec case approximates the potential inflow in a full-scale pilot project. For each model case, the dispersal of a tracer concentration within BRL was tracked though a three-year model run along with water quality constituents. The tracer study was used rather than an "age of water" analysis to define the potential influence of inflows through IRL.

Table 4. Summary of model test cases

Model Case	Specified Inflow	Model Run Duration
Case 0	No additional inflow	3 years
Case 1	1 m^3/sec	3 years
Case 2	2.5 m^3/sec	3 years
Case 3	5 m^3/sec	3 years
Case 4	10 m^3/sec	3 years

4.1.2.3.1 EFDC/HEM3D Results

Water quality model results are presented in a series of plots to illustrate the difference between the existing conditions in BRL and predicted conditions based on cases of increasing inflows of ocean water. The water quality constituent concentrations assigned to hypothetical pumped inflows to BRL were set to values listed in the most recent water quality monitoring report by Environmental Research and Design, Inc. as part of the ongoing monthly monitoring program (Harper, 2021). Concentrations of major constituents such as DO, TN, TP, NH_4, and nitrate + nitrite (NOx) are provided to approximate the overall water quality of Port water. Further, spatial variation of water quality constituents is reported from six stations, including a station at the west end of Port Canaveral near the locks. The monitoring report indicates good water quality as evidenced by high values of DO, low values of Chl-a, very lows values of TN, and moderate to low values of TP.

Figure 33 shows the predicted mid-depth net change in DO concentration after two years of model simulation. An increase in DO values is predicted for all cases, but confined to the immediate inflow area under Case 1 and Case 2. Under the higher inflow rates of Case 3 and Case 4, the influence moves to the northern most compartments of BRL. **Figure 34** compares predicted net change in DO concentrations in the model surface layer at numerical monitoring station BR16, south of the inflow point. Increasing DO concentrations corresponded with increasing flow rates. The maximum predicted increase in DO values reached about 4 milligrams per liter (mg/L) over the entire model run and occurred in the surface model layer under Case 4.

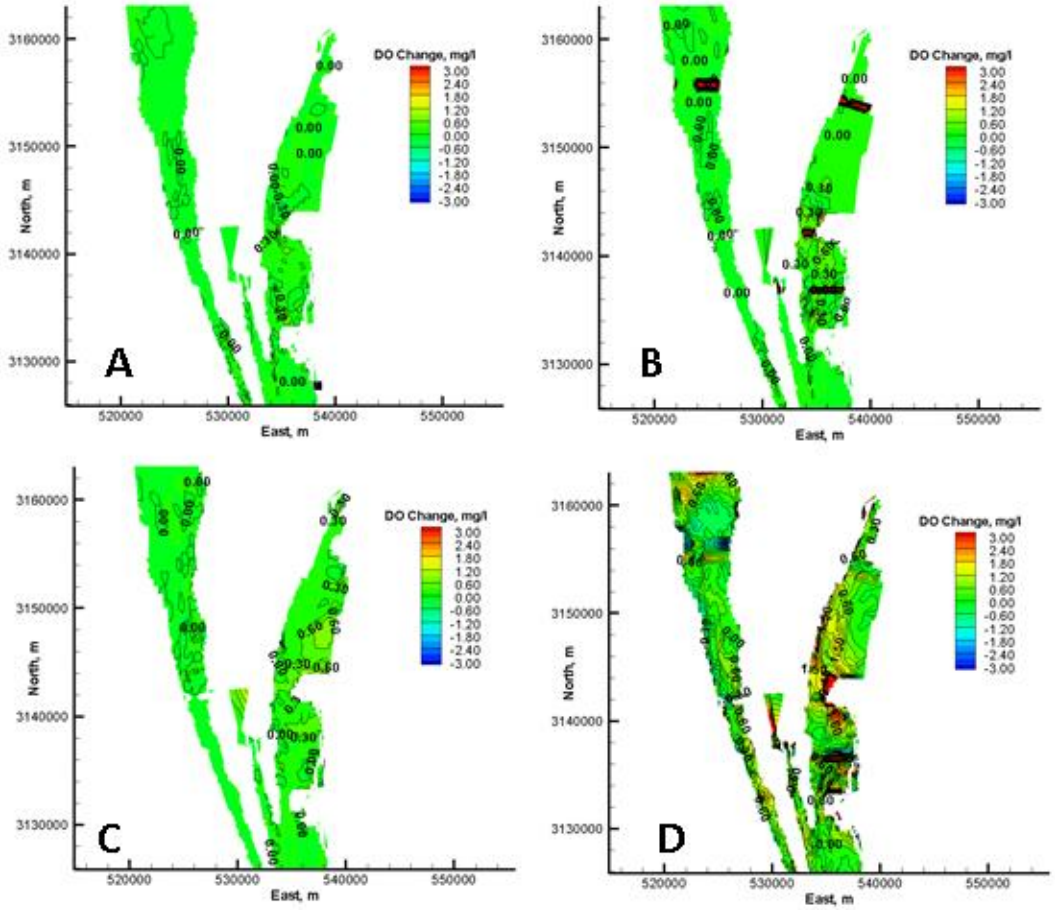

Figure 33. Comparison of predicted mid-depth net change in DO concentration in BRL after 730 days for Case 1 (A), Case 2 (B), Case 3 (C), and Case 4 (D)

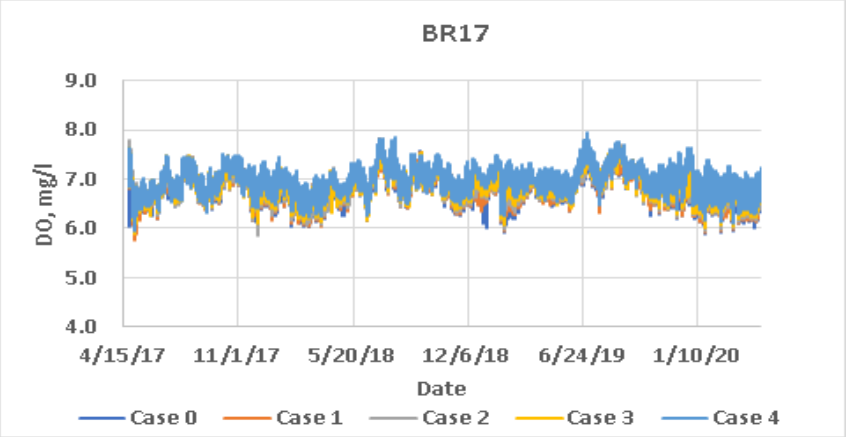

Figure 34. Comparison of predicted net change in surface layer DO concentrations at numerical monitoring station BR17 located to the south of the inflow point

The reduction in TN concentrations was the most apparent of potential benefits of the inflow. **Figure 35** shows the predicted mid-depth net change in TN concentrations under all four cases at two years into the model run. Reduction in TN concentration appears in all four cases and extends to the northernmost compartment of BRL in all cases. The predicted net TN concentration reduction was more than 2.5 mg/L under Case 3 and Case 4 in the northern compartments of BRL. South of the inflow point, the net reduction of TN concentration values were on the order of 1 mg/L or less in all cases (**Figure 35**). **Figure 36** and **Figure 37** demonstrate the spatial variation of TN concentrations. Model predictions at station BR6, north of Port Canaveral and the inflow point, show a clear reduction of TN concentration that reached a maximum of about 4 mg/L midway through the simulation. Predicted TN concentrations recorded at B23 in the southernmost row of numerical monitoring stations reached a net difference of about 1 mg/L between minimum (Case 0) and maximum (Case 4) prescribe inflow rates.

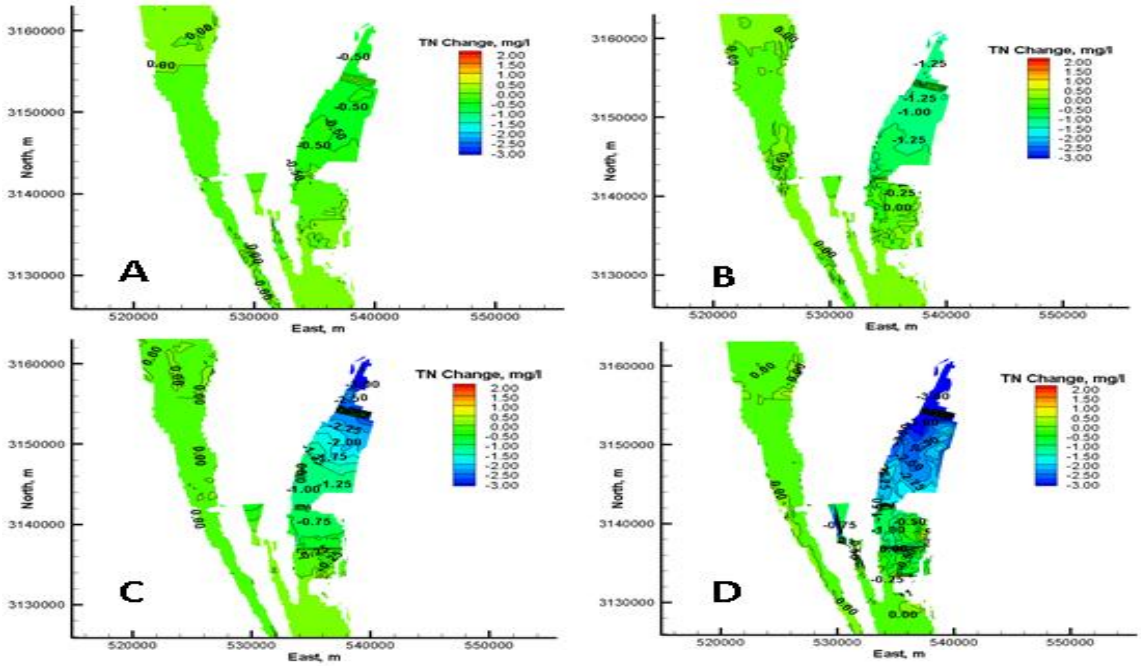

Figure 35. Comparison of predicted mid-depth net change in TN concentration in BRL after 730 days for Case 1 (A), Case 2 (B), Case 3 (C), and Case 4 (D)

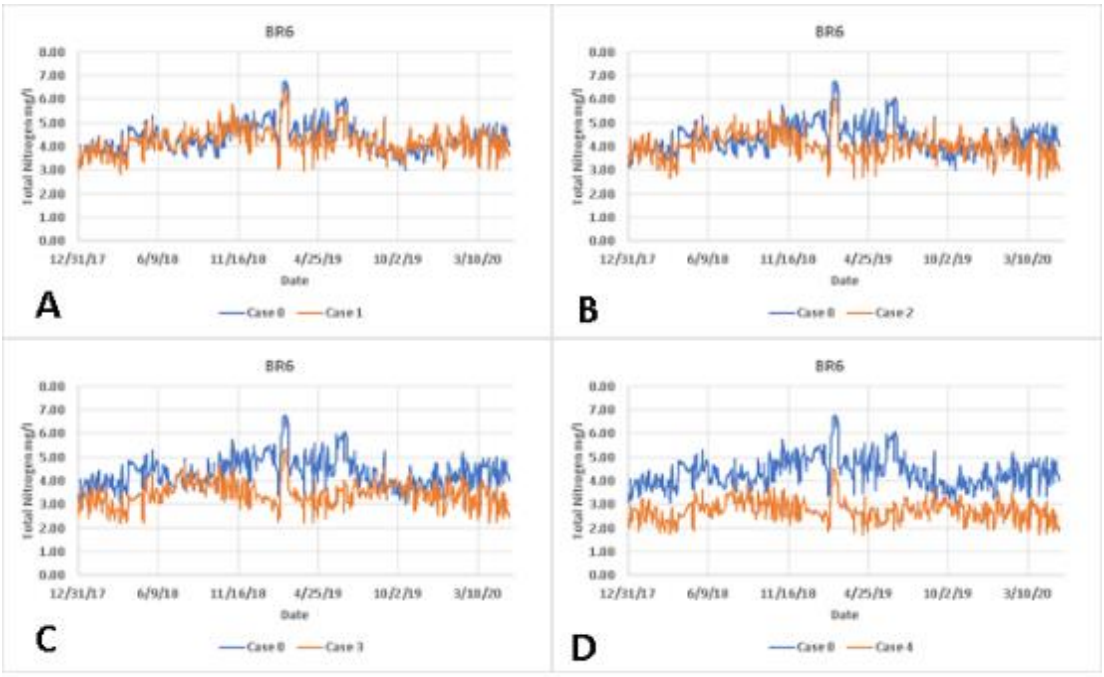

Figure 36. Comparison of predicted net change in surface layer TN concentrations for all cases at numerical monitoring station BR6 located to the north of the inflow point

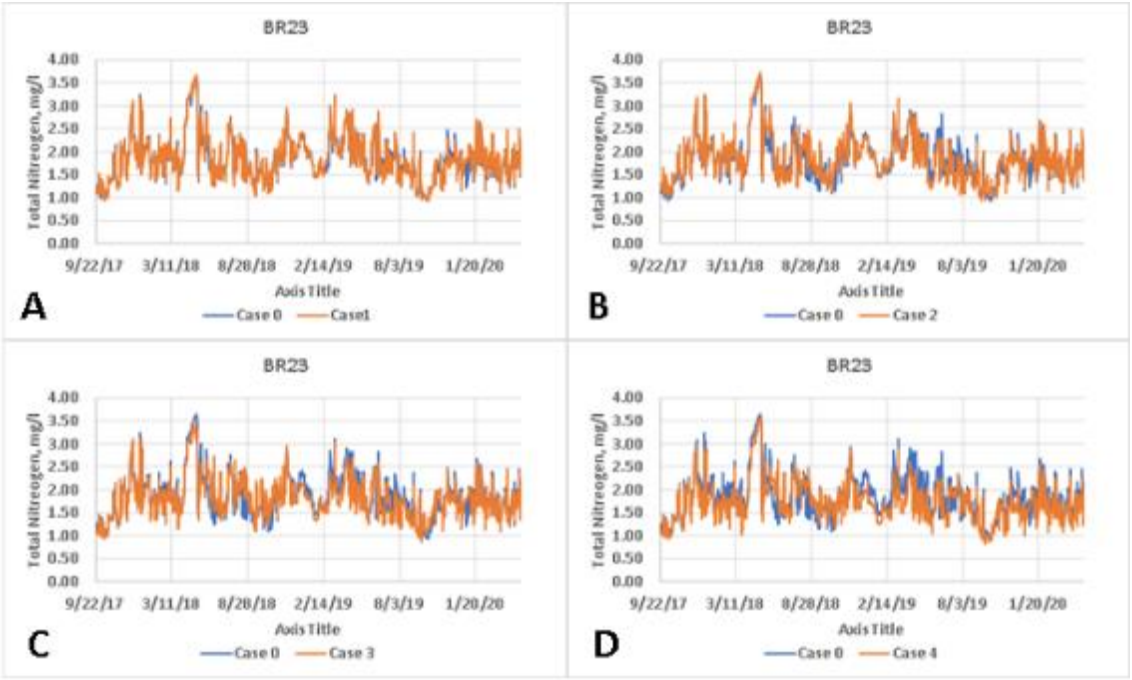

Figure 37. Comparison of predicted net change in surface layer TN concentrations for all cases at numerical monitoring station BR23

Predicted net change in TP concentrations followed a similar pattern to those of TN. The largest reductions occurred in the north compartments of BRL and tapered to a minimum south of the inflow location. TP water column concentration is generally lower than TN. **Figure 38** shows the predicted net change in TP concentration two years into the model runs. Reduction in TP

concentration begins under Case 2 (2.5 m^3/sec) and increases under Case 3 and Case 4. For most of the model run period, the measurable decrease in TP occurs from the inflow point and northward. This is consistent with the tracer analysis and analysis of ADCP flow direction.

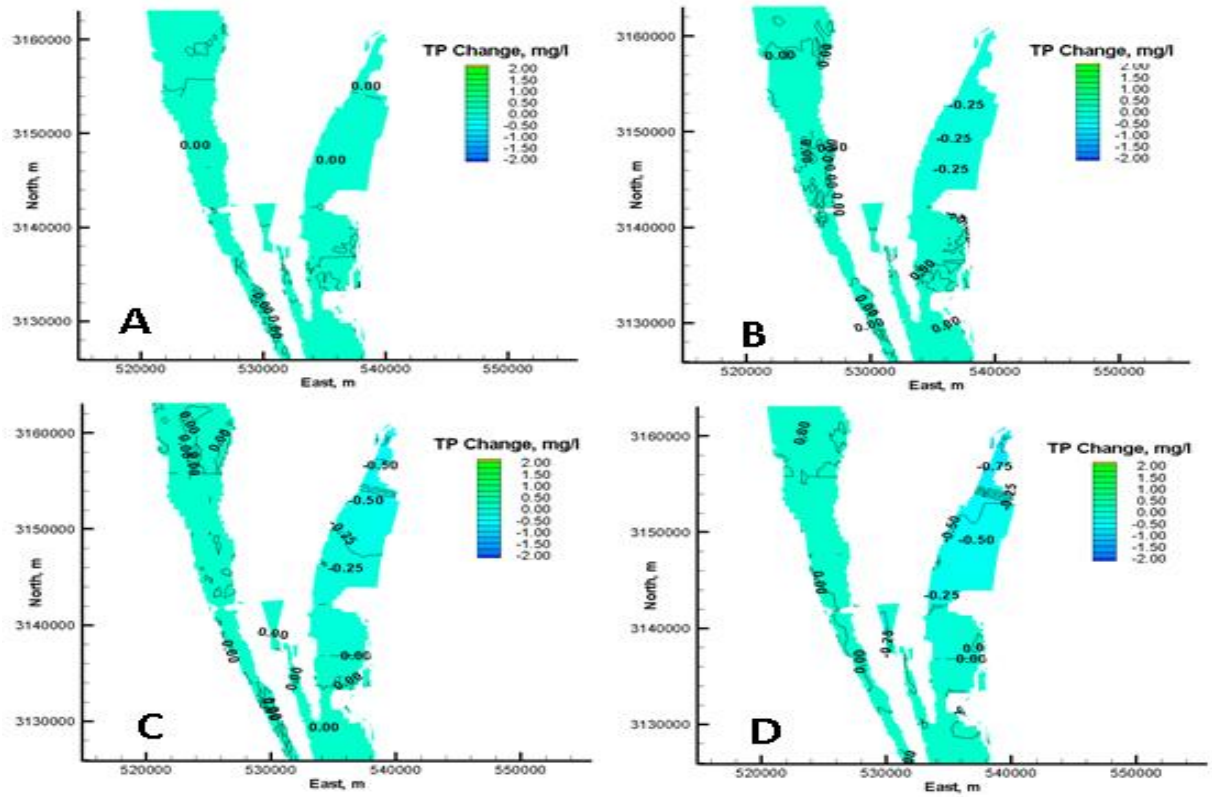

Figure 38. Comparison of predicted mid-depth net change in TP concentration in BRL after 730 days for Case 1 (A), Case 2 (B), Case 3 (C), and Case 4 (D)

Figure 39 and **Figure 40** compare predicted net TP concentration changes among the four inflow cases. The pattern is similar to that predicted for TN. The reduction in TP begins to appear under Case 2 and increases through Case 3 and Case 4. Predicted declines are larger north of the inflow point due to the circulation process. Maximum predicted reduction in TP concentration under Case 3 and Case 4 range from about 0.5 to 0.74 mg/L.

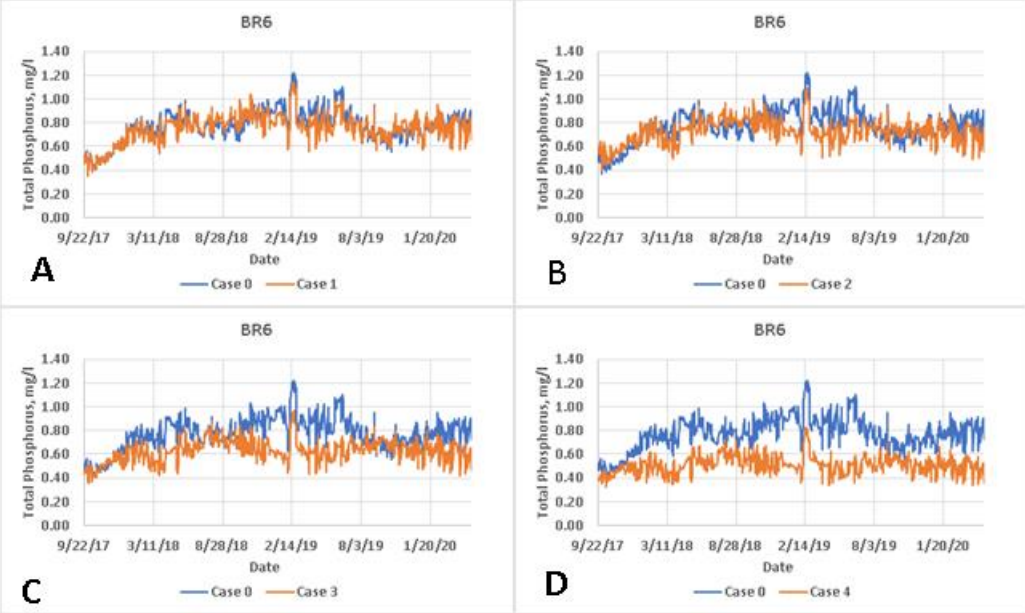

Figure 39. Comparison of predicted net change in surface layer TP concentrations for all cases at numerical monitoring station BR6 located to the north of the inflow point

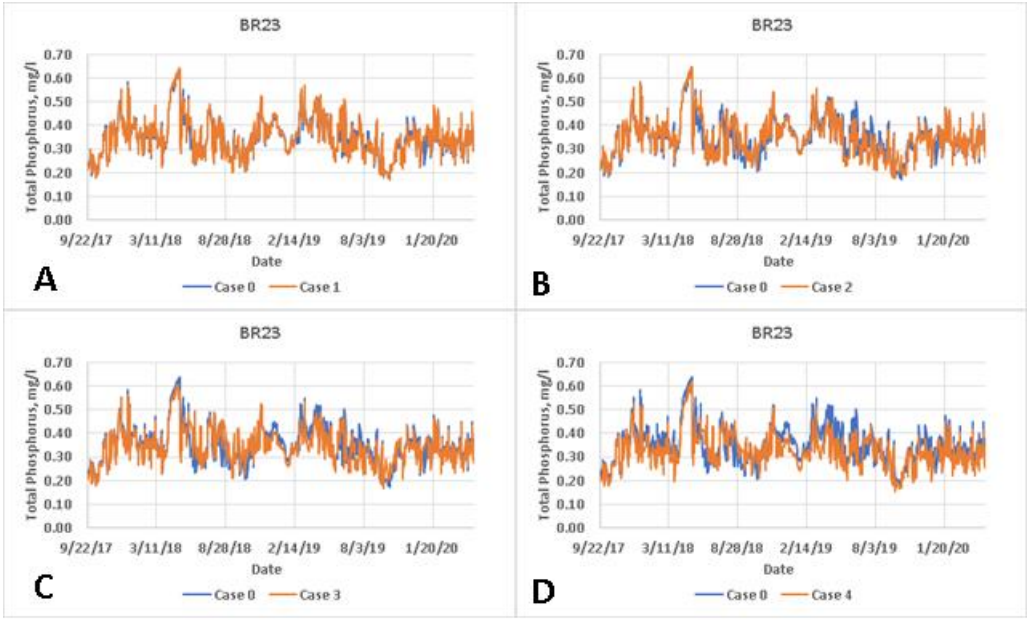

Figure 40. Comparison of predicted net change in surface layer TP concentrations for all cases at numerical monitoring station BR23

Model results of Chl-a concentration can be used as a guide to the potential benefits of enhanced inflows to mitigate HABs. Predicted Chl-a concentrations shown for selected stations demonstrate the potential for inflows to reduce episodes of high Chl-a concentrations that occurred in the model. Short events of slightly elevated Chl-a concentrations also appear in Case 0 model results, but were reduced in magnitude in cases including higher inflow rates. **Figure 41** presents model results for total Chl-a at numerical monitoring station BR6. Declines in Chl-a become noticeable beginning with Case 2 inflows and continue through Case 4. Under conditions of Case 3 (5

m^3/sec) and Case 4 (10 m^3/sec), higher Chl-a concentrations through extended periods of time seen in the Case 0 and Case 1 model data are substantially reduced. The pattern of Chl-a model results at numerical monitoring station BR17 (**Figure 42**) shows some reduction of peak concentration values beginning with Case 2 and substantial reductions in Case 3 and Case 4. The first Chl-a concentration peak that occurs in all four cases corresponds with the passing of Hurricane Irma in September 2017.

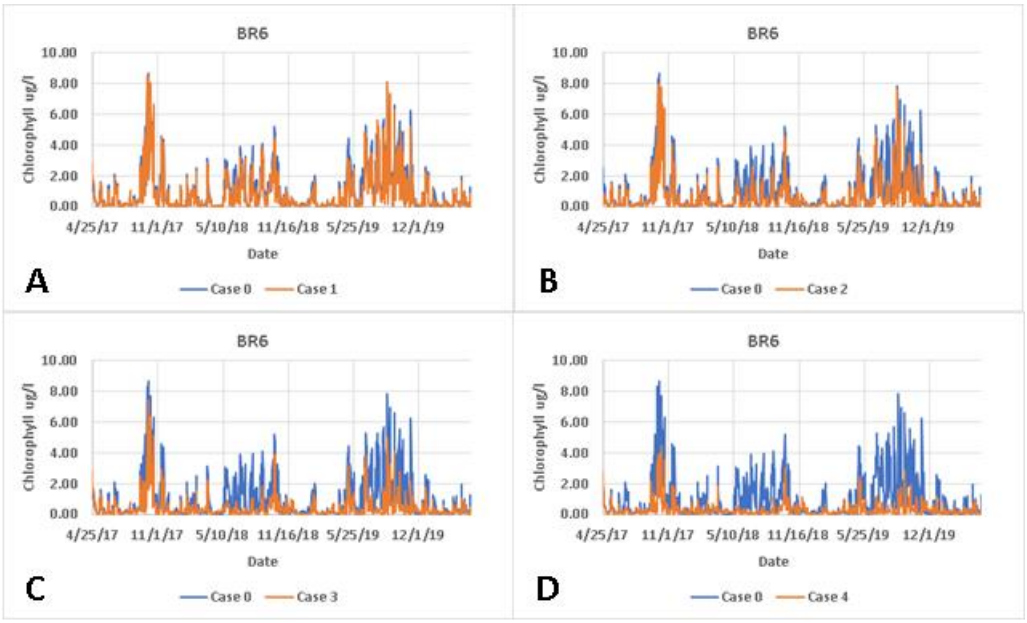

Figure 41. Model results for total Chl-a at numerical monitoring station BR6

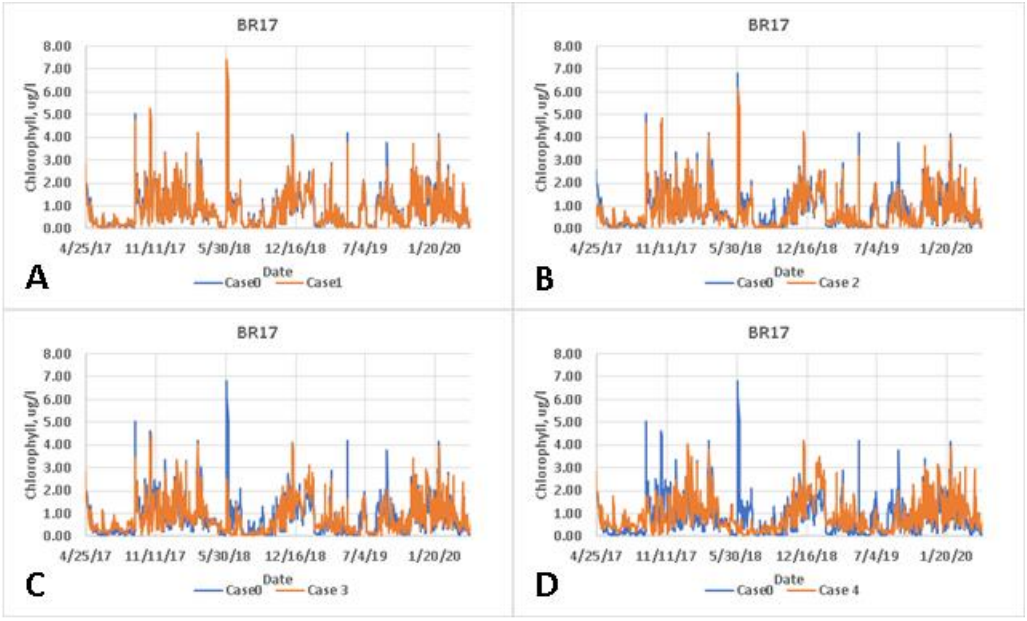

Figure 42. Chl-a model results at numerical monitoring station BR17

4.1.2.3.2 Potential for Distal Impacts on Water Quality

Concern has been expressed about the possibility that inflows to BRL from Port Canaveral could impact water quality at a location as far south as Sebastian Inlet. Model results show that changes in water quality reach Sykes Creek, but this is considered a positive impact since Sykes Creek is known for poor water quality and low DO values. Given the flow dynamics of BRL and IRL, a reasonable question is whether distal water quality can be impacted by the inflows. Thus far, no measurable difference in water quality constituent concentrations were found in the Sebastian Inlet area. Predicted TN and TP under Case 0 and Case 4 are nearly identical. **Figure 43** shows the predicted net change in TN and TP concentration at the throat section of Sebastian Inlet 60 km south of the BRL inflow point.

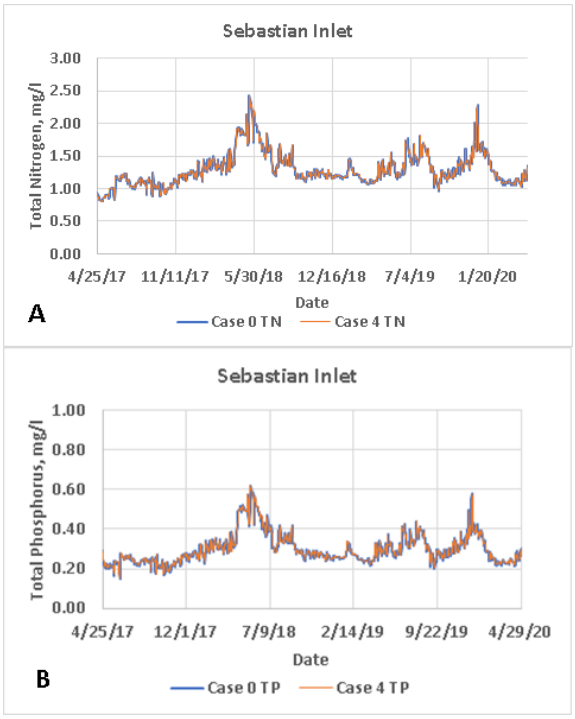

Figure 43. Predicted net change in TN (A) and TP (B) concentration a the throat section of Sebastian Inlet 60 km south of the BRL inflow point

4.1.2.3.3 Port Canaveral Coastal Processes Model

A numerical assessment of potential hydrodynamic and morphologic changes to the Canaveral Port system in response to inflow pumping was also conducted. The CMS was selected as the numerical modeling suite to simulate waves, hydrodynamics, morphology, and proposed outflow. Model configuration, including spatial and temporal coverage, was driven by a combination of model needs and available field data. The model spatial coverage was established to resolve both the processes in the coastal ocean and the flow through interior Port facilities.

Increased resolution of the model grid was included in the Port areas including the conveyance channel to the control structures, all turning basins, and inlet (**Figure 44**). Blue cells are active ocean cells while brown cells are inactive land cells. Darker areas are locations of increased grid refinement (smaller cells) while lighter areas are larger cell sizes. For this work, the cells representing the flow control structure are set to inactive to represent a closed condition. These cells can be switched to active ocean cells in future work.

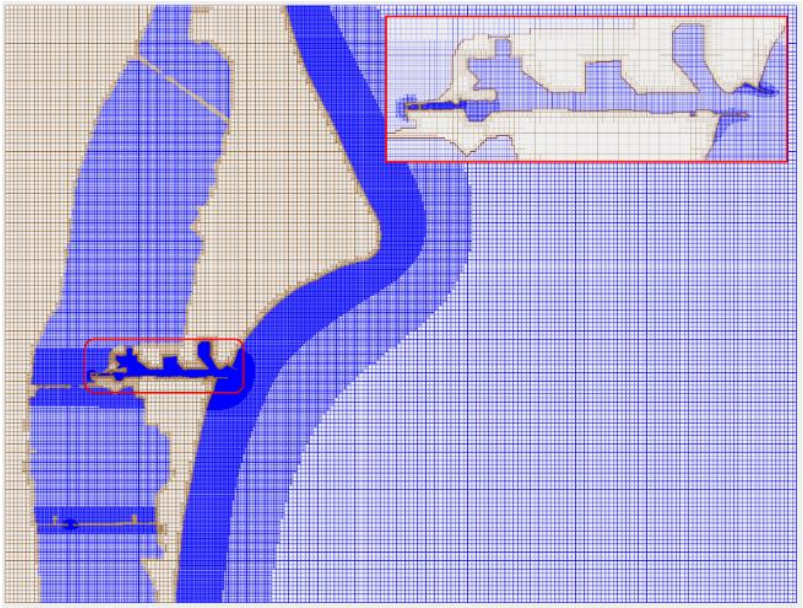

Figure 44. CMS flow grid with port detail (inset)

Potential flow changes from inflow pumping were investigated through simulation of three different flow scenarios: 1 m^3/sec, 2.5 m^3/sec, and 5 m^3/sec. Changes in flow and morphology through the Port facility were evaluated across the model alternatives under a closed sector gate condition. Four observation nodes were placed throughout the conveyance channel moving from the clamshell sector gates (Point 1) to the West Turning Basin (Point 4). Point 2 is westward of the State Road 104 overpass, and Point 3 is situated adjacent to the marina. Point 1 is immediately adjacent to the model flow output to represent the pumping system. The observation points in relation to the Port conveyance and control structure are shown in **Figure 45**.

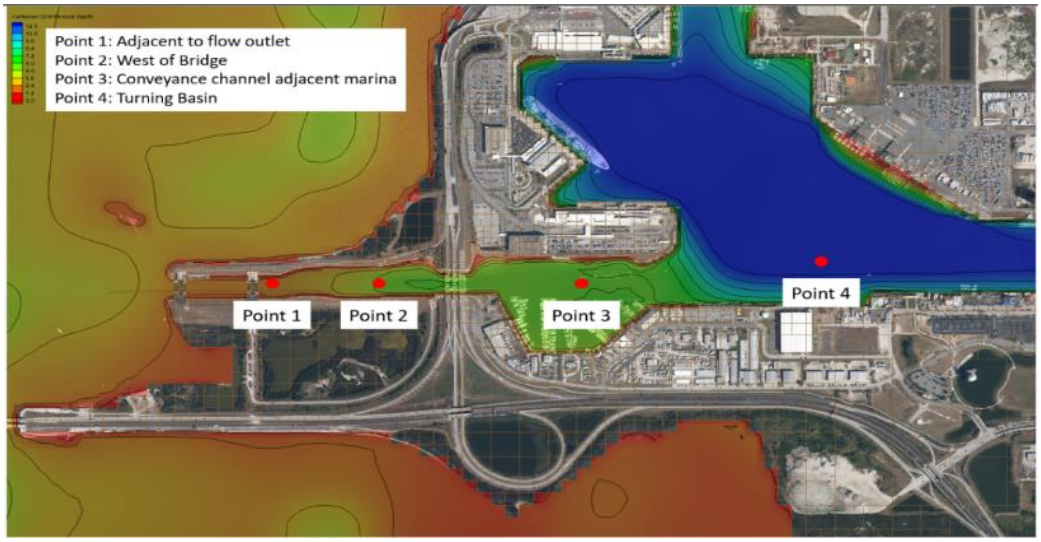

Note: Warmer colors indicate shallower water depths while cooler colors indicate deeper water depths. Plotted water depths in this image range from 0 to 12 m NAVD88.

Figure 45. Observation point locations

Figure 46 presents the computed flow for both the 1 m^3/sec alternative and existing conditions for comparison. At the 1 m^3/sec flow, Point 1 observed the most change in flow conditions as it is

located closest to the flow structure. At points 2 through 4, the model indicated no significant change in current magnitude or direction moving east through the Port.

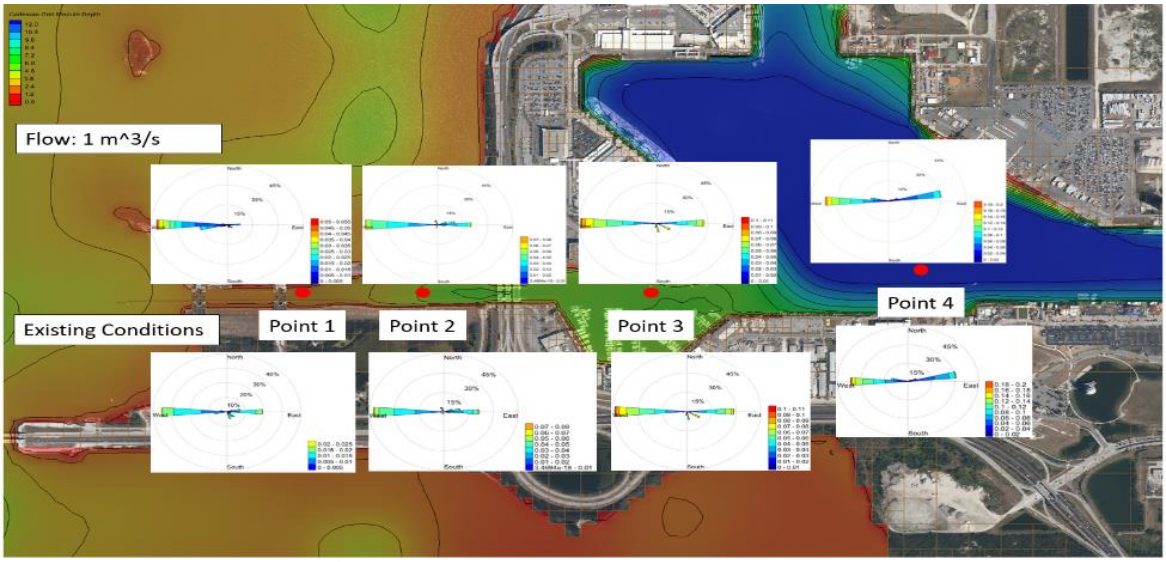

Figure 46. 1 m^3/sec flow rate alternative current directional plots

Computed flow for the 2.5 m^3/sec alternative is shown in **Figure 47**. Current direction at Point 1 is entirely directed towards the west and ebb flow (east) is eliminated. Ebb flow at Point 2 is reduced as well at the larger flow rate. Flow characteristics at points 3 and 4 are unchanged at this flow alternative. Flood dominance changes from the outward flow migrates through the conveyance channel with the incorporation of outward flow. The flow characteristics through the conveyance channel change at the 5 m^3/sec flow rate are shown in **Figure 48**. The flow rate at the observation nodes reduces in magnitude but the directionality is similar to the existing conditions. This reduction in flow rate is observed at points 1 through 3. The flow pattern at Point 4 compares well with the existing conditions. It should be noted that due to model stability requirements, the cell string was increased in length to distribute the flow over a greater distance.

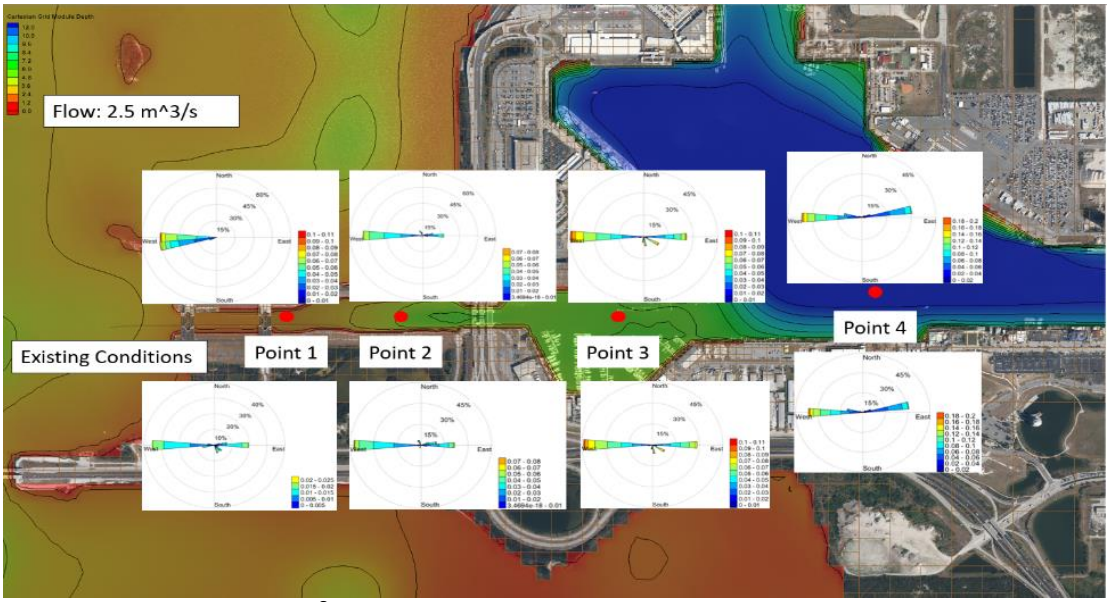

Figure 47. 2.5 m^3/sec flow rate alternative current directional plots

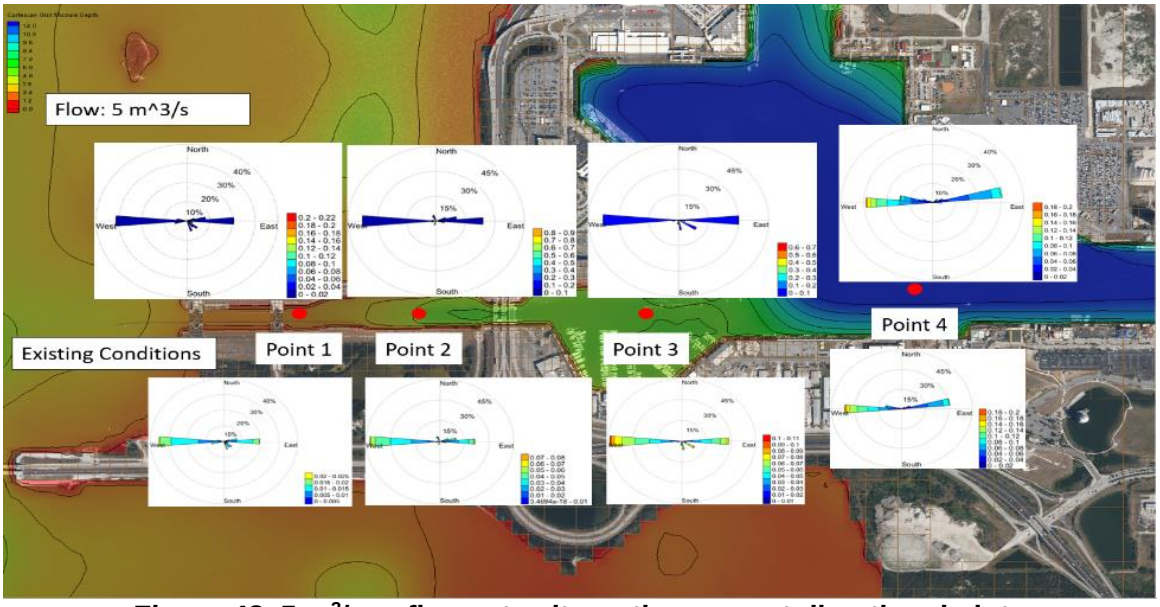

Figure 48. 5 m^3/sec flow rate alternative current directional plots

Computed morphology change was plotted for the existing conditions and all alternatives to evaluate the potential changes in sedimentation near the flow control structures. Erosion is represented by cool colors and sediment deposition is indicated by warmer colors. The color range spans from -0.5 m to 0.5 m and is taken from the final timestep of the simulation period. These plots represent three months of computed morphology change. With a dominance in flood directed flow, there is a potential for increased sedimentation near the sector gates.

Computed morphology change for the 1 m^3/sec flow alternative is shown in **Figure 49**. The existing condition is provided as an inset. Morphology patterns are similar to the existing conditions; however, the amount of deposition is predicted to increase with an outflow. This behavior is primarily observed adjacent to the flow control structure of the lock system. A distinct erosion pattern appears immediately adjacent to the outflow cell string on the southern shore indicating that scour protection would be required for an installation of this type.

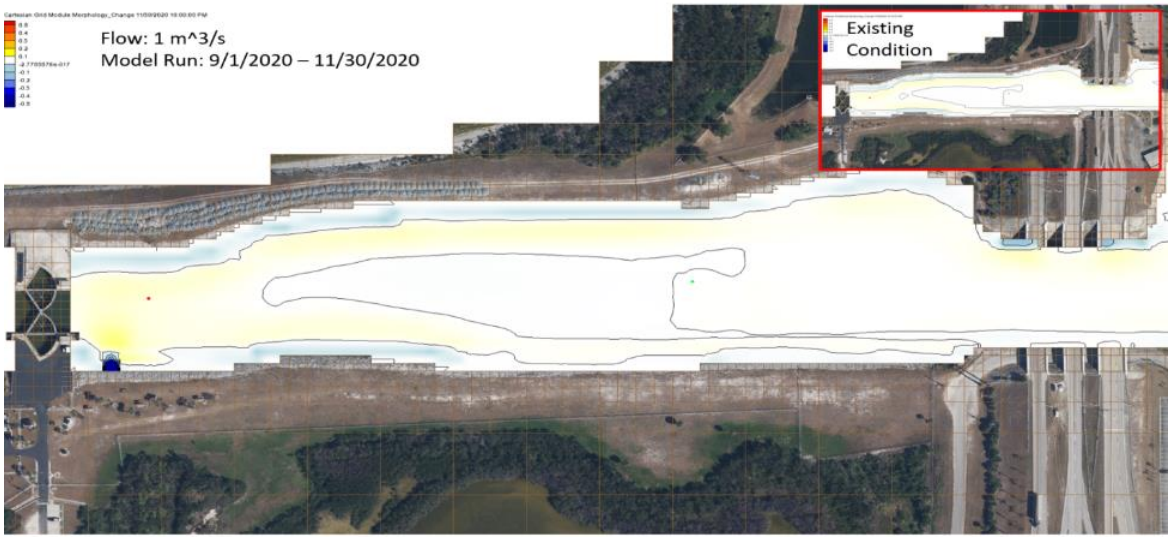

Figure 49. 1 m^3/sec flow alternative calculated morphology change

Figure 50 shows the computed morphology change for the 2.5 m^3/sec flow alternative. Sediment is predicted to increase in deposition immediately adjacent to the flow control structure. Scour near the outfall flow increases with increasing flow rate.

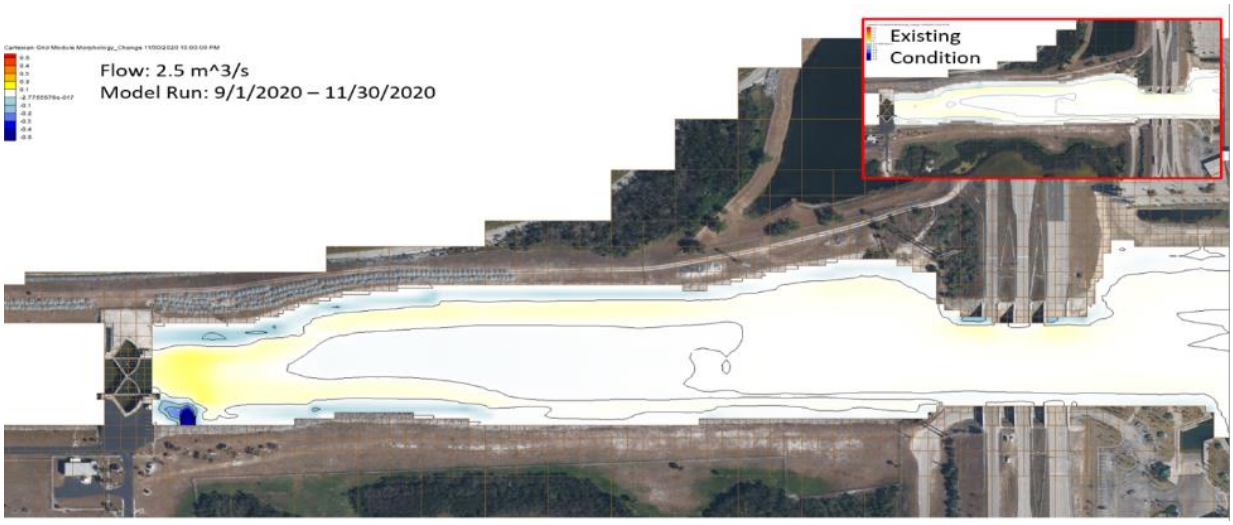

Figure 50. 2.5 m^3/sec flow alternative calculated morphology change

4.1.3 Conclusions

Predictions of major water quality constituent concentrations indicate that the potential benefit of prescribed inflows to BRL increases as the inflow rates are increased. Predicted concentrations of DO, TN, TP, and Chl-a under inflow rates of 1 m^3/sec (Case 1), 2.5 m^3/sec (Case 2), 5 m^3/sec (Case 3), and 10 m^3/sec (Case 4) were compared with the base condition (Case 0) of no additional inflows from the Port Canaveral. Potential benefits in terms of reduced concentration of TN and TP occur though all of the enhanced inflow cases, but most noticeable in Case 2, 3, and 4. Predicted improvements in water quality occur throughout BRL, but are most apparent in the northern compartments of the basins.

Predicted increased DO concentrations under the lower inflow rates of Case 1 and Case 2 reach a maximum of about 0.5 mg/L and are confined to the area near the inflow location. Under Case 3 and Case 4, DO concentrations increased by up to 4 mg/L at some locations and the area influenced by increased DO concentrations expanded to the north compartments of BRL.

The influence of inflows of sea water on Chl-a includes reductions in concentrations throughout the three-year model run, as seen at numerical monitoring station BR6, well north of the inflow point. Lower concentrations of Chl-a are more persistent at higher inflows of Case 3 and Case 4, but still apparent under Case 2. Predicted impacts on Chl-a also include “decapitation” of short-term spikes of higher Chl-a concentrations, even as the predicted time series of lower Chl-a concentrations under lower inflow rates remain similar.

Given the lower frequency reversing flow dynamics of BRL and IRL, the potential for distal impacts on water quality exists. Thus far, inspection of model data indicates no significant difference in water quality constituent concentrations beyond the BRL basin, Sykes Creek, and IRL compartment west of BRL.

4.2 Geochemistry (Task 2)

The objectives of the geochemistry task were to:

- Investigate temporal trends for geochemical processes (nutrient and oxygen cycling plus temperature and salinity regimes) in sediments and water near potential inflow locations. Resolve, temporally and spatially, the direct impacts of proposed inflow (seawater or Port water) on nutrient concentrations in the lagoon and calculate the quantity of nutrients that would be discharged into the coastal ocean using robust temporally resolved datasets.
- Determine how changes to temperature, salinity, and DO that could result from various levels of inflow would influence the geochemical cycling of N, P, and oxygen in lagoon water and sediments. Estimate/model the potential impacts of inflow towards indirect changes to nutrient concentrations in the lagoon.
- Resolve datasets for DO and nutrients in surface and bottom water in areas pursued for permitting. Determine if data from existing water quality sensors (approximately 0.5–1.0 m) can be extrapolated to conditions in the complete water column (e.g., bottom water) near proposed inflow location. Increase spatial resolution for bottom water DO monitoring.
- Determine how inflow plus geochemical processes and changes to these processes may influence water quality conditions to favor specific groups or types of algae (nutrient stoichiometry plus temperature and salinity regimes).

4.2.1 Approach

4.2.1.1 Field Sampling

Continuous vertical profiles for salinity, temperature, pH, oxidation reduction potential, and DO were obtained using a Yellow Springs Instruments (YSI) ProDSS. Discrete water samples were collected using a 1.7 liter (L) horizontal Niskin water sampler (General Oceanics) that was tripped at targeted depths using a weighted messenger. Water samples were filtered immediately after collection using Whatman 0.45 micrometer (µm) polypropylene syringe filters. Additional unfiltered samples were collected for processing in the laboratory. All water samples were transported to the laboratory in a cooler on ice in the dark.

Sediment samples were obtained using a 0.1 square meter (m^2) Ekman Grab that was lowered slowly from an anchored boat until it hit the bottom. This process was observed by Self-Contained Underwater Breathing Apparatus (SCUBA) to verify collection of 10–15 cm of stratified sediment and overlying water (**Figure 51**). Any standing water was siphoned off prior to sample collection. A 3 cm layer of surface sediments was subsampled from the grab using a clean spoon and placed in a 55 milliliter (mL) polycarbonate vial that was then sealed with parafilm.

Darkened, benthic (sediment) and “blank” chambers were used to determine fluxes of DO and nutrients from sediments and from suspended particles (water column respiration). Blank chambers containing HOBO U26 DO data loggers and mechanical stirrers were rinsed and then completely filled with bottom water. Water samples were obtained and immediately filtered through Whatman 0.45 µm polypropylene syringe filters and stored on ice until return to the laboratory. The volume of water removed for samples was replaced with bottom water and chambers containing no air were sealed and incubated for 1.5 to 2 hours. Chambers were kept in the shade at a constant in-situ temperature for the duration of the incubation. Following the incubation period, chambers were opened, and a final water sample was extracted and immediately filtered and placed on ice for transport to the laboratory.

Figure 51. Ekman Grab photographed by scientist with SCUBA descending through the water column (left) and settled in sediments with no visible disturbance to the sample (right)

Benthic chambers were pushed vertically into sediments without side-to-side movement to avoid creating channels that would allow water exchanges. Chambers were pushed at least 10 cm into the sediments to prevent burrowing organisms from creating channels. The height of each chamber was recorded to calculate the total volume of water in each chamber (e.g., Boynton et al., 2018). Once inserted, chambers were left open to the water column for 2–5 minutes to allow particles and sediments to settle and allow water to be exchanged with undisturbed bottom water. Water samples were obtained and immediately filtered using Whatman 0.45 µm polypropylene syringe filters. Chambers were then sealed with lids containing mechanical stirrers to keep the water well-mixed and prevent buildup of a concentration gradient at the sediment-water interface. HOBO U26 DO data loggers were mounted through an airtight seal in the lid of each chamber. The rate of DO decline was measured for 1.5 to 2 hours for sand and 20 to 45 minutes for mud. At the end of each deployment, a syringe was attached to a valve on top of the chamber and to extract a 60 mL water sample, which was immediately filtered and stored on ice (**Figure 52**). A sediment sample was also obtained and placed in a polycarbonate vial for analysis. At least 2 L of unfiltered bottom water was also collected for turbidity and Chl-a.

Sediment cores for laboratory incubation experiments were obtained by carefully pushing core barrels vertically into the sediments to avoid creating channels or resuspending/disturbing sediments. Cores were capped to create a vacuum, extracted from the sediment, and a cork immediately placed in the bottom of the core. Still underwater, caps were removed to prevent buildup of pressure as the cork was inserted fully. Expansion plugs were also inserted to prevent leaks. Caps were then replaced and the entire core, with no air, was placed in a dark cooler and transported to the laboratory. If any disturbance was noted, the core was discarded, and a new core was obtained. Large (at least 2 L) unfiltered water samples were collected for replacement of the overlying water at the beginning of laboratory incubation experiments.

Continuous monitoring of bottom water DO was carried out using Onset HOBO U26 DO data loggers which were deployed in polyvinyl chloride housings equipped with copper-based antifouling guards to promote reliable datasets collected over 14–30 day periods. Sensor housings were designed to keep sensor faces within 10 cm of the bottom based on developments during Phase 1 of this project. Sensors were lab calibrated immediately before each deployment,

and field data were validated at the beginning and end of each deployment by comparison with a calibrated YSI ProDSS data sonde.

Figure 52. Collecting water samples from a benthic chamber deployed in shallow water

4.2.1.2 Laboratory Analyses

Concentrations of NH_4, NOx, total dissolved nitrogen (TDN), PO_4, total dissolved phosphorus (TDP), and silica (SiO_2) were determined using a SEAL AA3 HR Continuous Segmented Flow Autoanalyzer. The NIST-traceable Dionex 5-Anion Standard was analyzed as a reference standard with each batch of samples to ensure accuracy. Values were consistently within the 95% confidence interval for the prepared standard. Analytical precision (relative standard deviation) for lab duplicates was <3% for nutrient analyses. pH was determined using Hach Sension1 pH meter and an Oakton field probe. The apparatus was calibrated using a three-point calibration immediately prior to use. Initial calibration verification was checked using a pH 7 buffer and was always better than 1%. Turbidity was determined on unfiltered samples using a Hach 2100 turbidimeter. The turbidimeter was calibrated prior to each use and checked periodically throughout the analyses. Concentrations of Chl-a were determined by vacuum filtering 50 mL of homogenized water through pre-combusted Whatman 0.7 µm pore size glass fiber filters. The fluorometer was initially calibrated using a Chl-a standard (Turner designs Part No. 10–850) and during sampling using a solid secondary standard (Turner Designs Part No. 10-AU-904). Concentrations of chloride, sulfate, and alkalinity were determined using a SEAL AQ400 discrete auto analyzer following manufacturer's methods.

Laboratory incubations were carried out in a manner consistent with previous studies (e.g., Cowan et al., 1996; Hammond et al., 2004; Boynton et al., 2018; Foster and Fulweiler, 2019). Intact sediment cores were placed in temperature-controlled recirculating water baths set to approximate in-situ conditions (**Figure 53**). Incubations were set up by removing caps and siphoning off overlying water, leaving about 1 cm of water to prevent disturbance of the sediment-water interface. Bottom water collected from the field site was slowly pumped into the chamber

using a floating diffuser to prevent disturbance of the sediment-water interface. Water was replaced before each incubation to ensure that starting water quality conditions were as close to in-situ conditions as possible and to remove any nutrient accumulation that had occurred between collection of each core and beginning of the incubation. At the beginning of each incubation, water samples were collected from each core. Water samples were immediately filtered using Whatman 0.45 µm polypropylene syringe filters and stored in a refrigerator until analysis. The volume of water removed for the initial sample was displaced by the HOBO U26 DO data logger and mechanical stirrer attached to the lid. Chambers were sealed and incubated for 1.5 to 2 hours. For experiments where DO was manipulated, mixed gases, air, and N were bubbled into each chamber to maintain constant DO concentrations. Following each incubation, a final water sample was extracted, immediately filtered, and stored in the refrigerator at 4 degrees Celsius (°C) until analysis. With each batch of laboratory incubations, a blank chamber containing unfiltered site water was processed for field incubations. Fluxes from the blank chamber were subtracted from values for chambers containing sediments to track water column and sediment processes.

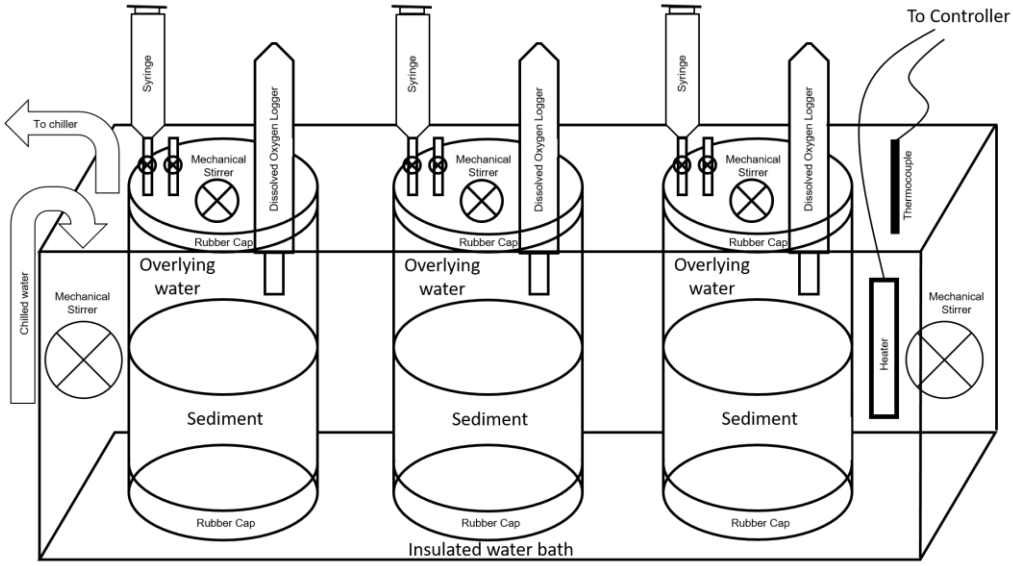

Figure 53. Schematic diagram of triplicate laboratory incubation chambers in an insulated, recirculating, temperature-controlled water bath

All sediment samples were weighed, freeze dried using a Labconco FreeZone 6 system, and reweighed to determine water content. Freeze dried samples were then powdered using a SPEX Model 8000 Mixer/Mill. Loss on ignition at 550 °C was determined following the method of Heiri et al. (2001). Values for loss on ignition estimated the fraction of organic matter in the sample. Concentrations of calcium carbonate were determined by heating the sediment that had been treated for loss on ignition at 550 °C to 950 °C following the method of Heiri et al. (2001). Average precisions for loss on ignition and calcium carbonate (relative standard deviation) were 2.0% and 1.0%, respectively.

4.2.1.3 Data and Statistical Analyses

Data and graphical analyses were carried out using Systat 12, SigmaPlot 10, Microsoft Excel 2016, ArcGIS (Version 10.2.2.3552), and HOBOware Pro 3.7.17. An alpha value to define statistical significance was set at 0.05. Least square linear regressions were calculated to determine relationships between individual pairs of parameters. All correlation coefficients are presented with a corresponding p-value. Comparisons of two independent groups of data were

carried out using two-tailed t-tests assuming equal variance, unless otherwise noted. Independent groups of data with p-values >0.05 were considered not significantly different from one another.

Prior to sampling, power analyses were carried out using G*Power 3.1 to determine minimum sample sizes required to obtain satisfactory power (0.8) for laboratory experiments showing linear regression between benthic fluxes and environmental parameters. A similar approach was used to determine the number of sites/samples required for comparison of the proposed treatment and reference areas using two-tailed tests. For all power analyses, the alpha error probability was set to 0.05 and power was set at 0.8. Effects sizes were estimated from preliminary means and standard deviations.

SOD was determined by subtracting the water column respiration (milligrams per liter per hour [mg/L/hr]) values for "blank" chambers from values obtained from benthic chambers. The total rate of oxygen utilization by sediments, accounting for the volume in the benthic chamber (DO used by sediments times the volume of the benthic chamber, calculated using the height of the chamber above the sediments) was divided by the surface area of sediment to yield values for SOD. Values for SOD are reported in micromoles per square meter per hour (µmoles/m^2/hr).

Benthic nutrient fluxes were determined from benthic and blank chambers by subtracting initial nutrient concentrations (µmoles) from final concentrations for both benthic and blank chambers. The changes in concentrations (µmoles) were then divided by the elapsed time (hours) of each incitation to yield rates in µmoles/hr. The rate of nutrient production/utilization in blank chambers was then subtracted from the rate calculated for benthic chambers, to determine the production/ utilization by sediments and particles independently. The rate (µmoles/hr) for the benthic chamber was then multiplied by the volume of the chamber, calculated using the height of the chamber above the sediments, to yield the amount of nutrients produced/used by sediments in the chamber per hour (µmoles/hr). This value was divided by the surface area of sediments in the chamber to yield a flux in µmoles/m^2/hr, consistent with units used in the literature (e.g., Boynton et al., 2018). A similar approach was used to determine nutrient fluxes from laboratory incubations. Nutrient fluxes were evaluated against the rate of oxygen utilization to ensure that linear nutrient production/utilization could be assumed. If the chamber went anaerobic during the deployment or oxygen use was non-linear, nutrient fluxes were flagged and not included in data interpretation.

4.2.2 Results

4.2.2.1 Temperature, Salinity, and Density

Long-term datasets for temperature and salinity were obtained for 2015 through July 2021 from sources including SJRWMD, NOAA National Data Buoy Center, Ocean Research and Conservation Association's Kilroys, and a network of sensors deployed and maintained by Florida Tech. The annual average lagoon temperature was about 25 °C and followed seasonal patterns with a range of about 17°C, with a minimum at approximately 15°C, typically reported during February, to a maximum of about 32°C, typically reported during August and September. Temperatures of seawater in Port Canaveral followed similar seasonal patterns; however, minimum temperatures during winter were higher, typically about 16°C and maximum temperatures during summer were lower, typically at about 31°C (e.g., **Figure 54**; data from multi-year analysis).

During winter 2020–2021 (Phase 2), the lowest temperature recorded near the proposed inflow location in the lagoon was 12.1°C (December 26, 2020), compared to 17.1°C in Port Canaveral. Overall, average temperatures during January 2020 and February 2021 were 0.9°C and 0.6°C cooler in the lagoon relative to Port Canaveral. Based on these data plus long-term datasets,

pumping during winter months could bring warmer water into the lagoon from the ocean. The lagoon also had a higher maximum temperature during August 2020 at 33.1°C, relative to 31.7°C in Port Canaveral. These data were consistent with results obtained during Phase 1 and with long-term datasets where typical spring-fall lagoon temperatures were 0.5–1.0°C warmer compared to water in Port Canaveral and adjacent coastal Atlantic Ocean.

Overall, salinity was lower in BRL compared to Port Canaveral. Vertical profiles for salinity in seawater from the proposed inflow location showed a gradient with the lowest salinities in surface water at 27–32 practical salinity unit (PSU), increasing with depth to 30–34 PSU (**Figure 55**).

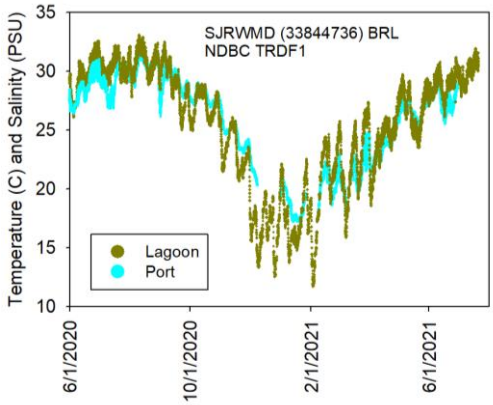

Note: Data obtained from SJRWMD site 33844736 and from National Data Buoy Center site TRDF1.

Figure 54. Temperature in BRL in the area of inflow and in Port Canaveral, the proposed source of inflow water

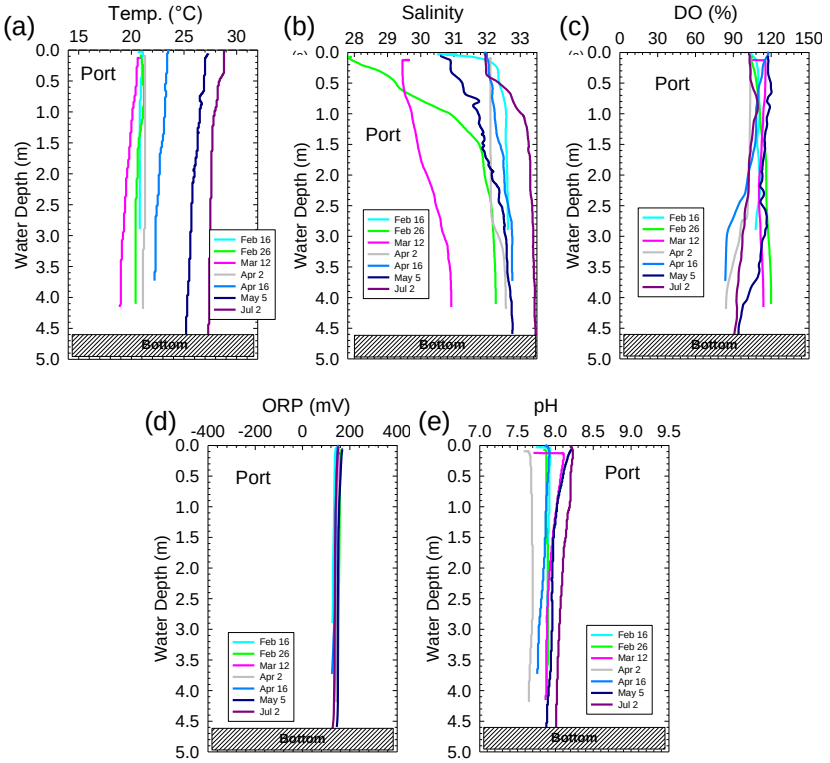

Figure 55. Vertical profiles for (a) temperature, (b) salinity, (c) DO, (d) oxidation reduction potential, and (e) pH in Port Canaveral during discrete sampling events

Using data for temperature and salinity, the water density was calculated as an indication of the likelihood of mixing or the degree of stratification that could occur if seawater were to be pumped into the system (**Figure 56** and **Figure 57**). Overall, consistent with lower salinity in the lagoon versus the Port, the density of water in BRL was 1,012 kilograms per cubic meter (kg/m^3) (average), 1.3% less dense than typical seawater at 1,025 kg/m^3. This seemingly small difference is enough to maintain discrete stratified layers and is greater than differences in density identified among existing layers observed during this study. For example, during Phase 1, discrete surface and bottom layers were identified at offshore sites based on temperature alone with densities of 1,022.9 kg/m^3 and 1,023.2 kg/m^3 for surface and bottom water, respectively, a difference of 0.03%. These data indicate that, regardless of mixing, inflow of seawater would preferentially support circulation in bottom water and at the sediment water interface either as a stratified layer of seawater or as a mixed water mass with a higher density than existing water in BRL.

Regardless the degree of mixing, inflow of seawater would stabilize temperature and salinity in the lagoon, producing slightly cooler (<1°C) lagoon water during summer months and potentially, if inflow occurred, warmer water during winter months. Salinity would increase slightly in the area of inflow and concentrations of DO would likely be more stable over time.

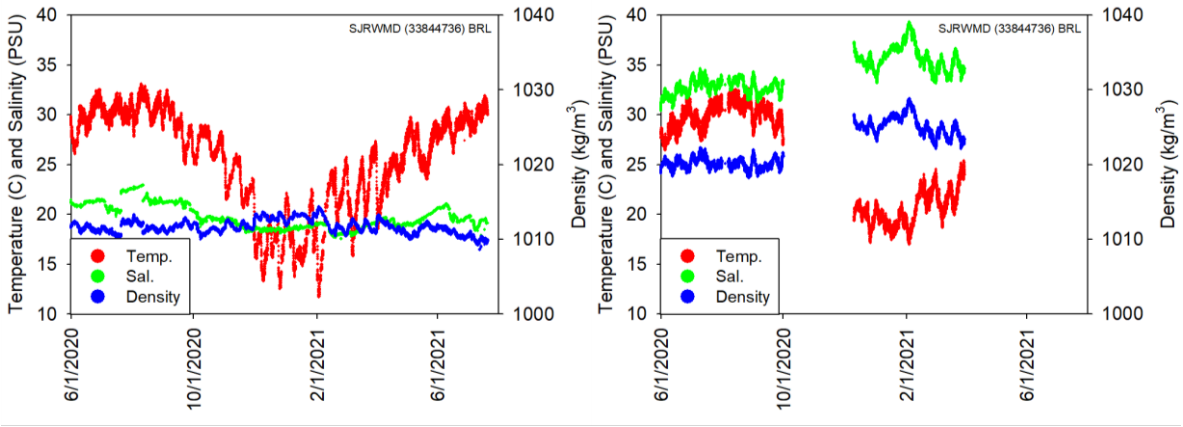

Figure 56. Temperature (red), salinity (green), and density (blue) in (a) BRL in the area of inflow and (b) in Port Canaveral

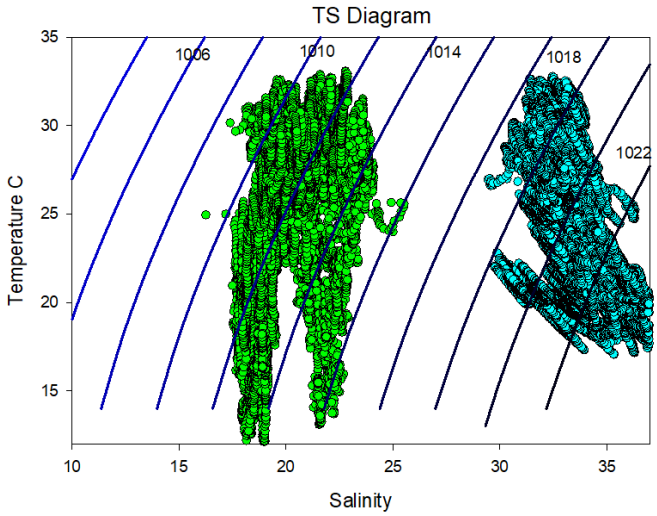

Figure 57. Temperature-salinity diagram showing data (2020–2021) from Port Canaveral (cyan on right) and the adjacent lagoon (light green on left)

Trends for salinity represent what can be expected based on the conservative properties of seawater. Although temperature is conservative, the shallow lagoon plus dark water and sediments are subject to more rapid heating relative to seawater, where changes to lagoon temperature may not behave conservatively. Other variables that, together with temperature and salinity, collectively describe water quality would likely experience less predictable variations as a result of inflow. For example, clearer and lower turbidity seawater typically has more stable DO.

4.2.2.2 Dissolved Nutrients

Nutrient data obtained during this study complement existing long-term IRL datasets. Collectively, these data were used to further evaluate potential impacts of inflow on nutrient concentrations by modeling the quantity of nutrients that would be removed through natural geochemical processes promoted by inflow relative to the quantity of nutrients that would likely be discharged through inlets to the coastal ocean.

Nutrient concentrations in Phase 2 were monitored through discrete sampling in Port Canaveral (proposed source of inflow water), BRL near the proposed inflow location, and reference site . As shown in **Table 5**, concentrations of dissolved nutrients in Port Canaveral were relatively low, with average concentrations of TDN, TDP, and SiO_2 at 23 ± 10 micromolar (µM), 0.37 ± 0.19 µM, and 11.9 ± 9.9 µM, respectively. Consistent with Phase 1, no significant vertical trends were observed for TDN, TDP, SiO_2, or speciation in Port Canaveral.

Dissolved nutrient concentrations in the lagoon were more variable compared to values for seawater from Port Canaveral (**Table 5**). However, trends for increases and decreases in nutrient concentrations over time tracked one another at the inflow and reference sites, suggesting that without treatment, these sites follow the same regional trends and are reasonable for comparisons during the proposed pilot study. Concentrations of TDN, TDP, and SiO_2 in lagoon samples were three to five times higher than values for seawater from Port Canaveral; no significant difference was identified for concentrations at the proposed inflow versus reference sites.

Table 5. Average nutrient concentrations for samples from the (1) lagoon reference site (n=17), (2) lagoon inflow site (n = 11), and (3) in Port Canaveral (n = 77).

Site	NH_4 (µM)	NOx (µM)	TDN (µM)	Dissolved Inorganic N (DIN) (µM)	Dissolved Organic N (DON) (µM)	PO_4 (µM)	TDP (µM)	Dissolved Organic P (DOP) (µM)	SiO_4 (µM)	Chloride (mM)	Sulfate (mM)	Alkalinity (mg/L)
Lagoon Reference	8.1 ± 11.7	1.1 ± 1.1	112 ± 21.2	9.2 ± 12.2	103 ± 10.4	0.25 ± 0.14	1.00 ± 0.34	0.8 ± 0.29	32 ± 31	238 ± 19	11.8 ± 0.8	74 ± 10.6
Lagoon Inflow	16 ± 24	0.5 ± 0.2	138 ± 47.9	17 ± 24	121 ± 42	0.35 ± 0.38	1.5 ± 0.9	1.2 ± 0.6	48 ± 86	251 ± 29	12.3 ± 1.6	79 ± 31
Port	3.0 ± 2.5	1.6 ± 5.1	23 ± 10	4.6 ± 5.5	18.5 ± 9.5	0.20 ± 0.11	0.37 ± 0.19	0.20 ± 0.16	11.9 ± 9.9	516 ± 137	26.3 ± 7.8	67.5 ± 6.7
Ocean (year1)	0.9 ± 0.2	0.3 ± 0.1	8 ± 2.4	1.2 ± 0.3	6.8 ± 2.4	0.06 ± 0.02	0.15 ± 0.05	0.09 ± 0.04	3 ± 1	466 ± 25	24 ± 2	69 ± 4

Differences in TDN and TDP between Port and lagoon samples were accompanied by variations in nutrient speciation. In the lagoon, a larger fraction of TDN was present as organic N. These data were consistent with trends observed for long-term datasets in IRL (e.g., SJRWMD). Higher concentrations of NH_4, especially relative to NOx, are known to stimulate blooms of *Aureoumbra lagunensis*, the brown tide species in IRL, and other harmful algal species, and large fractions of the TDN present as organic N indicate rapid recycling (e.g., Liu et al., 2001).

Overall, PO_4 and organic P accounted for 55% and 45% of the TDP in Port Canaveral (38% and 62% of the TDP at offshore sites during Phase 1) relative to 19% and 81% in the open lagoon (14% and 86% at the inflow site and 22% and 78% in the reference site).

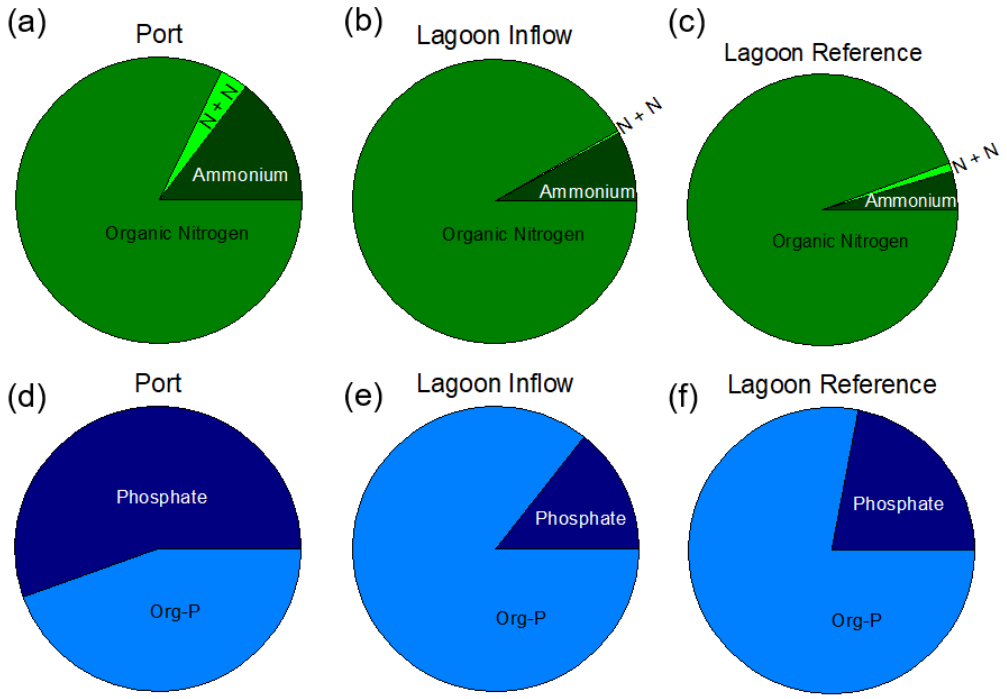

Figure 58. Pie diagrams showing the percent NH_4, percent NO_x, and percent organic N in (a) Port Canaveral, (b) BRL at the proposed inflow location, and (c) proposed reference site, and percent PO_4 and percent organic P in the water column in (a) Port Canaveral, (b) BRL at the proposed inflow location and (c) proposed reference site

Although total nutrient concentrations are frequently used as an indicator of the eutrophic state of an estuary, speciation and the relative abundance of bioavailable species of N:P:SiO_2 have consistently been shown to contribute to algal community composition, whereby at the same total concentrations, shifts in speciation, and relative abundance of N:P:SiO_2 can favor shifts from beneficial or less harmful photosynthesizers (e.g., seagrasses) to harmful species (e.g., *Aureoumbra lagunensis*) or vice versa (e.g., Choudhury and Bhadury 2015). Several species of harmful algae, including *Aureoumbra lagunensis,* the brown tide species in IRL, have been identified to use organic N and organic P (Liu et al., 2001), but are not able to use nitrate, complicating interpretations of water quality based on N:P. To provide a more complete picture, data are presented for both DIN:Soluble Reactive Phosphorus (SRP) and TDN:TDP.

Overall, DIN:SRP ratios varied among sample locations. For example, DIN:SRP in Port Canaveral averaged 20 ± 10 (median 22), consistent with ratios identified offshore during Phase 1 (offshore DIN:SRP = 20) and with ratios previously identified for the coastal Atlantic Ocean (Cavender-Bares et al., 2001; Martiny et al., 2014). The average ratio in seawater was more than two-fold lower than the average DIN:SRP ratio of 45 ± 56 for lagoon water; however, it was consistent with the median at 19 for lagoon samples during this study. The ratio for lagoon water during Phase 2 was higher than the average ratio identified during Phase 1 sampling; this difference was at least partially explained by sampling at predominantly northern sites during Phase 2. Higher N:P ratios in the northern lagoon were consistent with a trend identified during Phase 1 and supported by

results from Lapointe et al. (2020) showing a similar north-south pattern for the N:P ratios in seagrasses. Despite north-south trends that Lapointe et al. (2020) identified for seagrasses each species in their study had a relatively narrow range of N:P (*S. filiforme*, *T. testudinum* and *H. wrightii* range) and large differences in N:P have been shown to drive change in the composition of photosynthesizers (e.g., seagrasses versus algae, Hillebrand et al., 2013).

Ratios of TDN:TDP were higher than values for DIN:SPR. In Port Canaveral, TDN:TDP averaged 97 ± 75 (median 62) relative to 113 ± 46 (median 110) in the lagoon (119 ± 47 inflow and 109 ± 44 reference). These data reflect the larger fraction of TDN relative to P that is present in less bioavailable, organic forms. However, many small bloom-forming algae can use the organic forms of both N and P and high ratios of TDN:TDP are known to enhance the risk for *Aureoumbra lagunensis* blooms (Liu et al., 2001; DeYoe et al., 2007) whereby, some cyanobacteria and HAB dinoflagellates can store P within their cells (e.g., Hillebrand et al., 2013; Burford et al., 2014; Willis et al., 2015; Glibert et al., 2012; Accoroni et al., 2016).

Other studies have identified optimal $N:P_{opt}$ (molar) ratios (where limitation switches from N to P) for different groups of algae. For example, Hillebrand et al. (2013) reported the lowest $N:P_{opt}$ for diatoms at 14.9 increasing to 15.1 for dinoflagellates, 25.8 for cyanobacteria, and 27.0 for chlorophytes. At high N:P ratios, diatoms, which would generally be considered fast-growing, can be outcompeted by species, such as dinoflagellates, cyanobacteria, and chlorophytes, that have a higher optimal N:P ratios and are more frequently HAB-forming (Phlips et. Al., 2010). In the lagoon, high N:P ratios are preferred by HAB species such as *Pyrodinium bahamense var. bahamense, Aureoumbra lagunensis*, and *Akashiwo sanguinea*, which are commonly encountered in the northern IRL where muck and organic-rich sediments are prominent (e.g., Foster et al., 2019; **Figure 59**). Muck further promotes the dominance of HAB species by preferentially releasing NH_4, the preferred form of N of many harmful phytoplankton species, including *Pyrodinium bahamense var. bahamense* (e.g., Liu et al., 2001).

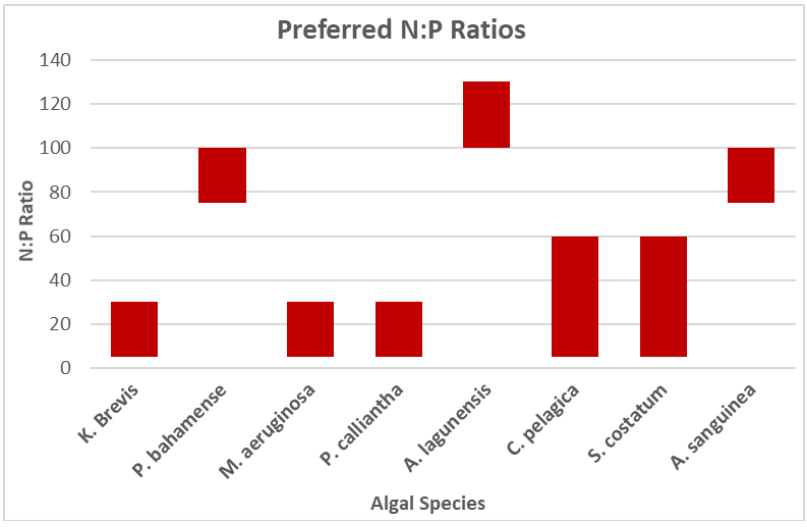

Figure 59. Preferred N:P ratios of selected algal species found in IRL: *K. brevis* (Vargo et. al, 2008), *P. bahamense* (Azanza et. al., 2004), *M. aeruginosa* (Smith et. al., 1993), *P. calliantha* (Guo et. al., 2017), *A. lagunensis* (Liu et. al., 2001), *C. pelagica* (Hauss et. al., 2012), *S. constatum* (Maso and Garces, 2006), and *A. sanguinea* (Chen et. al., 2019)

Based on global trends plus data from this study and long-term datasets, potential shifts in N:P ratios (DIN:SRP and TDN:TDP) should be considered for overall water quality and modeling and predicting algae blooms and bloom composition (Hillebrand et al., 2013). Based on the

importance of N:P ratios towards promoting certain algal groups, restoration efforts, including inflow, should be viewed not only as removing N or P but as regulating the ratio of these elements. Based on data for water in Port Canaveral, inflow water had both lower nutrient concentrations and lower ratios of both DIN:SRP and TDN:TDP, relative to the lagoon.

To use the most robust dataset available, five-year averages (2016–2021) for nutrient concentrations at sites near Sebastian Inlet were used to calculate discharges to the coastal ocean based on various inflow levels (**Table 6** and **Table 7**). These estimates do not account for nutrients that would be removed from the system via geochemical processes (see **Section 4.2.2.3**). Based on a proposed pilot pumping rate of 0.5 m^3/sec, 4.3 x 10^8 L of lagoon water would be discharged per day, or 1.6 x 10^{10} L per year (**Table 7**). An annual discharge of nutrients through inlets to the coastal Atlantic Ocean associated with the pilot project is estimated at 6.5 metric tons of N and 0.6 metric tons of P (**Table 7**). The discharge of dissolved nutrients is equal to about 0.5% and 0.4% of the annual total estimated inputs of N (1,400 tons/year) and P (140 tons/year) to IRL per year, respectively (Tetra Tech, 2021). Using average nutrient concentrations from **Table 6,** plus an average lagoon depth of 1.5 m and a surface area of 170 km^2 in BRL and 270 km^2 in northern IRL, standing stocks of N and P are estimated at about 300 metric tons and about 30 metric tons, respectively. Overall, maximum annual discharges from the pilot study would be equal to about 2% of the standing stock of N and P currently in the lagoon. The relatively small direct removal of N and P of the pilot project is expected because it is intended to treat only a small area as a test of this technique. Enhanced circulation is aimed at restoring natural ecosystem services (biogeochemical processes) that will remove/sequester N and P.

Table 6. Nutrient concentrations (five-year running averages) at stations near Sebastian Inlet (IRLI28) and Fort Pierce Inlet (IRLIRJ08) plus data from this study

Location	NH_4 (mg/L)	NOx (mg/L)	DIN (mg/L)	Organic N (mg/L)	TDN (mg/L)	PO_4 (mg/L)	TDP (mg/L)	DOP (mg/L)
Sebastian (IRLI28)	0.03 ± 0.03	0.01 ± 0.03	0.04 ± 0.06	0.37 ± 0.17	0.41 ± 0.23	0.01 ± 0.01	0.04 ± 0.02	0.025 ± 0.008
BRL (IRLB04)	0.05 ± 0.1	0.02 ± 0.03	0.07 ± 0.14	1.01 ± 0.12	1.08 ± 0.26	0.01 ± 0.01	0.03 ± 0.02	0.015 ± 0.003
Open Lagoon (this study)	0.12 ± 0.20	0.01 ± 0.01	0.13 ± 0.20	1.5 ± 0.4	1.7 ± 0.5	0.01 ± 0.01	0.04 ± 0.02	0.03 ± 0.01
Port (this study)	0.04 ± 0.04	0.02 ± 0.07	0.06 ± 0.08	0.26 ± 0.13	0.32 ± 0.14	0.01 ± 0.00	0.01 ± 0.01	0.01 ± 0.00

Table 7. Maximum tons of N and P predicted to be discharged to the coastal ocean per year from Sebastian Inlet from various inflow levels, if no geochemical removal occurred

Pumping Rate	L/day	L/year	NH_4 (tons/ year)	NOx (tons/ year)	DIN (tons/ year)	Organic N (tons/ year)	TDN (tons/ year)	PO_4 (tons/ year)	TDP (tons/ year)	DOP (tons/ year)
0.5 m^3/sec	$4.3*10^7$	$1.6*10^{10}$	0.5	0.2	0.63	5.8	6.5	0.2	0.6	0.39
2.5 m^3/sec	$2.2*10^8$	$7.9*10^{10}$	2.4	0.8	3.2	29	32	0.8	3.2	2.0
5 m^3/sec	$4.3*10^8$	$1.6*10^{11}$	4.8	1.6	6.4	59	66	1.6	6.4	4
10 m^3/sec	$8.6*10^8$	$3.2*10^{11}$	9.6	3.2	12.8	118	131	3.2	12.8	8
15 m^3/sec	$1.3*10^9$	$4.7*10^{11}$	14.1	4.7	18.8	174	193	4.7	18.8	11.8
20 m^3/sec	$1.7*10^9$	$6.3*10^{11}$	18.9	6.3	25.2	233	258	6.3	25.2	15.8

Table 8. Tons of N and P that are predicted to be brought into the lagoon with various inflow levels

Pumping Rate	L/day	L/year	NH4 (tons/ year)	NOx (tons/ year)	DIN (tons/ year)	Organic N (tons/ year)	TDN (tons/ year)	PO4 (tons/ year)	TDP (tons/ year)	DOP (tons/ year)
0.5 m^3/sec	$4.3*10^7$	$1.6*10^{10}$	0.69	0.14	0.82	4.18	5.00	0.10	0.18	0.00
2.5 m^3/sec	$2.2*10^8$	$7.9*10^{10}$	3.43	0.70	4.12	20.94	25.06	0.52	0.91	0.02
5 m^3/sec	$4.3*10^8$	$1.6*10^{11}$	6.96	1.42	8.34	42.41	50.75	1.06	1.84	0.03

Pumping Rate	L/day	L/year	NH4 (tons/ year)	NOx (tons/ year)	DIN (tons/ year)	Organic N (tons/ year)	TDN (tons/ year)	PO4 (tons/ year)	TDP (tons/ year)	DOP (tons/ year)
10 m^3/sec	$8.6*10^8$	$3.2*10^{11}$	13.91	2.84	16.68	84.81	101.50	2.12	3.68	0.06
15 m^3/sec	$1.3*10^9$	$4.7*10^{11}$	20.43	4.18	24.51	124.57	149.08	3.11	5.40	0.09
20 m^3/sec	$1.7*10^9$	$6.3*10^{11}$	27.39	5.60	32.85	166.98	199.83	4.17	7.24	0.12

Because inflow would create an exchange of water, nutrients brought from the coastal ocean into the lagoon should be subtracted from discharge estimates to determine net removal from the lagoon and net discharge into the ocean (not accounting for removal by decreased fluxes). Using the proposed pilot pumping rate of 0.5 m^3/sec, approximately 5.0 metric tons of N and 0.2 metric tons of P would be brought into the lagoon per year (**Table 8**). The net discharge of nutrients to the coastal ocean would be 1.5 metric tons of N and 0.4 metric tons of P per year during the pilot study. The direct discharge of nutrients would be greater if inflow water was obtained from offshore as reflected in data obtained during Phase 1 (**Table 5**). The comparison of standing stock (300 metric tons of N and 30 metric tons of P) relative to inputs (1,400 tons/year of N and 140 tons/year of P) illustrates the relative importance of geochemical nutrient cycling, where small changes to cycling can have large impacts on concentrations of bioavailable nutrients. Based on these data and calculations, the entire standing stock of nutrients in the lagoon is replaced about five times per year by inputs in current models including point sources, atmospheric deposition, stormwater runoff, groundwater seepage (baseflow), and muck.

Table 9. Tons of N and P that would be pumped into the lagoon associated with pumping seawater from offshore at various pumping rates (based on data from Phase 1)

Pumping Rate	L/day	L/year	NH_4 (tons/ year)	NOx (tons/ year)	DIN (tons/ year)	Organic N (tons /year)	TDN (tons/ year)	PO_4 (tons/ year)	TDP (tons/ year)	DOP (tons/ year)
0.5 m^3/sec	$4.3*10^7$	$1.6*10^{10}$	0.2	0.1	0.3	1	2	0.02	0.08	0.04
2.5 m^3/sec	$2.2*10^8$	$7.9*10^{10}$	1.0	0.3	1.3	5	9	0.1	0.4	0.2
5 m^3/sec	$4.3*10^8$	$1.6*10^{11}$	2.1	0.6	2.7	11	18	0.3	0.7	0.4
10 m^3/sec	$8.6*10^8$	$3.2*10^{11}$	4.2	1.2	5.4	21	36	0.6	1.4	0.9
15 m^3/sec	$1.3*10^9$	$4.7*10^{11}$	6.2	1.7	7.9	31	52	0.8	2.1	1.3
20 m^3/sec	$1.7*10^9$	$6.3*10^{11}$	8.3	2.3	10.6	42	70	1.1	2.8	1.8

4.2.2.3 Geochemical Nutrient Cycling (In-situ)

Due to the non-conservative nature of nutrients and strong benthic-pelagic coupling in shallow estuarine systems, processes in sediments and on particles make it difficult to estimate how the combined inflow and discharges of nutrients from the lagoon would change nutrient concentrations and ratios over time. To address these complex geochemical processes, nutrient and oxygen cycling were investigated in water from Port Canaveral and lagoon (both inflow and reference sites) and in laboratory experiments to determine how changes to temperature, salinity, and DO might influence geochemical nutrient cycling in the water column and sediments.

Water column respiration (dark) in IRL was highly variable and consumed oxygen at 0.19 ± 0.15 mg/L/hr. In Port Canaveral, water column respiration (dark) was about 30% lower at 0.12 ± 0.09 mg/L/hr Overall, water column respiration (dark) in the lagoon accounted for 50% to greater than 80% of the total respiration (sediments + water) and is a major contributor to hypoxia or anoxia, when it occurs (**Table 10**). The importance of water column processes is captured by the continuous DO data at the proposed inflow location and in Port Canaveral, where high rates of SOD and water column respiration lead to large diurnal fluctuations in DO concentrations in the lagoon, with lower magnitude diurnal cycles in seawater from Port Canaveral.

Table 10. Rates of water column respiration and SOD and relative importance of sediments towards total respiration for varying water depths (per 1m^2 of lagoon)

Note: Calculated using average rates of water column respiration (-0.19 mg/L/hr) and SOD (~3000 µmoles/m^2/hr = ~100 mg/m^2/hr) from sandy sediment.

Depth	DO Consumed by Sediment (mg/m^2/hr)	Water Volume/m^2 (L)	DO Consumed by Water (mg/hr)	Percent Consumed by Sediments
0.5	100	500	95	51
1.0	100	1,000	190	34
1.5	100	1,500	285	26
2.0	100	2,000	380	21
2.5	100	2,500	475	17

Water column respiration (dark) is accompanied by increased nutrient concentrations (particle fluxes). Previous studies have shown that these dark processes are relatively well matched, but opposite during light experiments to maintain nutrient concentrations over time (Ziegler and Benner, 1999). In that context, results presented here should be viewed as an indication of recycling rates and how particle exchanges during inflow may influence concentrations of dissolved nutrients over time. In the lagoon, NH_4, nitrate, DIN, organic N, and TDN (dark) increased by (median ± standard error) 0.05 ± 0.43 µM/hr, 1.8 ± 7.1 µM/hr, 1.9 ± 6.9 µM/hr, 4.6 ± 3.8 µM/hr, and 6.5 ± 10 µM/hr, respectively (**Table 11** and **Figure 60**). Releases of N associated with water column respiration in BRL were two to four times higher than particle fluxes from seawater in Port Canaveral with median values at 0.01 ± 0.9 µM/hr, 0.95 ± 1.9 µM/hr, 0.96 ± 2.0 µM/hr, 1.4 ± 6.0 µM/hr, and 2.4 ± 6.8 µM/hr for NH_4, nitrate, DIN, organic N, and TDN, respectively (**Table 11**). Releases of P from water column respiration were similar in BRL and Port Canaveral (PO_4 0.03 ± 0.03 µM/hr in the lagoon relative to 0.03 ± 0.12 µM/hr in the Port; **Table 11** and **Figure 61**). Based on these data, turnover times for TDN and TDP were two-fold and more than six-fold higher in lagoon water relative to seawater from Port Canaveral.

Table 11. Water column fluxes in Port Canaveral and in the adjacent lagoon (inflow and reference sites for dark conditions

Location	NH_4 (µM/hr)	NOx (µM/hr)	DIN (µM/hr)	Organic N (µM/hr)	TDN (µM/hr)	PO_4 (µM/hr)	TDP (µM/hr)	DOP (µM/hr)
Port Canaveral	0.01 ± 0.90	0.95 ± 19	0.96 ± 2.0	1.4 ± 6.0	2.4 ± 6.8	0.03 ± 0.12	0.07 ± 0.17	0.04 ± 0.07
Lagoon	0.05 ± 0.43	1.8 ± 7.1	1.9 ± 6.9	4.6 ± 3.8	6.5 ± 10	0.03 ± 0.03	0.04 ± 0.06	0.004 ± 0.06

Overall, data for water column recycling from this study indicate that inflow would bring water with lower rates of dark respiration (about 30% lower oxygen consumption) into the lagoon, thereby increasing resilience to hypoxia while also decreasing the rate of nutrient recycling. Because rates of N recycling were two to four times higher and rates of P recycling were similar in lagoon and Port Canaveral water, lower N:P ratios were identified for recycling in seawater from Port Canaveral. Based on data from this study, the water column recycling ratio of DIN:SRP for Port water was 10, relative to the DIN:SRP recycling ratio for lagoon water at 46. As expected, ratios for recycling of TDN:TDP were higher at 17 in the Port and 88 in lagoon water during this study. These rates were highly variable, responding to changes in water quality; nevertheless, these recycling ratios act to stabilize ratios of N to P in water over time. These recycling ratios followed patterns for ratios observed for the standing stock of nutrients observed in the Port and lagoon. Based on these data and consistent with global processes, water column recycling acts to buffer against changes to the relative abundance of N to P and helps to sustain algal communities over time. Inputs of seawater to the lagoon would decrease ratios of N:P recycling in the water column, likely leading to a lower N:P ratio of the standing stock of nutrients in the lagoon over time.

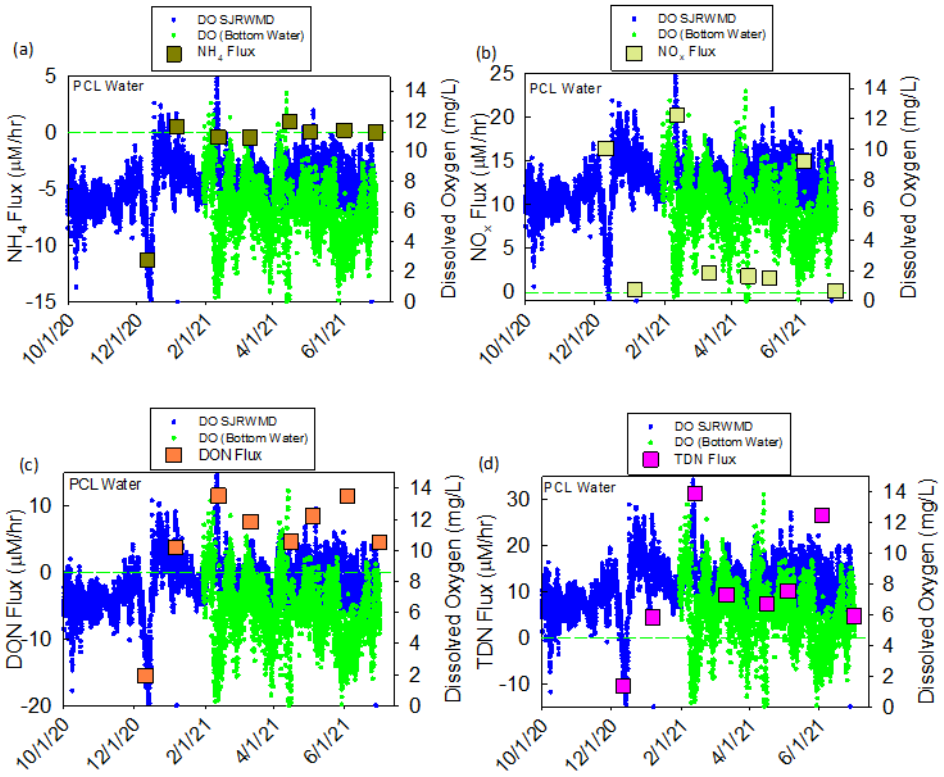

Note: Green and blue dotted lines show DO in the region at mid water depths (SJRWMD site IRLB04) and in bottom water at the inflow site.

Figure 60. Water column fluxes of (a) NH_4, (b) NO_x, (c) DON and (d) TDN

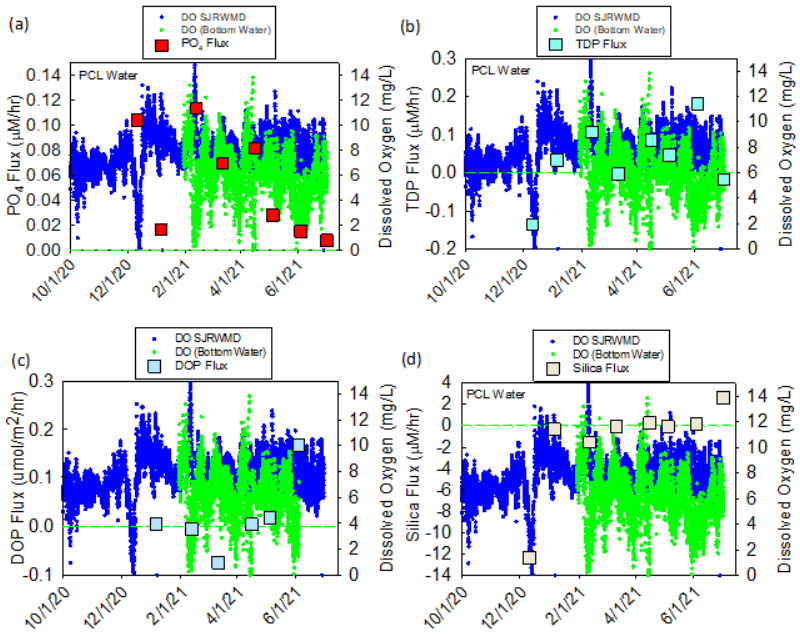

Note: Green and blue dotted lines show DO in the region at mid water depths (SJRWMD site IRLB04) and in bottom water at the inflow site.

Figure 61. Water column fluxes of (a) PO_4, (b) TDP, (c) DOP and (d) SiO_2

Benthic fluxes of N and P from muck are estimated to contribute more than 30% of the annual N and P loading to IRL (Tetra Tech, 2016; Fox and Trefry, 2018). These estimates are based only on fluxes from fine-grained, organic-rich sediments locally referred to as "muck." Because sand covers at least 90% of the lagoon bottom, non-trivial fluxes from sand need to be considered when evaluating the importance of internal nutrient sources and geochemical nutrient cycling. To evaluate the importance of these geochemical processes, nutrient residence times were calculated using benthic nutrient fluxes, long-term average nutrient concentrations in lagoon water (**Table 6**), and average lagoon depth of 1.5 meters. Data from this study serve as a baseline from which the importance of sandy sediments as both a source and sink of nutrients can be evaluated. Although this study focused on sandy sediments, non-trivial fluxes from muck would be influenced by changes to temperature, salinity, and DO.

During Phases 1 and 2 of this study, no significant trends for benthic nutrient fluxes versus the composition of sandy sediments were identified. There is an established pattern where sediment water and organic matter content were strongly correlated with benthic fluxes from fine-grained, organic-rich sediments (muck) throughout IRL (Fox and Trefry, 2018). The absence of a trend for sandy sediments is likely related to groundwater seepage into the lagoon (Pandit et al., 2017). Based on data from mini-seepage meters in this study, it is likely that benthic chambers deployed along the IRL western shoreline were influenced by groundwater seepage with rates ranging from less than 1 cm/day to 30 cm/day (Bethel Creek). During Phase 2, benthic chambers were focused along the BRL eastern shoreline near the inflow and reference sites.

Median ± standard deviation SOD for sandy sediments during this study and other projects was -3,100 ± 2,400 µmoles/m^2/hr (median 2,900 µmoles/m^2/hr, n = 53) lagoon-wide. Values during Phase 2 at the proposed inflow and reference sites were -2,500 ± 1,600 µmoles/m^2/hr (median 2,600 µmoles/m^2/hr, n = 22). Overall, DO concentrations in bottom water and rates of oxygen consumption varied together with lower bottom water DO identified during periods with higher oxygen demand (more negative SOD), except when DO in bottom water approached zero (i.e., December 2020, **Figure 62**). Overall, values for sandy sediment in IRL and BRL fit within a range of values previously reported for estuaries around the world, at -200 to -7,000 µmoles/m^2/hr (Boynton et al., 2018). Oxygen demand of muddy sediments was higher and more variable at -5,700 ± 4,600 µmoles/m^2/hr (n = 8); however, muddy sediments were investigated primarily during cooler months and average fluxes likely underestimate annual average values where SOD as high as -9,000 µmoles/m^2/hr were measured during summer months.

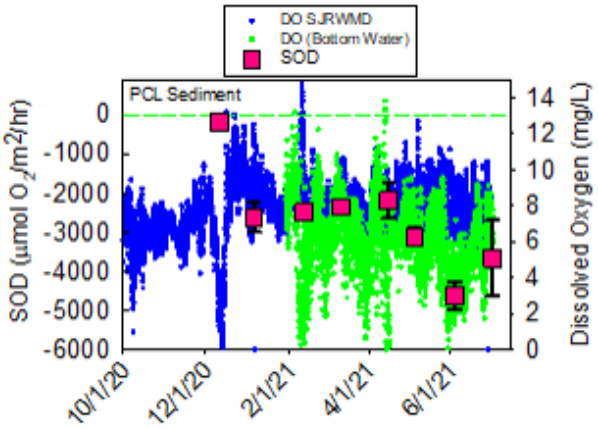

Note: Blue and green dotted lines show DO in mg/L at mid water depth (SJRWMD sensor IRLB04) and in bottom water, respectively.

Figure 62. SOD over time at the inflow site

During Phase 1, median ± standard deviation N fluxes varied among areas with sandy versus muddy sediments. Lagoon-wide, DIN was released from sandy sediments (median ± SE = 260 ± 170 µmoles/m^2/hr, 32 tons/km^2/year) primarily as NO_x (63% of DIN, 150 ± 150 µmoles/m^2/hr, 20 tons N/km^2/year), and NH_4 accounted for 37% of the DIN efflux from sandy sediments at 90 ± 60 µmoles/m^2/hr (11 tons N/km^2/year). During Phase 2, similar values were identified from higher resolution sampling at the inflow and reference sites, with a flux of DIN at 70 ± 52 µmoles/m^2/hr (8 tons/km^2/year). About 76% of the DIN flux was accounted for by NO_x at 53 ± 42 µmoles/m^2/hr (7 tons/km^2/year) and NH_4 accounted for 24% at 17 ± 21 µmoles/m^2/hr (1 ton/km^2/year). In about one-third of the chambers, NH_4 fluxes were directed into sediments, likely due to nitrification in aerobic surface sediments. During and shortly following hypoxic events (December 2020 and February 2021 on **Figure 63**), the flux of NH_4 was elevated as expected for anaerobic sediments.

During Phase 1, fluxes of DON were highly variable with median DON fluxes directed out of sediments for a median TDN flux from sandy sites at 290 ± 430 µmoles/m^2/hr (35 tons N/km^2/year). During Phase 2 at the inflow and reference sites, DON fluxes were highly variable and typically directed into sediments from overlying water with a median at -480 ± 52 µmoles/m^2/hr (**Figure 63**). Different outcomes from Phases 1 and 2 demonstrate the susceptibility of sediment processes to changing conditions, as well as variations among sites. Overall, sandy sediments represented both a source and a sink for N where small changes to fluxes had a dramatic impact on N supply or removal from the lagoon. With this, first of its kind in IRL, relatively limited dataset, event scale changes from seasonal patterns can be isolated yet. Continued sampling will help to resolve these differences that are critical to understanding N in this system.

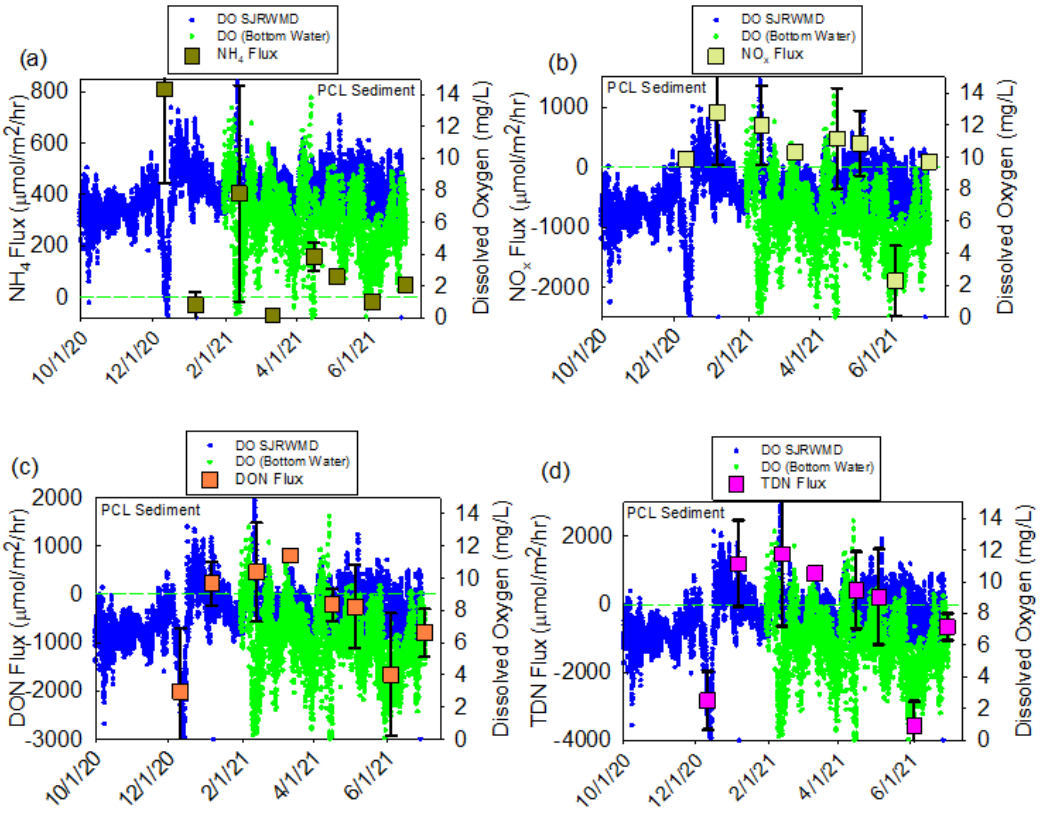

Note: Green and blue dotted lines show DO in the region at mid water depths (SJRWMD site IRLB04) and in bottom water at the inflow site.

Figure 63. Benthic fluxes of (a) NH_4, (b) NO_x, (c) DON and (d) TDN

At muddy sites (muck), fluxes of NO_x were directed from the water into sediments (-5 ± 19 µmoles/m^2/hr; -0.5 tons N/km^2/year), consistent with the use of nitrate as an oxidizing agent for the decomposition of organic matter in suboxic/anaerobic sediments. DIN releases from muddy sediments were 100% NH_4 at a median of 580 ± 460 µmoles/m^2/hr (71 tons N/km^2/year), greater than two-fold higher than DIN fluxes from sandy sediments and positive relative to negative TDN fluxes for sandy sediments. Based on data presented here, muddy sediments represented a significant source of reduced N to overlying water (70 tons/km^2/year). When applied to the surface area of muck**,** about 400–500 tons of N enter the lagoon per year from muck.

During Phase 1, at sandy sites through the lagoon, the median ± standard error PO_4 flux was 4.1 ± 8.1 µmoles/m^2/hr (1.1 ton/km^2/year). During Phase 2 at the inflow and reference sites, PO_4 flux was lower at 1.8 ± 0.6 µmoles/m^2/hr (0.5 tons/km^2/year). Wide ranges of values for P fluxes are not unexpected because P fluxes vary as a result of bacterial decomposition and concentration gradients, but also due to changing redox conditions in sediments and overlying water. As sediments and water become aerobic (oxic), P is scavenged by oxidized iron and aluminum while simultaneously aerobic decomposition of sediment organic matter can promote releases of PO_4 from sediments. Under anaerobic conditions, bacterial metabolism of organic matter slows; however, PO_4 can be released from reduced sediments, temporarily increasing fluxes (Cowan and Boynton, 1996; Boynton et al., 2018). Data presented show this change where sediments switch from a sink to a source of PO_4 (**Figure 64**). For example, during sampling in December 2020, bottom water DO at the inflow site was hypoxic at 1.3–1.5 mg/L and P fluxes were very high and directed out of sediments (18.8 ± 5.2 µmoles/m^2/hr, **Figure 64**). A similar, high P flux was identified in February 2021 (22 ± 12 µmoles/m^2/hr) immediately following a hypoxic event the night before. During subsequent sampling events (excluding December 2020 and February 2021), DO was greater than 5 mg/L at the time of sampling and P fluxes from the same location were lower at 0.38 ± 0.5 µmoles/m^2/hr (overall, 1.8 ± 0.5 µmoles/m^2/hr, **Figure 64**).

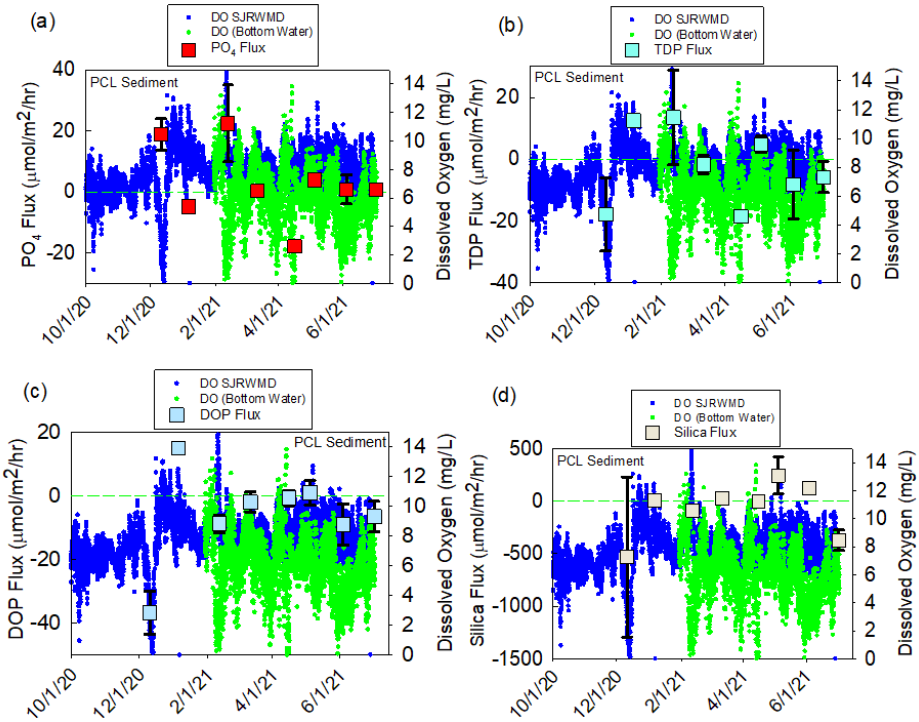

Note: Green and blue dotted lines show DO in the region at mid water depths (SJRWMD site IRLB04) and in bottom water at the inflow site.

Figure 64. Benthic fluxes of (a) PO_4, (b) TDP, (c) DOP and (d) SiO_2

Lagoon-wide DOP fluxes were directed into sandy sediments at -4.7 ± 4.9 µmoles/m^2/hr, consistent with mineralization of dissolved organic matter and a concentration gradient driving fluxes into sediments. Fluxes from the inflow and reference sites agreed well with Phase 1 data at -4.2 ± 0.6 µmoles/m^2/hr. Based on these datasets, the net TDP flux was directed into sandy sediments from overlying water at -0.6 µmoles/m^2/hr (-0.2 tons/km^2/year) for sites throughout the lagoon and -2.6 ± 0.7 µmoles/m^2/hr (-0.7 tons/km^2/year) at the inflow and reference sites.

At muddy sites, the median PO_4 flux was 12 ± 18 µmoles/m^2/hr (3.3 tons/km^2/year). Higher PO_4 fluxes in muddy/anaerobic sediments from IRL are consistent with data previously reported for other estuaries (e.g., Cowan and Boynton, 1996). Fluxes of DOP were also directed out of sediments at 8.8 ± 6.6 µmoles/m^2/hr (2.4 tons/km^2/year). Overall TDP fluxes were directed out of muddy sediments and the net flux of P was large and positive, compared to a flux directed into sandy sediments throughout the lagoon and at the inflow and reference sites (**Table 12**).

Table 12. Median ± standard error for benthic fluxes from sandy and muddy sediments in µmoles/m^2/hour for lagoon-wide sampling of sandy sediments during Phase 1 (lagoon-wide sand) and high resolution sampling at the proposed inflow and reference sites during Phase 2

Sediment	Oxygen	NH_4	NOx	DIN	PO_4	TDP	DOP
Lagoon-Wide Sand	-3,200 ± 900	90 ± 60	150 ± 150	260 ± 170	4.1 ± 8.1	-0.6	-4.7 ± 4.9
Inflow/ Reference	-2,500 ± 1,600	17 ± 21	53 ± 42	70 ± 52	1.8 ± 0.6	-2.6 ± 0.7	-4.2 ± 0.6
Muck	-4,300 ± 2,500	580 ± 460	-180 ± 200	400	12 ± 18	20 ± 23	8.8 ± 6.6

These data yielded trends in nutrient fluxes that were at least partially explained by changes to temperature and DO of bottom water. For example, during oxic conditions, sandy sediments were a sink for P (**Figure 64**); however, during or shortly following periods of hypoxia or anoxia, sandy sediments were a source of P to overlying water. During oxic conditions, sandy sediments promoted fluxes of NOx and during periods of hypoxia, sandy sediments were more frequently a large source of NH_4 (**Figure 63**). Pulses of bioavailable P can support algal growth and fluxes of reduced N during periods of hypoxia, preferentially support small, fast-growing algae like picocyanobacteria including *Aureoumbra lagunensis* (Liu et al., 2001).

Benthic nutrient and oxygen fluxes plus existing IRL nutrient concentrations were used to estimate residence (turnover) times for nutrients. Residence times indicate the theoretical amount of time required for all of a nutrient in the water column to be either re-generated or consumed. Short residence times for nutrients (hours to weeks) relative to water (months to years) indicate that water column processes and benthic-pelagic coupling buffer nutrient concentrations against changes resulting from external sources. Residence times based on fluxes alone were calculated. Using an average lagoon depth of 1.5 m, each 1 m^2 section of lagoon contains 1.5 m^3 or 1,500 L of water. Nutrient concentrations (µmoles/L, **Table 6**) times volume (1,500 L) yields the total quantity of nutrients (µmoles) in each 1 m^2 section. The total nutrient quantity was divided by fluxes (µmoles/m^2/hr) to yield residence times in hours. In sandy sediments, the residence time for NH_4 was about 140 hours, based on average nutrient concentrations at lagoon sites during this study. Water column respiration accounted for about 50% of the NH_4 recycling (**Table 13**).

NOx fluxes from sandy sediments were higher than NH_4 fluxes and concentrations in lagoon water were lower yielding turnover times ranging from about 10 to 20 hours (**Table 13**). Together, sediment DIN fluxes could replace TDN in the water column in about 100 days (2,600 hours).

Rapid recycling of NOx in the water column coupled with low concentrations yielded a turnover time of less than one hour. Water column processes accounted for 95% of NOx recycling (**Table 13**). Turnover times for NH_4 and NO_x from muck were 20 hours and 10 hours, respectively, where muck acted as a major source of NH_4 (70 tons/km^2/year) and a sink for NOx (-22 tons/km^2/year; **Table 12**). NH_4 could replace TDN in the water column overlying muck in approximately 13 days (300 hours). This decreases to less than 3 days when water column processes are included.

Turnover times for PO_4 from sandy sediments varied from 10 to 270 hours, or less than 1 to 11 days, compared to only 14 hours for areas with muck sediments (**Table 13**). To cycle the complete pool of dissolved P, it would take 500–1,100 hours, or 20–50 days, for sandy sediments and 60 hours, or 2–3 days, for muck. Water column processes appeared to be much more important compared to sediments for P cycling. Water column processes cycled the complete pool of TDP in just 32 hours and, in the adjacent Port, TDP was recycled in 5 hours. Due to rapid recycling in the water column, in areas with sandy sediments, benthic fluxes accounted for only 0.1% of the total recycling. In muddy areas, sediments accounted for 1% of the TP recycling.

Due to the large temporal and spatial variability in DO throughout the lagoon, turnover times for oxygen were highly variable. If the five-year average DO concentration is used, turnover times based on SOD alone ranged from 140 hours for sandy sites in the inflow area to 80 hours for mucky sites. When water column respiration and SOD are considered together, turnover times based on a 1.5-m deep water column were about 30 hours for sandy sites and 26 hours for muddy sites. Overall, sediments accounted for 26% and 32% of the total oxygen demand for areas containing sand and muck, respectively (**Table 10**). These short turnover times are consistent with observed nighttime (dark) decreases in DO observed throughout the lagoon in continuous monitoring networks. The Florida Tech network of bottom water DO sensors captures the importance of sediments towards oxygen consumption and nutrient recycling.

Table 13. Turnover times calculated using nutrient recycling in the water column and benthic fluxes, nutrient concentration in the water column, and an average depth of 1.5 m

Sediment	Oxygen (hours)	NH_4 (hours)	NOx (hours)	DIN to replace TDN (hours)	PO_4 (hours)
Water Column	40	170	0.4	60	10
Inflow/Reference	140	760	20	2600	270
Lagoon-Wide Sand	110	140	10	700	120
Muck	80	20	10*	460	10
Water + Sand	30	80	0.4	60	9
Sediment/Total	26%	55%	5%	-	0.1%

*removal by sediments

Despite the importance of benthic-pelagic coupling and short residence times for nutrients in shallow coastal systems, improved water quality that could result from artificial inflow would likely modify geochemical processes, possibly increasing or decreasing benthic fluxes into overlying water and changing residence times for nutrients. To address some of these potential changes, laboratory incubation experiments were carried out for water and sediments to investigate how changes to temperature, salinity, and DO might influence nutrients in the lagoon.

4.2.3 Laboratory Experiments

Geochemical responses to changes in water quality from enhanced ocean inflow were evaluated through a series of laboratory incubation experiments to simulate changes in temperature, salinity, and DO. These data provide insight into how nutrient cycling may respond to other processes,

including warming temperatures and enhanced rainfall. With respect to ocean inflow, the most likely results would be a small decrease in lagoon temperature, increase in salinity, and more stable DO. Consistent with data for temperature and DO, changes to water column salinity were used to isolate responses of sediments. intrinsic changes to particles during salinity adjustments confound interpretation of responses within the water column; therefore, changes to water column salinity are not discussed. No significant trends for N or P were identified for water column fluxes as a function of temperature, salinity, or DO (**Table 14**, **Table 15**, **Table 16**, and **Table 17**).

Table 14. Statistics for water column fluxes (dark) versus temperature (0–2 hours)

Plot	R^{2}*	P-value*
TDN and Temp	0.007	0.874
NH_4 and Temp	0.617	0.064
NO_x and Temp	0.490	0.122
DIN and Temp	0.548	0.093
DON and Temp	0.011	0.841
PO_4 and Temp	0.185	0.395
TDP and Temp	0.248	0.315
DOP and Temp	0.425	0.161
Silica and Temp	0.520	0.106
H^+ and Temp	0.001	0.944
DIN:SRP and Temp	0.490	0.122
TDN:TDP and Temp	0.154	0.442

Table 15. Statistics for water column fluxes (dark) versus temperature (2–18 hours)

Plot	R^{2}*	P-value*	Equation
TDN vs. Temp	0.004	0.908	-
NH_4 vs. Temp	0.524	0.104	-
NO_x vs. Temp	0.490	0.122	-
DIN vs. Temp	0.522	0.105	-
DON vs. Temp	0.085	0.575	-
PO_4 vs. Temp	0.140	0.464	-
TDP vs. Temp	0.110	0.521	-
DOP vs. Temp	0.017	0.807	-
Silica vs. Temp	0.510	0.111	-
H^+ vs. Temp	0.838	**0.010**	**H^+(nmol/hr) = -0.005[°C] + 0.17**
DIN:SRP vs. Temp	0.491	0.121	-
TDN:TDP vs. Temp	0.151	0.446	-

Table 16. Statistics for water column fluxes (dark) versus DO (0–2 hours)

Plot	R^{2}*	P-value*
TDN vs. DO	0.741	0.139
NH_4 vs. DO	0.349	0.409
NO_x vs. DO	0.726	0.148
DIN vs. DO	0.493	0.298
DON vs. DO	0.770	0.123
PO_4 vs. DO	0.054	0.767
TDP vs. DO	0.232	0.519
DOP vs. DO	0.271	0.479
Silica vs. DO	0.533	0.270
H^+ vs. DO	0.873	0.066
DIN:SRP vs. DO	0.001	0.976
TDN:TDP vs. DO	0.610	0.219

Table 17. Statistics for water column fluxes (dark) versus DO (2–18 hours)

Plot	R^2	P-value
TDN vs. DO	0.526	0.274
NH_4 vs. DO	0.243	0.507
NO_x vs. DO	0.041	0.799
DIN vs. DO	0.219	0.532
DON vs. DO	0.680	0.175
PO_4 vs. DO	0.365	0.396
TDP vs. DO	0.778	0.118
DOP vs. DO	0.733	0.144
Silica vs. DO	0.774	0.120
H^+ vs. DO	0.120	0.653
DIN:SRP vs. DO	0.152	0.610
TDN:TDP vs. DO	0.245	0.505

Table 18. Statistics for benthic fluxes versus temperature (0-2 hours)

Plot	R^2*	P-value*	Equation
TDN vs. Temp	0.008	0.778	-
NH_4 vs. Temp	0.275	0.080	-
NO_x vs. Temp	0.490	**0.025**	Y=-0.09x+2.33
DIN vs. Temp	0.267	0.086	-
DON vs. Temp	0.028	0.603	-
PO_4 vs. Temp	0.317	0.057	-
TDP vs. Temp	0.081	0.371	-
DOP vs. Temp	0.248	0.100	-
Silica vs. Temp	0.417	**0.023**	Y=27.0x-868
H^+ vs. Temp	0.096	0.328	-
DIN:SRP vs. Temp	0.058	0.452	-
TDN:TDP vs. Temp	0.142	0.227	-

Table 19. Statistics for benthic fluxes versus temperature (2-18 hours)

Plot	R^2*	P-value*	Equation
TDN vs. Temp	0.550	**0.006**	Y=3.5x-85.8
NH_4 vs. Temp	0.130	0.249	-
NO_x vs. Temp	0.488	**0.012**	Y=0.17x-0.43
DIN vs. Temp	0.123	0.264	-
DON vs. Temp	0.567	**0.005**	Y=4.0x-98
PO_4 vs. Temp	0.001	0.915	-
TDP vs. Temp	0.184	0.164	-
DOP vs. Temp	0.624	**0.002**	Y=0.12x-4.1
Silica vs. Temp	0.682	**0.001**	Y=14.9x-513
H^+ vs. Temp	0.022	0.647	-
DIN:SRP vs. Temp	0.0001	0.978	-
TDN:TDP vs. Temp	0.0767	0.384	-

To estimate how changes to temperature, salinity, and DO may influence geochemical processes within sediments, laboratory experiments with sandy sediments were carried out with temperatures ranging from 13 °C to 32 °C, salinities ranging from 0 to 34 PSU, and DO ranging from 0% (0 mg/L) to 100% (about 9 mg/L). Wide ranges of values for temperature, salinity, and DO were investigated to resolve changes among large natural variability while also controlling other variables. Incubations were carried out with multiple sampling intervals to investigate immediate responses (0–2 hours) to changes and responses after the initial change (2–18 hours).

Water column processes were tracked separately and subtracted from sediment fluxes allowing for sediment and water column processes to be evaluated independently.

Temperature was adjusted between 13 °C and 38 °C (±0.2 °C) using recirculating water baths to simulate the maximum annual range of temperatures. IRL sediments cores were slowly adjusted to the desired temperature within two hours of collection. After reaching the desired temperature, cores were allowed to equilibrate for at least one hour before overlying water was drained and replaced with new water from the collection site. Once temperature was stable for at least one hour, samples were collected and cores were stirred using air diffusers to maintain DO at 100%. Samples were collected at two and 18 hours after starting incubations.

Significant positive correlations were identified for TDN, NO_x, and DON (**Table 19**) from sandy sediments versus sediment temperature. NO_x fluxes were positively correlated with temperature but accounted for only a small (less than 1%) fraction of TDN. TDN increased by 3.5 µmoles/m^2/hr (0.4 tons/km^2/yr) per °C, virtually all as organic N, with sediments switching from a sink for N at temperatures below 25°C to a source of N into overlying water at temperatures above 25°C.

Based on data from Phase 1, fluxes of dissolved PO_4 from sandy sediments were positively correlated with temperature and increased from 0 µmoles/m^2/hr at 13 °C to 5 to 10 µmoles/m^2/hr at 32 °C. During Phase 2, a significant positive correlation was identified for DOP versus temperature (**Table 19**) and SiO_2 fluxes were positively correlated with sediment temperature increasing by 14.9 µM/m^2/hr per °C (**Table 19**).

Based on significant positive correlations between sediment temperature and NO_x, DON, TDN, PO_4, DOP, and SiO_2 fluxes, a potential decrease in water temperature from inflow would decrease inputs of these nutrients into the lagoon. For example, a 1 °C decrease in lagoon temperature would decrease PO_4 fluxes from sandy sediments by about 0.16 tons/km^2/year or about 15% from the current median at 1.1 ton/km^2/year (**Table 12**). Although lagoon-wide changes to temperature are likely to be small, small changes applied to large areas of the lagoon could have significant impacts on nutrient loading. Decreased nutrient inputs due to restoration of ecosystem services could be of more significance than decreased concentrations due to dilution by seawater.

Laboratory experiments were also carried out to evaluate potential uptake or releases of nutrients associated with changes in salinity. These experiments were carried out in water baths at 22 °C (laboratory temperature) and chambers were stirred using diffused air to maintain oxygen at 100% saturation. Before each experiment, overlying water was drained from cores and replaced with a mixture of site water plus deionized water (decreased salinity) or site water and added sea salt (higher salinity). Once overlying water was exchanged, cores were allowed to equilibrate for at least one hour before sampling.

During Phase 1, a significant correlation was identified for NO_x (flux (µmoles/m^2/hr) = -4.7 * [PSU] + 180) with a decrease in NO_x flux of 4.7 µmoles/m^2/hr (about 0.6 tons/km^2/hr) per PSU or about 3% per PSU from the median of 150 µmoles/m^2/hr (-20 tons N/km^2/year) for sandy sites. This trend likely represented short-term equilibrium processes during the shorter duration experiments in Phase 1. This same trend was not identified during Phase 2, likely because there was very little NO_x present in the cores. A significant correlation was identified for NH_4 flux versus salinity during the initial incubation period where NH_4 flux decreased by 0.84 µmoles/m^2/hr per PSU (**Table 20**). This equates to a decrease of about 1% per PSU from the median of 90 µmoles/m^2/hr (11 tons N/km^2/year) for sandy sites throughout the lagoon. These trends for small changes to N fluxes observed shortly after changes to salinity likely reflect lower concentrations in overlying water for

lower salinity samples. The absence of trends over the longer incubation periods (2–18 hours) suggest that small changes to salinity alone are not likely to influence geochemical N cycling.

Table 20. Statistics for benthic fluxes versus salinity (0-2 hours)

Plot	R^2*	P-value*	Equation
TDN vs. Salinity	0.002	0.886	-
NH_4 vs. Salinity	0.500	0.005	Y=-0.84x+29
NO_x vs. Salinity	0.036	0.553	-
DIN vs. Salinity	0.005	0.822	-
DON vs. Salinity	0.0001	0.978	-
PO_4 vs. Salinity	0.080	0.373	-
TDP vs. Salinity	0.137	0.237	-
DOP vs. Salinity	0.086	0.356	-
Silica vs. Salinity	0.092	0.339	-
H^+ vs. Salinity	0.201	0.144	-
DIN:SRP vs. Salinity	0.076	0.386	-
TDN:TDP vs. Salinity	0.022	0.649	-

No significant trends were identified for fluxes of dissolved PO_4 versus salinity during any of the experiments (**Table 20, Table 21**). These data suggest that no significant long-term changes to N or P cycling are expected based on changes to salinity.

Table 21. Statistics for benthic fluxes versus salinity (2-18 hours)

Plot	R^2*	P-value*	Equation
TDN vs. Salinity	0.032	0.576	-
NH_4 vs. Salinity	0.009	0.773	-
NO_x vs. Salinity	0.151	0.212	-
DIN vs. Salinity	0.012	0.733	-
DON vs. Salinity	0.061	0.437	-
PO_4 vs. Salinity	0.019	0.670	-
TDP vs. Salinity	0.040	0.532	-
DOP vs. Salinity	0.059	0.447	-
Silica vs. Salinity	0.657	**0.001**	Y=-0.28x-1.59
H^+ vs. Salinity	0.500	**0.010**	Y=2.65x-97
DIN:SRP vs. Salinity	0.236	0.120	-
TDN:TDP vs. Salinity	0.031	0.583	-

Although DO is not a conservative property of seawater, it is one of the water quality variables likely to change if seawater were to flow into the lagoon and it is one of the most important variables controlling nutrient cycling, infauna, epifauna, fish populations, and overall lagoon health. Changes to DO would likely result from: (1) a change in the solubility of oxygen due to changing temperature and salinity plus inflow of lower turbidity seawater with lower respiration, and (2) higher density seawater and enhanced circulation that could mix deep areas currently prone to stagnation and low DO events. To manipulate DO concentrations in the laboratory, cores were place in temperature stable water baths (22°C laboratory temperature) and continuously bubbled using mixed gases (air and N) to maintain DO concentrations between 0% (0 mg/L) and 100% saturation (7–8 mg/L).

Consistent with trends observed for in-situ benthic chambers, significant positive correlations were identified for organic and total N versus DO concentrations in bottom water (**Table 22**). In both the field and laboratory, sediments switched from a sink of organic N and TN to a source, as DO concentrations increased above 6–8 mg/L. These data show a 15 tons/km^2/year increase in

TDN fluxes, almost all as organic N, per mg/L increase in DO. This result is likely tied to the higher rates of decomposition in sediments yielding higher fluxes of organic N and TN. In the laboratory, following an initial pulse of organic N and TDN, aerobic sediments were a net sink for organic N and TDN (-82 ± 89 µmoles/m^2/hr) and anaerobic sediments were sometimes a source of organic N and TDN to overlying water (119 ± 240 µmoles/m^2/hr), with a significant negative correlation identified between TDN flux and DO over the 2–18 hour incubation (**Table 22**, **Table 23**).

Table 22. Statistics for benthic fluxes versus DO (0–2 hours)

Plot	R^2*	P-value*	Equation
TDN and DO	0.686	**0.002**	Y=124x-761
NH_4 and DO	0.021	0.673	-
NO_x and DO	0.368	0.048	
DIN and DO	0.014	0.730	-
DON and DO	0.633	**0.003**	Y=122x-733
PO_4 and DO	0.500	**0.033**	Y=-0.9x+1.06
TDP and DO	0.279	0.095	-
DOP and DO	0.252	0.116	-
Silica and DO	0.0001	0.978	-
H^+ and DO	0.007	0.802	-
DIN:SRP and DO	0.016	0.709	-
TDN:TDP and DO	0.165	0.215	-

Table 23. Statistics for benthic fluxes versus DO (2–18 hours)

Plot	R^2	P-value	Equation
TDN and DO	0.371	**0.047**	Y=-15x+52
NH_4 and DO	0.420	**0.031**	Y=2.3x-14.9
NO_x and DO	0.174	0.202	-
DIN and DO	0.370	**0.047**	-
DON and DO	0.474	**0.019**	Y=-17.5x+66.6
PO_4 and DO	0.042	0.545	-
TDP and DO	0.146	0.247	-
DOP and DO	0.077	0.409	-
Silica and DO	0.214	0.152	-
H^+ and DO	0.064	0.454	-
DIN:SRP and DO	0.453	**0.023**	Y=2.8x-15.0
TDN:TDP and DO	0.429	**0.029**	Y=11.4x-32.0

Fluxes of dissolved PO_4 decreased at higher concentrations of bottom water DO (**Table 22**).These observations were consistent with data from the field study, where PO_4 fluxes from hypoxic sediments were typically higher and positive from anaerobic sediments (19 ± 11 µmoles/m^2/hr in December 2020 and February 2021), compared to a negative median flux (-4.4 ± 7.3 µmoles/m^2/hr) under aerobic conditions during all other sampling events. Laboratory incubations with multiple sample intervals captured changes to nutrient cycling that resulted from the initial change in P. Longer term sampling captured the more stable fluxes at new DO concentrations. Variable responses are consistently identified in the literature (Foster and Fulweiler, 2019), mostly due to the complexities of the N and P cycles.

4.2.3.1 Discussion of Experimental Results

No significant correlations were identified between water column nutrient fluxes and changes to temperature, salinity, or DO. Although no changes were observed, mixing seawater with differing turnover times into lagoon water would, in and of itself, influence nutrient cycling in the inflow area. Significant positive correlations were identified for NO_x, TDN, PO_4, DOP, and SiO_2 versus

sediment temperature (**Table 19**), indicating that lower temperature would decrease internal loading of these nutrients into IRL. Shortly after changing salinity, significant negative correlations were identified between NH_4 and nitrate fluxes; however, there were no significant correlations beyond initial pulses of NH_4 and nitrate released following a decrease in salinity. Significant positive correlations were identified between DO and both DON and TDN (**Table 22**); however, after initial releases, significant negative correlations were identified between DON and TDN and DO and a positive correlation between NH_4 and DO (**Table 23**).

Significant correlations were identified between N and P and temperature plus DO, but not salinity. Using equations from statistically significant relationships, quantities of nutrients that could be removed or prevented from entering the lagoon in response to changes in temperature or DO were calculated. Because these responses are scalable depending on the magnitude of change to temperature or DO and the lagoon area that experiences change (km^2), results are presented per °C and per mg/L per km^2 (**Table 24**).

Table 24. Expected changes to fluxes of N and P resulting from an increase in temperature of 1°C and an increase in DO of 1 mg/L

Media	Change in N flux	Change in P flux
Sediment	0.4 tons/km^2/year/°C	0.16 tons/km^2/year/°C
Sediment	1.8 tons/km^2/year/mg/L	-0.9 µmoles/m^2/hr (0.24 tons/km^2/year/mg/L)

Using a simple mixing model for temperature, a current residence time for water in the northern lagoon (about 300 days; Smith, 1993), inflow of seawater at 0.5 m^3/sec, and average difference in temperature in the lagoon and in Port Canaveral (0.5°C), the average change in lagoon temperature over various spatial scales with inflow was calculated and used to estimate decreases in N and P loading from sandy sediments. Even though the change in temperature would be greater if mixing occurred over a smaller area, small changes over larger areas would have more impact on decreasing fluxes and internal nutrient loading. For example, if mixing from the pilot study (0.5 m^3/sec) occurred over 5 km^2, 0.6 tons of N and 0.3 tons of P would be prevented from entering the lagoon each year based on a decrease in temperature of 0.23°C. If mixing occurred throughout the entire 170 km^2 of BRL, 1.6 tons of N and 0.7 tons of P would be prevented from entering the lagoon each year based on a 0.02°C decrease in temperature over 170 km^2. Based on these data and calculations, the nutrients removed via changes to benthic fluxes is expected to be greater than the nutrients that would be discharged to the coastal ocean. Additional benefits are expected based on increased DO concentrations; however, these improvements are less easily modeled. These data suggest that a pilot inflow project would yield net removal of N and P from the combined lagoon-ocean system, where decreased nutrient concentrations resulting from changes to internal cycling are expected to exceed changes to resulting from direct exchanges of water. Although trends were statistically significant, varying responses over different time intervals and large natural variability resulted in lower than expected statistical power. For this reason, caution was used when extrapolating these small changes over large areas and the plan is to focus future efforts in developing trends.

Laboratory experiments carried out to estimate the potential impacts of pumping on geochemical nutrient cycling showed that lower lagoon temperature and higher DO led to significant decreases in benthic fluxes for N and P. These observations suggest that geochemical responses to inflow would contribute to decreasing nutrient concentrations, mitigating discharges to the coastal ocean. Data obtained during this study illustrate the importance of DO towards regulating fluxes and cycling of dissolved nutrients. Despite the relative importance of DO towards predicting nutrient fluxes, few data are available for bottom water DO near the sediment-water interface where DO influences benthic fluxes. To that end, Florida Tech established a network of DO

sensors to aid in modeling efforts and better understand benthic-pelagic coupling in this system. These observations are consistent with recent studies showing that sediments play a key role in maintaining hypoxic conditions in bottom water (e.g., Rabouille et al., 2021).

Due to the dependence of biogeochemical nutrient cycling on DO, it is not possible to accurately model nutrient fluxes, turnover times, or nutrient concentrations without a detailed picture of DO. To assist modeling efforts, long-term datasets for DO concentrations from IRL and BRL were obtained from SJRWMD (**Figure 65**). Most sensors record DO at fixed depths, often at or above mid-depth of the water column, which can miss events that are restricted to the near bottom. For example, the SJRWMD sensors had average depths during 2019 to 2021 of about 0.5–1.5 m. DO data from these sensors showed annual trends relatively consistent with variations in DO solubility. For example, at a salinity of 25 PSU (average for IRL), DO solubility increases from 6.4 mg/L at 32 °C to 8.7 mg/L at 15 °C. In addition to this DO range (at 100%), values sometimes fell below saturation during summer with some instances of hypoxia (less than 2 mg/L) recorded by existing sensors located in the middle of the water column. Consistent with the more limited dataset from Phase 1, during winter months, DO in bottom water at sandy sites typically tracked patters for DO at 0.5–1.5 m; however, during summer months, bottom water DO was often lower and less stable, especially following peaks in DO concentrations (**Figure 65**).

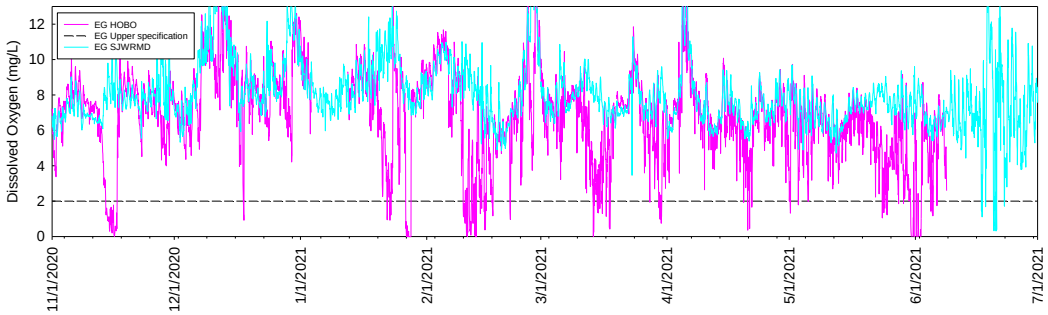

Figure 65. DO concentrations near Eau Gallie in bottom water (<10 cm above the bottom; cyan line) and mid-depths 1-1.5m (pink line) with the dashed black line at 2 mg/L for hypoxic conditions

Sensors deployed in BRL near the reference site showed stark differences for DO in bottom water overlying muck versus sand, although the sensors are only about 200-m apart (**Figure 66**). These data are consistent with SOD differences among substrates from -3,200 µmoles/m^2/hr for sandy sites (lagoon-wide average) and -4,300 µmoles/m^2/hr for muddy sites (during winter months).

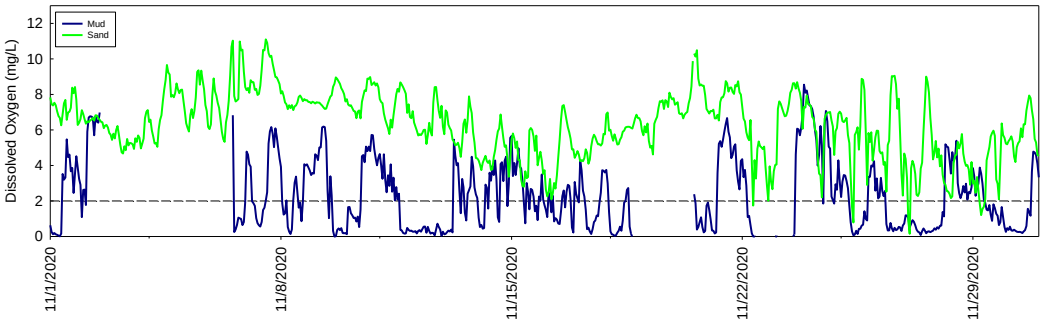

Figure 66. Bottom water DO near the reference site at sites containing muck (blue line) and sand (green line) with the dashed black line at 2 mg/L for hypoxic conditions

In Port Canaveral, DO concentrations followed patterns similar to those observed in the adjacent lagoon; however, diurnal fluctuation in the Port were much less. For example, DO in the lagoon varied by 4–6 mg/L on a daily basis, relative to diurnal variations of only 1–2 mg/L in Port Canaveral. Temporal and spatial differences in bottom water DO can drive spatial and temporal changes, where sediments alternate between sinks and sources of nutrients. Changes to DO in bottom water lead to changes in concentrations and the relative abundance of bioavailable N and P with implications to algal community composition and density. As a result, data for bottom water DO are essential to improving lagoon modeling, not only for this project but for nutrient loading or HAB models.

N and P loading from muck deposits were calculated and modeled based on estimates for the current surface area of muck present in the lagoon at a given time. Despite covering less than 10% of the lagoon bottom, muck is a significant source of N and P to overlying water while also acting as a large sink for DO (Fox and Trefry, 2018). To assist modeling efforts and better resolve the relative importance of muck versus sand, data for known IRL muck deposits have been synthesized into a single map (**Figure 67**).

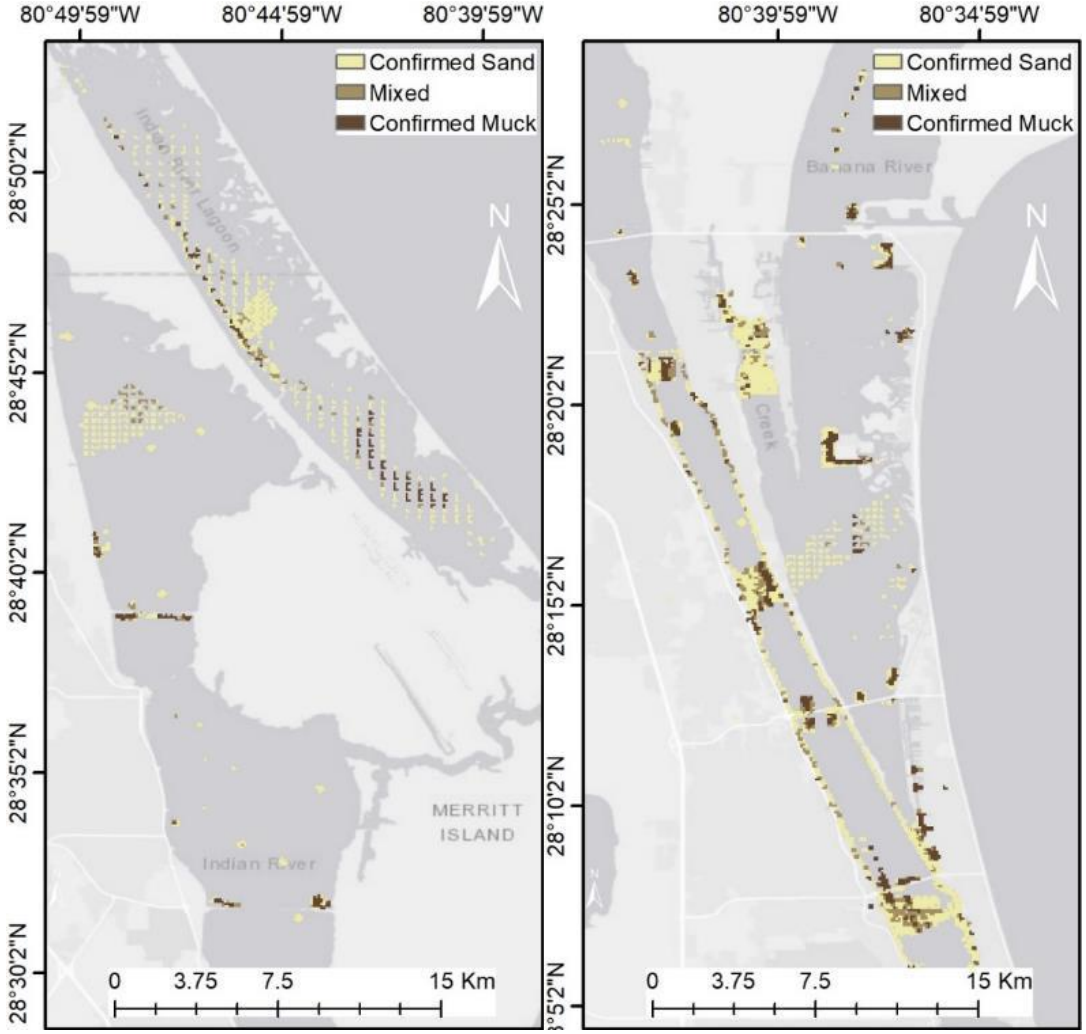

Figure 67. Map of the northern IRL, Mosquito Lagoon, and BRL with locations of confirmed sand, mixed sand and muck, and muck with 100-m resolution

4.2.4 Conclusions

Eutrophication of coastal marine ecosystems around the world has become increasingly common due to enhanced nutrient loading from adjacent watersheds (Brady, et al., 2013; Diaz and Rosenberg, 2008). As the eutrophic state progresses, sediment mineralization becomes increasingly important as a nutrient source to overlying water as seen in IRL (Cowan and Boynton, 1996; DiDonato et al., 2006; Seitzinger 1988; Kemp et al., 1990; Fox and Trefry, 2018). In eutrophic systems, HABs contribute to occurrences of hypoxia and anoxia, where even short events can promote loss of ecosystem services. Loss of these ecosystem services over time and space create positive feedback loops sustaining eutrophication. Distinct differences in the ability of poorly flushed versus well flushed estuaries to cope with eutrophication have been observed throughout the literature, where poorly flushed estuaries with long residence times, like IRL, more readily retain nutrients to promote algal blooms, loss of seagrass beds, hypoxia, and loss of ecosystem services (Defne and Ganju, 2015; Kemp et al., 1992; Twilley et al., 1999). Within this conceptual framework, impacts of enhanced inflow of seawater into IRL were evaluated for the potential to: (1) directly decrease nutrient concentrations, and (2) promote water column and sediment processes that would help to restore ecosystem services to remove or prevent N and P from entering the lagoon.

Temperatures in Port Canaveral and coastal Atlantic Ocean were moderate relative to more variable and extreme temperatures in the lagoon, with 0.5–1°C cooler temperatures in Port Canaveral during March to November and, in some cases, 4–5°C warmer temperatures during winter months. Salinity was higher in Port Canaveral than in the lagoon, leading to distinct densities among the lagoon (1,008–1,016 kg/m^3) and Port (1,018–1,028 kg/m^3) water masses. These data indicate that inflow of seawater and a mixed water mass would favor circulation in bottom water, on average decreasing temperature, raising salinity (slightly) and helping to raise and stabilize concentrations of DO at the sediment-water interface.

Concentrations of TDN and TDP were lowest at offshore sites; however, concentrations in Port Canaveral were five-fold and three-fold lower than concentration in IRL. If the proposed pilot inflow project (0.5 m^3/sec) were to occur, 6.5 tons of N and 0.6 tons of P would be discharged from the lagoon, mostly through Sebastian Inlet to the Atlantic Ocean. Seawater from Port Canaveral would bring 5 tons of N and 0.2 tons of P for a maximum net discharge, assuming no change to internal nutrient cycling, of 1.5 tons of N and 0.4 tons of P per year, which represent 0.1% of the N and 0.3% of the P annual input removal. While this small pilot project would have little impact at the lagoon scale, changes at the inflow site would facilitate a scientifically sound study of inflow in a well-defined area while preserving reference sites and mitigating adverse impacts. Data from the pilot study could then be used to determine the scale of a full-sized project to achieve desired improvement to water quality.

Water column and sediment biogeochemical responses to changes in temperature, salinity, and DO were investigated using a combination of field and laboratory experiments. Sediment and water column incubations in the field were used to establish current rates of nutrient fluxes and cycling from sandy sediments and water in the lagoon and to serve a baseline to evaluate changes over time. Benthic fluxes from sandy sediments could replace all the N in the water column in about 7 days to less 1 day via recycling, and sediments accounted for only 10% of the total N cycling. The complete pool of dissolved P could be completely removed by oxic sandy sediments in about 18 days, and recycling in the water column replaced the dissolved P in less than two days. Sediments accounted for about 10% of the TDP cycling. At sandy sites, TDN fluxes were highly variable and, on average, directed into sediments; however, fluxes of NH_4 and nitrate were directed out of sediments. TDP was directed into sandy sediments and PO_4 had a positive flux.

No significant correlations were identified between water column fluxes of N or P and changes to temperature, salinity, or DO. Despite this, lower rates of recycling in the proposed inflow water and lower N:P ratios would, when mixed, help to slow recycling and lead to lower N:P ratios, which would help to promote beneficial photosynthesizers. In laboratory incubation experiments, significant positive correlations were identified between benthic fluxes of NO_x, TDN, PO_4, DOP, and SiO_2 versus sediment temperature. Collectively, these data show that lowering lagoon temperatures, a likely result of inflow, would help to reduce inputs of N and P by approximately 1.6 tons of N and 0.7 tons of P, resulting in additional removal of N and P by sediments. Based on laboratory experiments, no long-term changes in nutrient cycling are expected from changes to salinity. In both field measurements and laboratory experiments, low DO promoted release of PO_4 and NH_4, which are known to promote HABs. In contrast, higher, stable concentrations of DO promoted removal of PO_4 while also promoting fluxes of nitrate over NH_4, both changes that support beneficial photosynthesizers. Lower lagoon temperatures and higher, stabilized bottom water DO from inflow would support lower nutrient concentrations and ratios promoting nutrient species that are more favorable to beneficial photosynthesizers.

Concentrations of DO in bottom water followed general seasonal patterns observed at mid-depths reported by other existing monitoring networks; however, bottom water experienced frequent periods of hypoxia or anoxia, likely due to proximity to sediments, responsible for 20–50% of the total respiration. These new data are essential towards improving lagoon models from this study and other nutrient loading or HAB models. The Florida Tech network of bottom water DO sensors showed lower DO concentrations overlying muck deposits compared to sand. Concentrations of DO in Port Canaveral tracked concentrations in lagoon water, both in response to changes in solubility over time. Despite similarities in long-term trends, diurnal fluctuations in Port Canaveral were much less than those in the lagoon, due mostly to 30% lower rates of dark respiration in Port Canaveral and almost monthly instances of hypoxia observed in the lagoon.

4.3 Biology (Task 3)

The objectives of the biology task were to:

- Continue documenting baseline biological characteristics in BRL near the proposed inflow location to gain knowledge of annual variability and seasonal impacts. Categories of biological characteristics monitored include fish community; eDNA; and seagrasses, rooted algae, drift algae, benthic fauna, and phytoplankton/harmful algae.
- Build predictive models relating oceanic inflow-associated abiotic factors with key metrics of fish-community structure.
- Investigate the influence of algal blooms on fish community structure in BRL.

4.3.1 Approach

4.3.1.1 Fish Community Modeling

The fish community models were built to predict the effects of salinity, temperature, DO, latitude, and longitude on four key metrics of community structure and relative abundance of eight key species of interest (SoI). Multiple linear regressions, using the most recent FWC FWRI FIM program fish community data (FWRI, 2009; Paperno, 2002), were used to investigate the individual and combined effects of each predictive variable on key metrics of fish community structure for the available data range, 1996–2018.

The abiotic predictive variables (salinity, temperature, and DO) were indicated by the Phase 1 work as the strongest determinants of fish community structure in IRL (Johnson et al., 2020). This

previous work, consultations with local experts, and personal observations indicated a strong influence of spatial heterogeneity of BRL fish community structure; therefore, the spatial variables of latitude and longitude were included as descriptors in the models. The models were built to project changes in alpha-diversity (species richness), Shannon diversity index (H, a combined measure of relative abundance and evenness), Pielou's evenness index (J, a combined measure of richness and evenness), and mean community trophic level (a representation of the trophic ecology of the system). Both H and J were calculated following Troast et al. (2020) and trophic level was calculated for each sample as the relative abundance weighted mean of the constituent community following Blanchard (2018). Each species' individual trophic levels were retrieved from FishBase (Froese et al., 1992; Froese and Pauly, 2020) where possible.

The SoI were selected based on discussions with the FWC laboratory in Melbourne, Florida, and as recommended by the external reviewers of the Phase 1 report (Florida Tech, 2020). These were the Bay Anchovy, *Anchoa mitchilli*; Sheepshead, *Archosargus probatocephalus*; Spotted Seatrout, *Cynoscion nebulosus*; Mangrove Snapper, *Lutjanus griseus*; Pinfish, *Lagodon rhomboides*; Black Drum, *Pogonias cromis*; Red Drum, *Sciaenops ocellatus*; and Gulf Pipefish, *Syngnathus scovelli*. For species abundance models, analyses were performed in tandem, including and excluding outliers in the source data, to determine which approach may be more useful. Outliers were defined as any abundance more than two standard deviations above the mean. Candidate models targeting SoI abundance and community structure metrics, which involved all possible combinations of the available descriptive factors, were evaluated and the best models were selected using Akaike's Information Criterion (Aho et al., 2014). Models were trained using a randomly drawn half of the available FWC data for each gear type deployed within BRL. The model performance was evaluated by using them to blindly predict the other half of available data. This report focuses on gear 20, a small seine, which catches primarily small fishes (i.e., anchovies or juveniles), and gear 160, a much larger seine, which is inefficient at capturing small fish but is adept at catching larger animals (i.e., adult sportfish). As they have different biases and efficiencies, each gear was analyzed separately.

Each model was then used to project changes in the dependent variable (i.e., SoI abundance or community metric) as a result of changing mean conditions due to various inflow scenarios, where abiotic projections were available. All inflow scenarios were plotted with reference to the base over the span of nine months, the entirety of available abiotic projections, to determine the temporally explicit and net impacts on the SoI or community metric being projected.

For evaluations of fish and Chl-a, two long-term data sets were used: SJRWMD Chl-a concentration and dominant phytoplankton species data from 2002–2018, and FWC FWRI FIM fish community data for the same time span. Spearman Rank Correlations (Zar, 1999) were used to look for associations of Chl-a with the time series mean relative abundances the eight SoI and four metrics of community structure. Analyses of Variance (ANOVA) (Zar, 1999) were used to look at the influence of the interaction of Chl-a and time on the four metrics of community structure.

Data from the SJRWMD monitoring program were used to begin investigating potential associations between algal blooms and the BRL fish community. The data provided include monthly measurements of Chl-a concentrations, in micrograms per liter (µg/L), in BRL from 2002–2018, which were used as a proxy measurement for microalgal density and primary productivity in the water column (Huot et al., 2007) as indicators of algal density. These Chl-a records were matched with the fish data provided by FWC. Where multiple fish samples were available for a single month, the mean abundance among the samples for that month was used. A series of Spearman Rank correlations (Zar, 1999) were performed to test for associations between median Chl-a concentrations and relative abundances of the eight SoI and four community structure

metrics. These data were plotted over time to allow for visual inspection of the associations, which will be more comprehensively analyzed in planned future phases.

To begin laying the groundwork for these analyses, a series of ANOVA (Zar, 1999) was used to examine the importance of the interaction of time and Chl-a concentrations on the metrics of community structure. IRL has been substantially different since 2011 (Kamerosky et al., 2015) and BRL is likely no exception. A strong influence of time in these analyses is expected and the 2011 superbloom likely marks a state shift, after which the community likely behaves differently. Details are still limited about how the BRL fish community is being affected. This effort is aimed at determining which SoI and metrics of community structure show the strongest association with Chl-a concentrations, and which metrics of community structure are most heavily influenced by the interaction of time and Chl-a.

A short period of an extensive literature survey was conducted to gather information on the patterns of fish movement and habitat use in IRL, particularly near the proposed inflow location. The results of this meta-analysis, focusing on two commercially and recreationally important species of fish (Red Drum, *Sciaenops ocellatus*; and Seatrout *Cynoscion nebulosus*), are summarized. The association between patterns of fish abundance variation and environmental parameters including DO, salinity, temperature, and pH in BRL are examined at the proposed pilot pumping site and the Patrick Air Force Base area during the 1996–2018 monitoring period of the FWC-FIM program to infer intra-IRL variation in habitat utilization of the SoI.

4.3.1.2 eDNA Characterization

To investigate biological community response to enhanced inflow using eDNA sampling, three approaches were initiated in Phase 1 and continued in Phase 2. The first eDNA approach leverages the power of sampling before and after enhanced inflow at pre-determined reference sites. This before-after-control-impact (BACI) experimental design is commonly used in ecological studies when sites cannot be randomly assigned and the timing and location of impact are known (Smokorowski and Randall, 2017). To improve detection of environmental impacts, the traditional BACI design was modified to include supplemental reference sites (Underwood, 1994). The second approach investigates regional biodiversity patterns using complimentary metrics to track changes in community diversity that may result from the proposed pilot project. Under this framework, biodiversity was characterized at site, basin, and regional scales to determine how communities are structured across the central IRL and BRL. This baseline can then be used track any changes in community similarity/dissimilarity that may result from the proposed pilot inflow, or other perturbations. The third approach uses randomization tests to detect differences in site-specific measures of taxonomic distinctness from a fixed baseline derived from a master IRL species list. The value of this approach is both its insensitivity to sample size and ability to track improvements or declines in site diversity against a fixed baseline (Clarke and Warwick, 2001).

Data quality, sample collection, processing, and analysis followed developing best practices, including strict procedures to minimize both false positives and false negatives detections (Eble et al., 2020). False positives are a significant concern in eDNA sampling because of the potential for contamination with exogenous deoxyribonucleic acid (DNA) and cross-contamination between samples during field sampling or laboratory analyses. To minimize cross-contamination, established contamination management guidelines were followed that included thorough decontamination of equipment and laboratory work surfaces with bleach and ultraviolet light, and the addition of negative controls at each step in the workflow to ensure detection and removal of contaminated samples (Ficetola et al., 2016). To minimize false negatives, established sampling guidelines were followed to minimize DNA degradation and extensive primer testing was conducted to ensure sufficient detection of target taxa.

For Phase 2, eDNA field collections were coordinated with project team members to support collection of 101 water samples from IRL. Three replicate 500 mL water samples were collected at sites 1–12 and sites 24–26 (**Figure 68**) in April and July 2021. An additional twenty 500 mL samples were collected at site 2 in January 2021 to allow estimation of sample sufficiency and power. Together with Phase 1 sampling, 185 IRL water samples were collected and preserved to support assessment of pumping impacts.

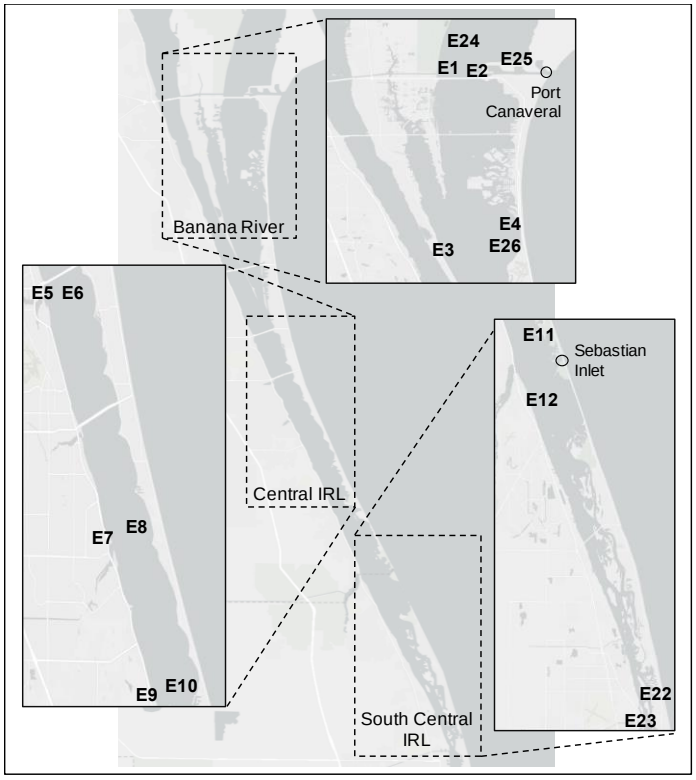

Note: Sites E22 and E24 were sampled in Phase 1 to determine the location of the proposed pilot pumping system and were not sampled in Phase 2. Sites E24–E26 were established in Phase 2 to improve resolution of regional biodiversity patterns and direct testing of inflow impacts.

Figure 68. Map of the central IRL and BRL with insets depicting Phases 1 and 2 eDNA study sites in BRL, central IRL, and south central IRL

Marker development and sequencing focused on fishes using mitochondrial primers for 16S ribosomal ribonucleic acid (rRNA; Deagle et al., 2007; Berry et al., 2017). A subset of filtered samples were analyzed using taxa specific mitochondrial primers for 16S rRNA (Berry et al., 2017) and cytochrome oxidase subunit I (COI; Leray et al., 2013) targeting crustaceans and metazoans, respectively. To prepare samples for paired-end sequencing on the Miseq sequencing platform (Illumina), eDNA was extracted from half of each mixed cellulose ester filter using the Dneasy Blood and Tissue extraction kits (Qiagen Inc.), followed by polymerase chain reaction (PCR) inhibitor removal using the OneStep PCR Inhibitor Removal kit (Zymo Research). The remaining half of each filter was archived for future analyses. Once the DNA was extracted, sequencing libraries were prepared by amplifying eDNA using a two-step PCR process (Cruaud et al., 2017). Samples were quantified using a Qubit 4 Fluorometer (Invitrogen) and cleaned using the EZNA Cycle Pure Kit (Omega Bio-Tek). Resulting tagged amplicons were pooled in equimolar concentrations, size-selected using a PippinHT (Sage Science), and bi-directionally sequenced (paired-end sequencing) on the University of Central Florida Illumina MiSeq system using both

V2 and V3 reagent kits. Sequencing data were then demultiplexed using the Illumina MiSeq software and downloaded for processing and analysis.

To ensure accurate taxonomic assignment, paired-end sequence reads were filtered and trimmed in Rstudio (Rstudio Team, version 1.3.959) using the DADA2 pipeline (Callahan et al., 2016). Gene-specific, demultiplexed sequences were trimmed to remove amplicon primers and low-quality bases (median quality score < 30) at the beginning and end of the sequence, filtered to remove sequences with ambiguous base calls (max N = 0; max E = 2) and Phix control reads, and dereplicated and denoised based on read identify and quality. Forward and reverse reads with $\geq$20 base pairs overlap were then merged to obtain full denoised sequences, after which chimeras were removed and an exact amplicon sequence value table was constructed to provide a summary of the unique DNA sequences detected in each sample. Amplicon sequence variants were blasted against the National Center for Biotechnology Information's GenBank nucleotide database using the Basic Local Alignment Search Tool with the default parameters on the University of Central Florida COOMBS computer cluster.

Successful resolution of biodiversity patterns is determined by both the sufficiency and power of the sampling strategy (Li et al., 2020). With low sample sufficiency many species present at a site may go undetected, potentially increasing variability among samples and decreasing the power to resolve differences in species occurrence between sites and within sites over time, when significant differences exist. To address this issue, the samples needed to reliably resolve site diversity were estimated by analyzing the diversity of fish detected in 20 replicate water samples collected in January 2021 from the site just south of Port Canaveral locks (E2). Because sample power is also determined by sample variance, a separate power analysis was conducted for the proposed BACI experimental design using estimates of species richness and group standard deviation derived from the Port Canaveral samples.

Three eDNA approaches were initiated to investigate community response to inflow:

1. BACI experimental design to investigate differences in species occurrence both before and after enhanced inflow at the pre-determined reference sites.
2. Assessment of regional biodiversity patterns at site, basin, and regional scales to track changes in community similarity/dissimilarity that may result from enhanced inflow, or other perturbations.
3. Monitoring changes in community taxonomic structure over time relative to a fixed baseline to track biodiversity recovery or loss.

Four measures of site-specific diversity were estimated for each site across seasonal samples analyzed to date (fall, winter, and spring). Samples collected in July 2021 are being processed and will be analyzed as part of the proposed next phase. The four site-specific diversity metrics examined were the total number of species (species richness), Shannon diversity index (log base *e*; Shannon, 2001), and two estimates of sample taxonomic distinctness (average distinctness and variation in distinctness; Warwick and Clarke, 1995). Taxonomic distinctness measures the relatedness of species within a sample as defined by traditional Linnaean taxonomy. Estimates of both average and variation in taxonomic distinctness are useful alternative measures of diversity that are insensitive to sample size (Clarke and Warwick, 2001), sensitive to environmental disturbance (Warwick and Clarke, 1995), and a direct compliment to standard richness-related like the Shannon diversity index (Gallardo et al., 2011). Sample taxonomy was assessed for assigned species across the taxonomic levels of genus, family, order, and class with an unlimited number of lineage paths and equal path weights (Clarke and Warwick, 2001).

4.3.1.3 Benthic Fauna, Seagrasses, and Phytoplankton

Seagrasses, benthic infauna, and phytoplankton are key communities because their responses are ecologically important and they most impacted by pollution in the lagoon. There are some historical and publicly available records for IRL seagrasses and fishes that can inform the status and trends of these communities. However, the historical data are not tailored to the potential inflow site. It is critical that pumping and ecological sampling sites be tightly aligned to reliably investigate the extent of any impacts, both in severity and area influenced. This is particularly true for benthic sessile organisms that will be unable to leave the region of greatest impact and will therefore be subjected to the most extreme environmental changes.

4.3.1.3.1 Seagrass, Rooted Algae, and Drift Algae

At selected locations (**Figure 69**), transects 100-m long were surveyed perpendicular to the shoreline to document the presence of seagrasses and drift algae. Quadrats were laid down every 10-m along the transect lines, and seagrasses and drift algae were scored according to standard methods Measurements included seagrass visual estimate percent cover (coverage upon imagining the seagrass crowded into corner of quadrat at a high density), seagrass percent coverage or occurrence (proportion of 100 quadrat sub-squares having at least 1 blade of seagrass), seagrass density (number of shoots per area), seagrass canopy height (length of blade from sediment to tip), drift algae percent occurrence (proportion of 100 quadrat sub-squares having any drift algae), drift algae biomass estimate (coverage upon imagining drift algae crowded into corner of quadrat), and drift algae canopy height (Virnstein and Morris, 1996; Morris et al., 2001). This sampling strategy was repeated quarterly for all sites. Power analysis was conducted on data to confirm the sampling viability to make statistical determinations of impacts.

4.3.1.3.2 Benthic Fauna Methods

Sediment grabs for infaunal analysis were collected at the 50-m mark along all seagrass transects (**Figure 69**) via petite Ponar grab (n = 3 per transect). Triplicate samples were collected at each station. This sampling strategy was repeated quarterly for all sites. Sampling and identification of infauna were conducted consistently with other IRL benthic studies (Mason, 1998; Cooksey, 2007) and were tested for correlations with sediment parameters, including percent organic content (dry weight), percent water content by weight, and percent silt/clay content (dry weight), as well as environmental parameters. Biological communities were summarized as biodiversity (Shannon-Wiener Diversity Index), species richness, and overall abundances. Where appropriate, statistical analyses included two-way ANOVAs (factors of site and year), principle components analysis (comparing biological parameters between years as a multivariate function of multiples sediment and water column environmental conditions), and non-metric multidimensional scaling (NMDS; community analyses with the basic summary biological parameters) with post hoc analysis of similarity. Power analysis was conducted on some data to confirm the viability of sampling for making statistical determinations of infauna impacts of restored inflow.

4.3.1.3.3 Phytoplankton/Harmful Algae Methods

Phytoplankton were sampled via plankton tows for cell identification, and via whole water samples for flow cytometer analysis. Samples were collected in conjunction with the infauna sampling schedule and locations shown in **Figure 69**. Four plankton tows were conducted quarterly at the proposed inflow site (n = 4). Tows used a 20-µm mesh plankton net towed for approximately two minutes. Flow rate and submersion time were recorded and used to estimate volume processed for each plankton sample. Samples were preserved in 4% buffered formaldehyde to await enumeration and identification via microscopy. Whole water samples for flow cytometry were collected at every station (n = 5) using a bottle to collect unfiltered water approximately 0.5 m below the surface of the water. These samples were set on ice and processed in the flow

cytometer immediately upon returning from the field. This sampling strategy was repeated quarterly for all sites. NMDS graphs were used to group the phytoplankton communities based upon similarity and as a function of year, season, and location/site. Analysis of similarity and permutational multivariate ANOVA (PERMANOVA) were used to evaluate the strength and significance of NMDS outcomes.

Note: Blue dots = infauna sampling stations inside IRL. Green dots = seagrass transect and associated infauna stations. All dots, infauna sample n = 3. Yellow dashed line = plankton tow location. Whole water flow cytometer samples were collected at all infauna sampling stations (blue and green dots, n = 4 per station).

Figure 69. Samples collected and station locations for the proposed pilot inflow site (A) Banana River North (BRN) near Port Canaveral and (B) reference site for treatment comparisons Banana River South (BRS) near Patrick Air Force Base

4.3.2 Results

4.3.2.1 Fish Community Modeling

Phase 2 fish community modeling efforts were focused on developing predictive models capable of projecting changes in the abundances of eight SoI and four key metrics of community structure. Four of the targeted models (gear 160: *Anchoa mitchilli* and *Syngnathus scovelli*; gear 20: *Pogonias cromis* and *Lutjanus griseus*) could not be generated as there were not enough occurrences in the source data to support the effort. Models of species abundance, excluding outliers, were better able to predict validation data than those including outliers and, therefore,

the outlier-excluded projects are presented here. No metrics of community structure were subjected to outlier-excluded analyses as it would not be ecologically meaningful to do so.

Model projections were produced for 0.5, 1, 2.5, 5, and 10 m^3/sec enhanced inflow scenarios, as well as the no inflow change, base, scenario for all models where sufficient abiotic project data were available. The Task 1 team provided salinity projections for all scenarios, temperature projections for all but the 10 m^3/sec scenario, and DO projections for the base and 5 m^3/sec scenarios. With the data provided, changes in abundance for 26 different species*gear*pumping scenario combinations and 23 community structure metric*gear*pumping scenario combinations were projected. The projected base scenario value was subtracted from each increased inflow scenario's projections for the entire projected timeline to calculate a total projected net effect for each scenario (**Figure 70**). Most of abundance projections, 20 of the 26, suggest net positive increases in abundance over a nine-month period, while a notable few suggest net decreases. For community structure, the model projections were more varied with 11 projecting increases in the metric modeled and 12 projecting decreases (**Table 25**).

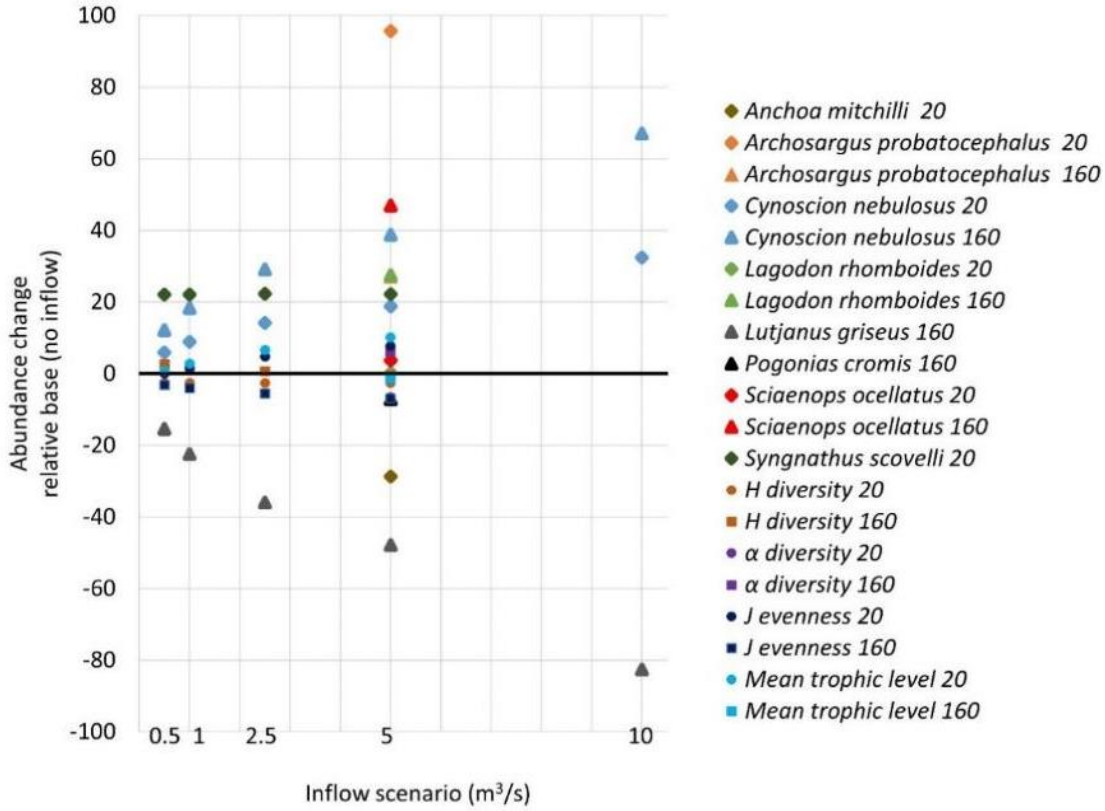

Note: Positive values represent increases in the modeled parameter relative to the base scenario, negatives represent decreases. For abundance projections, gear type 20 is shown by diamonds, and gear type 160 is shown by triangles. For community structure projections, gear type 20 is represented by circles while 160 is shown as squares. The reader is cautioned against making comparisons between species here

Figure 70. Net effect of nine months for each pumping scenario on all fish populations and community structure metrics for which sufficient source data and abiotic projection data were available

Table 25. Net effects of enhanced inflow projected by each model

Note: Gray cells represent models which were generated but were unable to provide projections due to a lack of input data. Red cells represent net reductions, and green cells represent net increases.

Modeled parameter	Gear	0.5 m^3/sec	1 m^3/sec	2.5 m^3/sec	5 m^3/sec	10 m^3/sec
Anchoa mitchilli	20				-28.68	
Anchoa mitchilli	160	Insufficient data				
Archosargus probatocephalus	20				95.70	
Archosargus probatocephalus	160				27.15	
Cynoscion nebulosus	20	5.89	8.89	14.12	18.80	32.46
Cynoscion nebulosus	160	12.17	18.36	29.18	38.84	67.06
Lagodon rhomboides	20				0.21	
Lagodon rhomboides	160				27.45	
Lutjanus griseus	20	Insufficient data				
Lutjanus griseus	160	-15.41	-22.49	-35.98	-47.83	-82.60
Pogonias cromis	20	Insufficient data				
Pogonias cromis	160				-7.20	
Sciaenops ocellatus	20				3.71	
Sciaenops ocellatus	160				46.95	
Syngnathus scovelli	20	22.05	22.13	22.32	22.25	
Syngnathus scovelli	160	Insufficient data				
H diversity	20	-2.56	-2.59	-2.63	-2.60	
H diversity	160	2.68	1.99	0.67	-0.56	
α diversity	20				-6.62	
α diversity	160				6.08	
J evenness	20	-0.01	1.62	4.76	7.69	
J evenness	160	-3.17	-4.00	-5.57	-6.92	
Mean trophic level	20	0.78	2.80	6.64	10.20	
Mean trophic level	160				-1.34	

4.3.2.1.1 Fish and Chl-a

BRL Chl-a concentrations range from 0.350–135.250 µg/L between 2002 and 2018. However, from 2002–2010, Chl-a never exceeded 19.45 µg/L with a mean value of 6.68 µg/L. From 2011–2018, the mean Chl-a concentration was 24.36 µg/L, exceeding the maximum value of all preceding years. This pattern is demonstrated by a moderately strong association between Chl-a concentration and time ($p<0.001$, $S = 618503$, $rho = 0.563$). Spikes in Chl-a concentrations, exclusively in 2011 and after, co-occur with a prevalence of cyanobacteria during the known HAB events in 2011, 2016, and 2018. When looking at the influence of this interaction between time and Chl-a concentrations on the metrics of community structure, it is unsurprising to see all metrics of community structure were significantly affected. The one exception to this statement was no significant influence of the community sampled by gear type 160 (**Table 26**).

Table 26. Statistics for two-way ANOVAs

Dependent: fish community structure metrics. Independent: time and Chl-a concentrations.

Gear type	Descriptor	Factor	F	P
160	α	Time	30.464	<0.001
		Chl-a	75.483	<0.001
		Time*Chl-a	3.969	0.046
160	H	Time	31.680	<0.001
		Chl-a	0	0.985
		Time*Chl-a	102.220	<0.001
160	J	Time	5.268	0.022
		Chl-a	50.209	<0.001
		Time*Chl-a	87.369	<0.001

Gear type	Descriptor	Factor	F	P
160	Trophic Level	Time	9.459	0.002
		Chl-a	85.495	<0.001
		Time*Chl-a	1.231	0.267
20	α	Time	193.92	<0.001
		Chl-a	27.610	<0.001
		Time*Chl-a	31.150	<0.001
20	H	Time	14.830	<0.001
		Chl-a	9.560	0.002
		Time*Chl-a	18.010	<0.001
20	J	Time	9.406	0.002
		Chl-a	1.777	0.183
		Time*Chl-a	6.660	0.010
20	Trophic Level	Time	140.192	<0.001
		Chl-a	1.962	0.162
		Time*Chl-a	5.190	0.023

All metrics of community structure were also significantly associated with Chl-a concentrations, save Pielou's evenness for the gear type 20 fish community, with the associations being primarily negative and relatively weak. The only positive associations were found with mean trophic level of the fish community from gear type 20, and the alpha diversity of the fish community from gear type 160. All associations were relatively weak, possibly due to the strong influence of time which could not be captured in these preliminary analyses. Such an interaction would be visible in **Figure 71**, but there is indication of such a pattern.

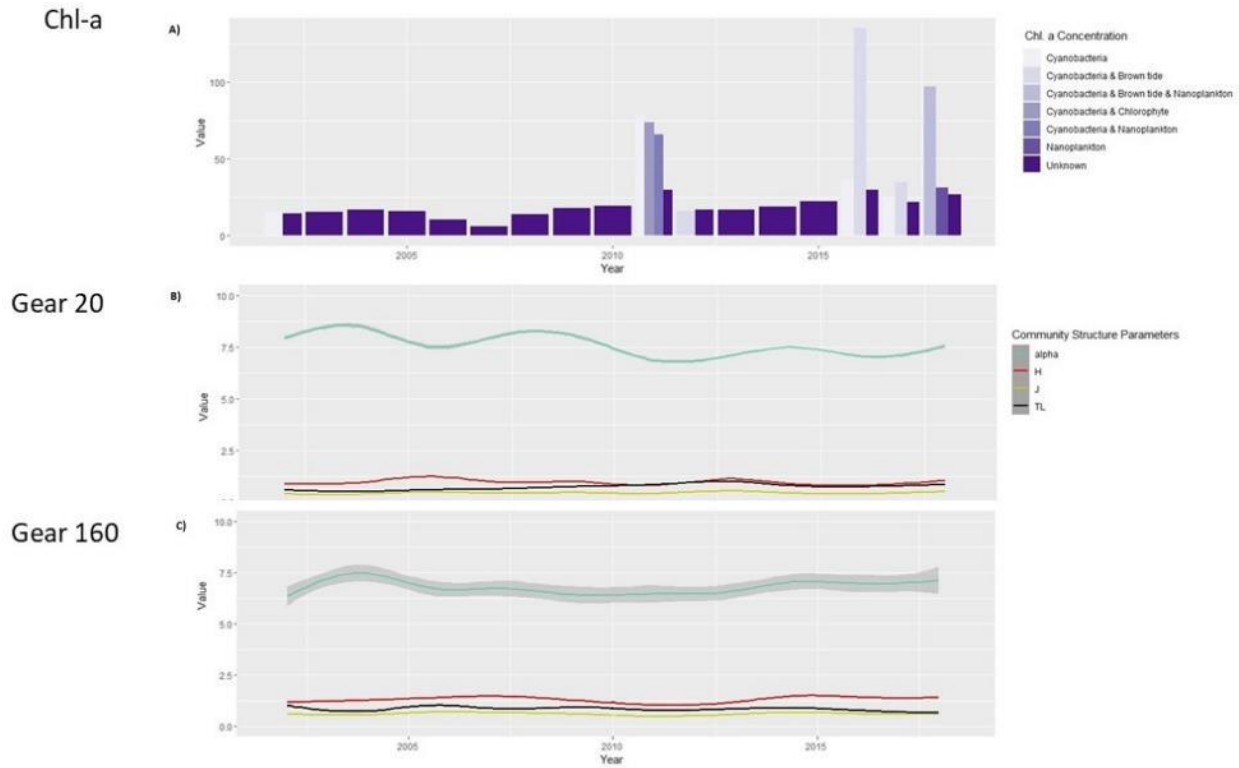

Note: Colors in plot A represent the dominant phytoplankton species present, when known. Shaded regions around the lines in the bottom two plots represent the standard error of the mean.

Figure 71. Plots of Chl-a concentrations (A) and BRL fish community structure metrics for gears type 20 (B) and 160 (C) from 2002–2018

Nearly all fish populations showed significant associations with Chl-a concentrations in BRL (**Table 27**). Only *Anchoa mitchilli* and *Lagodon rhomboides,* from gear type 20, showed no association. Most of the associations were, however, very weak. *Pogonias cromis* and *Syngnathus scovelli* abundances, being the only exceptions, had moderately strong associations to Chl-a, but in different directions, positively and negatively, respectively.

Table 27. Spearman Rank correlations between each SoI and Chl-a in BRL

Species	Gear	S	rho	P
Anchoa mitchilli	20	90595843	0.042	0.223
Anchoa mitchilli	160	Insufficient data		
Archosargus probatocephalus	20	88201793	0.068	0.051
Archosargus probatocephalus	160	2025176393	0.172	<0.001
Cynoscion nebulosus	20	103448862	-0.09	0.007
Cynoscion nebulosus	160	2123212110	0.132	<0.001
Lagodon rhomboides	20	98570020	-0.04	0.229
Lagodon rhomboides	160	2210494529	0.096	<0.001
Lutjanus griseus	20	76737404	0.189	<0.001
Lutjanus griseus	160	2789936992	-0.14	<0.001
Pogonias cromis	20	82853763	0.124	<0.001
Pogonias cromis	160	1534390098	0.372	<0.001
Sciaenops ocellatus	20	87560645	0.074	0.032
Sciaenops ocellatus	160	2341575504	0.042	0.036
Syngnathus scovelli	20	129120010	-0.36	<0.001
Syngnathus scovelli	160	Insufficient data		

Visual inspection of these patterns (**Figure 72**) suggests that 2011 may have marked a state shift for the BRL fish community, with a strong decline in nearly all SoI. Notably *Syngnathus scovelli*, currently being evaluated as a potential indicator species for IRL health (personal communication, Dr. Richard Paperno, FWC), and *Lagodon rhomboides,* an important forage fish throughout IRL, have both experienced a steady decline since the 2011 event. All SoI show patterns with typical time-lagged responses to algal blooms, suggesting individual species time series break-point-analyses would be useful to understand the interplay between BRL's abiotic and biotic stressors on these SoI to predict how increased inflow may influence them.

4.3.2.1.2 Fish Movement

Among the studies examined, three are summarized here: (1) Tremain, Harnden, and Adams (2003) Multidirectional movements of sportfish species between an estuarine no-take zone and surrounding waters of the Indian River Lagoon, Florida; (2) Reyier, Lowers, Scheidt, and Adams (2011) Movement patterns of adult Red Drum, *Sciaenops ocellatus*, in shallow Florida lagoons as inferred through autonomous acoustic telemetry; and (3) Reyier, Scheidt, Stolen, Lowers, Halloway-Adkins, and Ahr (2020) Residency and dispersal of three species from a coastal marine reserve: Insights from a regional-scale acoustic telemetry network. These studies make compelling conclusions that are relevant to this project. First, Red Drum and Seatrout exhibit very strong site fidelity, meaning their movement within their post-settlement habitat is very limited, an average of less than 0.10 km per day. Second, long distance movement, ranging from 150 to 650 km are associated with known species-specific spawning period. And third, life-history stage specific movement within IRL are apparent.

An examination of the 1996–2018 FWC-FIM monitoring data indicate that the pattern of variation in the mean total fish abundance and species-specific mean abundance of Red Drum and Seatrout are correlated to the pattern of variation in DO, salinity, temperature, and pH. This covariation also differs between the proposed pilot pumping site and Patrick Air Force Base site

(**Figure 73** and **Figure 74**). A decrease in temperature and salinity and an increase in pH between 2015 and 2018 are associated with the decrease in abundance of Red Drum and Seatrout in BRL (**Figure 73**). This pattern differs from that of the Patrick Air Force Base site **(Figure 74**).

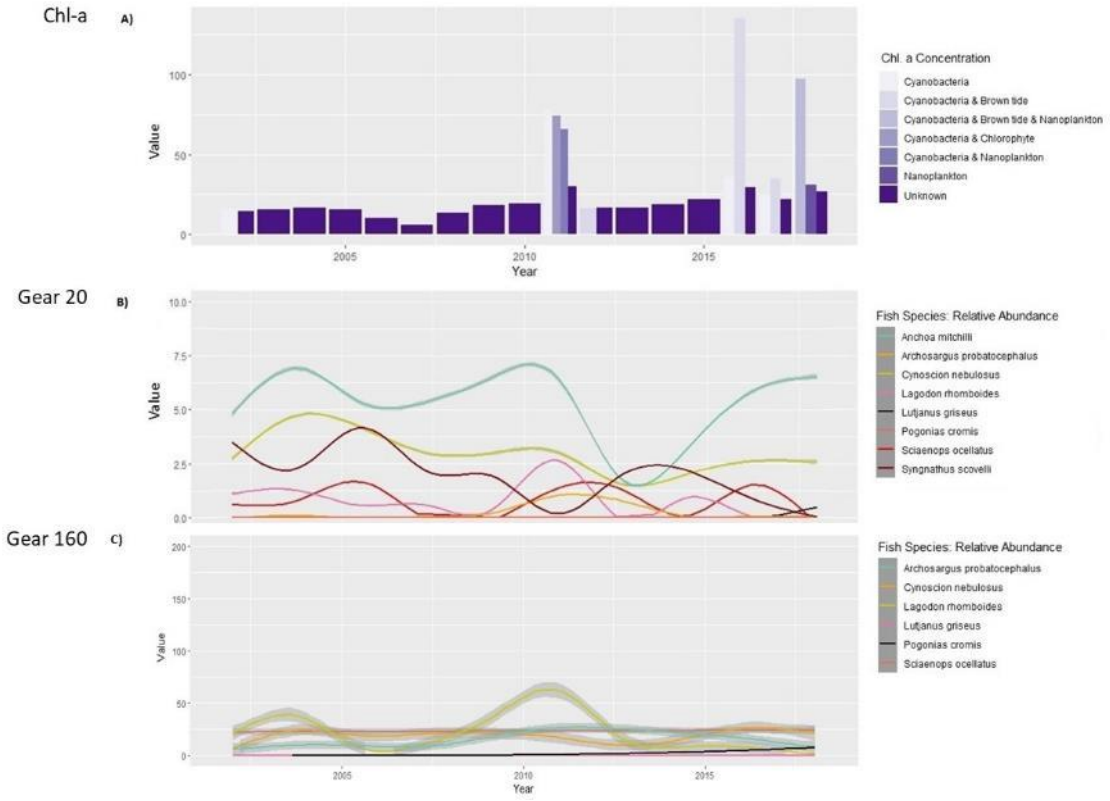

Note: Colors in plot A represent the dominant phytoplankton species present, when known. Shaded regions around the lines in the bottom two plots represent the standard error of the mean.

Figure 72. Plots of BRL Chl-a concentrations (A), and relative fish abundances for gears type 20 (B) and 160 (C) from 2002–2018

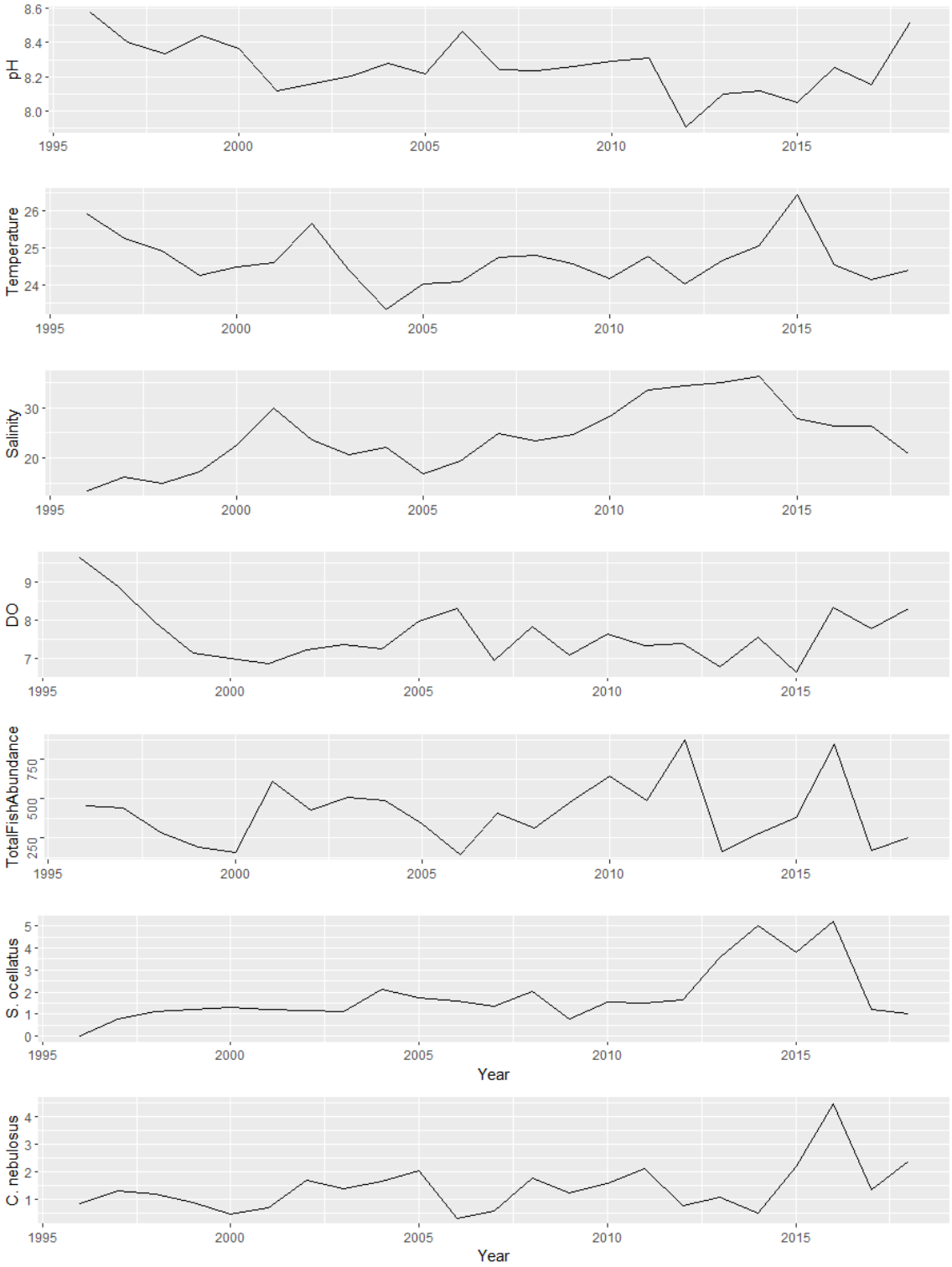

Figure 73. Patterns of variation in mean fish abundance and environmental factors in BRL between 1996 and 2018

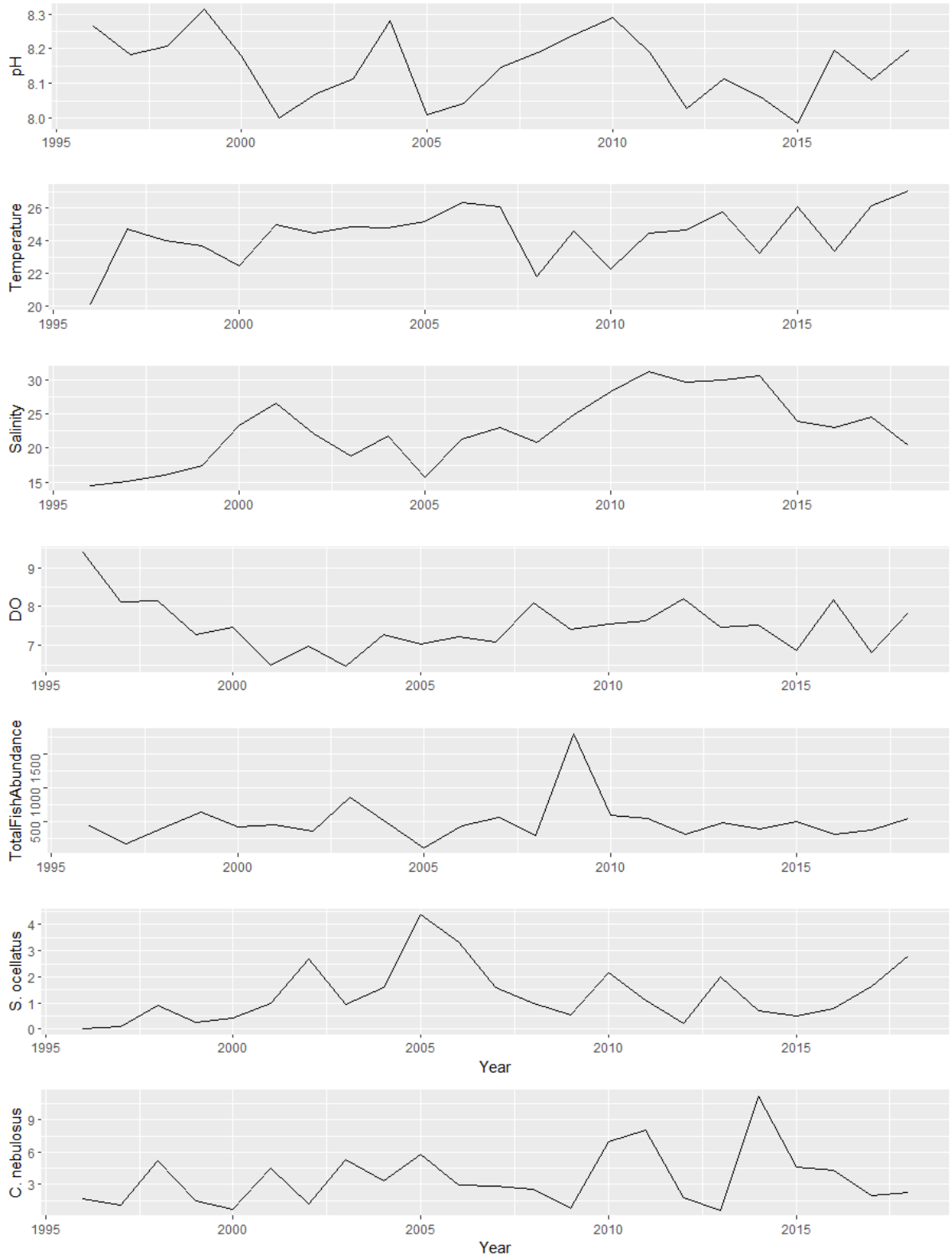

Figure 74. Patterns of variation in mean fish abundance and environmental factors in the Patrick Air Force Base area of IRL between 1996 and 2018

4.3.2.2 eDNA

Paired-end sequencing on the Miseq platform was initiated in Phase 1 with an analysis of samples collected at IRL sites E1–E12 and E22 and E23 during fall 2019 and winter 2020. Phase 2 sequencing was directed towards samples collected at sites E1–E12 and E24–E26 during spring 2021 using the fish specific 16s rRNA primer set. An additional 20 samples collected just south of the Port Canaveral Lock in winter 2021 were sequenced during Phase 2 using both fish and crustacean specific 16s rRNA primer sets along with the COI primer set targeting metazoan diversity. Samples collected in July from sites E1–E12 and E24–E26 were archived for analysis during the proposed pilot project. Four sequencing runs were completed resulting in a combined 22.4 million sequences generated during Phases 1 and 2 (**Table 28**). Following optimization of sequence quality control parameters, a combined 13.9 million sequences passing sequence filtering and processing were used to identify unique exact amplicon sequence variants present in the sequence libraries (**Table 29**).

A combined 4,439 unique amplicon sequence variants were identified across all sequencing runs resulting in 107 unique species level identifications (**Table 29**). Most unique taxa detected (89) were generated from libraries prepared using the fish specific 16s rRNA primers. Test libraries developed for crustaceans and metazoans were overwhelmed by sequencing of both non-target and highly abundant target taxa. The COI test libraries produced no informative species level identifications. The crustacean libraries predominately generated sequences from uncultured bacteria and an unidentified marine copepod (family *Canuellidae*). Seven fishes and 9 crustaceans were identified to species level in the crustacean libraries. Additional optimization of both the metazoan and crustacean marker sets is required.

Table 28. Summary of Miseq run quality control and filtering with run name, number of reads generated (input), and number of reads passing quality control

Run	Input	Filtered	DenoisedF	DenoisedR	Merged	No chimera
Marker test: 16s-fish, 16s-crustacean, & COI	361,033	315,798	317,201	317,170	314,774	313,437
Pilot study baseline: 16s-fish	745,379	617,860	617,201	616,630	607,085	596,888
Fall & winter IRL samples: 16s-fish	8,625,029	3,833,754	3,827,848	3,823,693	3,589,083	3,555,313
Spring IRL samples: 16s-fish	12,659,527	10,334,864	10,276,005	10,274,805	10,259,505	9,471,121

Table 29. Number of sequence reads, amplicon sequence variants, and number of unique species detected for target taxa

Target taxa	Reads	Amplicon Sequence Variants	Species
Elasmobranchii & Actinopterygii	13,874,072	3,939	89
Crustaceans	62,687	500	17

Of the 89 species detected in the fish-specific 16s rRNA libraries, 77 were confirmed to occur in IRL. An additional 12 species not known to occur in IRL or Florida's Atlantic coast were reassigned to genus level. Of the 77 confirmed IRL species, 28 were unique to sites in south central IRL (including 13 species unique to sites E22 and E23 in Vero Beach), while 25 species detected at one or more sites in the central or south central IRL were not detected in BRL. Taken together, 16s rRNA sequencing of 185 IRL samples identified a diverse community of 77 species representing 63 genera, 39 families, 23 orders, and 3 classes of fish. Teleosts were the dominant class of fish detected (67 species). Nine Chondrichthyes species were detected, including two that are not known to occur in IRL or Atlantic coast and likely reflect species level misassignment. One species from class Actinopteri was detected (Longnose gar; *Lepisosteus osseus*).

Species accumulation curves generated from 20 samples collected at site E2 indicate the current replication of three samples per site each season is sufficient to resolve a majority (57%) of the fish diversity detected in the full dataset. An average of 12 species were detected in each set of three samples, out of a combined total of 21 species. Species richness projections are well resolved with three replicates. Sample sufficiency is further improved with regional within basin replication, which varied from 6–12 sample replicates per season. This same pattern was seen in power analyses, with the power of the BACI design to detect differences among sites each season (n = 6–12) near or exceeding the accepted 80% power threshold (**Figure 75**). Estimated power based of the BACI design to detect differences among sites across all four seasons is lower (57%; n = 24). However, for simplicity, power analyses assumed a two-way ANOVA, which inflated within the sample residual variance by combining seasonal samples into a single group. The statistical approach currently planned for the BACI design is to apply a mixed model using a PERMANOVA framework to accommodate seasonal effects (Anderson, 2005). This approach is commonly used to test the simultaneous response of multiple variables to one or more factors and is expected to significantly increase power by diminishing residuals (Anderson, 2014).

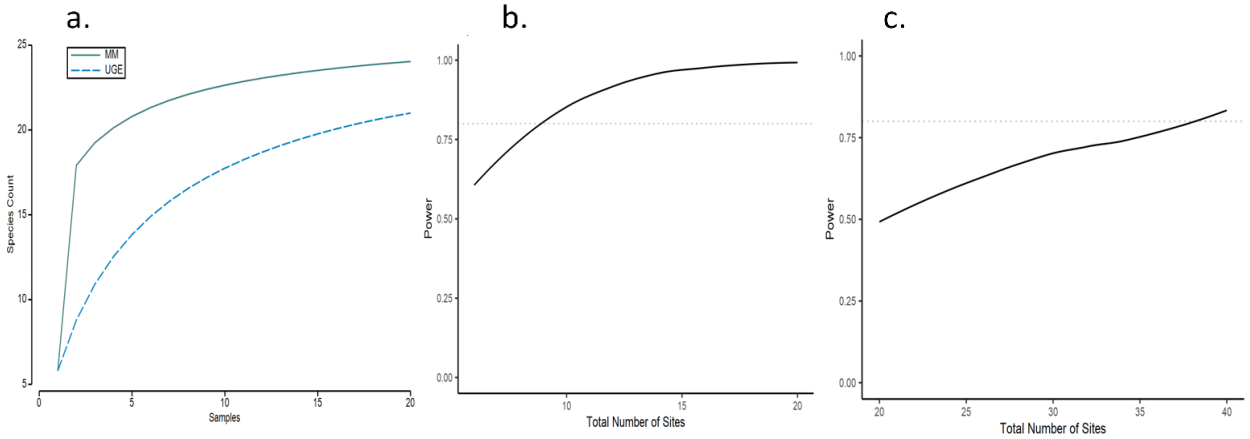

Figure 75. Estimates of sample sufficiency and power derived from 20 samples collected at site E2 with (a) Ugland-Gray-Elligsen and Michaelis-Menten estimates of species richness derived and estimated power of the BACI design with 2-way ANOVA for (b) seasonal species richness and (c) projected, combined annual species richness

The four selected measures of within site diversity (richness, Shannon diversity, average taxonomic distinctness, and variation in taxonomic distinctness) for combined fall, winter, and spring collections show a general trend of increasing diversity from north to south (**Figure 76**). In each case, average diversity was lowest in BRL and highest in the south central IRL. Sites E22–E26 were not included in cumulative analyses but within season comparisons show a similar trend of declining diversity with increasing latitude. Richness and Shannon diversity measures were highly correlated ($R^2 = 0.98$, $p < 0.001$) indicating they provide similar information about site diversity. The correlation between richness or Shannon diversity and taxonomic distinctness was also significant but less pronounced ($R^2 = 0.41$, $p = 0.02$), with site-specific differences revealing additional information for monitoring impacts during experimental pumping. Variation in taxonomic distinctness was uncorrelated with, and therefore complimentary to, each of the other measures ($R^2 > 0.6$, p = NS).

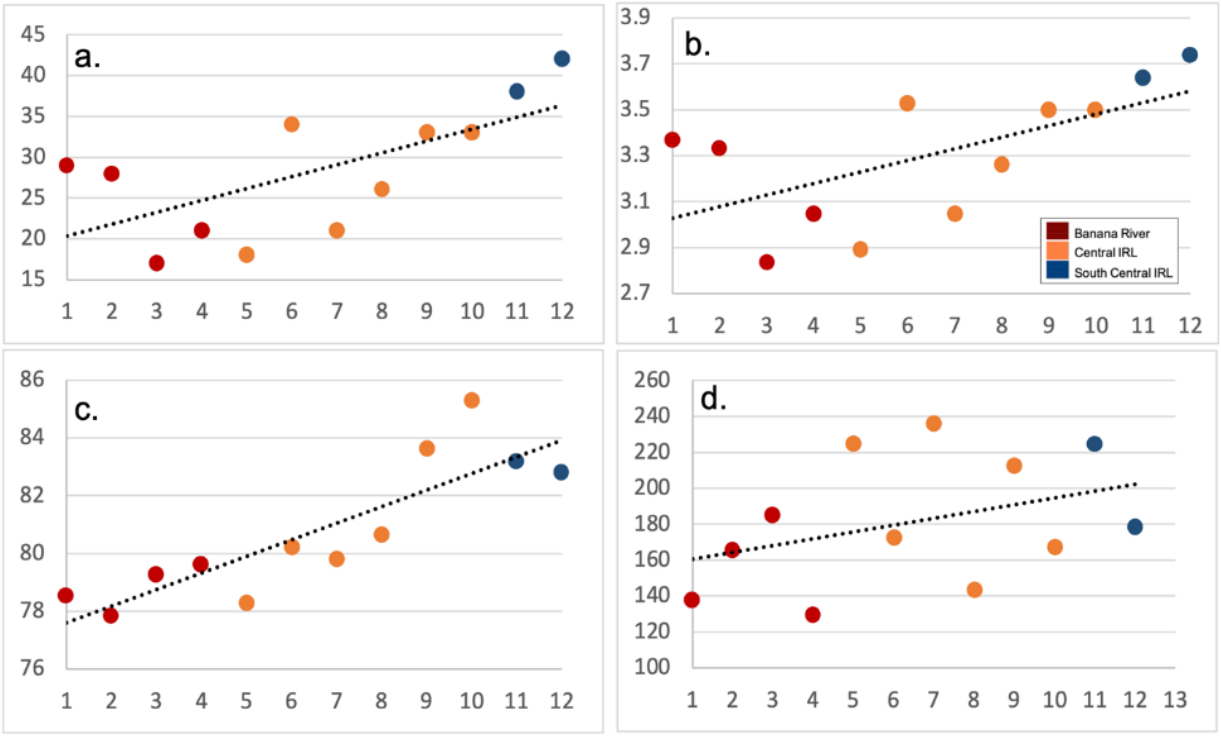

Figure 76. Estimates of fish diversity for sites E1–E12 for combined fall, winter, and spring collections with (a) species richness, (b) Shannon diversity, (c) average taxonomic distinctness, and (d) variation in taxonomic distinctness

An assessment of community response to enhanced inflow will be conducted with the proposed pilot project. To inform on the appropriateness of the designated approach and provide additional information on how fish biodiversity is structured across the survey area, pairwise similarity/dissimilarity among sampled sites were evaluated using the Sørenson similarity index and estimates of taxonomic similarity derived from site-based estimates of taxonomic distinctness (**Table 30**). With the exception of site E6, there was a consistent pattern of higher similarity among sites within regional basins than between sites in different basins. Within basin similarity estimates ranged between 59.0–72.5 for the Sørenson index and 80.0–87.0 for taxonomic similarity, while estimates of similarity for comparisons between sites in different basins ranged between 49.0–55.0 and 75.4–77.2 for Sørenson and taxonomic similarity, respectively.

A combination of cluster plots and similarity profile permutation tests were used to depict statistically significant similarities/dissimilarities among sites and regions. Statistically significant patterns of site similarity/dissimilarity were examined for each season for which data were available (fall, winter, and spring) and on the combined three season dataset. Seasonal analyses of site groupings support the general pattern of greater within site than between site similarity, highlighting significant regional differences in fish eDNA detections across seasons, including in all comparisons with samples collected in the fall and winter at sites E22 and E23. The relationship between individual sites varies somewhat among seasons; however, both the Sørenson index and estimates of taxonomic similarity show BRL sites consistently clustering together and most different from the south central IRL sites. This same pattern can be seen in the combined three season datasets, with significant differences in fish community structure generally aligning with basin boundaries and greatest dissimilarity occurring between BRL and south central IRL sites.

Table 30. Pairwise estimates of IRL fish community similarity based on (a) Sørenson similarity index and (b) taxonomic similarity

Note: BRL sites are shown in red, central IRL sites in yellow, and south central IRL sites in blue.

a.	E1	E2	E3	E4	E5	E6	E7	E8	E9	E10	E11	E12
E1	-											
E2	73.7	-										
E3	60.9	62.2	-									
E4	64.0	69.4	68.4	-								
E5	55.3	69.6	57.1	66.7	-							
E6	57.1	51.6	43.1	47.3	46.2	-						
E7	60.0	57.1	68.4	57.1	56.4	61.8	-					
E8	61.8	63.0	60.5	59.6	68.2	66.7	68.1	-				
E9	54.8	65.6	56.0	51.9	58.8	50.7	51.9	67.8	-			
E10	51.6	55.7	52.0	51.9	47.1	59.7	51.9	57.6	72.7	-		
E11	50.7	48.5	40.0	44.1	32.1	41.7	37.3	46.9	62.0	50.7	-	
E12	53.5	51.4	47.5	50.8	46.7	44.7	44.4	58.8	69.3	61.3	72.5	-

b.	E1	E2	E3	E4	E5	E6	E7	E8	E9	E10	E11	E12
E1	-											
E2	84.6	-										
E3	77.4	76.9	-									
E4	81.6	85.3	83.2	-								
E5	76.6	85.2	81.1	83.1	-							
E6	76.2	69.4	65.5	71.3	68.8	-						
E7	80.0	77.6	84.2	81.0	81.0	80.4	-					
E8	81.5	80.0	76.3	80.9	84.5	83.3	86.8	-				
E9	76.5	83.3	73.6	76.7	82.4	73.1	77.0	84.7	-			
E10	74.8	74.4	69.6	75.6	72.5	80.3	76.3	80.7	87.9	-		
E11	74.6	73.0	67.3	74.2	67.5	72.8	74.9	76.9	82.3	79.4	-	
E12	75.2	75.1	68.8	75.9	72.3	73.4	74.6	82.1	85.1	83.2	87.0	-

Site groupings highlight fish communities shaped by regional differences in both abiotic factors (e.g., temperature and salinity) and perturbation history, including eutrophication (e.g., Mouillot et al., 2005; Gallardo et al., 2011; Tweedley et al., 2017). The relatively high similarity of sites within BRL provides further support for the value of the BACI design to directly test pumping impacts against within basin sites.

The demonstrated sensitivity of taxonomic distinctness measures to anthropogenic impacts provides an opportunity to track biodiversity loss or recovery over time in response to the proposed pilot inflow project or other anthropogenic impacts. The list of IRL fishes maintained by the Smithsonian Fort Pierce Field Station was used to develop funnel plots depicting the average taxonomic distinctness and variation in taxonomic distinctness of all IRL fishes with 95% confidence intervals reflecting sampling effort (i.e., number of species detected). With a few exceptions, site distinctness measures mapped onto the respective confidence funnel reinforce the general pattern of increasing similarity among sites within basins compared to sites in different basins (**Figure 77**). Exceptions highlight the unique taxonomic diversity of individual sites (e.g., E9–E12) and the relatively low taxonomic diversity of BRL sites. Sites E9–E12 in the south central IRL standout as having fish communities that are both species rich and taxonomically diverse.

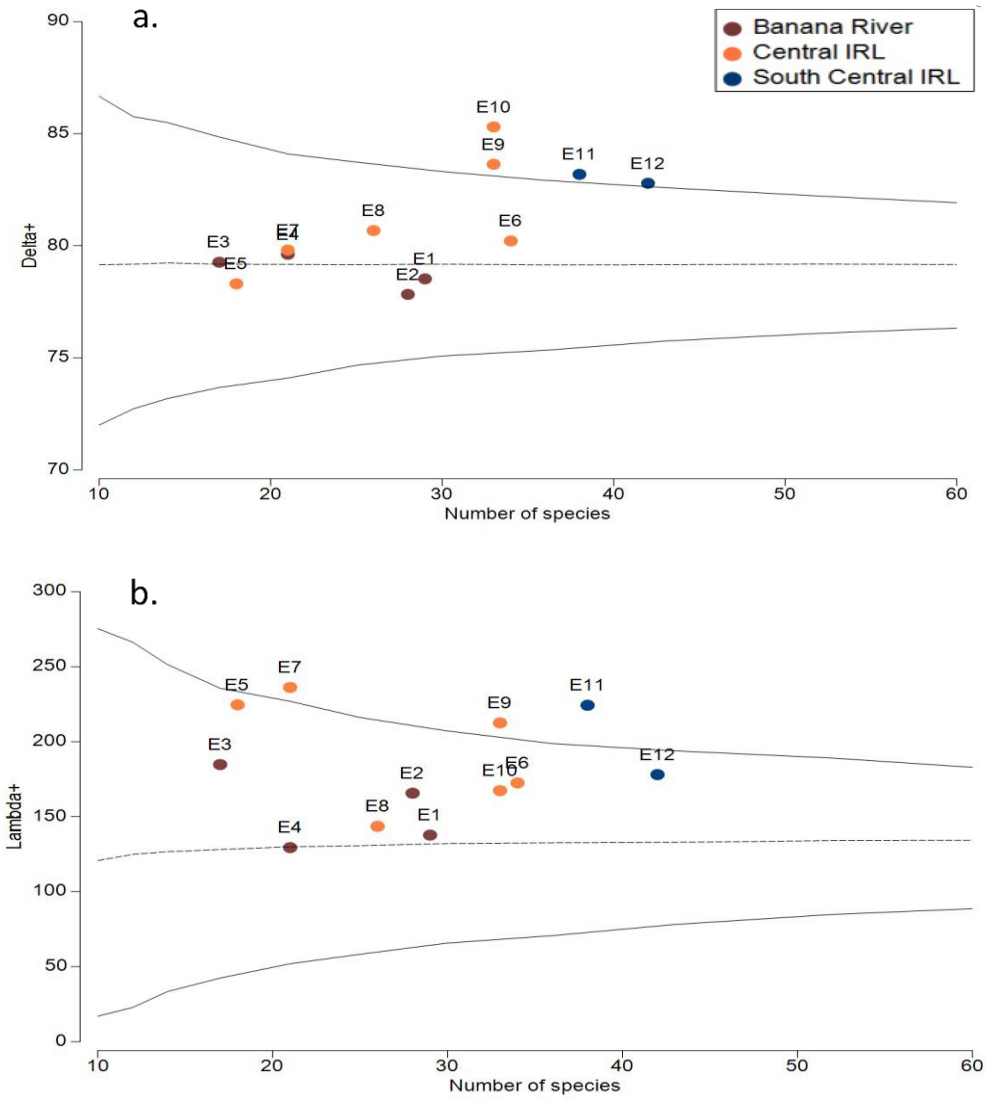

Note: Site specific taxonomic distinctness estimates from eDNA detections are color coded by region.

Figure 77. Fixed reference funnel plots with 95% confidence interval for (a) average taxonomic distinctness and (b) variation in taxonomic distinctness of all IRL fishes

4.3.2.3 Benthic Fauna, Seagrasses, and Phytoplankton

4.3.2.3.1 Seagrass, Rooted Algae, and Drift Algae

An attempt was made to find the nearest seagrass beds to the proposed inflow site. Within IRL, seagrasses are patchy and, when present, vary from sparse to abundant at the selected seagrass locations examined for this study. The primary species of seagrass observed at all locations was the seagrass *Halodule wrightii*. Abundances of seagrass, in terms of percent cover, are presented in **Figure 78**. Seagrass percent cover was greatest in Phase 1 summer, ranging from 0–9% and 0–6% at BRS and BRN, respectively. Canopy heights were highest in the summer (Quarter 3, **Figure 79**), as high as 5.7 cm at BRS.

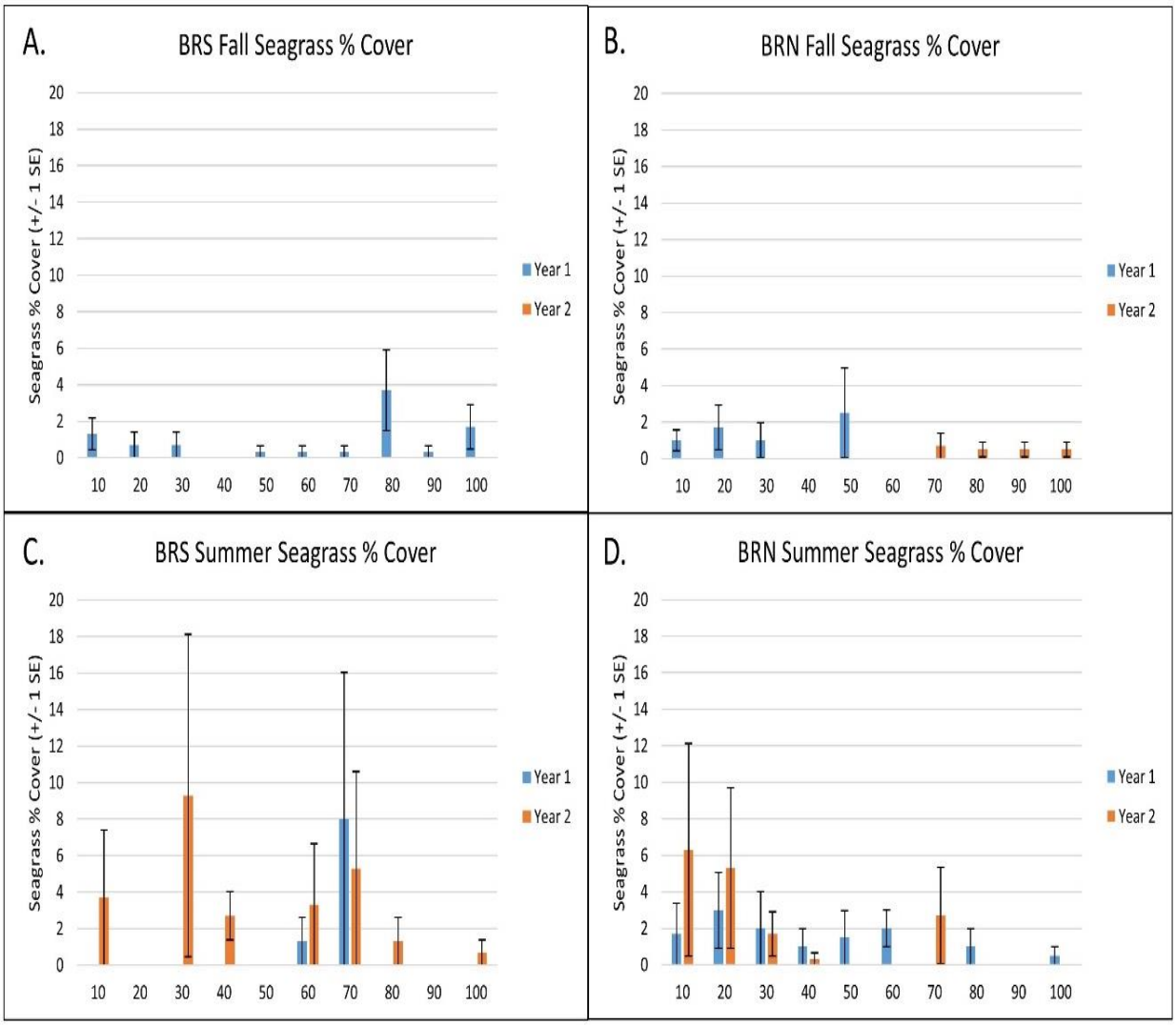

Note: Blue bars = Phase 1 of baseline sampling (RLI1); orange bars = Phase 2 of baseline sampling (RLI2).

Figure 78. Seagrass mean percent cover in fall (A and B) and summer (C and D), comparing Phases 1 and 2 for transects nearest the proposed inflow crossover point at A) BRS in the fall, B) BRN in the fall, C) BRS in the summer, and D) BRN in the summer

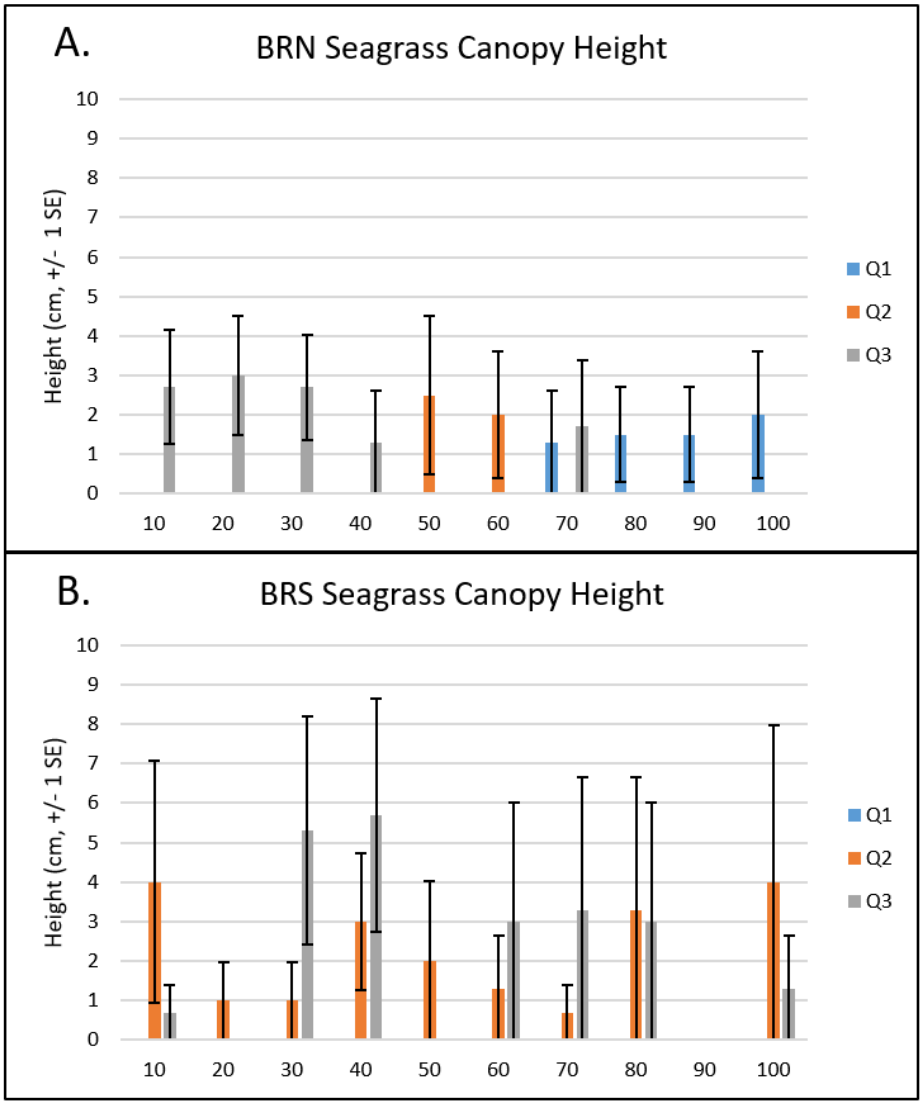

Note: Q1 is winter, Q2 is spring, and Q3 is summer.

Figure 79. Seagrass mean seasonal canopy height during Phase 2 (2021) for A) BRN (proposed crossover location) and B) BRS (reference site)

Epiphytes growing on shoal grass blades showed different seasonal patterns based on site and were most abundant at BRN in the spring and summer (**Figure 80**).

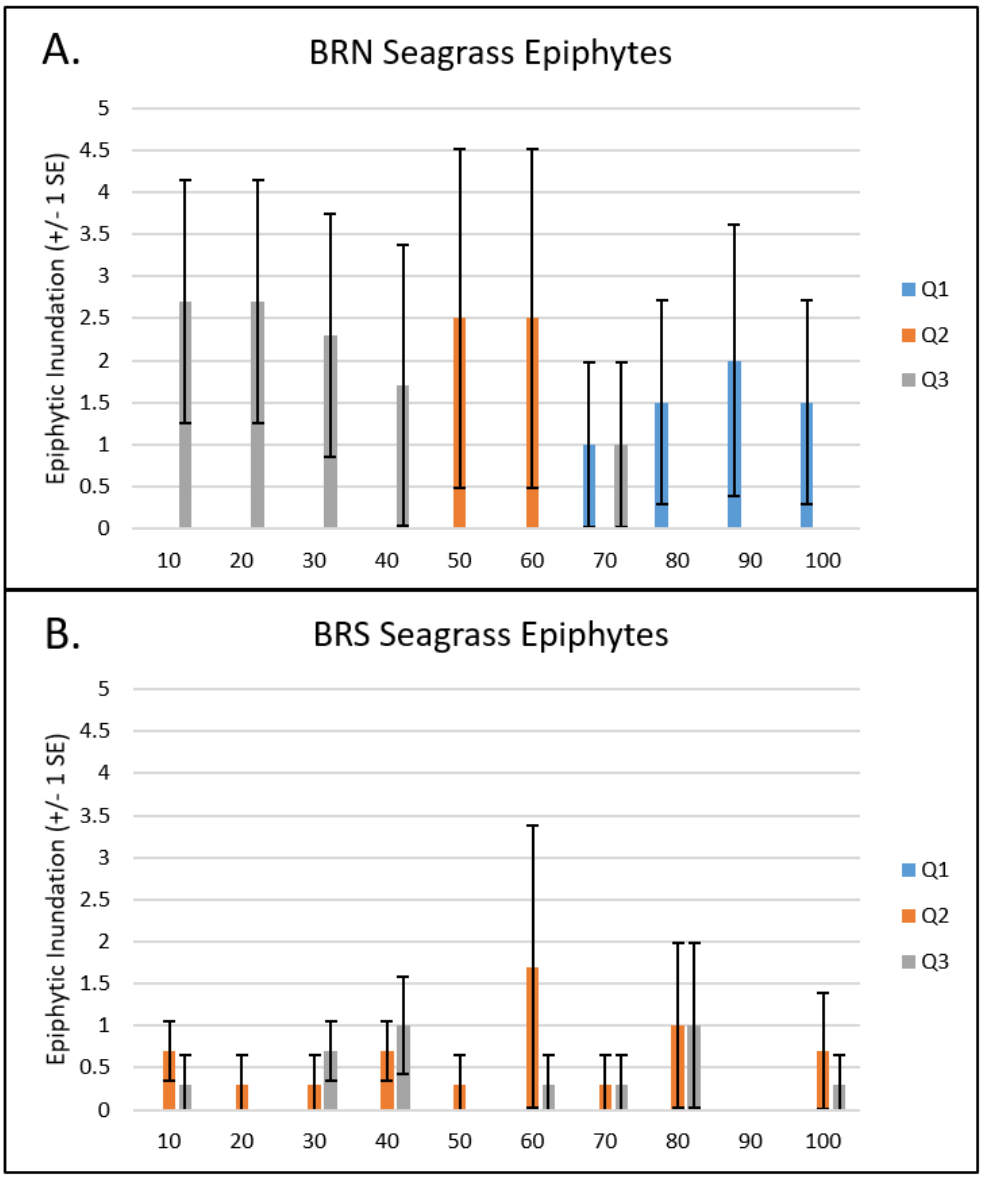

Note: Q1 is winter, Q2 is spring, and Q3 is summer. "Inundation" is a subjective determination of the relative abundance of epiphytes on a scale of 0-5.

Figure 80. Epiphyte mean seasonal inundation during Phase 2 (2021) for A) BRN (proposed crossover location) and B) BRS (reference site)

Rooted alga of the genus *Caulerpa* had the greatest coverage in the summer, particularly at the proposed inflow site BRN (2–68% in Phase 1, 4–52% in Phase 2) (**Figure 81**). Drift algae was absent in the fall of both years, but had a strong presence in the summer both at BRN and BRS, particularly in Phase 2 (0–33%) (**Figure 82**). Results of the power analysis on benthic/drift vegetation ranged from 0.04 to 0.83, with the highest power being for drift algae percent cover in the winter.

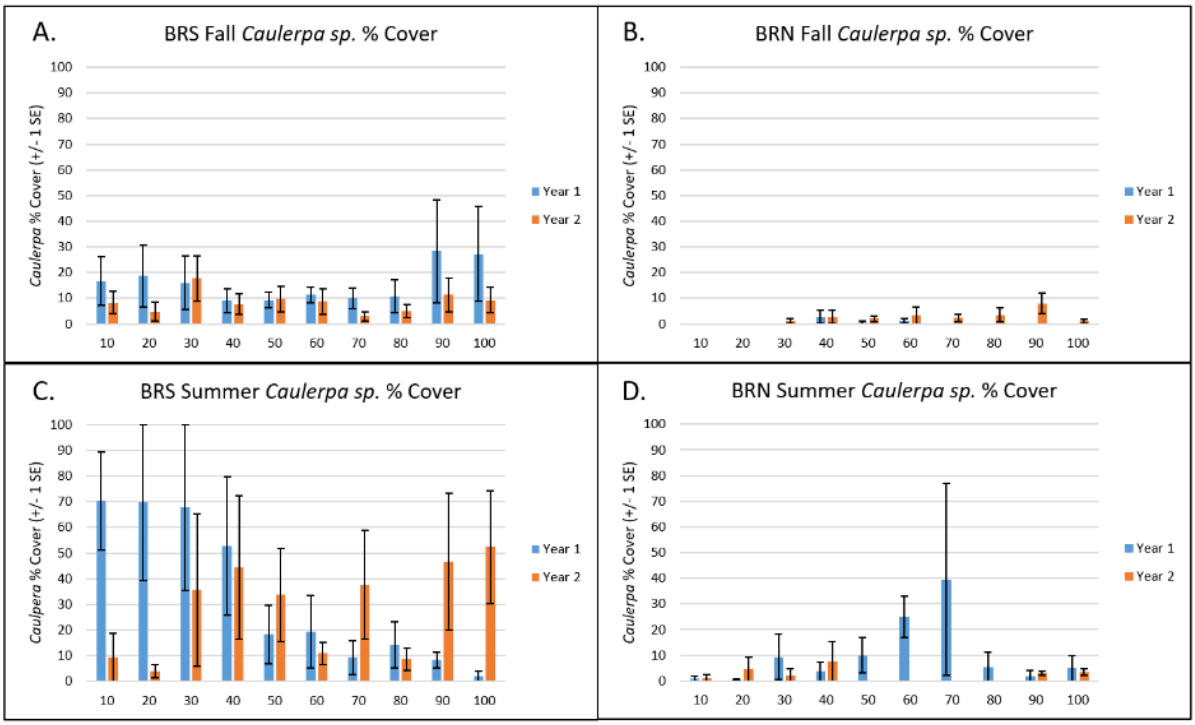

Figure 81. Rooted algae (Caulerpa sp.) mean percent cover during Phases 1 and 2 for the proposed crossover location (BRN – B and D) and reference site (BRS – A and C), comparing fall (A and B) and summer (C and D)

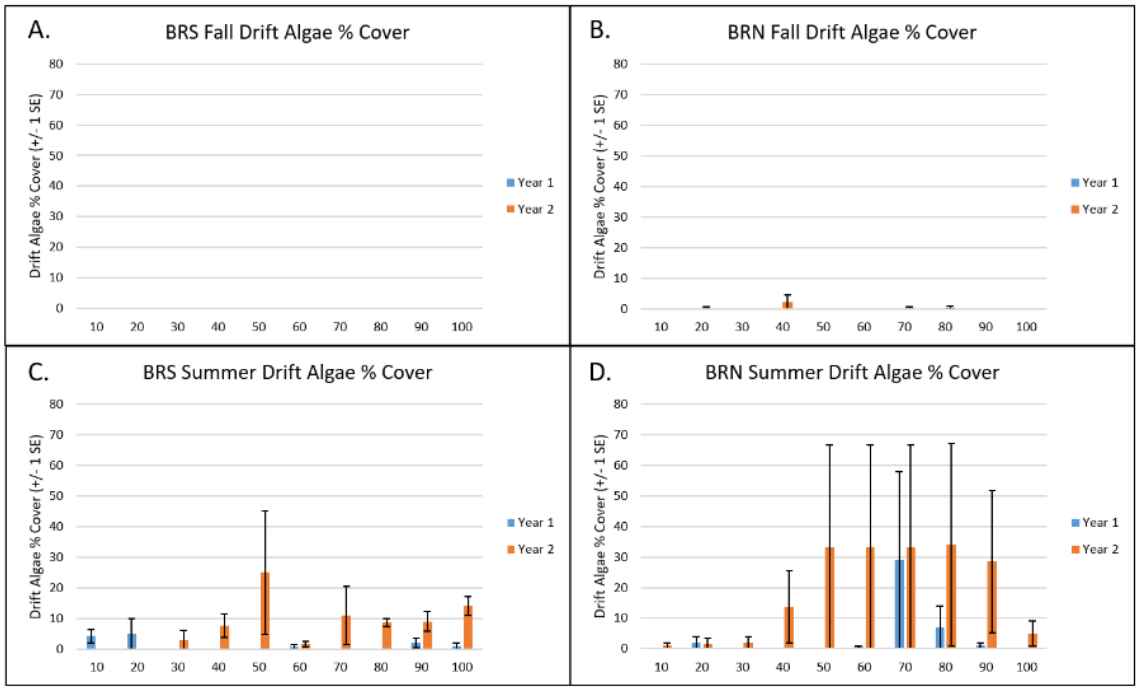

Figure 82. Drift algae mean percent cover during Phases 1 and 2 for the proposed crossover location (BRN – B and D) and reference site (BRS – A and C), comparing fall (A and B) and summer (C and D)

4.3.2.3.2 Benthic Fauna

Species universally present, or almost universally present, at both locations and throughout all seasons and years are the polychaetes *Alitta succinea*, *Capitella capitata*, *Ctenodrilus serratus*, *Glycera americana*, *Hypereteone heteropoda*, *Paradiopatra hispanica*, and *Pectinaria gouldii*; amphipod crustaceans *Ampelisca abdita*, *Cerapus tubularis*, *Cymadusa compta*, and *Eusirus cuspidatus*; ostracod crustacean *Eusarsiella zostericola*; peanut worm *Phascolion cryptus*; phoronid *Phoronis* sp.; gastropods *Acteocina canaliculata* and *Phrontis vibex*; and bivalves *Anomalocardia cuneimeris*, *Mulinia lateralis*, and *Parastarte triquetra*.

Infaunal densities in bare sediments ranged from 1.9–4.0 x 10^4 organisms m^{-2} in Phase 1. In Phase 2, there was evidence of a large recruitment event near the proposed inflow site, with densities approaching 1.5 x 10^5 organisms m^{-2}. Infauna living amongst seagrasses ranged from 4.3–4.7 x 10^4 m^{-2} in Phase 1 (BRN and BRS, respectively), and densities dropped to 1.0 x 10^4 and 1.2 x 10^4 m^{-2} in Phase 2 (BRS and BRN, respectively). Two-way ANOVA results are reported in infauna in **Figure 83** with letters indicating significance at the alpha = 0.05 level.

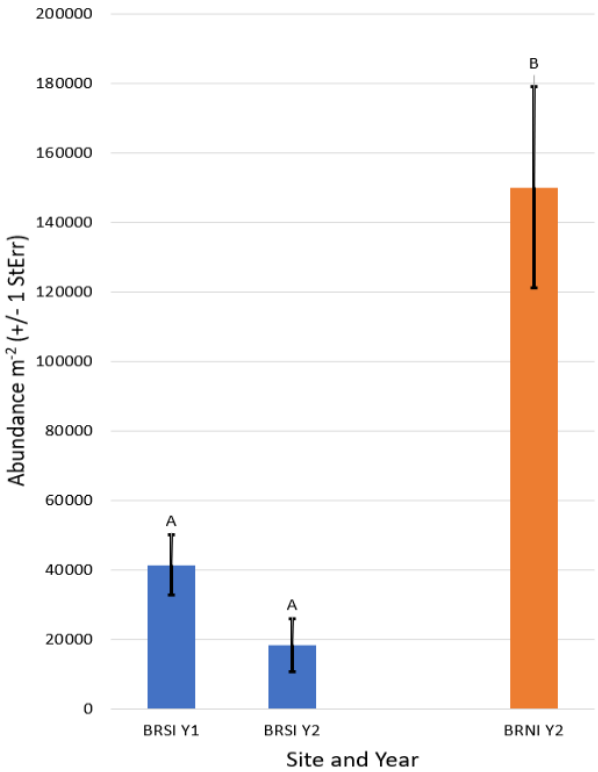

Note: Samples were not collected in Phase 1 spring because of the global pandemic and a COVID-19 outbreak in the lab.

Figure 83. Mean spring general infauna abundances at the proposed inflow site (BRN – orange) and reference site (BRS – blue) during Phases 1 and 2 ($p < 0.001$)

The polychaete annelid *Alitta succinea* and the bivalve *Parastarte triquetra* were selected as focal species due to their high densities and consistent presence. In bare sediments, *A. succinea* densities ranged from 2 x 10^2 worms m^{-2} (BRS inside lagoon, Phase 2) to 1.6 x 10^3 m^{-2} (BRN inside lagoon, Phase 2) (**Figure 84**). When amongst seagrass sediments, *A. succinea* densities ranged from near zero to as high as 1.1 x 10^3 animals m^{-2} (**Figure 85**). *P. triquetra* were most abundant in the fall, and especially abundant at the BRS inside lagoon reference site during Phase 1 (5.7 x 10^3 clams m^{-2}, **Figure 86**).

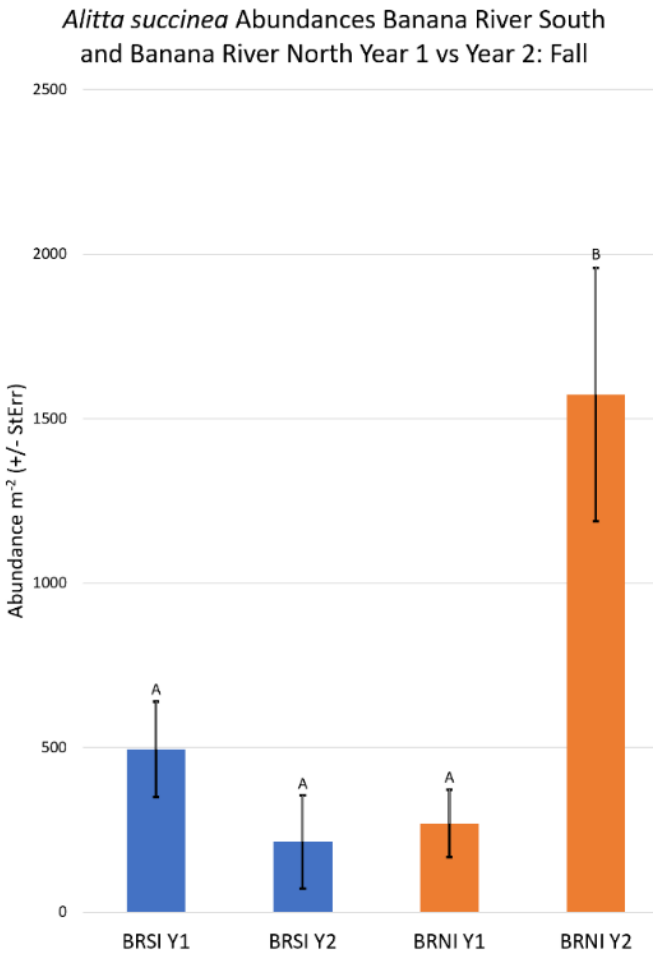

Figure 84. Mean abundance of the infaunal polychaete *Alitta succinea* at the proposed inflow site (BRN – orange) and reference site (BRS – blue) during Phases 1 and 2 (p = 0.006)

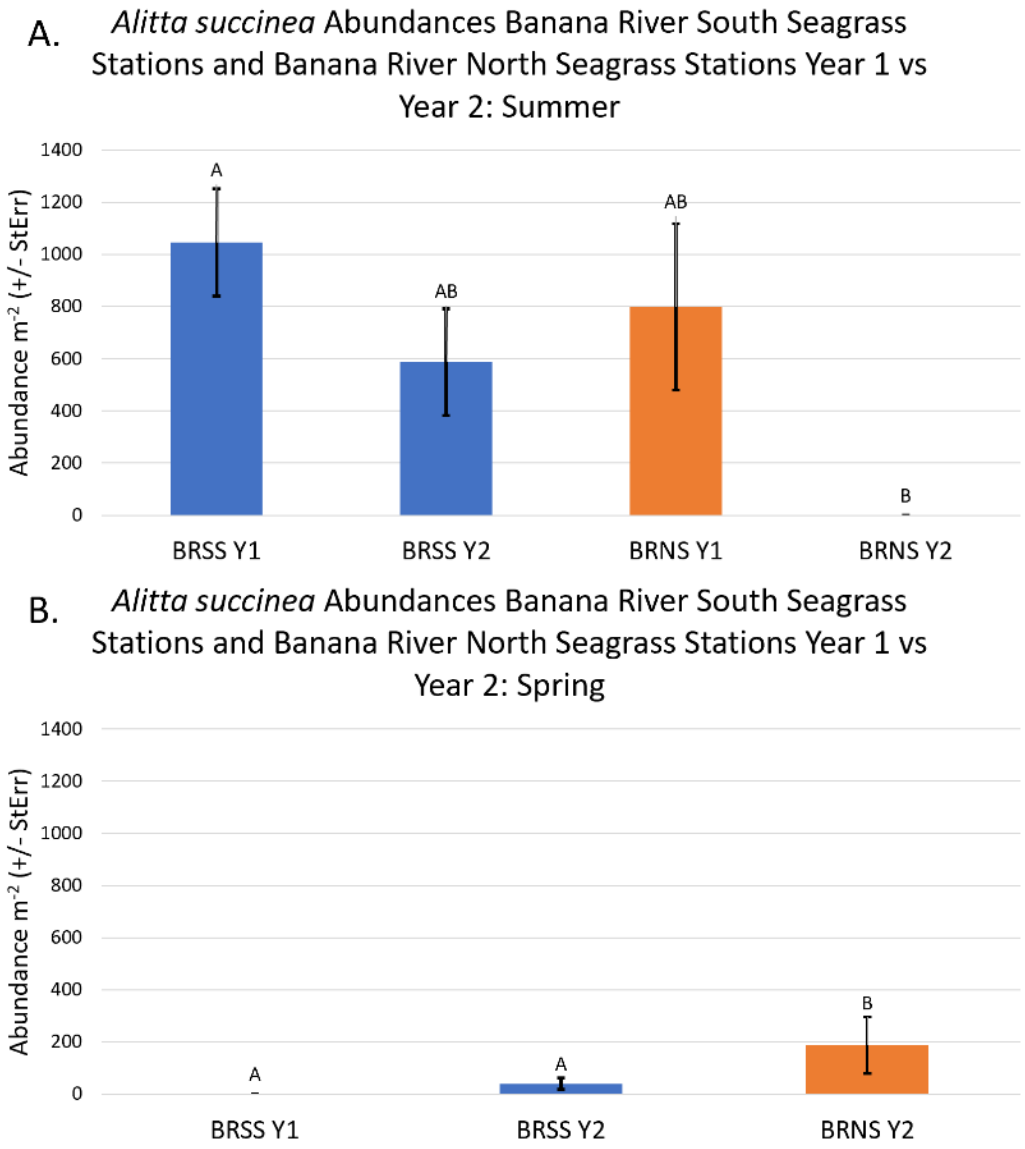

Figure 85. Mean abundance of the infaunal polychaete *Alitta succinea* in seagrass-associated sediments at the proposed inflow site (BRN – orange) and reference site (BRS – blue) during Phases 1 and 2 in the A) summer (p = 0.044) and B) spring (p = 0.006)

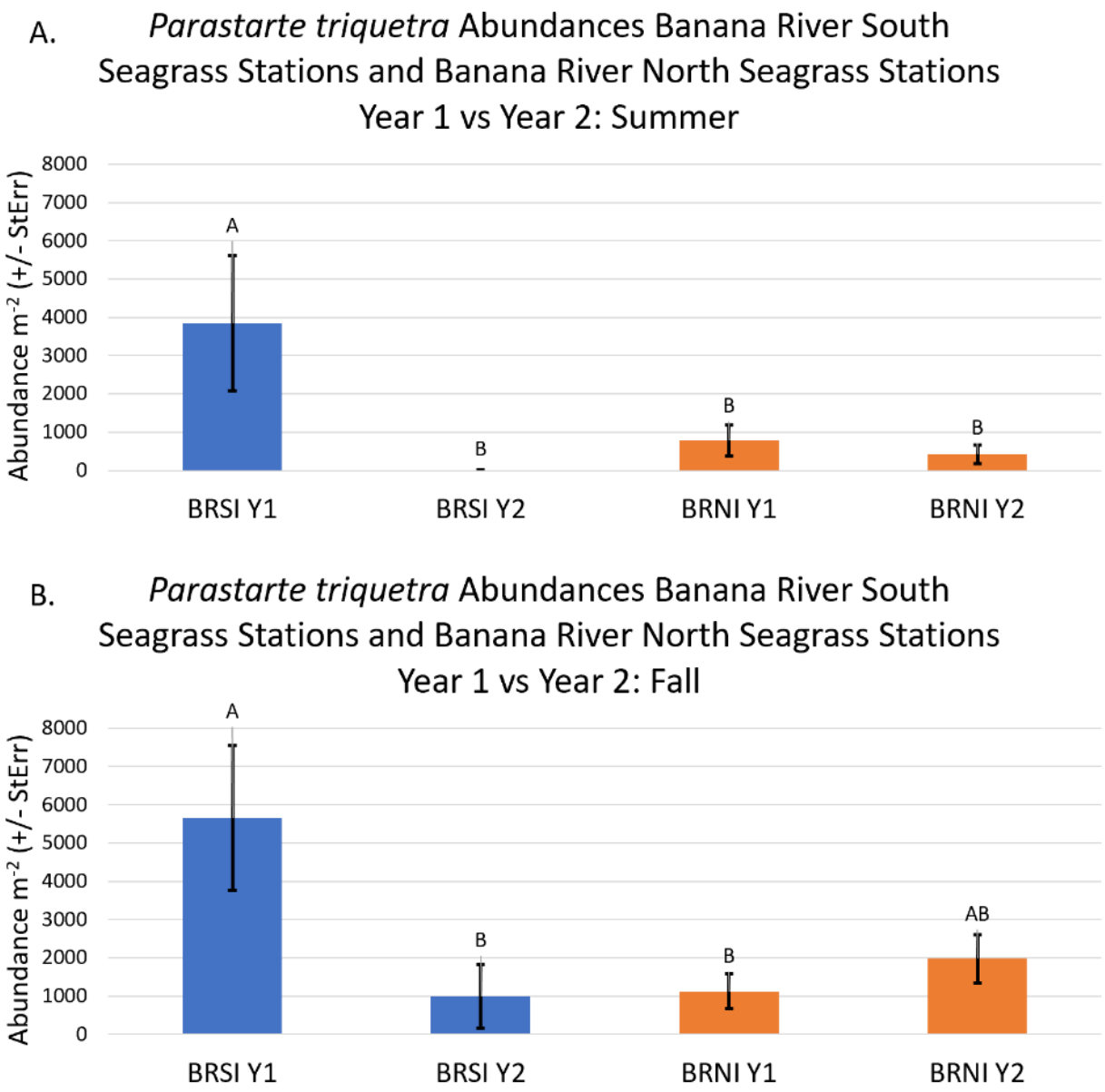

Figure 86. Mean abundance of the infaunal brown gem clam *Parastarte triquetra* in seagrass-associated sediments at the proposed inflow site (BRN – orange) and reference site (BRS – blue) during Phases 1 and 2 in A) summer (p = 0.01) and B) fall (p = 0.02)

Infaunal species richness was 4–13.7, with the highest at BRS inside lagoon during the fall of Phase 1. Biodiversity ranged from 0.5–1.8, no matter the site, year, season, or whether they were found in bare sediments or seagrass sediments (**Figure 87** and **Figure 88**).

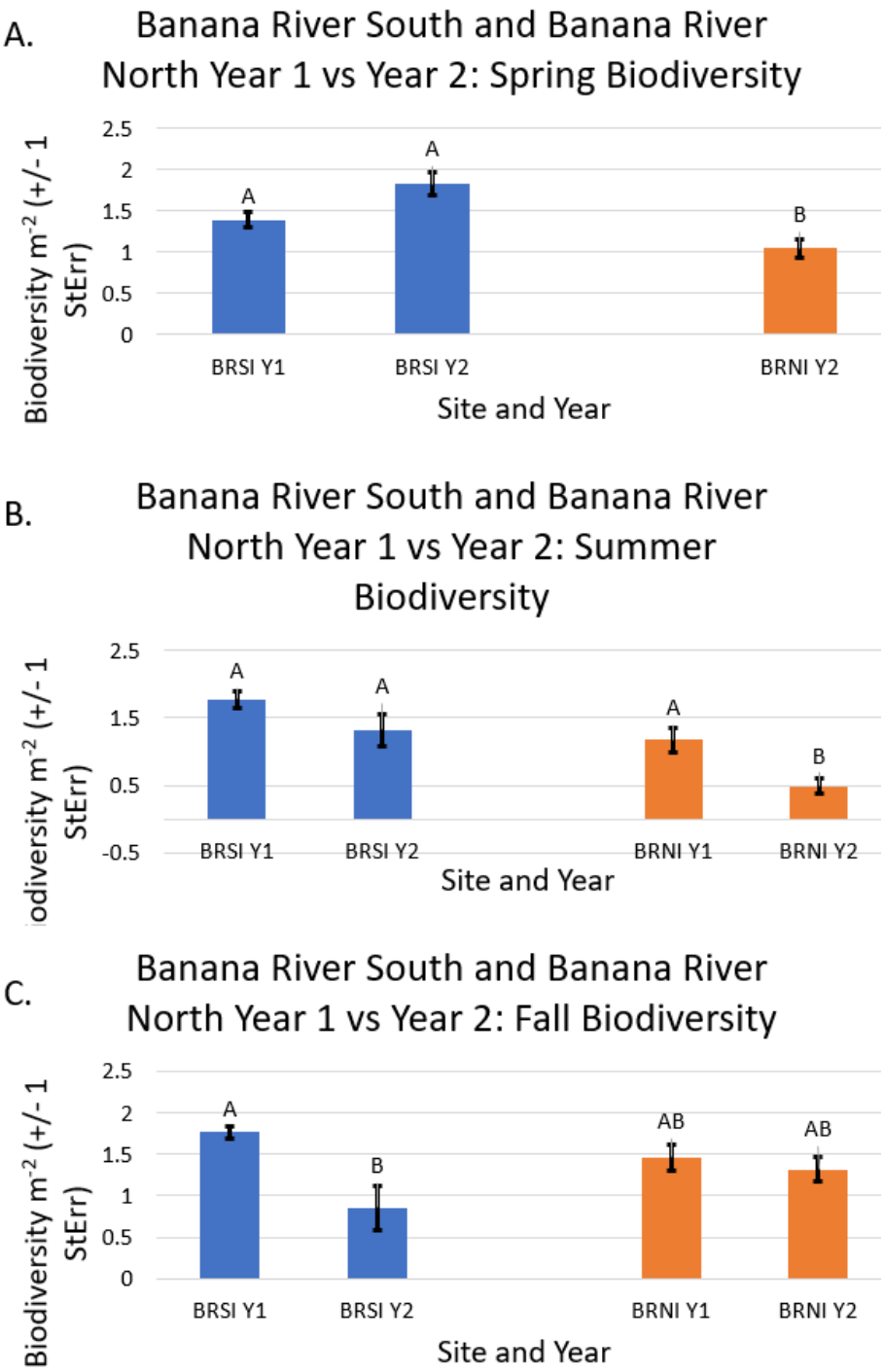

Figure 87. Mean benthic fauna biodiversity for bare sediments at the proposed inflow site (BRN – orange) and reference site (BRS – blue) during Phases 1 and 2 during A) spring (p = 0.002), B) summer (p = 0.001), and C) fall (p = 0.012) seasons

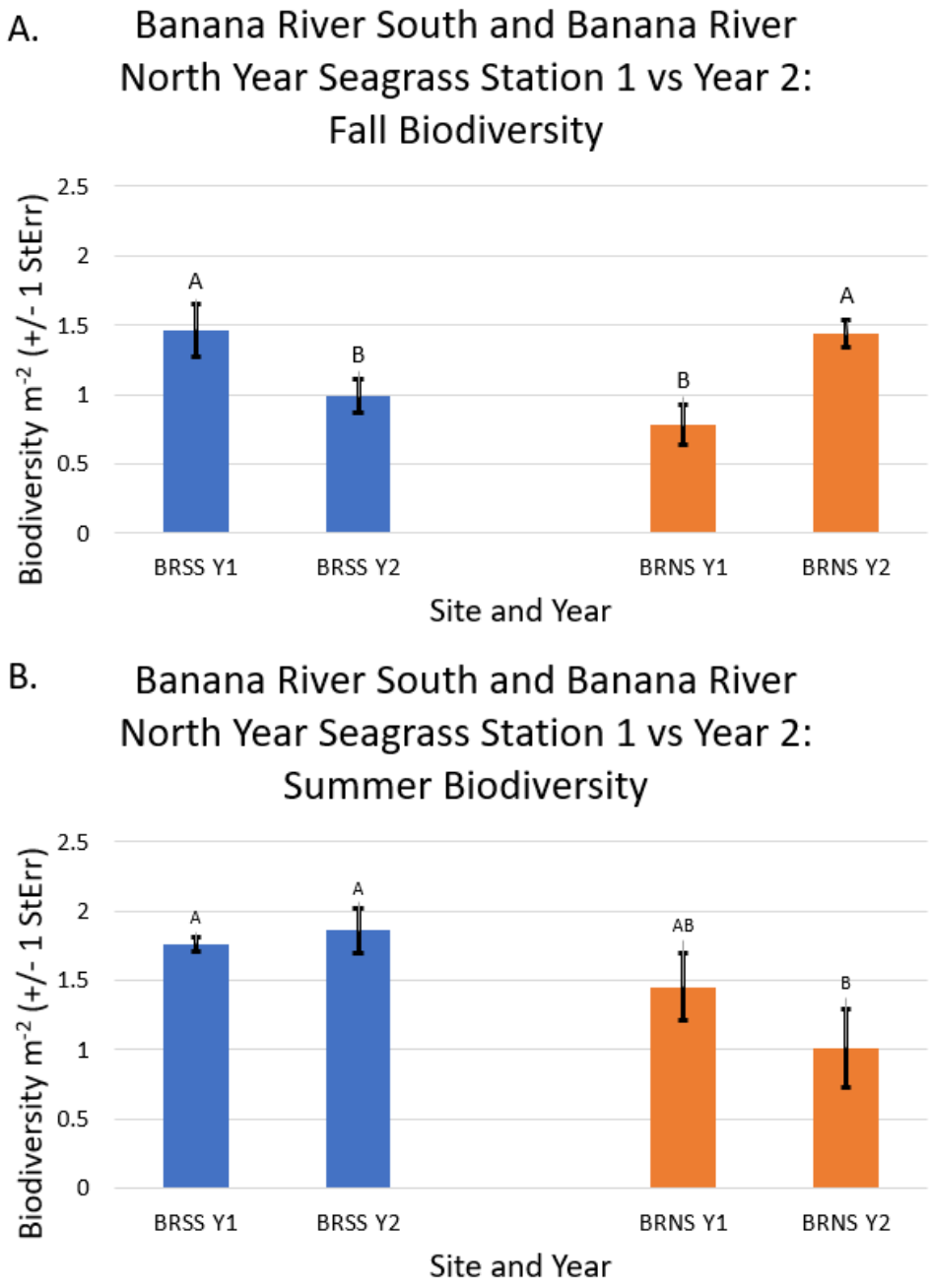

Figure 88. Mean benthic fauna biodiversity for seagrass-associated sediments at the proposed inflow site (BRN – orange) and reference site (BRS – blue) during Phases 1 and 2 during A) fall ($p < 0.001$) and B) summer ($p = 0.006$) seasons

Principle components analysis revealed that sediment conditions (percent organic content, percent silt-clay content, and percent water content) were the most influential environmental factors impacting the site, followed by bottom water DO. NMDS plots show considerable overlap from one year to the next in community data, whether looking at biodiversity, species richness or abundance (**Figure 89**). Results of power analysis on species diversity was as high as 0.83 and indicated that power should be sufficient for analysis with the current sample design.

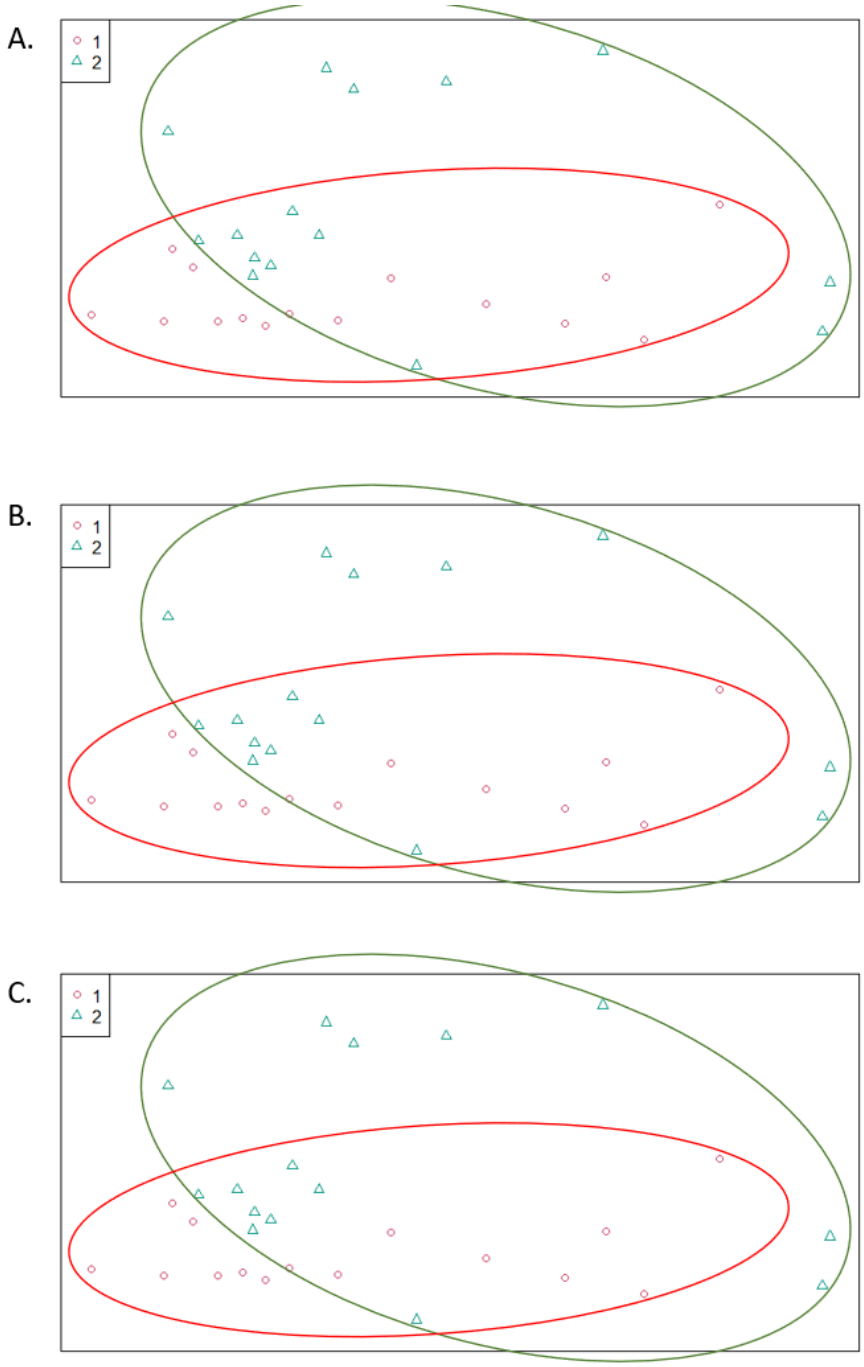

Note: Ellipses represent distinct groups based on similarity of the community.

Figure 89. NMDS of the benthic infauna community data at BRN seagrass stations in Phases 1 and 2, namely A) biodiversity, B) species richness, and C) abundance

NMDS was also used to examine patterns of seagrass coverage, and there were some significant differences based on year, season, and site (**Figure 90**).

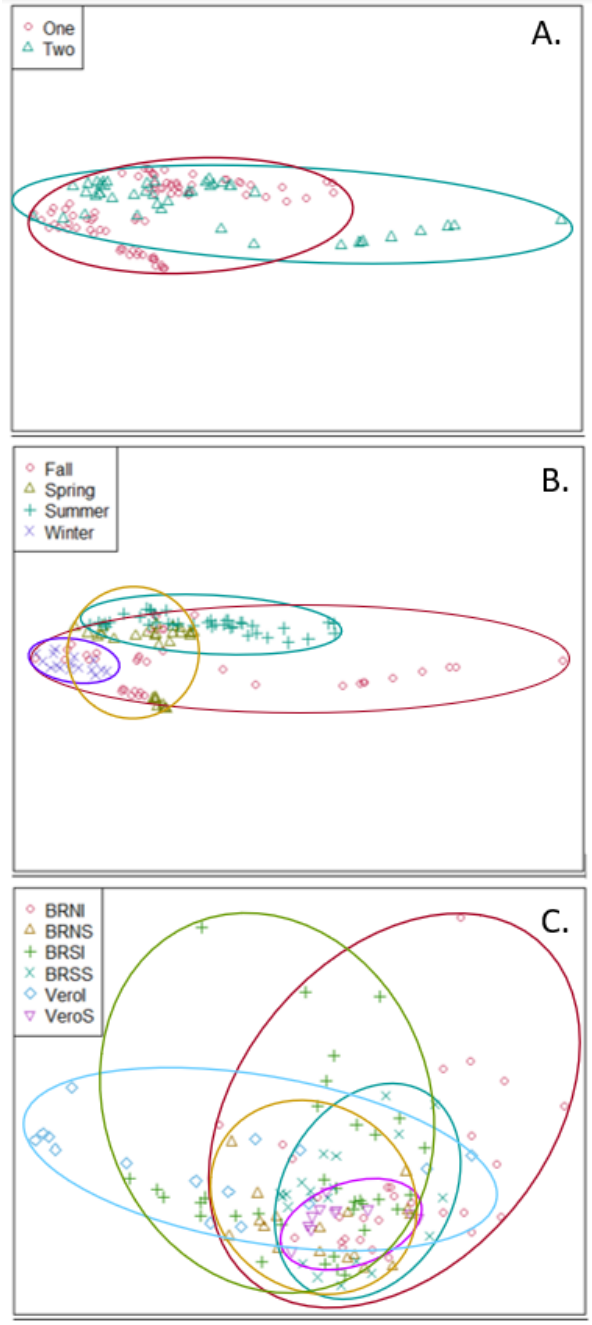

Site legend: BRNI = BRN in lagoon; BRNS = BRN seagrass; BRSI = BRS in lagoon; BRSS = BRS seagrass; VeroI = Vero Beach in Bethel Creek; VeroS = Vero Beach seagrass.

Figure 90. NMDS plots of seagrass percent cover as a function of environmental and other biological factors with aggregation of seagrasses according to A) year (p = 0.001), B) season (p = 0.001), and C) site (p = 0.001)

4.3.2.3.3 Phytoplankton/Harmful Algae

Diatom species that were dominant during most seasons and locations included *Chaetoceros* spp., *Coscinodiscus* spp., *Cylindrotheca closterium*, *Navicula* spp., *Nitzschia* spp., *Odontella* spp., *Pleurosigma* spp., and *Rhizosolenia* spp. Diatoms of the genus *Pseudo-nitzschia* are known to cause HABs via the production of domoic acid. Dinoflagellates that were frequently present, often in high numbers, included *Ceratium* spp. And *Prorocentrum* sp. Other dinoflagellates present,

sometimes in high numbers, and known to produce toxins and create harmful conditions included *Gonyaulax* spp., *Gymnodinium* spp., and *Pyrodinium bahamense*. The most abundant phytoplankton were non-cyanobacterial cells less than 40-µm, which tended to be more abundant in the estuary near the region of the proposed for restored inflow, especially in Phase 2 (**Figure 91**). Cyanobacteria densities measured by phycocyanin pigment presence range from nearly absent to $4x10^7$ cells L^{-1}, and were especially abundant during 2021. Cyanobacteria detected by the presence of phycoerythrin pigment were more consistently present and peaked at about the same order-of-magnitude as phycocyanin-bearing cells.

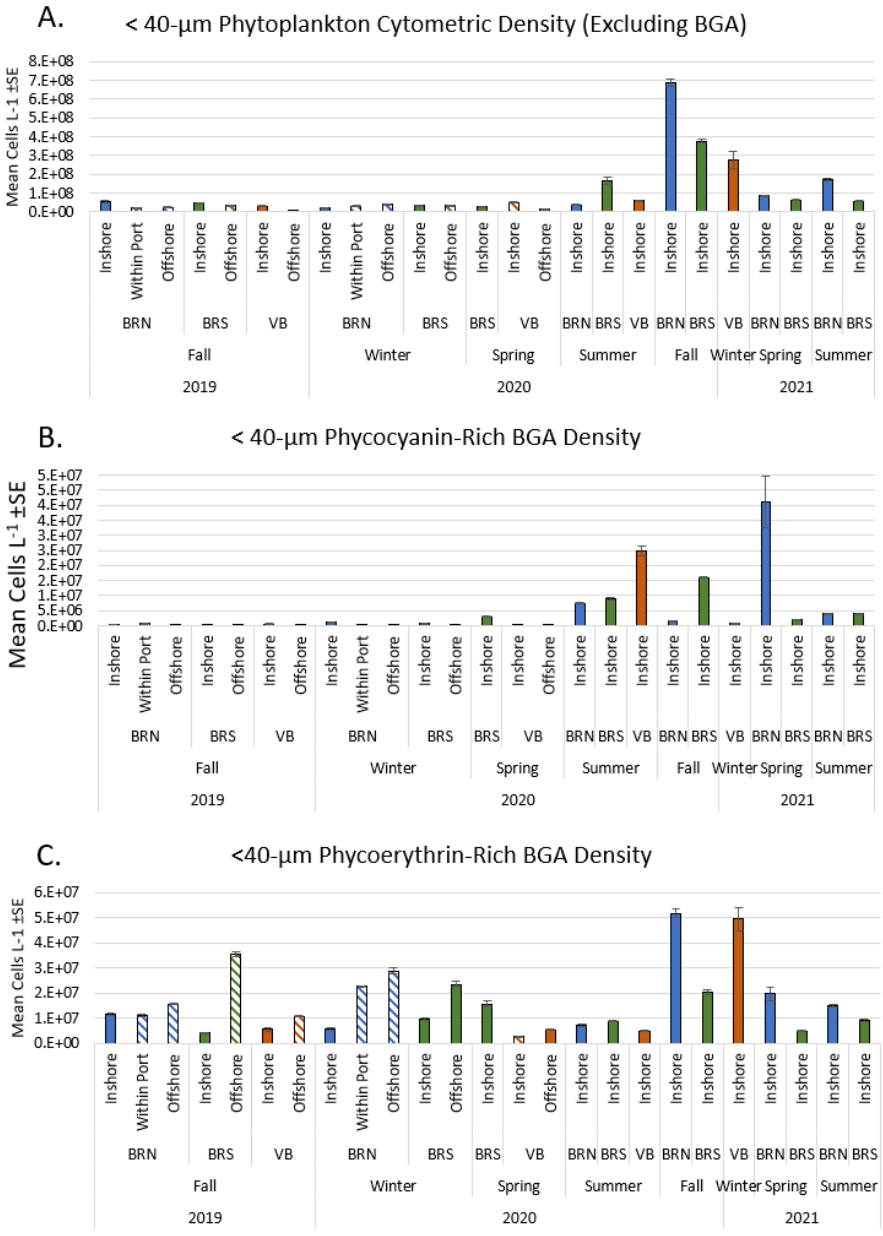

Note: Sites are BRN, BRS, and Vero Beach. "Inshore" is within the estuary. "Offshore" is coastal.

Figure 91. <40-µm phytoplankton densities for A) non-cyanobacteria, B) cyanobacteria as indicated by phycocyanin presence, and C) cyanobacteria as indicated by phycoerythrin presence

Larger phytoplankton (greater than 25-µm due to tow net mesh size) were mostly diatoms and dinoflagellates. The greatest abundances was $4.5x10^3$ – $5.9x10^3$ cells L^{-1} at BRS (**Figure 92**).

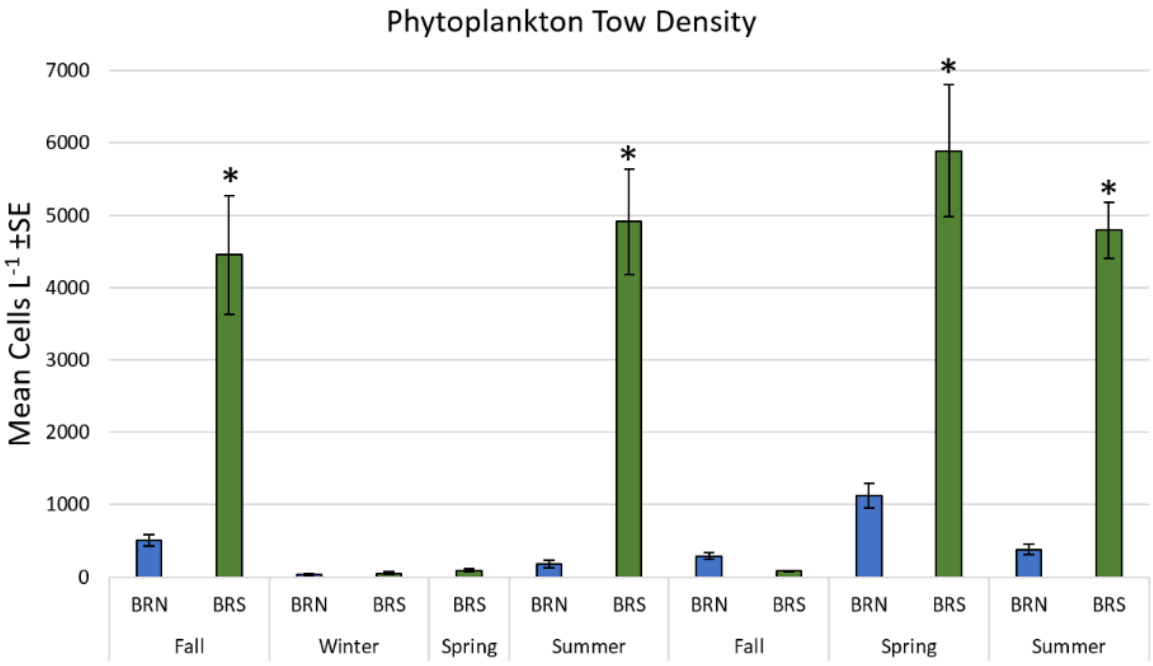

Figure 92. >25-µm phytoplankton mean densities inside and outside of the proposed inflow site (BRN) and reference (BRS), seasonally from fall 2019 to summer 2021

Phytoplankton biodiversity, species richness, and evenness were calculated for tow plankton (**Figure 93**).

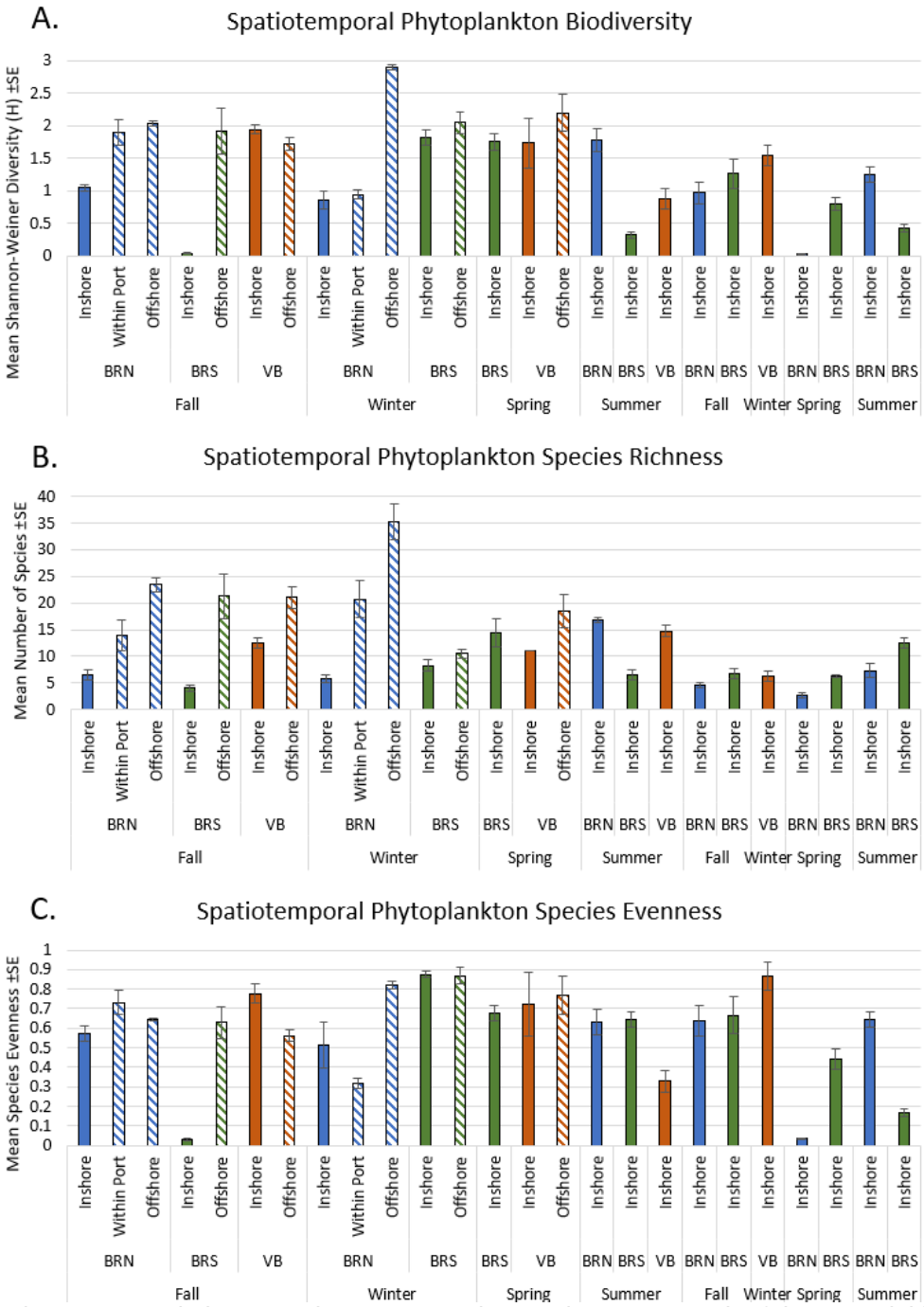

Note: Comparisons are made between the estuary and coastal ocean at each of the potential inflow sites ("offshore"), the latter during the first year of sampling only.

Figure 93. Phytoplankton mean Shannon-Weiner Diversity Index (A), mean species richness (B), and mean community evenness (C)

NMDS plots to group communities based on relative species abundances show communities fall out based on season and location (**Figure 94**, stress 0.15–0.24, analysis of similarity R = 0.23-0.99, $p<0.05$). Estuarine plankton communities were most distinct from one another when compared via pooled seasons per site (**Figure 94**, panel B).

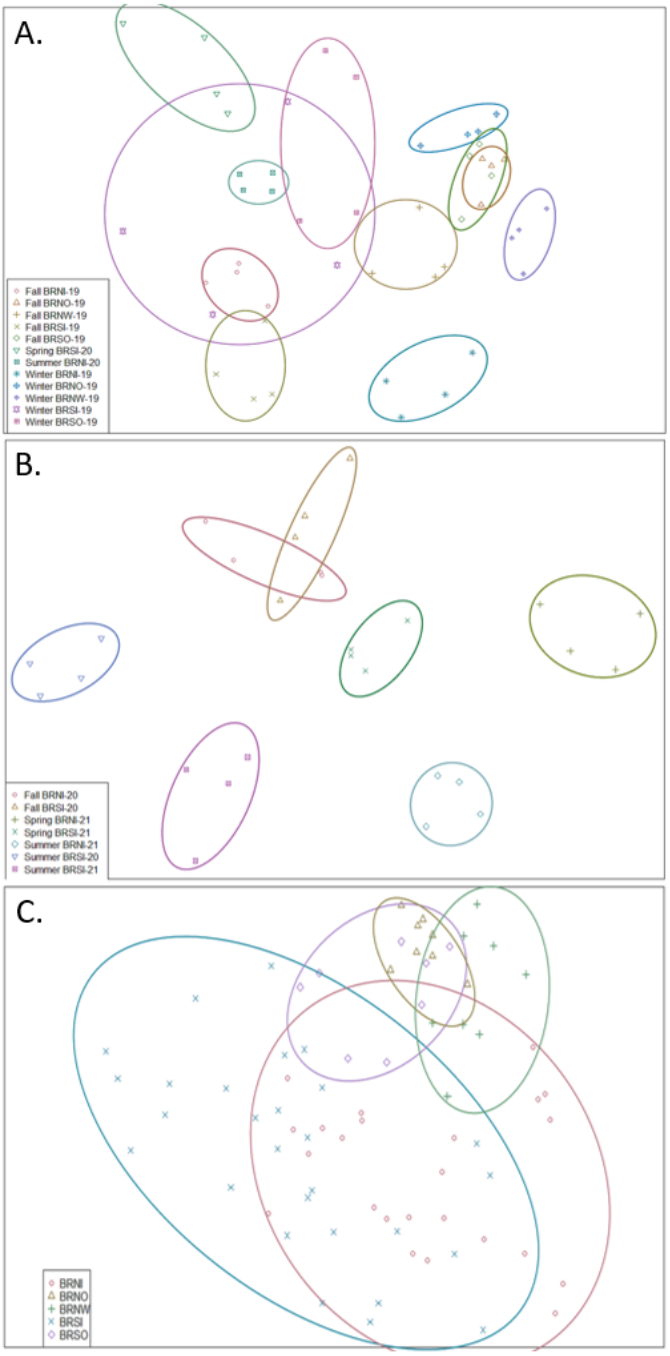

- **n-MDS Stress** 0.1941613
- **ANOSIM**
  - Anosim R: 0.9689
  - P<0.05
- **PERMANOVA**
  - F-statistic: 15.703
  - MS: 0.97178
  - R^2= 0.82753
  - P<0.05

- **n-MDS Stress** 0.1495578
- **ANOSIM**
  - Anosim R: 0.9999
  - P<0.05
- **PERMANOVA**
  - F-statistic: 30.425
  - MS: 1.08996
  - R^2= 0.89683
  - P<0.05

- **n-MDS Stress** 0.2429391
- **ANOSIM**
  - Anosim R: 0.2338
  - P<0.05
- **PERMANOVA**
  - F-statistic: 6.247
  - MS: 1.44352
  - R^2= 0.26033
  - P<0.05

Note: Symbols represent BRN (inside estuary, within port, and outside coastal – BRNI, BRNW, and BRNO, respectively) and BRS (inside estuary and outside coastal – BRSI and BRSO, respectively). Outer coastal and port sites (BRNO, BRNW, and BRSO) were sampled only in Phase 1.

Figure 94. NMDS associations of >25-µm phytoplankton communities based on species and abundances, comparing A) seasons and locations for Phase 1 (2019–2020); B) seasons and locations for Phase 2 (2020–2021); and C) locations only with seasons and years pooled

4.3.3 Conclusions

4.3.3.1 Fish Community Modeling

In Phase 1, the team concluded that the variation in fish community structure, abundance, and distribution in IRL are associated with variation in salinity, temperature, and DO and identified SoI for further study (Florida Tech, 2020; Johnson et al., 2020). In Phase 2, the team built predictive models to quantify the strength of the relationships between these environmental factors and metrics of fish responses. The models were used to provide preliminary projections of nine months of change in abundance and fish community structure.

Seven of the models were able to predict the fish responses with more than 95% accuracy, and only two, Red Drum from gear type 20 and Pinfish from gear type 160, had accuracy less than 50%. The poor performance of the Red Drum model likely stems from the noise generated from lumping all age groups into one abundance estimate. It is known that Red Drum undergo several ontogenetic habitat shifts, preferring structured seagrass beds and mangroves early in life and then shifting toward more open areas as they grow (Bacheler et al., 2009; Moulton et al., 2017; Reyier et al., 2011; Stunz et al., 2001) with complex movement patterns increasing the complexity further (Adams and Tremain, 2000). With changing habitat preferences comes different driving factors of abundance and capture probability. Accurately modeling this species will require a more intensive spatiotemporally mediated age-structured population modeling approach. The Pinfish model showed poor predictive performance, with less than 10% accuracy. Most age classes of Pinfish are captured in gear 160, with 460 records in the BRL data used in this study. They are known to be a hardy fish that capitalizes on many different structured habitats and can frequently be found moving through open water. Habitat and age-structured species distribution models are needed to accurately model the dynamic relationship between this species, and many other fish populations, and changes in the IRL abiotic and biotic conditions.

These results support an important conclusion that each species is expected to respond to increased inflow differently. The valuable recreational sportfish Sheepshead, Spotted Seatrout, and Red Drum; ecologically and economically valuable Pinfish; and ecologically important Gulf Pipefish are projected to increase in abundance. The valuable recreational sportfish Gray Snapper and Black Drum, as well as one of the most abundant low trophic-level fishes, Bay Anchovy, are projected to decrease. Lacking a more nuanced understanding of the complex ecological feedback mechanisms at work in BRL, the fish community response to increasing inflow cannot be generalized yet. Efforts can now be focused on building knowledge of the mechanistic details (i.e., trophic feedbacks, ontogenetic differentiation in movement, spatiotemporal breakpoints).

Significant responses were shown to increased inflow by some of Florida's most economically, ecologically, and recreationally valuable fishes. These models were produced using the best fish community data available for IRL but each net is known to have its own set of biases, strengths, and weaknesses (FWRI, 2009). To overcome these limitations, the FIM program deploys a large number of different types of nets. With the different biases of the nets, the data are not comparable so they must be discussed independently. As a result, each model offers only a piece of the picture. It is also important to note that these initial results are based on projected water quality data, which are still preliminary. As the water quality projections are updated, the fish abundance and community structure models will also be updated. In addition, what is lacking is a mechanistic understanding of the observed patterns. Increased oceanic inflow will result in change. Absent that mechanistic understanding of the patterns, any change in the system drivers will weaken the models' predictive power. These models do not account for ecological feedback loops, interactions between species, ontogenetic changes, density dependent factors, recruitment, or

behavior; all of which are known to be important. The Phase 2 study represents an important and necessary next step toward evaluating the potential impacts of increased oceanic inflow into IRL, but is not the final necessary step.

4.3.3.1.1 Fish and Chl-a

The preliminary analyses of algal associations with fish abundances and community structure suggest significant influences of algae. Negative associations were expected and found, as algal blooms are known to cause physiological stress to fishes (Altieri and Gedan, 2015; Cochrane et al., 2009; Feyrer et al., 2015; Glibert et al., 2014; Macusi et al., 2015). However, some significant positive associations were noted for Black Drum and Gray Snapper with Chl-a. These species are associated with structured benthos so it is possible that the low oxygen conditions typical late in algal blooms (Altieri and Gedan, 2015) push them out making them more readily captured by nets. Along with the abiotic stress algal blooms cause in fishes, they may also influence fish behavior, which could skew their probability of occurring in the FIM data. Further investigations into the mechanisms behind these associations are needed to understand what role they play in altering projections made by the models.

4.3.3.1.2 Fish Movement

The initial meta-analysis of the movement and habitat use of IRL fishes suggests very strong site fidelity associated with spawning episodes and ontogenetic change in habitat and food requirements (Reyier et al., 2020, 2011; Tremain et al., 2004). These findings suggest that changes in IRL water and habitat quality influence recruitment and survivorship of fishes. The association in patterns of variation between fish abundance and water/habitat quality is not unique to IRL; it appears to be ubiquitous in estuarine ecosystems in Florida and the country. Maintenance of optimal environmental conditions and preventing large fluctuations in environmental parameters though mitigating mechanisms, such as the proposed pilot project, may promote the sustainability of estuarine-fish communities.

4.3.3.2 eDNA

Using a combination of samples collected during Phases 1 and 2, detection patterns for fishes were evaluated across the south central IRL, central IRL, and BRL. Sampling during Phase 1 allowed initiation of seasonal sampling and a direct examination of diversity at three candidate sites. Seasonal sampling was completed in Phase 2 with the addition of three sites in BRL to improve resolution of local diversity patterns. Comparison of species occurrence at the designated Phase 2 experimental (E1 and E2) and reference sites (E4 and E26) highlighted the similarity of the fish community prior to initiation of the proposed pilot experiment and demonstrate the strength of the BACI design.

Within site diversity measured by species richness, Shannon diversity, average taxonomic distinctness, and variation in taxonomic distinctness demonstrated a significant decline in diversity from south to north, with the lowest diversity occurring in BRL. A comparison of diversity measures shows that while species richness and Shannon diversity provide similar information about site diversity, both measures of taxonomic distinctness provide complimentary data that, when considered in combination with either of the richness measures, can provide a more detailed understanding of biodiversity structure and response to impacts.

Pairwise estimates of site similarity/dissimilarity highlight the presence of regional drivers of fish diversity, with sites within basins more similar than to sites in other basins. Comparisons with the highest dissimilarity were between sites in BRL and south central IRL. This is in line with previous studies of IRL fishes and ongoing fish modeling that show regional differences in fish diversity

and community structure, and a general pattern of decreasing diversity with increasing latitude (Gilmore, 1981; Snelson, 1983; Tremain and Adam, 1995; Paperno et al., 2001).

Similarity patterns based on eDNA varied somewhat with seasons, likely reflecting seasonal variation in species abundance patterns and habitat in response to changes in temperature, salinity, and ontogenic habitat shifts (Virnstein, 1990; Paperno et al., 2001). However, a clear pattern was seen across all seasons and within the combined dataset confirming patterns indicated in the pairwise tests. Relatively high similarity was seen among sites within each region, with a few exceptions. In the central IRL, fishes detected at sites E9 and E10 were more similar to sites E11 and E12 near Sebastian Inlet than to sites further north, which were less diverse and more distinct. Similarity among adjacent sites may in part be explained by the high site fidelity IRL fishes exhibit. Gilmore (1981) and others have noted the unique diversity of fish communities within or adjacent to IRL inlets, and declining diversity with increasing distance from the inlet. This pattern is thought to reflect both the complexity of habitats found around inlets and the opportunity provided to directly access the lagoon (Gilmore, 1981; Snelson, 1983). Impacts from declining water quality and increasingly frequent HABs are not evenly distributed across IRL, and northern IRL and BRL appear to be particularly vulnerable (Badylak & Phlips, 2004; Phlips et al., 2011).

In line with expectations based on the high frequency of HAB outbreaks in BRL (Gallardo et al., 2011; Phlips et al., 2011), site-specific estimates of taxonomic distinctness compared against a fixed baseline highlight the low taxonomic diversity of fish detected in BRL and comparatively higher taxonomic diversity of fishes in the central and south central IRL. A significant negative bias in measures of taxonomic distinctness has been seen in response to increasing eutrophication levels in freshwater invertebrates (Gallardo et al., 2011), marine plants (Mouillot et al., 2005), and estuarine fishes (Tweedley et al., 2017). More commonly employed diversity measures provided useful data on the status and drivers of biodiversity; however, taxonomic distinctness measures were the only diversity measures to show a direct relationship with water quality condition (Gallardo et al., 2011). This is thought to be because as impacts increase, higher taxonomic groups that are represented by one or a few species are lost. The loss of one or a few species will have little effect on richness-based diversity measures. Yet, the loss of less specious taxonomic groups and maintenance of taxa containing a high number of closely related species will drive down estimates of both average taxonomic distinctness and variation in taxonomic distinctness (Clarke and Warwick, 2001). This pattern can be seen with eDNA detections from BRL revealing a low diversity fish community, even when species richness is relatively high. Sites E9–E12 near Sebastian Inlet stand out as having fish communities that are both species rich and taxonomically diverse, as expected for sites that are buffered against eutrophication impacts (Gallardo et al., 2011; Phlips et al., 2011).

4.3.3.3 Benthic Fauna, Seagrasses, and Phytoplankton

Literature suggests that IRL species may have minimal direct impacts from an influx of coastal water. Species present in estuaries can typically withstand large fluctuations in salinity and temperature compared to ocean species. For instance, fish are among the most motile of estuarine populations, yet an enhanced ability to osmoregulate in changing conditions is required (Allen et al., 2006). Additional examples include estuarine molluscs, which must be adapted to extreme fluctuations of salinity and pollutants (Levinton et al., 2011). Estuarine phytoplankton have a wider salinity tolerance than oceanic phytoplankton, and coastal phytoplankton are intermediate in their tolerance (Brand, 1984). In addition, there is an existing ocean connection through the Port Canaveral Lock, which opens to vessel passage an average of 48 times daily and water levels can change by 3 to 4 feet as water moves from the ocean/port to the estuary (Berman, 2019). With the open lock comes the opportunity for migration, larval transport, and gene flow between coastal and estuarine populations. Diatoms may be transported with water, or

on the boats (Sweat et al., 2017). However, indirect impacts of modest inflow may impact the estuarine ecosystem, such potentially new predators and competitors being introduced, or a shift in existing community balance. Continued biological monitoring throughout the pilot inflow project is critical for documenting changes.

4.3.3.3.1 Seagrass, Rooted Algae, and Drift Algae

Seagrasses provide habitat for other organisms, and a protective nursery for vulnerable developmental stages. They are a food source for numerous animals, and serve to stabilize sediments (Zieman, 1982; Dawes et al., 1995). There are seven species of seagrasses known to occur in IRL estuary; however, the shoal grass *Halodule wrightii* dominates and was the only species documented in the study surveys. Coastal surveys were too deep (>10 m) to conduct via snorkeling, but hundreds of sediment grab samples did not yield incidental seagrass capture. Video evidence by tethered remotely operated vehicle showed no *H. wrightii* on the coastal side of proposed inflow location. Further south in coastal waters, there are likely *H. wrightii* beds living subtidally at depths not possible in the turbid northern IRL. *H. wrightii* would likely inhabit the coastal sites in this study were it not for unhospitable depths and water clarity.

The environmental tolerances of *H. wrightii* are broad. It is eurythermal and euryhaline, with likely optimal temperature tolerance range of 20–30 °C (McMillan, 1982) and reported in Florida to withstand salinities of at least 12–38.5 parts per thousand (Phillips, 1960). *H. wrightii* is also flexible with regard to nutrient and organic sediment levels and can be found in sediments ranging from silty mud to sand with limited organic material (Phillips, 1960). It seems unlikely that *H. wrightii* would be directly harmed by the abiotic environmental changes from restored lagoon inflow. If water clarity improves, *H. wrightii* may even be able to recruit into deeper parts previously inaccessible due to depth and photosynthesis limitations. If the water column becomes less eutrophic, or if sediments have less silt and organic material, shoal grass could benefit from a less polluted and stressful environment. Shoal grass is considered a tolerant pioneer species (Gutierrez, 2010) and, if there is dramatic water quality and sediment improvement, shoal grasses could experience competition for space with other seagrass species. Sufficient information is lacking to predict how *H. wrightii* might be impacted by changes in herbivory or competition due to a shifting ecosystem driven by restored inflow.

Herbivorous fish known to graze on *H. wrightii* include Pinfish (*Lagodon rhomboides*), Surgeonfish (*Acanthurus bahianus* and *A. coeruleus*), and Parrotfish (*Scarus taeniopterus*, *S. iseri*, and *Sparisoma aurofrenatum*). Increases in these fish due to restored inflow would likely increase grazing pressure on *H. wrightii*. The West Indian Manatee is a voracious grazer on *H. wrightii*, but it is not anticipated that restored inflow will greatly change manatee presence directly. Monitoring of seagrasses and grazers during a pilot study would provide data on how inflow impacts seagrasses through water quality changes and, possibly, a shift in grazers.

Results of power analysis on benthic/drift vegetation generally ranged from 0.05–0.35. To differentiate treatments with statistical significance, sample sizes would need to be increased due to the extreme variability of benthic/drift vegetation. Continued monitoring of seagrasses and other vegetation is essential to document and detect any dramatic crashes or improvements in response to a restored inflow pilot study.

4.3.3.3.2 Benthic Fauna

Benthic fauna are key indicators of local environmental conditions due to their unique life histories and, therefore, an important component of monitoring. Their benthic and sessile nature (relative to fishes) renders them unable to easily escape when sediment or water column conditions shift. For this reason, discussion is focused on species whose abundance and presence has been

confirmed in baseline sampling. Infaunal species from prominent taxa dominating the IRL benthic community include six benthic fauna that are abundantly present near the proposed inflow and reference sites. They are considered to hold ecological importance.

The gammarid amphipod *Cymadusa compta* is a ubiquitous amphipod found in throughout IRL in almost all benthic habitats (Zimmerman, 1979; Stoner, 1983). *C. compta* feeds on drift algae, epiphytes, and phyto-detritus (Zimmerman et al., 1979), which are abundantly available in IRL. Temperature and salinity changes in IRL due to inflow are unlikely to directly force the displacement of *C. compta* given its broad physical and chemical tolerances, although if water quality changes were to successfully reduce drift algae, epiphytes, and detritus, *C. compta* might be impacted by reduced food availability. Pinfish and other benthic foraging fish are important predators on *C. compta* (Stoner, 1979 and 1983; Nelson, 1995), and environmental shifts that impact those fish populations could well have an indirect impact on benthic prey like *C. compta*.

The gammarid amphipod *Cerapus tubularis'* distribution, tolerances, and life history are not well-described in the literature, especially for Florida and IRL (NOAA National Benthic Inventory; Felder and Camp, 2009). However, it is consistently present in IRL in medium abundances. It is absent from coastal samples so it should be monitored for impacts due to inflow during a pilot project. This species may be an important food source for benthic foraging fish (Stoner, 1979), and there is the potential for indirect trophic web impacts if inflow changes the ratio of predators.

The gammarid amphipod *Gammarus mucronatus* is thought to occur in brackish estuaries and coastal sediments from the Gulf of St. Lawrence (Nova Scotia) to the Gulf of Mexico (Bousfield, 1969 and 1973). *G. mucronatus* is recognized as strongly eurythermal (Fredette and Diaz, 1986) and euryhaline (Bousfield, 1973), and are not likely to be displaced by seawater influx. They are an important part of the diet of benthic foraging fish, such as the Pinfish *Lagodon rhomboids* (Nelson, 1979 and 1980), Surgeonfish, and Parrotfish. Seawater impact on those fish populations may indirectly impact *G. mucronatus*.

The ostracod crustacean *Eusarsiella zostericola* is eurythermal, occurring from Maine to the Gulf of Mexico, and can tolerate salinities from 22–36 PSU (Kornicker, 1967 and 1986). *E. zostericola* was observed within all IRL sites in all seasons. They are not commonly found in coastal sediments. *E. zostericola* has been an invasive species in some parts of the world, but has not been documented to displace species, nor does it have recognizable trophic impacts through grazing on prey or serving as food for predators (Ruiz et al., 2011).

The bivalve mollusc *Parastarte triquetra* is subtropical to tropical, found from Florida through most of the Caribbean (Abbott and Morris, 1995), and is considered a characteristic species of IRL, where it can occur in densities exceeding 2 x 104 m^{-2} (Mikkelsen et al., 1995). *P. triquetra* was found within IRL at all sites in all seasons. Relatively little is known about the tolerances, life history, and ecological interactions of this bivalve.

The gastropod mollusc *Acteocina canaliculata* is eurythermal, occurring in Maine, the mid-Atlantic, Florida, throughout the Caribbean, and as far south as Suriname (Brunel et al., 1998,; Rosenberg et al., 2009). They are found in sediments with >38% silt-clay content (Kennish et al., 2004; Flanagan et al., 2018). In IRL, this level of silt-clay tends to accompany polluted organic sediments. Coastal sediments rarely have this level of silt-clay, and may explain why *A. canaliculata* was not found at the coastal sites. Franz (1971) collected individuals in water that varied 28–31 PSU in salinity, but their occurrence throughout IRL makes it almost certain they can withstand lower salinities.

It is recommended that monitoring of benthic fauna be ongoing before, during, and after the implementation of a pilot inflow project. Continued baseline monitoring ahead of pilot pumping is advisable to have a better understanding of the biology and ecology. Biological populations are variable, and that variation increases with seasonal changes. The pre-pilot monitoring data will help to differentiate changes due to inflow (Giovannoni and Vergin, 2012; Kroodsma et al., 2018).

4.3.3.3.3 Phytoplankton/Harmful Algae

Phytoplankton are drifting microalgae of various taxa (e.g., dinoflagellates, diatoms, nanoflagellates), and can be responsible for harmful or toxic algal blooms. Phytoplankton, by definition, drift with currents. Monitoring their distributions is challenging, because they are variable and patchy in time and space (Bengfort et al., 2006; Trudnowsky et al., 2016; Breier et al., 2018). Phytoplankton data were collected using two different methods for this evaluation.

There are at least 82 species of diatoms comprising the phytoplankton community in the proposed IRL inflow and reference sites. At least one of these genera (Pseudo-nitzschia) is a known toxin (domoic acid) producer and a HAB species in other systems. Pseudo-nitzschia has not, however, contributed to the IRL HABs of concern within the last decade. There are least 16 species of dinoflagellates confirmed to occur near the proposed inflow site. At least four genera or species (*Gymnodinium*, *Dinophysis*, *Gonyaulax*, and *Pyrodinium bahamense*) are known toxin producers and form HABs in other systems. Only *P. bahamense*, however, has bloomed and created trophic web toxicity in IRL within the last decade. Most of the IRL HABs have been smaller cells that are difficult to identify without genetic confirmation. There have been substantial HABs of the smaller-celled bloom species measured in this study, including non-cyanobacterial cells, cyanobacteria with phycocyanin pigments, and cyanobacteria with phycoerythrin pigments. These species play a role in the planktonic ecosystem, and could be directly or indirectly impacted by changes in estuarine water quality.

HABs caused by phytoplankton create turbidity and attenuate light and have caused the death of tens-of-thousands-of-acres of IRL seagrasses (Tetra Tech, 2016). Should an inflow project be implemented, one of the most positive potential outcomes would be a reduction in frequency and severity of IRL HABs. For the toxic and otherwise harmful dinoflagellates, diatoms, and cyanobacteria, there are now baseline lists and concentrations at the inflow site. With continued monitoring of phytoplankton and HABs, seasonal variation will be better understood and treatment impacts more certain.

5 References

Abbott, R.T. and Morris, P.A. 1995. A Field Guide to Shells: Atlantic and Gulf Coasts and the West Indies. New York: Houghton Mifflin, 73.

Accoroni, S., Romagnoli, T., Pichierri, S., and Totti, C. 2016. Effects of the bloom of harmful benthic dinoflagellate Ostreopsis cf. ovata on the microphytobenthos community in the northern Adriatic Sea. Harmful Algae, 55, 179-190.

Adams, D.H. and Tremain, D.M. 2000. Association of large juvenile red drum, Sciaenops ocellatus, with an estuarine creek on the Atlantic coast of Florida. Environ. Biol. Fishes 58, 183–194. https://doi.org/10.1023/A:1007614930445.

Adams, D.H., Tremain, D.M., Paperno, R., and Sonne, C. 2019. Florida lagoon at risk of ecosystem collapse. Science, 365(6457), 991-992.

Aho, K., Derryberry, D., and Peterson, T. 2014. Model selection for ecologists: the worldviews of AIC and BIC. Ecology 95, 631–636.

Allen, L., Lokyavich, M., Cailliet, G., and M. Horn. 2006. Ch.5 Bays and Estuaries, In: The Ecolog of Marine Fishes: California and Adjacent Waters (eds: Allen, L, Pondella, D., and M. Horn). University of California Press, Berkeley. 659 pp.

Almasi, M. 1985. The Importance of Inlets and Sea Level in the Development of Hutchinson Island and the Indian River Lagoon. In: The Indian River Lagoon: Proceedings of the Indian River Resources Symposium. D. Barile (ed). The Marine Resources Council, Rockledge Florida.

Altieri, A.H. and Gedan, K.B. 2015. Climate change and dead zones. Glob. Chang. Biol. 21, 1395–1406. https://doi.org/10.1111/gcb.12754.

Anderson, M.J. 2005. Permutational multivariate analysis of variance. Department of Statistics, University of Auckland, Auckland, 26, 32-46.

Anderson, M.J. 2014. Permutational multivariate analysis of variance (PERMANOVA). Wiley statsref: statistics reference online, 1-15.

Azanza, R.V., Siringan, F.P., San Diego-Mcglone, M.L., Yniguez, A.T., Macalalad, N.H., Zamora, P.B., Agustin, M.B., and Matsuoka, K. 2004. Horizontal dinoflagellate cyst distribution, sediment characteristics and benthic flux in Manila Bay, Philippines. Phycological Research 52(4):376-386.

Bacheler, N.M., Paramore, L.M., Burdick, S.M., Buckel, J.A., and Hightower, J.E. 2009. Variation in movement patterns of red drum (Sciaenops ocellatus) inferred from conventional tagging and ultrasonic telemetry. Fish. Bull. 107, 405–419.

Badylak, S. and Phlips, E. J. 2004. Spatial and temporal patterns of phytoplankton composition in subtropical coastal lagoon, the Indian River Lagoon, Florida, USA. Journal of plankton research, 26(10), 1229-1247.

Bengfort, M., Feudel, U., Hilker, F.M., and Malchow, H. 2014. "Plankton blooms and patchiness generated by heterogeneous physical environments." Ecological complexity 20 (2014): 185-194.

Berman, D. 2019. Canaveral Lock at Port Canaveral to close to boaters for four months for repairs. Florida Today, 30 July 2019. https://www.floridatoday.com/story/news/2019/07/30/canaveral-lock-port-canaveral-close-four-months-repairs/1864684001/.

Berry, T.E., Osterrieder, S.K., Murray, D.C., Coghlan, M.L., Richardson, A.J., Grealy, A.K., Stat, M., Bejder, L., and Bunce, M. (2017). DNA metabarcoding for diet analysis and biodiversity: A case study using the endangered Australian sea lion (Neophoca cinerea). Ecology and Evolution, 7(14), 5435-5453.

Bilskie, M.V., Bacopoulos, P., and Hagen, S.C. 2019. Astronomic tides and nonlinear tidal dispersion for a tropical coastal estuary with engineered features (causeways): Indian River lagoon system. Estuarine, Coastal and Shelf Science, 216, 54-70.

Blanchard, J.R. 2018. A confluence of invasion, behavioral, and theoretical ecology: what drives ephemeral metacommunity re-assembly? Florida International University. https://doi.org/10.25148/etd.FIDC006532.

Blanchard, J.R., Santos, R.O., and Rehage, J.S. 2021. Sociability interacts with temporal environmental variation to spatially structure metapopulations: A fish dispersal simulation in an ephemeral landscape. Ecol. Modell. 443. https://doi.org/https://doi.org/10.1016/j.ecolmodel.2021.109458.

Bluff Manufacturing. 2019. Crossover Ramp. Retrieved from Bluff Manufacturing, Inc.: www.bluffmanufacturing.com/yard-ramps/crossover-ramps-fracking-ramps/#gsc.tab=0.

Bluff Manufacturing. 2021. Quote 110363.

Bonte, D., Van Dyck, H., Bullock, J.M., Coulon, A., Delgado, M., Gibbs, M., Lehouck, V., Matthysen, E., Mustin, K., Saastamoinen, M., Schtickzelle, N., Stevens, V.M., Vandewoestijne, S., Baguette, M., Barton, K., Benton, T.G., Chaput-Bardy, A., Clobert, J., Dytham, C., Hovestadt, T., Meier, C.M., Palmer, S.C.F., Turlure, C., and Travis, J.M.J., 2012. Costs of dispersal. Biol. Rev. 87, 290–312. https://doi.org/10.1111/j.1469-185X.2011.00201.x.

Bousfield, E.L. 1969. New records of Gammarus (Crustacea: Amphipoda) from the Middle Atlantic Region. Chesapeake Science 10:1-17.

Bousfield, E.L. 1973. Shallow-water gammaridean Amphipoda of New England. Cornell University Press, Ithaca, New York. 312p.

Boynton, W.R., Ceballos, M.A.C., Bailey, E.M., Hodgkins, C.L.S. Humphrey, J.L., and Testa, J.M. 2018. Oxygen and nutrient exchanges at the sediment-water interface: a global synthesis and critique of estuarine and coastal data. Estuaries and Coasts 41:301-333.

Brady, D.C., Testa, J.M., Di Toro, D.M., Boynton, W.R., and Kemp, W.M. 2013. Sediment flux modeling: calibration and application for coastal systems. Estuarine, Coastal and Shelf Science 117:107-124.

Brand, L. 1984. The salinity tolerance of forty-six marine phytoplankton isolates. Estuarine, Coastal and Shelf Science, 1984, Volume 18, Issue 5.

Brech, A. 2004. Neither Ocean Nor Continent: Correlating the Archaeology and Geomorphology

of the Barrier Islands of East Central Florida. MS Thesis, University of Florida, Gainesville.

Breier, R.E., Lalescu, C.C., Waas, D., Wilczek, M., and Mazza, M.G. 2018. "Emergence of phytoplankton patchiness at small scales in mild turbulence." Proceedings of the national academy of sciences 115, no. 48 (2018): 12112-12117.

Brunel, P., Bosse, L., and Lamarche, G. 1998. Catalogue of the marine invertebrates of the estuary and Gulf of St. Lawrence. Canadian Special Publication of Fisheries and Aquatic Sciences, 126. 405 p.

Burford, M.A., Davis, T.W., Orr, P.T., Sinha, R., Willis, A., and Neilan, B.A. 2014. Nutrient-related changes in the toxicity of field blooms of the cyanobacterium Cylindrospermopsis raciborskii. FEMS Microbiology and Ecology 89:135–148, https://doi.org/10.1111/1574-6941.12341.

Callahan, B.J., McMurdie, P.J., Rosen, M.J., Han, A.W., Johnson, A.J.A., and Holmes, S.P. 2016. DADA2: High-resolution sample inference from Illumina amplicon data. Nature Methods, 13, 581-583. doi: 10.1038/nmeth.3869.

Carere, C. and Gherardi, F. 2013. Animal personalities matter for biological invasions. Trends Ecol. Evol. 28, 5–6. https://doi.org/10.1016/j.tree.2012.10.006.

Cavender-Bares, K.K., Karl, D.M., and Chisholm, S.W. 2001. Nutrient gradients in the western North Atlantic Ocean: Relationships to microbial community structure and comparison to patterns in the Pacific Ocean. Deep-Sea Research I 2373-2395.

CDM Smith in association with Taylor Engineering. 2014. Preliminary Concept Design for Artificial Flushing Projects in the Indian River Lagoon – Phase I Literature Review/Preliminary Site Selection. Prepared for the St. Johns River Water Management District.

CDM Smith in association with Taylor Engineering. 2015. Preliminary Concept Design for Artificial Flushing Projects in the Indian River Lagoon – Phase II Conceptual Design/Project Refinement. Prepared for the St. Johns River Water Management District.

CDM Smith in association with Taylor Engineering. 2017. Conceptual Design for Artificial Flushing Projects in the Indian River Lagoon, Draft Report August 2017, Conceptual Design and Conceptual Cost Estimates for Pilot Testing. Prepared for the St. Johns River Water Management District.

Chen, B., Kang, W., and Hui, L. 2019. Akashiwo sanguinea blooms in Chinese waters in 1998–2017. Marine Pollution Bulletin, 149, 110652.

Choudhury, A.K. and Bhadury, P. 2015. Relationship between N:P:Si ratio and phytoplankton community composition in a tropical estuarine mangrove ecosystem. Biogeosciences Discussions 12:2307-2355.

Clarke, K.R. and Warwick, R.M. 2001. A further biodiversity index applicable to species lists: variation in taxonomic distinctness. Marine ecology Progress series, 216, 265-278.

Cochrane, K., De Young, C., Soto, D., and Bahri, T. 2009. Climate change implications for fisheries and aquaculture: Overview of current scientific knowledge.

Comprehensive Everglades Restoration Plan. 2006. Guidelines for Manatee Conservation During Comprehensive Everglades Restoration Plan Implementation. Retrieved from U.S. Fish and Wildlife Service: www.fws.gov/verobeach/MammalsPDFs/CERPManateeGuidelines120806.pdf?spcode=A007.

Cooksey, C. and Hyland, J. 2007. Sediment quality of the Lower St. Johns River, Florida: An integrative assessment of benthic fauna and general characteristics. Marine Pollution Bulletin 54:9–21.

Cowan, J.L.W. and Boynton, W.R. 1996. Sediment-water oxygen and nutrient exchanges along the longitudinal axis of Chesapeake Bay: seasonal patterns, controlling factors and ecological significance. Estuaries 19:562-580.

Cruaud, P., Rasplus, J.Y., Rodriguez, L.J., and Cruaud, A. 2017. High-throughput sequencing of multiple amplicons for barcoding and integrative taxonomy. Scientific reports, 7(1), 1-12.

Dawes C.J., Hanisak D., and Kenworthy, J.W. 1995. Seagrass biodiversity in the Indian River Lagoon. Bull Mar Sci 57: 59-66.

Deagle, B.E., Gales, N.J., Evans, K., Jarman, S.N., Robinson, S., Trebilco, R., and Hindell, M.A. 2007. Studying seabird diet through genetic analysis of faeces: a case study on macaroni penguins (Eudyptes chrysolophus). PLoS One, 2(9), e831.

Defne, Z. and Ganju, N.K. 2015. Quantifying the residence time and flushing characteristics of a shallow, back-barrier estuary: application of hydrodynamic and particle tracking models. Estuaries and Coasts 38:1719-1734.

DeYoe, H.R., Buskey, E.J., and Jochem, F.J. 2007. Physiological responses of Aureoumbra lagunensis and Synechococcus sp. to nitrogen addition in a mesocosm experiment. Harmful Algae, 6(1), 48-55.

Diaz, R.J., and Rosenberg, R. 2008. Spreading dead zones and consequences for marine ecosystems. Science 321:926-929.

DiDonato, G.T., Murrell, E.M., Lores, M.C., Smith, L.M. and Caffrey, J.M. 2006. Benthic nutrient flux in a small estuary in northwest Florida (USA). Gulf and Caribbean Research 18:15-26.

Dutka-Gianelli, J., Taylor, R., Nagid, E., Whittington, J., and Johnson, K., 2011. Habitat Utilization and Resource Partitioning of Apex Predators in Coastal Rivers of Southeast Florida, Library. https://doi.org/FWRI Library No. F2771-07-11-F.

Eble, J.A., Daly-Engel, T.S., DiBattista, J.D., Koziol, A., and Gaither, M.R. 2020. Marine environmental DNA: Approaches, applications, and opportunities. Advances in Marine Biology, 86(1), 141-169.

ElectricRate. 2020. Electricity Rates By State. Retrieved from https://www.electricrate.com/electricity-rates-by-state/.

FDEP. 2013. Indian River Lagoon Basin, Banana River Lagoon Basin Management Action Plan.

Felder, D.L., and Camp, D.K. 2009. eds. Gulf of Mexico origin, waters, and biota: Biodiversity. Texas A&M University Press.

Feyrer, F., Cloern, J.E., Brown, L.R., Fish, M.A., Hieb, K.A., and Baxter, R.D. 2015. Estuarine fish communities respond to climate variability over both river and ocean basins. Glob. Chang. Biol. 21, 3608–3619. https://doi.org/10.1111/gcb.12969.

Ficetola, G.F., Taberlet, P., and Coissac, E. 2016. How to limit false positives in environmental DNA and metabarcoding?

Flanagan, A.M., Flood, R.D., Frisk, M.G., Garza, C.D., Lopez, G.R., et al. 2018. The relationship between observational scale and explained variance in benthic communities. PLoS One; San Francisco Vol. 13, Iss. 1, (Jan 2018): e0189313. DOI:10.1371/journal.pone.0189313.

Florida Tech. 2020. Restore Lagoon Inflow Research (Phase 1) Summary Report.

Foster, S.Q. and Fulweiler, R.W. 2019. Estuarine sediments exhibit dynamic and variable biogeochemical responses to hypoxia. Journal of Geophysical Research: Biogeosciences 124:737-758.

Fox, A.L. and Trefry, J.H. 2018. Environmental dredging to remove fine-grained, organic-rich sediments and reduce inputs of nitrogen and phosphorus to a subtropical estuary. Marine Technology Society 52: 42-57.

Franz, D.R. "Development and metamorphosis of the gastropod Acteocina canaliculata (Say)." Transactions of the American Microscopical Society (1971): 174-182.

Fredette, T.J. and Diaz, R.J. 1986. Life history of Gammarus mucronatus Say (Amphipoda: Gammaridae) in warm temperate estuarine habitats, York River, Virginia. Journal of Crustacean Biology 6:57-78.

Froese, R., Palomares, M.L.D., and Pauly, D. 1992. Draft user's manual of FishBase, a biological database on fish. ICLARM Software.

Froese, R. and Pauly, D. 2020. FishBase [WWW Document]. World Wide Web Electronic Publication. www.fishbase.org.

FWC. 2021. 2021 Preliminary Manatee Mortality Table with 5-Year Summary From: 01/01/2021 To: 08/27/2021. Marine Mammal Pathobiology Laboratory.

FWRI. 2009. Fisheries-Independent Monitoring Program Procedure Manual.

Gallardo, B., Gascón, S., Quintana, X., and Comín, F. A. 2011. How to choose a biodiversity indicator–Redundancy and complementarity of biodiversity metrics in a freshwater ecosystem. Ecological indicators, 11(5), 1177-1184.

Ghosh, A.K., Pattnaik, A.K., and Ballatore, T.J. 2006. Chilika lagoon: restoring ecological balance and livelihoods through re-salinization. Lakes Reserv. Res. Manag. 11, 239–255. doi: 10.1111/j.1440-1770.2006.00306.x.

Gilmore, R.G. 1995. Environmental and Biogeographic Factors Influencing Ichthyofaunal Diversity: Indian River Lagoon. Bull. Mar. Sci. 57, 153–170.

Gilmore, R.G., Donohoe, C.J., Cooke, D.W., and Herrema, D.J. 1981. Fishes of the Indian River Lagoon and adjacent waters, Florida. Harbor Branch Foundation. Inc., Tech. Rpt, (41), 1-36.

Giovannoni, S.J. and Vergin, K.L. 2012. "Seasonality in ocean microbial communities." Science 335, no. 6069 (2012): 671-676.

Glibert, P.M., Dugdale, R.C., Wilkerson, F., Parker, A.E., Alexander, J., Antell, E., Blaser, S., Johnson, A., Lee, J., Lee, T., Murasko, S., and Strong, S. 2014. Major - but rare - spring blooms in 2014 in San Francisco Bay Delta, California, a result of the long-term drought, increased residence time, and altered nutrient loads and forms. J. Exp. Mar. Bio. Ecol. 460, 8–18. https://doi.org/10.1016/j.jembe.2014.06.001.

Glibert, P.M., Burkholder, J.M., and Kana, T.M. 2012. Recent insights about relationships between nutrient availability, forms, and stoichiometry, and the distribution, ecophysiology, and food web effects of pelagic and benthic Prorocentrum species. Harmful Algae, 14, 231-259.

Google. 2021. Google Earth. Retrieved from earth.google.com/web/@28.40800523,-80.63589592,4.26711183a,1057.64197548d,30.00002933y,0h,0t,0r.

Guo, H., Guan, C., Yang, L., and Lu, D. 2017. Pseudo-nitzschia species. Conditions promoting extreme Pseudo-nitzschia events in the eastern Pacific but not the western Pacific, PICES Report No. 53:20-27.

Gutierrez, M. A., Cardona, A. A., and Smee, D. L. 2010. Growth patterns of shoal grass Halodule wrightii and manatee grass Syringodium filiforme in the western Gulf of Mexico. Gulf and Caribbean Research, 22(1), 71-75.

Hammond, D.E., Cummins, K.M., McManus, J., Berelson, W.M., Smith, G., and Spagnoli, F. 2004. Methods for measuring benthic nutrient flux on the California margin: comparing shipboard core incubations to in situ lander results. Limnology and Oceanography 2:146.

Harper, H.H. 2021. Canaveral Port Authority Water Quality Monitoring Program. Prepared for Canaveral Port Authority Environmental Plans and Programs, 31p.

Hauss, H., Franz, J.M., and Sommer, U. 2012. Changes in N: P stoichiometry influence taxonomic composition and nutritional quality of phytoplankton in the Peruvian upwelling. Journal of sea Research, 73:74-85.

Harwood, D.W. 2003. Review of Truck Characteristics as Factors in Roadway Design. Transportation Research Board.

Heiri, O., Lotter, A.F., and Lemcke, G. 2001. Loss on ignition as a method for estimating organic and carbonate content in sediments: reproducibility and comparability of results. Journal of Paleolimnology 25:101-110.

Hillebrand, H., Steinert, G., Boersma, M., Malzahn, A., Meunier, C.L., Plum, C., and Ptacnik, R. 2013. Goldman revisited: Faster-growing phytoplankton has lower N:P and lower stoichiometric flexibility. Limnology and Oceanography 58:2076-2088.

Humphries, R. and Robinson, S. 1995. Assessment of the success of the Peel Harvey estuary system management strategy-a western Australian attempt at integrated catchment management. Water Sci. Technol. 32, 255–264. doi: 10. 2166/wst.1995.0619.

Huot, Y., Babin, M., Bruyant, F., Grob, C., Twardowski, M.S., and Claustre, H. 2007. Does chlorophyll a provide the best index of phytoplankton biomass for primary productivity studies? Biogeosciences Discuss. 4, 707–745.

IRL National Estuary Program. 2020. Looking Ahead to 2030: A 10-Year Comprehensive Conservation and Management Plan for the Indian River Lagoon, Florida.

Johnson, K.B., Turingan, R.G., Eble, J., Shenker, J., and Blanchard, J.R. 2020. Restore Lagoon Inflow Research Project (Phase 1) Task 2, Biological Monitoring.

Kaiser, M.J. 2017. FERC pipeline decommissioning cost in the U.S. Gulf of Mexico, 1995–2015. Retrieved from Marine Policy, Volume 82, Pages 167-180: https://doi.org/10.1016/j.marpol.2017.05.006.

Kemp, W.M., Sampou, P., Caffrey, J., Mayer, M., Henriksen, K., and Boynton, W.R. 1990. Ammonium recycling versus denitrification in Chesapeake Bay sediments. Limnology and Oceanography 35:1545-1563.

Kemp, W.M., Sampou, P.A., Garber, J., Tuttle, J., and Boynton, W.R. 1992. Seasonal depletion of oxygen from bottom waters of Chesapeake Bay: relative roles of benthic and planktonic respiration and physical exchange processes. Marine Ecology Progress Series 85:137.

Kennish, M.J., Haag, S.M, Sakowicz, G.P., and Durand, J.B. 2004. Benthic Macrofaunal Community Structure along a Well-Defined Salinity Gradient in the Mullica River-Great Bay Estuary. Journal of Coastal Research, suppl. Special Issue; Fort Lauderdale Vol. SI, Iss. 45: 209-226.

Kornicker, L.S. 1967. A study of three species of Sarsiella (Ostracoda: Myodocopina). Proceedings of the United States National Museum 122(3594): 1–46, 4 pls.

Kornicker, L.S. 1986. Sarsiellidae of the Western Atlantic and Northern Gulf of Mexico, and revision of the Sarsiellinae (Ostracoda: Myodocopina).

Kroodsma, D.A., Mayorga, J., Hochberg, T., Miller, N.A., Boerder, K., Ferretti, F., Wilson, A., Bergman, B., White, T.D., Block, B.A., Woods, P., Sullivan, B., Costello, C., and Worm, B. 2018. Tracking the global footprint of fisheries. Science 359, no. 6378 (2018): 904-908.

Lapointe, B.E., Herren, L.W., Brewton, R.A., and Alderman, P.K. 2020. Nutrient over-enrichment and light limitation of seagrass communities in the Indian River Lagoon, an urbanized subtropical estuary. Science of the Total Environment 699:134068.

Lefebvre, L.W., Provancha, J., Slone, D., and Kenworthy, W. 2016. Manatee grazing impacts on a mixed species seagrass bed. Marine Ecology Progress Series. 564. 10.3354/meps11986.

Leray, M., Yang, J.Y., Meyer, C.P., Mills, S.C., Agudelo, N., Ranwez, V., Boehm, J.T., and Machida, R.J. 2013. A new versatile primer set targeting a short fragment of the mitochondrial

COI region for metabarcoding metazoan diversity: application for characterizing coral reef fish gut contents. Frontiers in zoology, 10(1), 1-14.

Levinton, M.D., Ralston, D., Starke, A., and Allam, B. 2011. Climate change, precipitation and impacts on an estuarine refuge from disease. PLoS One, 6 (2011), p. e18849.

Li, F., Zhou, Y., Zhang, X., Tang, J., Yang, Q., Zhang, Y., Luo, Y., Hu, J., Xue, W., Qiu, Y., He, Q., Yang, B., and Zhu, F. 2020. SSizer: determining the sample sufficiency for comparative biological study. Journal of molecular biology, 432(11), 3411-3421.

Li, Y., Tang, C., Wang, C., Anim, D., Yu, Z., and Acharya, K., 2013. Improved Yangtze River Diversions: Are they helping to solve algal bloom problems in Lake Taihu, China, Ecological Engineering, Vol. 51, 104-116. doi:10.1016/j.ecoleng.2012.12.077.

Lillebo, A.I., Neto, J.M., Martins, L., Verdelhos, T., Leston, S., and Cardoso, P.G. 2005. Management of a shallow temperate estuary to control eutrophication: the effect of hydrodynamics on the system's nutrient loading. Estuar. Coast. Shelf S. 65, 697-707.

Liu, H., Laws, E.A., Villareal, T.A., and Buskey, E.J. 2001. Nutrient-limited growth of aureoumbra lagunensis (pelagophyceae), with implications for its capability to outgrow other phytoplankton species in phosphate-limited environments. Journal of Phycology 37(4): 500-508.

Macusi, E.D., Abreo, N.A.S., Cuenca, G.C., Ranara, C.T.M., and Deepananda, A. 2015. The Potential Impacts of Climate Change on Freshwater Fish, Fish Culture and Fishing Communities. J. Nat. Stud. 14, 1689–1699. https://doi.org/10.1017/CBO9781107415324.004.

Marine Resources Council. 2018. Indian River Lagoon Health Update.

Martiny, A.C., Vrugt, J.A., and Lomas, M.W. 2014. Concentrations and Ratios of Particulate organic carbon, nitrogen, and phosphorus in the Global Ocean. Scientific Data 140048(2014).

Maso, M., Garces, E. 2006. Harmful microalgae blooms (HAB); problematic and conditions that include them. Marine pollution bulletin 53(10-12)620-630.

Mason, W.T., Jr. 1998. Macrobenthic monitoring in the lower St. Johns River, Florida. Environmental Monitoring and Assessment 50:101-130.

McMillan, C. 1982. Reproductive physiology of tropical seagrasses. Aquatic Botany 14 (1982): 245-258.

Mikkelsen, P.M., Mikkelsen, P.S., and Karlen, D.J. 1995. "Molluscan biodiversity in the Indian River lagoon, Florida." Bulletin of Marine Science 57, no. 1 (1995): 94-127.

Mouillot, D., Gaillard, S., Aliaume, C., Verlaque, M., Belsher, T., Troussellier, M., and Do Chi, T. 2005. Ability of taxonomic diversity indices to discriminate coastal lagoon environments based on macrophyte communities. Ecological Indicators, 5(1), 1-17.

Moulton, D.L., Dance, M.A., Williams, J.A., Sluis, M.Z., Stunz, G.W., and Rooker, J.R. 2017. Habitat Partitioning and Seasonal Movement of Red Drum and Spotted Seatrout. Estuaries and Coasts 40, 905–916. https://doi.org/10.1007/s12237-016-0189-7.

Morris, L., Hall, L., Miller, J., Lasi, M., Chamberlain, R., Virnstein, R., and Jacoby, C. 2021. Diversity and distribution of seagrasses as related to salinity, temperature, and availability of light in the Indian River Lagoon, Florida. 84. 119-137.

Morris, L.J., Hall, L.M., and Virnstein, R.W. 2001. Field guide for fixed seagrass transect monitoring in the Indian River Lagoon. St. Johns River Water Management District, Palatka, Florida.

MWI Pumps. 2020. Axial Flow Pump Curves: Pump Bowl Performance Curves. Retrieved from MWI Pumps - Moving Water Industries: mwipumps.com/axial-flow-curves/.

MWI Pumps. 2021. Quote From MWI Pumps.

Nelson, W.G. 1979. Experimental studies of selective predation on amphipods: Consequences for amphipod distribution and abundance. Journal of Experimental Marine Biology and Ecology 38:225-245.

Nelson, W.G. 1980. The biology of eelgrass (Zostera marina L.) amphipods. Crustaceana 39:59-89.

Nelson, W.G. 1995. Amphipod crustaceans of the Indian River Lagoon: current status and threats to biodiversity. Bulletin of Marine Science 57:143-152.

NOAA National Benthic Inventory: https://products.coastalscience.noaa.gov/nbi/.

ODOT. 2014. Hydraulics Design Manual. Retrieved from Oregon Department of Transportation: www.oregon.gov/odot/GeoEnvironmental/Docs_Hydraulics_Manual/HDM_Complete.pdf.

Pandit, A., Heck, H.H., Berber, A., Al-Taliby, W., and Mamoua, K. 2017. Sediment Survey and Fluxes of Nutrients from Sediments and Groundwater in the Northern Indian River Lagoon, Florida (Part III). Annual report submitted to SJRWMD for Contract # 27815.

Paperno, R. 2002. Age-0 Spot (Leiostomus xanthurus) from Two Estuaries Along Central Florida's East Coast: Comparisons of the Timing of Recruitment, Seasonal Changes in Abundance, and Rates of Growth and Mortality. Florida Scientist 65:85–99.

Paperno, R., Mille, K. J., and Kadison, E. 2001. Patterns in species composition of fish and selected invertebrate assemblages in estuarine subregions near Ponce de Leon Inlet, Florida. Estuarine, Coastal and Shelf Science, 52(1), 117-130.

Peterson, J.K., Hansen, J.W., Laursen, M.B., Clausen, P., Carstensen, J., and Conley, D.J. 2008. Regime Shift in a Coastal Marine Ecosystem, Ecological Applications, 497-510.

Phillips, R.C. 1960. Observations on the ecology and distribution of the Florida seagrasses. Professional Paper Series No. 2. Florida State Board Conserv Mar Lab, St. Petersburg, FL.

Phlips, E.J., Badylak, S., Christman, M.C., and Lasi, M.A. 2010. Climatic trends and temporal patterns of phytoplankton composition, abundance and succession in the Indian River Lagoon, Florida, USA. Estuaries and Coasts, 33: 498-512.

Phlips, E.J., Badylak, S., Christman, M., Wolny, J., Brame, J., Garland, J., Hall, L., Hart, J., Landsberg, J., Lasi, M., Lockwood, J., Paperno, R., Scheidt, D., Staples, A., and Steidinger, K. 2011. Scales of temporal and spatial variability in the distribution of harmful algae species in the Indian River Lagoon, Florida, USA. Harmful Algae, 10(3), 277-290.

Provancha, J.A., and Hall, C.R. 1991. Observations of associations between seagrass beds and manatees in east Central Florida. Florida Scientist 54:87-98.

Provancha, J.A. and Provancha, M.J. 1988. Long-term trends in abundance and distribution of manatees (*Trichechus manatus*) in the northern Banana River, Brevard County, Florida. Marine Mammal Science, 4: 323–328.

Rabouille, C., Lansard, B., Owings, S.M., Rabalais, N.N., Bombled, B., Metzger, E., Richirt, J., Eitel, E.M., Boever, A.D., Beckler, J.S., and Taillefert, M. 2021. Early Diagenesis in the Hypoxic and Acidified zone of the northern Gulf of Mexico: is organic matter recycling in sediments disconnected from the water column? Frontiers in Marine Science. 8:604330. doi: 10.3389/fmars.2021.604330.

Reyier, E.A., Lowers, R.H., Scheidt, D.M., and Adams, D.H. 2011. Movement patterns of adult red drum, Sciaenops ocellatus, in shallow Florida lagoons as inferred through autonomous acoustic telemetry. Environ. Biol. Fishes 90, 343–360. https://doi.org/10.1007/s10641-010-9745-3.

Reyier, E.A., Scheidt, D.M., Stolen, E.D., Lowers, R.H., Holloway-Adkins, K.G., and Ahr, B.J. 2020. Residency and dispersal of three sportfish species from a coastal marine reserve: Insights from a regional-scale acoustic telemetry network. Glob. Ecol. Conserv. 23, e01057. https://doi.org/10.1016/j.gecco.2020.e01057.

Rosenberg, G., Moretzsohn, F., García, E. F. 2009. Gastropoda (Mollusca) of the Gulf of Mexico, Pp. 579–699 in: Felder, D.L. and D.K. Camp (eds.), Gulf of Mexico–Origins, Waters, and Biota. Texas A&M Press, College Station, Texas.

RSMeans. 2021. Retrieved from RSMeans Data Online from Gordian: rsmeansonline.com/ManageEstimate.

Ruiz, G., Fofonoff, P., Steves, B., and Dahlstrom, A. 2011. "Marine crustacean invasions in North America: a synthesis of historical records and documented impacts." In in the Wrong Place-Alien Marine Crustaceans: Distribution, Biology and Impacts, pp. 215-250. Springer, Dordrecht.

Saberi, A. and Weaver, R. 2016. Simulating Tidal Flushing Response to the Construction of a Low-Crested Weir Connecting Port Canaveral to the Banana River, Florida. Journal of Waterway, Port, Coastal, and Ocean Engineering 10.1061/(ASCE)WW.1943-5460.0000337, 05016002.

Schallenberg, M., Larned, S.T., Hayward, S., and Arbuckle, C. 2010. Contrasting effects of managed opening regimes on water quality in two intermittently closed and open coastal lakes. Estuar. Coast. Shelf S. 86, 587–597. doi: 10.1016/j.ecss.2009.11.001.

Scheidt, D. 2021a. Recent Seagrass Trends in the Banana River at Kennedy Space Center, Florida In Support of Restore Lagoon Inflow Project: Prepared by Herdon Solutions Group. Kennedy Space Center Environmental Monitoring, NASA.

Scheidt, D. 2021b. Summary of Manatee Use Trends in the Banana River at Kennedy Space Center, Florida In Support of Restore Lagoon Inflow Project, Florida Tech: Prepared by Herdon Solutions Group. Kennedy Space Center Environmental Monitoring, NASA.

Seitzinger, S.P. 1988. "Denitrification in freshwater and coastal marine ecosystems: ecological and geochemical significance." Limnology and Oceanography 33:702-724.

Shannon, C.E. 2001. A mathematical theory of communication. ACM SIGMOBILE mobile computing and communications review, 5(1), 3-55.

Sigua, G.C., Steward, J.S., and Tweedale, W.A. 2000. Water-Quality Monitoring and Biological Integrity Assessment in the Indian River Lagoon, Florida: Status, Trends, and Loadings (1988-1994). Environmental Management 25:199-209.

Sih, A., Cote, J., Evans, M., Fogarty, S., and Pruitt, J. 2012. Ecological implications of behavioural syndromes. Ecol. Lett. 15, 278–89. https://doi.org/10.1111/j.1461-0248.2011.01731.x.

Smith, N.P. 1993. Tidal and nontidal flushing of Florida's Indian River Lagoon. Estuaries 16:739-746.

Smokorowski, K.E. and Randall, R.G. 2017. Cautions on using the Before-After-Control-Impact design in environmental effects monitoring programs. Facets, 2(1), 212-232.

Snelson Jr, F.F. 1983. Ichthyofauna of the northern part of the Indian River Lagoon System, Florida. Florida Scientist, 187-206.

Spiegel, O., Leu, S.T., Bull, C.M., and Sih, A. 2017. What's your move? Movement as a link between personality and spatial dynamics in animal populations. Ecol. Lett. 20, 3–18. https://doi.org/10.1111/ele.12708.

Stauble D.K., Da Costa, S.L., Monroe, K.L., and Bhogal, V.K. 1988. Inlet Flood Tidal Delta Development through Sediment Transport Processes. In: Aubrey D.G., Weishar L. (eds) Hydrodynamics and Sediment Dynamics of Tidal Inlets. Lecture Notes on Coastal and Estuarine Studies, vol 29. Springer, New York, NY. https://doi.org/10.1007/978-1-4757-4057-8_18.

Stoner, A.W. 1979. Species-specific predation on amphipod Crustacea by the pinfish Lagodon rhomboides: Mediation by macrophyte standing crop. Marine Biology 55:201-207.

Stoner, A.W. 1983. Distributional ecology of amphipods and tanaidaceans associated with three sea grass species. Journal of Crustacean Biology 3:505-518.

Stunz, G.W., Levin, P.S., and Minello, T.J. 2001. Selection of estuarine nursery habitats by wild-caught and hatchery-reared juvenile red drum in laboratory mesocosms. Environ. Biol. Fishes 61, 305–313.

Sweat, L.H., Swain, G., Hunsucker, K., and Johnson, K.B. 2017. Transported biofilms and their influence on subsequent macrofouling colonization. Biofouling 33(5):433-449.

Tetra Tech, Inc. 2016. Save our Indian River Lagoon Project Plan for Brevard County, Florida.

Tetra Tech, Inc. 2021. Save Our Indian River Lagoon Project Plan 2021 Update for Brevard County, Florida.

Tremain, D.M. and Adams, D.H. 1995. Seasonal variations in species diversity, abundance, and composition of fish communities in the northern Indian River Lagoon, Florida. Bulletin of Marine Science, 57(1), 171-192.

Tremain, D.M., Harnden, C.W., and Adams, D.H., 2004. Multidirectional movements of sportfish species between an estuarine no-take zone and surrounding waters of the Indian River Lagoon, Florida. Fish. Bull. 102, 533–544.

Troast, B., Paperno, R., and Cook, G.S. 2020. Multidecadal shifts in fish community diversity across a dynamic biogeographic transition zone. Diversity and Distributions 26, 93–107. https://doi.org/10.1111/ddi.13000.

Trudnowska, E., Gluchowska, M., Beszczynska-Möller, A., Blachowiak-Samolyk, K., and Kwasniewski, S. 2016. "Plankton patchiness in the Polar Front region of the West Spitsbergen Shelf." Marine Ecology Progress Series 560 (2016): 1-18.

Tweedley, J.R., Warwick, R.M., Hallett, C.S., and Potter, I.C. 2017. Fish-based indicators of estuarine condition that do not require reference data. Estuarine, Coastal and Shelf Science, 191, 209-220.

Twilley, R.R., Cowan, J., Miller-Way, T., Montagna, P.A., and Mortazavi, B. 1999. Benthic Nutrient Fluxes in Selected Estuaries in the Gulf of Mexico. In Biogeochemistry of Gulf of Mexico Estuaries, by J.R. Pennock, R.R. Twilley Eds. T.S. Bibnchi, 163-209. John Wiley & Sons.

Underwood, A.J. 1994. On beyond BACI: sampling designs that might reliably detect environmental disturbances. Ecological applications, 4(1), 3-15.

USACE. 1882. Annual Report of the Chief of Engineers, United States Army. Washington, D.C., Appendix J: 1233.

U.S. Department of Energy. 2001. Pump Life Cycle Costs. Retrieved from Office of Industrial Technologies Energy Efficiency and Renewable Energy: https://www.energy.gov/sites/prod/files/2014/05/f16/pumplcc_1001.pdf.

Vargo, G.A., Heil, C.A., Fanning, K.A., Dixon, L.K., Neeley, M. B., Lester, K., Ault, D., Murasko, S., Havens, J., Walsh, J., and Steven, B. 2008. Nutrient availability in support of Karenia Brevis blooms on the central West Florida Shelf: What keeps Karenia blooming? Continental Shelf Research, 28:73-98.

Virnstein, R.W. 1990. The large spatial and temporal biological variability of Indian River Lagoon. Florida Scientist, 249-256.

Virnstein, R.W. and Morris, L.J. 1996. Seagrass preservation and restoration: a diagnostic plan for the Indian River Lagoon. St. Johns River Water Management District.

Warwick, R.M. and Clarke, K.R. 1995. New\'biodiversity\'measures reveal a decrease in taxonomic distinctness with increasing stress. Marine ecology progress series, 129, 301-305.

Wijnhoven, S., Escaravage, V., Daemen, E., and Hummel, H. 2010. The decline and restoration of a coastal lagoon (Lake Veere) in the Dutch Delta. Estuar. Coast. 33, 1261–1278. doi: 10.1007/s12237-009-9233-1.

Willis, A., Adams, M.P., Chuang, A.W., Orr, P.T., O'Brien, K.R., Burford, M.A. 2015. Constitutive toxin production under various nitrogen and phosphorus regimes of three ecotypes of cylindrospermopsis raciborskii ((Woloszynska) Seenayya et Subba Raju). Harmful Algae, 47:27-34.

Zar, J.H. 1999. Biostatistical Analysis, fourth. ed, Prentice Hall New Jersey. Pearson education.

Zarillo, G.A. 2015. Indian River Lagoon Numerical Model Flushing Experiments.

Zarillo, G.A. 2018. Numerical Model Flushing Experiments Final Report Submitted to the Wisher Indian River Lagoon National Estuary Program and Canaveral Port Authority. 36pp.

Zarillo, G.A., Watts, I., Brehin, F, and Erickson, L. 2013. State of Sebastian Inlet 1943-201: An Assessment of Inlet Morphologic Processes, Shoreline Changes, Sediment Budget and Management Strategies. Report to the Sebastian Inlet Management District. 161pp.

Ziegler, S.E., and Brenner, R. 1999. Dissolved organic carbon cycling in a subtropical seagrass-dominated lagoon. Marine Ecology Progress Series, 188:51-62.

Zieman, J.C. 1982. Ecology of the seagrasses of south Florida: a community profile. No. FWS/OBS-82/25. Virginia Univ: Charlottesville, VA (USA). Dept Environ Sci.

Zimmerman, R., Gibson, R., and Harrington, J. 1979. Herbivory among gammaridean amphipods from a Florida seagrass community. Marine Biology 54:41-47.

Appendix A Task 1 – Modeling and Engineering Report

Restore Lagoon Inflow Research (Phase 2)
Task 1, Modeling and Engineering

PREPARED FOR

Florida Department of Education
325 W Gaines Street
Tallahassee, FL 32399

PREPARED BY

Robert J. Weaver, Gary A. Zarillo
Florida Institute of Technology
150 West University Boulevard
Melbourne, FL 32901

August 2021

Table of Contents

List of Tables

List of Figures

Acknowledgements

We would like to thank the following Florida State Legislators, regulatory permitting agencies, and the growing number of organizations that have consulted on the project in support of lagoon science. We would also like to thank the many students and technicians who's dedicated effort and passion helps to make this project possible.

Elected Representatives

Representative Thad Altman
Senator Debbie Mayfield
Representative Randy Fine

Permitting Agencies

U.S. Army Corps of Engineers
Florida Department of Environmental Protection
St. Johns River Water Management District

Project Consultants and/or Partners

Canaveral Port Authority
Applied Ecology

Photographs on cover: Series of photographs from field days on board the Florida Tech workboat. Leftmost image: Encrusted acoustic doppler current profiler (ADCP) raised on board for servicing. Middle image: Close up photograph of ADCP quadrapod on board for servicing. Rightmost image: Student monitoring side-scan sonar towfish during the search for instrument station 3. *Photo credit:* R.J. Weaver

List of Acronyms

ADCIRC	Advanced Circulation
ADCP	Acoustic Doppler Current Profiler
BRL	Banana River Lagoon
°C	Degrees Celsius
CMS	Coastal Modeling System
CT	Conductivity-Temperature
DO	Dissolved Oxygen
EFDC	Environmental Fluid Dynamics Code
FDEP	Florida Department of Environmental Protection
Florida Tech	Florida Institute of Technology
ft	Feet
GIS	Geographic Information System
HAB	Harmful Algal Bloom
HBOI	Harbor Branch Oceanographic Institution
HDPE	High-density Polyethylene
HEM3D	Hydrodynamic-Eutrophication Model Three-Dimensional
HYCOM	Hybrid Coordinate Model
IRL	Indian River Lagoon
km	Kilometer
LOBO	Land/Ocean Biogeochemical Observatory
m	Meter
m^3/sec	Cubic Meters Per Second
mg/L	Milligrams Per Liter
MWI	Moving Water Industries
NAD83	North American Datum of 1983
NASA	National Aeronautics and Space Administration
NAVD88	North American Vertical Datum of 1988
NDBC	National Data Buoy Center
NOAA	National Oceanic and Atmospheric Administration

ODOT	Oregon Department of Transportation
ORCA	Ocean Research and Conservation Association
PT	Pressure Transducer
PVC	Polyvinyl Chloride
RMSE	Root Mean Square Error
SJRWMD	Saint Johns River Water Management District
SWAN	Simulating Waves Nearshore
SWIL	Spatial Watershed Iterative Loading
TN	Total Nitrogen
TP	Total Phosphorus
µg/L	micrograms per liter
USACE	U.S. Army Corps of Engineers
USEPA	U.S. Environmental Protection Agency
USFWS	U.S. Fish and Wildlife Service
USGS	U.S. Geological Survey

Task Summary

The health of coastal waterbodies continues to be threatened by climate change and changes in population. Our changing climate will increase contributors to eutrophication. Projected changes in agricultural lands and precipitation combine to increase the transport of fine sediments and nutrients to coastal waters. Rising sea levels and associated changes in the coastal water table will result in groundwater contamination due to inundated septic and sewer systems. The groundwater will carry these waste products to the coastal estuaries and bays. As more of the coastal wetlands become degraded by human development and sea level rise inundating the system, the natural filtration system becomes lost. With coastal populations continuing to rise disproportionally to inland regions, there has never been more pressure on the coastal waterbodies as they receive the increased nutrient loading.

For restricted estuaries and lagoons, like the Indian River Lagoon (IRL), the influx of nutrients is particularly damaging due to high residence times and impaired flushing. As communities explore solutions for eutrophication and poor water quality, one possible solution to consider is hydraulically engineering the waterbody to mechanically bring ocean water into the system. Ocean water inflow projects, if designed properly, can improve the flushing rate and decrease the residence times for restricted estuaries and lagoons.

Hydrological engineering of waterbody systems that are impaired has been managed in various locations throughout the world, and a common result has been an improvement in water quality. Existing international projects in India (Ghosh et al., 2006), Netherlands (Wijnhoven et al., 2010), New Zealand Schallenberg et al., 2010), China (Li et al., 2013), Australia (Humphries and Robinson, 1995), Denmark (Peterson, et al., 2008), Portugal (Lillebo et al., 2005), as well as projects in the United States including Florida (Landers-Atkins Planners, Inc., 1987; Burgess, 2020), New York (National Park Service and U.S. Army Corps of Engineers [USACE] 2017; Olin et al., 2020; National Park Service 2018), and California (Port of Los Angeles Engineering Division, 2006) can provide guidance as coastal communities seek effective and beneficial method to combat eutrophication.

With a second year of funding from the Florida legislature, Florida Institute of Technology (Florida Tech) faculty continued to explore customized solutions for improving water quality in our IRL. Task 1 of the Restore Lagoon Inflow Research Phase 2, Modeling and Engineering, is focused on developing the engineering design for a viable inflow structure; determining the change in flow, salinity, and temperature that would be caused by bringing in ocean water into the IRL; and collect data that can be used to calibrate and validate the numerical models.

Objectives of Task 1 are to:

1. Conduct numerical model predictions of hydrodynamics, flushing rate, and water quality with/without enhanced inflow using the Environmental Fluid Dynamics Code (EFDC) and Three-Dimensional Hydrodynamic-Eutrophication Model (HEM3D) modeling at a 2-year time scale.
2. Conduct salinity, water temperature, and water level predictions over a minimum of a 2-year time scale with/without enhanced inflow.
3. Support the Biological Monitoring Team and other project teams with model produced environmental data.
4. Setup and run a coastal processes model to provide predictions of sediment transport, shoaling, and currents within Port Canaveral with/without enhanced inflows.

5. Collect flow and water level data supporting model verification at verification Dragon Point, Sykes Creek, and the Barge Canal.
6. Build an archive of model data to support permit activities.
7. Advance the design of a temporary inflow structure in preparation for permitting.
8. Initiate the permitting for a temporary pumping station, transporting seawater from the ocean into the Banana River Lagoon (BRL).

This second phase of the study builds on the Phase 1 results to develop a design for an inflow structure, and further baseline data and modeling on existing water quality, biological parameters, and hydrologic conditions at potential locations for future temporary permitted inflow test structure. The modeling and engineering research proceeded in parallel with biological and water quality monitoring in advance of a proposed, temporary pilot-pumping project.

Engineering Key Findings:

- Small scale pilot pumping structure capable of pumping 0.5 cubic meters per second (m^3/sec) is designed and estimated to cost $551,000 to construct, $50,000 to operate for one year, and $112,000 to decommission once the pilot project is ended.
- Salinity in BRL is highly variable, and increased groundwater seepage following major rainfall events can result in water near the bed being less saline than the surface water.
- Water levels naturally fluctuate as much as 2.5 feet [ft] (75 centimeters) between annual high and low water periods, indicating that BRL and IRL can handle the slight increases in water level predicted by the EFDC model of 1 to 7 centimeters with no adverse impacts.

Modeling Key Findings:

- Water quality calculations based on prescribed inflow rates of sea water from Port Canaveral indicate potential water quality benefits to BRL.
- Dissolved oxygen concentrations in the BRL are predicted to increase according to increases of the prescribed inflow rates under which water quality improvements begin to appear in the BRL at an inflow rate of 2.5 m^3/sec.
- Water column total nitrogen (TN) and total phosphorus (TP) concentrations are predicted to be reduced at inflow rates at and above 2.5 m^3/sec.
- Predicted chlorophyll concentrations are also reduced and concentration spikes mitigated by inflow of seawater.
- Potential water quality benefits at inflow rates of 2.5 m^3/sec and higher are predicted to spread to the northern most compartment of the BRL.
- A survey of circulation dynamics from acoustic doppler current profiler (ADCP) data supported by model tracer studies, indicates that seasonally reversing flow direction in the BRL and IRL may limit the measurable impacts of inflows to the BRL, Sykes Creek, and IRL to the west of BRL.
- Reversing flows that confine waters masses in the north compartments of the BRL for extended periods may set the physical conditions that trigger and promote harmful agal blooms (HABs) in the BRL.
- Examination of predicted water quality constituent concentrations at the throat of Sebastian Inlet 60 kilometers to the south of the sea water inflow point indicates no detectable changes in water quality with enhanced inflow.

1 Introduction

The Indian River Lagoon (IRL) is a shallow (less than 5 meter [m]) bar-built, lagoon type estuary that extends 250 kilometers (km) along the central east coast of subtropical Florida and ranges in width from 1 to 9 km (Sigua et al., 2000; **Figure 1**). The IRL is poorly flushed across most of its length, with limited exchange with the ocean occurring through five engineered and stabilized inlets (Ponce de Leon, Sebastian, Fort Pierce, St. Lucie, and Jupiter; Kjerfve 1986; Smith 1990, 1993). The northern portion of the IRL is micro tidal and tidal flushing between sub-basins is negligible (Saberi and Weaver 2016; Zarillo 2015). Limited IRL circulation combined with several decades of increasing anthropogenic impacts have led to declining water quality and more severe and more frequent harmful algal blooms (Marine Resource Council 2018; Tetra Tech 2020), increasing the risk of ecosystem collapse (Adams et al., 2019).

Historically and prior to the development of human infrastructure, the IRL system was episodically connected to the coastal ocean through storm produced cuts and persistent tidal inlets that migrated alongshore under the net southward wave produced drift of littoral sediments (Zarillo et al., 2013). This process over geological time resulted in a system of wash over platforms and tidal inlet flood shoals upon which extensive human infrastructure has been built on the barrier islands bounding the east side of the IRL (Stauble et al., 1988; Zarillo et al., 2013). Correspondingly, historical development of coastal Florida resulted in a major expansion of the IRL watershed from Brevard County to Martin County due to construction of the canal system and associated water control structures.

As a result of the expanding human infrastructure, existing natural tidal inlets have been stabilized by jetty construction coupled with shore protection projects that involve repeated beach restoration projects that can have a 50-year planning horizon. This has resulted in the prevention of the natural tidal inlet migration process, episodic storm cuts, and barrier over wash events that previously provided exchanges between the coastal ocean and the IRL. Limited coastal ocean exchanges coupled with watershed expansion and related eutrophication (nutrient loading) of the lagoon has resulted in a trend of declining water quality over the past 60 years.

Eutrophication of coastal marine ecosystems has become increasingly common due to enhanced nutrient loading from adjacent watersheds (Brady et al., 2013; Diaz and Rosenberg 2008). As the eutrophic state progresses, sediment mineralization becomes an increasingly important source of nutrients and can sustain eutrophication through the dry season as well as destabilize the trophic state of an estuary (Cowan and Boynton 1996; DiDonato et al., 2006; Seitzinger 1988; Kemp et al., 1990). Extended periods of eutrophication can lead to a shift from seagrass-dominated ecosystems to degraded, algae-dominated systems (DiDonato et al., 2006).

A distinct difference in the ability to cope with eutrophication has been observed among estuaries with varying geomorphologies and residence times or flushing times for water (Twilley et al., 1999; Defne and Ganju 2015). Poorly flushed estuaries with long residence times, like IRL, more readily retain nutrients to promote algal blooms, loss of seagrass beds, hypoxia, and loss of ecosystem services (Defne and Ganju 2015; Kemp et al., 1992; Twilley et al., 1999). Conversely, well-flushed estuaries with shorter residence times have greater resilience to the impacts of eutrophication (Defne and Ganju 2015). Historically, estuarine flushing has been controlled by fluvial discharge, tides, wind mixing, geomorphology of the estuary, as well as other forcing over longer timescales (Defne and Ganju 2015; Csanady 1978; Jassby and Van Nieuwenhuyse 2005).

Different approaches to managing the eutrophication have been applied around the world, including hydrologic engineering of the system. Hydrologic engineering is used to encompass any

method of remediation that involved changing the flow patterns into and/or out of a system. Hydrological engineering of impaired waterbody systems has been managed in various locations throughout the world, and a common result has been an improvement in water quality. Existing international projects in India (Ghosh et al., 2006), Netherlands (Wijnhoven et al., 2010), New Zealand Schallenberg et al., 2010), China (Li et al., 2013), Australia (Humphries and Robinson, 1995), Denmark (Peterson, et al., 2008), Portugal (Lillebo et al., 2005), as well as projects in the United States in Florida (Landers-Atkins Planners, Inc., 1987; Burgess, 2020) , New York (National Park Service and U.S. Army Corps of Engineers [USACE] 2017; Olin et al., 2020; National Park Service 2018), and California (Port of Los Angeles Engineering Division, 2006) can provide guidance as coastal communities seek effective and beneficial method to combat eutrophication.

Hydrologic engineering in the form of enhanced circulation in the IRL may contribute toward lowering nutrient concentrations that support the onset and proliferation of algal blooms. Another potential benefit may be to increase the concentration of dissolved oxygen (DO) yielding enhanced resilience to anoxia and fish kills. The main benefits of decreased nutrient concentrations and possibly increased DO would likely result from changes to geochemical cycling, with spatially limited impacts from direct dilution by seawater. Results from Phase 1 of this study were consistent with literature and suggest that enhanced circulation could lead to decreased concentrations of nutrients in areas of the IRL with enhanced circulation.

The objectives of this Phase 2 effort are to continue to explore customized solutions for improving water quality in our lagoon with a pilot project to investigate the impacts of restoring periodic historical ocean inflows. This is not a proposal for an artificial inlet. Rather, this second phase of the study builds on the Phase 1 results to further develop baseline data and modeling on existing water quality, biological parameters, and hydrologic conditions at the most feasible location for a future, temporary, permitted inflow test structure. Phase 2 modeling and engineering research proceeded in parallel with biological and water quality monitoring in advance of a proposed, temporary pilot pumping project.

1.1 Study Area

The Banana River Lagoon (BRL) is a sub-basin of the IRL that lies between Cape Canaveral and Merritt Island and extends from the National Aeronautics and Space Administration (NASA) Kennedy Space Center to Dragon Point. The BRL is poorly flushed with no direct connection to the ocean, which leads to some of the longest water residence times in the IRL system. According to the Florida Department of Environmental Protection (FDEP), it takes approximately 2 years for the water to flush in the BRL (FDEP 2013). The northern section of BRL was historically connected to the IRL by a series of natural channels that have become increasingly restricted with continued upland development. Prior to the development of the barrier island, each sub-basin of the IRL was subjected to episodic over washing and breaching of the barrier island by storms as evidenced by the numerous relict tidal inlet shoals and expansive wash over sediment fans. This historical inflow would bring ocean water into regions of the IRL and enhance the circulation in the estuary.

This study was carried out to evaluate possible impacts of enhanced circulation in the BRL with an emphasis at two primary locations: (1) north BRL considered as a likely inflow site (centered near 28.407, -80.638), and (2) central BRL evaluated as a reference area where any impacts of inflow would be minimized due to geomorphological conditions that limit circulation (centered near 28.287, -80.6100). The control area was selected based on evaluation of models to identify candidate locations with limited circulation associated with proposed pumping volumes, followed

by comparison of water depth and bottom type at candidate sites versus the proposed inflow location.

Note: Red circles show a 1 km radii around the proposed pumping location and reference site for scale.

Figure 1. Map of the study area showing potential pumping location in the north BRL and the reference site in the central BRL

1.2 Objectives for Task 1: Modeling and Engineering

- Conduct numerical model predictions of hydrodynamics, flushing rate, and water quality with/without enhanced inflow using the Environmental Fluid Dynamics Code (EFDC) and Three-Dimensional Hydrodynamic-Eutrophication Model (HEM3D) modeling at a 2-year time scale.
- Conduct salinity, water temperature, and water level predictions over a minimum of a 2-year time scale with/without enhanced inflow.
- Support the Biological Monitoring Team and other project teams with model produced environmental data.

- Setup and run a coastal processes model to provide predictions of sediment transport, shoaling, and currents within Port Canaveral with/without enhanced inflows.
- Collect flow and water level data supporting model verification at verification Dragon Point, Sykes Creek, and the Barge Canal.
- Build an archive of model data to support permit activities.
- Advance the design of a temporary inflow structure.
- Initiate the permitting for a temporary pumping station, transporting seawater from the ocean into the BRL.

1.3 Methods

The project approach included a combination of numerical modeling and continued data collection to provide quantification of the influence of enhanced inflows on flushing rates and water quality in the north BRL assuming pumping produced inflows from the west compartment of Port Canaveral. The overall approach was designed to meet permit requirements governed by federal and state regulations. The permitting process was initiated based on the final site and design determination.

The modeling team evaluated IRL inflow scenarios based on the pilot scale parameters designed to mimic water exchanges with the coastal ocean that were historically produced by episodic over washing and breaching of the barrier island by storms as evidenced by the numerous relict tidal inlet shoals and expansive washover sediment fans.

The Phase 2 project approach for modeling included continued assessment of flushing rates using the EFDC environmental modeling platform. This model code was successfully applied in Phase 1 of the project to assess and compare pumping and water control structure scenarios for the BRL and central IRL. In Phase 2, the model predictions were extended to include calculation of water quality constituents using the water quality module contained within the EFDC modeling platform.

The U.S. Environmental Protection Agency (USEPA) supported EFDC/HEM3D includes features and capabilities that make it superior and more applicable to shallow estuarine environments than other models. The model computational grid area extends from Ponce de Leon Inlet north of the Mosquito Lagoon into the IRL compartments extending to the Fort Pierce Inlet. This multi-parameter finite difference model represents estuarine flow and material transport in three dimensions and has been extensively applied to shallow estuarine environments in Florida and other coastal states.

The EFDC model was coupled with the water quality model. The kinetic processes included in the HEM3D water quality model were derived and updated from the Chesapeake Bay three-dimensional water quality model, CE-QUAL-ICM (Cerco and Cole 1994). A detailed description of the water quality model is provided by Park et al. (1995) and Tetra Tech (2007). Earlier water quality models, such as the Water Quality Analysis Simulation Program (Ambrose et al., 1993) used biochemical oxygen demand to represent oxygen demanding organic material. The HEM3D water quality model is carbon based. The four algae species are represented in carbon units. The three organic carbon variables play an equivalent role to biochemical oxygen demand. Organic carbon, nitrogen, and phosphorous can be represented by up to three reactive sub-classes, refractory particulate, labile particulate and labile dissolved.

In order to produce useful predictions for BRL and IRL, water quality boundary conditions are applied to guide the calculation. Some of these inputs had already been developed under a recent project sponsored by FDEP and Brevard County, FL. Predictions of the water quality at several locations in the IRL system were based on existing and projected dredging of muck deposits. For this project, watershed-based and tributary-based nutrient loads were specified along with measured and assumed nutrient flux rates from benthic sediments. The flux rate of nutrients specified in the sediment diagenesis sub-model (**Figure 2**) was the basis of model comparisons with and without muck dredging. Similar comparisons for scenarios with and without enhanced inflow to BRL require substantial knowledge of existing nutrient flux rates from sediment in BRL, along with concentrations of water quality constituents contained in the water inflows from Port Canaveral. Thus, there is close coordination between the Numerical Modeling Team and Geochemical Team.

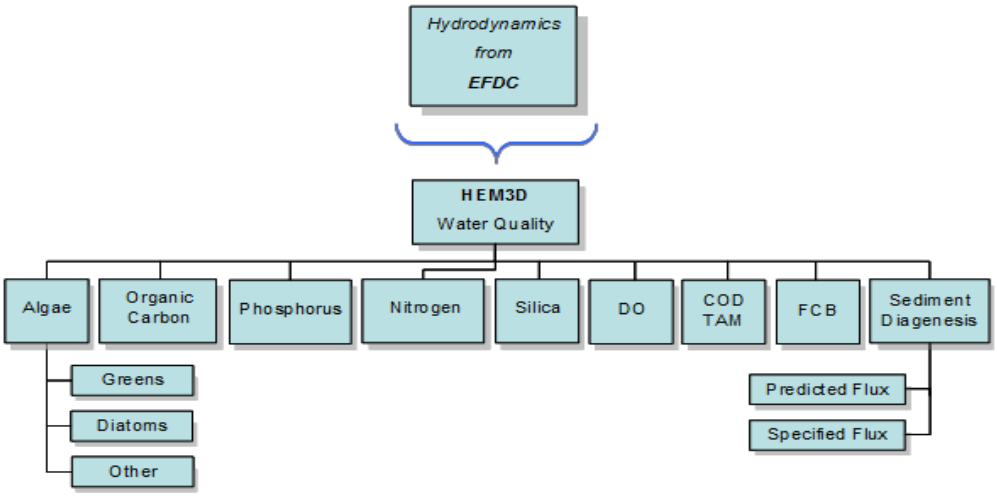

Figure 2. Flowchart for the water quality module of HEM3D

Additional updates to the modeling scheme to produce water quality model boundary conditions include watershed inputs from Spatial Watershed Iterative Loading (SWIL) model and the groundwater inflow predictions compiled by Florida Tech (Dr. Pandit and his team). The SWIL model was developed for FDEP to incorporate more available data, more recent conditions, and more temporally fine datasets to support predictions of nutrient inflows from the sub-basins of the IRL system. SWIL-predicted nutrient inflows through the close of 2017 supported the in-estuary water quality predictions for the FDEP-Brevard County muck dredging assessment (Zarillo and Listopad 2020).

SWIL is a custom ESRI ArcGIS toolset, originally designed to provide a continuous monthly simulation of runoff (surface and baseflows) over a 16-year period, yielding robust representation of pollutant loadings and freshwater volumes in the IRL. Under the Restore Lagoon Inflow Research project, the SWIL model of the IRL watershed sub-basis was updated to produce predictions of nutrient loads though the end of June 2020. In Phase 1 of this project, groundwater inputs, in terms of inflows through the sediment benthic boundary, were linked to the EFDC model grid. By extending EFDC modeling to include water quality predictions, Dr. Pandit and his team updated the groundwater inflow predictions to include nutrient concentrations. This, in combination with the other nutrient boundary conditions, provide a more complete representation of the IRL nutrient budget and facilitate sensitivity tests based on the proposed enhanced inflows

to the BRL. Further details on the setup, operation, and results of the EFDC/HEM3D model are provided in a later section of this report.

An additional modeling approach was conducted to evaluate potential impacts within the Port Canaveral Basin from pumping water from west compartment of Port Canaveral into the BRL. The enhanced flows have been evaluated for effects on the Port's circulation and the potential for altering sedimentation rates. The model predictions are performed using the USACE Coastal Modeling System (CMS) that has already been established in the project area to assess enhanced inflows in earlier studies (Zarillo 2015, 2018). The previous studies did not include sediment transport calculations, which were added to the updated application. The CMS is widely used by the coastal engineering community for analysis of tidal inlets, beach fill performance, and storm produced changes in coastal morphology. CMS is a vertically averaged finite volume model that includes empirically calculated vertical processes such as water column suspended sediment concentration profiles. Experience has shown that CMS produces useful predictions of hydrodynamics, sediment transport, and topographic change. For this project, model simulations included a full set of boundary conditions consisting of water level time series, wind forcing, and wave forcing. CMS-Flow produced predictions of water level and circulation and was coupled with the CMS-Wave model to provide wave forcing and wave-current interaction, which are important in establishing the sediment transport regime at the entrance of Port Canaveral.

The modeling effort is supported by continued baseline sampling of the water quality and hydrodynamic properties of BRL. As stated in the Phase 1 project, these data are crucial in supporting Phase 2 of the project to identify a location and design for a pilot project to evaluate controlled, temporary inflows from the coastal ocean. The modeling team continued collection of current velocity and water level data at key locations in BRL including Kars Park, east end of the Barge Canal near the west boundary of Port Canaveral, inflow basin, Sykes Creek, southern BRL at Lansing Island, and south boundary of BRL at Dragon Point. The water level and flow data were applied to verify performance of the hydrodynamic model. New sensors were deployed in the inflow basin. A transect of four instruments was deployed in the cove out into the BRL just south of the Canaveral Locks. These four stations measured salinity, temperature, and water depth. In addition to the instruments deployed and services by the Task 1 team, the geochemical data collected by Dr. Fox and his team were crucial to establishing boundary conditions for the water quality model.

The engineering team, including graduate and undergraduate student interns, assimilated research results from project Tasks 1, 2, and 3 in response to questions and concerns as they arose from permitting agencies and stakeholders. During the pre-application meetings, issues were discussed and a determination of permitting requirements established. Appropriate design modifications were made based on the input from stakeholders. Working with the support of experts from Tetra Tech, the structure design developed by the Florida Tech Task 1 team to the 20% level during Phase 1 was advanced to the >60% design level during Phase 2. The location and scope of the pilot was finalized, and the final temporary design has been presented to agencies and stakeholders for comment.

This final report provides a detailed account of the results obtained during Phase 2. First the engineering design process is provided with the result being the >60% design needed for permitting. Second, summaries of the long-term water level stations and four salinity, temperature, and depth stations located in the proposed inflow basin are discussed. In addition to providing model guidance, the results address concerns around water level increases and salinity fluctuations. The results from the ADCP deployment are also presented. These flow data are critical for model calibration, but also provide insight into the natural cycling of water through the

BRL. Finally, the numerical modeling efforts are presented. The modeling provided guidance for planning of a full-scale system. With a validated numerical model capable of predicting changes to the water quality in the BRL and IRL, managers will be able to address questions that stakeholders may have in a clear and concise manner. The model enables managers to predict the outcome of an intervention in the design phase to enable a more robust design.

2 Inflow Design

The project objectives included advancing the design of a temporary inflow structure in preparation for permitting, and initiating the permitting for a temporary pumping station, transporting seawater from the ocean into the BRL. To achieve these objectives the inflow design was advanced to >60% and shared with USACE for comment.

The stakeholder input has been assimilated into the pilot project pumping design. A flow rate of 0.5 cubic meters per second (0.5 m^3/sec) was set and the pump intake is proposed to be located east of the State Road 401 bridge and west of the Canaveral Locks. An optimal path for the pipeline has been identified after discussion with Port Canaveral, St. Johns River Water Management District (SJRWMD), and Tetra Tech, with the discharge into the BRL in a semi-enclosed basin just south of the locks.

The current engineering design for pilot pumping is based on past work funded by SJRWMD and produced by CDM Smith (2014, 2015, and 2017) and modified to meet the flow rate needs of this project. The intake structure was modified from the published design in CDM Smith (2017) to minimize the impact to the channel banks. The outfall structure is similar to the design in CDM Smith (Figure No.3-3 in CDM Smith 2017), modified for the new location.

The inflow structure will be located inside Canaveral Inlet, directly behind the fendering wall that protects the lock system, shown in **Figure 3**, while the outflow structure will be located on the bank of the BRL on the left side of Mullet Road, also shown in **Figure 3**. The pipe will run over land and will cross Mullet Road inside of the USACE property.

Figure 3. Location of inflow and outflow structures inside Port Canaveral (Google, 2021)

The locations of the inflow structure and pipe road crossing were specifically chosen so the public will have minimal interference with the pipe and pump system. Also, placing the inflow structure behind the fender wall will allow the intake structure to have substantial protection during a storm event since the maximum wave height behind the fender wall will be nominal. The site selection of the pipe and pump system allows for a large range of influence since it would feed directly into BRL, enabling it to flush BRL.

2.1 Site Description

The bathymetry was needed for the complete structural design of the pipe and pump system to determine the elevation difference from the inflow structure to the outflow structure, which was used in the Bernoulli equation calculations. It was also needed to determine the depth at the location of the intake to ensure there will be adequate clearance to avoid sediment entrainment. Finally, the bathymetry was needed for the design of the outflow structure and riprap pad to ensure the bank will be stable and erosion is mitigated. **Figure 4** shows the bathymetry plot inside of the Canaveral Inlet near the lock, where the inflow structure will be located, and **Figure 5** shows the bathymetry plot in BRL near Mullet Road, where the outflow structure will be located.

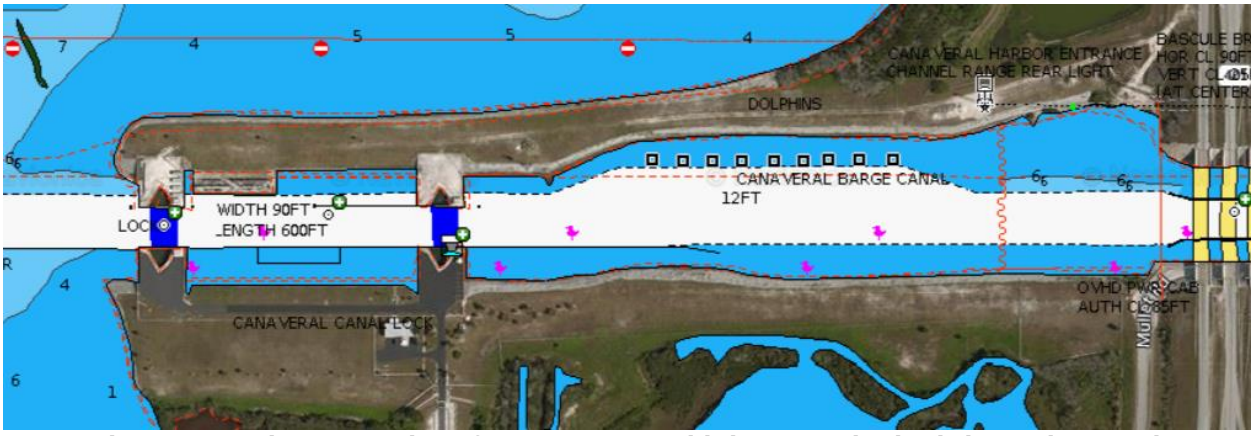

Figure 4. Bathymetry plot of Port Canaveral inlet near the lock (Garmin, 2021)

The Port Canaveral Inlet channel has an average depth of 12 feet (ft) or 3.7 m in the center with a steep gradient towards the north and south banks. The depth is unknown behind the fender wall, so a bathymetry survey will need to be taken before finalizing the inflow structure design.

Figure 5. Bathymetry plot of BRL near Mullet Road (Garmin, 2021)

BRL near Mullet Road is very shallow with a mild slope; the sub-basin that water will be flushing into from the pipe and pump system is between 0 to 2 ft (0 to 0.6 m) deep.

In both Garmin bathymetry plots, shown in **Figure 4** and **Figure 5**, mandatory depths, such as the depth where the inflow and outflow structures will be placed, are missing. To aid in the design of the pipe and pump system, professional surveys were taken by Oceanside Solutions of the Canaveral Inlet (**Figure 6**) and BRL (**Figure 7**). The contours shown are one-foot and the vertical datum used for land elevations was North American Vertical Datum of 1988 (NAVD88); North American Datum of 1983 (NAD83) was used for the horizontal datum.

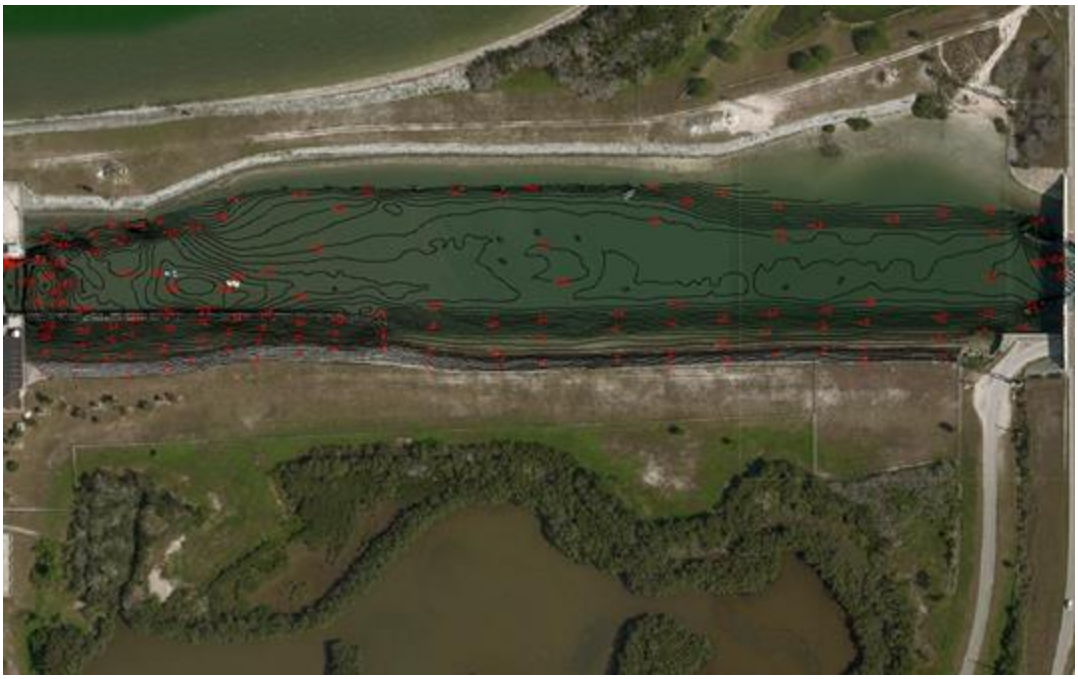

Figure 6. Oceanside Solutions Canaveral Inlet survey (Oceanside Solutions, 2021)

Figure 7. Oceanside Solutions BRL survey (Oceanside Solutions, 2021)

2.2 Proposed Structure

The proposed structure to aid in flushing out the BRL for a one-year pilot study of the physical, chemical, and biological effects is a pipe and pump system. The complete structural design of the system will include the design of five components: the pipeline itself, recommended pump to be used, design of a ramp for vehicles to drive over the pipe, design of an inflow structure where the

pump intake will be located, and design of an outfall structure where the water will flow out of the system and into BRL.

The design of the pipeline and determination of the recommended pump to be used are formulated around a flow rate of 0.5 m^3/sec. The design of a ramp for vehicles to drive over consisted of first selecting a design vehicle that the ramp is accessed by. The ramp, created by Bluff Manufacturing, incorporates a steel frame that will be placed on top of the pipeline with a path for the pipeline to travel underneath the ramp.

The inflow structure will be placed behind the Canaveral Lock fender wall, where it will be protected from wave activity and from boats navigating through the lock. The inflow structure will consist of the pump intake in a vertical orientation and a 90-degree bend so the pipeline will run parallel to the water surface until it contacts the ground. The intake will be surrounded by a cage structure to ensure manatees, fish, and other marine animals do not get sucked into the pipe or harmed from the intake propellers. The intake and pipe portion that hangs over water will be supported by pairs of piles evenly spaced along the pipeline so that the pipeline does not exceed its maximum deflection. The pile pairs will have two H members connecting them, with one H member running along the bottom of the pipe and the other H member running along the top of the pipe to keep it from moving. The electric drive unit of the pump will be placed on land near the pipeline on top of a skid frame.

The outflow structure will be placed on the west side of Mullet Road so the fresh ocean water will feed directly into BRL, enabling it to flush BRL and IRL. The outflow structure will consist of a riprap pad that the water will initially fall onto before it flows into BRL. The riprap pad will dissipate the energy of the flowing water, helping to minimize erosion of the bank. The riprap pad will contain riprap rocks with a filter fabric underneath. The filter fabric will be protected from the rough edges of the riprap rock by a thin layer of sand.

A pipe and pump system was chosen as the proposed structure for adding flowing water into the IRL due to its feasibility and practicality of construction and operation. The construction of the system will cause minimal disturbance to infrastructure and is relatively inexpensive compared to other design options and the benefits it will produce. The system can be used as a temporary structure to study the physical, chemical, and biological effects of introducing ocean water into the IRL or as a permanent structure if the inflow proves to be beneficial. Lastly, the system is easy to control, and the pipe can be blocked off at any time.

Once across the road, the pipeline will continue west-southwest to the shrub line, and then cross the fence heading south on the west side of the access road. To minimize impact to the existing mangroves, the pipeline outfall will use the existing access points to BRL that have been cleared.

The concerns of both U.S. Fish and Wildlife Service (USFWS) and USACE will be addressed in the final design. This includes manatee and fish exclusion, with a flow intake area large enough that the intake velocity at the grate will preclude fish and manatee from becoming trapped.

2.2.1 Pipeline and Pump

Bernoulli's principle states that the sum of mechanical energy, potential energy, and kinetic energy along a streamline is constant, shown by Bernoulli's equation below (Qin and Duan 2017):

$$P + \frac{\rho V^2}{2} + \rho g z = constant \qquad [1]$$

where P is the pressure at a point along the streamline, ρ is the density of the fluid, V is the velocity of the fluid at a point along the streamline, g is gravity, and z is the elevation at the point along the streamline above a reference point.

By applying a streamline to the entire pipe system being designed and choosing the two streamline points to be one inside of the intake and one near the pipe exit, and by dividing equation 1 by ρg, equation 1 can be rewritten as equation 2, where γ is the specific weight of the fluid:

$$\frac{P1}{\gamma} + \frac{V1^2}{2g} + z1 = \frac{P2}{\gamma} + \frac{V2^2}{2g} + z2 \text{ [2]}$$

For a more complete equation, terms must be added to equation 2 to account for major head losses due to friction, minor head losses due to fixtures within the pipe system, and the head gained from using a pump. The final form of Bernoulli's equation used for the design of the pipe system is below:

$$\frac{P1}{\gamma} + \frac{V1^2}{2g} + z1 + h_p = \frac{P2}{\gamma} + \frac{V2^2}{2g} + z2 + h_{l(major)} + h_{l(minor)} \quad \text{[3]}$$

where h_p is the total dynamic head loss, $h_{l(major)}$ is head lost to friction, and $h_{l(minor)}$ is head lost to ten 45-degree bends and one 90-degree bend.

The equations used for major and minor head losses are below, where f is the friction factor, L is the length of the pipe, and k_l is the minor loss coefficient for the pipe components or fittings:

$$h_{l(major)} = \frac{fLV^2}{2gD} \quad \text{[4]}$$

$$h_{l(minor)} = \sum \frac{k_l V^2}{2g} \quad \text{[5]}$$

The friction factor for the major head loss term, 0.015, is found using the Moody Diagram, shown in **Figure 8**; the value of the minor loss coefficient for a 45-degree bend, 0.4, and for a 95-degree bend, 0.9, can be found in **Figure 9** (Penn State University 2015).

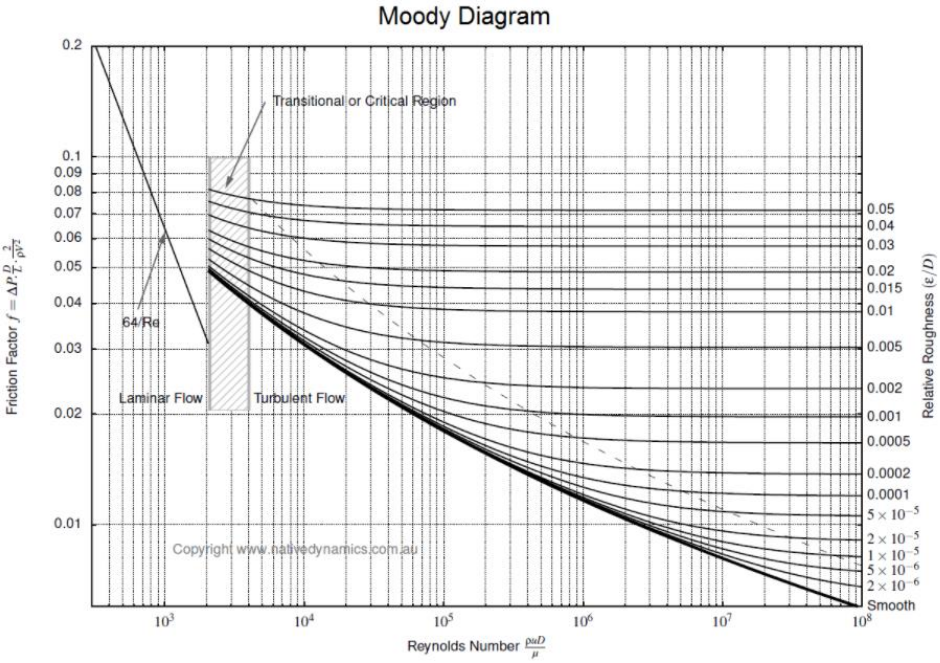

Figure 8. Moody diagram (Native Dynamics 2012)

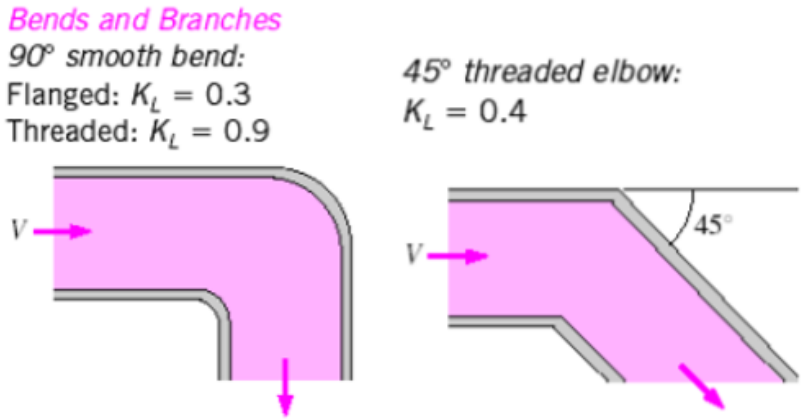

Figure 9. Minor loss coefficient for 90-degree bend and 45-degree bend (Penn State University 2015)

After rearranging the Bernoulli equation, the total dynamic head loss can be solved for each desired diameter of pipe. **Table 1** shows the various calculated values discussed above for a 16-inch (0.41 m), 20-inch (0.51 m), and 24-inch (0.61 m) diameter pipe.

Table 1. Pipe calculations for losses with differing pipe diameters

Pipe Diameter (inches)	16	20	24
Velocity in Pipe (feet/second)	12.647	8.094	5.621
hlmajor (ft)	33.472	10.968	4.408
hlminor (ft)	11.926	4.885	2.356
Total Dynamic Head Loss (ft)	47.882	16.871	7.254

There are two main types of power associated with a pump: hydraulic power and shaft power. The hydraulic pump power is the power that will be transmitted to the fluid, and it depends on the necessary flowrate, density of the fluid, and total head losses from the pipe system, which are previously calculated using Equation 7 and solving for the h_p term. The equation for hydraulic pump power is below (He et al., 2019) for the calculation in International System of Units:

$$P(hydraulic) = \frac{h_p \rho Q}{76} \quad [6]$$

The shaft pump power is the power that is applied to the shaft to obtain the specified flowrate, given the head; it is highly dependent on the hydraulic pump power, along with the efficiency of the pump, typically found in the pump's manufacturer manual on the pump bowl performance curves. The equation for shaft pump power is below (He et al., 2019):

$$P(shaft) = \frac{P(hydraulic)}{\eta} \quad [7]$$

where η is the efficiency of the pump.

Once the total dynamic head losses are calculated for the pipe and pump system, the required hydraulic power, in horsepower, for a pump can be calculated using Equation 6 and the required shaft power, also in horsepower, can be calculated based on the pump efficiency, found on the pump bowl performance curves. The Moving Water Industries (MWI) Pumps Hydraflo™ Hydraulically Driven Submersible Pump was chosen for the project. The pump comes in two different options, axial flow and mixed flow, depending on the diameter of the pipe and the total head losses calculated for that diameter. The overall performance ranges can be seen below in **Figure 10**, with axial flow pumps shown in blue and mixed flow pumps shown in yellow.

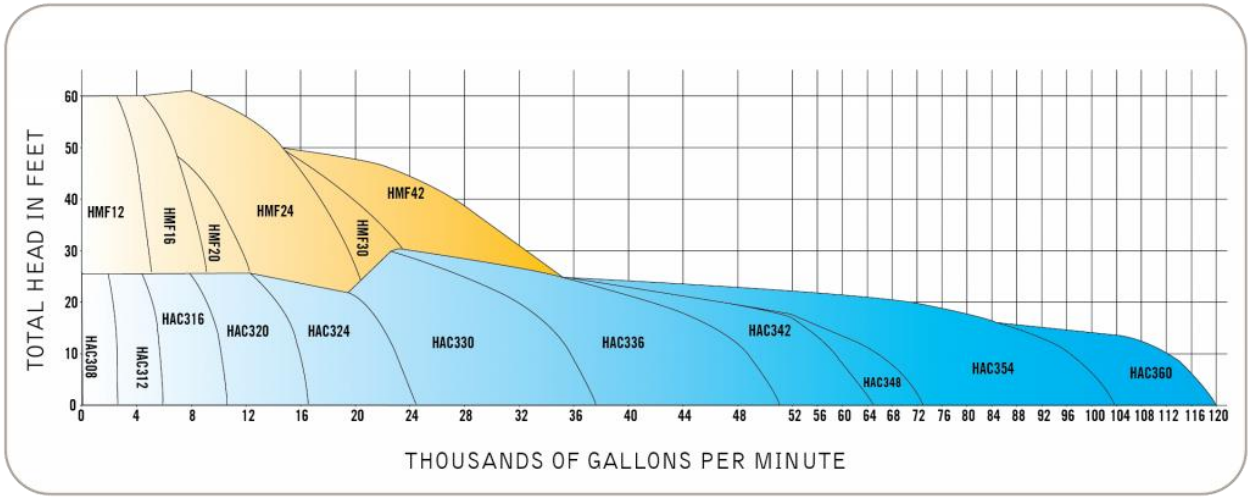

Figure 10. Overall performance ranges for MWI Pumps Hydraflo™ (2020)

For a 16-inch (0.41 m) diameter pipe, based on **Figure 10** above, an MWI mixed flow pump would be needed to achieve the required head and horsepower. The chosen mixed flow model and performance curve can be seen in **Figure 11**. For a pipe with a diameter of 16 inches (0.41 m), the calculated total head loss is 47.881 feet (14.594 m) and the pump efficiency would be 80%, requiring a shaft power of 123 horsepower.

For a 20-inch (0.51 m) diameter pipe, based on **Figure 10** above, an MWI axial flow pump would be needed to achieve the required head and horsepower. The chosen axial flow model and performance curve can be seen in **Figure 12**. For a pipe with a diameter of 20 inches (0.51 m), the calculated total head loss is 16.870 feet (5.142 m) and the pump efficiency would be 79%, requiring a shaft power of 44 horsepower.

For a 24-inch (0.61 m) diameter pipe, based on **Figure 10** above, an MWI axial flow pump would be needed to achieve the required head and horsepower. The chosen axial flow model and performance curve can be seen in **Figure 13**. For a pipe with a diameter of 24 inches (0.61 m), the calculated total head loss is 7.254 feet (2.211 m) and the pump efficiency would be 82%, requiring a shaft power of 18 horsepower.

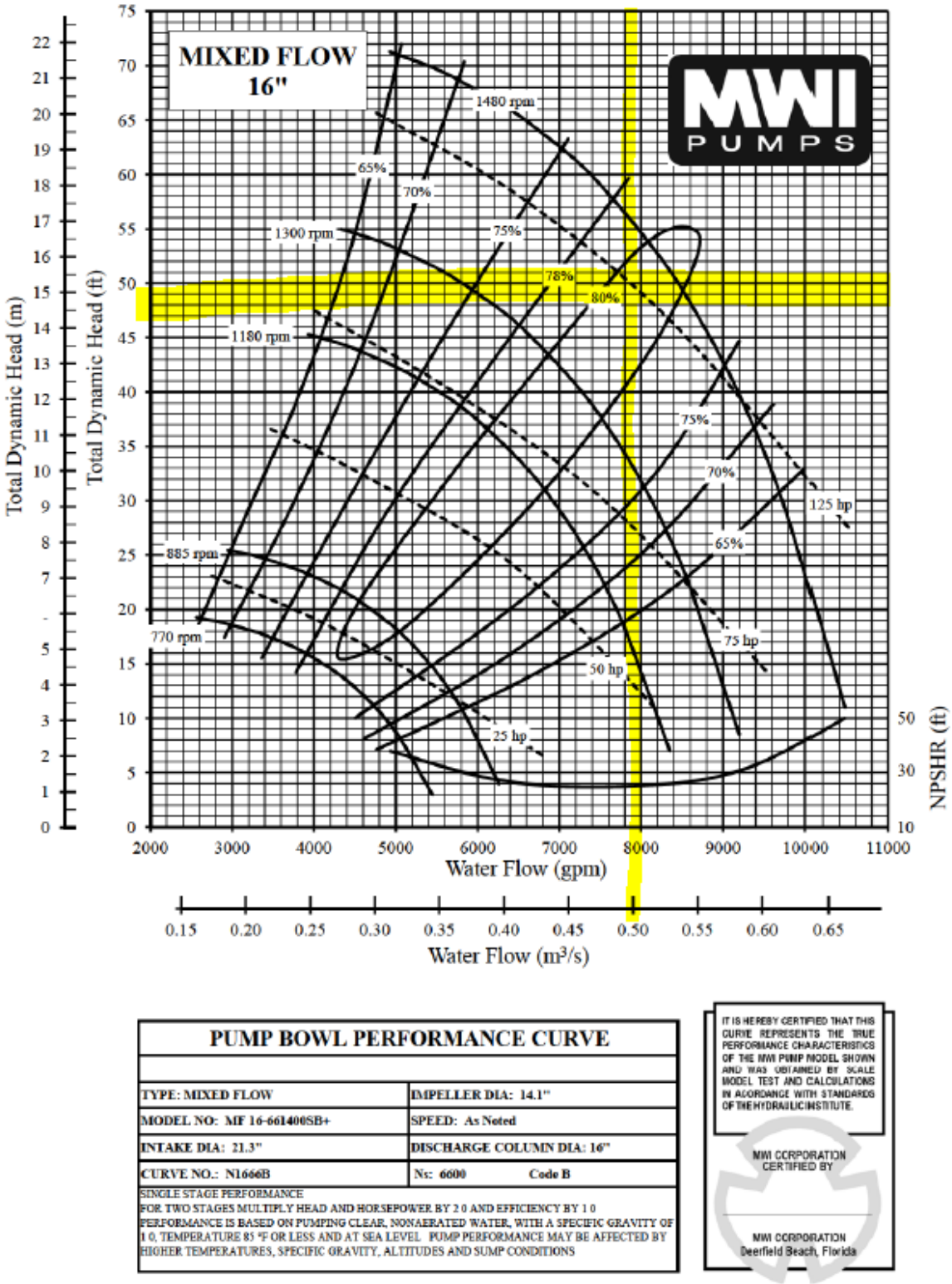

Figure 11. Performance curve for mixed flow 16-inch diameter pump (MWI Pumps 2020)

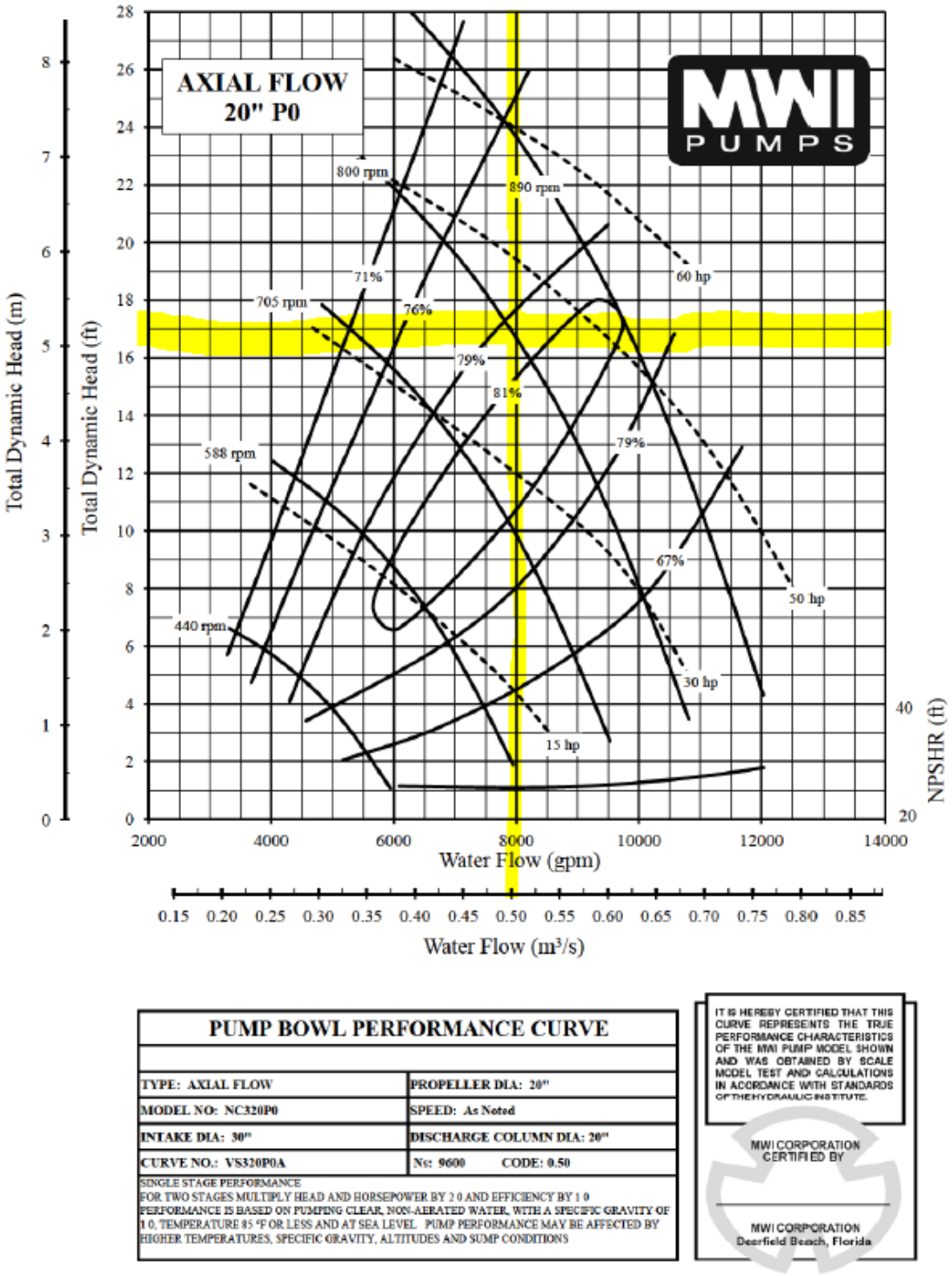

Figure 12. Performance curve for axial flow 20-inch diameter pump (MWI Pumps 2020)

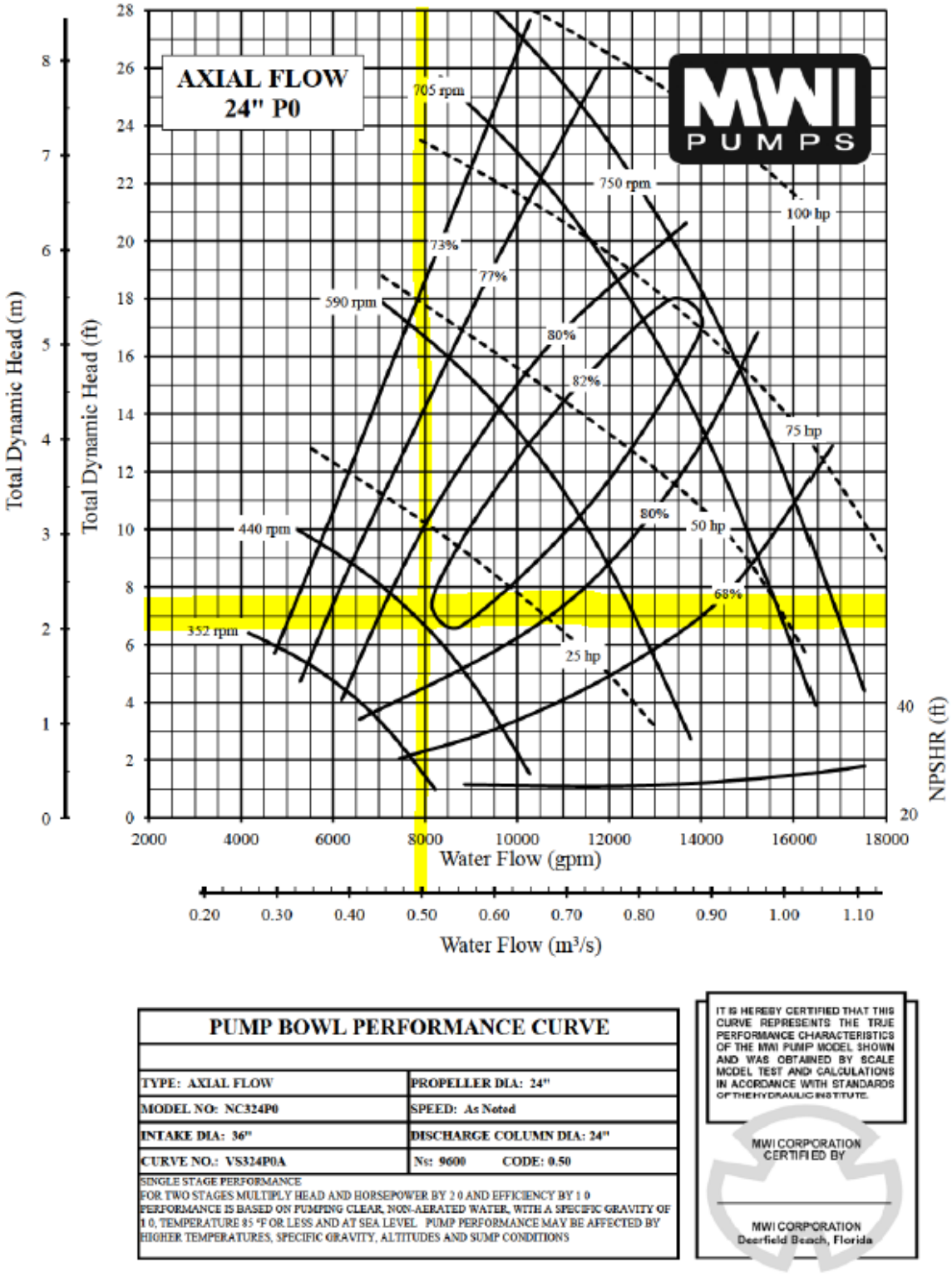

Figure 13. Performance curve for axial flow 24-inch diameter pump (MWI Pumps 2020)

Table 2 shows the various calculated values discussed above for a 16-inch (0.41 meter), 20-inch (0.51 meter), and 24-inch (0.61 meter) diameter pipe.

Table 2. Pipe calculations for power with differing pipe diameters

Pipe Diameter (inches)	16	20	24
Pump Hydraulic Power (horsepower)	98	35	15
Pump Efficiency (%)	0.80	0.79	0.82
Pump Shaft Power (horsepower)	123	44	18
Pump type (MWI Pumps)	mixed flow HMF16	axial flow HAC316	axial flow HAC316

The most feasible pipe diameter was determined to be 20 inches (0.51 m), due to the required hydraulic power and shaft power. All diameters have a similar pump efficiency at the needed flow rate, so pump efficiency was not a factor in determining the diameter to choose. Other factors that played a role in the decision are height constraints when designing a ramp for vehicles to drive over along with annual cost savings by using an axial flow pump compared to a mixed flow pump.

For the remainder of the pipe and pump system design, a high-density polyethylene (HDPE) 20-inch (0.51 m) inner diameter pipe will be used with an MWI Pumps Hydraflo™ HAC316 pump fitted with a 20-inch discharge flange. The MWI Hydraflo™ pump will be made out of 316 stainless steel since the intake will be placed in salt water.

The majority of the pipe's path from the inflow structure to the outflow structure is uninhabited land with very few disruptions; however, the pipe must eventually cross an access road to get to the outflow basin. To protect the pipe from the general public, the pipe will be laid across the road inside of USACE property, just south of the Lock. **Figure 14** shows where the pipe will cross the access road with an arrow pointing to the location of the crossing.

Figure 14. Location of pipe road crossing (Google 2021)

Information worth noting about the road crossing area is that the length of the road is about 50 feet (15.2 m), without interfering with the gate to the south and the turn in the road to the north; the width of the road is about 20 feet (6.1 m). Since the pipe will be above ground, a ramp must be added so traffic is able to get inside USACE property. Due to construction on the locks, trucks may need access to this road to get necessary equipment on the other side, also.

To successfully design a ramp for cars and trucks to cross over the pipeline, a design vehicle needed to be chosen. The design vehicle chosen for the ramp design is an intermediate semitrailer WB-40 since equipment may need to be trucked in for repairs to the locks. The WB-40 truck has a length of 45.5 feet (13.9 m), width of 8 feet (2.4 m), and wheelbase of 40 feet (12.2 m) (Harwood et al., 2003). **Figure 15** shows more complete dimensions of the design vehicle used (Harwood et al., 2003). The maximum weight of the semitrailer is 80,000 pounds (36,287 kilograms) with a fully loaded trailer and the maximum axle load for a tandem axle is 34,000 pounds (15,422 kilograms) (Harwood et al., 2003).

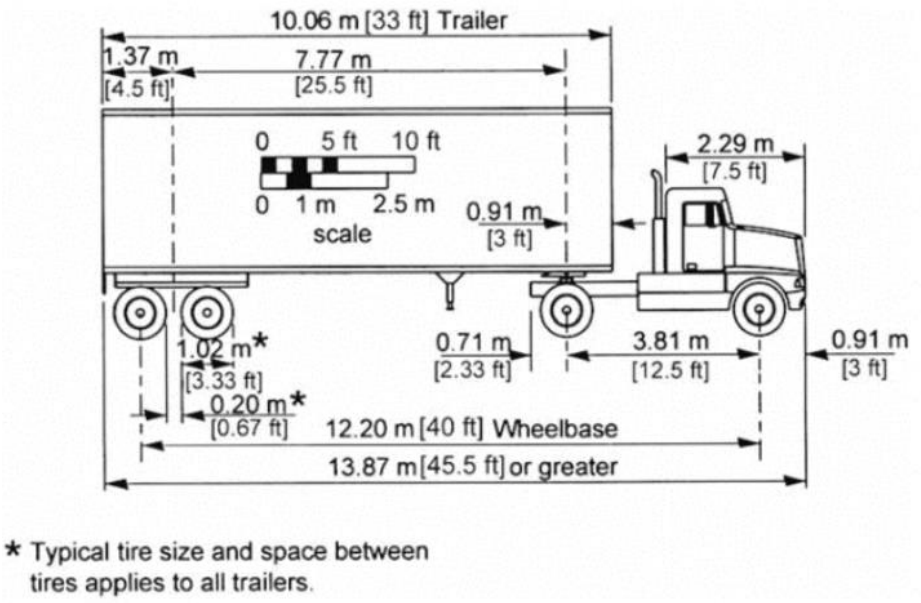

Figure 15. Semitrailer WB-40 dimensions (Harwood et al., 2003)

Manufacturing companies, such as Bluff Manufacturing, make crossover ramps out of heavy-duty steel to protect pipes and allow heavy equipment to pass over the obstacle. Bluff Manufacturing crossover ramps can accommodate equipment up to 160,000 pounds (72,575 kilograms) (Bluff Manufacturing 2021). The Crossover Ramp Worksheet with site specific dimensions was sent to Bluff Manufacturing to receive a quote for the production and freight of a ramp that fits the project location. **Figure 16** displays a picture of what the ramp would look like while **Figure 17** displays the ramp engineering drawing from Bluff Manufacturing (Bluff Manufacturing 2021). A top view of the location and ramp placement on the proposed site is provided in **Figure 18**.

Figure 16. Bluff Manufacturing crossover ramp (Bluff Manufacturing 2021)

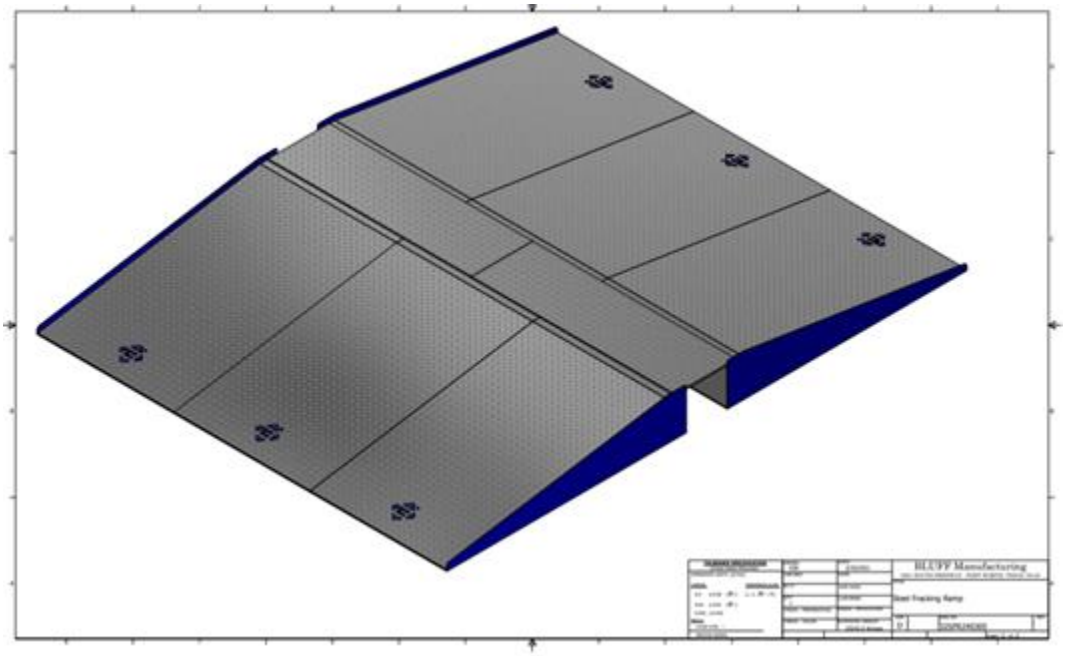

Figure 17. Bluff Manufacturing design of ramp (Bluff Manufacturing 2021)

Figure 18. AutoCAD drawing of ramp structure top view

The inflow structure is designed based on the MWI Pumps Hydraflo™ model HAC316 pump specifications and dimensions; the pump will be fitted with a 20-inch discharge flange. The standard vertical Hydraflo™ pump, shown in **Figure 19**, will be submerged and located inside of an inflow cage while the electric drive unit, shown in **Figure 20**, will be located on land and on top of a pump skid (MWI Pumps 2020).

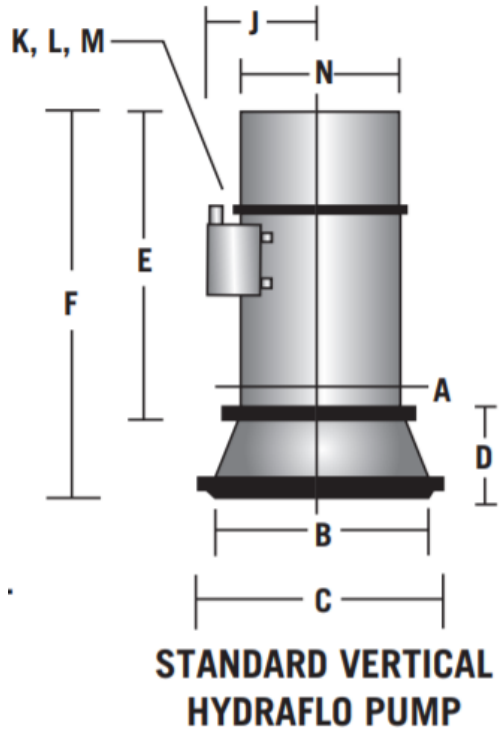

Figure 19. Standard vertical Hydraflo™ pump (MWI Pumps 2020)

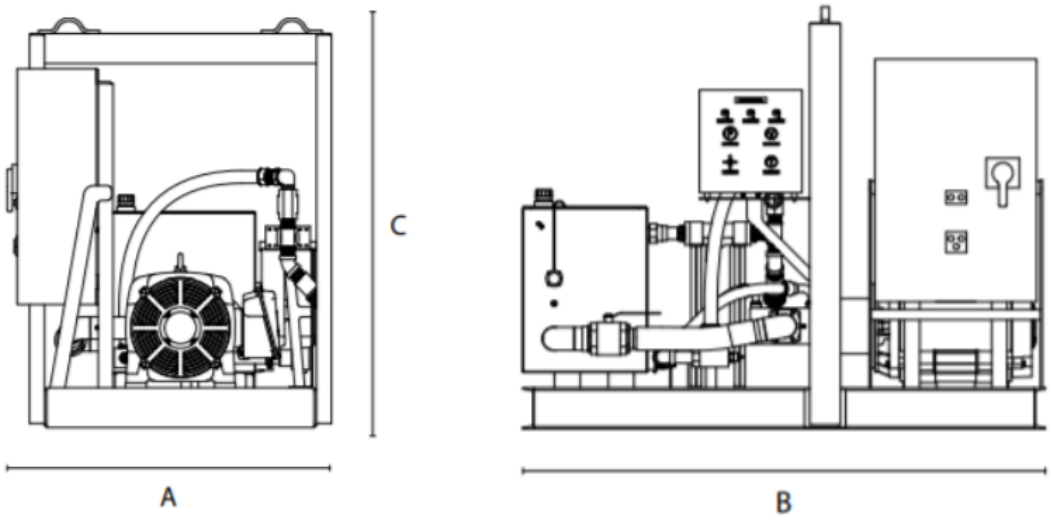

Figure 20. Electric drive unit (MWI Pumps 2020)

The inflow structure will be located behind the fenders of the lock system, where it will be the most protected from human impacts and wave activity. The approximate location is shown in **Figure 21**; the distance from the fender wall to the bank is 65.6 feet (20 m) and the depth is 3.3-6.6 feet (1-2 m). The electric drive unit will be placed on land near the pipeline on top of a skid frame and will be connected to the Hydraflo™ pump via steel conduit supply and return hoses.

Figure 21. Location of inflow structure (Google 2021)

The MWI Pumps Hydraflo™ model HAC316 will be installed with a vertical orientation. The minimum dimension requirement for the pump intake clearance, minimum water level for pump starting, and minimum water level for pump shut off can all be found in **Figure 22**, along with the maximum pump centerline to backwall spacing, which will be used for the distance between the pump centerline to the first pile being used to support the weight of the pump. Additional standard pump dimensions for the Hydraflo™ model HAC320 can be found in **Figure 23**, and the electric drive unit dimensions can be found in **Figure 24**.

Vertical Hydraflo Water Pump Single Stage Dimension Guide U.S.

NOTES:

1. Dimensions shown are minimum and can be increased when required.
2. Dimensions shown are based on an equal elbow and pipe diameter.
3. Strainer bars on intake extend below intake flange opening.
4. Depth of sump should always be designed liberally to accommodate possible future decreasing intake water levels and to maximize the potential draw down.

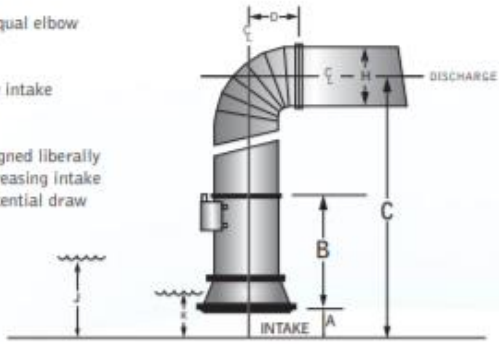

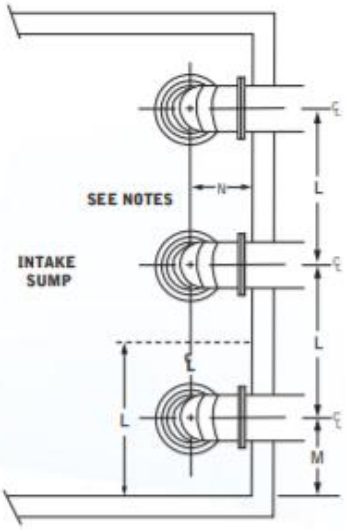

Model	A RECOMMENDED INTAKE CLEARANCE in.	B HYDRAFLO PUMP LENGTH in.	C SUMP FLOOR TO HORIZONTAL CENTERLINE OF DISCHARGE in.	D CENTERLINE OF INTAKE BELL TO DISCHARGE FLANGE in.	H DISCHARGE PIPE DIAMETER in.	J MINIMUM WATER LEVEL FOR PUMP STARTING in.	K MINIMUM WATER LEVEL FOR PUMP SHUT OFF in.	L MINIMUM PUMP SPACING in.	M MINIMUM PUMP SIDE WALL CLEARANCE in.	N MAXIMUM PUMP CENTERLINE TO BACKWALL SPACING in.
HAC308	5	29	42	9	8.6	25	13	24	12	9
HAC312	7	29	48	13	12.8	32	13	36	18	14
HAC316	10	33	58	16	16.0	40	15	48	24	18
HAC320	12	39	71	20	20.0	47	17	60	30	23
HAC324	14	42	80	24	24.0	56	24	72	36	27
HAC330	18	52	100	30	30.0	69	25	90	45	34
HAC336	22	63	121	36	36.0	82	32	108	54	41
HAC342	25	64	131	42	42.0	94	32	126	63	47
HAC348	29	58	134	48	48.0	105	46	144	72	54
HAC354	32	82	169	54	54.0	117	46	162	81	61
HAC360	36	120	216	60	60.0	131	49	180	90	68
HMF12	6	33	51	13	12.8	31	13	32	16	12
HMF16	9	42	67	16	16.0	39	15	43	21	16
HMF20	10	54	85	20	20.0	45	17	53	27	20
HMF24	13	59	96	24	24.0	57	23	64	32	24
HMF30	16	77	123	30	30.0	58	23	80	40	30
HMF42	22	108	172	42	42.0	91	33	112	56	42

Figure 22. Vertical Hydraflo™ water pump setup minimum dimensions (MWI Pumps 2020)

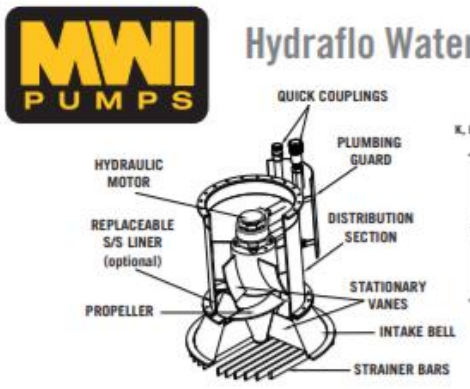

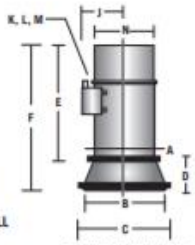

STANDARD VERTICAL HYDRAFLO PUMP

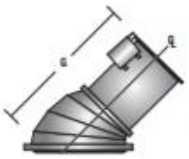

OPTIONAL ANGLE HYDRAFLO PUMP

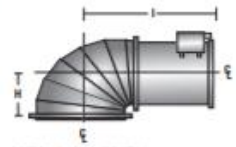

OPTIONAL HORIZONTAL HYDRAFLO PUMP

Hydraflo Water Pump - Single Stage Physical Data

	HOUSING DIAMETER		INTAKE OPENING DIAMETER		INTAKE FLANGE OUTER DIAMETER		STANDARD VERTICAL INTAKE FLANGE TO FLANGE		PUMP HOUSING FLANGE TO FLANGE		STANDARD INTAKE FLANGE TO DISCHARGE FLANGE		OPTIONAL INTAKE (NOTE 2) 45° HORIZONTAL INTAKE FLANGE TO DISCHARGE FLANGE		OPTIONAL INTAKE (NOTE 2) 90° INTAKE FLANGE TO HOUSING CENTERLINE		OPTIONAL INTAKE (NOTE 2) 90° INTAKE CENTERLINE TO VERTICAL DISCHARGE FLANGE	
	A		B		C		D (Note 1)		E (Note 3)		F		G		H		I	
	in.	mm.	in.	mm.	in.	mm.	in.	mm.	in.	mm.	in.	mm.	in.	mm.	in.	mm.	in.	mm.
HAC308	8.75	222	12	305	16	405	6.375	162	17.5	445	23.875	606	28.75	730	9.13	232	29.06	738
HAC312	13	330	18	457	22	559	6.375	162	22.25	565	28.625	727	37.63	956	11.63	295	35.44	900
HAC316	16.75	425	24	610	28	711	8.375	213	24.5	622	32.875	835	42.31	1075	15.38	391	42.38	1076
HAC320	20.75	527	30	762	34	864	8.375	213	30.5	775	38.875	987	50.81	1291	17.00	432	50.63	1286
HAC324	25	635	36	914	39.5	1003	11	279	30.5	775	41.5	1054	52.44	1332	20.38	518	54.75	1391
HAC330	31	787	45	1143	50	1270	12.5	318	39.25	997	51.75	1314	66.38	1686	23.50	597	67.81	1722
HAC336	37.25	946	54	1372	60.125	1527	14.75	375	48.375	1229	63.125	1603	81.50	2070	27.38	695	81.50	2070
HAC342	43.25	1099	63	1600	70.25	1784	14.75	375	49	1245	63.75	1619	82.44	2094	31.50	800	88.31	2243
HAC348	49.75	1264	72	1829	78.25	1988	17	432	60	1524	77	1956	102.50	2604	35.00	889	104.69	2659
HAC354	56.25	1429	81	2057	89.25	2267	21.75	552	60	1524	81.75	2076	102.50	2604	36.88	937	106.31	2700
HAC360	62	1575	90	2286	98.125	2492	24.75	629	60	1524	84.75	2153	105.06	2669	39.50	1003	113.13	2873

	HOUSING CENTERLINE TO PLUMBING GUARD		HOSE CONNECTION DIAMETER OF HOSE			FLANGE AT DISCHARGE (NOTE 4)						STANDARD VERTICAL PUMP VOLUME		STANDARD VERTICAL PUMP WEIGHT	
	J		K	L	M	N						APPROXIMATE		APPROXIMATE	
	in.	mm.	SUPPLY	RETURN	CASE DRAIN	NUMBER OF HOLES	DIAMETER OF HOLES in.	DIAMETER OF HOLES mm.	BOLT CIRCLE DIAMETER in.	BOLT CIRCLE DIAMETER mm.	OUTER DIAMETER in.	OUTER DIAMETER mm.	cu.ft.	cu.mts.	lbs.	kg.
HAC308	10	254	0.75	1	-	8	0.5625	14.29	10.75	273	12.75	324	4.42	0.125	170	77
HAC312	12	305	1	1.25	0.75	12	0.5625	14.29	14.875	378	16	406	8.02	0.227	300	136
HAC316	15	381	1.25	1.5	0.75	12	0.5625	14.29	19	483	20.8125	529	17.1	0.484	550	249
HAC320	19	483	1.25	1.5	0.75	18	0.5625	14.29	22	559	24.125	613	227.7	6.448	925	420
HAC324	22	559	1.5	1.5	0.75	20	0.5625	14.29	26.375	670	28.625	727	44.24	1.253	1500	680
HAC330	26	660	1.5-2.0	2.0	0.75	24	0.5625	14.29	32.75	832	34.125	867	95	2.690	2200	998
HAC336	30	762	1.5-2.0	2.0	0.75	28	0.75	19.05	40.625	1032	43.125	1095	158.21	4.480	3400	1542
HAC342	33	838	1.5-2.0	2.0	0.75	30	0.75	19.05	45.5	1156	49.5	1257	215	6.088	4000	1814
HAC348	40	1016	1.5-2.0	2.0	0.75	24	0.875	22.23	51.625	1311	54.1875	1376	604	17.103	7000	3175
HAC354	45	1143	(2)2.0	(2)2.0	[illegible]	24	0.875	22.23	57.625	1464	60.1875	1529	604	17.103	8500	3856
HAC360	48	1219	(2)2.0	(2)2.0	[illegible]	50	0.8124	20.64	63	1600	66.125	1680	604	17.103	10000	4536

Figure 23. Vertical Hydraflo™ water pump additional dimensions (MWI Pumps 2020)

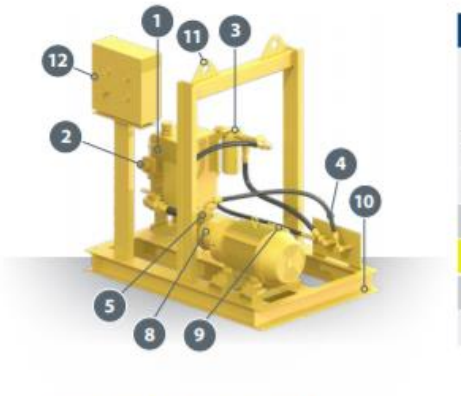

GENERAL INFORMATION							
Drive Model Number	Water Pump	Hydraulic Reservoir		Hose Connection (in.)			Electric Motor (BHP Range)
		Gals.	Ltrs.	Return	Supply	Case Drain	HP @ 1800 RPM
800	8"	10	38	1	0.75	0.75	≤35
1200	12-16"	10	38	1.25	1	0.75	36-70
2000	20"	15	57	1.5	1.25	0.75	76-100
2400	24"	22	83	1.5	1.5	0.75	101-200
3000	30-42"	40	151	2	2	0.75	201-350

STANDARD FEATURES

1. Oil reservoir/heat exchanger
2. Hydraulic oil level switch gauge
3. Return filter
4. Quick couplers
5. Relief valve
6. Suction strainer
7. Hydraulic pump
8. Coupling
9. Electric motor
10. Heavy-duty skid frame
11. Lifting eyes
12. Control panel
    A. Suction strainer vacuum gauge
    B. Hydraulic system pressure gauge
    C. Oil temperature gauge
    D. Failure reset
    E. System loading valve
13. Electric motor starter panel (optional)

Items not shown: 6, 7, 13

DIMENSIONS

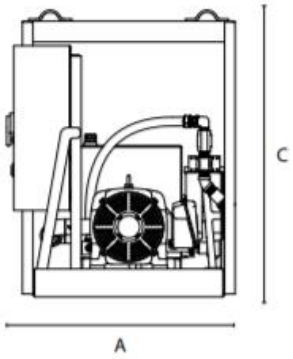

PHYSICAL DATA								
Drive Model Number	General Dimensions							
	A		B		C		Dry Weight (Approx.)	
	Ft.	Mts.	Ft.	Mts.	Ft.	Mts.	lbs	kg
800	4.00	1.22	6.00	1.83	5.60	1.71	1750	795
1200-2000	4.25	1.30	7.50	2.29	5.60	1.71	2100	950
2400	4.50	1.37	10.00	3.05	5.60	1.71	3000	1360
3000	5.19	1.58	12.50	3.81	6.67	2.03	4100	1860

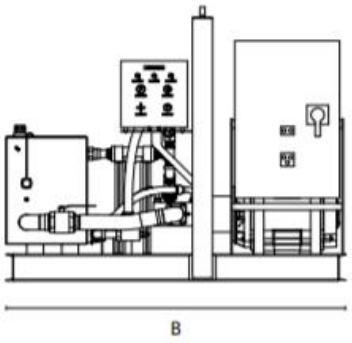

Figure 24. Electric drive unit dimensions (MWI Pumps 2020)

2.2.2 Inflow Structure

Side view and front view AutoCAD drawings of the dimensions of the inflow structure are shown in **Figure 25** and **Figure 26**. Using the maximum pump centerline to backwall spacing, the first group of support piles are located 23 inches (0.58 m) away from the centerline of the intake. Additional support pile groups are needed along the length of the pipe, and this spacing was calculated to be 20.9 feet (6.4 m) from the center of each pile (shown in **Figure 26**).

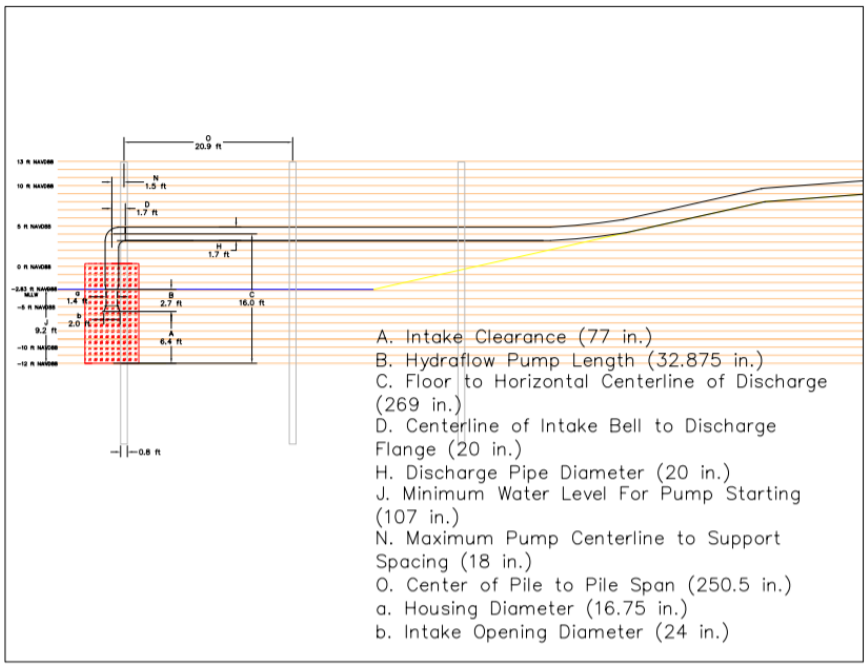

Nicole McClain
Florida Institute of Technology
Inflow Structure Side View

Figure 25. AutoCAD drawing of inflow structure side view

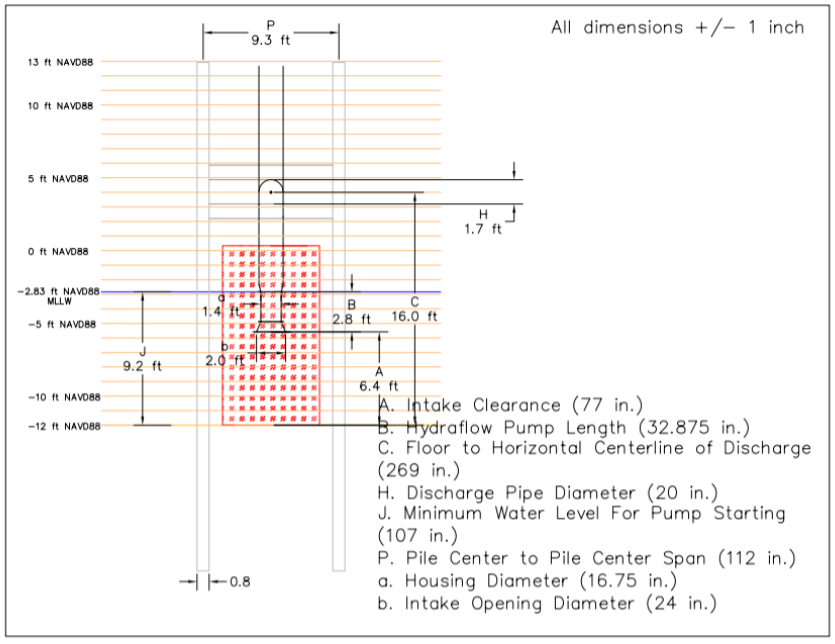

Nicole McClain
Florida Institute of Technology
Inflow Structure Front View

Figure 26. AutoCAD drawing of inflow structure front view

A side view AutoCAD drawing of the dimensions of the electric drive unit structure is shown in **Figure 27**. A top view of the where the inflow structure will be placed at the project site is displayed in **Figure 28**.

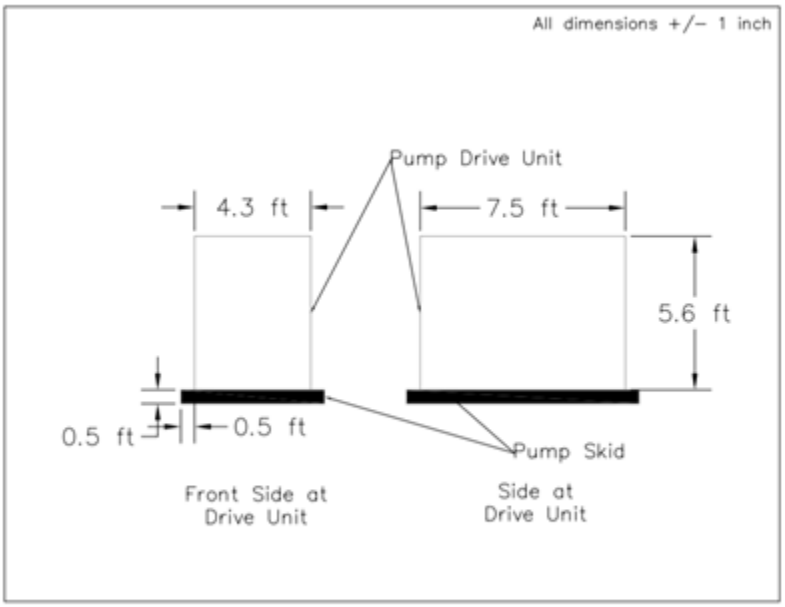

Figure 27. AutoCAD drawing of drive unit structure side view

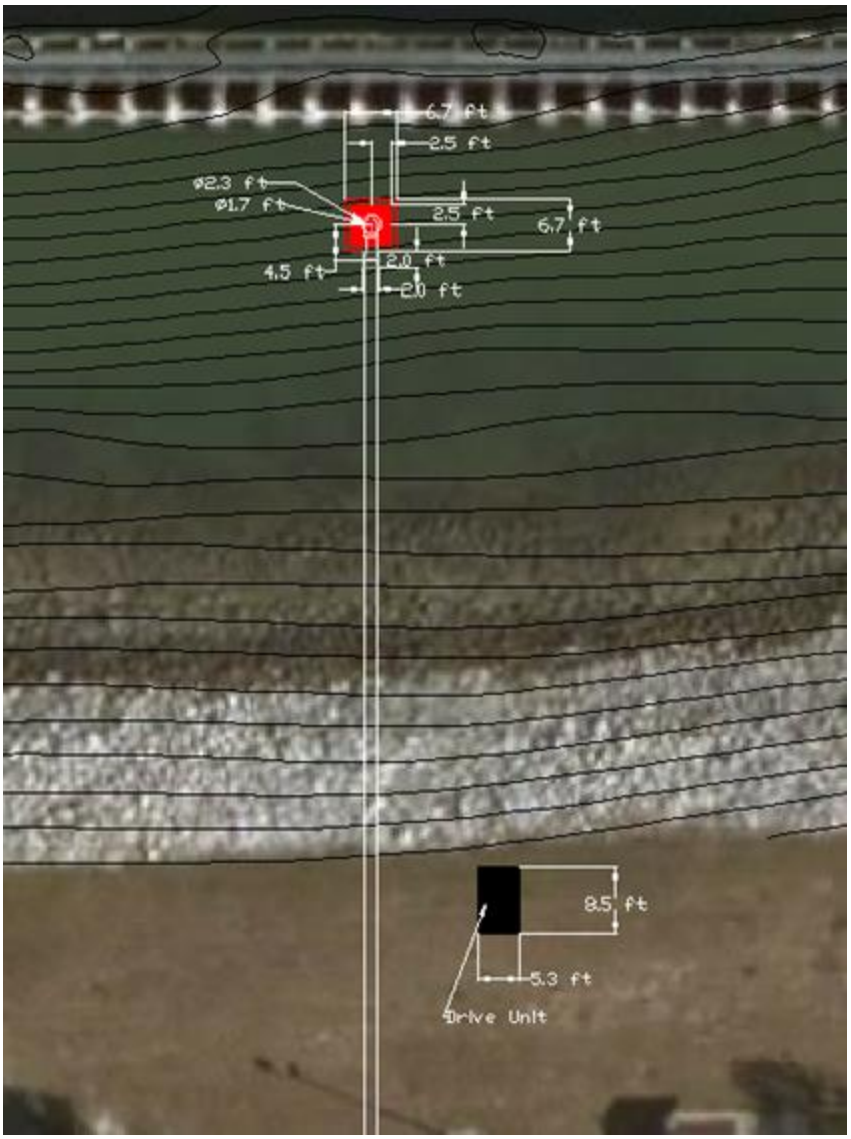

Figure 28. AutoCAD drawing of inflow structure top view

To calculate an appropriate pile spacing that will be able to support the weight of the pipe and pump, the allowable pipe deflection is first calculated to be 5% of the pipe diameter, or 1 inch (0.03 m) for the 20-inch (0.51 m) diameter pipe being used (American SpiralWeld Pipe Company 2014). The maximum pipe deflection can then be calculated for the entire length of the pipeline over water with each pile acting as a pinned support, vertical section of the pipe and seawater acting as a point load, and horizontal section of the pipe and seawater acting as a uniformly distributed load. **Figure 29** shows the deflection diagram for the portion of the pipe and pump system that will be supported by piles. When using a pile spacing of 20.9 feet (6.4 m), the maximum pipe deflection equals 0.000565 inches (0.0144 millimeters), giving the pipeline ample leeway in deflection.

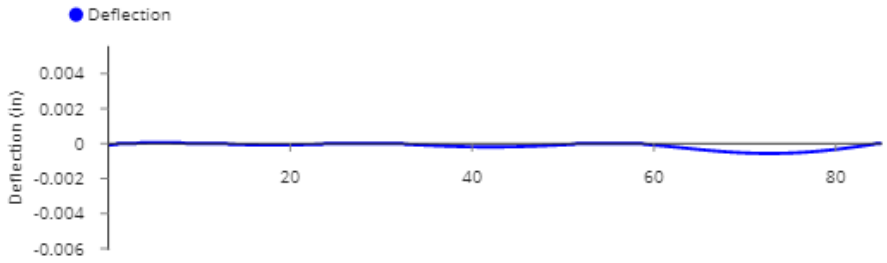

Figure 29. Deflection diagram for portion of pipe and pump system supported by piles

When piles are grouped together, the stresses transmitted by the piles to the soil will overlap, which reduces the load-bearing capacity of the piles (Das 2019). The minimum center-to-center pile spacing used is 3.5D, so when using 12-inch (0.30 m) diameter square piles, the grouped piles must be spaced at least 42 inches (1.07 m). In each group of piles for the inflow structure, the spacing was calculated to be 112 inches (2.84 m) so that the piles do not interfere with the cage structure (**Figure 26**).

A minimum intake clearance was calculated to ensure particles of fine sediment will not be sucked into the pump intake. The initiation of particle movement can be represented by the dimensionless parameter known as the Shields parameter, ψ (El Shamy et al., 2018). The Shields parameter is used to express the ratio of the shear forcing, created by water flow, acting on a sediment particle that is resting on the top of the bed to the weight of a single particle water (Stachurska and Staroszczyk 2019; El Shamy et al., 2018). The equation for Shields parameter is below (Dean and Dalrymple 2002):

$$\psi = \frac{\tau_b}{(\rho_s - \rho) g d_{50}} \quad [8]$$

where τ_b is the shear stress at the bed, ρ_s is the density of the sediment particle at the bed, ρ is the density of the fluid, and d is the sediment grain diameter. The shear stress of the bed can further be equated to:

$$\tau_b = \frac{1}{8} \rho f U_b^2 \quad [9]$$

where f is the Darcy-Weisbach friction coefficient. The Darcy-Weisbach friction coefficient has an inverse relationship with the drag coefficient:

$$C_d = \frac{f}{4} \quad [10]$$

When plugging the shear stress equation into the Shields parameter equation and substituting the drag coefficient for the Darcy-Weisbach friction coefficient, equation 8 becomes:

$$\psi = \frac{\frac{1}{2} \rho U_b^2 C_d}{(\rho_s - \rho) g d_{50}} \quad [11]$$

For sediment entrainment to be eliminated in the pipe and pump system, the intake must be placed a calculated distance above the bed, so that the flow of water inside of the intake will not initiate sediment movement. If the calculated Shields number exceeds the critical Shields number, ψ_c, the particles at the bed would begin to move (El Shamy et al., 2018). The critical Shields number must be plugged into Equation 11, and the velocity must be solved for. With the calculated

velocity at the bed that will initiate sediment movement, the area of a flow hemisphere around the intake can be computed, and then a radius of this flow hemisphere can be obtained. This radius value will also be the minimum intake clearance for which sediment entrainment will not occur.

The particle used for the evaluation of Shields parameter is coarse silt, which has a particle diameter of 0.00246 inches (0.0624 mm); shown in **Figure 30**, the critical Shields number for a coarse silt particle is 0.109 (Berenbrock and Tranmer, 2008).

Particle classification name	Ranges of particle diameters		Shields parameter (dimensionless)	Critical bed shear stress (τ_c) (N/m^2)
	φ	mm		
Coarse cobble	-7 – -8	128 – 256	0.054 – 0.054	112 – 223
Fine cobble	-6 – -7	64 – 128	0.052 – 0.054	53.8 – 112
Very coarse gravel	-5 – -6	32 – 64	0.05 – 0.052	25.9 – 53.8
Coarse gravel	-4 – -5	16 – 32	0.047 – 0.05	12.2 – 25.9
Medium gravel	-3 – -4	8 – 16	0.044 – 0.047	5.7 – 12.2
Fine gravel	-2 – -3	4 – 8	0.042 – 0.044	2.7 – 5.7
Very fine gravel	-1 – -2	2 – 4	0.039 – 0.042	1.3 – 2.7
Very coarse sand	0 – -1	1 – 2	0.029 – 0.039	0.47 – 1.3
Coarse sand	1 – 0	0.5 – 1	0.033 – 0.029	0.27 – 0.47
Medium sand	2 – 1	0.25 – 0.5	0.048 – 0.033	0.194 – 0.27
Fine sand	3 – 2	0.125 – 0.25	0.072 – 0.048	0.145 – 0.194
Very fine sand	4 – 3	0.0625 – 0.125	0.109 – 0.072	0.110 – 0.145
Coarse silt	5 – 4	0.0310 – 0.0625	0.165 – 0.109	0.0826 – 0.110
Medium silt	6 – 5	0.0156 – 0.0310	0.25 – 0.165	0.0630 – 0.0826
Fine silt	7 – 6	0.0078 – 0.0156	0.3 – 0.25	0.0378 – 0.0630

Figure 30. Particle classification with particle diameter and Shields parameter (Berenbrock and Tranmer 2008)

The drag coefficient value used for the calculation is the drag coefficient of a sediment particle at the bed. Shown in **Figure 31**, the drag coefficient for a sediment particle varies based on the bed geometry; a drag coefficient of 0.35 was chosen for the calculation of the velocity at the bed (Dwivedi, Melville, Shamseldin, and Guha 2010).

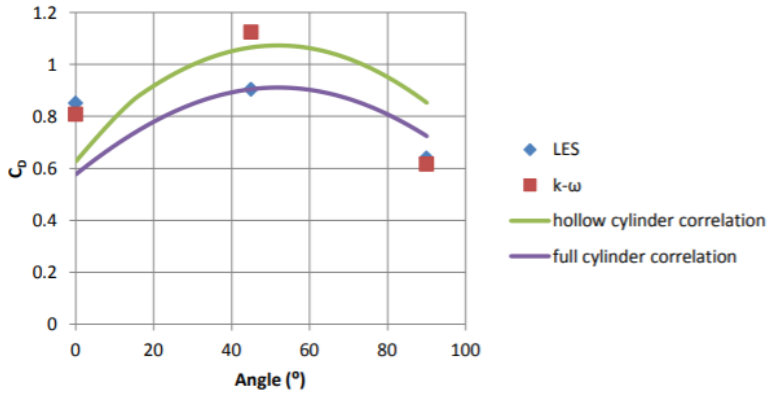

Figure 31. Drag coefficient for a hollow cylinder (Franzluebbers 2013)

The velocity value for initial particle movement was calculated to be 0.046 ft per second (0.0140 m per second); the velocity value can then be used to determine the radius of the suction hemisphere. With a particle velocity of 0.046 ft per second (0.0140 m per second), the radius of the suction hemisphere is calculated to be 6.4 ft (1.9 m). In other words, the intake must be at least 6.4 ft (1.9 m) above the seabed to ensure particles smaller than coarse silt will not get sucked into the pump intake.

Using **Figure 22** and the minimum water level for pump starting a minimum water depth can be calculated for the location of the pump. The minimum water depth needed for the pump intake is 9.2 ft (2.8 m) to satisfy both the minimum water level required for the pump to start and the minimum depth needed to avoid fine sediment particle entrainment.

To protect the marine animals in the area, such as manatees and fish, and to protect the pump from human impacts, the pump will be surrounded by a cage structure with grated screens on the side. The cage will be placed on the seabed and the pipe and intake pump will be lowered vertically inside of the cage. An AutoCAD drawing of the cage structure with screens to keep out manatees and other important marine life is shown in **Figure 32**. For the protection of manatees, the maximum grating space should be 8 inches (0.20 m) apart (Comprehensive Everglades Restoration Plan 2006). For the protection of small fish, the grating should be 1 inch by 4 inches (0.03 m by 0.10 m) (USFWS 2019). The grating that will be used on the caged inflow structure will be 1 inch by 4 inch (0.03 m by 0.10 m) galvanized steel grating installed with the 4 inch (0.10 m) dimension aligned to the horizontal plane.

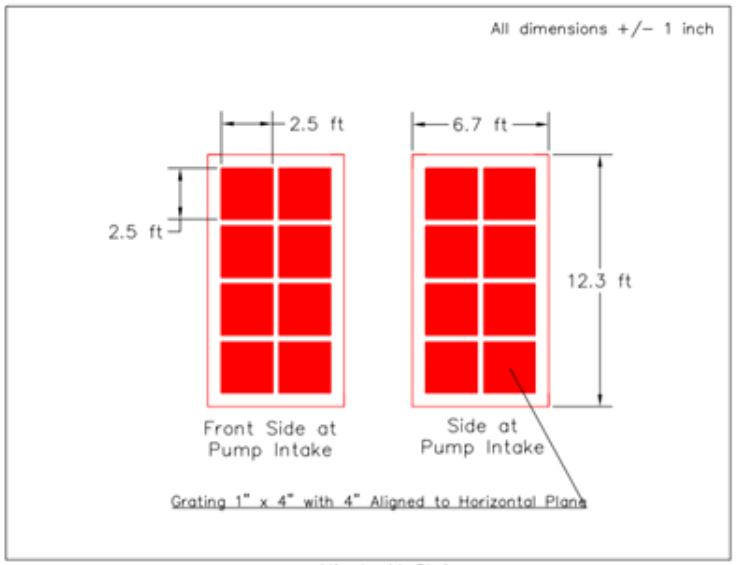

Figure 32. AutoCAD drawing of cage structure with screening

2.2.3 Outflow Structure

The outflow structure is designed based on the Hydraulics Manual from the Oregon Department of Transportation (ODOT). An energy dissipator is needed at the pipe outlet so that the bank is protected from erosion as the water flows out of the pipe and into BRL. Energy dissipators can be designed in many different forms, including unlined pools, internal dissipators, riprap pads, riprap lined basins, drop structures, and complex dissipators (ODOT 2014). The design of the outflow

structure for the pipe and pump system will specifically examine riprap pads and riprap lined basins.

Riprap pad dissipators allow the flowing water to cross over riprap before it enters the waterbody it is flowing into, causing a considerable decrease in hydraulic energy from the flow (ODOT 2014). Riprap pads are often used for projects where a low cost and easily constructed dissipator are needed, the flow from the pipe outlet has moderate to low velocity and depth, and fish passage is not required (ODOT 2014). An example of a riprap pad dissipator is shown in **Figure 33**.

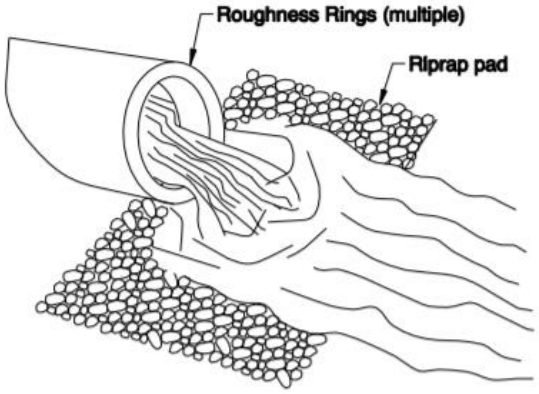

Figure 33. Riprap pad dissipator example (ODOT 2014)

Riprap lined basin dissipators allow the flowing water to collide with water already in the basin, again causing a considerable decrease in hydraulic energy from the flow (ODOT 2014). In this scenario, the riprap lining protects the soil from scour and erosion as water flows into the basin (ODOT 2014). Riprap lined basins are often used for projects where fish passage is desired, flow depths and velocities exceed acceptable values for a riprap pad, and the pool is not a safety hazard to the public (ODOT 2014). **Figure 34** shows an example of a riprap lined basin dissipator.

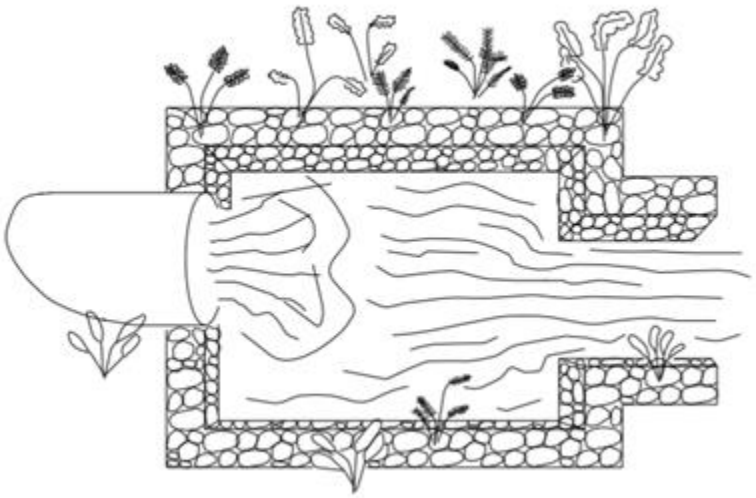

Figure 34. Riprap lined basin example (ODOT 2014)

The main hydraulic characteristics that determine the type and size of the energy dissipator needed, along with the class of riprap rock, are brink depth and Froude number (ODOT 2014).

Equivalent brink depth is defined as the hypothetical depth of flow at the brink, or outlet of the pipe. The equation for equivalent brink depth is below (ODOT 2014):

$$y_e = \left(\frac{a}{2}\right)^{0.5} \quad [12]$$

where y_e is the equivalent brink depth and a is the cross-sectional area of flow.

Froude number is a dimensionless parameter that expresses the ratio of the inertial force of flowing water to the force of gravity. The equation for Froude number is below (ODOT 2014):

$$Fr_e = \frac{v}{(32.2y_e)^{0.5}} \quad [13]$$

where Fr_e is the equivalent Froude number of the flow at the brink, v is the average flow velocity, and y_e is the equivalent brink depth.

For the pipe and pump system, the equivalent brink depth is calculated to be 0.93 feet (0.29 m) while Froude number is calculated to be 1.845. With the calculation of brink depth and Froude number, the ODOT Energy Dissipator Selection Charts can be used to determine the type of energy dissipator and the class of riprap rock needed. **Figure 35** shows the appropriate chart for the pipe and pump system.

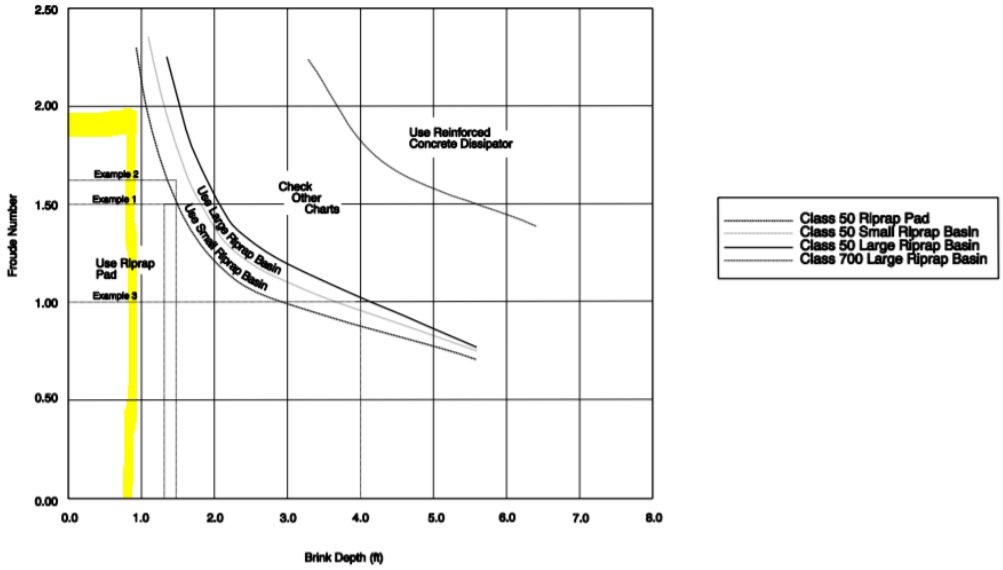

Figure 35. ODOT energy dissipator selection chart (ODOT 2014)

From **Figure 35**, it was determined that a Class 50 riprap pad is an adequate energy dissipator for the pipe and pump system. The characteristics of Class 50 riprap are shown in **Figure 36**. The dimensions of the riprap pad are then calculated using the ODOT riprap pad dimensions figures, shown in **Figure 37** and **Figure 38**.

Standard Riprap Class	D_{50} (feet)	W_{50} (lbs)	D_{100} (feet)	W_{100} (lbs)
Class 50	0.56	15	0.83	50
Class 100	0.66	25	1.05	100
Class 200	0.93	70	1.32	200
Class 700	1.32	200	2.01	700
Class 2000	2.01	700	2.85	2000

Figure 36. Characteristics of standard riprap classes (ODOT 2014)

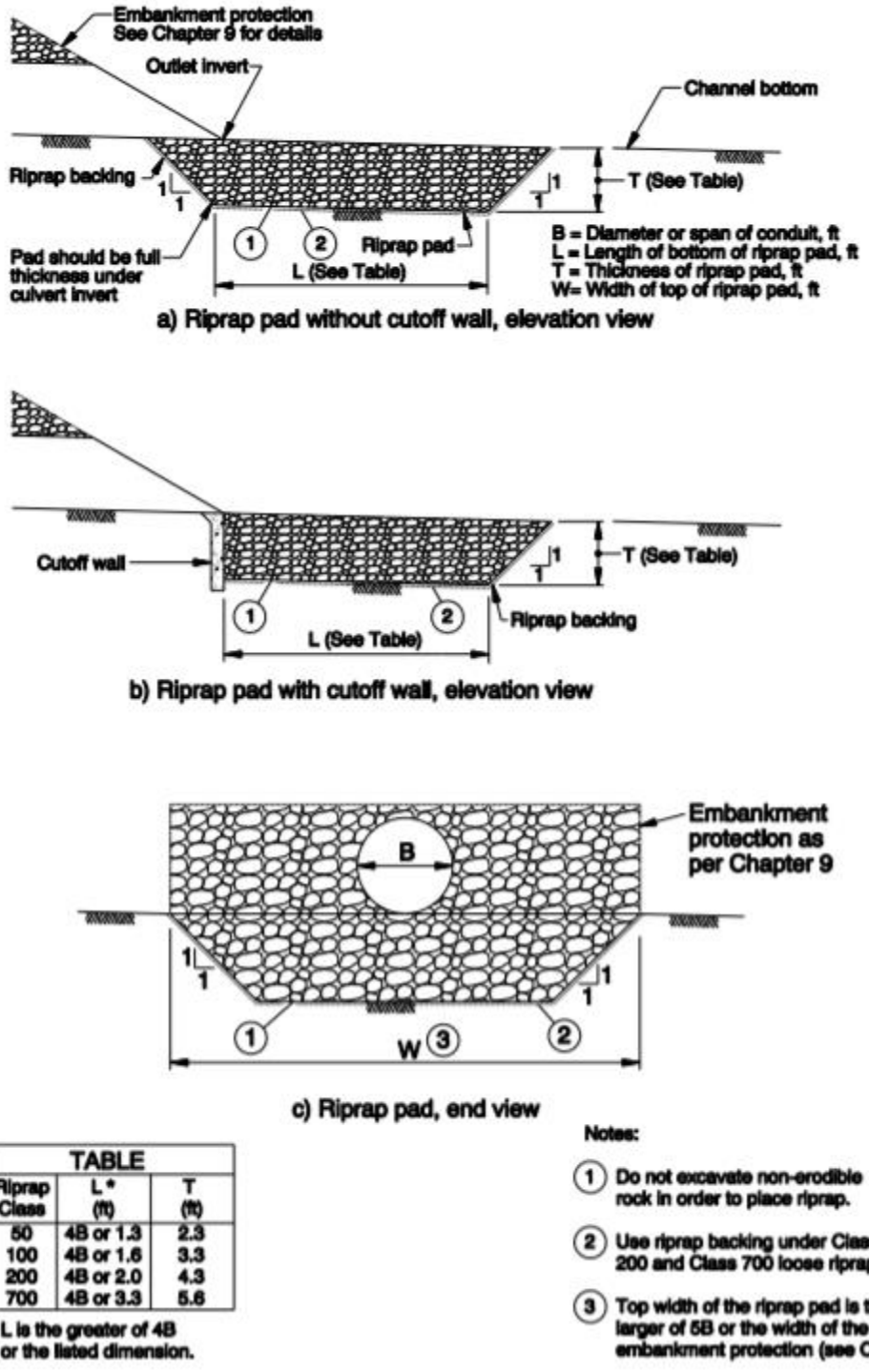

TABLE		
Riprap Class	L * (ft)	T (ft)
50	4B or 1.3	2.3
100	4B or 1.6	3.3
200	4B or 2.0	4.3
700	4B or 3.3	5.6

* L is the greater of 4B or the listed dimension.

Notes:

1. Do not excavate non-erodible rock in order to place riprap.
2. Use riprap backing under Class 200 and Class 700 loose riprap.
3. Top width of the riprap pad is the larger of 5B or the width of the embankment protection (see Chapter 9).

Figure 37. Dimensions of riprap pad (ODOT 2014)

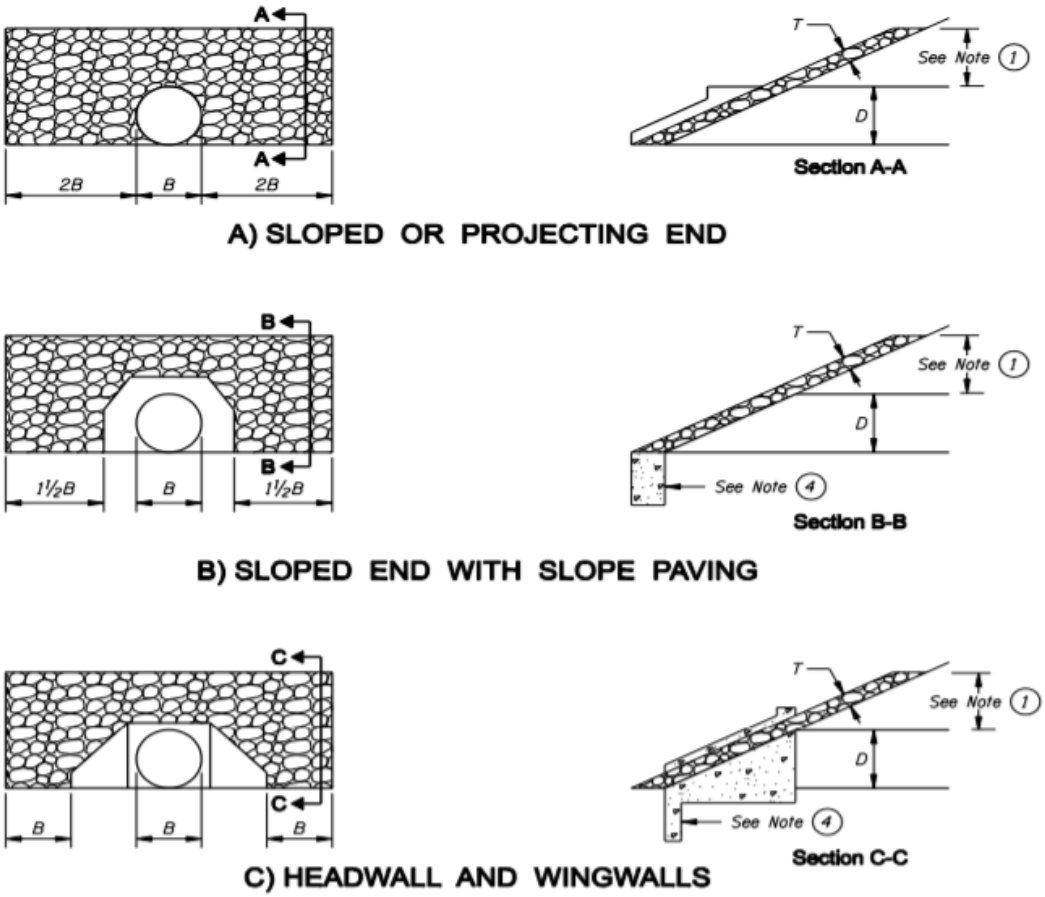

Figure 38. Dimensions of riprap pad continued (ODOT 2014)

The dimensions of the riprap pad were calculated to be 6.67 feet in length, 8.35 feet in width, and 2.3 feet in thickness (2.03 m in length, 2.55 m in width, and 0.70 m in thickness). The riprap pad toe must extend past mean lower low water (a distance of 37.7 feet [11.5 m]) to prevent erosion of the toe. The thickness of the riprap blanket must be 12 inches (0.30 m) (ODOT 2014). Underneath the riprap, a geotextile, non-woven filter fabric will be placed on the foundation; a 2-inch (0.05 m) sand layer is also needed on top of the filter fabric to protect it from ripping when coming into contact with the riprap rocks. A side view AutoCAD drawing of the dimensions of the outflow structure is shown in **Figure 39** and a top view of the outflow structure location is shown in **Figure 40**.

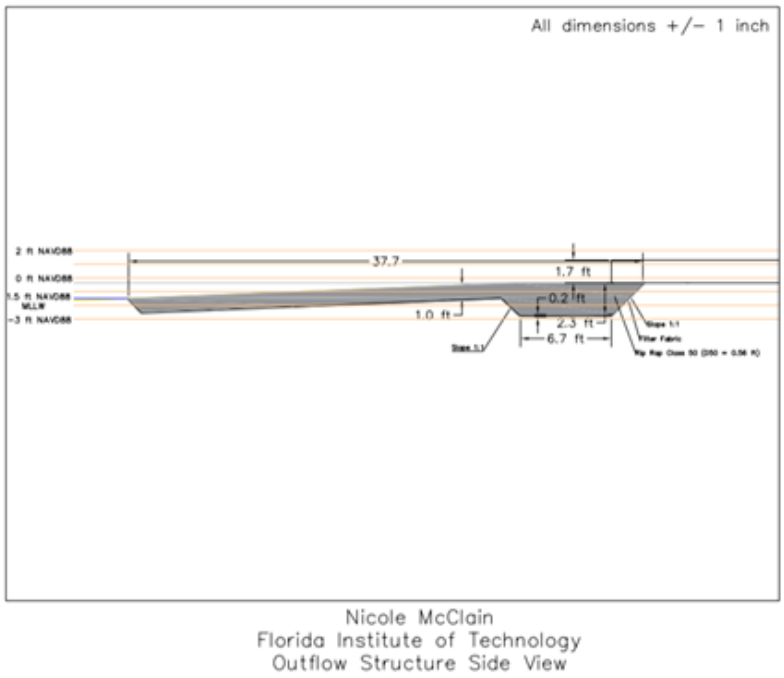

Figure 39. AutoCAD drawing of outflow structure side view

Figure 40. AutoCAD drawing of outflow structure top view

2.3 Cost Analysis

The cost analysis of the pipe and pump system will include an analysis of first costs during the construction of the system, an analysis of annual costs expected over the span of the first year, and an analysis of decommissioning costs of the system. The overall project cost, including first costs, annual costs, and decommissioning costs, is estimated to be $711,245.32.

The analysis of first costs during construction will be broken into five parts based on the construction of the different components that make up the system. Prices for each component of the cost estimate come from standard material costs listed by RSMeans unless otherwise noted.

The cost analysis for the pipeline, shown in **Table 3**, includes 1,000 linear feet of 24-inch HDPE pipe DR 11 (inner diameter = 19.374 inches and outer diameter = 24 inches), ten 45 degree 24-inch HDPE DR 11 elbows, and five thrust anchors. The total cost of the pipeline portion of the design is $93,635.00.

Table 3. Pipeline cost analysis (RSMeans 2021; Development Services Department 2009)

Item	Number	Units	Per Unit Cost	Total Cost
24-inch HDPE Pipe DR 11 (ID 19.374 in, OD 24 in)	1,000	Linear Feet	$86	$86,000
24-inch HDPE Elbow DR 11 - 45 degree	10	EA	$540	$5,400
Thrust Anchor	5	EA	$447	$2,235
Pipeline Total				***$93,635***

The cost analysis for the pump, shown in **Table 4**, comes from a quote from MWI Pumps and includes one MWI HAC316 Hydroflo™ pump made out of 316ss materials, one 1600E electric drive unit in a skid configuration, one 75 horsepower at 1800 revolutions per minute electric motor, one auto start/stop control panel with floats, and one 50-foot set of hydraulic hoses. The total cost of the pump portion of the design is $149,092.

Table 4. Pump cost analysis (MWI Pumps, 2021)

Item	Number	Units	Per Unit Cost	Total Cost
MWI HAC316 Hydraflo™ Pump – 316ss Materials 1600E Electric Drive Unit – Skid Configuration 75 horsepower @ 1800 revolutions per minute Electric Motor Auto Start/Stop Control Panel with Floats 50’ Set of Hydraulic Hoses – Stainless Quick Disconnect Fittings	1	EA	$149,092	$149,092
Pump Total				***$149,092***

The cost analysis for the ramp structure, shown in **Table 5**, comes from a quote from Bluff Manufacturing and includes one steel fracking ramp and freight from Fort Worth, Texas to Melbourne, Florida via C&H Freight. The total cost of the ramp structure portion of the design is $49,806.

Table 5. Ramp structure cost analysis (Bluff Manufacturing 2021)

Item	Number	Units	Per Unit Cost	Total Cost
Bluff Manufacturing Steel Fracking Ramp (32SFR240305)	1	EA	$46,556	$46,556
Freight from Fort Worth, Tx to Melbourne, Fl Via C & H	1	EA	$3,250	$3,250
Ramp Structure Total				***$49,806***

The cost analysis for the inflow structure, shown in **Table 6**, includes one 24-inch stainless steel type 316 90 degree elbow, 260 linear ft of stainless steel for the cage frame, 1-inch by 4-inch galvanized steel grating, six timber piles, the cost for pile driving equipment setup and labor for driving the piles, and 51 linear ft of steel H beam. The total cost of the inflow structure portion of the design is $31,196.25.

Table 6. Inflow structure cost analysis (RSMeans 2021; Midwest Steel Supply 2021; McMaster-Carr 2021; LK Goodwin 2021)

Item	Number	Units	Per Unit Cost	Total Cost
24-inch Stainless Steel Type 316 90 degree Elbow	1	EA	$169.25	$169.25
Cage Frame - Stainless Steel Square Tube 2-inch by 2-inch	260	Linear Feet	$7.00	$1,820.00
Galvanized Steel Grating 15W4 – 1-inch by 4-inch (non-serrated)	5	EA	$852.00	$4,260.00
Timber Pile - 50-59 feet long	6	EA	$688.00	$4,128.00
Pile Driving Set Up - Equipment and Labor	1	EA	$10,250.00	$10,250.00
Pile Driving - Labor for Crew	12	Hours	$800.00	$800.00
Steel H Beam – 8-inch by 15-inch	51	Linear Feet	$19.00	$969.00
Inflow Structure Total				***$31,196.25***

The cost analysis for the outflow structure, shown in **Table 7**, includes ten tons of riprap and rock lining (D50=0.56 ft, W100=50 pounds), 40 square yards of nonwoven geotextile fabric, and two and a half cubic yards of sand (RSMeans 2021). The total cost of the outflow structure portion of the design is $438.

Table 7. Outflow structure cost analysis (RSMeans 2021)

Item	Number	Units	Per Unit Cost	Total Cost
Riprap and Rock Lining (D_{50}=0.56 feet, W_{100}=50 pounds)	10	Tons	$32.61	$326.10
Geotextile Fabric - Non-woven	40	Square Yards	$1.36	$54.40
Sand	2.5	Cubic Yards	$23.00	$57.50
Outflow Structure Total				***$438.00***

For the complete design of the pipe and pump system, the costs of each individual component of the design are summed. A 30% contractor mobilization and overhead cost is added to the final project price; a contingency of 40% is also added for miscellaneous site work and uncertainties. The total first cost of the pipe and pump system is $551,084.33, shown in **Table 8**.

Table 8. Total first cost for pipe and pump system

Structure	Total Cost
Pipeline	$93,635.00
Pump	$149,092.00
Ramp	$49,806.00
Inflow	$31,196.25
Outflow	$438.00
Subtotal	$324,167.25
Contractor Mobilization, Overhead, and Profit (30%)	$97,250.18
Contingency (40%)	$129,666.90
Total	***$551,084.33***

The analysis of annual costs expected over the span of one year includes two main cost categories: operational costs and maintenance costs. Operational costs include the cost of electricity for the pump to run 24 hours a day for 365 days, or one full year. Maintenance costs include the cost of pump maintenance and the cost of expected maintenance to the pipeline. A contingency of 40% is added to account for increased electricity costs and unexpected maintenance costs. The total annual cost of the pipe and pump system is $47,578.63, shown in **Table 9**.

Table 9. Total annual cost for pipe and pump system (U.S. Department of Energy 2001; ElectricRate 2020)

Item	Number	Units	Per Unit Cost	Total Cost
Electricity	287423	Kilowatt Hours	$0.1165	$33,484.73
Routine Maintenance	1	EA	$500.00	$500.00
Subtotal				$33,984.73
Contingency (40%)				$13,593.89
Total				***$47,578.63***

The analysis of decommissioning costs expected at the end of the project's lifespan includes the removal of different components that make up the system. A 30% contractor mobilization and overhead cost is added to the final project price; a contingency of 40% is also added for miscellaneous site work and uncertainties. The total decommissioning cost of the pipe and pump system is $112,582.37, shown in **Table 10**.

Table 10. Total decommissioning cost for pipe and pump system (RSMeans 2021; Kaiser 2017; CDM Smith 2017)

Item	Number	Units	Per Unit Cost	Total Cost
Riprap Removal	10	Tons	$33.25	$332.50
Pile Removal - Equipment and Labor	1	EA	$10,250.00	$10,250.00
Pile Removal - Labor for Crew	12	Hours	$800.00	$9,600.00
Pipeline Removal (On Ground)	850	Feet	$11.40	$9,691.29
Pipeline Removal (Over Water)	150	Feet	$57.01	$8,551.14
Safety Signs	5	Days	$2,000.00	$10,000.00
Diver, Boat, Misc.	5	Days	$3,560.00	$17,800.00
Subtotal				$66,224.92
Contractor Mobilization, Overhead, and Profit (30%)				$19,867.48
Contingency (40%)				$26,489.97
Total				***$112,582.37***

2.4 Design Summary

The design was developed working with partners and stakeholders. Once the work was passed onto Tetra Tech, where the official 60% design plan set was generated, this design plan was shared with USACE for comment.

3 Water Level, Salinity, and Temperature

Phase 2 included upgrading of existing long-term water level sensors in BRL and IRL, as well as the addition of new sensors in the project area to measure water level, salinity, and temperature. Instruments were deployed in the semi-enclosed basin where the port water will be discharged

into BRL. The data collected will be used for model validation and serve baseline data should the pilot project get approval.

3.1 Long-term Water Levels

Existing long-term water level stations have been collecting data with some gaps since winter of 2014. For this project, the three stations were upgraded with real time data collection and reporting system purchased from OnSet, HOBO RX2100 Station - CELL-4G. In April 2021, student researchers installed the solar powered HOBO instruments at each of the three long-term water level locations in the IRL: Kars Park on Merritt Island, Lansing Island in Indian Harbour Beach, and Riverside Park in Sebastian (**Figure 41**).

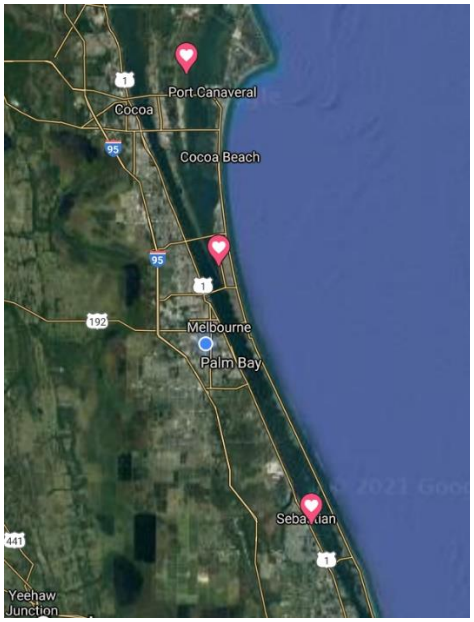

Figure 41. Location of long-term water level gauges at Kars Park on Merritt Island, Lansing Island in Indian Harbour Beach, and Riverside Park in Sebastian

The HOBO instruments include up to eight connection ports for possible data reading devices, a cellular connection to the internet, and a solar panel that powers the entire system. These new instruments are used to replace the old HOBO U20 water level and temperature loggers that required a physical offload of data every time the device runs out of memory.

The previous HOBO instrument was removed from the pipe and the distance from the cap was measured. The main housing was screwed into a nearby piling facing towards the south for optimal solar conditions. Braid fishing line was used to tie the sensor to the cap of the polyvinyl chloride (PVC) pipe. The length of fishing line was measured and then the sensor was lowered into the pipe until it touched the surface of the water. This position on the line was marked with tape and we then subtracted the known length of line from the length of the new tape position to find a beginning reference water depth. A slot was drilled in the PVC pipe so the wire could be inserted, and the cap can be placed back on top. The instruments are hanging by fishing line with slack in the wire so there is always a known distance that the instrument is suspended within the pipe. The top of each PVC cap is a surveyed position above the mean water level, allowing for the location of the sensor to be calculated.

The northern-most sensor is located at the end of a pier off of Kars Park across the lagoon from the Barge Canal (**Figure 42**). This sensor is closest of the three to the inflow project site and provides a record of the water levels in the northern BRL.

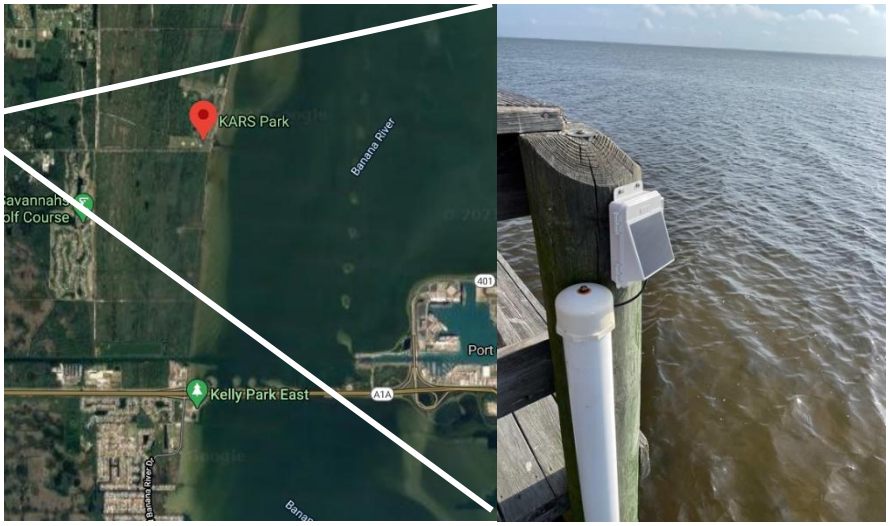

Figure 42. Northern-most station at Kars Park in Merritt Island, FL, which is west of the proposed inflow site in the northern BRL

The second sensor is located at the end of a residential pier on Lansing Island (**Figure 43**). This location provides measurements of water level in the southern BRL.

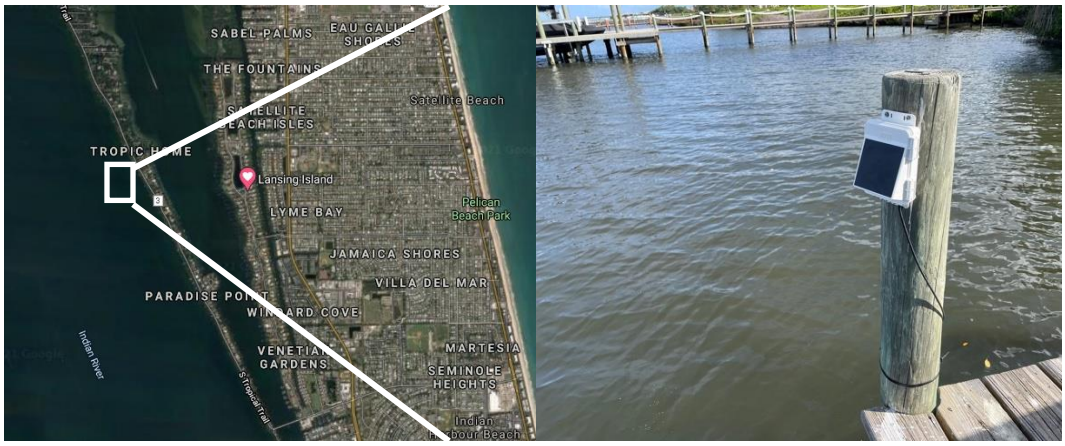

Figure 43. Lansing Island station, located at the southern end of BRL

The southern-most sensor is located at the end of the Riverview Park fishing pier in Sebastian, FL (**Figure 44**). This sensor is located near the Sebastian Inlet, the closest inlet to the study site with a direct access to the Atlantic Ocean.

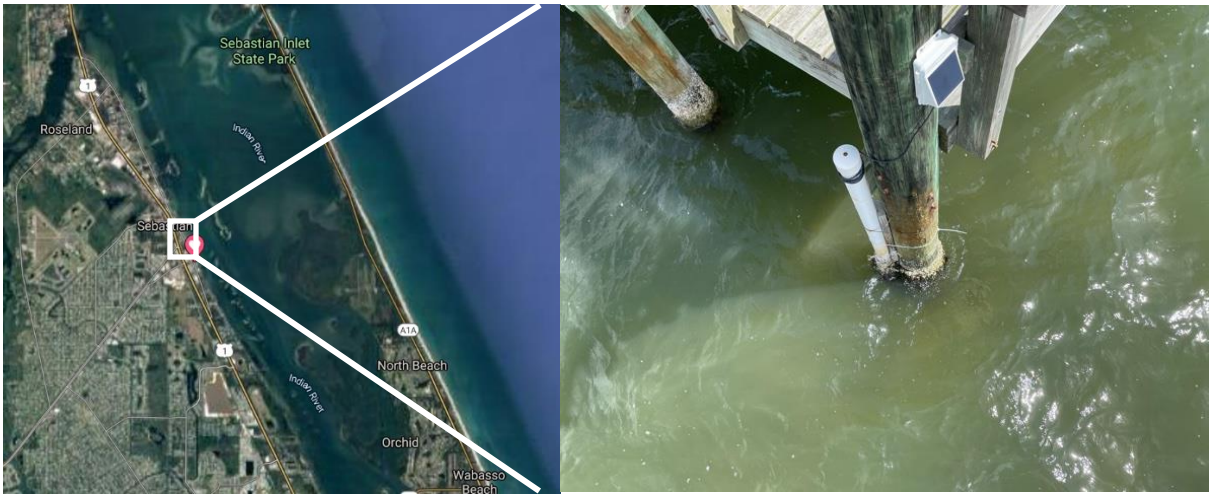

Figure 44. Southern-most station, located at Riverside Park in Sebastian, FL, located near the inlet closest to the inflow project and source of most of the tidal flow to BRL

The live readout of water level, temperature, and pressure plots from all three locations (**Figure 45**) can be viewed using here https://dashboard.hobolink.com/public/11961/Dashboard%2003-31-2021-04-15-2021%2020:39:32.

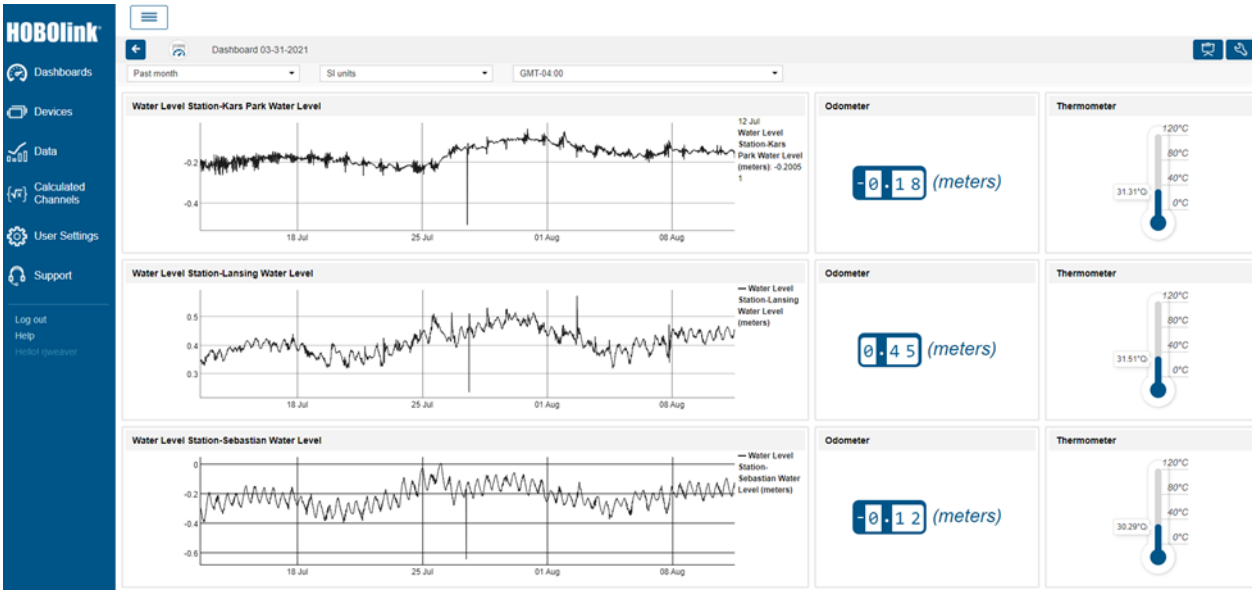

Figure 45. Screen shot from the live data reporting site provided by HOBO link

The three locations were surveyed in last year by Brevard County and that survey data were used to convert the water level data to NAVD88. The long-term water level data show very small water level fluctuations in the northern BRL (closest to the study site) on the order of a few centimeters. Larger water level fluctuations are driven by meteorological disturbances. On a longer time scale, the water levels vary on a seasonal basis, with higher water levels in late fall and lower water levels in the summer, as seen in the 2.5-year record from November 2014 to June 2017 (**Figure 46**).

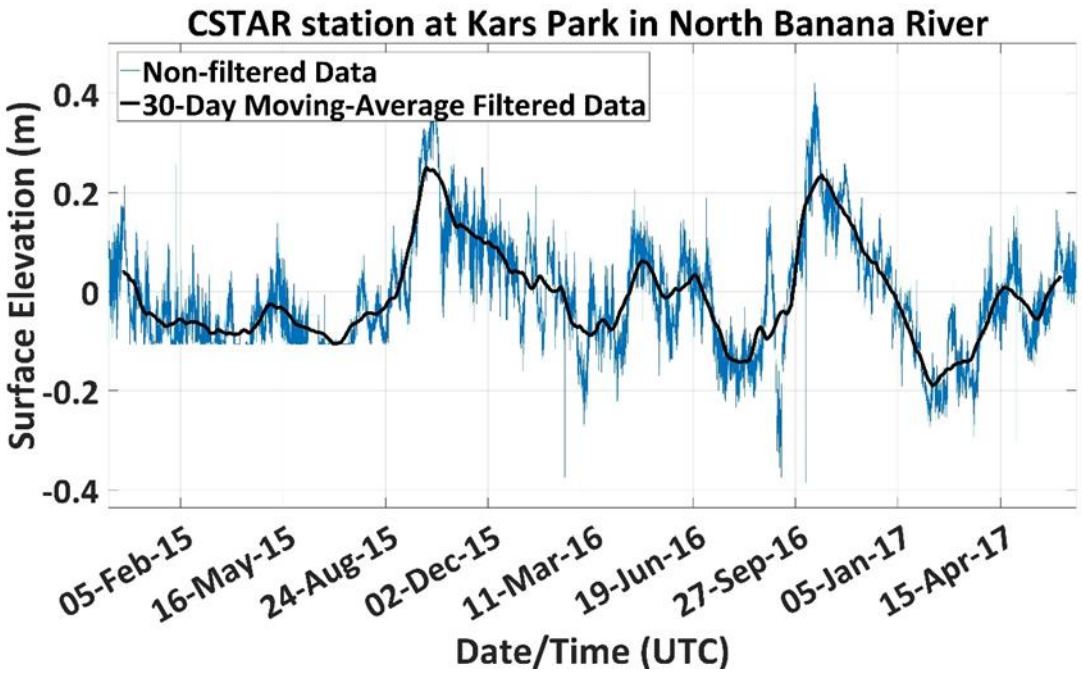

Figure 46. Long-term water level record for northern BRL station at Kars Park

Our research team will continue to monitor the long-term water level and temperature data collected by these stations.

3.2 Salinity, Temperature, and Depth at the Inflow Site

During Phase 2 of the project, four new instrument stations were deployed to monitor mean water level fluctuations, salinity, and land temperature along a transect within the inflow project site in the BRL at Port Canaveral (**Figure 47**). Stations 1, 2, and 3 contain a conductivity-temperature sensor (CT) and pressure transducer (PT) attached to a cinderblock and placed at the bottom of the lagoon. While station four only contains CT sensors (**Figure 47**), it is important to note that station 4 was originally deployed with a single bottom-mounted CT, another CT was deployed at this station on the date of the first data retrieval (January 15, 2021) located just under the buoy to monitor the difference between bottom and surface values of salinity and temperature.

Figure 47. Locations of the four salinity and depth instrument stations in the project area

After each data offload and instrument servicing, the instrument stations were kept at the same locations, as seen in **Figure 47**; however, it must be noted that during deployment 7, station 3 was not able to be located. At first, it was believed that the buoy may have been stuck under another vessel, and simply unable to be seen from the deployment boat. After returning to the site, the buoy was still not visible, and searches were conducted around the immediate area to retrieve the instruments. As of July 27, 2021, buoy 3 still has not been retrieved.

Multiple changes were made during the deployments which were designed to positively affect the results measured by the instruments. Notably, the team deployed anti-biofouling apparatus consisting of pool noodles covering the body of the instruments, and zinc oxide cream around the instrument's sensors. This made both the deployment process easier, by making the instruments easier to clean with less biofouling, and ensured accurate data were being recorded by the instruments. The improved anti-fouling method was implemented starting on May 12, 2021. Originally the team was fastening the instruments onto the cinder block, which held the entire apparatus under water. This was another factor leading to less accurate results as the block was sinking into the soft sediment on the lagoon floor, thus the sensor was also being covered by the muck. Instead, the team began to fasten the instruments about a foot above the cinder block to ensure that it would not become buried. This may affect the pressure/water level results slightly, but in turn will improve in the data.

3.2.1 Station 1

The instruments on this buoy required a simple data offload, instrument clean and redeploy. Nothing out of the ordinary was witnessed. This station is located deep into the cove just seaward of where the outfall will be located. The conductivity / temperature probe data shows highly varying salinity over the duration of the deployment (upper and middle plots in **Figure 48**). The temperature data are more continuous and captures the gradual warming of BRL into the summer months (bottom plot in **Figure 48**).

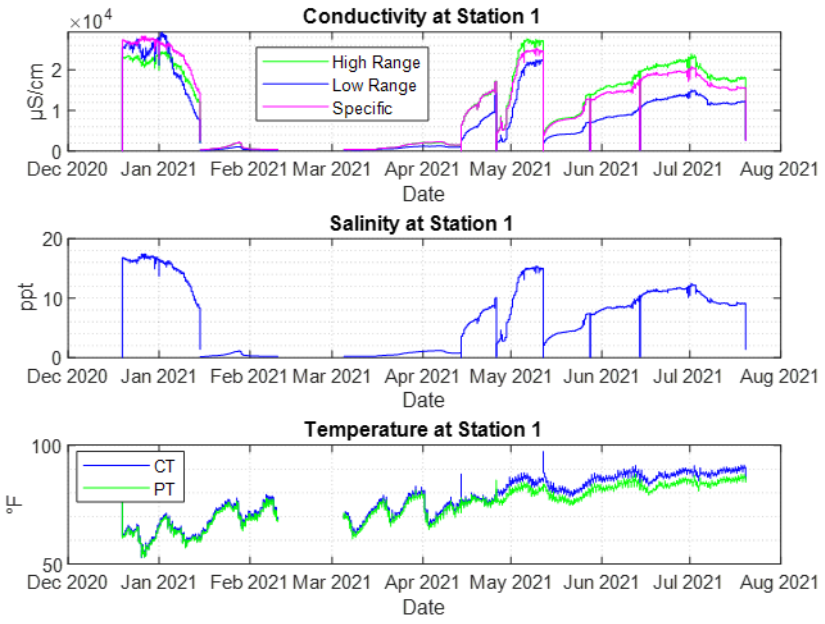

Figure 48. Raw conductivity/temperature data from station 1 with recorded conductivity (top) is converted to salinity (middle), and temperature (bottom) containing both the temperature from the pressure sensor, PT (green) and conductivity sensor, CT (blue)

About two-thirds of the way through the first dataset, we noticed the salinity values started to decrease. The main suspect was biofouling on the sensor altering the readings. One may notice the conductivity, and salinity for the second dataset are extremely low and have no correlation to the previous dataset. The cause of this remains unknown, though the main suspect is fouling. There could still be a significant amount of fouling altering the readings, or the sensors could have been damaged during cleaning. One way to prevent these issues is to take the instruments back to the lab in between deployments and ensure they are all clean and working properly before redeployment. There is no noticeable discrepancy between the first and second datasets for the temperature plots on both instruments. This is because the temperature sensor is encased in the instrument housing and not exposed to biofouling.

Deployment 3 began on March 5 around 11:00 a.m., while deployment 8 concluded on July 20 around 11:15 am. The blank space between mid-February and early March is thought to be caused by the instruments filling up with data and this issue was not addressed until the third deployment on March 5. Anti-fouling measures were installed during deployment 5 (May 12), and the results following seem to be much more feasible. More data will need to be collected using this anti-fouling apparatus to determine if accurate data are now being recorded for salinity and conductivity. The temperature data are more accurate and was seemingly unaffected by biofouling. The results show daily variance, while steadily rising through the transition of seasons.

The pressure readings for station 1 were more accurate and dependable then the conductivity and salinity data. The pressure data are converted into water level (depth). The water level for station 1 ranged from about 1.25 to 1.75 meters, which is to be expected for the shallow inlet where it is located (**Figure 49**). The water level fluctuations are mostly dependent on atmospheric disturbances. The BRL is a wind dominated system.

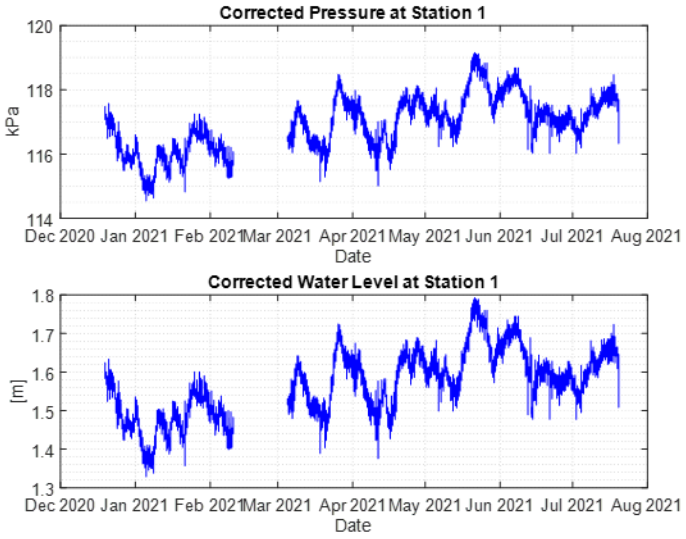

Figure 49. Corrected pressure and calculated water level at station 1

3.2.2 Station 2

This station followed the same procedure as the first station and saw the same errors as posed previously. This suggests that the same issues occurred (**Figure 50**). The data from the CT sensor indicate the same issues with conductivity, which will translate to the calculated salinity. The temperature data (bottom plot blue line) is in agreement with the temperature sensor on the pressure instrument (bottom plot green line). Both recorded the increasing temperature as summer set in.

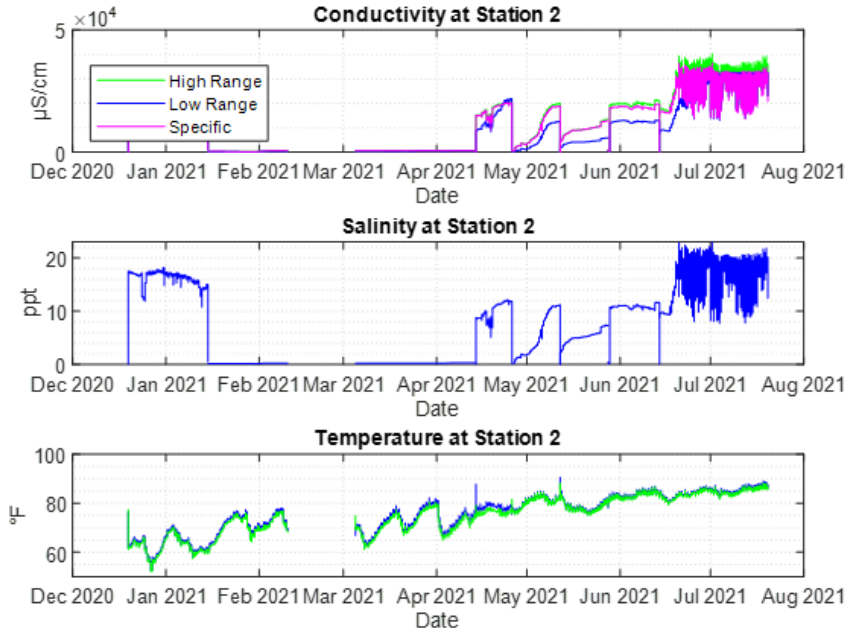

Figure 50. Raw CT data from station 2 where recorded conductivity (top) is converted to salinity (middle) and temperature (bottom) from the pressure sensor, PT (green) and the conductivity sensor, CT (blue)

After the anti-fouling measures were implemented, it seemed that the salinity and conductivity for this station were reasonable. Deployment 8, however, beginning on June 14, had a significant amount of noise. This could be caused by being dragged by a boat, as the same results were not collected by the other stations. As more data are collected, the belief is that the positive trend will continue, and more accurate results for salinity and conductivity will be recorded.

As seen in at station 1, station 2 recorded daily water level variation on the order of centimeters, and monthly fluctuations on the order of tens of centimeters (**Figure 51**). This is consistent with the measurements being recorded across BRL at the long-term water level station at Kars Park. While station 1 had a water level of 1.5 m, station 2 water level is around 2-2.25 m, which is the change you would expect from the lagoon as you move toward the center of the basin.

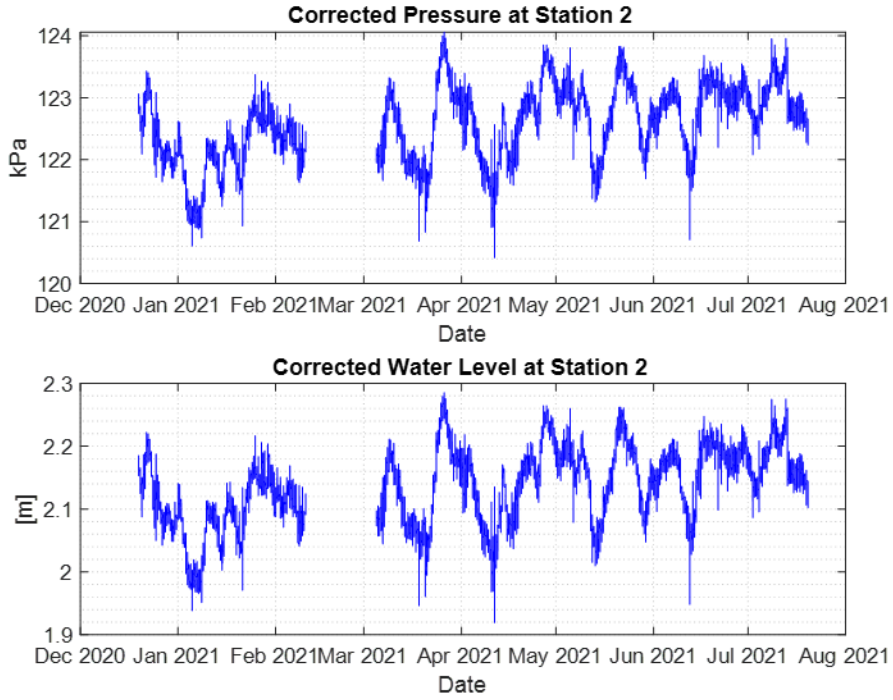

Figure 51. Corrected pressure and calculated water level at station 2

The shallow cove where the inflow project is proposed will see large water level responses to wind events in this micro tidal region of the IRL.

3.2.3 Station 3

The same procedures as implemented for the first two stations, were applied to station 3. The instruments included the same model PT and CT sensors. This station had significant experimental error compared to stations 1 and 2. As previously mentioned, station 3 was found to be missing when the team was on deployment 7. It is thought that the buoy line was most likely cut by a passing boat and the buoy was dragged away by the current, or that the keel from a larger vessel moored nearby impacted the instrument dragging it through the soft sediment bottom and burying the instrument in the muck. At this time station 3 has still not been retrieved, so the data for this station are shorter than the others, only continuing through May 28.

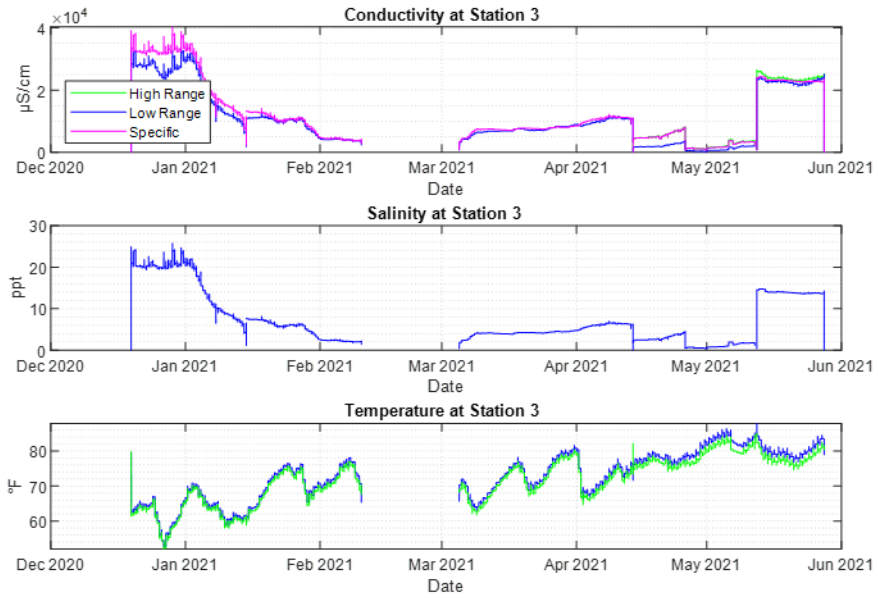

Figure 52. Raw CT data from station 3 with recorded conductivity (top) converted to salinity (middle) and temperature (bottom) from the pressure sensor, PT (green) and the conductivity sensor, CT (blue)

Note that the salinity readings for the second deployment are very similar to the concluding readings of the first deployment and suggest the instrument was not cleaned properly (**Figure 52**). The pressure readings for station 3 had more variation compared to the other stations (**Figure 53**). During deployment 5, the buoy for station 3 was originally not found but then discovered under a nearby boat. The increase in pressure found in the beginning of May is thought to be caused by a shift in the sensor caused by being dragged by the boat. During deployment 6 (mid-May to June), the change in pressure was most likely caused by a change in sensor location. The team needed to redeploy the station at a different location to move the buoy away from the boat it was previously stuck under. No follow up could be made to this conclusion as buoy 3 was missing before it could be recollected.

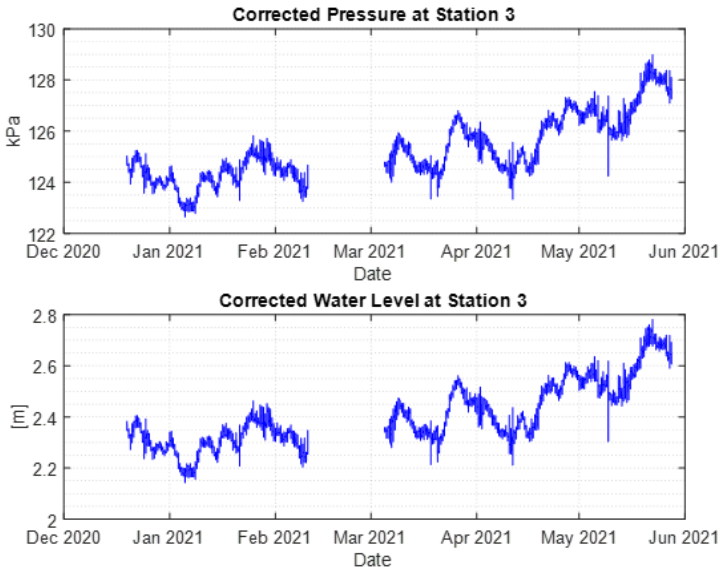

Figure 53. Corrected pressure and calculated water level at station 2

A team with a side scan sonar went to the last known location and could not find the instrument array. Most likely the array was impacted by a large sailboat moored in the cove and buried in fine sediment.

3.2.4 Station 4

This station has no PT sensor, only bottom mounted (**Figure 54**), and later added surface mounted (**Figure 55**) CT sensors. The primary purpose of this was to study the mixing between the surface and bottom layers. The first deployment data technically do not exist for the surface mounted CT and is marked by an array of zeros.

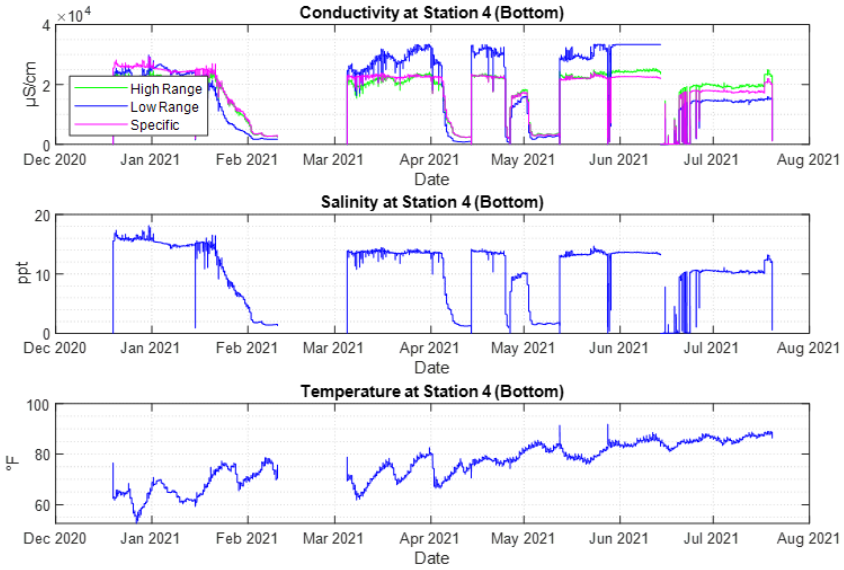

Figure 54. Bottom mounted CT sensor at station 4

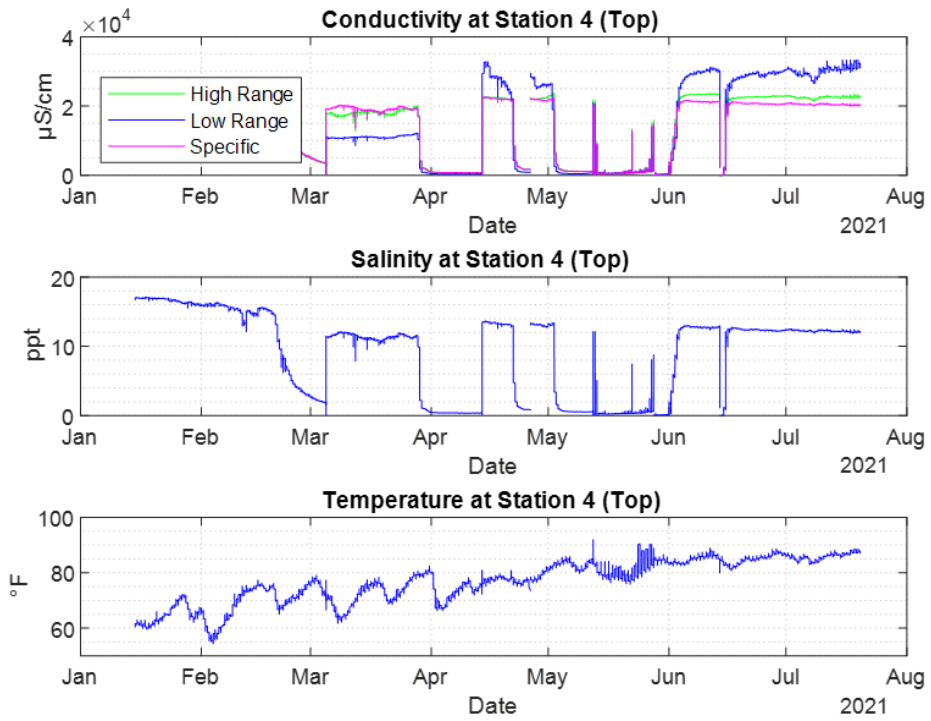

Figure 55. Surface/top mounted CT at station 4

The team incorporated the anti-fouling apparatus on both the top and bottom sensors. For the bottom sensors, which were located on all the previous stations, there was no issue with buoyancy. When the team attached the apparatus to the surface sensor of station 4, the sensor began to float. The data collected on deployment 6, between May 12, 2021 and May 28, 2021, are inaccurate due to the sensor floating on the surface and not recording water data. This was fixed during deployment 6, and between May 28, 2021 and July 20, 2021 is when the sensor was recording more accurate data.

After analyzing these plots, it is important to note that the salinity from the surface mounted CT gauge was reading higher than the bottom mounted gauge. This could be due to groundwater seepage. This suggests that the water is not completely mixed and there is something causing a change in salinity between the surface and seafloor. We see a similar trend towards the end of both data sets of decreasing salinity values and is expected from biofouling.

As more data are taken, it will be interesting to analyze the correlation between temperature, salinity, and water levels to better understand how much the salinity and water levels are fluctuating with the mean. The next step is to properly maintain the sensors and ensure they will be taking accurate data. This may include taking them to the lab for heavy cleaning and redeploying with an antifouling coat. The data will be much more significant if these steps are taken. The instruments are scheduled to be serviced within the next 10 days, although the sooner the better since some instruments are suspected to be recording faulty data. A summary of all the plots are shown below.

3.2.5 Analysis

The figure below was formed using data from the Melbourne Airport Weather History. The daily precipitation is given in inches per day over the time span of December 19, 2020 through July 20,

2021. Data were attempted to be taken from the Merritt Island database but could not be found. Melbourne Airport was the closest and most reliable data found.

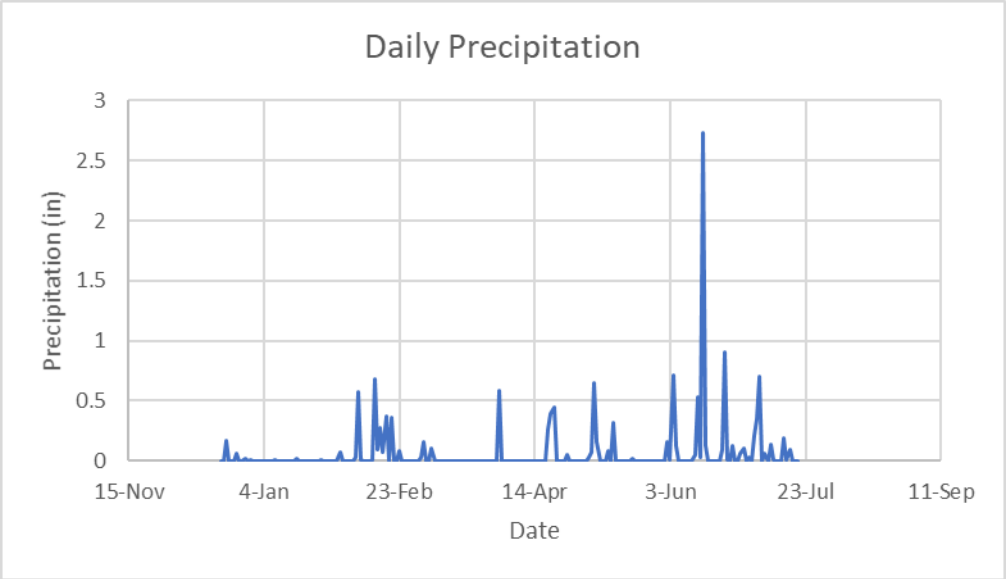

Figure 56. Daily precipitation data from Melbourne Airport Weather History, December 19, 2020 – July 20, 2021

By analyzing the daily precipitation near the location of the instruments, the team hoped to find a correlation between rainfall and the measured variables such as water pressure and salinity.

Based on the proximity of the stations, it was expected that very little variation in the water level would exist. The data for each of the pressure sensors, converted to water levels confirm that each station saw fluctuations on the order of tens of centimeters over monthly intervals (**Figure 57**). Higher frequency fluctuations on the order of several centimeters was measured over daily intervals. Over the 8 month record collected during Phase 2, seasonal fluctuation of approximately 0.5m was recorded.

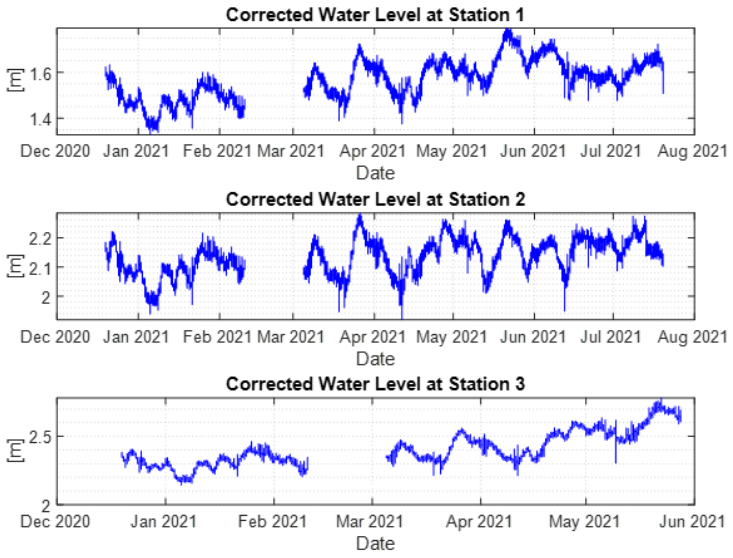

Figure 57. Water level from each of the three stations (1, 2, and 3)

As expected in Florida, much of the rainfall occurs in the spring/summer months. Simultaneously looking at the trend of the water level, it seems that compared to December and January, the water level during the later deployments entering the summer is increasing. Also, based on the data taken from the Melbourne airport, a significant amount of rain occurred in February, and there does seem to be a spike of water level entering February (**Figure 56**).

With an increase of rainfall, we would expect a decrease in salinity. Based on the data collected, there is not a clear signal of the rainfall at Melbourne Airport in the salinity data at the project site (**Figure 58**). Since rainfall is highly localized, it will be important to locate a rainfall data source in closer proximity to the study site. A large portion of the salinity data collected so far has been affected by bio-fouling and other unknown factors (e.g. possible groundwater seepage). Collaboration with project partners on data analysis will help to better understand the data.

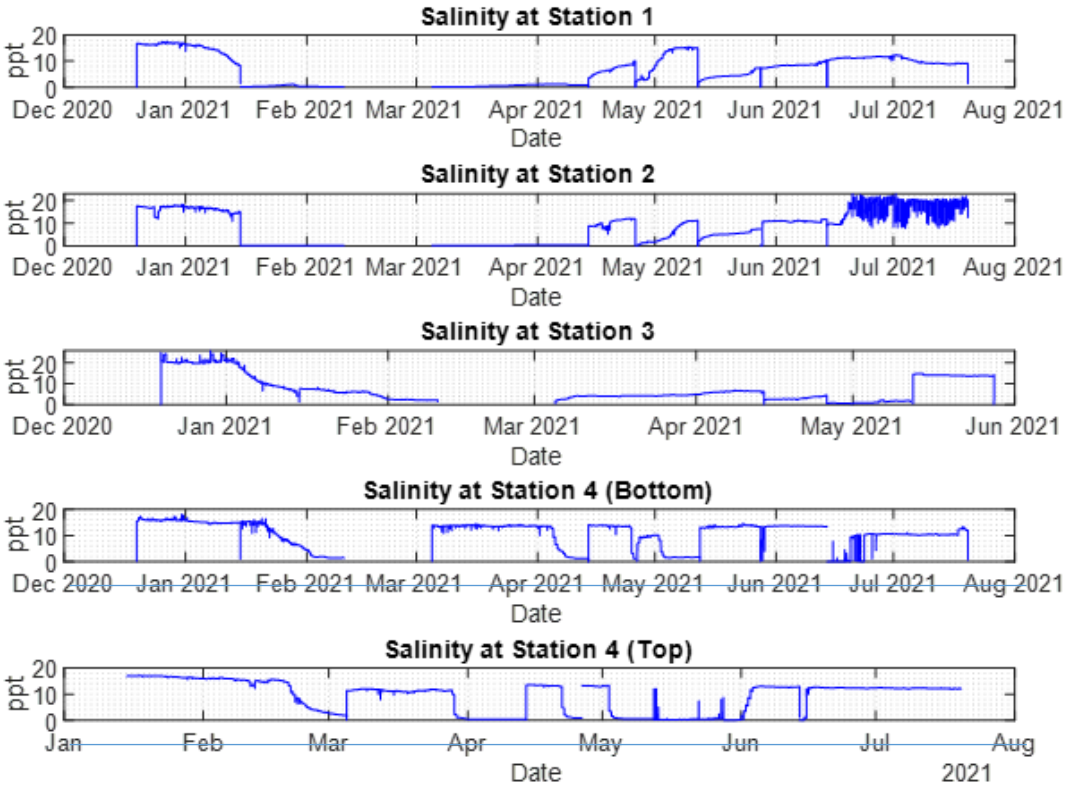

Figure 58. Salinity from each of the 4 stations with both the surface and bottom record at station 4 plotted

It is interesting to note that at station 4 where both top (surface) and bottom sensor were deployed, there are several periods where the salinity near the lagoon bottom was lower than at the surface (**Figure 58**) bottom two plots. This would indicate that there is a source of freshwater entering the lagoon through the bottom at this location. The times when this occurrence is most pronounced are late February, May, and July. These time periods coincide with heavy rainfall events (**Figure 56**). It is expected that groundwater seepage into the lagoon would increase following a rainfall event as the groundwater is recharged by the precipitation. Local precipitation would cause the surface sensor to record fresher than the bottom. This is seen in the March to April time period, as well as the June time period. To better understand the salinity fluctuations, more accurate local rainfall data are needed in addition to resolving issues with instrument fouling.

As more data are taken, it will be interesting to analyze the correlation between temperature, salinity, and water levels to better understand fluctuations and timescales. The next step is to continue proper maintenance of the sensors and ensure they are calibrated. This may include removing them from the field, them to the lab, heavy cleaning, and redeploying with an antifouling coat.

3.3 Data Summary

The long-term water level data establish a yearly cycle of high and low water in the IRL (**Figure 46**). This cycle is also experienced in the coastal ocean as measured by the National Oceanic and Atmospheric Administration (NOAA) station at Trident Pier. The BRL at the location of the inflow project experiences a water level fluctuation of as much as 0.6 m (2 ft) over the course of a year, with the high water occurring around October and the low water occurring around July (**Figure 46**). There is a smaller peak in the high water around May, which follows a low that occurs around February. This smaller cycle fluctuation is on the order of 20 centimeters (0.65 ft) change in water level over 3 months.

Water level data indicates that the BRL historically experiences fluctuating water levels. A study by Saberi and Weaver (2016) found that under extreme inflow conditions (e.g., over 400 m^3/sec during spring high tide) the maximum increase in mean water level would be approximately 4.5 centimeters in the BRL. Even at the high inflow modeled by Saberi and Weaver (2016), the increase in water level is well within the natural range of water level fluctuations for this basin. Having the ability to manage the inflow would allow for the system to shut down during the highest water period (e.g. late September through November).

The salinity and temperature data collected at the proposed project site indicates a system with high variability. Salinity fluctuations are common and can be wide ranging. Regular inflow of ocean water with a near constant salinity would buffer these wide swings in salinity measured during Phase 2 of the project.

One potential source of freshwater is groundwater seepage after large rain events. The freshwater enters the lagoon through the bed creating lower salinities at the bottom than at the surface. Inflow will enhance the mixing and stabilize the salinity levels.

4 ADCP Data Analysis

4.1 Background

At the beginning of 2020, ADCP were deployed in BRL. Three ADCPs were deployed in strategic locations to record current velocities and directions (**Figure 59**). These data are initially intended to verify computational models, which estimate the flow patterns within this basin. However, the data are useful in interpreting the flow directly and analysis thereof provides insight into additional causal factors relating the flow in this basin to systemic phenomenon.

4.2 Introduction

Three ADCP units were deployed in BRL at locations chosen for their proximity to inflows and outflows. Dragon Point is located at the very southern tip of BRL, where it interfaces directly with IRL. The Barge Canal runs east-to-west connecting BRL to IRL and is intersected by Sykes Creek. The third ADCP is located at the southern end of Sykes Creek, which bisects Merritt Island and allows for additional flow from IRL, as well as from freshwater sources.

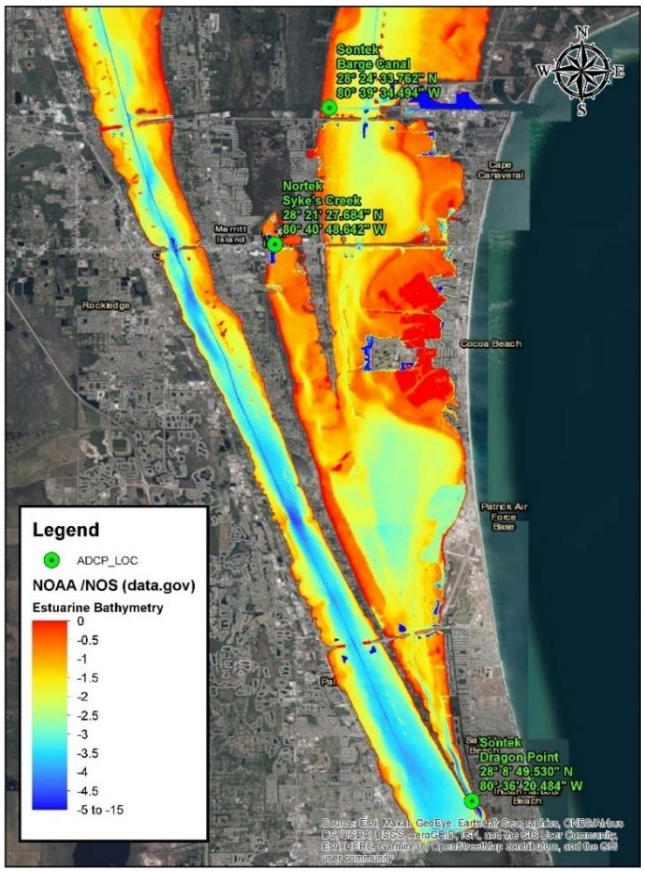

Figure 59. ADCP deployment locations and approximate bathymetry

The three ADCPs include two refurbished Sontek Argonauts deployed at Dragon Point and Barge Canal and one new Nortek Aquadopp profiler deployed at Sykes Creek. Periodic maintenance was performed on each system according to the schedule in **Table 11**. The maintenance requirements included data collection, ensuring adequate memory availability, battery replacement, removing biofouling, and general inspection of components and connections. Every visit entailed data retrieval, and battery replacement was performed periodically. Insufficient memory in the Nortek system situated at Sykes Creek necessitated a lengthy surface interval of two months during April and May 2020. The longest interval between maintenance periods was experienced by the unit located at Barge Canal and lasted 170 days. Longer service intervals, while suboptimal, were unavoidable due to the COVID pandemic, personnel shortage, and weather. The rage of data displayed in this report is from January 1, 2020 to July 20, 2021.

Table 11. Deployment and maintenance record for ADCP units in BRL

Date Deployed	Date Retrieved	Duration (days)	Unit	System	Task
31-Dec-19	02-Mar-20	62	Barge Canal	Sontek	Data Retrieval
02-Mar-20	01-Apr-20	30	Barge Canal	Sontek	Data Retrieval
01-Apr-20	11-Jun-20	71	Barge Canal	Sontek	Data & Batteries
11-Jun-20	29-Jul-20	48	Barge Canal	Sontek	Data Retrieval
29-Jul-20	15-Jan-21	170	Barge Canal	Sontek	Data & Batteries
15-Jan-21	14-Apr-21	89	Barge Canal	Sontek	Data Retrieval
14-Apr-21	07-Jun-21	54	Barge Canal	Sontek	Data & Batteries
07-Jun-21	22-Jul-21	45	Barge Canal	Sontek	Data Retrieval

Date Deployed	Date Retrieved	Duration (days)	Unit	System	Task
17-Jan-20	18-Mar-20	61	Dragon Point	Sontek	Data Retrieval
19-Mar-20	05-Jun-20	78	Dragon Point	Sontek	Data & Batteries
05-Jun-20	07-Aug-20	63	Dragon Point	Sontek	Data Retrieval
07-Aug-20	21-Nov-20	106	Dragon Point	Sontek	Data & Batteries
21-Nov-20	26-Feb-21	97	Dragon Point	Sontek	Data Retrieval
26-Feb-21	26-May-21	89	Dragon Point	Sontek	Data & Batteries
26-May-21	27-Jul-21	62	Dragon Point	Sontek	Data Retrieval
28-Feb-20	30-Mar-20	31	Sykes Creek	Nortek	Data & Memory
29-May-20	29-Jul-20	61	Sykes Creek	Nortek	Data & Batteries
29-Jul-20	20-Aug-20	22	Sykes Creek	Nortek	Data Retrieval
20-Aug-20	20-Nov-20	92	Sykes Creek	Nortek	Data & Batteries
20-Nov-20	14-Apr-21	145	Sykes Creek	Nortek	Data & Batteries
14-Apr-21	20-Jul-21	97	Sykes Creek	Nortek	Data & Batteries

4.3 Data Processing and Quality Control

The systems were deployed in shallow, warm waters and data quality suffered from increased biofouling and a low signal-to-noise ratio. Data loss was significant after three months of continual deployment without a service interval to replace batteries. It is as-yet unclear what contributed to the loss in data quality but it is assumed that battery power and biofouling are the main culprits.

The ADCPs maintain a blanking distance, or minimum distance to first cell of measurement in the water column, and record ten cells or “bins” meaning individual depth interval of averaged current speed and direction. For example, a cell or bin size of 0.1 m averages the currents and direction over 0.1 m of water, and the intervals extend from the first cell above the blanking distance to the maximum distance calculated by taking the product of the number of bins and individual bin size. In the case of the Nortek system, the blanking distance is 0.21 m and each bin is 0.1 centimeters so the maximum column of water measured is 1.21 m, which is slightly below the average water level above this unit of approximately 1.79 m. The Sontek ADCPs record past a blanking distance of 0.4 m with a bin size of 0.3 m for the Barge Canal ADCP to an average depth of 2.4 m and 0.5 m for the Dragon Point ADCP to an average depth of 4.85 m.

Quality control of these data entails the rejection of any bin higher than the recorded water level. Additional criteria for acceptable data is a signal-to-noise ratio at least above 3 decibels. The graphics below illustrate the binned current velocities, quality controlled for depth and signal-to-noise ratio. **Figure 60** shows a 2-month gap from March 30 to May 30, which was necessary to upgrade the memory of the system. The gap shown during the months of February and March was due to poor signal quality, likely due to battery power but also could have been caused by excess biofouling. When this system was serviced in mid-April, it was covered and surrounded by worm rock remnants and might have been buried during that time.

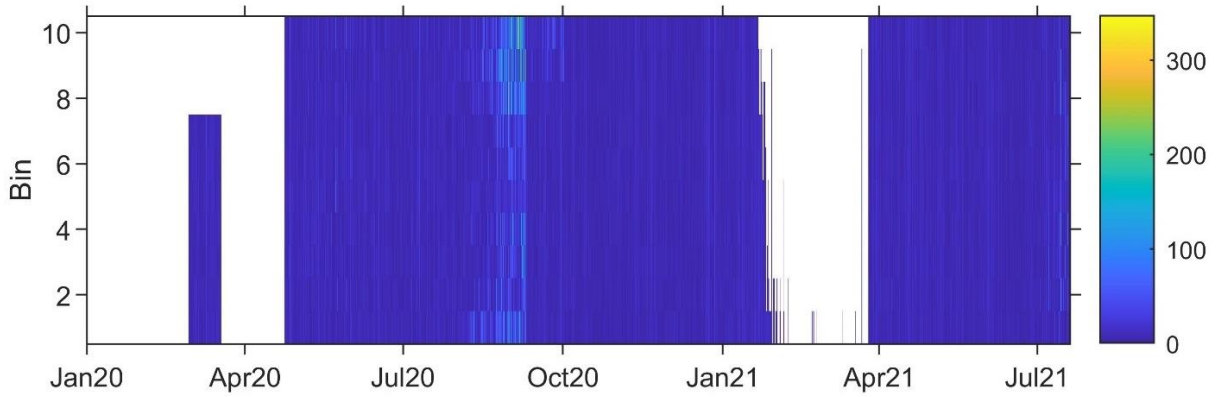

Figure 60. Quality controlled binned current velocities at Sykes Creek

Figure 61 shows a gap caused by poor quality data from October 2020 to February 2021. This is assumed to be due to battery power issues resultant from the long interval of 218 days between battery replacement. As previously stated, the long service interval of 170 days was due to pandemic restrictions at the time. Poor quality data occurring in March and April 2021 was more likely due to biofouling but could have also arisen because of battery power issues.

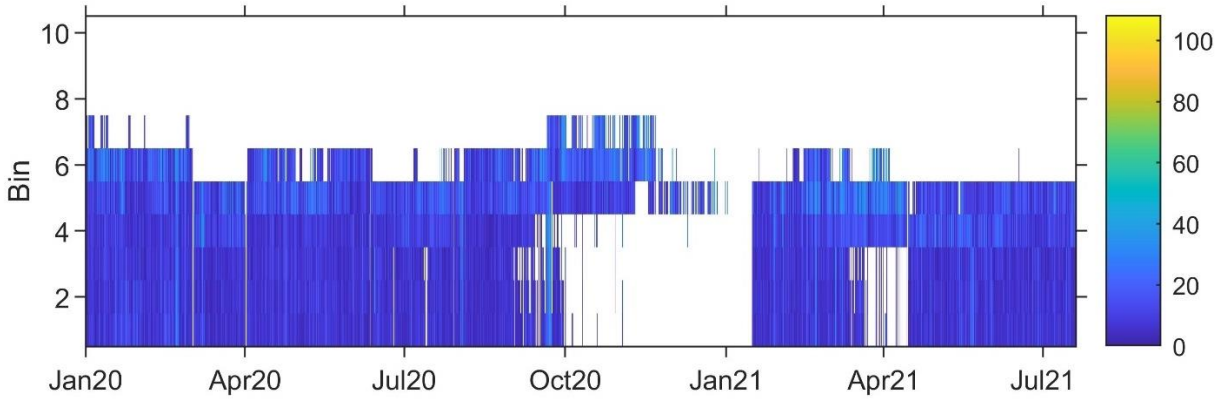

Figure 61. Quality controlled binned current velocities at Barge Canal

Figure 62 shows near total loss of data from the deployment between August and November 2020, which is most likely due to power issues. The poor-quality data at the end of July 2021 are most likely due to excess biofouling on the transducer heads.

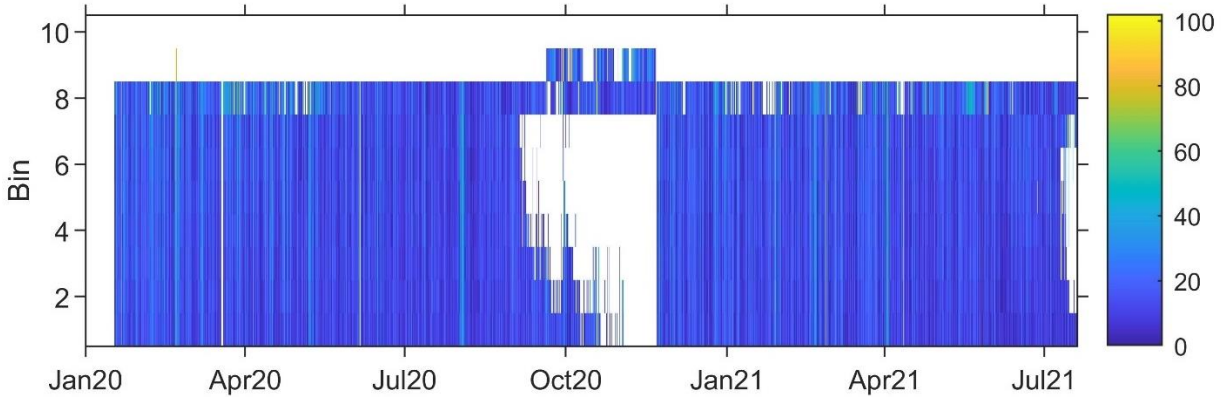

Figure 62. Quality controlled binned current velocities at Dragon Point

While it is possible to glean some useful information from the binned plots, it is far more useful to average the velocities for each record across the water column. Applying this method to these data presents complications when dealing with large gaps. To maximize the utility of these data, the velocities are averaged for every bin in the water column for each record. This skews data by adding weight to the few remaining bins that pass quality control and thus must be treated with caution but useful information can still be elucidated. A 24-hour moving average is also calculated and plotted for a better indication of long-term trends.

The direction of the currents were also subject to quality control, and their display via rose-plot is weighted based on the corresponding bin velocity and then averaged to better illustrate the direction of flow. Below are plots of depth-averaged current velocities and associated moving averages, and are followed by the velocity-weighted direction of the currents. The 2-month break in recording to retrofit additional memory into the Nortek Aquadopp deployed at Sykes Creek as seen in **Figure 63** is clearly visible during April and May 2020. There is a large spike in current velocities presented in this time series in October and November 2020, which is as-yet inexplicable and the data pass quality control. The gap present in March and April 2021 is due to data recorded at the noise floor of the unit, which indicates very poor return to the instrument. This seems to be correlated with excess biofouling but could have been compounded by a lack of battery capacity. The currents at Sykes Creek flow predominantly south (**Figure 64**). This does not vary with season and only a proportion of directionality changes with the tides. A possible reason for this is the inflow from both ends of the Barge Canal and inflow from the northern extent Sykes Creek.

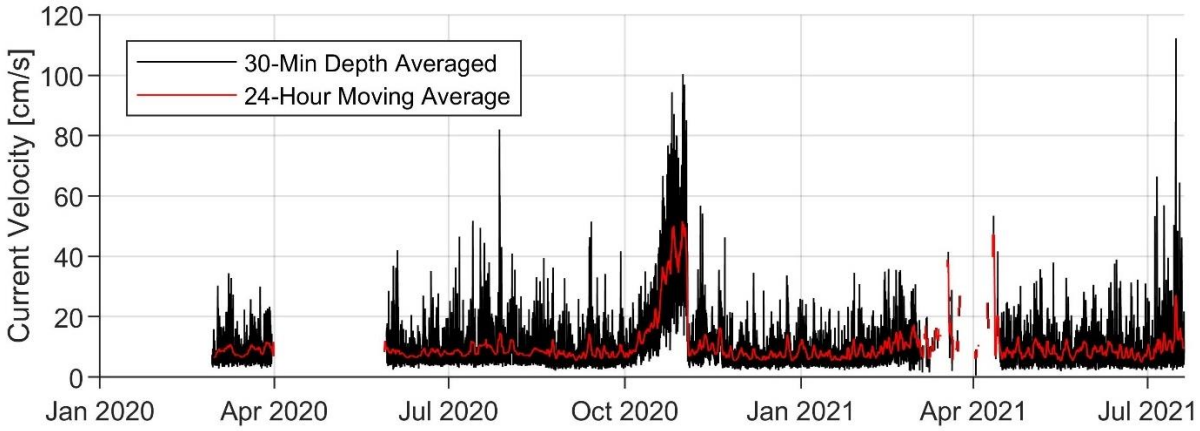

Figure 63. Time series of depth-averaged current velocities at Sykes Creek

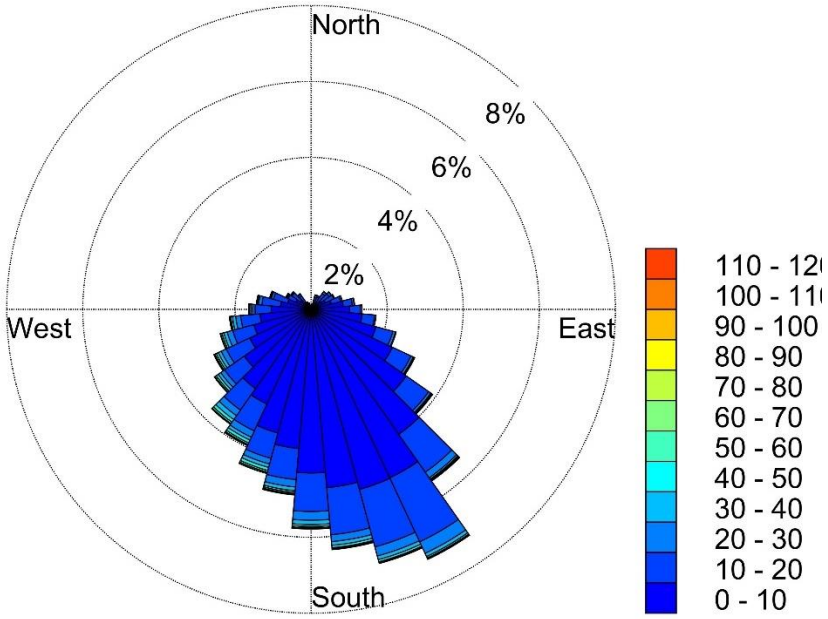

Figure 64. Rose plot of current direction at Sykes Creek

In bin 5, nearer the surface of the water column, more consistent data could be collected due to quality. This is likely due to the higher transmissibility of lower-frequency signals in fluid and perhaps more or larger scatterers (**Figure 65**). In any case, to mitigate issues of the depth-averaged velocities being skewed toward the higher rate of transport as indicated in **Figure 66**, the anomalous increase in current velocities during October and November 2020 seem to disappear and the increase in velocities experienced from February through April 2021 remain. There seems to be a similar condition in the previous year. The direction of currents at Barge Canal, as shown in **Figure 67**, oscillate from east to west with some proportion flowing south. No significant proportion of these currents flow to the north. Between October 2020 and February 2021, these data suffered from poor quality in all but one bin, potentially weighting the current velocities in that range slightly higher and more erratic.

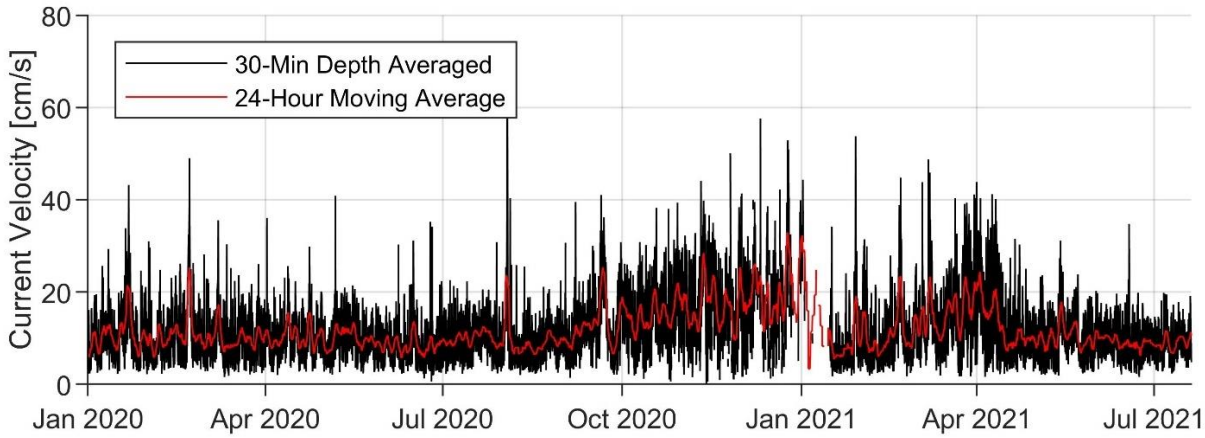

Figure 65. Time series of depth-averaged current velocities at Barge Canal

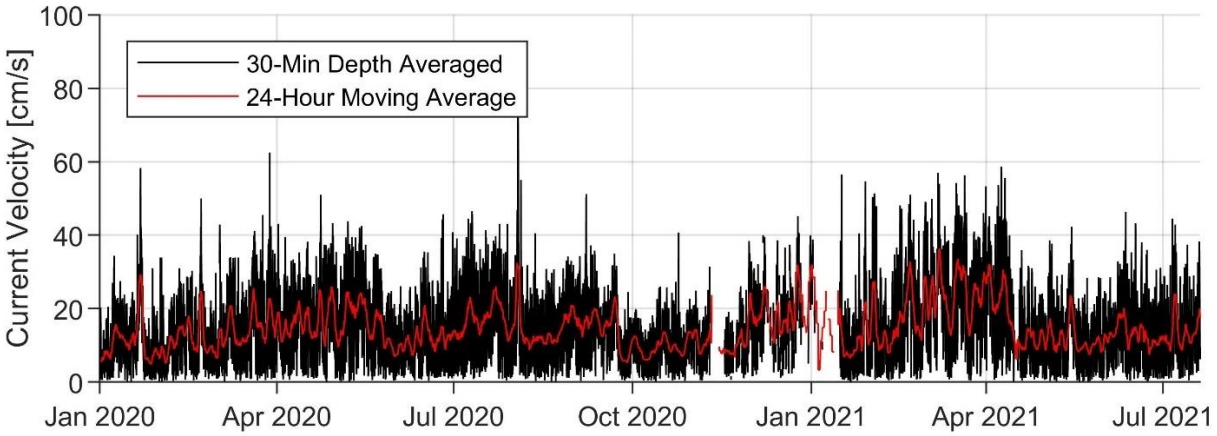

Figure 66. Time series of bin 5 current velocities at Barge Canal

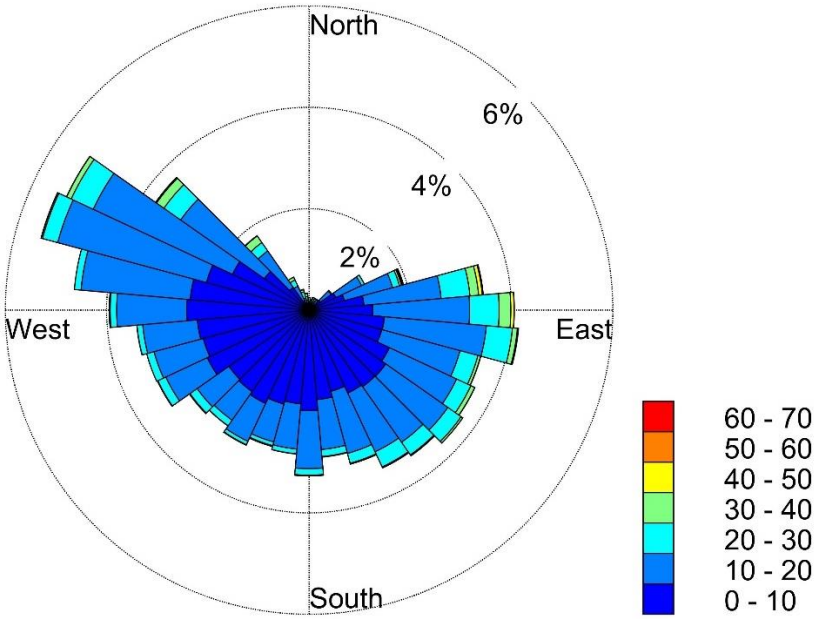

Figure 67. Rose plot of current direction at Barge Canal

The data for Dragon Point, as shown in **Figure 68**, are also marked by inconsistent quality during the October and November 2020 timeframe, and the moving average does not indicate any significant oscillation or trend.

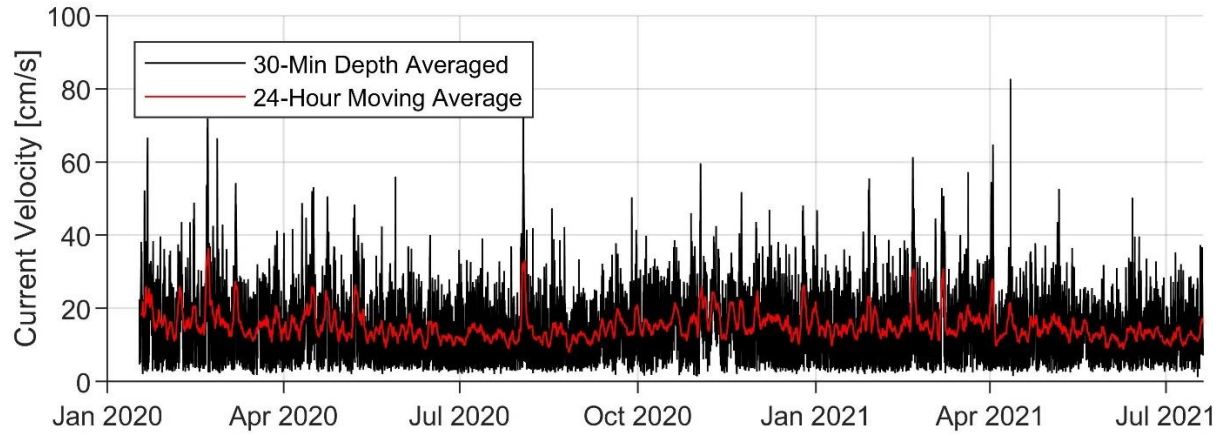

Figure 68. Time series of depth-averaged current velocities at Dragon Point

Figure 69 depicts the time series of only bin 8, near the surface of the water column over the ADCP at Dragon Point. In this bin, a longer term oscillation in current magnitude is apparent around April 2020 and 2021. The direction of the currents at Dragon Point, as shown in **Figure 70**, are from southeast to northwest, which is expected because the channel in which it is located goes in the same directions.

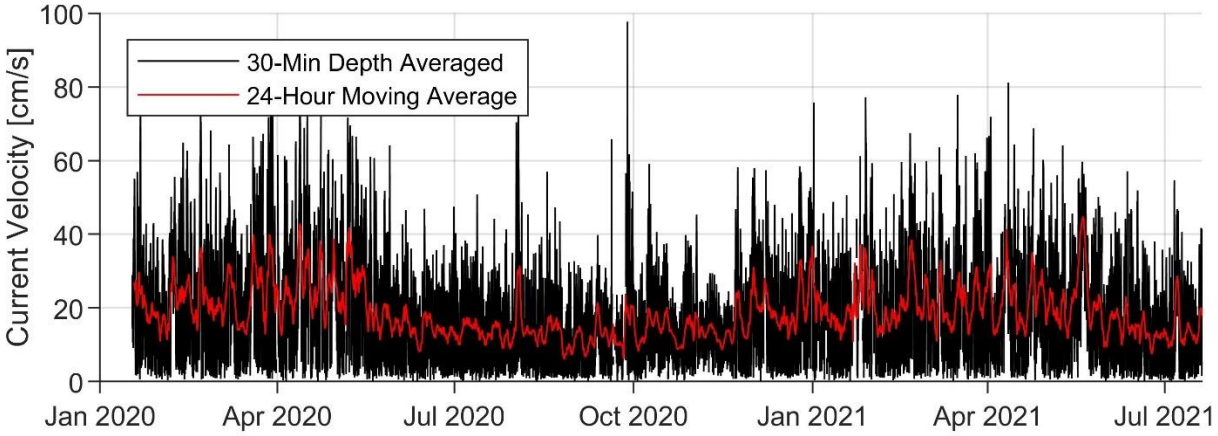

Figure 69. Time series of bin 8 current velocities at Dragon Point

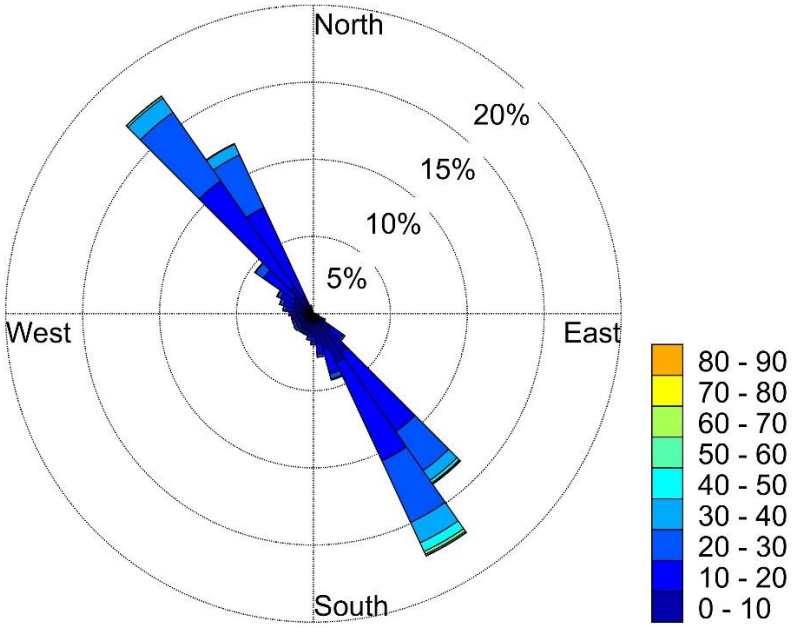

Figure 70. Rose plot of current direction at Dragon Point

For comparison, **Figure 71** shows the 24-hour moving averages of the current velocities at each station. Based on this plot, the anomalous nature of the November spike in current velocity at Sykes Creek is apparent. It is difficult to glean any longer-term understanding from this time series.

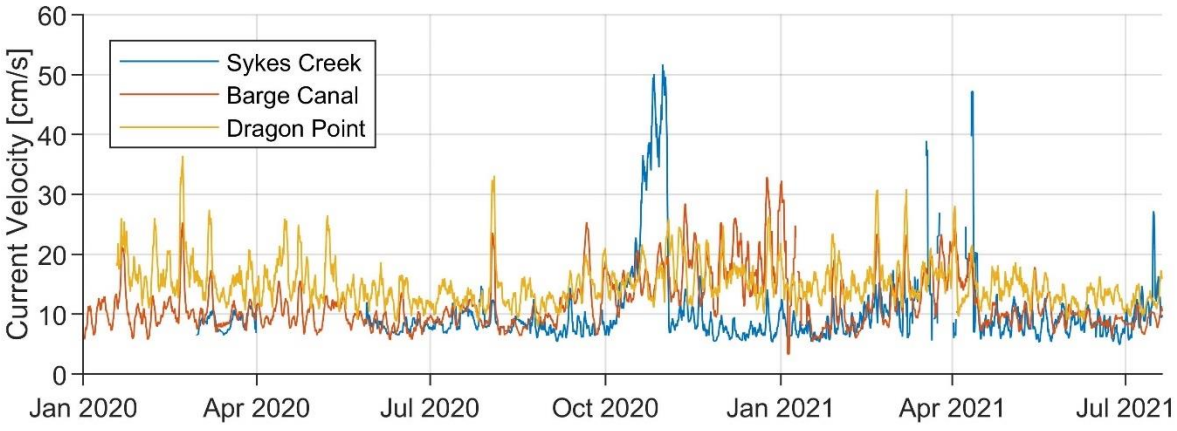

Figure 71. Combined 24-hour moving average of current velocities

Figure 72 depicts the depth-averaged current velocities in a 24-hour moving average for Sykes Creek, solely for bin 5 in a 24-hour moving average for Barge Canal and likewise bin 8 for Dragon Point. The increase in current velocities around April 2020 and 2021 are more apparent for Dragon Point and Barge Canal. For Sykes Creek, data gaps prevent useful interpretation during these time periods but some indication of increased current is present in the vicinity of April 2021.

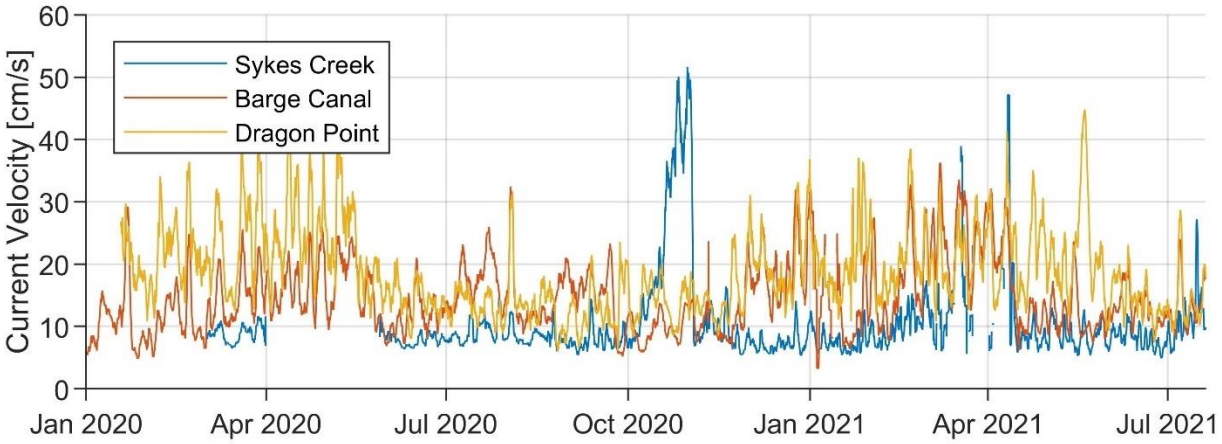

Figure 72. Combined 24-hour moving average of binned current velocities

The hydrostatic pressure, as recorded on the instruments and shown in **Figure 73**, is reported in dBar, which is approximately equal to one meter of depth per dBar. These time-series have been demeaned to better show correlation and a trend of increased water level is apparent between September and November 2020. It remains to be seen whether this trend repeats this coming fall 2021.

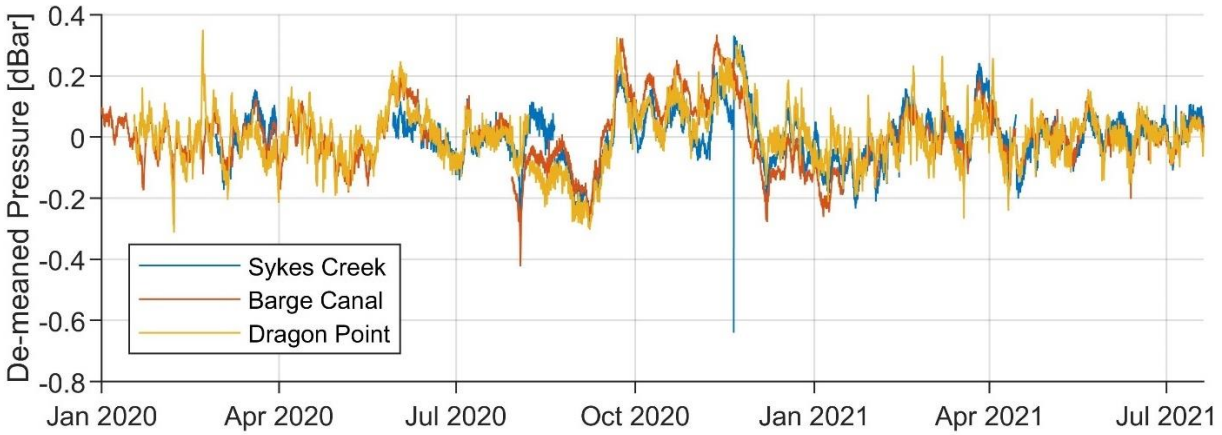

Figure 73. Combined demeaned pressure time series

The temperature of the water at each location varies predictably and seasonally with seemingly higher variation in late winter to early spring (**Figure 74**). Daily variation is greater at Sykes Creek and Barge Canal than at Dragon Point due to the depth of the units, Dragon Point being the deepest, but the pattern of oscillation in temperature looks the same at each unit.

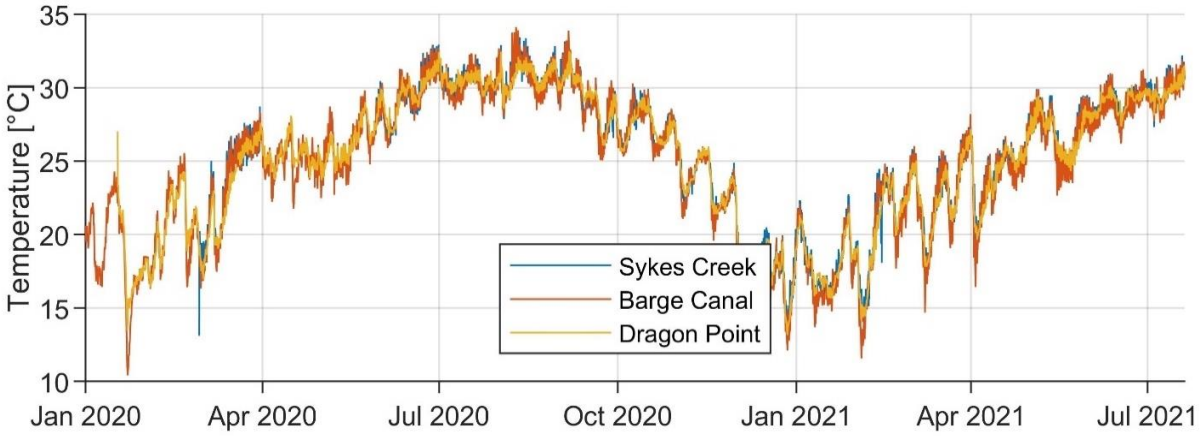

Figure 74. Temperature time series

4.4 Analysis

These data were analyzed to find relationships between the data collected and environmental factors, such as water level and wind. Trident Pier at Cape Canaveral is the primary source of data and is sourced from NOAA's National Data Buoy Center (NDBC) (TRDF1). It is also useful to compare transport through the Florida Current to draw conclusions about the contributors to overall water level. These data were sourced from NOAA's Atlantic Oceanographic and Meteorological Laboratory's Western Boundary Time Series.

There is very little tidally influenced water level fluctuation in BRL. This is because the fluid flux at its boundaries are relatively constrained. One might assume that the water level at the Atlantic Ocean would have little effect, considering the locks at the Port restrict any flux and the next inlet is 35.4 km south of the southern opening to BRL and another 30 km north to the Barge Canal. However, a long-term relationship is seen when the water level in BRL is compared to the flux in the Gulf Stream (**Figure 75**). As shown in **Figure 75**, the water levels recorded at the three ADCPs and Trident Pier's 24-hour moving average of water levels track well. In **Figure 76**, the inverse relationship between Florida Current transport and the BRL water levels is apparent.

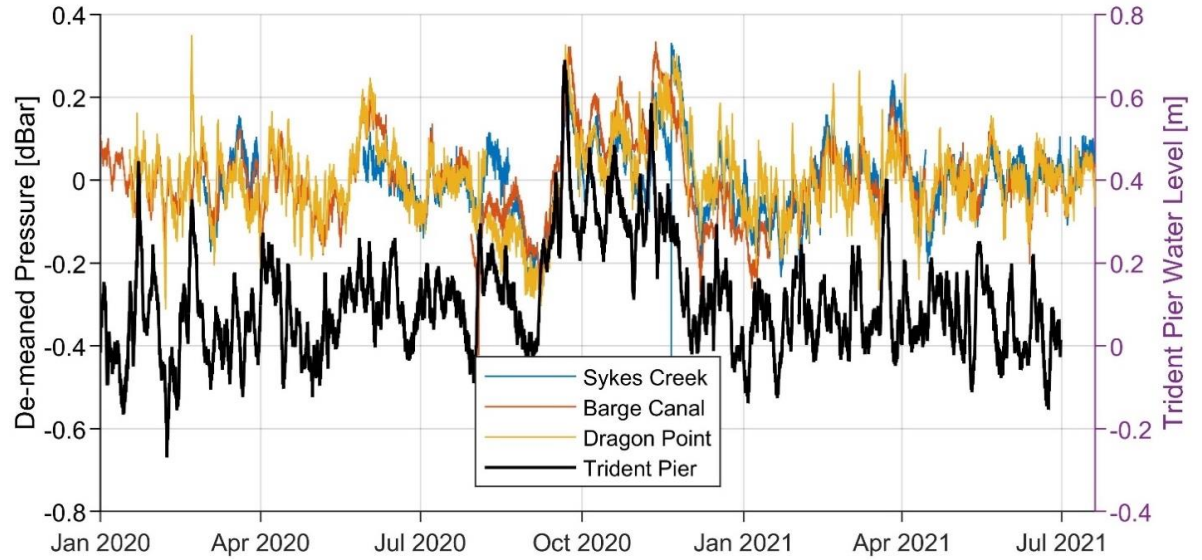

Figure 75. Water levels at ADCPs and Trident Pier

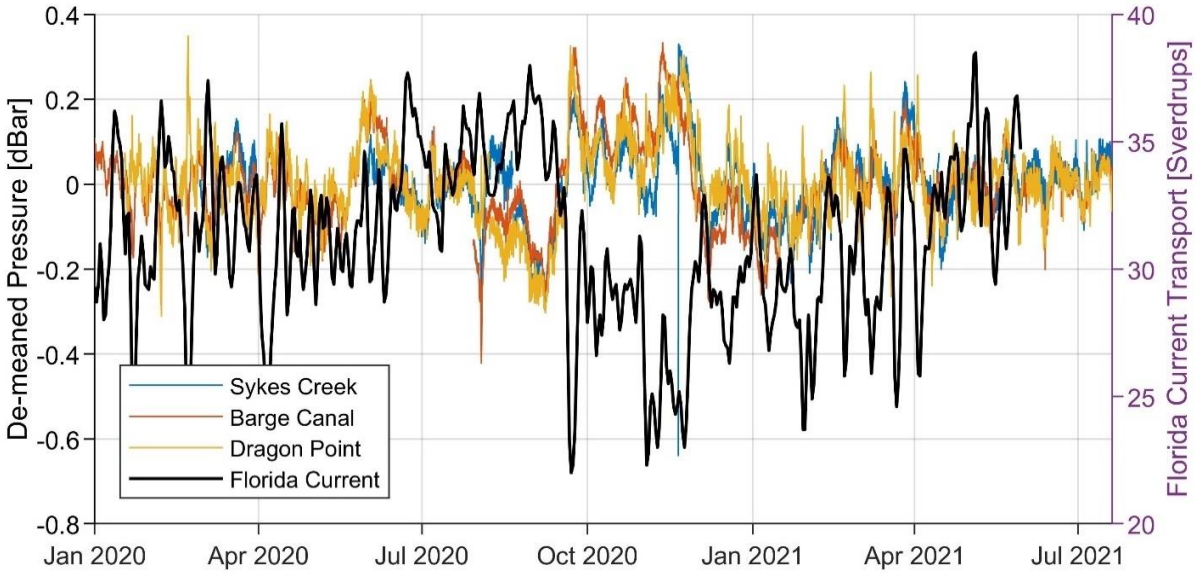

Figure 76. BRL water levels and Gulf Stream flux

The inverse relationship between Gulf Stream flux and water level is also apparent in the water level data from Trident Pier subject to a 24-hour moving average as shown in **Figure 77**.

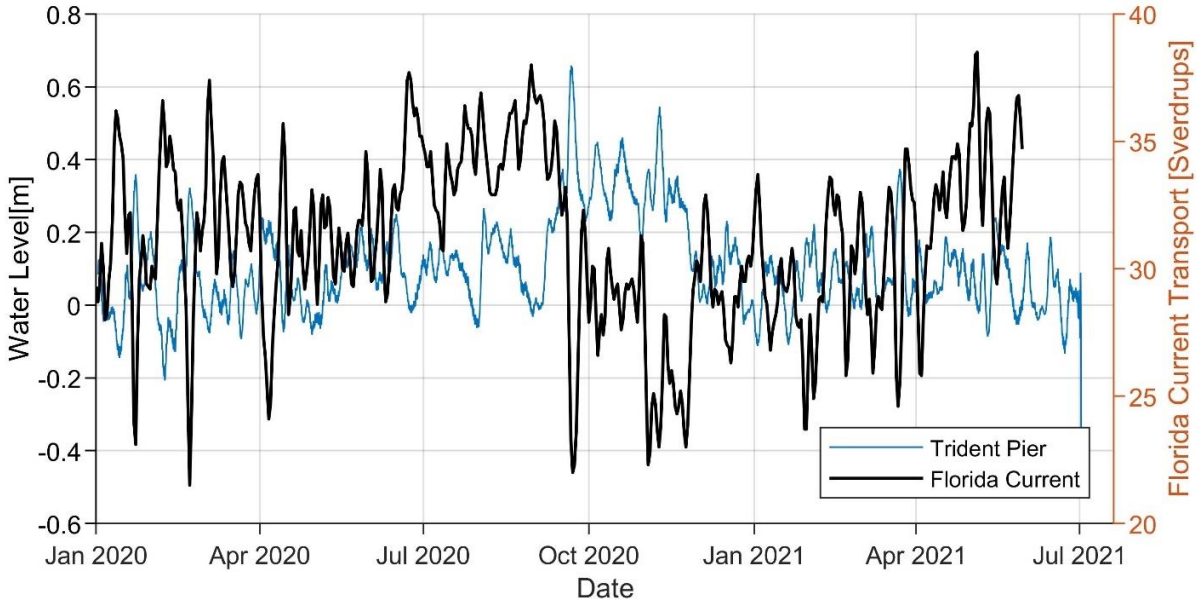

Figure 77. Trident Pier water levels and Gulf Stream flux

The Gulf Stream is powered by winds just north of the equator and differential heating, which draw water north from the equator to the Arctic. This pressure pulls in nearby water, drawing down sea levels, especially near the coast, as it is transported north. During the cooler months, with less differential heating, the Gulf Stream slows down and less water is pulled from the coast, leading to higher coastal sea levels. This obviously has an effect on water levels in IRL and BRL as hydrostatic head seeks equilibrium. During the warmer periods, more water is transported to

the north along the Gulf Stream and coastal sea levels are drawn down, as is the water level of BRL.

The flow in BRL in this northern compartment, which is essentially a restricted basin, was thought to be primarily driven by the wind, but these data suggest that coastal sea level and to a limited extent tides influence the direction of the current at Dragon Point.

The frequency spectrum of water levels at Trident Pier as depicted in **Figure 78** clearly shows the semi-diurnal tidal signal having the most influence over water levels, which occurs every 12.4 hours. Smaller spectral peaks occur at 23.8 and 25.8 hours, or diurnal, intervals. **Figure 79** depicts the frequency spectrum of the changes in direction of currents at Dragon Point. Energy in both of these occurs at 2.23E-5 Hz or 12.4 hours, which corresponds to the semi-diurnal tidal cycle. Smaller spectral peaks also occur at 23.8 and 25.8 hours in both datasets, which corresponds to the diurnal tide. These three correlations indicate the influence of tidal forcing on the directionality of currents at Dragon Point. However there is substantial energy distributed over lower frequencies in the Dragon Point record indicating influence by sea levels fluctuation and wind.

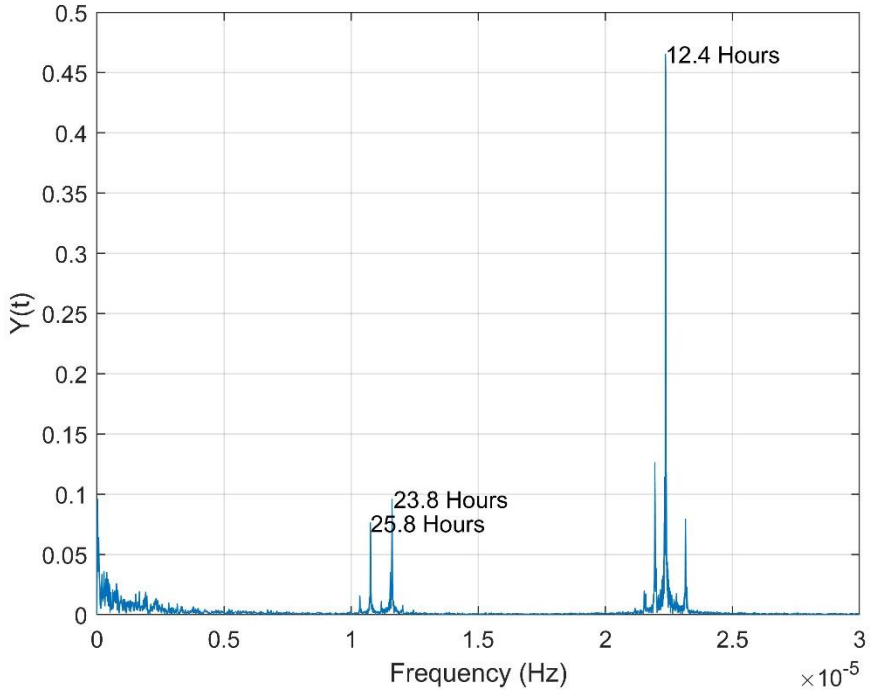

Figure 78. Frequency spectrum of changes in water level at Trident Pier

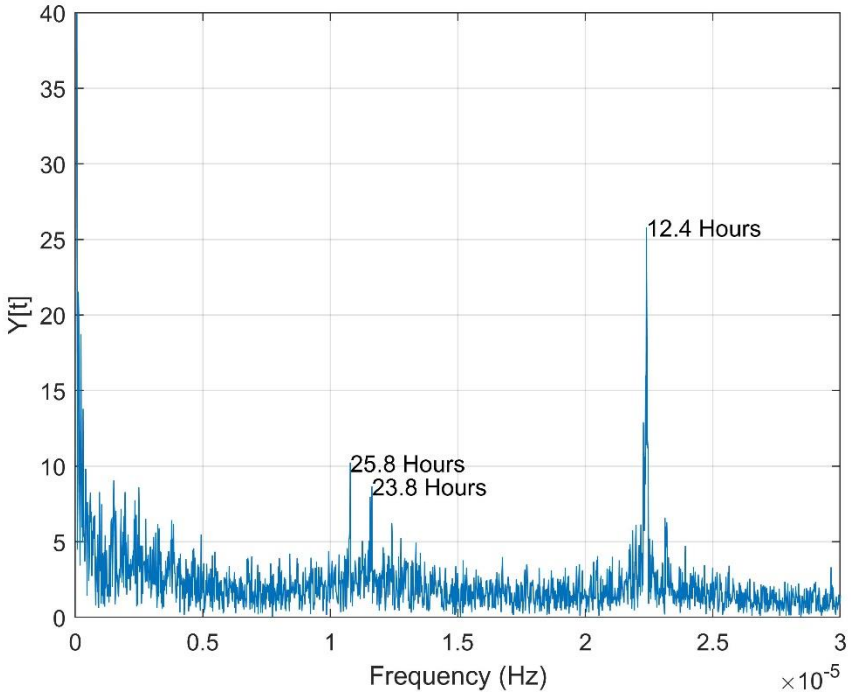

Figure 79. Frequency spectrum of changes in direction at Dragon Point

Similar peaks can be seen in the frequency spectrum for directional changes at Barge Canal. The semi-diurnal tidal influence here is less pronounced and the 23.9 hour, assumed to be the diurnal tidal signal, fluctuation has a greater impact as can be seen in **Figure 80**. Similar to that of Barge Canal, the frequency spectrum of directionality of Sykes Creek currents, as depicted in **Figure 81**, shows greater influence at the diurnal cycle but oscillations in current direction are not induced over background at the semi-diurnal tidal signal for this time series. Higher energy levels distributed over lower frequencies again indicate other factors that influence current direction including sea level and wind forcing.

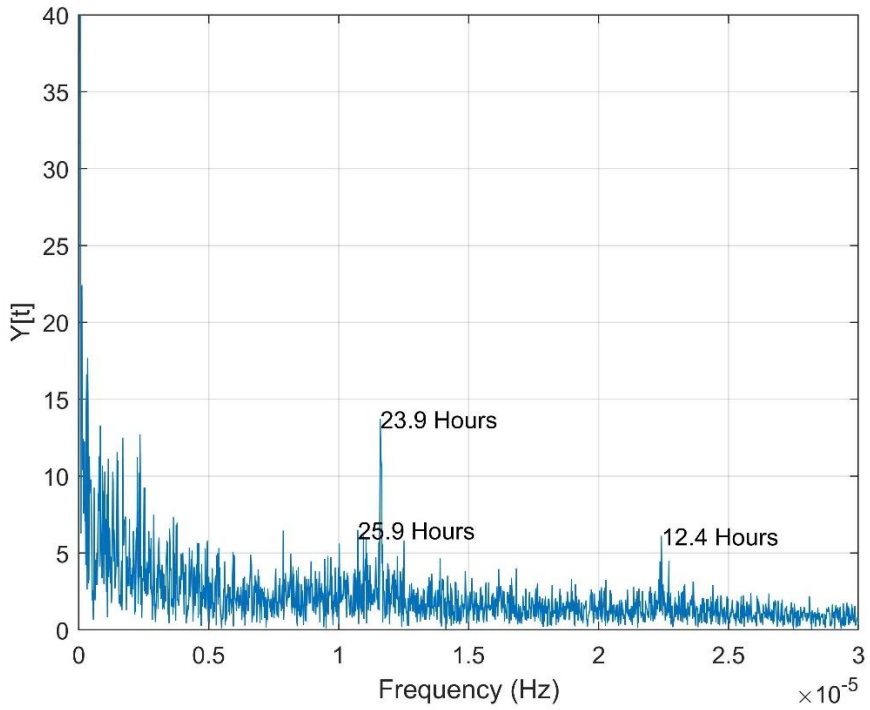

Figure 80. Frequency spectrum of changes in direction at Barge Canal

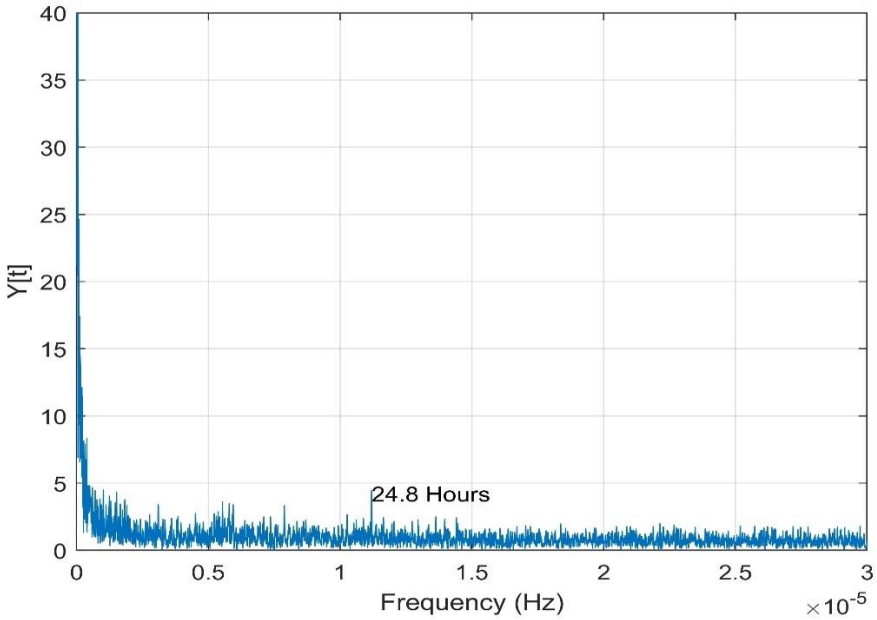

Figure 81. Frequency spectrum of Changes in Direction at Sykes Creek.

While these spectral plots indicate a relationship between current direction and tides, the tidal influence in the velocity of the currents and the shorter period water levels fluctuations of BRL are harder to resolve. Based on pressure data collected at each ADCP, the tides have a small effect on the water levels in BRL but are distinguishable in the frequency spectrum. The following pressure data have been filtered by subtracting a moving average of 12.5 hours from the time series which is then subject to a moving average of 6.5 hours to remove high frequency oscillations to better resolve the tidal influence in the time series. The filtered pressure data

frequency spectrum, as shown in **Figure 82**, clearly indicate tidal influence at the predictable diurnal and semi-diurnal tides.

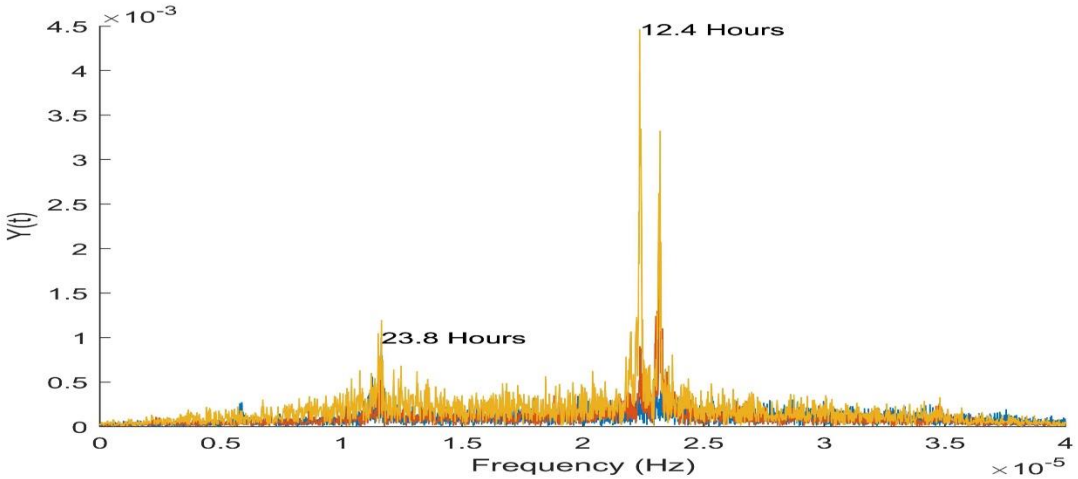

Figure 82. Frequency spectrum of water levels at 3 ADCP locations

Figure 83, **Figure 84**, and **Figure 85** show week-long snapshots of the pressure time series superimposed with the water level at Trident Pier to better illustrate the tidal influence. Being 34 km from Sebastian Inlet, the tidal influence in BRL is small enough to be almost unnoticeable compared to lower frequency water level changes. As shown in the figures, the oscillation in water level in BRL resulting from the tide is a few centimeters at maximum.

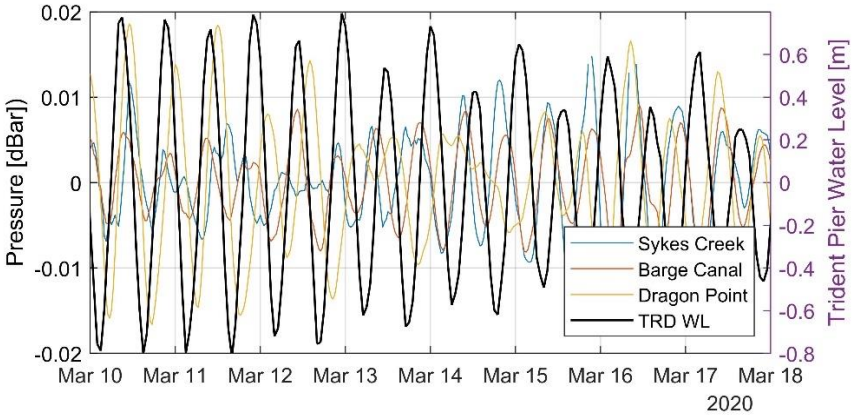

Figure 83. Filtered pressure and water level snapshot March 10-17, 2020

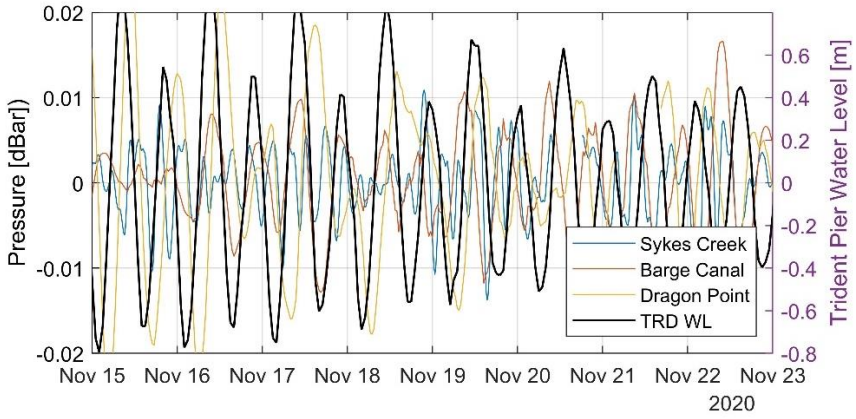

Figure 84. Filtered pressure and water level snapshot November 15-22, 2020

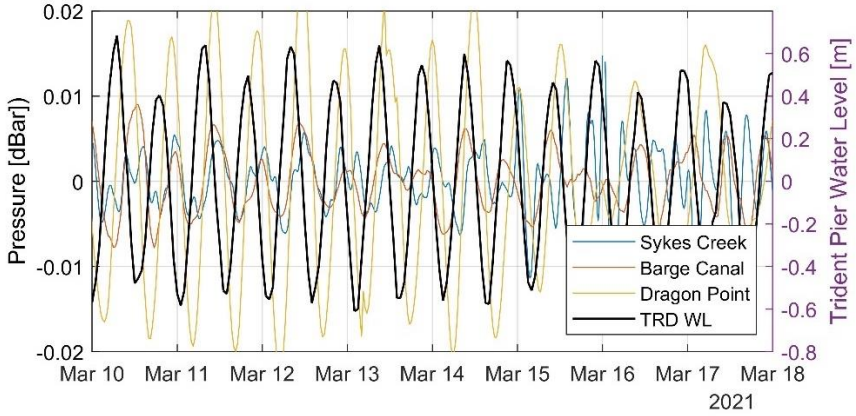

Figure 85. Filtered pressure and water level snapshot March 10-17, 2021

To better resolve the flow patterns for BRL, it is helpful to also filter the directional data similarly to the pressure data, with a 6.5 hour moving average. This helps clarify the directional trends and allows for better interpretation (**Figure 86** and **Figure 87**).

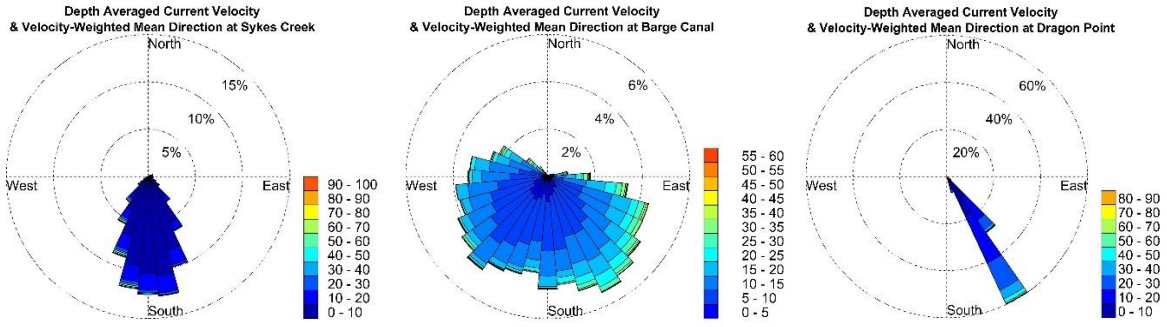

Figure 86. Filtered directional rose plots during south flow

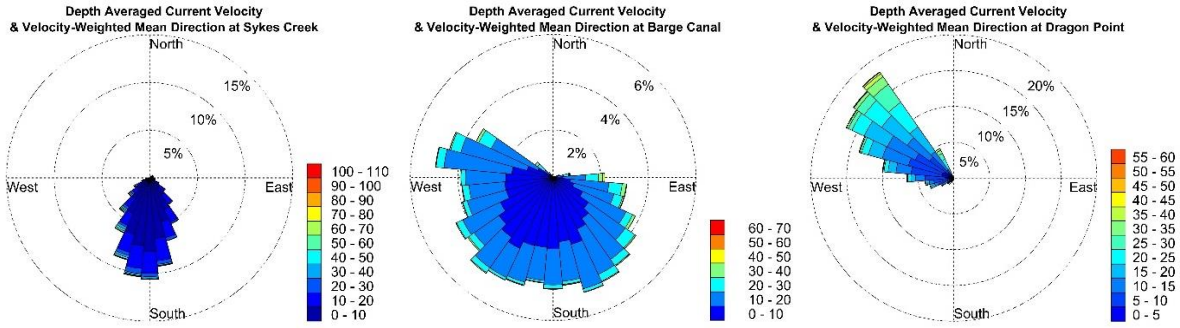

Figure 87. Filtered directional rose plots during north flow

Figure 88 shows the southward flow of the currents in BRL and the northern flow, respectively. Sykes Creek never reverses flow to the north and the flows around the ADCP at the Barge Canal are ambiguous but there is a visible east-west oscillation in these rose plots.

During a northward flow, water masses pass Dragon Point into BRL. By the time this flow pattern reaches the Barge Canal, there is likely hydraulic pressure from both ends as the influx from Dragon Point begins to be influenced by lowering water levels of the coastal ocean. This results in variable currents in the Barge Canal station and, instead of circulating out into IRL, this water is forced into Sykes Creek and reintroduced into BRL. Flows though at Barge Canal are also potential impacted by the isolation caused by the intersection of State Roads 520 and 528 through IRL and BRL. **Figure 88** shows both the south (left) and north (right) current directions exemplifying a time varying reversing circulation pattern.

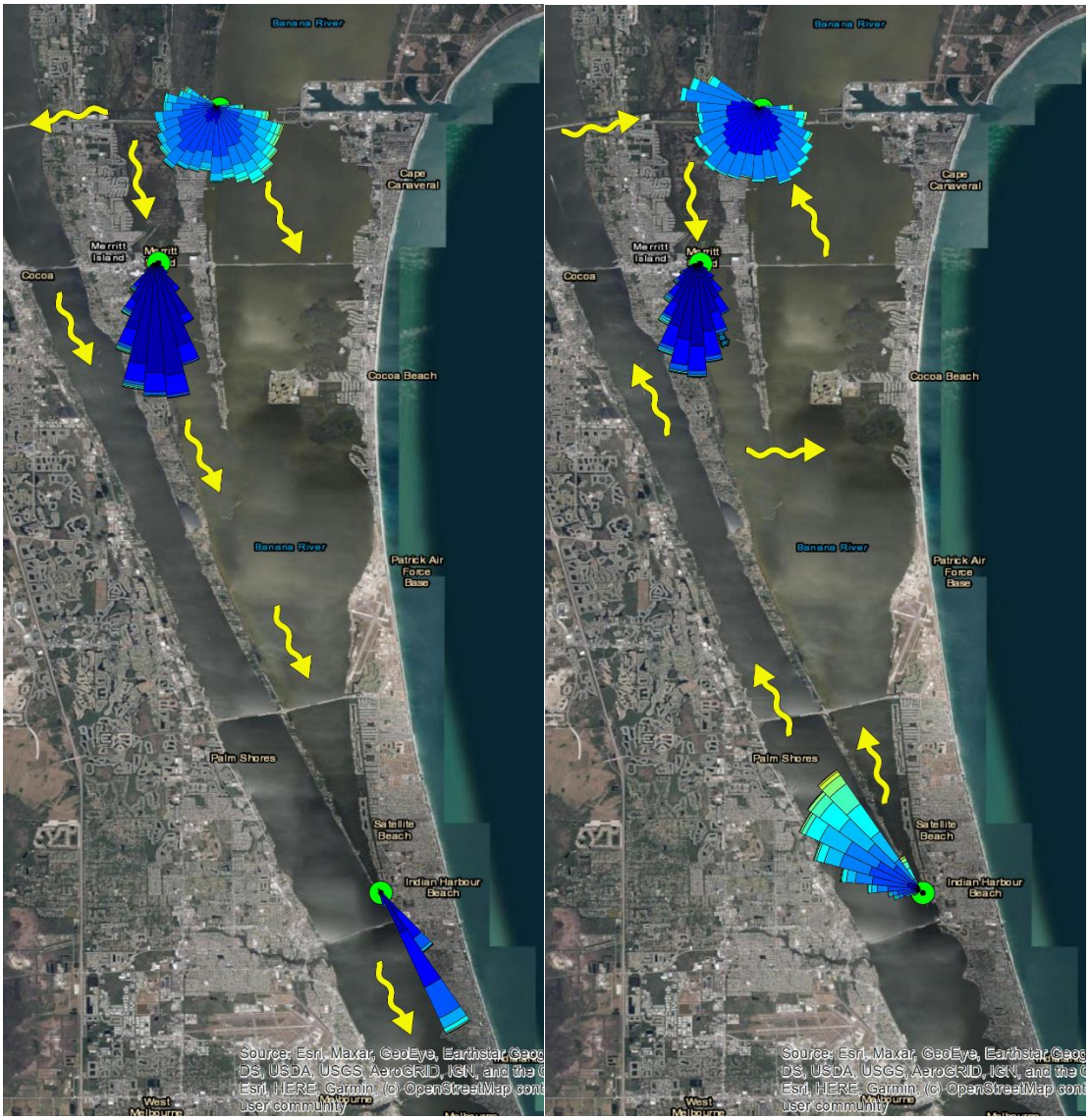

Figure 88. South and north directed current patterns

5 Introduction to Hydrodynamic and Water Quality Modeling

The model applied to meet the project objectives is the USEPA-supported EFDC model (Tetra Tech 2007). The model includes features and capabilities that make it applicable to shallow estuarine environments. The project area extends from the Mosquito Lagoon into the IRL compartments extending to the Fort Pierce Inlet. EFDC/ HEM3D was developed and refined at the Virginia Institute of Marine Science over the time period of 1988–1995 (Hamrick 1992). This multi-parameter finite difference model represents estuarine flow and material transport in three dimensions and has been extensively applied to shallow estuarine environments in Florida and other coastal states. A few examples include the central IRL (Zarillo and Surak 1994; Zarillo and Yuk 1996), Lake Jesup, Florida (Zarillo 2001), Loxahatchee River Estuary in south Florida (Zarillo 2004), Lake Worth Lagoon, Florida (Zarillo 2003), and more recently to the IRL for muck dredging evaluations (Zarillo and Listopad, 2021).

6 EFDC Description

6.1 Hydrodynamic Model Formulation

EFDC's hydrodynamic scheme solves the three-dimensional, vertically hydrostatic, free-surface, turbulent-averaged primitive equations of motion for a variable density fluid (Tetra Tech 2007). Also solved are the dynamically coupled transport equations for turbulent kinetic energy, turbulent length scale, salinity, and temperature. **Figure 89** shows a flow diagram of the various components of the EFDC model. The Mellor-Yamada level 2.5 turbulence closure scheme, as modified by Galperin and others (Galperin 1988), is implemented for the two turbulence parameter equations used in the model. The time integration of the momentum and continuity equations uses a second-order, semi-implicit, three-time-level, leap frog-trapezoidal method, with an insertion of a two-time level trapezoidal step to suppress the mode generated by the three-level scheme. The barotropic and baroclinic modes are split with a method that is implicit in the horizontal for the barotropic, and in the vertical for the baroclinic. Thus, the solution is a finite difference scheme with an internal-external mode splitting procedure to separate the internal shear or baroclinic mode from the external free surface gravity wave or barotropic mode. The external mode solution is semi-implicit, and simultaneously computes the two-dimensional surface elevation field by a preconditioned conjugate gradient procedure. The external solution is completed by the calculation of the depth averaged barotropic velocities using the new surface elevation field. Advection is handled with an upwind difference technique described in Hamrick (Hamrick 1992 and 1994). The EFDC model can be used to drive a number of external water quality models using internal linkage processing procedures described by Tetra Tech (2007).

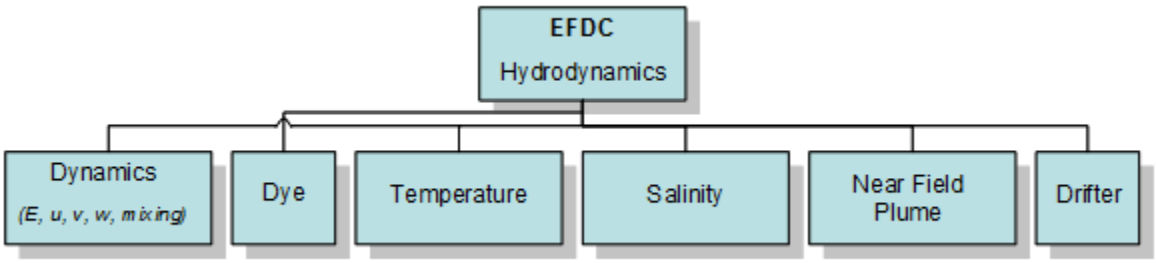

Figure 89. Flow diagram for the EFDC hydrodynamic and transport model (Tetra Tech 2009)

6.2 Water Quality Model Overview

The EFDC model can be directly coupled with the water quality model. The kinetic processes included in the HEM3D water quality model have been derived and updated from the Chesapeake Bay three-dimensional water quality model, CE-QUAL-ICM (Cerco and Cole 1994). A detailed description of the water quality model is provided by Park et al. (1995) and Tetra Tech (2007). **Table 12** lists the model's complete set of state variables. **Figure 90** presents a schematic flow chart of interactions among water quality variables in EFDC/HEM3D. Earlier water quality models, such as the Water Quality Analysis Simulation Program (Ambrose et al., 1993), used biochemical oxygen demand to represent oxygen demanding organic material, and the HEM3D water quality model is carbon based. The four algae species are represented in carbon units. The three organic carbon variables play an equivalent role to biochemical oxygen demand. Organic carbon, nitrogen, and phosphorous can be represented by up to three reactive sub-classes: refractory particulate, labile particulate, and labile dissolved. The use of the sub-classes allows a more

realistic distribution of organic material by reactive classes when data are used to estimate distribution factors.

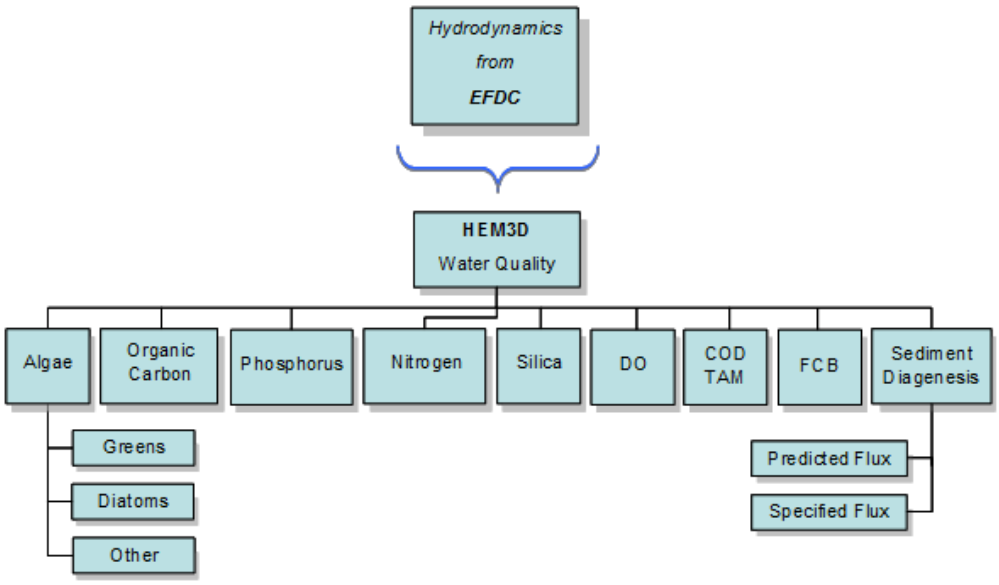

Figure 90. Flowchart for the water quality module of HEM3D (Hamrick,2008)

Table 12. List of water quality variables that can be calculated by the EFDC/HEM3D model

(1) cyanobacteria **Bc**	(12) labile particulate organic nitrogen **LPON**
(2) diatom algae **Bd**	(13) dissolved organic nitrogen **DON**
(3) green algae **Bg**	(14) ammonia nitrogen **NH_4**
(4) refractory particulate organic carbon **RPOC**	(15) nitrate nitrogen **NO_3**
(5) labile particulate organic carbon **LPOC**	(16) particulate biogenic silica **SAP**
(6) dissolved organic carbon **DOC**	(17) dissolved available silica **SAD**
(7) refractory particulate org. phosphorus **RPOP**	(18) chemical oxygen demand **COD**
(8) labile particulate organic phosphorus	(19) dissolved oxygen **DO**
(9) dissolved organic phosphorus **DOP**	(20) total active metal **TAM**
(10) total phosphorus **TP**	(21) fecal coliform bacteria **FCB**
(11) refractory particulate organic nitrogen **RPON**	

7 EFDC Model Setup

Application of the EFDC model to inflow studies in the IRL leverages the modeling platform built to assess the benefits of muck dredging in the IRL (Zarillo and Listopad 2020). Under this project, the model grid was initially developed along with external and internal model boundary conditions.

These were updated and modified for the present inflow evaluation project. The following subsection provides an overview of the model development and update to the inflow project.

7.1 Model Computational Grid

Figure 91 shows the overall extent of the IRL model grid that extends from Ponce Inlet on the north to just south the Fort Pierce Inlet at the south end. The model grid includes 10,094 active computational cells in the horizontal and 5 layers in the vertical dimension.

The model grid was designed as a layer in the ArcGIS software platform. A recent set of aerial images was used as a background over which a data layer was hand drawn to fit the model grid to shoreline boundaries and other morphologic features of the IRL system. Care was taken to include extensive marsh and mangrove areas, as well as include the details of the numerous causeway-bridge combinations within the IRL system. The EFDC model software platform includes grid generating software. Once a boundary fitted curvilinear orthogonal grid is visualized as a Geographic Information System (GIS) layer. The grid generator uses a subscripted array of cell types and the x,y coordinates of the corner points of all water cells to produce model input files that numerically represent the model grid. A time-consuming step in the grid generation process can be to digitize the water cell corner points. To speed this process, Applied Ecology, Inc. developed a digitizing tool that operates under ESRI ArcGIS^{TM} 10.3. (Listopad 2017). The hand drawn grid layer is opened by the tool and the coordinates of the cell corner points are digitized in order, row by row from the southwest corner of the grid to the northeast corner of the grid. The grid tool assigns I (row) and J (column) indices to each set of cell coordinates. The subscripted list of cell coordinates, along with an or ordered two-dimensional array of cell types and depth value inputs are then used by the grid generator to calculate an ordered list of cell dimensions (file dxdy.out) and a file specifying horizontal cell center coordinates and cell orientations(file lxly.out). These files are restated as input files along with the control and boundary forcing information.

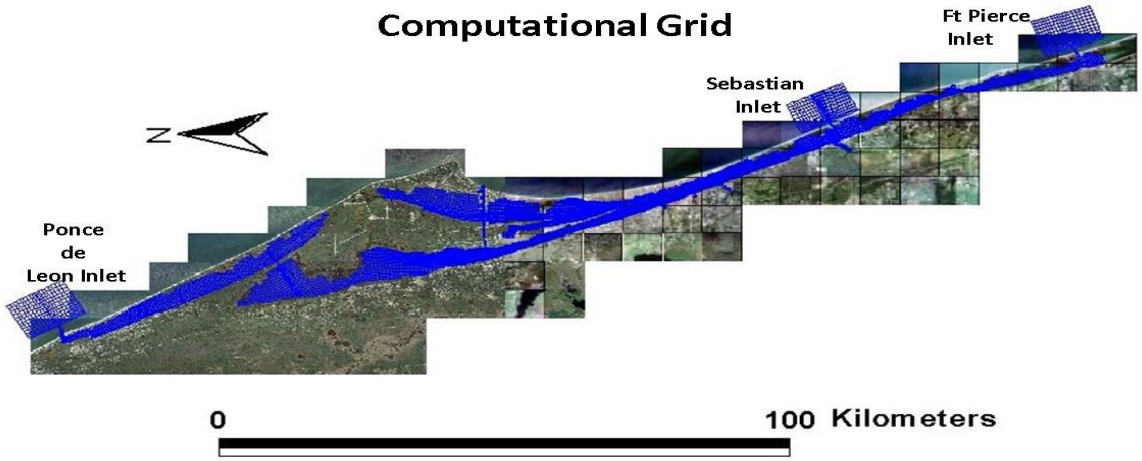

Figure 91. Model computational grid extending from Ponce de Leon Inlet to Fort Pierce Inlet

Data sets have been assembled from a wide range of sources and evaluated for use in the model. Among the most important data sets are those maintained by SJRWMD, by the U.S. Geological Survey (USGS) under sponsorship by SJRWMD, and Harbor Branch Oceanographic Institution's (HBOI) Land/Ocean Biogeochemical Observatory (LOBO). Data from these stations include time series of water level, salinity, temperature, discharge, and meteorological parameters. These data

sources were used to either set internal model boundary conditions, such as freshwater inflow, or to check the calibration of the model for salinity and water temperatures. Another important source of data applied to the model was estimates of groundwater inflows into the lower layer of the EFDC model to simulate groundwater flux. At the time scale of this project, the contribution of groundwater is secondary to the overall hydrologic balance of the system but can be of increasing importance at the longer time scales of a decade or longer in which the major balance is between evaporation and groundwater flux. Groundwater flows were provided by the work of Mamoua et al. (2019) under an ongoing IRL groundwater assessment project that includes both data collection and modeling. Data from meteorological stations maintained by the SJRWMD and the National Weather Service are used to setup air sea interaction boundary conditions for the hydrodynamic model.

The major model input files are listed in **Table 13**. For each of the of the model time series files listed in

Table 13, the complete available data record is loaded in the model boundary input file. Although the available data sets are generally of high quality, having been quality controlled levelled to NAVD88 with respect to water level, they are limited in time span, especially for the model boundaries that extend into the coastal ocean at Ponce de Leon, Sebastian Inlet, and Fort Pierce Inlet.

Table 13. Major EFDC input files

Input File	Description
efdc.inp	Main control file
aser.inp	Atmospheric forcing time-series file.
cell.inp	Horizontal cell type identifier file.
dxdy.inp	File specifying horizontal grid spacing or metrics, depth, bottom elevation, bottom roughness and vegetation classes for either Cartesian or curvilinear orthogonal horizontal grids.
Dye.inp	Initial numerical tracer assigned to selected model cells.
lxly.inp	File specifying horizontal cell center coordinates and cell orientations.
pser.inp	Water level time series.
qser.inp	Volumetric source-sink time-series file. Including groundwater (inflow-outflow).
salt.inp	File with initial salinity distribution for cold start, salinity stratified flow simulations.
sser.inp	Salinity time-series file.
temp.inp	File with initial water temperature distribution for cold start, salinity stratified flow simulations.
tser.inp	Temperature time-series file.
wser.inp	Wind speed and direction.

To provide water level time series at model cells in the coastal ocean offshore of Ponce de Leon Inlet, Sebastian Inlet, and Fort Piece Inlet, predicted time series of water elevation were provided at these locations from the Advanced Circulation (ADCIRC) model as described in other sections. Since ADCIRC only provides water level time series in the tidal frequency band, it is important to add lower frequency components that include water level oscillations outside the frequency of the tides. This signal can include seas level shifts of up to 1 m at time scales of a few weeks to seasonal (Zarillo 2019). **Figure 92** is an example of the water level time series applied offshore on Ponce de Leon Inlet.

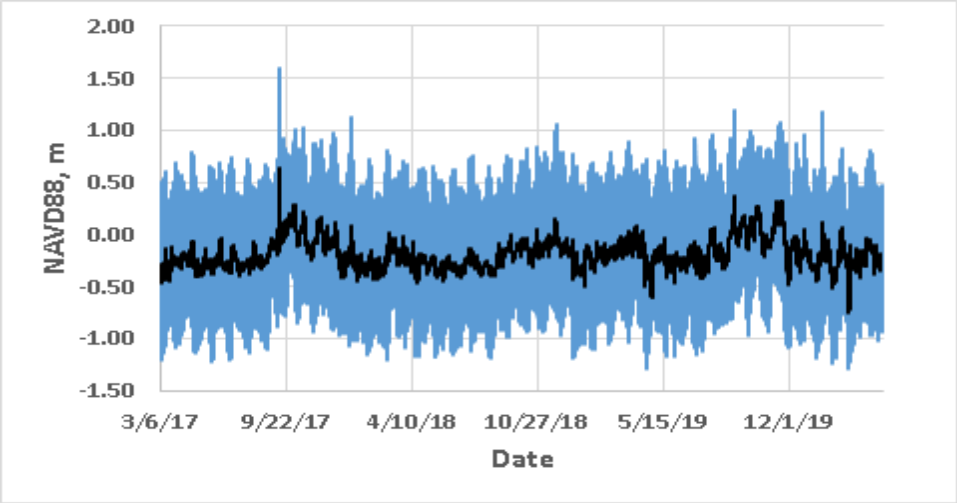

Note: Black line shows the non-tidal sea level, whereas the blue line shows the combined series. Storm surge related to passing of Hurricane Irma in September of 2017 is seen in the time series.

Figure 92. Water level time series applied to model boundary cells offshore of Ponce de Leon Inlet showing the combined tidal and sea level signals

Non-tidal water levels combined with the ADCIRC model data were derived by filtering measured data at NOAA Station 8721604 at the Trident Pier, Cape Canaveral. Observations show that non-tidal sea levels are coherent at regional spatial scales, as seen in **Figure 93** illustrating tidal and filtered non-tidal water level records from Trident Pier and from measured data at Sebastian Inlet 65 km to the south.

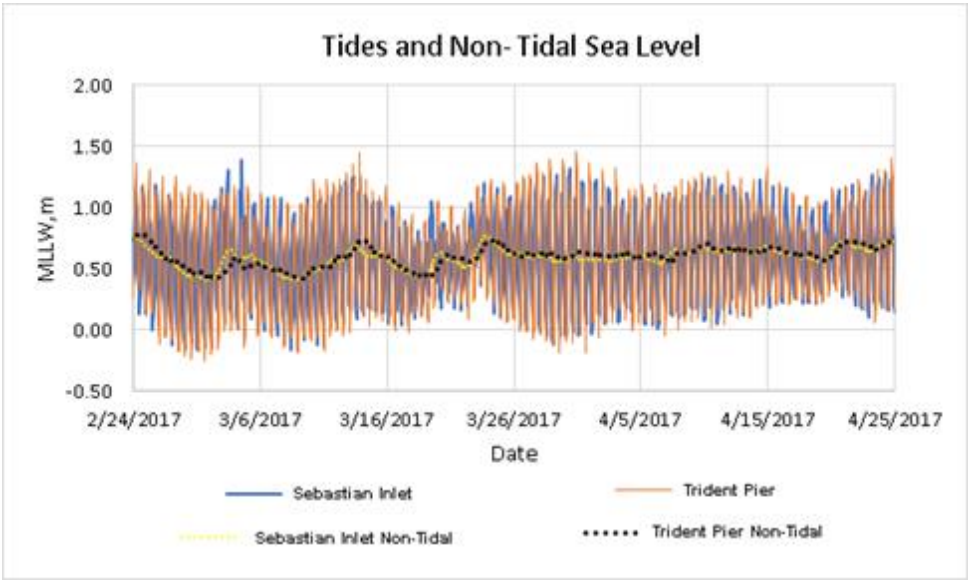

Figure 93. Measured tidal and non-tidal water level records from NOAA Station 8721604 (Trident Pier, Cape Canaveral, FL) and Sebastian Inlet

Salinity and water temperature time series were assigned to the coastal ocean model boundary cells offshore of Ponce de Leon Inlet, Sebastian Inlet, and Fort Pierce Inlet. These data were provided from the archive of model runs maintained by the Hybrid Coordinate Model (HYCOM) Consortium (https://www.hycom.org/). **Figure 94** is an example of salinity and water temperature data provided by HYCOM assigned to the surface layer of offshore model cells at Sebastian Inlet.

Similar HYCOM time series of salinity and water temperature were assigned to model boundary cells offshore of Ponce de Leon Inlet and Fort Pierce Inlet.

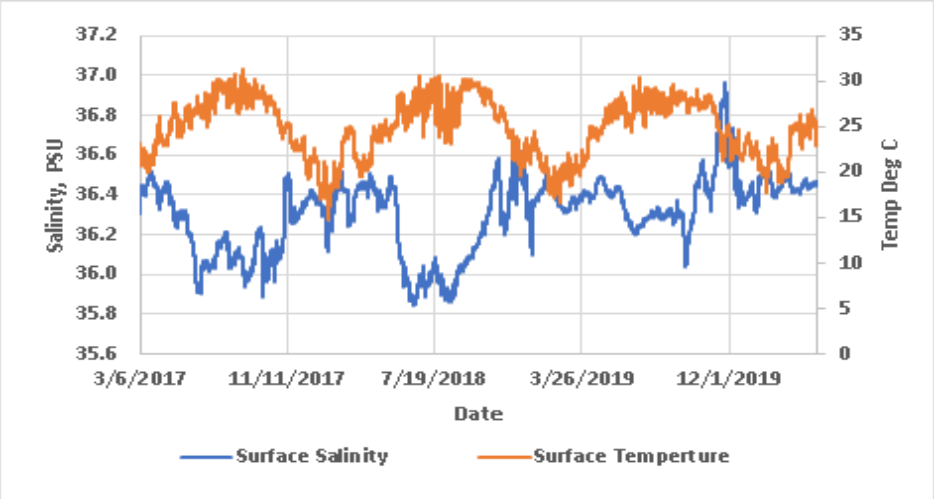

Figure 94. Example of salinity and water temperature data provided by HYCOM for offshore model cells at Sebastian Inlet

8 Water Quality Model Setup

To activate the water quality calculations within EFDC/HEM3D, various input files are applied and controls set in the main water quality control input file (WQWC.INP). **Table 14** lists the required files and their function within the model. Similar to the hydrodynamic portion of the model, water quality data to drive and calibrate the model are derived from existing historical sources, ongoing data collection efforts sponsored by SJRWMD, and the SWIL watershed model (Applied Ecology, 2015). **Figure 95** shows the distribution of water quality monitoring stations maintained throughout the IRL system.

The water quality parameter concentrations and coefficients controlling the kinetics of the nutrient and sediment cycles initially have been set from a review of available water quality data from the IRL and from recent studies of sediment geochemistry by Trefry and Fox (2020). During the calibration process, kinetics and coefficients for each variable are adjusted to improve the performance of the water quality calculations with respect to measured data. For example, kinetics constants and coefficients for the water column and sediment model input files are adjusted for model calibration and operation using information collected during several years of a project to determine the environmental impacts of muck dredging sponsored by Brevard County (Florida Tech 2021).

Table 14. Summary of major EFDC/HEM3D water quality input files

Model Input File	Description
efdc.inp	Primary controlling input file for EFDC hydrodynamics and water quality transport options
wq3dwc.inp	Kinetics constants and coefficients for the water column
wq3dsd.inp	Kinetics constants and coefficients for the sediment model
cwqsr01-21.inp	Time-series to be applied to model boundary conditions for water quality state variables 1-21
wqpsl.inp	Time-series river and point source loads for variables 1-21
BENFN	Time series of the benthic fluxes for the different sediment zones

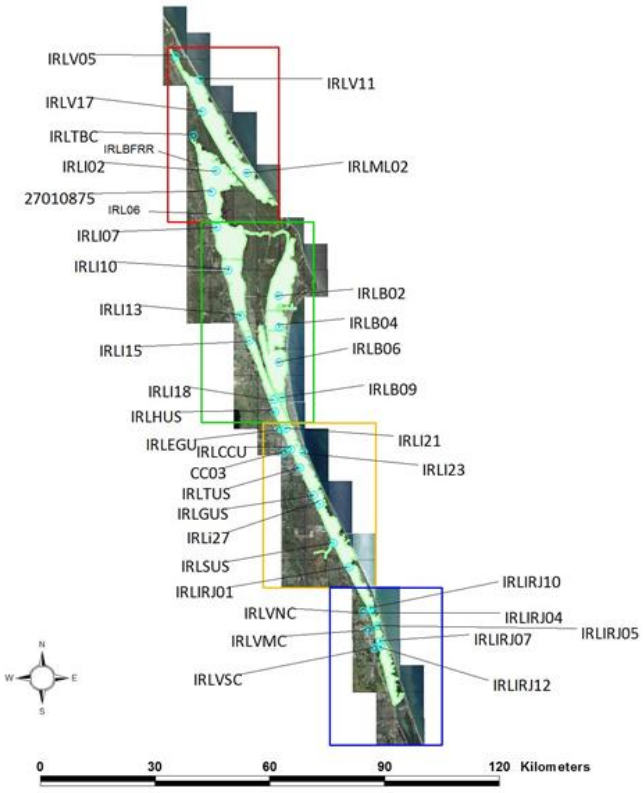

Figure 95. Location of water quality monitoring station maintained by SJRWMD

8.1 Watershed Inputs

Watershed inputs were assembled from two sources including the Hydrological Simulation Program - FORTRAN watershed sub-basin models available from SJRWMD and SWIL model developed by Applied Ecology, Inc. **Figure 96** shows the watershed sub-basins linked to the IRL model. Time series of surface water flows, base flows, and major nutrient classes produced by the SWIL model are applied as inputs to model runs, along with freshwater inflows from major USGS gauging stations associated with water control structures connected to Turkey Creek and Sebastian River. Surface water, baseflow, and USGS gauged flow data are placed in model input file qser.inp (see **Table 14**). SWIL watershed model output is available as monthly loads of total phosphorus (TP) and total nitrogen (TN) from 1995 through 2020. Likewise, stormwater runoff and baseflow volumes are provided as monthly volumes. **Figure 97** shows an example of output from the SWIL watershed model from the Turkey Creek sub-basin.

Time series of water quality data from SWIL and from selected SJRWMD monitoring stations are specified as input to the EFDC/HEM3D model in file wqpsl.inp (see **Table 14**). In this file, time series of water quality data are linked to specific sets of water cells in the model grid that connect to the watershed sub-basins shown in **Figure 96**.

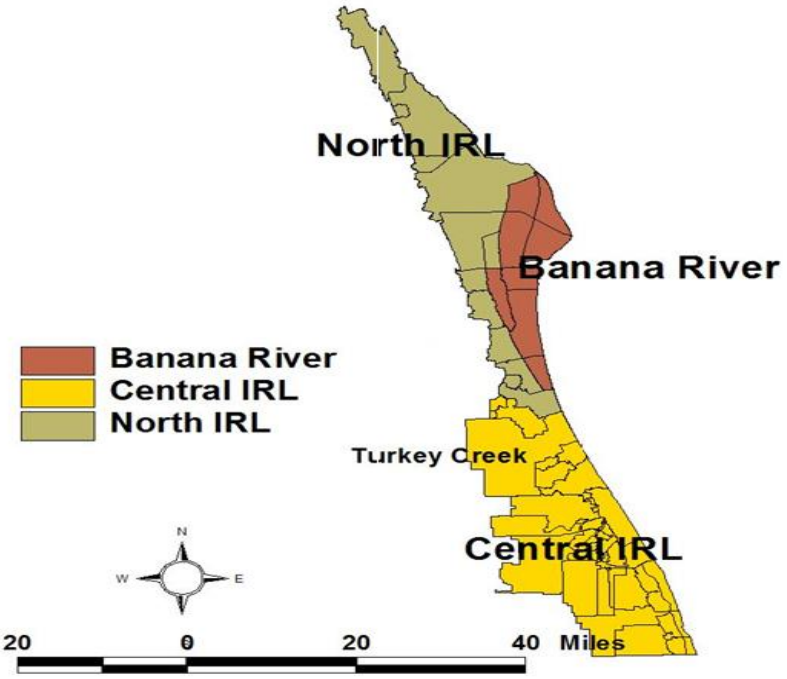

Figure 96. Boundaries of the watershed model sub-basin links to the IRL model

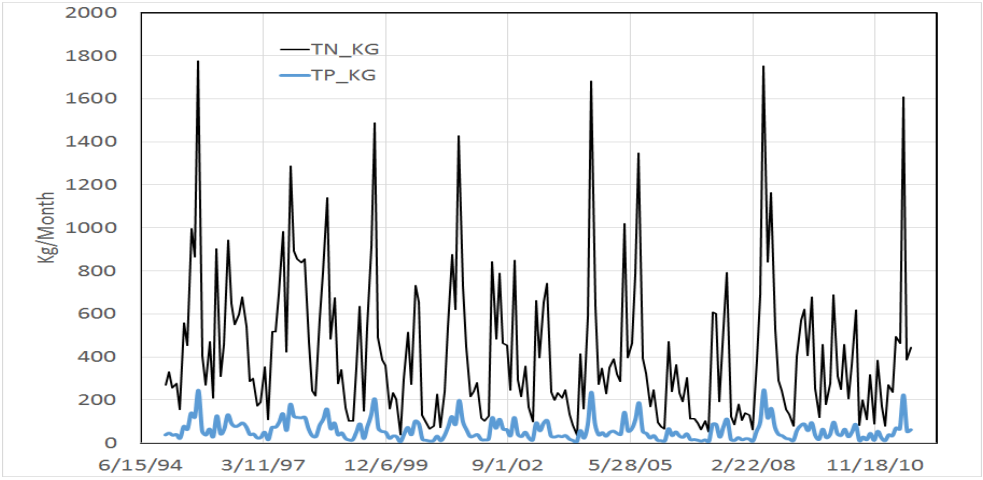

Figure 97. Example of TN and TP inputs to the EFDC/HEM3D model from the SWIL watershed model, with inputs received from the Turkey Creek sub-basin (AEI, 2016)

8.2 Sediment Diagenesis Model Setup

The EFDC/HEM3D sediment diagenesis model is based on formulations modified from the Chesapeake Bay Model and includes 27 state variables and fluxes (Table 15). This sub model, as applied in the IRL, is a key element in calibrating and running the water quality model. Three basic processes are included in the sediment sub model: depositional flux of particulate organic matter from water the column, diagenesis (decay) of particulate organic matter in sediments, and flux of substances produced by diagenesis. Benthic sediments are represented by two layers. The upper layer can be oxic or anoxic, whereas the lower layer is always anoxic. The diagenesis model is schematically represented in **Figure 98**.

Table 15. Sediment model state variables (Tetra Tech, 2007)

(1) particulate organic carbon G1 class in layer 2	(15) nitrate nitrogen in layer 1
(2) particulate organic carbon G2 class in layer 2	(16) nitrate nitrogen in layer 2
(3) particulate organic carbonG3 class in layer 2	(17) phosphate phosphorus in layer 1
(4) particulate organic nitrogen G1 in layer 2	(18) phosphate phosphorus in layer 2
(5) particulate organic nitrogen G2 in G2layer 2	(19) available silica in layer 1
(6) particulate organic nitrogen G3 in layer 2	(20) available silica in layer 2
(7) particulate organic phosphorus G1 in layer 2	(21) ammonia nitrogen flux
(8) particulate organic phosphorus G2in layer 2	(22) nitrate nitrogen flux
(9) particulate organic phosphorus G3 in layer 2	(23) phosphate phosphorus flux
(10) particulate biogenic silica in layer 2	(24) silica flux
(11) sulfide/methane in layer 1	(25) sediment oxygen demand
(12) sulfide/methane in layer 2	(26) release of chemical oxygen demand
(13) ammonia nitrogen in layer 1	(27) sediment temperature
(14) ammonia nitrogen in layer 2	

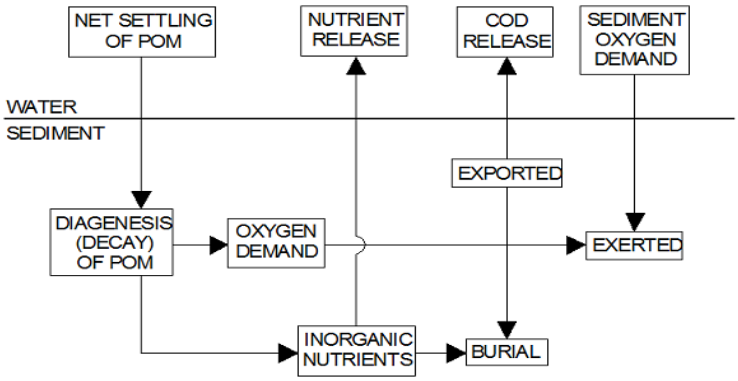

Figure 98. Sediment diagenesis schematic (Tetra Tech, 2007)

The kinetics of the sediment model are controlled within file wq3dsd.inp listed in **Table 14**. The recent data collected by Trefry and Fox (2015) indicate high rates of loading of ammonium and phosphate to the water column by muck sediments. Dr. Fox is also performing laboratory experiments of nutrient flux from muck sediments sampled from the Turkey Creek area where muck was to be dredged. Within the sediment diagenesis model, fluxes of these and other nutrients are calculated using the benthic flux of nutrients specified in the BENFN water quality input file (**Table 14**).

9 Model Verification

9.1 Hydrodynamic Model

Model calibration results for the IRL model developed at Florida Tech were described in an earlier project report (Zarillo and Listopad 2016). However, there was an update of model boundary conditions in the coastal ocean for this project, an additional validation on model performance was conducted.

Figure 99 compares observed and model water levels at the Wabasso Bridge in north Indian River County, where a long-term water level sensor has been maintained by the USGS on behalf of SJRWMD. The time period shown in **Figure 99** is within the time period in which the latest round of model predictions were made. The root mean square error (RMSE) of the comparison is 0.055 m (5.4 centimeters) and the ratio between RMSE and the range of observed values of water level is 0.037 representing an error of 6.1% In the original calibration and validation exercise, the observations to model companions were 7.7% and 9.4%, respectively (Zarillo and Listopad 2016).

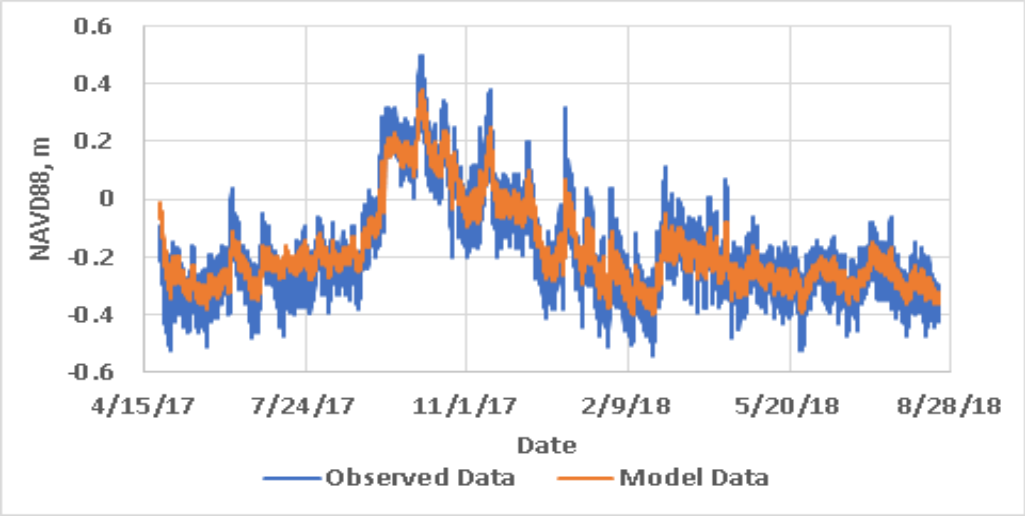

Figure 99. Observed and predicted water levels at Wabasso Bridge, north Indian River County, FL

An additional water level comparison was made between observed and model data in Haulover Canal connecting the southern end of the Mosquito Lagoon with the north compartments of the IRL. Observed data were from the USGS Haulover Canal monitoring station midway along the Canal. **Figure 100** shows the comparison in which the model data followed the trends of the observed data, but do not completely reproduce shorter term water level variation. The RMSE for this comparison is 9.7 centimeters representing a match error 13.8% of the total observed range of water level.

Both water level comparisons show that the hydrodynamic model captures the annual high stand of sea level in the IRL that is forced by coastal sea levels responding to large variations in the Gulf Stream. Capturing this phenomenon is important since the total annual range of sea level can vary by more than 0.7 m in comparison to an average depth of about 1 m in IRL. The physics of the relationship between the Gulf Stream flux and coastal ocean sea level is explained in Ezer et al., 2013.

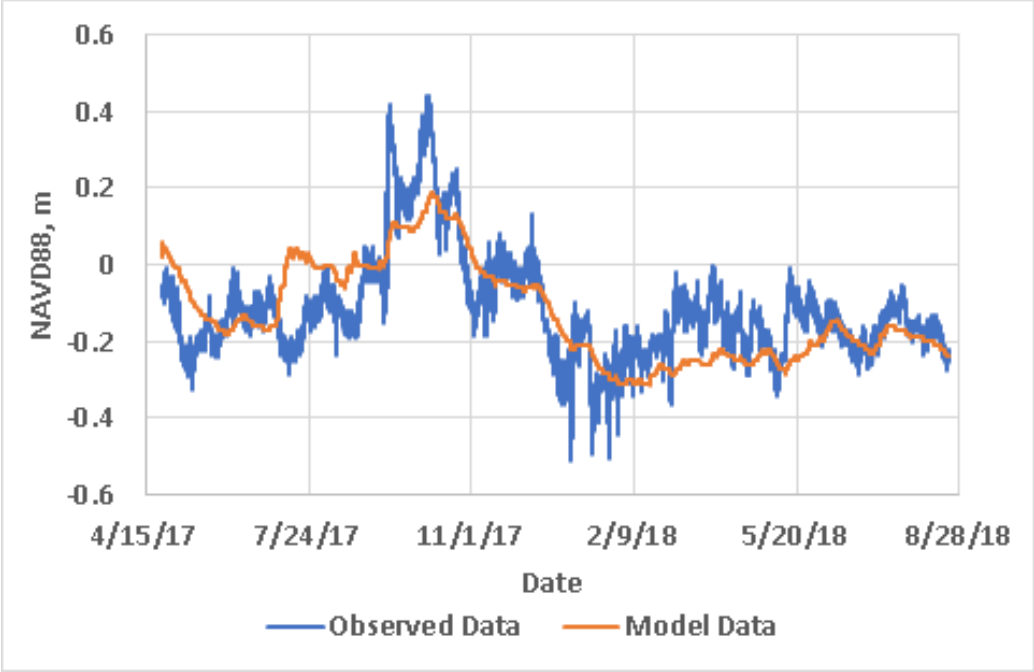

Figure 100. Observed and predicted water levels at Haulover Canal, north Brevard County, FL

Calibration and validation of model salinity and water temperature data were provided (Zarillo and Listopad 2016). However, since the HYCOM time series are an update of outer model boundary conditions, a comparison of observed and model salinity data and water temperature data was made within the 2018-2019 period that corresponds to a portion of the model productions runs. data. **Figure 101** compares model predicted salinity values with observed salinity data recorded by LOBO Station IRL-SB. This station is located in the Intracoastal Waterway to the west of Sebastian Inlet. The observation to model data comparison was made for the surface layer of the model, which represents the upper 20% of the water column. The RMSE for the comparison is about 2.7 practical salinity units representing an error of about 12%, which is comparable to the calibration and validation error values reported earlier (Zarillo and Listopad 2016).

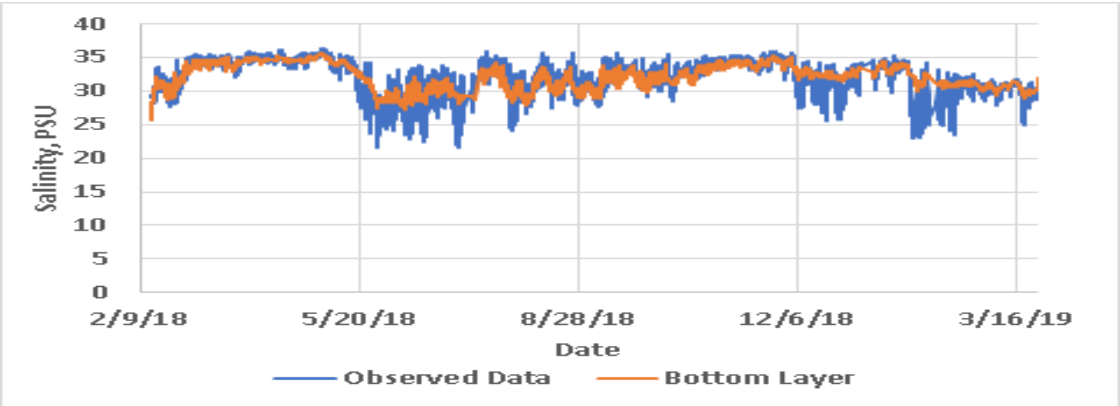

Figure 101. Comparison of observed and model salinity values recorded at LOBO Station IRL-SB in the IRL near Sebastian Inlet

Figure 102 compares water temperature observations with model data at LOBO Station IRL-SB the IRL near Sebastian Inlet. The RMSE for the comparison is 2.68 degrees Celsius (˚C) for a

relative percentage error of about 18.% when comparing the RMSE value to the range of observed values.

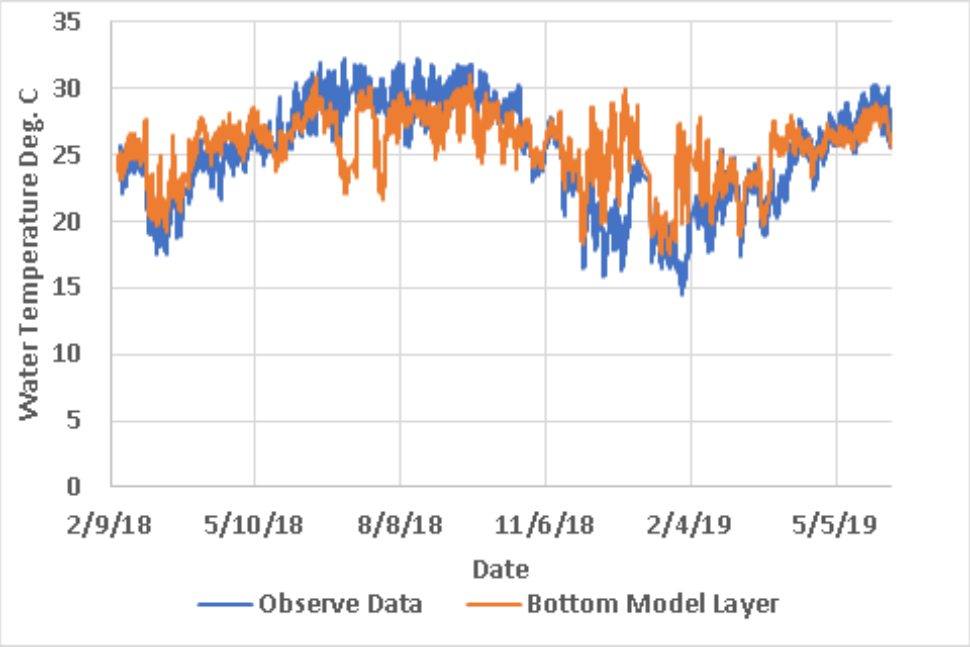

Figure 102. Comparison of observed and model water temperature values recorded at LOBO Station IRL-SB near Sebastian Inlet

10 Water Quality Model Verification

Verification of the EFDC/HEM3D water quality calculations in the IRL system is an ongoing process. Operation of the water quality model depends on a number of input files that contain measured data from a variety of sources (see **Section 7**). However, at this stage of development, predictions of water quality constituent concentrations in the water column show good agreement with measured data. Inputs from the SWIL watershed model are still undergoing refinement to provide details of nitrogen and phosphorus species components of TN and TP loads. Chemical species such and phosphate, nitrate + nitrite, and labile and refectory components in the total loads are only estimated. Thus, in the model-observation comparisons, only TN and TP are considered in addition to total chlorophyll and DO concentrations. In the following sections, graphical comparisons between observed and model data are made at locations where continuous observed water quality data are available and at locations in BRL where data from SJRWMD are available on a quality basis.

10.1 DO Comparisons

A comparison of model and observed DO concentrations is based on data from monitoring stations maintained by the HBOI LOBO. Data can be inspected and downloaded at http://fau-hboi.loboviz.com/ge/. **Figure 103** shows LOBO monitoring stations near the south end of the EFDC model computational grid. Comparisons are made at the SBLOBO and VBLOBO stations shown in the figure.

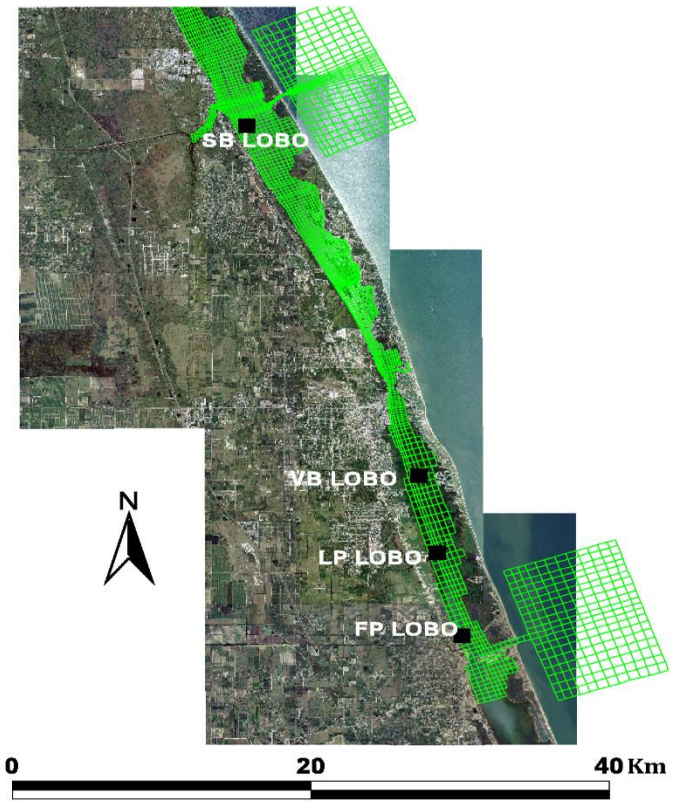

Figure 103. Location of the HBOI LOBO water quality monitoring station in IRL between Fort Pierce Inlet and Sabastian Inlet

Figure 104 shows a comparison between observed and modeled DO at SBLOBO located in the IRL near Sebastian Inlet (see **Figure 103**). The RMSE calculated between measured and model data at this location is 2.11 milligrams per liter (mg/L) or about 13% of the observed range of measure data values. There are numerous gaps in the measured data as can be seen in **Figure 104**. However, according to the HBOI LOBO program specifications (http://fau-hboi.loboviz.com/qa/), water quality sensors are factory calibrated every 12 months and undergo a calibration check against laboratory analysis of collected water samples. Based on a comparison with previous model studies based on the EFDC/HEM3D, the model performance can be considered good and comparable with other EFDC/HEM3D model applications (USEPA 2000; Park et al., 2005; Hamrick and Ji 2008).

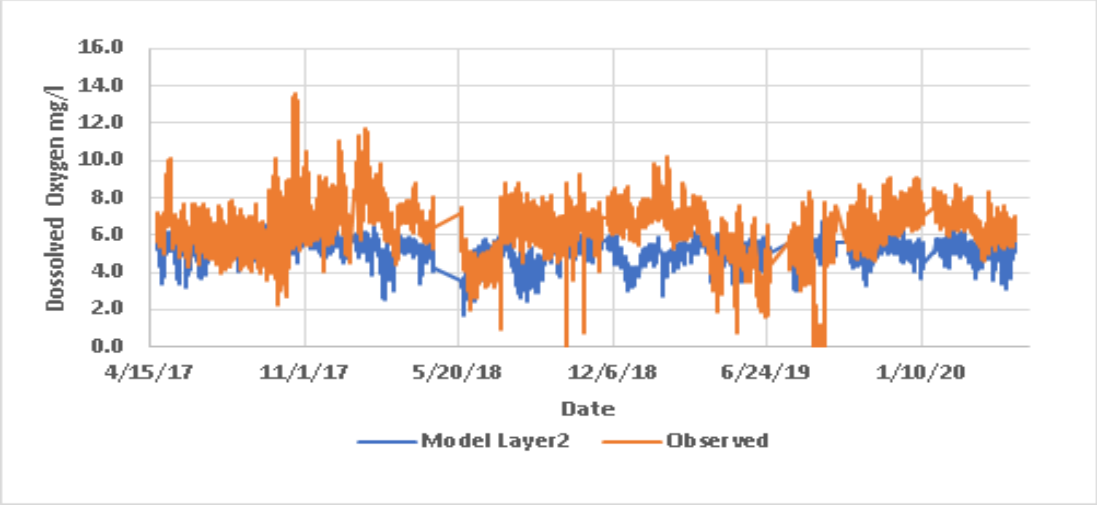

Figure 104. Model and observed DO time series at station SBLOBO

Figure 105 shows model and observed DO concentrations at station VBLOBO shown in **Figure 103**. The RMSE between the observed and model data is 1.81 mg/L, which is about 16% of the observed range of measured values. The measured DO time series at both LOBO stations appears to have very low and declining values in spring 2018 during a period of time when a noticeable gap in the measured data occurred at SBLOBO.

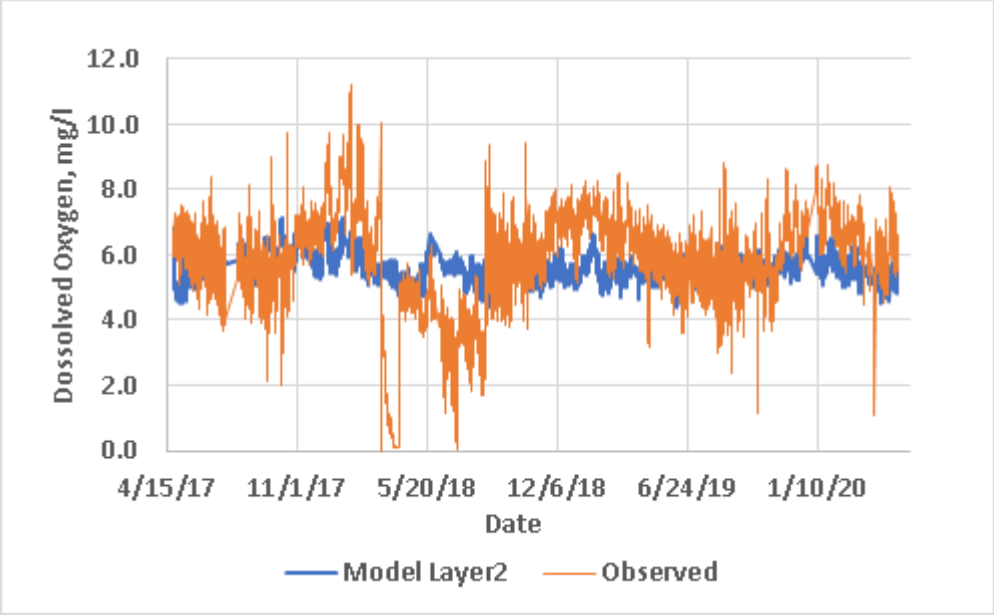

Figure 105. Model and observed DO time series at station VBLOBO

Figure 106 shows the location of the SJRWMD long-term water quality monitoring station (IRLB04) in BRL in the vicinity of the hypothetical inflows evaluated in this study. One of the locations includes a recent continuous DO monitoring station that has been maintained since 2014. **Figure 107** compares measured and model DO values at this location. The RMSE DO comparison is 2.12 mg/L, which is about 14% percent of the observed range of DO values.

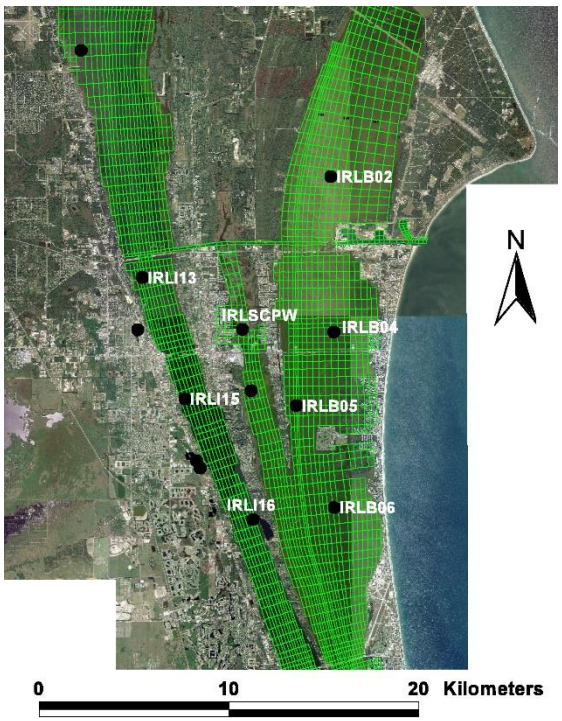

Figure 106. Location of SJRWMD long term water quality monitoring stations in the BRL with IRLB04 shown in the center of the BRL

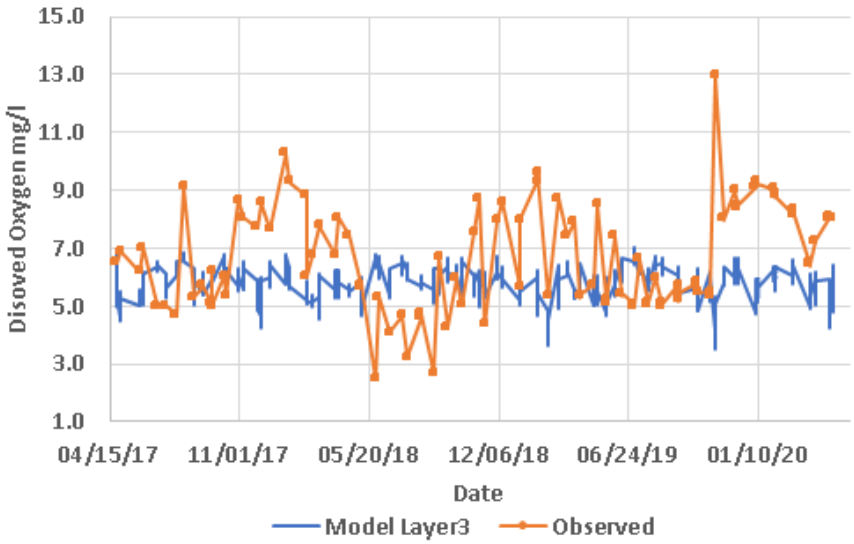

Figure 107 Measured and modeled DO values at IRLB04

10.2 Chlorophyll Comparisons

The HBOI LOBO monitoring project provides observed chlorophyll water column concentrations at four locations that are within the EFDC model domain. LOBO station locations with respect to the model computational grid are shown in **Figure 103**. At station SBLOBO, the model and observed data chlorophyll are well matched to within a RSME of 2.39 micrograms per liter (µg/L), which is about 10% of the observed range of observed values. At station VBLOBO, the RSME comparison is 3.83 about 12% of observed range of values.

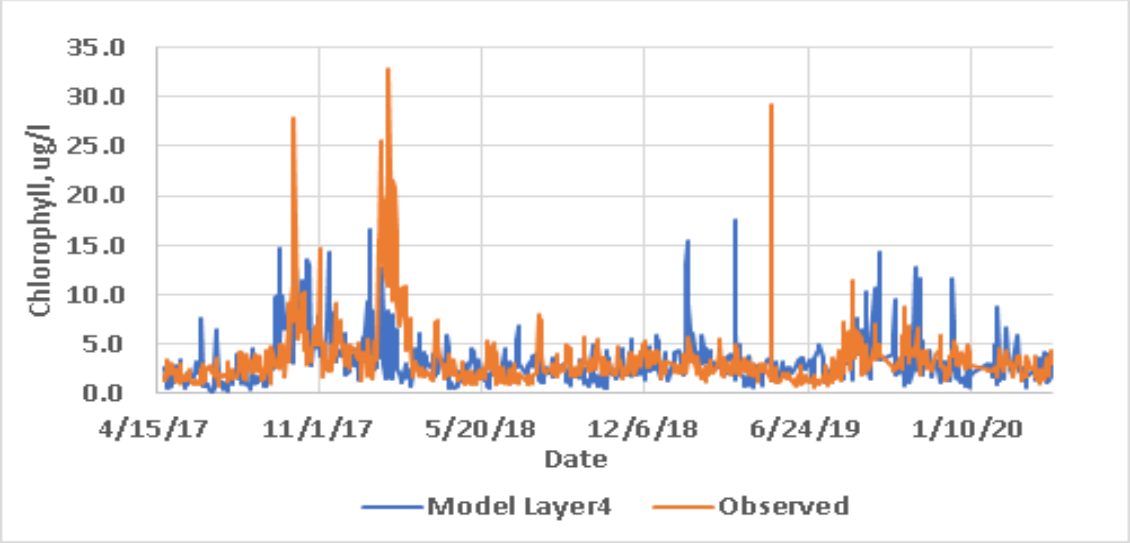

Figure 108. Comparison of model and observed total chlorophyl values at station SBLOBO

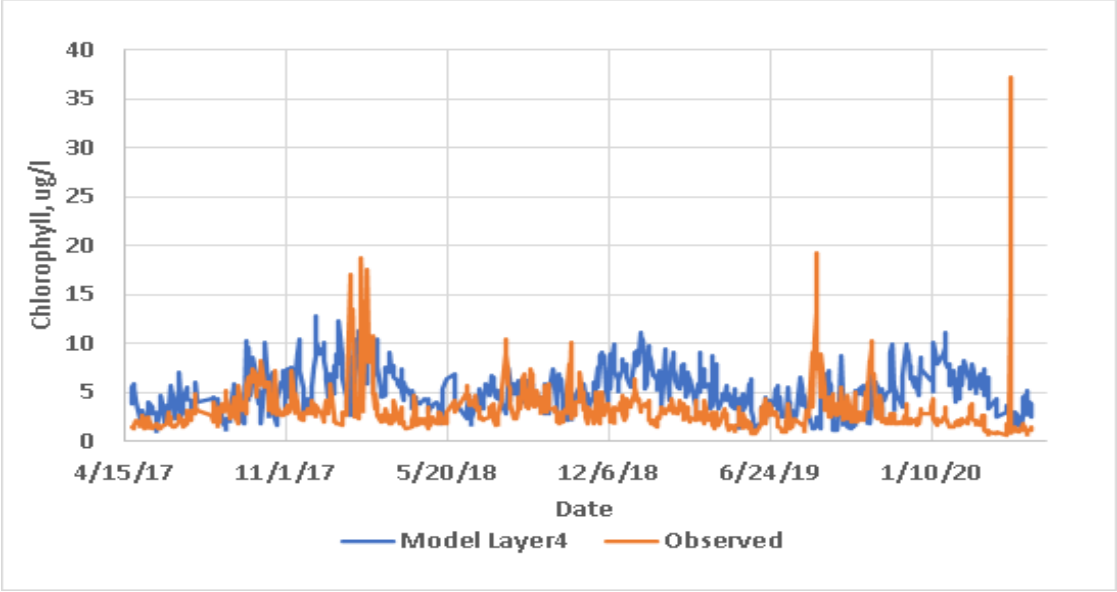

Figure 109. Comparison of model and observed total chlorophyl values at station VBLOBO

10.3 TN Comparisons

TN water column concentration comparisons are made between observed and model data at selected stations in BRL. Water quality data from these locations are available at quarterly intervals from the SJRWMD water quality monitoring program. There are no continuous water quality data available in this area with the exception of DO data collected at station IRLB04, which was compared with model data in **Section 10.1**.

Model TN values at stations IRLB04 and IRLB04 in BRL (**Figure 106**) compare well with observed values (**Figure 110** and **Figure 111**). The RSME comparisons are 0.44 mg/L and 0.46 mg/L, which are 14% and 17% of the observed ranges of values, respectively.

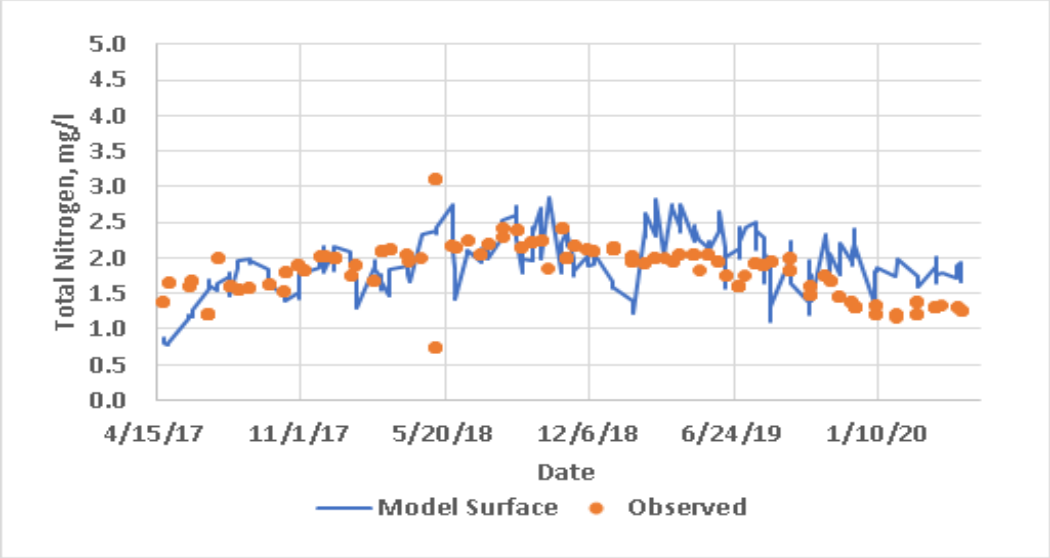

Figure 110. Comparison of model and observed total TN values at station IRLB04

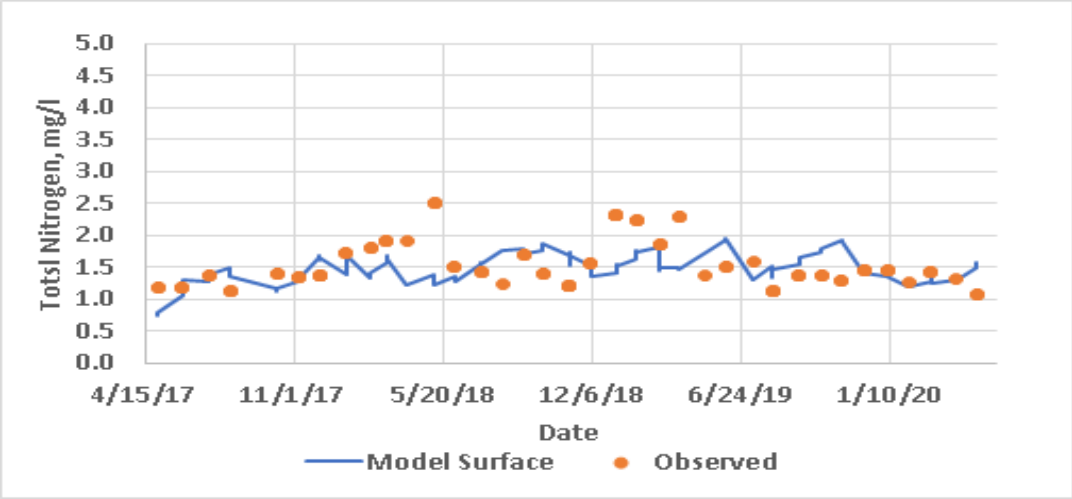

Figure 111. Comparison of model and observed total TN values at station IRLB06

10.4 TP Comparisons

Companions of model and observed TP values are shown in **Figure 112** and **Figure 113**. Model values are higher than observed values for most of the time series comparisons. However, the predicted values are well within an order of magnitude and overlap with measures during the 3-year model run values for a period in 2018. Further model refinement is expected to close the gap between model and observations when the SWIL watershed model providing more detail on phosphorus species is completed.

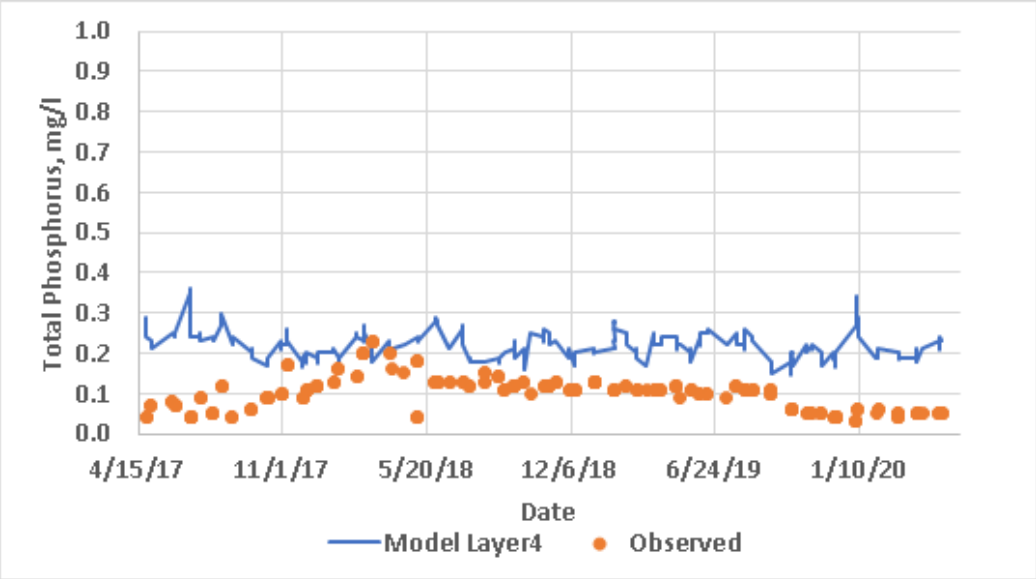

Figure 112. Comparison of model and observed TP values at station IRLB04

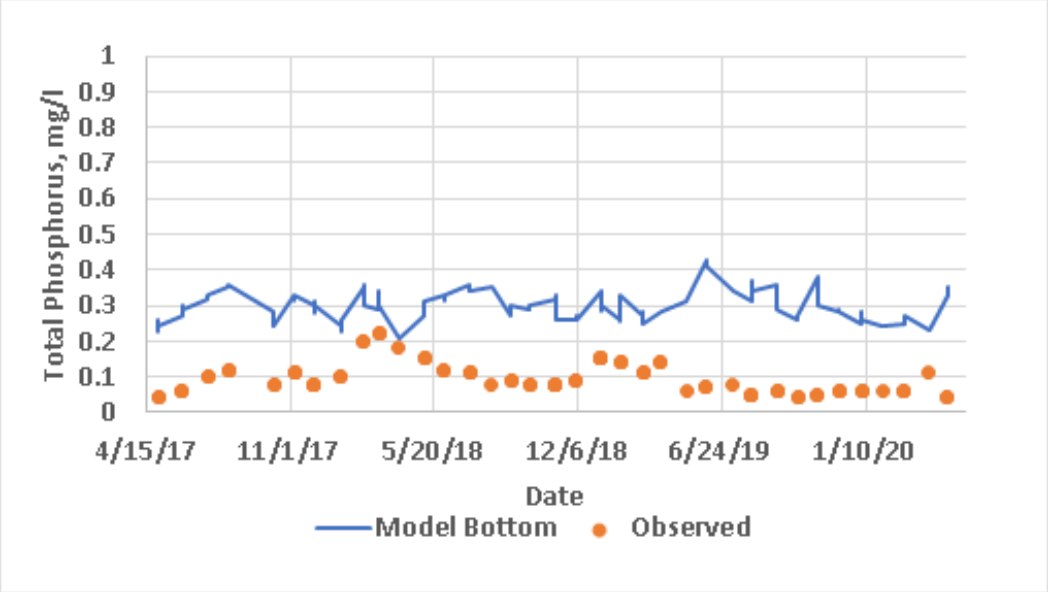

Figure 113. . Comparison of model and observed TP values at station IRLB06

10.5 Summary of Water Quality Model to Observation Comparisons

Table 16 summarizes the comparisons between model data and observations for major water quality constituents calculated by the EFDC/HEM3D model. Predicted water column concentrations of major water quality constituents agree remarkably well with observed values given the limitations of both the observed data and watershed loadings into the model. DO, chlorophyll, and TN predictions are comparable to predictions proved by EFDC in other model applications to Florida and other estuaries. Predicted TP values are only considered slightly high in terms of absolute values and well within an order of magnitude in terms of predictions that are on the order of a fraction of 1 mg/L. Further refinement of all predictions are expected with the application of the updates SWIL model now under development. The water quality model

permeance is considered appliable to testing of enhanced inflow cases described in the following sections of this report.

Table 16. Summary of model to observation comparisons for major water quality constitutions

Location/Parameter	RSME	RSME/Range
SBLOBO DO	2.11 mg/L	14%
VBLOBO DO	1.81 mg/L	13%
IRLB04 DO	2.12 mg/L	16%
SBLOBO Chlorophyll	2.39 µg/L	10%
VBLOBO Chlorophyll	3.83 µg/l	12%
IRLB04 TN	0.46 mg/L	14%
IRLB06 TN	0.44 mg/L	17%
IRLB04 TP	0.12 mg/L	54%
IRLB06 TP	0.11 mg/L	50%

11 Model Run Definitions

Table 17 lists the model runs cases that were used to assess the potential benefits of prescribed enhanced inflows to BRL though the west end of the Port Canaveral basin. **Figure 114** shows the location on the EFDC model grid cell where inflows were specified. As listed in **Table 17**, five model cases were run beginning with the exiting condition in which no additional inflows were sets followed by progressive inflows of 1 m^3/sec, 2.5 m^3/sec, 5 m^3/sec, and 10 m^3/sec. In this progression, an inflow of 1 m^3/sec approximates the potential prescribed inflow in a full scale pilot project that may be conducted in the near future. For each model case, the dispersal of an assigned tracer concentration within BRL was tracked though a 3-year model run along with a section of water quality constituents. The tracer study was applied rather than an “age of water” analysis to help define the total regional extent of potential influence of hypothetical inflows though the sub-basins of the IRL.

Table 17. Summary of model test cases

Model Case	Specified Inflow	Model run duration
Case 0	No additional inflow	3 years
Case 1	1 m^3/sec	3 years
Case 2	2.5 m^3/sec	3 years
Case 3	5 m^3/sec	3 years
Case 4	10 m^3/sec	3 years

Figure 114. Location of model prescribed inflows to BRL

12 Tracer, Salinity, and Water Temperature Model Results

12.1 Tracer Study

Tracer study model runs were designed to indicate the potential dispersal of tagged water particles under existing and enhanced inflow cases and provide a guide to the spatial extent of water quality impacts under potential enhanced inflow cases. The five model test cases investigated are listed in **Table 17**. In each case, 100 mg/L of tracer was assigned to each of the model cells in the BRL. Under the existing case without a prescribed pumped inflow from Port Canaveral, model results show that BRL is poorly flushed and likely has a long residence time with respect to exchange of water with other compartments of the IRL. **Figure 115** provides a regional view of the IRL showing high concentrations of tracer in the BRL. **Figure 116** provides details of tracer concentration in the BRL and indicates exchanges of water across the Barge Canal to the west of Port Canaveral and movement to the south end of Merritt Island and into the central IRL basin. Concentrations remain particularly high in the north compartments of the BRL, remaining at 80% or more of the original concentration the start of the model run.

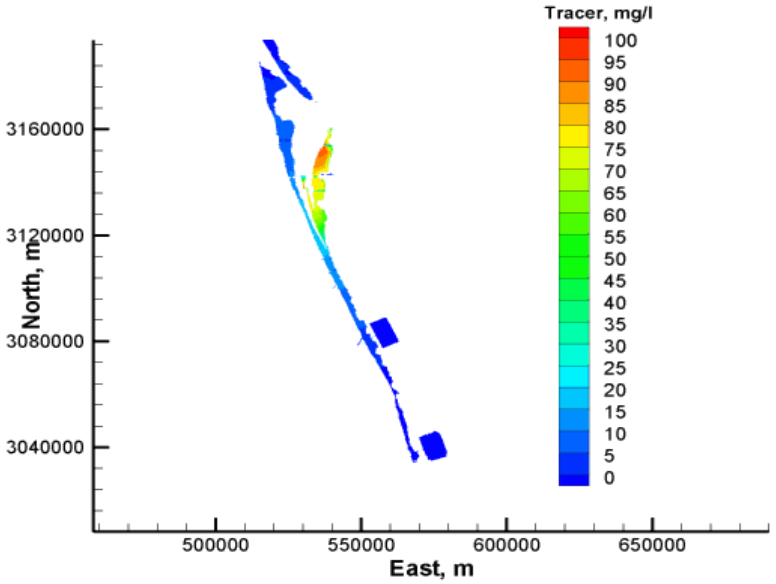

Figure 115. Tracer concentrations after 500 days of simulation under Case 0

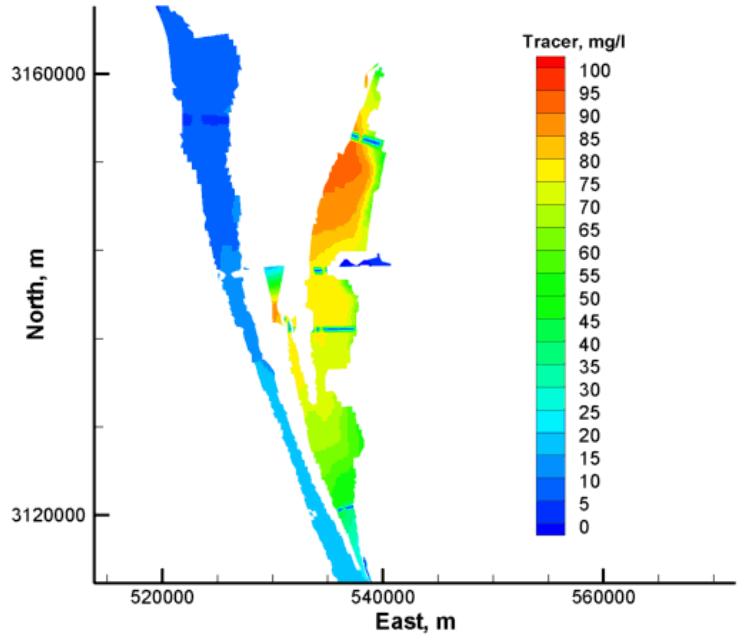

Figure 116. Details of tracer concentrations after 500 days of simulation under Case 0

Figure 117 compares tracer concentration at 100 days and 235 days into the model run under the existing Case 0. showing that the tracer concentration can be reduced in the BRL by lowering seasonally lower sea levels and increased by seasonally rising sea level in the coastal ocean that can reverse outflows from the BRL to inflows. This cycle repeated three times during the three-year model run in reaction to sea level changes in the coastal ocean forced by variations in Gulf Stream flow (Zarillo et al., 2021; Ezer et al., 2013).

The relatively low rate of 1 m^3/sec inflow assigned to Case 1 was able to mitigate the higher concentration in the BRL at day 235 under Case 0 as shown in **Figure 118**. A comparison among all four model cases is shown in **Figure 119**. Since the differences among the enhanced flow

cases are not easily resolved in the color codes plots, a comparison among the cases at numerical monitoring station BR17 is presented (**Figure 120**), which is near the center of the BRL to south of the inflow point. Here, the differences among the five model cases are resolvable in data from the surface layer of the model. A full graphic digital archive of model tracer study results is maintained and can be bound into a digital archive for further study. The plot demonstrates the decline of tracer concentration with higher inflow rates among the text cases. It is notable that a steady decline does not occur among the case results indicating changing and reversing flows in the BRL linked to changing coastal sea levels. Tracer concentration at BR17 under Case 0, having no prescribed inflow, does not undergo a significant decline and over on portion of the run period increase slightly above the initial concentration.

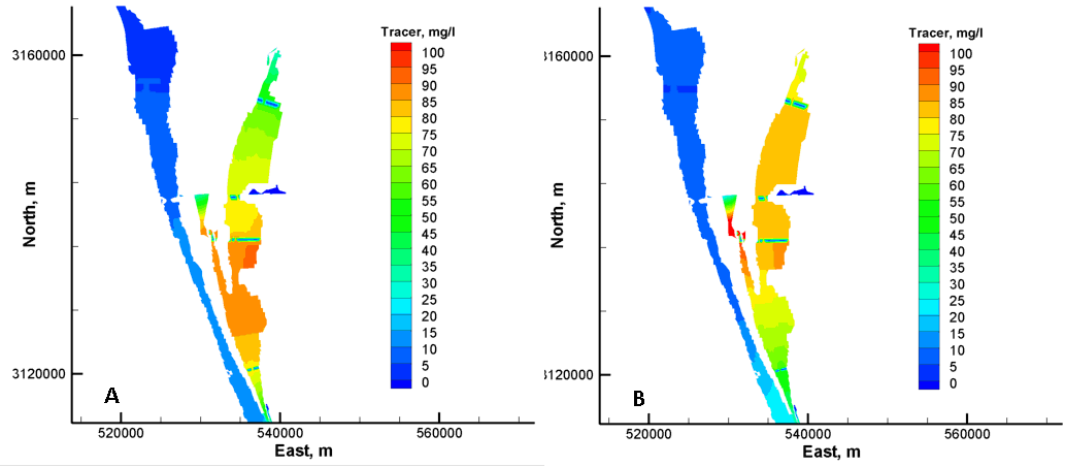

Figure 117. Comparison of tracer concentration at 100 days (A) and 235 days (B) into the 3-year model run

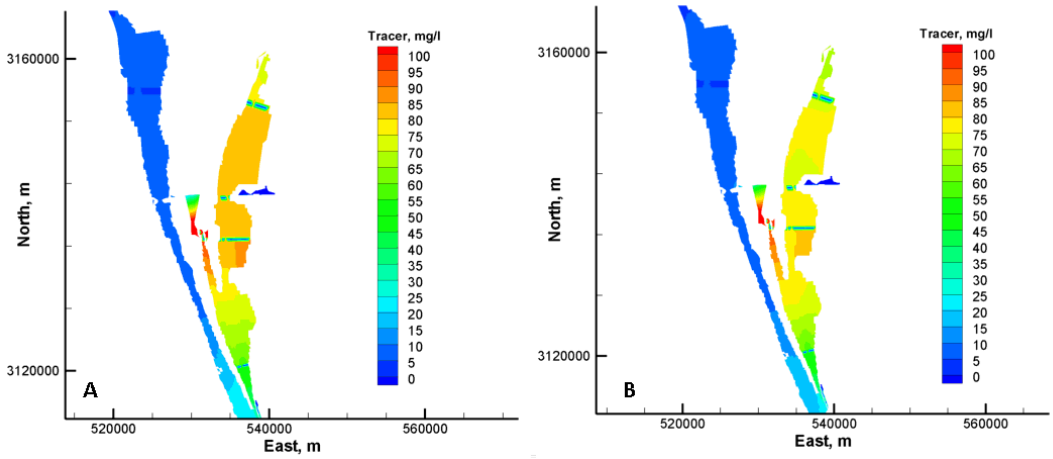

Figure 118. Comparison of tracer concentration at 235 days under Case 0 (A) and Case 1 (B)

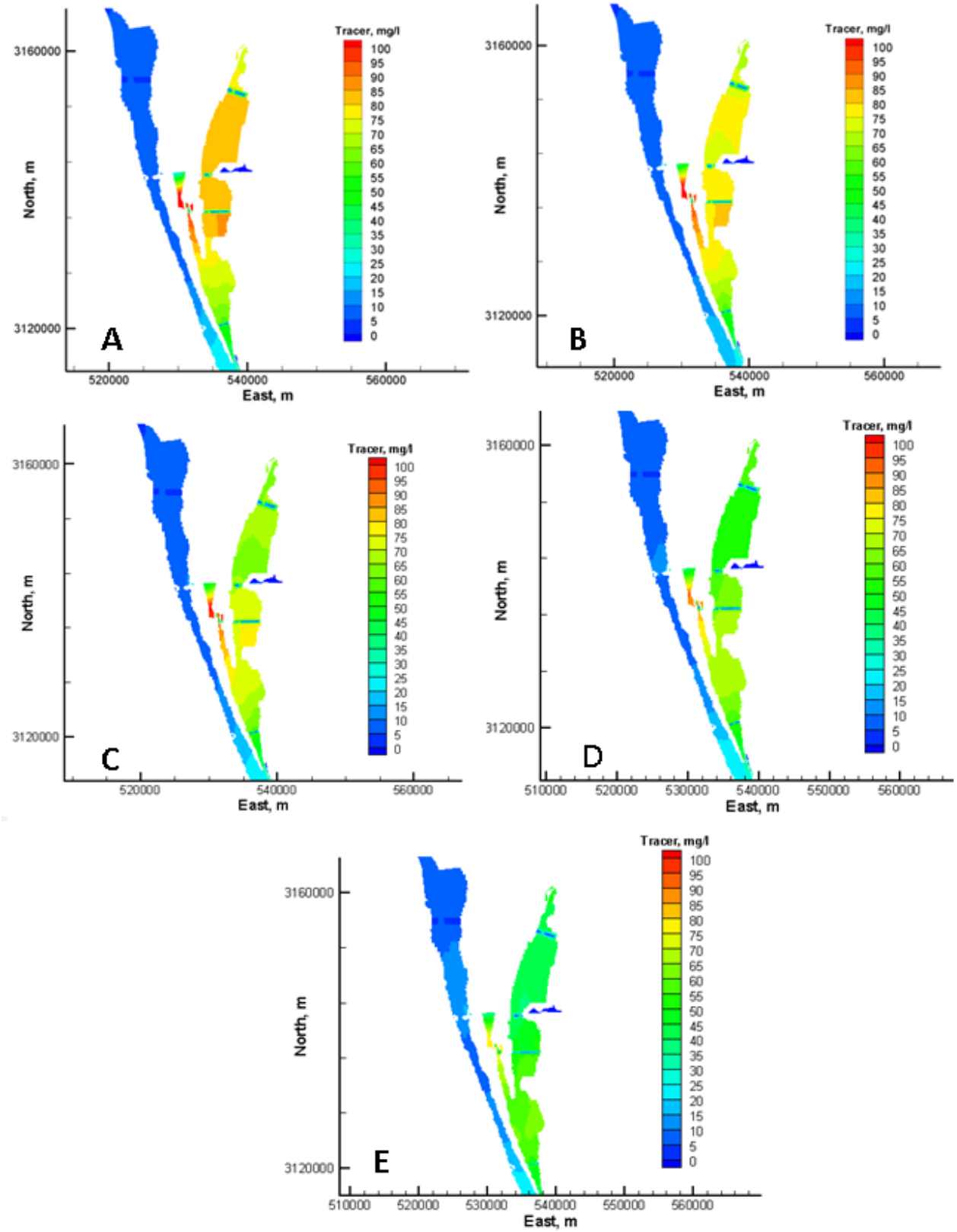

Figure 119. Comparison of tracer concentration at 235 days under model Case 0 (A), Case 1 (B), Case 2 (C), Case 3 (D), and Case 4 (E)

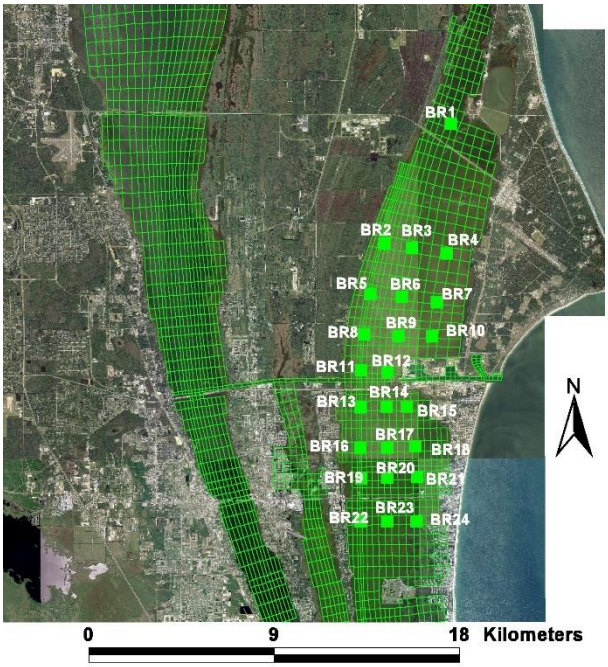

Figure 120. Location of 24 numerical monitoring stations set up in the BRL to capture output of tracer concentration data along with predicted salinity and temperature values over the 3-year model run

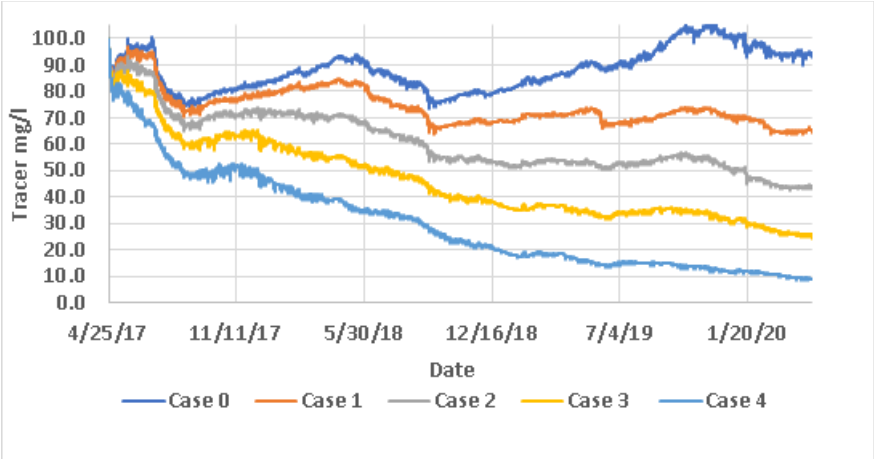

Figure 121. Comparison of tracer concentrations at numerical monitoring station BR17 under the 5 model cases over the 3-year model run

12.2 Salinity

The influence on salinity on the BRL under hypothetical pumping scenarios was presented in the 2020 Phase 1 report for this project. However, impact on the salinity regime under the five cases in enhanced inflow considered under Phase 2 are briefly reviewed here. A set of model animation files were generated from the EFDC model output files for each case and a selection of plots and extracted from the animations and time series are shown in the figures that follow.

Figure 122 compares predicted surface salinity after 1-year of simulation for each of the five cases. As the hypothetical inflows progress from 1 m^3/sec to 10 m^3/sec, a detectible increase in

surface salinity is seen in BRL along with an increased predicted in the Sykes Creek area situated between the BRL and IRL basin to the west. In **Figure 122**, panels A through E represent the progression of the model Cases 0 (no enhanced inflow) through Case 4 (10 m^3/sec inflow). Higher salinity in Sykes Creek results from the net circulation system described from the ADCP, discussed earlier in this report.

Figure 123 and **Figure 124** show the progression of predicted surface salinity at monitoring stations BR6 to the north of the inflow location and station BR17 south of the inflow point. Both stations record increases in surface salinity produced by each of the enhanced inflow cases. Model results are similar to those described in the Phase 1 report. Larger hypothetical inflows of ocean water produced larger increases in salinity. Differences in salinity compared to the existing Case 1 varied through the 3-year model run and ranged from minimal increases to up to a range of 10 to 15 PSU for under the largest pumping rate of 10 m^3/sec.

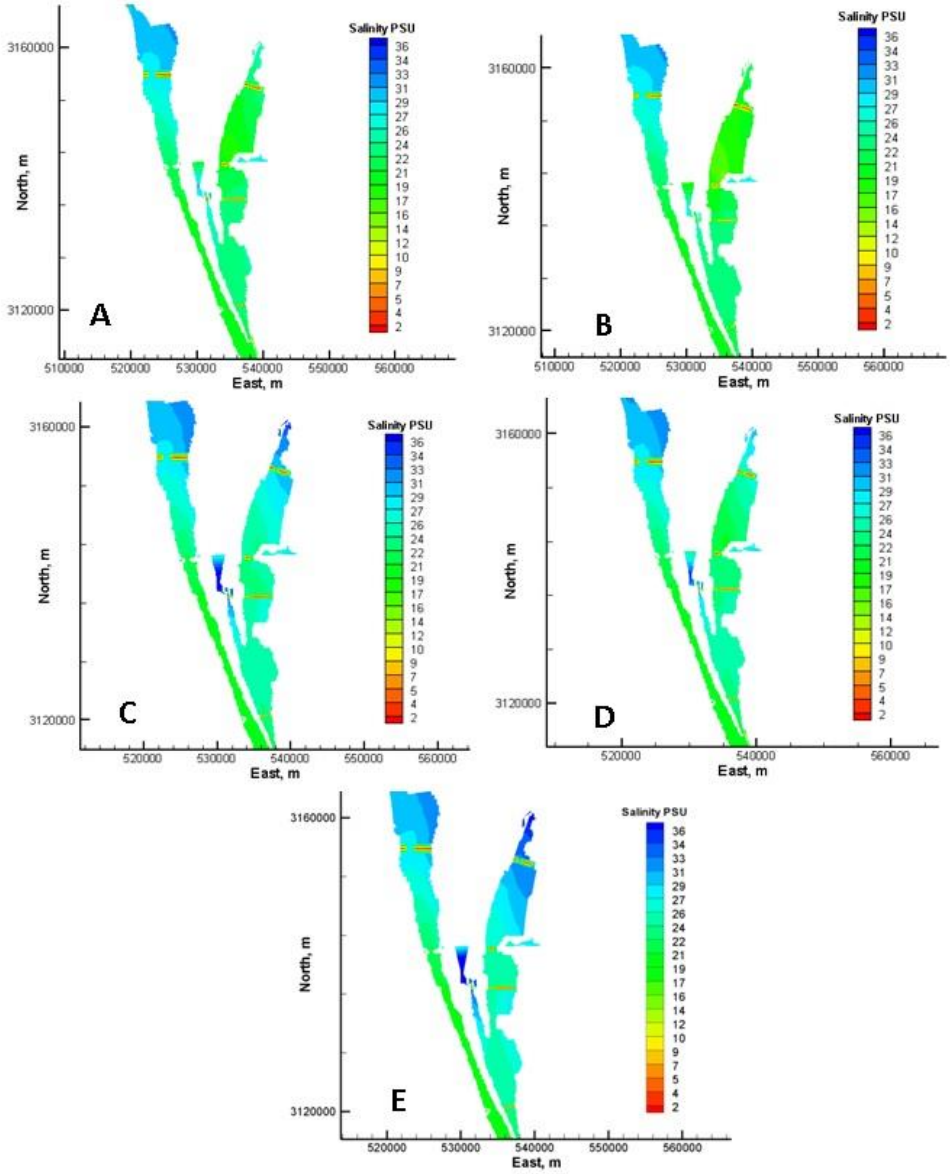

Figure 122. Comparison of predicted net change in surface salinity after 365 days for Case 0 (A), Case 1 (B), Case 2 (C), Case 3 (D), and Case 4 (E)

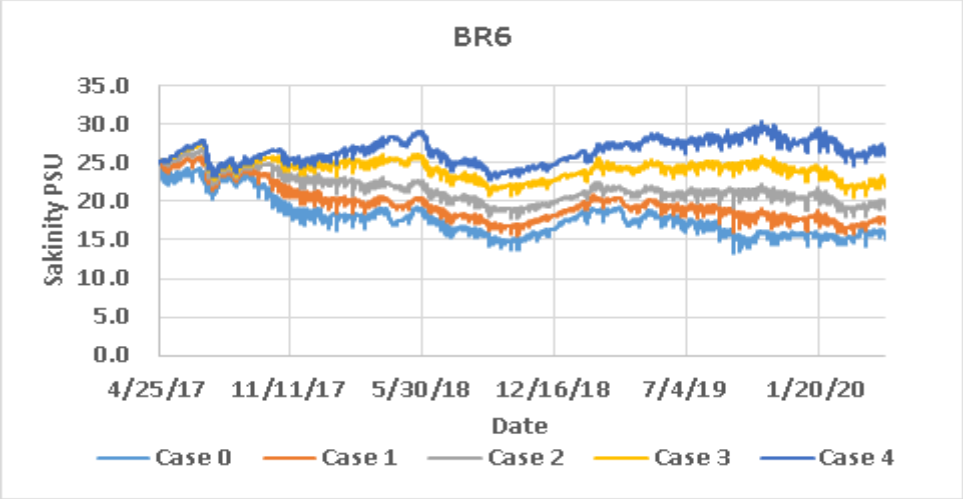

Figure 123. Comparison of surface salinity at numerical monitoring station BR6 under the 5 model cases over the 3-year model run

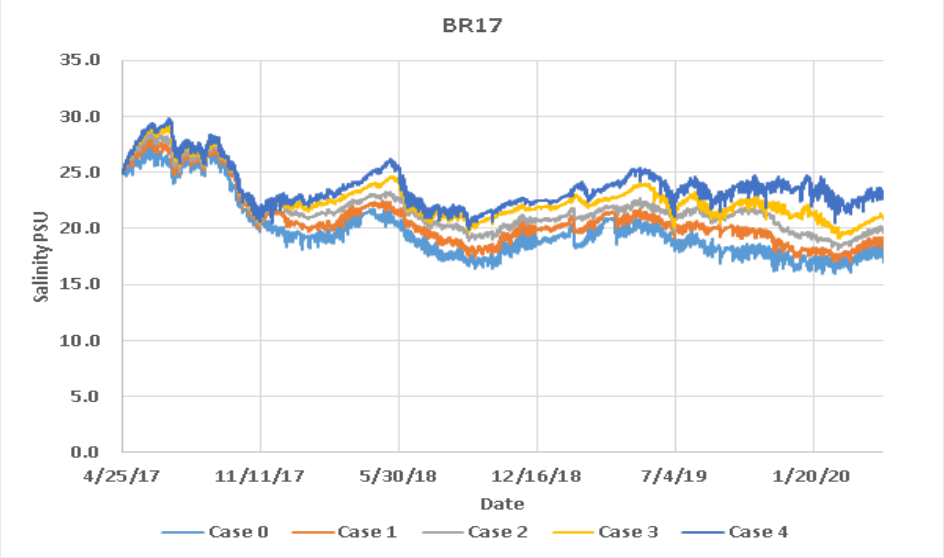

Figure 124. Comparison of surface salinity at numerical monitoring station BR14 under the 5 model cases over the 3-year model run

12.3 Water Temperature

Predicted surface water temperature at 365 days into the 3-year model run for each model case is shown in **Figure 125**. Water temperature pattern is similar among the cases. However, the influence of water temperatures from imported coastal ocean water is visibly detectable in Case 4 that specified a pump rate of 10 m^3/sec. (**Figure 125D**). **Figure 126** and **Figure 127** compare the time series of surface water temperature among the model cases at numerical monitoring station BR6 to the north of the inflow point and at station BR17 to the south of the inflow (**Figure 120**). Each plot also shows the net difference between Case 0, having no enhanced flow specified and Case 4 assigned an inflow of 10 m^3/sec. Under Case 4, the influence of seawater temperatures pumped into the BRL from Port Canaveral ranges from a near zero impact to temperature decreases on the order of 1 to 5 °C. However, at times when the ocean water temperatures are higher, the net difference is an increase in BRL water temperature compared to

Case 0. The average predicted difference between Case 0 and Case 4 is a surface water temperature decrease of -0.88 °C. and -1.27 °C. at stations BR6 and BR17. The comparison among the other cases also indicated a net decrease in water temperature. The difference is about -0.1 °C. under Case 1, which specifies an inflow rate of 1 m^3/sec.

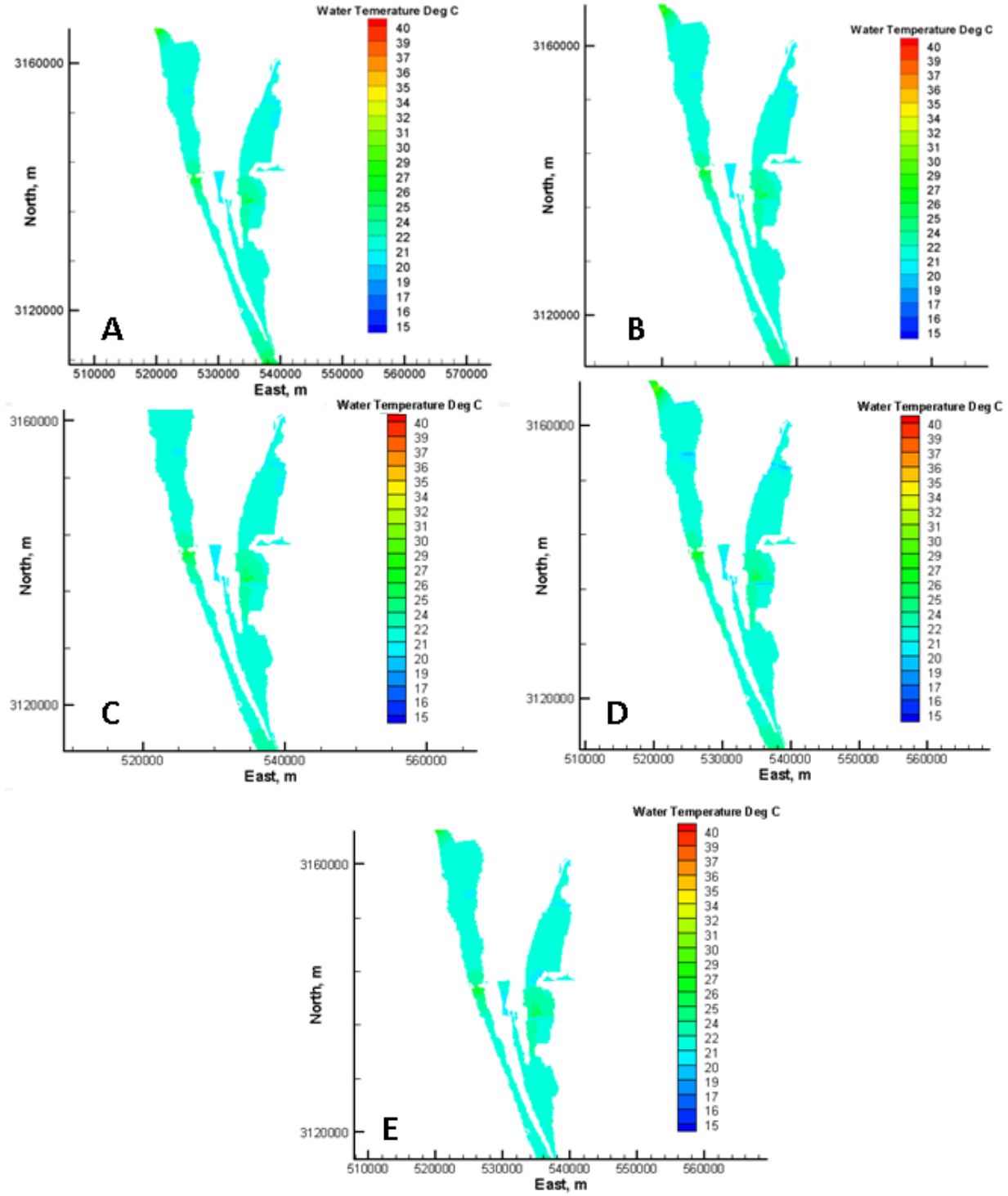

Figure 125. Comparison of predicted net change in surface water temperature after 365 days for Case 0 (A), Case 1 (B), Case 2 (C), Case 3 (D), and Case 4 (E)

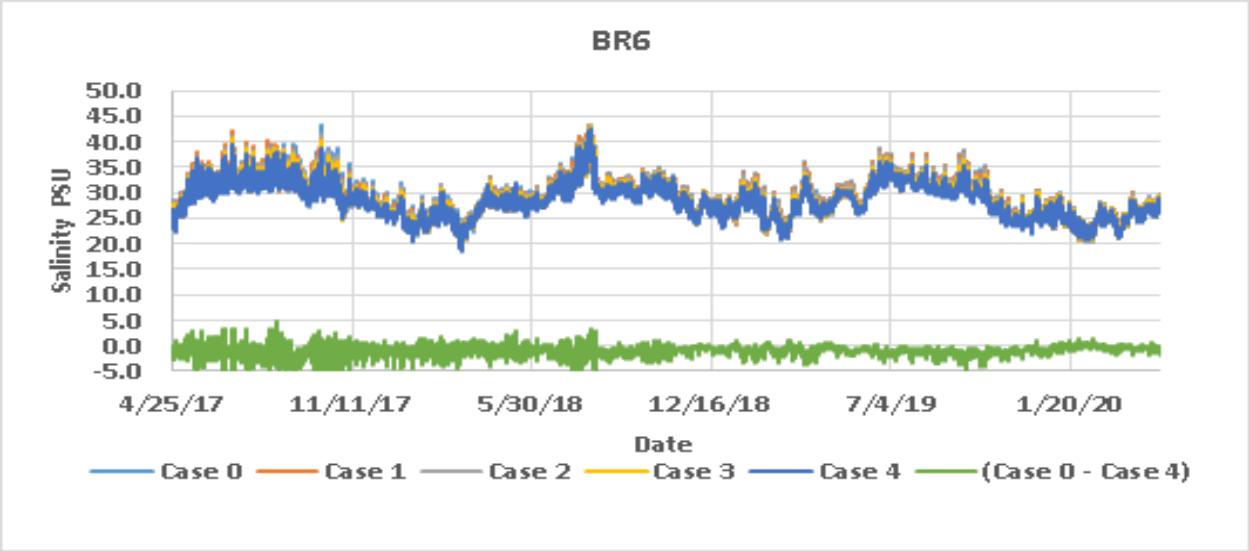

Figure 126. Comparison of surface water temperature at numerical monitoring station BR6 under the 5 model cases over the 3-year model run, showing the predicted difference between Case 0 and Case 4

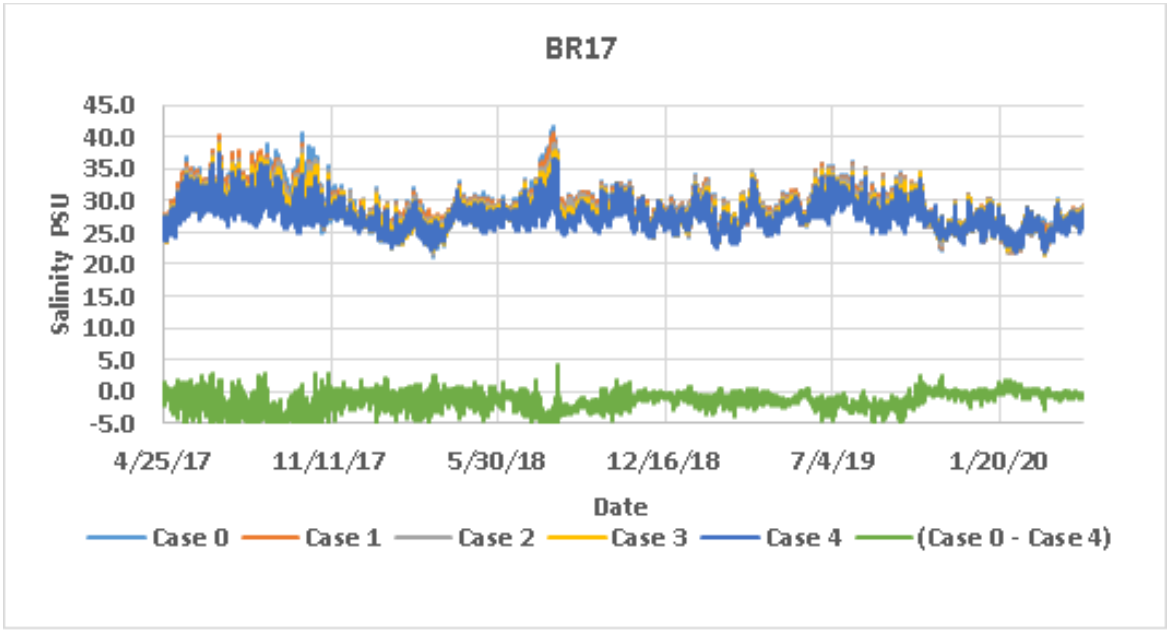

Figure 127. Comparison of surface water temperature at numerical monitoring station BR17 under the 5 model cases over the 3-year model run

13 Water Quality Model Results

13.1 Introduction

Water quality model results are presented in a series of plots that provide a visual perspective on the difference between the existing conditions in BRL and predicted water quality conditions based on cases of increasing inflows of ocean water pumped from Port Canaveral (**Table 17**).

The water quality constituent concentrations assigned to hypothetical pumped inflows to the BRL from Port Canaveral were set to values listed in the most recent water quality monitoring report by Environmental Research and Design, Inc. as part of the ongoing monthly monitoring program (Harper 2021). The data listed in the report are mostly from April 2021. Whereas all forms of nitrogen, phosphorous, and other parameters assimilated by the EFDC/HEM3D model boundaries are not reported, concentrations of major constituents such as DO, TN, TP, ammonium, and nitrate + nitrite are adequate for approximating the overall water quality of Port water. Further, spatial variation of water quality constituents is reported from six stations within the confines of the Port, including a station near the west end of Port Canaveral near the locks. The monitoring report indicates good water quality as evidenced by high values of DO, low values of chlorophyll, very lows values of TN, and moderate to low values of TP.

Water quality model results are reported in four subsections including DO, TN, TP, and total chlorophyll. The DO, TN, and TP comparisons among the cases are presented in both global contour plots covering the BRL and selected time series at site-specific monitoring stations. Comparison among the cases for total chlorophyll concentrations are presented at selected numerical monitoring stations (**Figure 120**). The contour plots represent the predicted net change in water quality constituent concentrations with respect to the existing Case 0.

13.2 DO

Figure 128 shows the predicted mid-depth net change in DO concentration after two years of model simulation. An increase in DO values is predicted for all cases, but confined to the immediate inflow area under Case 1 and Case 2. Under the higher inflow rates of Case 3 and Case 4, the influence of more oxygenated coastal ocean water disperses to the northern most compartments of the BRL. A comparison of net DO change among all cases at numerical monitoring station BR6 is shown in **Figure 129**. The comparisons between Case 0 (no inflow) and Case 4 (10 m^3/sec) is shown for the surface layer of the model.

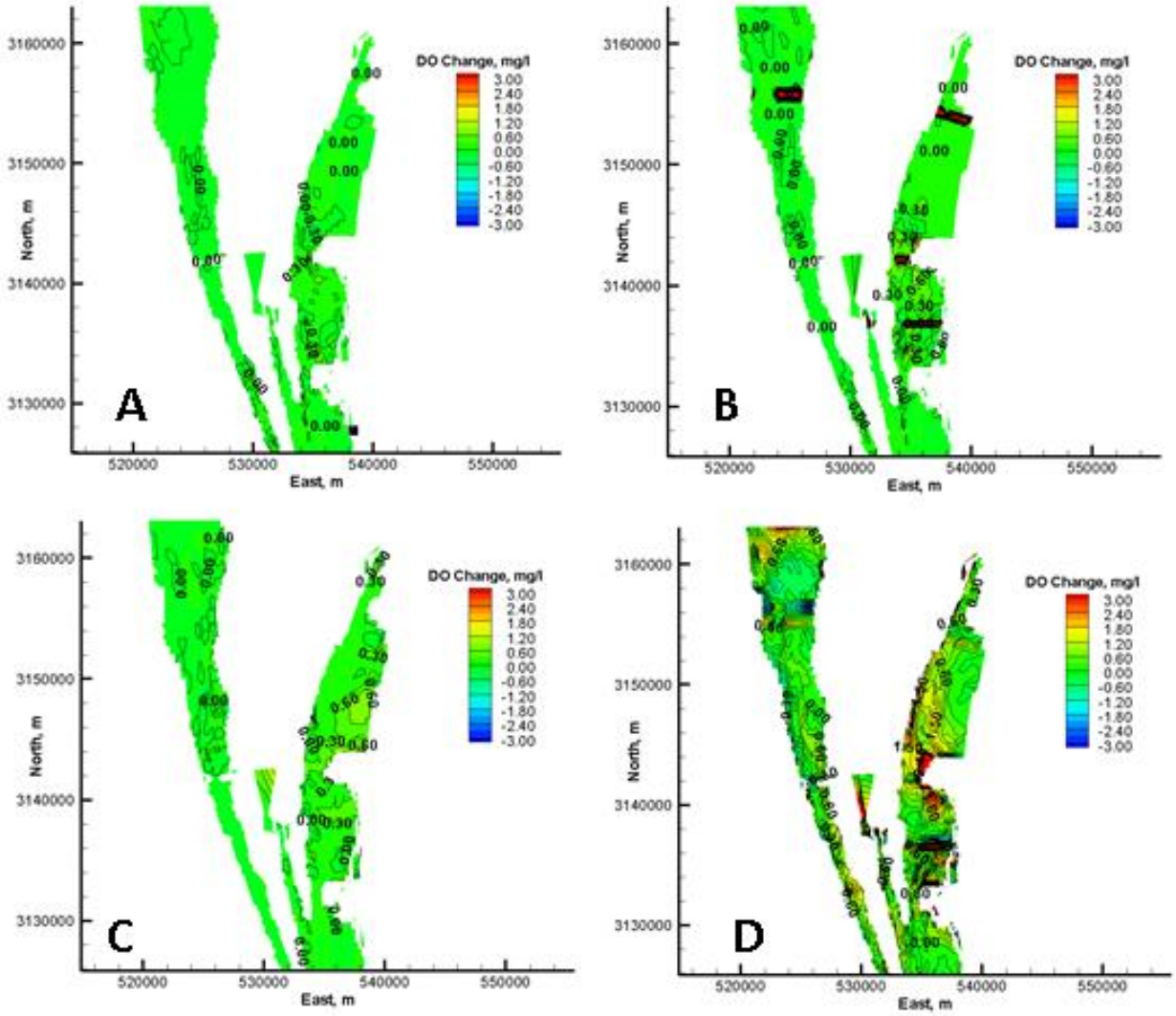

Figure 128. Comparison of predicted mid-depth net change in DO concentration after 730 days for Case 1 (A), Case 2 (B), Case 3 (C), and Case 4 (D)

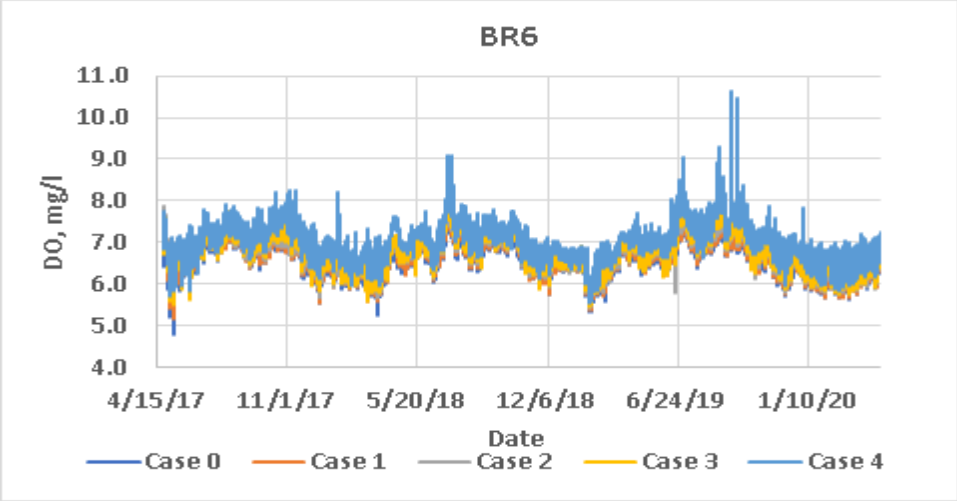

Figure 129. Comparison of predicted net change surface layer DO concentrations at numerical monitoring station BR6 located to the north of the inflow point

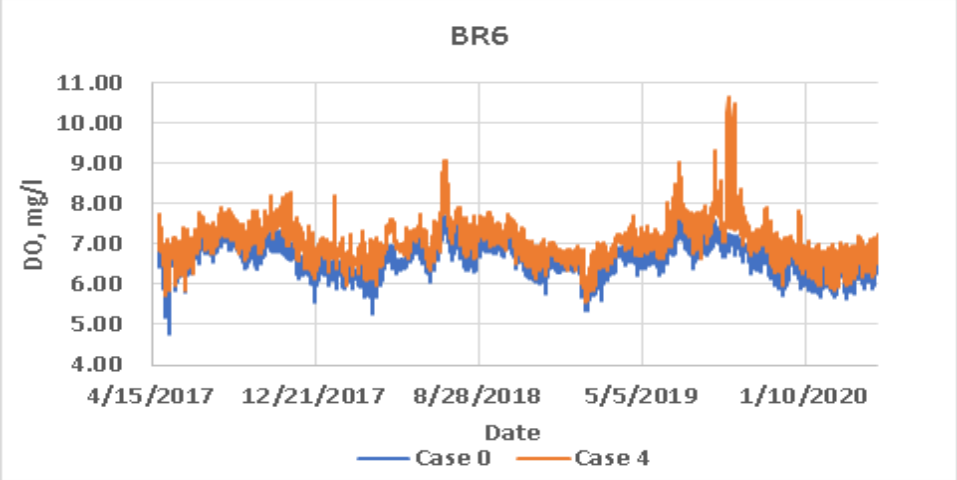

Figure 130. Comparison of Case 0 and Case 4 predicted net change in surface layer DO concentrations at numerical monitoring station BR6

Figure 131 compares predicted net change in DO concentrations in the model surface layer at numerical monitoring station BR16 south of the inflow point. Increasing DO concentrations corresponded with increasing flow rates. The comparison between Case 0 and Case 4 in **Figure 132** indicates a maximum increase in DO of of about 1 mg/L at this location for the highest inflow rate of 10 m^3/sec. The maximum predicted increase in DO values reached about 4 mg/L over the entire model run and occurred in the surface model layer under Case 4.

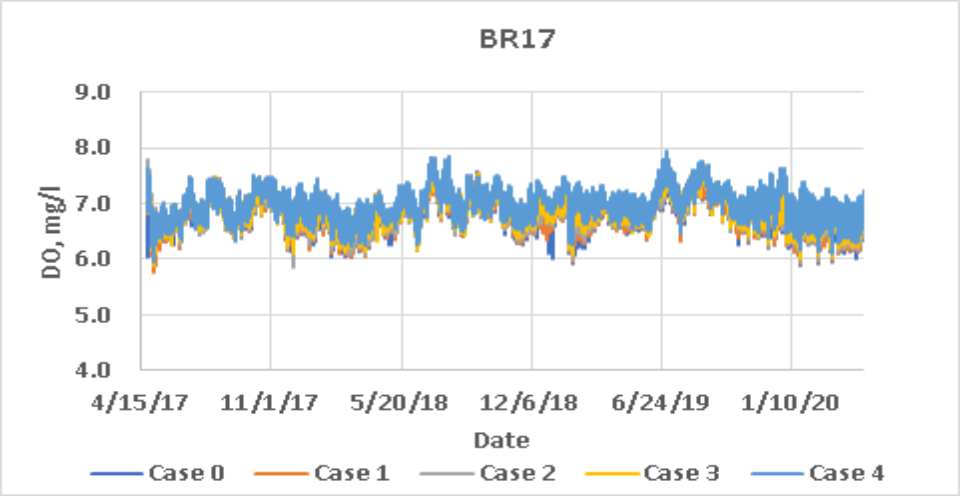

Figure 131. Comparison of predicted net change in surface layer DO concentrations at numerical monitoring station BR17 located to the south of the inflow point

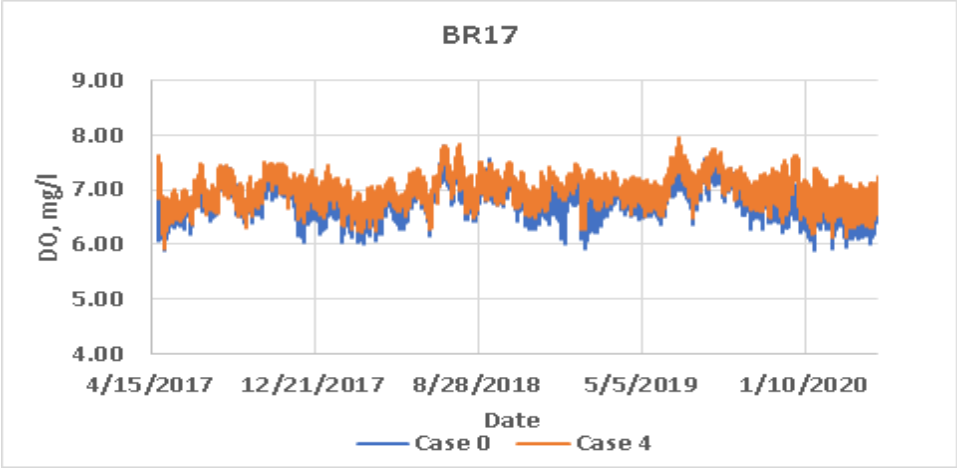

Figure 132. Comparison of Case 0 and Case 4 predicted net change in surface layer DO concentrations at numerical monitoring station BR6

13.3 TN

The reduction in TN concentrations was the most apparent of potential benefits of the inflow prescribed in the model runs. **Figure 133** shows the predicted mid-depth net change in TN concentrations under all four cases at two years into the model run. Reduction in TN concentration appears in all four cases and extends to the northernmost compartment of the BRL in all cases. The predicted net reduction TN concentration reached to more than 2.5 mg/L under Case 3 and Case 4 in the north compartments of the BRL. South of the inflow point, the net reduction of TN concentration values were on the order of 1 mg/L or less in all cases (**Figure 133**).

Figure 134 and **Figure 135** demonstrate the spatial variation of TN concentrations in the BRL. Model predictions at station BR6 well north of Port Canaveral and the inflow point show a clear reduction of TN concentration that reached a maximum of about 4 mg/L midway through the simulation. Predicted TN concentrations recorded at B23 in the southernmost row of numerical monitoring stations (**Figure 120**) reached a net difference of about 1 mg/L between minimum (Case 0) and maximum (Case 4) prescribe inflow rates.

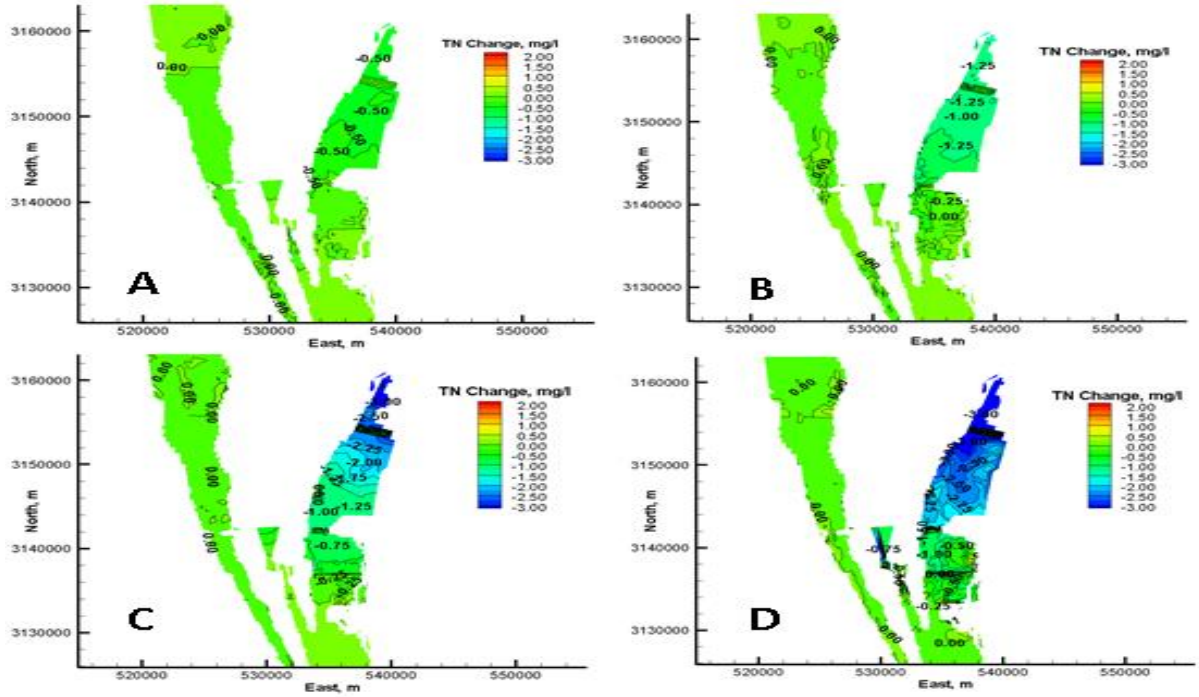

Figure 133. Comparison of predicted mid-depth net change in TN concentration after 730 days for Case 1 (A), Case 2 (B), Case 3 (C), and Case 4 (D)

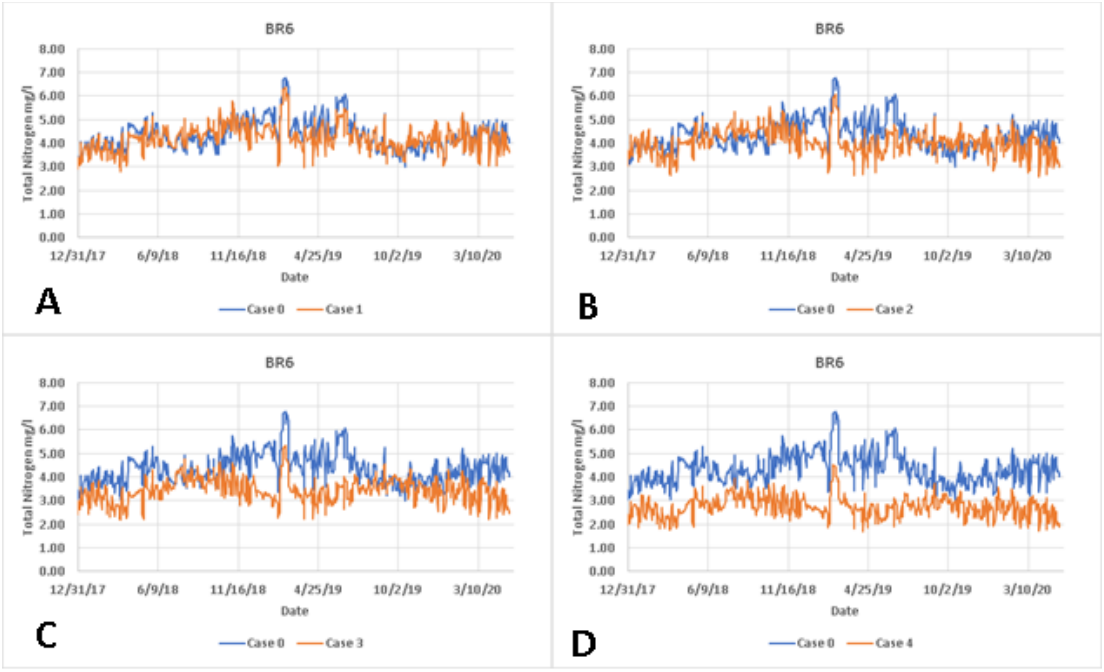

Figure 134. Comparison of predicted net change in surface layer TN concentrations for all cases at numerical monitoring station BR6 located to the north of the inflow point

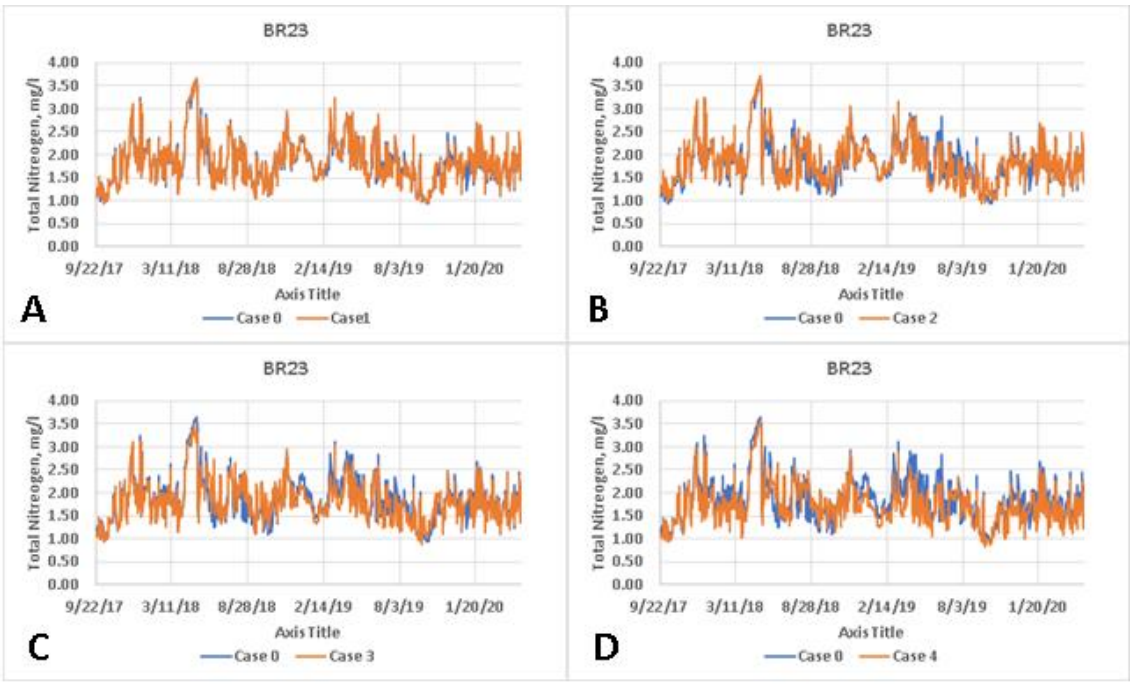

Figure 135. Comparison of predicted net change in surface layer TN concentrations for all cases at numerical monitoring station BR23

13.4 TP

Predicted net change in TP concentrations followed a similar pattern to those of TN. The largest reductions occurred in the north compartments of the BRL and tapered to a minimum south of the inflow location. Water column concentration of TP is generally lower than TN in the IRL and other estuaries. Thus, the absolute magnitude of predicted net reduction in the BRL relative to the inflow rates is lower. **Figure 136** shows the predicted net change in TP concentration two years into the model runs. Reduction in TP concentration begins to persist under Case 2 (2.5 m^3/sec inflow and increase as the inflow rates are increased under Case 3 and Case 4. For most of the model run period the measurable decrease in TP occurs from the inflow point and northward. This is consistent with the tracer analysis and analysis of flow direction from the ADCP data. Net circulation in the BRL can be northward for periods of time moving tracer and inflows to the north. This transport in the longer term is balanced by west transport through the Barge Canal and south transport through Sykes Creek as seen in the ADCP analysis (Section 4). The north directed net transport is balanced in the longer term by reversals in circulation to the south. This process is reflected the tracer results showing both increases and decreases in tracer concentration in the BRL as the overall tracer concentration decreased through the model runs.

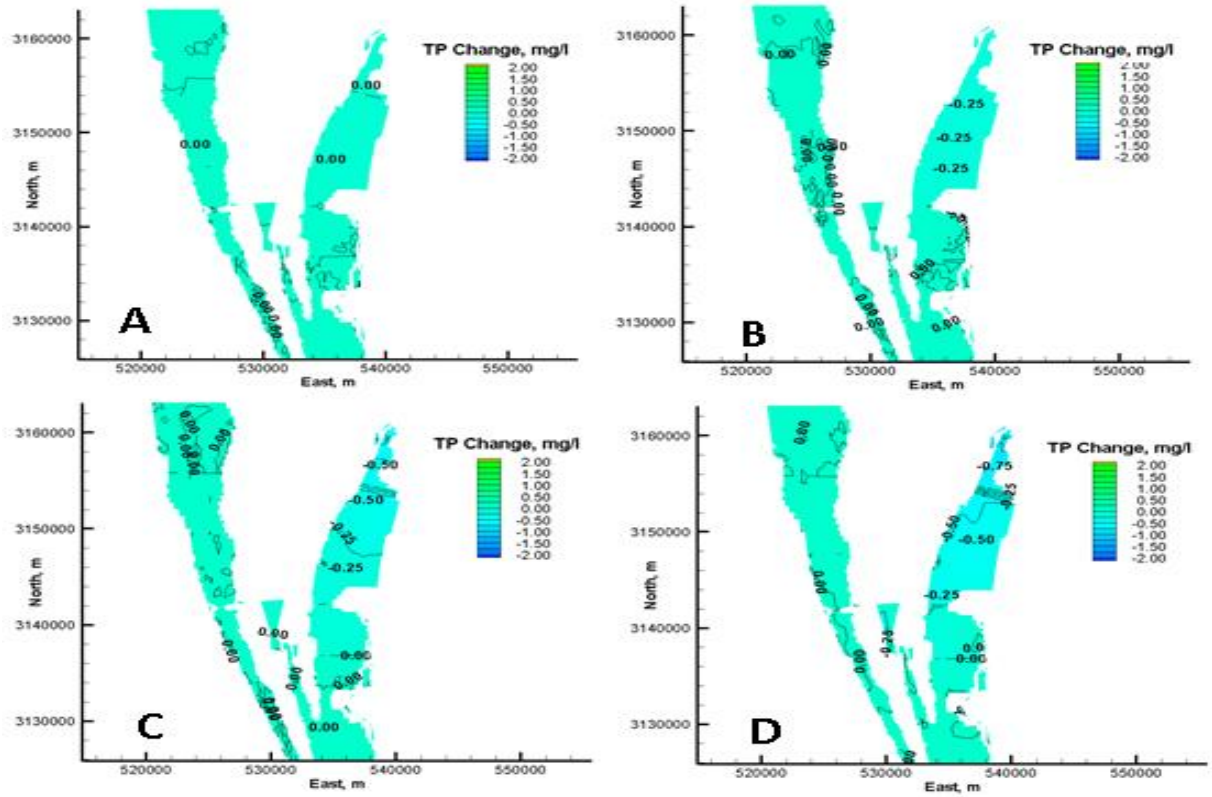

Figure 136. Comparison of predicted mid-depth net change in TP concentration after 730 days for Case 1 (A), Case 2 (B), Case 3 (C), and Case 4 (D)

Figure 137 and **Figure 138** compare predicted net TP concentration changes among the four inflow cases. The pattern is similar to that predicted for TN. The reduction in TP begins to appear under Case 2 and increases through Case 3 and Case 4. Predicted declines are larger north of the inflow point due to the circulation process explained in the previous section. Maximum predicted reduction in TP concentration under Case 3 and Case 4 range from about 0.5 to 0.74 mg/L.

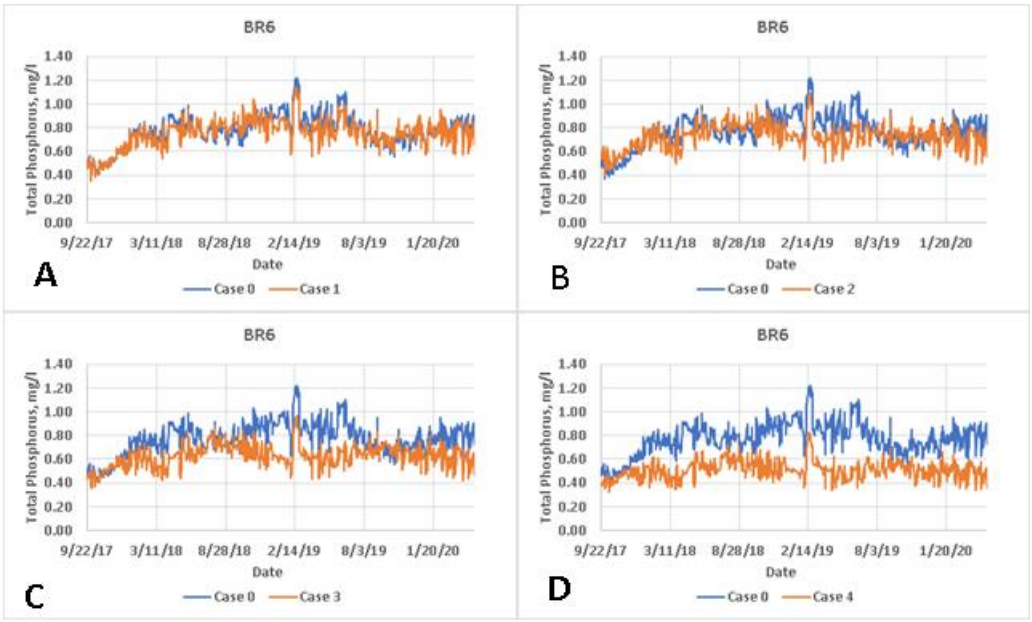

Figure 137. Comparison of predicted net change in surface layer TP concentrations for all cases at numerical monitoring station BR6 located to the north of the inflow point

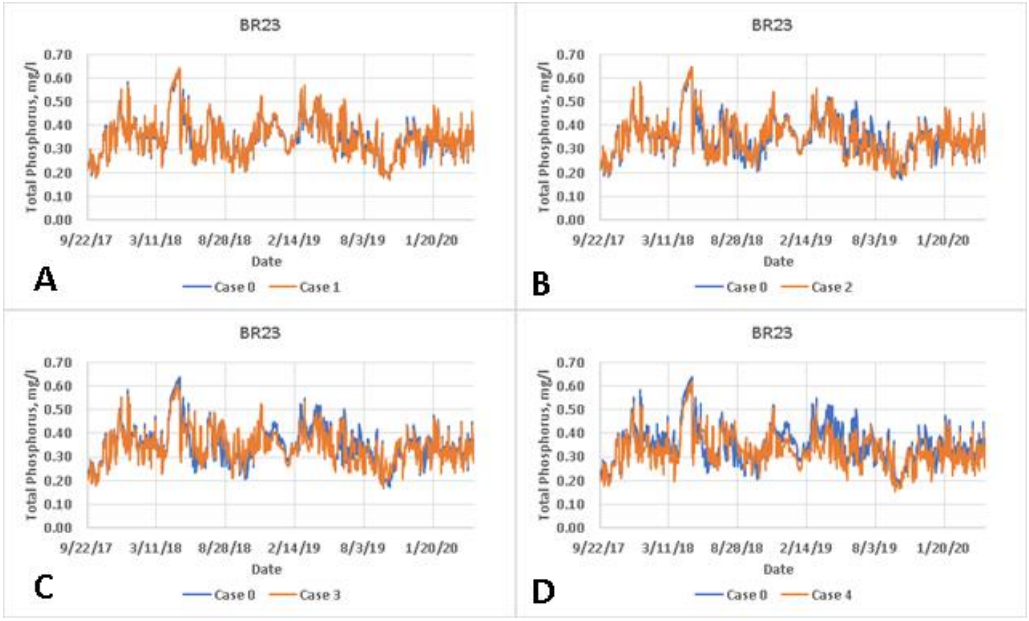

Figure 138. Comparison of predicted net change in surface layer TP concentrations for all cases at numerical monitoring station BR23

13.5 Chlorophyll

Chlorophyll concentrations can be used as a marker for conditions potentially leading to HABs. The ability of the EFDC/HEM3D water quality model to reproduce observed total chlorophyll concentrations with reasonable accuracy is documented under **Section 6**. Model results of chlorophyll concentration on the BRL can be used as a guide to the potential benefits of enhanced inflows to mitigate HABs. Predicted chlorophyl concentrations shown for selected stations

demonstrate the potential for inflows to reduce episodes of high chlorophyll concentrations that occurred in the model. A review of measured total chlorophyll data from the HBOI LOBO monitoring stations between Sebastian Inlet and Fort Pierce Inlet shows several events of higher concentrations that occur in the 2017 to 2020 period (see **Figure 108** and **Figure 109**). Short events of slightly elevated chlorophyll concentrations also appears in Case 0 model results, but were reduced in magnitude in cases including higher inflow rates. Total chlorophyll model concentrations obtained in the BRL area are similar to concentrations of chlorophyll reported quarterly by SJRWMD for the 2017 to 2020 time period ranging from about 2 to 14 mg/L. Further adjustment of watershed inputs to the EFDC/HEM3D will be required to optimize chlorophyll predictions for HAB simulations. This effort will also require more continuous and more accurate field measurements of chlorophyll components. However, model results thus far indicate that EFDC/HEM3D is capable of HAB simulations. An example of algal boom predictions using the EFDC model, Wu and Xu (2011) were able to reproduce trends of chlorophyll-a concentrations. However, errors were 45% to 98% relative to measured data. In ongoing work for IRL, we are able to achieve a match between model and measured total chlorophyll of 10% to 12% in an area that is influenced by river and canal inflows for which some water quality data are available.

Figure 139 presents model results for total chlorophyll at numerical monitoring station BR6 in the BRL (see **Figure 120**). Declines in chlorophyll become noticeable beginning with Case 2 inflows and continue through Case 4. Under conditions of Case 3 (5 m^3/sec inflow) and Case 4 (10 m^3/sec), higher chlorophyll concentrations through extended periods of time seen in the Case 0 and Case 1 model data are substantially reduced. The pattern of chlorophyll model results at numerical monitoring station BR17 (**Figure 140**) shows some reduction of peak concentration values beginning with Case 2 and substantial reductions in Case 3 and Case 4. The first chlorophyll concentration peak that occurs in all four cases corresponds with the passing of Hurricane Irma in September 2017.

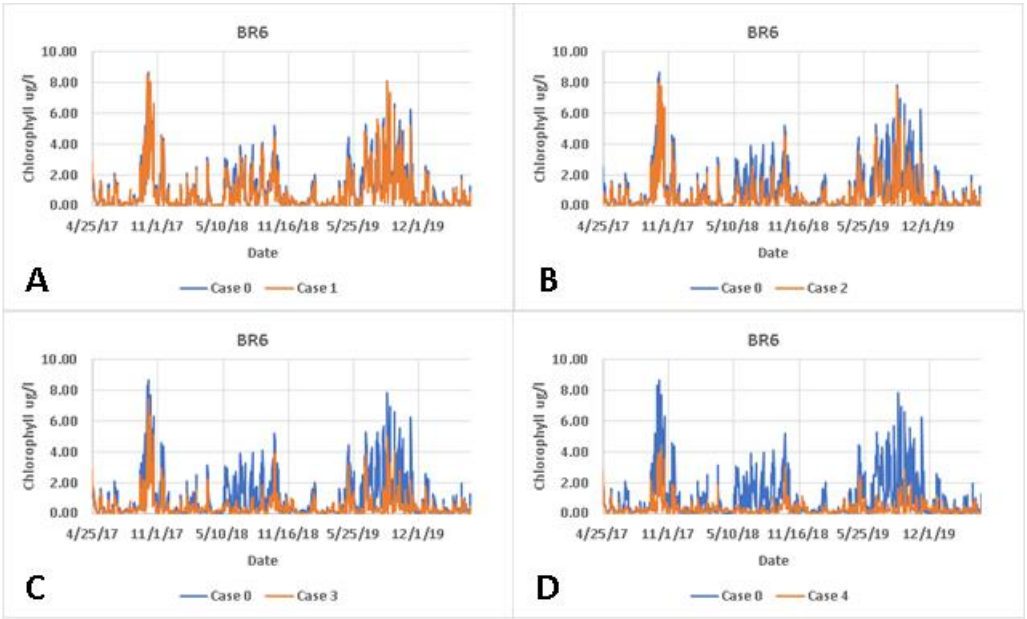

Figure 139. Model results for total chlorophyll at numerical monitoring station BR6 in BRL

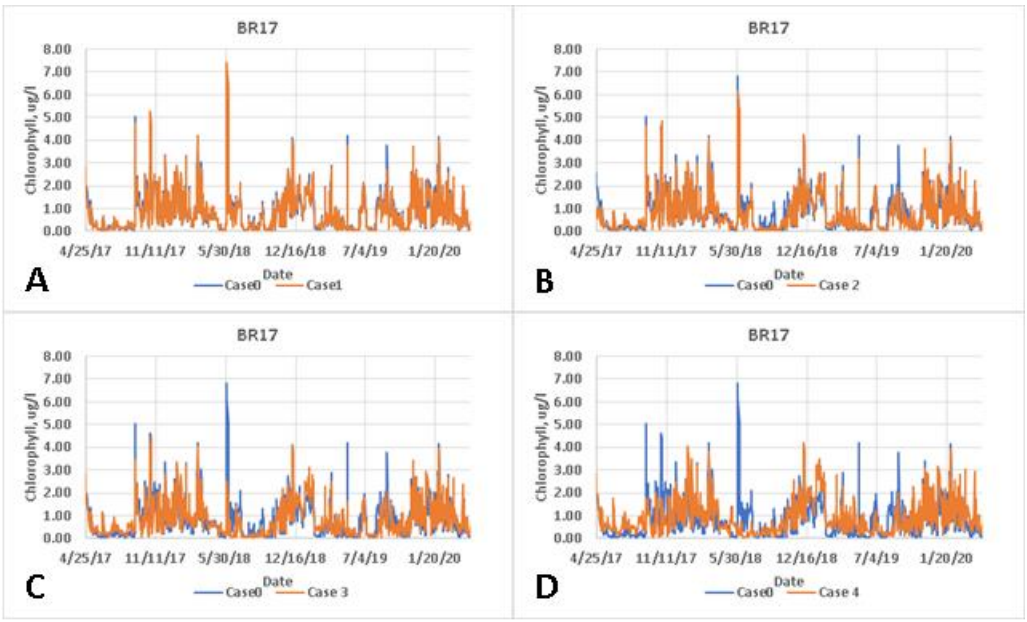

Figure 140. Chlorophyll model results at numerical monitoring station BR17

13.6 Potential for Distal Impacts on Water Quality

Concern has been expressed about the possibility of inflows to the BRL from Port Canaveral could impact water quality a distal location as far south as Sebastian Inlet. Model results show that changes in water quality reach Sykes Creek as seen in **Figure 133** and **Figure 136**. This is considered a positive impact since Sykes Creek is known for poor water quality and low DO values. Analysis of ADCP data in **Section 4** show a circulation pathway at times northward along the BRL and west across the Barge Canal, followed by southward flow into Sykes Creek. This net circulation carries the influence of inflows from Port Canaveral into Sykes Creek and potentially west into the IRL. This net circulation pattern at times reverses to a south directed flow in both the BRL and IRL. The driving force for this reversing circulation pattern is under investigation, but may be linked to rise and fall of coastal elves driven by Gulf Stream dynamics.

The results of the tracer analysis conducted are consistent with the ADCP analysis indicating reversals in flow direction that cause both declines and increases in tracer concentration over the three-year model period. This indicates some directional “sloshing” of the BRL and IRL water masses, both north and south, likely dependent on chances in coastal ocean sea levels and wind direction.

Given the flow dynamics of the BRL and IRL, a reasonable question is whether distal water quality can be impacted by the inflows. Thus far, no measurable difference in water quality constituent concentrations were found in the Sebastian Inlet area. **Figure 141** shows the predicted tracer concentration at the throat of Sebastian Inlet 60 km south of the inflow point. Minor peaks on the order of 10^{-3} mg/L occur early in the three-year model period. The first peak corresponds with the passing of Hurricane Irma in September 2017. Consistent with the near zero dispersion of tracer well to the south of the BRL, predicted TN and TP under Case 0 and Case 4 are nearly identical. **Figure 142** shows the predicted net change in TN (A) and TP (B) concentration at the throat section of Sebastian Inlet 60 km south of the BRL inflow point.

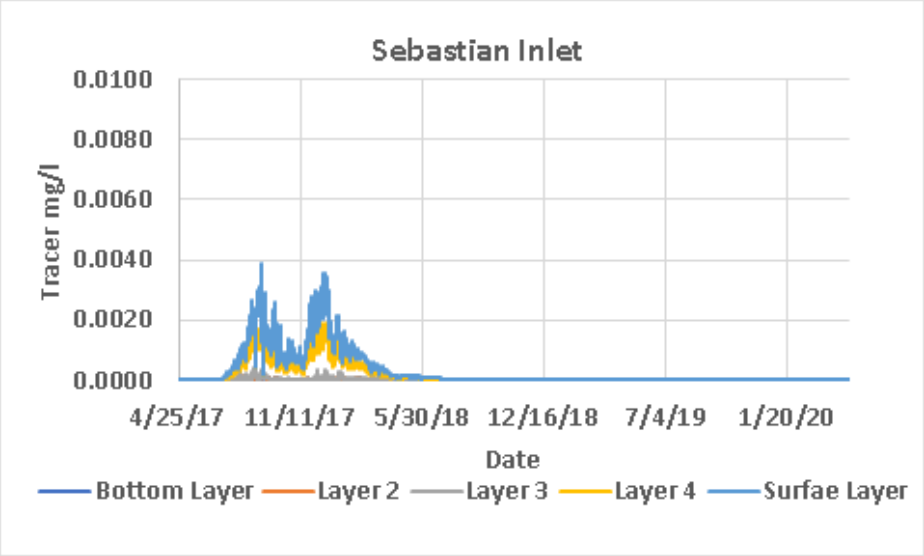

Figure 141. Predicted concentration of tracer within the throat of Sebastian Inlet under Case 4 with the first concentration peak corresponding with the occurrence of Hurricane Irma in September 2017

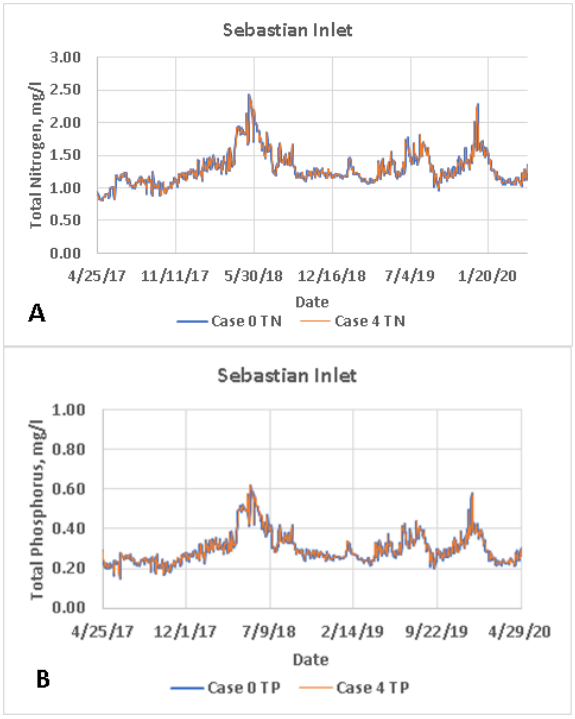

Figure 142. Predicted net change in TN (A) and TP (B) concentration a the throat section of Sebastian Inlet 60 km south of the BRL inflow point

14 Conclusions from Water Quality Model Predictions

Predictions of major water quality constituent concentrations indicate that the potential benefit of prescribed inflows to the BRL increases as the inflow rates are increased. Predicted concentrations of DO, TN, TP, and chlorophyll under inflow rates of 1 m^3/sec (Case 1), 2.5 m^3/sec (Case 2), 5 m^3/sec (Case 3), and 10 m^3/sec (Case 4) were compared with the base condition

(Case 0) of no additional inflows from the Port Canaveral. Potential benefits in terms of reduced concentration of TN and TP occur though all of the enhanced inflow cases, but most noticeable in Case 2, 3, and 4. Predicted improvements in water quality occur throughout the BRL, but are most apparent in the northern compartments of the basins as seen in **Figure 133** and **Figure 136**, which depict the net predicted reductions of TN and TP, respectively.

Predicted increased DO concentrations under the lower inflow rates of Case 1 and Case 2 reach a maximum of about 0.5 mg/L and are confined to the BRL area proximal to the inflow location. Under Case 3 and Case 4, DO concentrations increased by up to 4 mg/L at some locations and the area influenced by increased DO concentrations expanded to the north compartments of BRL.

The influence of inflows of sea water on chlorophyll includes reductions in concentrations throughout the three-year model run as seen at numerical monitoring station BR6, well north of the inflow point. Lower concentrations of chlorophyll are more persistent at higher inflows of Case 3 and Case 4, but still apparent under Case 2. Predicted impacts on chlorophyll also include “decapitation” of short-term spikes of higher chlorophyll concentrations, even as the predicted time series of lower chlorophyl concentrations under lower inflow rates remain similar.

Given the lower frequency reversing flow dynamics of the BRL and IRL, the potential for distal impacts on water quality exists. Thus far, inspection of model data indicates no significant difference in water quality constituent concentrations beyond the BRL basin, Sykes Creek, and compartment of the IRL west of the BRL.

15 Port Canaveral Coastal Processes Model

This work provides a numerical assessment of potential hydrodynamic and morphologic changes to the Cape Canaveral Port system in response to the incorporation of a pumping system within the conveyance channel. The intent of the proposed pumping system is to provide additional seawater exchange from the coastal Atlantic Ocean to IRL and BRL. Potential changes in current magnitude and direction were investigated, as well as predicted changes in morphology near the control structure. Additionally, the distance away from the proposed pumping system.

15.1 Numerical Model

The motivation of this numerical modeling study is to investigate the impact of a potential pumping system to support water quality and additional flushing to IRL and BRL. The CMS was selected as the numerical modeling suite to simulate waves, hydrodynamics, morphology, as well as the proposed outflow as a cell string. **Figure 143** schematizes the processes simulated by the CMS model suite and the information passed between the Wave and Flow modules.

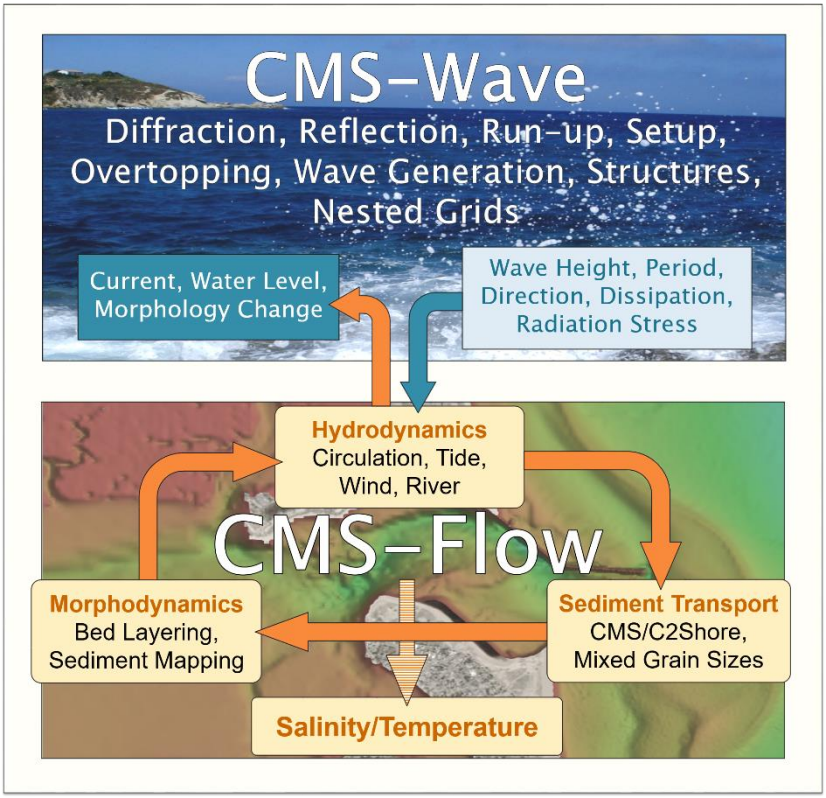

Figure 143. CMS components (USACE 2021)

The CMS is developed and maintained by the Coastal Inlets Research Program, which is a program within the Coastal and Hydraulics Laboratory of the Engineer Research and Development Center located in Vicksburg, Mississippi. This model is specifically designed for tidal inlets and the complex processes associated with them. The CMS model is run in a closely coupled approach with inline steering between the Wave and Flow modules. The model also employs an implicit numerical solution scheme and run on a desktop computer with multiple threads.

Numerical model configuration, including spatial and temporal coverage, was driven by a combination of model needs and available field data. The model spatial coverage was established to resolve both the processes in the coastal ocean and the flow through interior port facilities. This section describes the methodology for grid development and selection of boundary conditions.

15.1.1 Grid Configuration

Figure 144 provides the spatial coverage of both the flow and wave model grids in the Google Earth interface with the location of wave buoys (yellow) and boundary condition nodes (black diamonds).

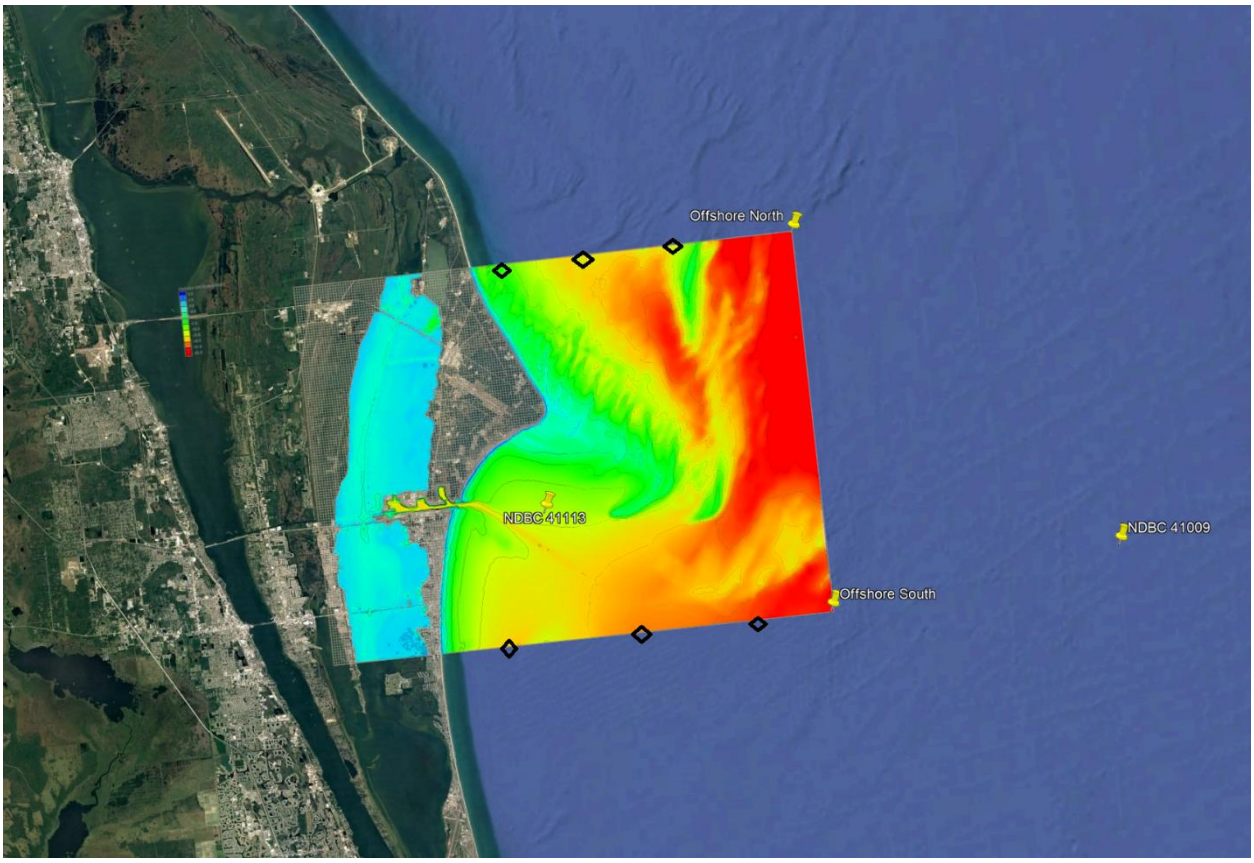

Figure 144. Numerical model spatial coverage with NDBC buoys

Warmer colors indicate deeper depths while cooler colors indicate shallower depths. The model grid includes the coastal ocean to a depth of 22 m in the offshore areas. Spatial coverage includes Cape Canaveral and BRL and provides representation of the NASA Parkway to the north, State Road 528/Bee Line causeway, and Wes Cocoa Beach and East Merritt Island Causeway.

The flow model grid uses a quadtree telescoping grid approach that optimizes grid refinement and model run time. Increased resolution was included in the Port areas including the conveyance channel to the control structures, all turning basins, and the inlet. **Figure 145** is a graphic of the CMS flow telescoping grid for the complete domain and detail of the port facility as an inset.

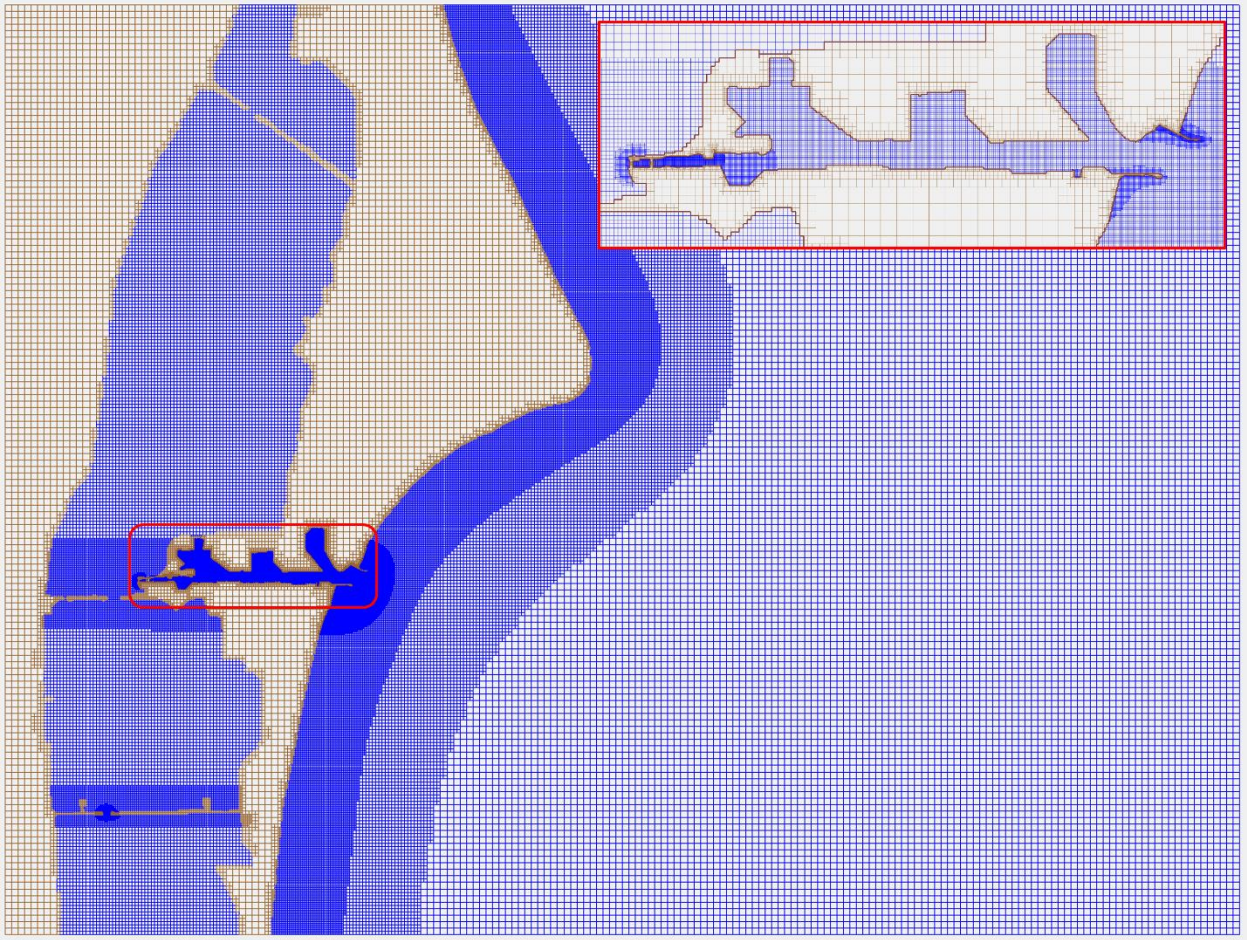

Figure 145. CMS flow grid with port detail (inset)

Blue cells are active ocean cells while brown cells are inactive land cells. Darker areas are locations of increased grid refinement (smaller cells) while lighter areas are larger cell sizes. For this work, the cells representing the flow control structure are set to inactive to represent a closed condition. These cells can be switched to active ocean cells in future work. The CMS flow grid spans 30 km cross shore to a water depth of 22 m and approximately 23 km alongshore. Grid refinement includes five levels ranging from 160 m in the offshore areas to 5 m in the interior Port areas. The finer resolution was dictated by the width of the conveyance channel, which is approximately 76 m wide including the riprap bank protection. General guidance on resolving processes in numerical model grids is at least 5-7 cells are needed to properly resolve flow through a channel. Due to the anticipated complexity of the flow conditions in this area and the primary study interest, the conveyance channel was set to 5 m to include 16 active ocean cells across the conveyance channel. A total of 103,442 cells are in the flow grid with 91,954 specified as active ocean cells.

The CMS wave grid has a rectilinear configuration and with a spatially varying refinement technique focused on providing good representation of waves as they approach the inlet. The wave grid spatial coverage is slightly larger than the flow grid to enable passing information between the modules and match the offshore boundary condition location. A total of 102,816 active ocean cells are in the wave grid and span 41 km cross shore and 24 km alongshore. Jetties and shoreline armoring throughout the port are represented in the wave grid as rubble mound

breakwater low permeability. **Figure 146** provides an image of the CMS wave grid with the jetties and interior structures specified as brown icons.

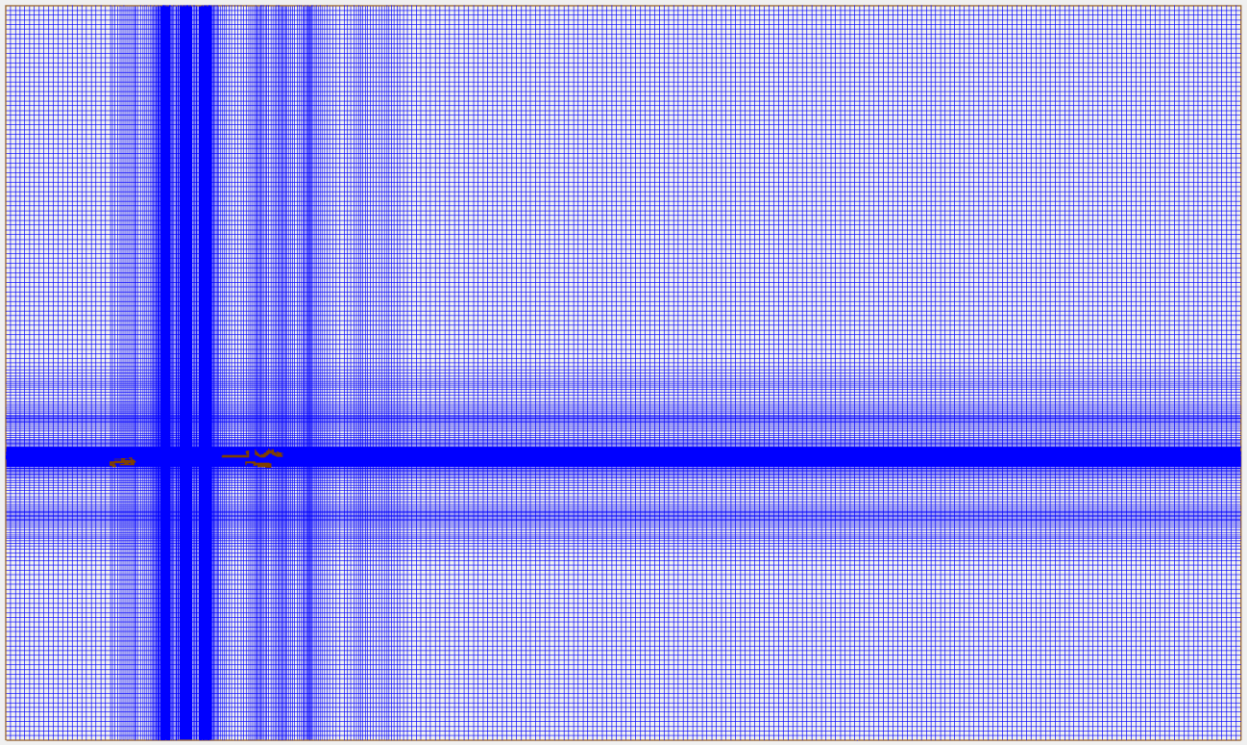

Figure 146. CMS wave grid and structures

15.2 Boundary Conditions

Numerical model temporal coverage was three months of September 1, 2020, through November 30, 2020. The CMS wave model is driven by a combination of a wave input spectra and winds. Two NDBC directional wave buoys are located offshore of Cape Canaveral. NDBC 41009 and 41113 reside in 42 m and 9.8 m water depth, respectively. **Figure 147** shows the location of the NDBC buoy locations with Google Earth imagery.

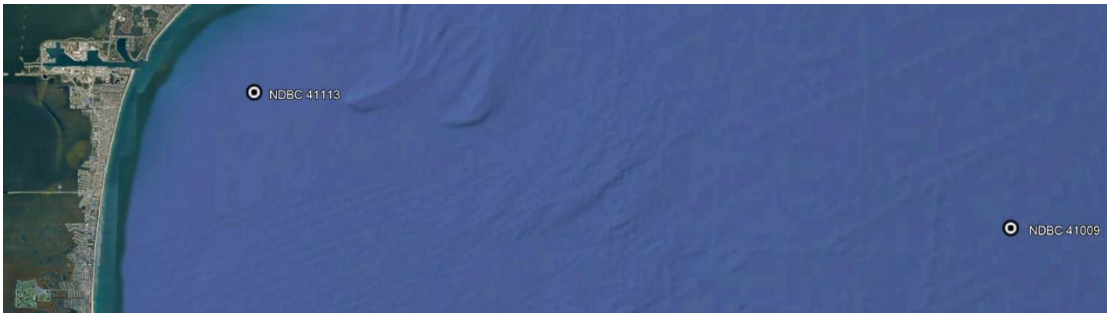

Figure 147. NDBC buoy locations

NDBC 41009 was used as the offshore boundary for the wave model for both wave spectra and wind. Wave data from NDBC 41113 was also obtained for the simulation period to determine model skill. The CMS model was run with existing conditions and showed good agreement with water surface elevation at Trident Pier. Figure **148** plots the wave height, dominant wave period,

and mean wave direction for the simulation period at the offshore buoy location. Three energetic events are observed in the wave record in late September, late October and mid November 2020.

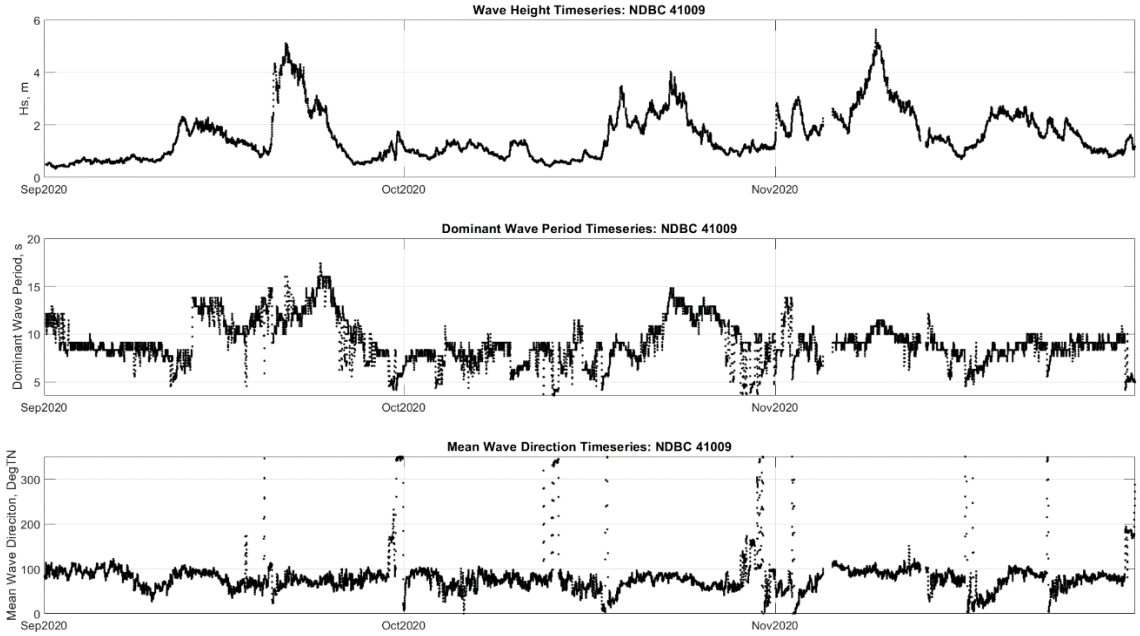

Figure 148. Wave timeseries for NDBC 41009, September–November 2020

Maximum wave height for this observation period is 5.6 m with an average height of 1.6 m. **Figure 149** presents a directional plot of wave height. Waves predominantly come from the north at this location and observation period.

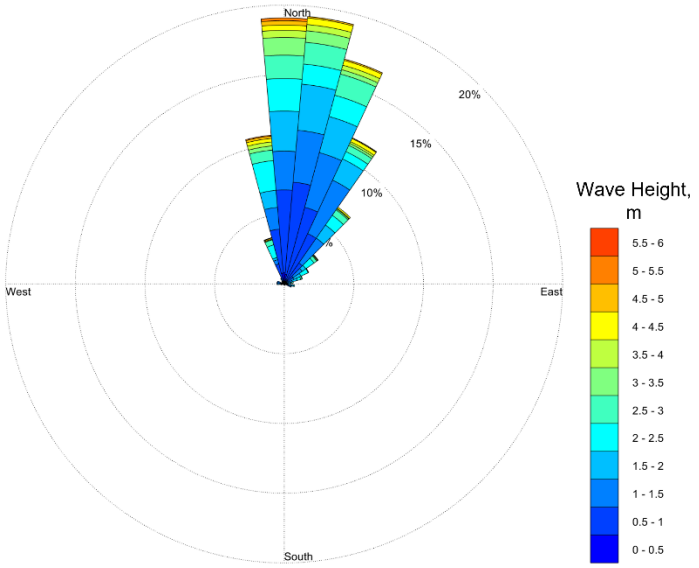

Figure 149. Wave height directional plot

The flow model is driven by an offshore water surface elevation timeseries and wind data observed at the Trident Pier, Port Canaveral NOAA Station (8721604). HYCOM provided water surface elevation boundary conditions. Black diamond markers in **Figure 144** represent the offshore flow boundary configuration using global simulated wave data. This approach was used

to resolve the complex flow patterns around the Cape. Steering between the wave and flow model occurred in three-hour intervals.

15.3 Model Approach

Potential flow changes from implementation of a pumping structure were investigated through simulation of three different flow scenarios: 1 m^3/sec, 2.5 m^3/sec, and 5 m^3/sec. Outflow is represented by a cell string with the total outflow distributed across the cell string nodes. Cell string was situated adjacent to the sector gate on the southern bank and discharges southward.

15.4 Inlet Flow Analysis

Changes in flow and morphology through the Port facility were evaluated across the model alternatives under a closed sector gate condition. Four observation nodes were placed through the conveyance channel moving from the clamshell sector gates (Point 1) to the West Turning Basin (Point 4). Point 2 is westward of the State Road 104 overpass and Point 3 is situated adjacent to the marina. Point 1 is immediately adjacent to the location of the model flow output to represent the pumping system. Location of the observation points in relation to the port conveyance and control structure is diagrammed in **Figure 150**.

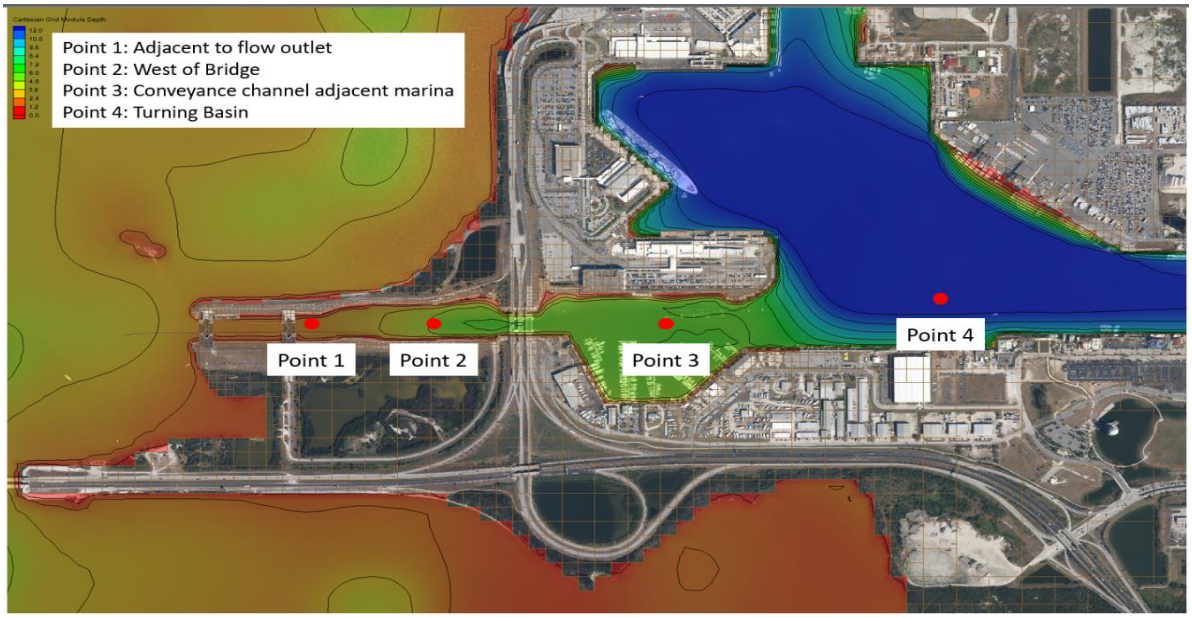

Note: Warmer colors indicate shallower water depths while cooler colors indicate deeper water depths. Plotted water depths in this image range from 0 to 12 m NAVD88. 2018 aerial images are included with the model grid for clarity.

Figure 150. Observation point locations

The current magnitude and direction changes through the Port conveyance were evaluated using a series of directional plots at each observation node. Directional plots indicate the direction of flow as well as representing the magnitude and occurrence of flow. Directional convention indicates where flow is moving towards. All values of current magnitude are in meters per second. Model results of existing conditions and model alternatives is presented in the following sections. Directional plots use the entire model run.

15.4.1 Existing Conditions

Figure 151 represents the computed flow conditions for the existing condition model run and depicts the flow through the conveyance channel. This model run serves as a baseline for comparison. Flow at nodes 1 through 3 are primarily bi-directional along the conveyance channel moving in an east-west direction. The flood current to the west dominates in both magnitude and incidence indicating a flood dominant regime. Flow speeds increase at Point 3 but maintain a flood dominance. At Point 4, the ebb flow is deflected northward as the flow moves into the turning basin.

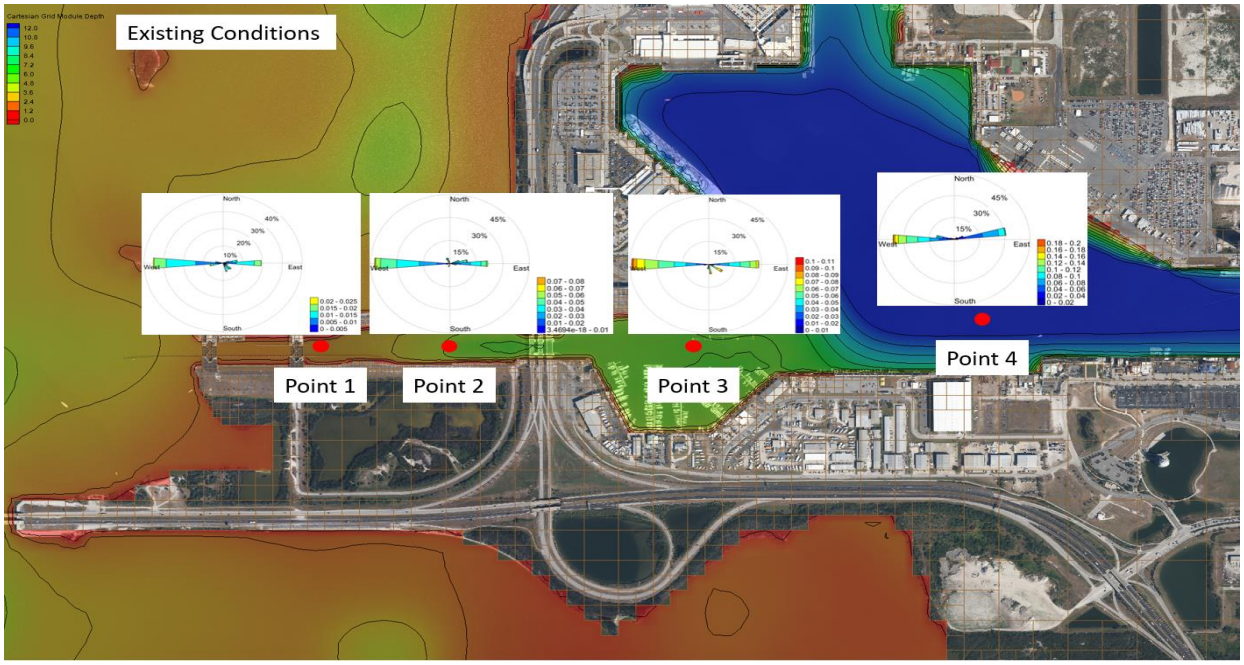

Figure 151. Existing conditions current directional plots

15.4.2 Model Alternative 1 m^3/sec Flow

Figure 152 presents the computed flow for both the 1 m^3/sec alternative and the existing conditions for comparison. At the 1 m^3/sec flow alternative, Point 1 observed the most change in flow conditions as compared to the other observation points. This point is located closest to the flow structure and the location of the outflow. At points 2 through 4, the model indicated no significant change in current magnitude or direction moving east through the port.

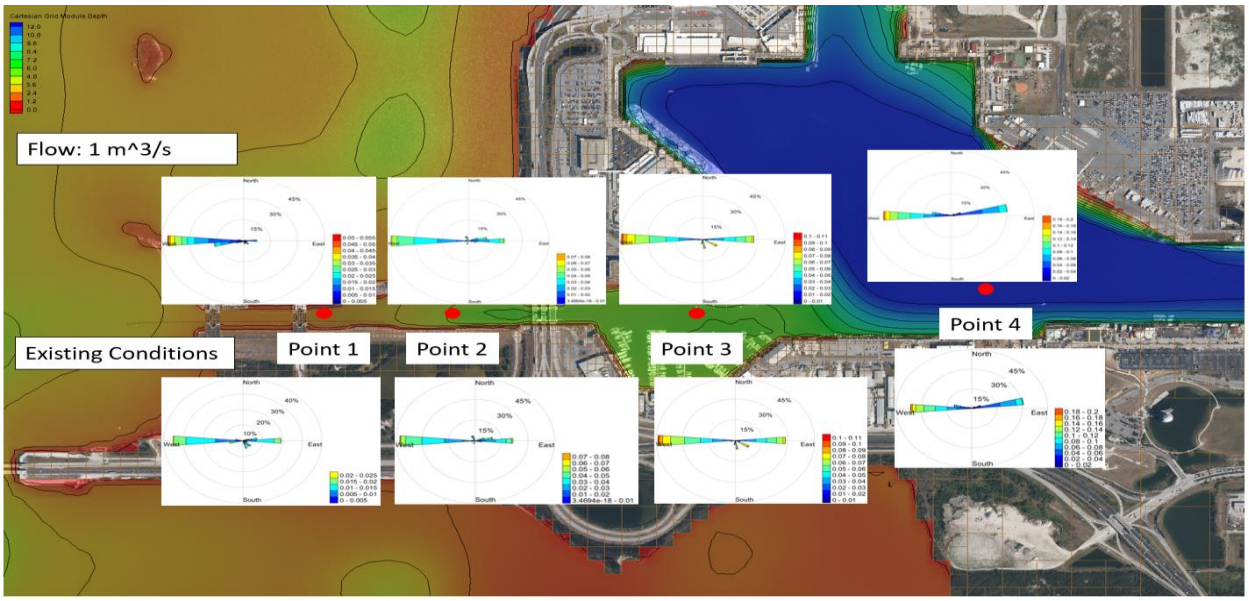

Figure 152. 1 m^3/sec flow rate alternative current directional plots

15.4.3 Model Alternative 2.5 m^3/sec Flow

Computed flow for the 2.5 m^3/sec alternative is shown in **Figure 153**. Current direction at Point 1 is entirely directed towards the west and ebb flow (east) is eliminated at the 2.5 m^3/sec flow rate. Ebb flow at Point 2 is reduced as well at the larger flow rate. Flow characteristics at points 3 and 4 are unchanged at this flow alternative. Flood dominance changes from the outward flow migrates through the conveyance channel with the incorporation of outward flow.

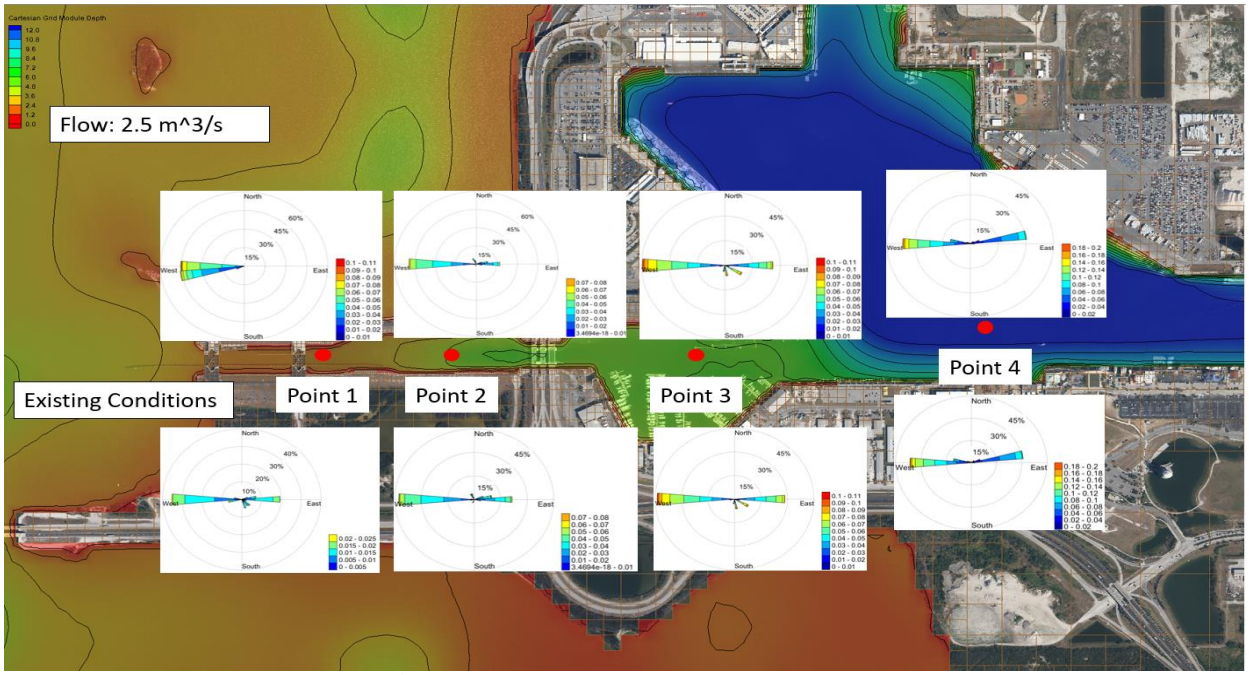

Figure 153. 2.5 m^3/sec flow rate alternative current directional plots

15.4.4 Model Alternative 5 m³/sec Flow

The flow characteristics through the conveyance channel change at the 5 m³/sec flow rate are shown in **Figure 154**. The flow rate at the observation nodes reduces in magnitude but the directionality is similar to the existing conditions. This reduction in flow rate is observed at points 1 through 3. The flow pattern at Point 4 compares well with the existing conditions. It should be noted that due to model stability requirements, the cell string was increased in length to distribute the flow over a greater distance.

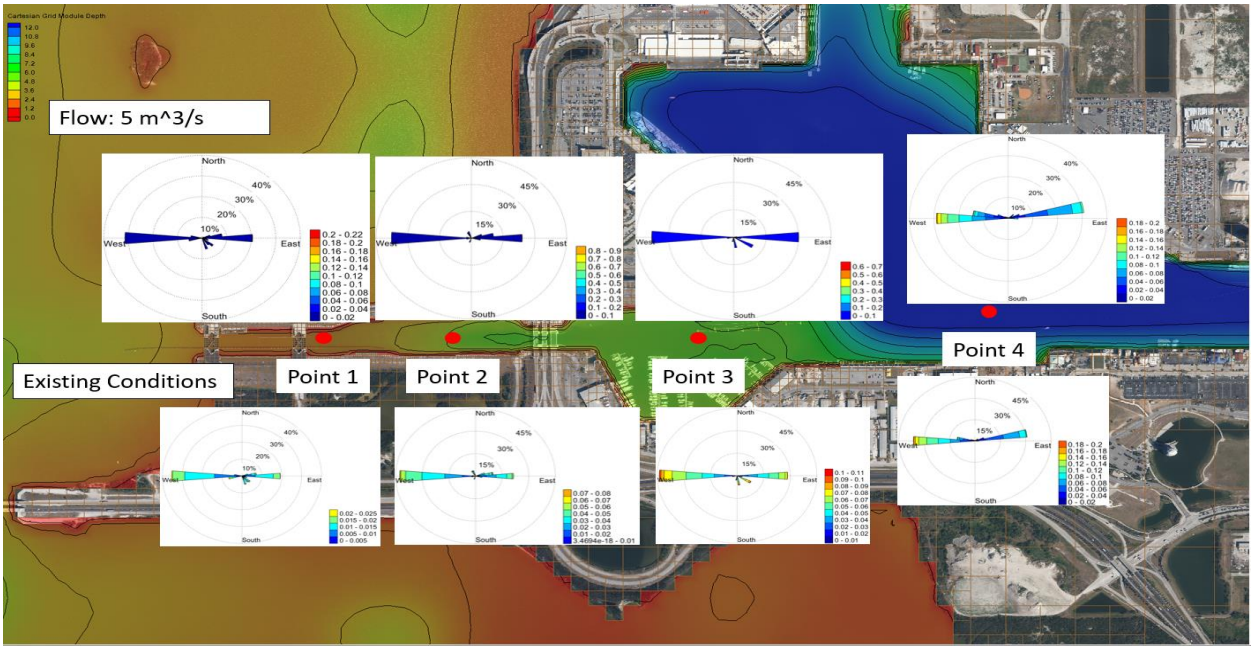

Figure 154. 5 m³/sec flow rate alternative current directional plots

15.5 Morphology Change

Computed morphology change was plotted for the existing conditions and all alternatives to evaluate the potential changes in sedimentation near the flow control structures. Morphology change plots are represented as difference plots where erosion is represented by cool colors and sediment deposition is indicated by warmer colors. Null or no predicted change is represented by while. In all figures, color range spans from -0.5 m to 0.5 m and is taken from the final timestep at the end of the simulation period. These morphology change plots represent 3 months of computed morphology change. With a dominance in flood directed flow, there is a potential for increased sedimentation near the sector gates.

15.5.1 Existing Conditions

Figure 155 shows the computed morphology change for the existing conditions model run. Material is predicted to deposit in the middle of the conveyance channel while sediment is predicted to erode from the banks.

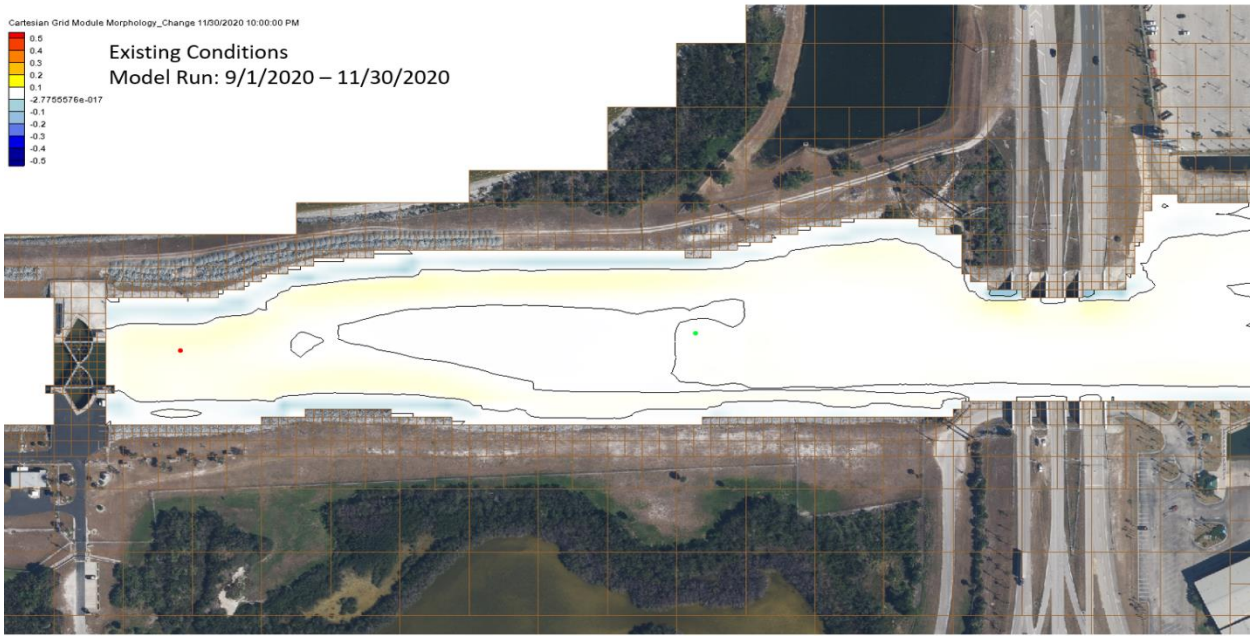

Figure 155. Existing conditions calculated morphology change

15.5.2 Model Alternative 1 m³/sec Flow

Computed morphology change for the 1 m^3/sec flow alternative is shown in **Figure 156**. The existing condition is provided as an inset. Morphology patterns are similar to the existing conditions however the amount of deposition is predicted to increase with an outflow. This behavior is primarily observed adjacent to the flow control structure of the lock system. A distinct erosion pattern appears immediately adjacent to the outflow cell string on the southern shore indicating that scour protection would be required for an installation of this type.

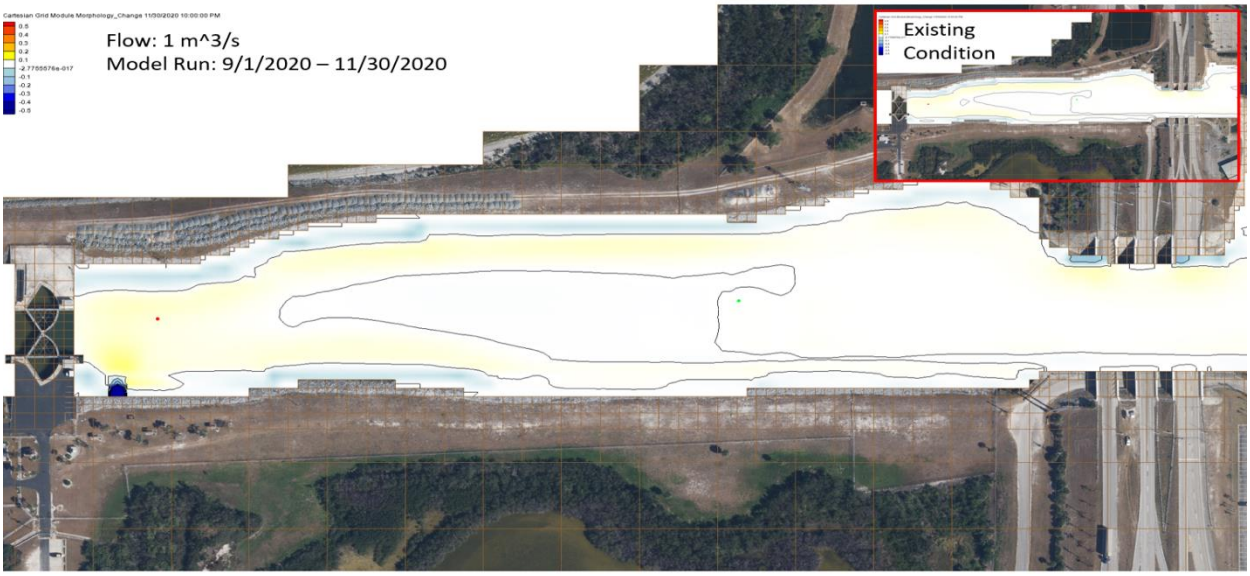

Figure 156. 1 m^3/sec flow alternative calculated morphology change

15.5.3 Model Alternative 2.5 m^3/sec Flow

Figure 157 shows the computed morphology change for the 2.5 m^3/sec flow alternative. Sediment is predicted to increase in deposition immediately adjacent to the flow control structure. Scour near the outfall flow increases with increasing flow rate.

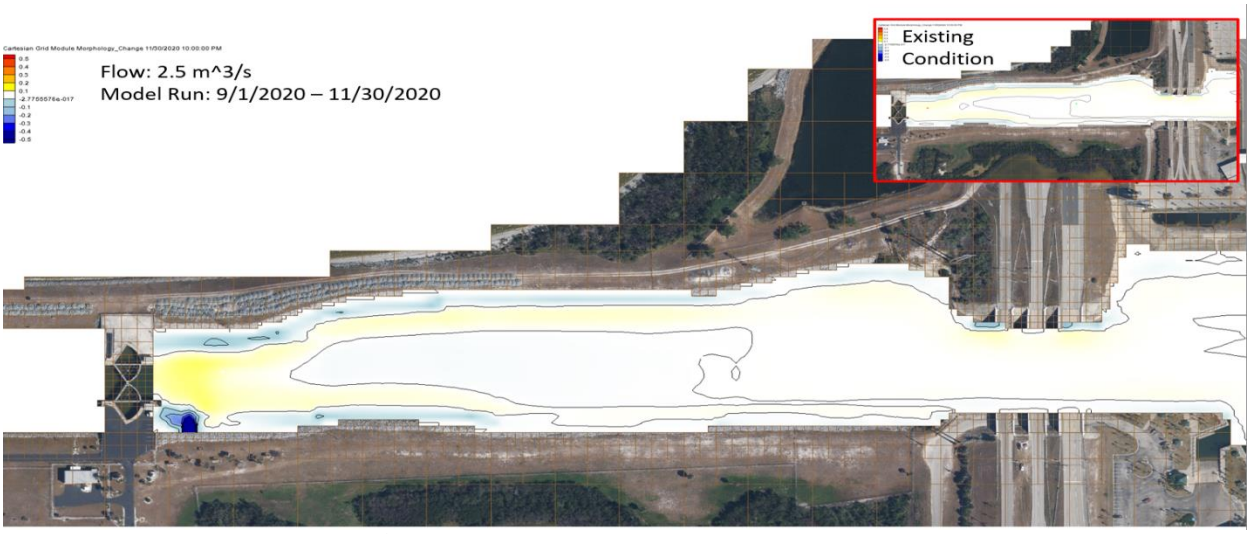

Figure 157. 2.5 m^3/sec flow alternative calculated morphology change

16 Next Steps – Future Work

Each component of Task 1 Modeling and Engineering will have a unique path forward. The ultimate goal is to improve the water quality in the IRL for future generations and create a more resilient IRL able to weather inputs brought by future climate change.

16.1 Inflow Design

The +60% design has been shared with USACE for comment. The next step will be to work with the stakeholders, including USACE, to finalize the design for the permit application. The engineering team will continue to work with Tetra Tech to address any requests for additional information or modifications to the design.

The engineering team will continue to look at alternate methods for transporting ocean water into the IRL. At scales greater than those proposed for the pilot project, a pump system is inefficient. At the larger scales needed to effect a significant change in the water quality of the IRL, a new path for ocean water will have to be used. Just as Denmark has been using a sluice to provide exchange between the coastal ocean and enclosed lagoon (Peterson, et al., 2008), the most efficient method would be a passive mechanism. One such mechanism would be to modify the gates at Canaveral Locks to allow tidal exchange on the flood tide. To provide better evidence for the benefits of such large-scale exchange, a manuscript that was written during Phase 2 will be completed and submitted for publication in a peer reviewed journal.

Future work includes the permit application. To begin this process, a project sponsor needs to be identified and named on the permit application. If permitting goes smoothly, the pilot project could be permitted in 6-9 months, at which point construction could begin. Construction of the pilot can happen relatively quickly, and it could be possible to start pumping water within the year. If

permitting hits snags, the permit process could take over a year. Once permitted, the construction could happen quickly with funding to support the project.

It is difficult to put a timeline on a full-scale inflow project. With support from the public and legislature, any project could happen in a shortened timeline. Permitting for the full-scale project will be shortened due to the work put in with the pilot project. Even shortened, it is estimated that permitting would take 9-18 months. The construction timeline will depend on the structure design. A safe estimate for construction of the full-scale inflow would be one year beyond permit approval.

16.2 Water Level, Salinity, and Temperature Gauges

The long-term water level and temperature stations that have been recording since 2014 will continue to operate. The stations were surveyed last year to NAVD88 vertical datum. The team will continue to work to adjust the historical data to this new datum, and all new data cataloged will be converted to the NAVD88 datum. These three stations require regular maintenance, which currently will be maintained on a quarterly schedule.

The water level, salinity, and temperature stations in the inflow project site were serviced during the last week of Phase 2 funding. We will continue to offload data and service the instruments on a quarterly schedule. Currently there are only three of these stations as station 3 was lost in the last month of Phase 2.

The temperature and water level data from these stations are consistent and have been checked against the long-term data sensor across BRL from the site. Work will continue to evaluate the salinity data, as salinity has the greatest uncertainty. Work is underway to validate the conductivity sensor data at these locations. Phase 3 will allow for validation of the salinity data, and generation of more reliable data, with antifouling measures implemented in Phase 2 and future implementation of a more rigorous calibration protocol.

Should the pilot project receive funding and obtain permits to operate, the sensor array located at the inflow site will provide valuable performance data. The data collected will provide guidance for collocating an additional real-time sensor, like the long-term water level sensors, that can measure salinity and temperature. This will allow researchers to track the progress of the ocean inflow in real time.

The timeline for upgrading sensors in the project area is 3-6 months. Once funding is received, the instrumentation will be acquired and the team will seek authorization to mount the instrumentation on preexisting structures. Obtaining authorization or permitting for mounting on existing structures can take time. The team will allot 2-5 months to acquire authorization. Once authorization is granted, installation is quick and data collection can start. The remaining instrumentation is currently on a quarterly servicing schedule, this schedule would increase with additional funding. The ongoing monitoring effort combined with the planned enhancements to monitoring systems will allow an additional level of confidence in coincident model predictions over the entire BRL by providing for further model validation within the pilot project period

16.3 ADCP and Hydrodynamic Modeling

With the data collected by the Florida Tech researchers, as well as pre-existing Ocean Research and Conservation Association (ORCA) and HBOI instrumentation, two-dimensional circulation models, such as ADCIRC, can be calibrated and validated. During fall 2021, researchers in the modeling and engineering group performed multi-year simulations to capture the seasonal fluctuations in water levels in the IRL. In order for the water level in the IRL to increase by up to 2

ft (0.6 m), a significant volume of water must be exchanged among the compartments of the IRL and BRL. This process has not been documented in previous studies. Our data collection and models will be able to help better understand the natural flushing cycles that occur between late summer and winter in the IRL.

The ADCP deployments carried out in the latter part of Phase 1 and continued through Phase 2 produced new knowledge of IRL and BRL circulation patterns. These deployments should continue through the project hiatus to establish a multi-year record of IRL circulation patterns to capture interannual variations in estuarine circulation linked to the large sea level oscillations in the coastal ocean that have been observed at multiyear time scales. The EFDC/HEMD model in both Phase 1 and Phase 2 produced results that document the potential benefits of enhanced flows from Port Canaveral into the BRL. Under Phase 2, the modelling expanded to include a potential benefit to the water quality of the BRL. Model results were encouraging and will be continued by improving the coupling between the SWIL model and in-estuary EFDC model. In particular, refinements of the SWIL model to include the components of TN and TP are like to improve the already well calibrated performance of the EFDC model. Model predictions of chlorophyll and the potential for predict HAB situations are also encouraging and will be improved by further adjustments to the various rates and coefficients that help to guide calculations of the equations of state for water quality constituents.

16.4 Water Quality Modeling

The EFDC/HEM3D model in both Phase 1 and Phase 2 produced results that document the potential benefits of enhanced flows from Port Canaveral into the BRL. Under Phase 2, the modeling expanded to include potential benefits to the water quality of the BRL. Model results were encouraging. The next step will be to continue improving the coupling between the watershed SWIL model and the in-estuary EFDC model. In particular, refinements of the SWIL model to include the components of TN and TP are like to improve the already well calibrated performance of the EFDC model. This will require an estimated 12-month effort.

Model predictions of chlorophyll and the potential for predict HAB situations are also encouraging and can be improved by further adjustments to the various rates and coefficients that guide calculations of the equations of state for water quality constituents. The effort to predict HAB conditions is enhanced by the ADCP survey of circulation dynamics and by EFDC model tracer studies. Reversed flow direction of either north or south flow in the BRL and central IRL that can have a frequency of a month or longer may set the physical conditions that trigger and promote HABs in BRL. Coupling this phenomenon, variations in water quality and the occurrence of HABs will be investigated as part of the proposed Phase 3. An additional effort is required to quantify water quality inputs through the tidal inlets that connect the coastal ocean to the IRL system. This will require a thorough search for nearshore coastal ocean water quality data including evidence of HAB triggers that may be associated with Gulf Stream dynamics. Along with continued monitoring and further calibration of ongoing models, this effort should extend over a 12-month period in Phase 3.

16.4.1 ADCIRC Modeling of Circulation

With the data collected by the Florida Tech researchers, as well as pre-existing ORCA and HBOI instrumentation, two-dimensional circulation models such as ADCIRC can be calibrated and validated. The team is waiting for a response form ORCA to a request for data. With the ORCA data and our project data, the team will seek to improve the model predictive capabilities. The timeline for completion of the ADCIRC modeling and validation against in-situ data would be one year of funded research. That year would involve the collection of updated data from third parties,

extended modeling of the system using the latest published modeling framework, and final analysis of the results.

16.5 Pilot Project

A pilot pumping project is an important final step to fully integrate all components of the Restore Lagoon Inflow Research project. During this proposed phase, all monitoring and modeling components will converge to fully verify hydrodynamic and water quality predictions at a local scale in the area around the inflow point. Water quality predictions of the Phase 2 project indicate an increase in DO levels and decrease in water quality nutrient concentrations in the BRL. These impacts should be locally realized at the scale of the pilot project. Modeling and monitoring specific to the zone around the inflow point will allow validation at a local scale the predicted improvements in water quality, and will provide an improved level of confidence that the broader BRL will respond as predicted under the higher inflow cases tested under Phase 2. Potential influence of exporting flows from the Port Canaveral basin on circulation in the Port can be verified by continuing to maintain the ADCP station that is now deployed in the Port.

17 References

Bluff Manufacturing. 2019. Crossover Ramp. Retrieved from Bluff Manufacturing, Inc.: www.bluffmanufacturing.com/yard-ramps/crossover-ramps-fracking-ramps/#gsc.tab=0.

Bluff Manufacturing. 2021. Quote 110363.

Brady, D.C., Testa, J.M., Di Toro, D.M., Boynton, W.R., and Kemp, W.M. 2013. Sediment flux modeling: calibration and application for coastal systems. Estuarine, Coastal and Shelf Science 117:107-124.

CDM Smith in association with Taylor Engineering. 2014. Preliminary Concept Design for Artificial Flushing Projects in the Indian River Lagoon – Phase I Literature Review/ Preliminary Site Selection.

CDM Smith in association with Taylor Engineering. 2015. Preliminary Concept Design for Artificial Flushing Projects in the Indian River Lagoon – Phase II Conceptual Design/Project Refinement.

CDM Smith in association with Taylor Engineering. 2017. Conceptual Design for Artificial Flushing Projects in the Indian River Lagoon, Draft Report August 2017, Conceptual Design and Conceptual Cost Estimates for Pilot Testing.

Cerco, C.F. and Cole, T. 1994. Three-dimensional eutrophication model of Chesapeake Bay. J. Environ. Eng., 119, 1006-1025.

Comprehensive Everglades Restoration Plan. 2006. Guidelines for Manatee Conservation During Comprehensive Everglades Restoration Plan Implementation. Retrieved from U.S. Fish and Wildlife Service: www.fws.gov/verobeach/MammalsPDFs/CERPManateeGuidelines120806.pdf?spcode=A007.

Cowan, J.L.W. and Boynton, W.R. 1996. Sediment-water oxygen and nutrient exchanges along the longitudinal axis of Chesapeake Bay: seasonal patterns, controlling factors and ecological significance. Estuaries 19:562-580.

Csanady, G.T. 1978. The arrested topographic wave. Journal of Physical Oceanography 8:47-62.

Das, B.M. and Sivakugan, N. 2019. Principles of Foundation Engineering. Cengage Learning.

Dean, R.G. and Dalrymple, R.A. 2002. Coastal Processes with Engineering Applications. Cambridge University Press.

Defne, Z. and Ganju, N.K. 2015. Quantifying the residence time and flushing characteristics of a shallow, back-barrier estuary: application of hydrodynamic and particle tracking models. Estuaries and Coasts 38:1719-1734.

Development Services Department. 2009. Unit Price List. Retrieved from City of San Diego: https://www.sandiego.gov/sites/default/files/legacy/development-services/pdf/industry/pricelist.pdf.

Diaz, R.J. and Rosenberg, R. 2008. Spreading dead zones and consequences for marine ecosystems. Science 321:926-929.

DiDonato, G.T., Murrell, E.M., Lores, M.C., Smith, L.M., and Caffrey, J.M. 2006. "Benthic nutrient flux in a small estuary in northwest Florida (USA)." Gulf and Caribbean Research 18:15-26.

El Shamy, U., Krueger, P., An, Z., and Abdelhamid, Y. 2018. Experimental and Numerical Modeling of Surface Erosion. Retrieved from IFCEE: https://ascelibrary.org/doi/pdf/10.1061/9780784481639.018.

ElectricRate. 2020. Electricity Rates By State. Retrieved from https://www.electricrate.com/electricity-rates-by-state/.

Ezer, T., Atkinson, L.P., Corlett, W.B., and Blanco, J.L. 2013. Gulf Stream's induced sea level rise and variability along the US mid-Atlantic coast, J. Geophys. Res. Oceans, 118, 685–697.

FDEP. 2013. Banana River Lagoon Basin Management Action Plan. Retrieved from https://floridadep.gov/sites/default/files/banana-river-lagoon-bmap.pdf.

Garmin. 2021. Navionics ChartViewer. Retrieved from webapp.navionics.com/?lang=en#boating/menu@undefined&key=ogklDnfdkN.

Ghosh, A.K., Pattnaik, A.K., and Ballatore, T.J. 2006. Chilika lagoon: restoring ecological balance and livelihoods through re-salinization. Lakes Reserv. Res. Manag. 11, 239–255. doi: 10.1111/j.1440-1770.2006.00306.x.

Google. 2021. Google Earth. Retrieved from earth.google.com/web/@28.40800523,-80.63589592,4.26711183a,1057.64197548d,30.00002933y,0h,0t,0r.

Harper, H.H. 2021. Canaveral Port Authority Water Quality Monitoring Program. Prepared for Canaveral Port Authority Environmental Plans and Programs, 31p.

Harwood, D.W. 2003. Review of Truck Characteristics as Factors in Roadway Design. Transportation Research Board.

He, X., Jiao, W., Wang, C., and Cao, W. 2019. Influence of Surface Roughness on the Pump Performance Based on Computational Fluid Dynamics. Retrieved from IEEE Access: DOI 10.1109/ACCESS.2019.2932021.

Humphries, R. and Robinson, S. 1995. Assessment of the success of the Peel Harvey estuary system management strategy-a western Australian attempt at integrated catchment management. Water Sci. Technol. 32, 255–264. doi: 10. 2166/wst.1995.0619.

Jassby, A.D., and Nieuwenhuyse, E.E. 2005. Low dissolved oxygen in an estuarine channel (San Joaquin River, California): mechanisms and models based on long-term time series. San Francisco Estuary and Watershed Science 3(2).

Kaiser, M.J. 2017. FERC pipeline decommissioning cost in the U.S. Gulf of Mexico, 1995–2015. Retrieved from Marine Policy, Volume 82, Pages 167-180: https://doi.org/10.1016/j.marpol.2017.05.006.

Kemp, W.M., Sampou, P., Caffrey, J., Mayer, M., Henriksen, K., and Boynton, W.R. 1990. Ammonium recycling versus denitrification in Chesapeake Bay sediments. Limnology and Oceanography 35:1545-1563.

Kemp W.M., Sampou P.A., Garber J., Tuttle J., and Boynton W.R. 1992. Seasonal depletion of oxygen from bottom waters of Chesapeake Bay: relative roles of benthic and planktonic respiration and physical exchange processes. Marine Ecology Progress Series 85:137.

Kjerfve, B. 1986. Comparative Oceanography of Coastal Lagoons. Retrieved from Estuarine Variability, 63-81: https://doi.org/10.1016/b978-0-12-761890-6.50009-5.

Li, Y., Tang, C., Wang, C., Anim, D., Yu, Z., and Acharya, K., 2013. Improved Yangtze River Diversions: Are they helping to solve algal bloom problems in Lake Taihu, China, Ecological Engineering, Vol. 51, 104-116. doi:10.1016/j.ecoleng.2012.12.077.

Lillebo, A.I., Neto, J.M., Martins, L., Verdelhos, T., Leston, S., and Cardoso, P.G. 2005. Management of a shallow temperate estuary to control eutrophication: the effect of hydrodynamics on the system's nutrient loading. Estuar. Coast. Shelf S. 65, 697-707.

McMaster-Carr. 2021. Retrieved from McMaster-Carr: https://www.mcmaster.com/u-bolts/u-bolts-6/.

Midwest Steel Supply. 2021. Retrieved from Midwest Steel and Aluminum: https://www.midweststeelsupply.com/store/hotrollsteelbeam.

MWI Pumps. 2020. Axial Flow Pump Curves: Pump Bowl Performance Curves. Retrieved from MWI Pumps - Moving Water Industries: mwipumps.com/axial-flow-curves/.

MWI Pumps. 2021. Quote From MWI Pumps.

Native Dynamics. 2012. Pressure Loss in Pipes. Retrieved from Neutrium: neutrium.net/fluid-flow/pressure-loss-in-pipe/.

ODOT. 2014. Hydraulics Design Manual. Retrieved from Oregon Department of Transportation: www.oregon.gov/odot/GeoEnvironmental/Docs_Hydraulics_Manual/HDM_Complete.pdf.

Penn State University. 2015. Minor Losses. Retrieved from Penn State University: www.me.psu.edu/cimbala/me320web_Spring_2015/pdf/Minor_losses.pdf.

Peterson, J.K., Hansen, J.W., Laursen, M.B., Clausen, P., Carstensen, J., and Conley, D.J. 2008. Regime Shift in a Coastal Marine Ecosystem, Ecological Applications, 497-510.

RSMeans. 2021. Retrieved from RSMeans Data Online from Gordian: rsmeansonline.com/ManageEstimate.

Saberi, A. and Weaver, R. 2016. Simulating Tidal Flushing Response to the Construction of a Low-Crested Weir Connecting Port Canaveral to the Banana River, Florida. J. Waterway, Port, Coastal, Ocean Eng.10.1061/(ASCE)WW.1943-5460.0000337, 05016002.

Schallenberg, M., Larned, S.T., Hayward, S., and Arbuckle, C. 2010. Contrasting effects of managed opening regimes on water quality in two intermittently closed and open coastal lakes. Estuar. Coast. Shelf S. 86, 587–597. doi: 10.1016/j.ecss.2009.11.001.

Seitzinger, S.P. 1988. Denitrification in freshwater and coastal marine ecosystems: ecological and geochemical significance. Limnology and Oceanography 33:702-724.

Sigua, G.C., Steward, J.S., and Tweedale, W.A. 2000. Water-Quality Monitoring and Biological Integrity Assessment in the Indian River Lagoon, Florida: Status, Trends, and Loadings (1988-1994). Environmental Management 25:199-209.

Smith, N. 1990. Computer Simulation of Tide-Induced Residual Transport in a Coastal Lagoon. Journal of Geophysical Research, Vol. 95, No. Ci0, Pages 18,205-18,211.

Stauble, D.K., Da Costa, S.L., Monroe, K.L., and Bhogal, V.K., 1988. Inlet Flood Tidal Delta.

Tetra Tech, Inc. 2007. The Environmental Fluid Dynamics Code Theory and Computation Volume 3: Water Quality Module. Fairfax, VA.

Tech Tetra, Inc. 2016. Save Our Indian River Lagoon Project Plan for Brevard County, Florida.

Tetra Tech, Inc., and CloseWaters LLC. 2020. Save Our Lagoon Project Plan for Brevard County, Florida.

Tetra Tech, Inc. 2021. Restore Lagoon Inflow Research Pilot Project Indian River, FL.

U.S. Department of Energy. 2001. Pump Life Cycle Costs. Retrieved from Office of Industrial Technologies Energy Efficiency and Renewable Energy: https://www.energy.gov/sites/prod/files/2014/05/f16/pumplcc_1001.pdf.

USFWS. 2019. Fish Passage Engineering Design Criteria. Retrieved from U.S. Fish and Wildlife Service: www.fws.gov/northeast/fisheries/pdf/USFWS-R5-2019-Fish-Passage-Engineering-Design-Criteria-190622.pdf.

Weaver, R. and Zarillo, G.A. 2020. Restore Lagoon Inflow Research (Phase I) Task 1 - Modeling and Engineering. Prepared for the Florida Department of Education.

Wijnhoven, S., Escaravage, V., Daemen, E., and Hummel, H. 2010. The decline and restoration of a coastal lagoon (Lake Veere) in the Dutch Delta. Estuar. Coast. 33, 1261–1278. doi: 10.1007/s12237-009-9233-1.

Wu, G. and Xu, Z. 2011. Prediction of algal blooming using EFDC model: Case study in the Daoxiang Lake. Ecological Modelling 222 (2011) 1245–1252.

Zarillo, G.A. 2015. Indian River Lagoon Numerical Model Flushing Experiments.

Zarillo, G.A. 2018. Numerical Model Flushing Experiments Final Report Submitted to the Wisher Indian River Lagoon National Estuary Program and Canaveral Port Authority. 36pp.

Zarillo, G.A. and Listopad, C. 2020. Hydrologic and Water Quality Model for Management and Forecasting within Brevard County Waters of the Indian River Lagoon. Final Project Report to Brevard County Natural Resources Management Department. 128pp.

Zarillo, G.A., Watts, I., Brehin, F, and Erickson, L. 2013. State of Sebastian Inlet 1943-201: An Assessment of Inlet Morphologic Processes, Shoreline Changes, Sediment Budget and Management Strategies. Report to the Sebastian Inlet Management District. 161pp.

Appendix B Task 2 – Geochemistry Report

Restore Lagoon Inflow Research (Phase 2)
Task 2, Geochemistry

PREPARED FOR

Florida Department of Education
325 W Gaines Street
Tallahassee, FL 32399

PREPARED BY

Austin Fox
Assistant Professor of Ocean Sciences
afox@fit.edu
Florida Institute of Technology
150 West University Boulevard
Melbourne, FL 32901

August 2021

Table of Contents

List of Tables

List of Figures

Acknowledgements

I would like to thank our representatives in the Legislature and the public for overwhelming support of lagoon science. We thank Robert Salonen for his efforts that made this research at Florida Tech possible. I would also like to thank Jeff Eble for his leadership and interest in the collective science, and the other PIs on this project for their collaboration and support. Finally, I would like to thank the students and technicians helping to support this project. I would especially like to thank Abigail Gering, Stacey Fox, Tyler Provoncha, and Iulia Bibire.

Cover Photo: Proposed inflow location in the northern Banana River Lagoon looking southwest at the A1A causeway: Photo credit: Austin Fox

List of Acronyms

BRL	Banana River Lagoon
°C	Degrees Celsius
cm	Centimeter
DIN	Dissolved Inorganic Nitrogen
DO	Dissolved Oxygen
DON	Dissolved Organic Nitrogen
DOP	Dissolved Organic Phosphorus
Florida Tech	Florida Institute of Technology
HAB	Harmful Algal Bloom
IRL	Indian River Lagoon
kg/m^3	Kilograms Per Cubic Meter
km	Kilometer
L	Liter
LOI	Loss on Ignition
m	Meter
m^2	Square Meter
m^3/sec	Cubic Meters Per Second
mg/L	Milligrams Per Liter
mg/L/hr	Milligrams Per Liter Per Hour
mL	Milliliter
N	Nitrogen
NDBC	National Data Buoy Center
NH_4	Ammonium
NOx	Nitrate + Nitrite
O	Oxygen
OM	Organic Matter
ORP	Oxidation Reduction Potential
P	Phosphorus
PO_4	Orthophosphate
PSU	Practical Salinity Unit

PVC	Polyvinyl Chloride
SCUBA	Self-Contained Underwater Breathing Apparatus
SiO_2	Silica
SJRWMD	St. Johns River Water Management District
SOD	Sediment Oxygen Demand
SRP	Soluble Reactive Phosphorus
TDN	Total Dissolved Nitrogen
TDP	Total Dissolved Phosphorus
µm	Micrometer
µM	Micromolar
µmoles/m2/hr	Micromoles Per Square Meter Per Hour

Task Summary

Distinct differences in the ability of poorly-flushed versus well-flushed estuaries to cope with eutrophication have been consistently reported where poorly-flushed estuaries with long residence times, like the Indian River Lagoon (IRL), more readily retain nutrients to promote algal blooms, loss of seagrass beds, hypoxia, and corresponding loss of ecosystem services (Twilley et al., 1999; Defne and Ganju 2015; Kemp et al., 1992; Twilley et al., 1999). In contrast, well-flushed estuaries with shorter residence times have greater resilience to the impacts of eutrophication (Defne and Ganju 2015). Loss of ecosystem services that would, in healthy systems, remove or sequester nutrients over time and space creates a positive feedback loop helping to sustain eutrophication. This study was intended to investigate whether or not inflow of seawater would help to break the cycle of eutrophication and hypoxia by (1) directly decreasing nutrient concentrations through mixing and (2) promoting water column and sediment processes that would help to restore ecosystem services by either removing or preventing nitrogen (N) and phosphorus (P) from entering the lagoon. Key geochemical findings from this study are presented below:

- Inflow of seawater from Port Canaveral would bring cooler (0.5-1 degrees Celsius [°C]), saltier (~10 practical salinity units [PSU]), denser water from the Port (1,018-1,028 kilograms per cubic meter [kg/m^3]) into the lagoon (1,008-1,016 kg/m^3) favoring circulation in bottom water, helping to lower lagoon temperature while raising and stabilizing concentrations of dissolved oxygen at the sediment-water interface.
- Concentrations of total dissolved nitrogen (TDN) and total dissolved phosphorus (TDP) in Port Canaveral (23 ± 10 micromolar [µM] TDN, 0.37 ± 0.19 µM TDP) were 5-fold and 3-fold lower than concentrations in the IRL. A scaled test of inflow at 0.5 cubic meters per second (m^3/sec) from Port Canaveral would have a maximum net discharge of 1.5 tons of N and 0.4 tons of P per year, quantities that would increase current discharges by less than 1%. Discharges to the coastal ocean are estimated to be smaller in magnitude than removal of N and P resulting from restoration of ecosystem services.
- No significant correlations were identified between water column cycling (particle fluxes) of N or P and changes to temperature, salinity, or dissolved oxygen (DO). Lower rates of recycling in Port Canaveral and lower N:P ratios (dissolved inorganic nitrogen (DIN): soluble reactive phosphorus (SRP) 45 in the lagoon, 20 in Port Canaveral; TDN:TDP 113 in the lagoon, 97 in Port Canaveral) would, when mixed, help to increase rates of nutrient removal in the lagoon while promoting lower N:P ratios that are less favorable to some harmful algal bloom (HAB) species.
- Fluxes of TDN and TDP were highly variable and on average directed into sandy sediments at -400 micromoles per square meter per hour (µmoles/m^2/hr) and -06 µmoles/m^2/hr, respectively. In contrast, muddy “mucky” sediments were a source of N and P to overlying water.
- Significant positive correlations were identified between benthic fluxes of nitrate + nitrite (NO_x), TDN, orthophosphate (PO_4), dissolved organic phosphorus (DOP), and SiO_2 (silica) versus sediment temperature. Lower temperatures associated with the proposed pilot study (0.5 m^3/sec) were calculated to prevent 1.6 metric tons of N and 0.7 metric tons of P from entering the lagoon each year. Using average costs for removal of N and P from the Brevard County Save Our Indian River Lagoon Project Plan (Tetra Tech, 2021; $384 per pound of N and $4,650 per pound of P), estimated load reductions would be valued at more than $9 million per year.
- Under hypoxic conditions (<2 milligrams per liter [mg/L]), sediments were a source of dissolved PO_4 to overlying water (18.8 ± 5.2 µmoles/m^2/hr) and at higher DO

concentrations (>5 mg/L), sediments were a net sink for dissolved PO_4. Low DO also promoted preferential fluxes of ammonium versus nitrate, a shift that supports HAB species at low DO concentrations.

- Concentrations of DO in bottom water, where it has the greatest impact on nutrient cycling, reflected rates of sediment oxygen demand both temporally at the same site and spatially across sites. In other words, higher sediment oxygen demand results in lower bottom water DO. Concentrations of DO in bottom water were typically lower and more frequently hypoxic than concentrations measured at mid depths, where most monitoring currently occurs. Through this project a network of bottom water DO sensors was established and we hope to find support for long term maintenance of this network to provide essential data to lagoon modelers and stakeholders.
- Overall, data to date support a limited test of inflow as part of a multifaceted approach to lagoon restoration.

1 Introduction

1.1 Background

Globally, eutrophication of coastal marine ecosystems has become increasingly common due to enhanced nutrient loading from adjacent watersheds (Brady et al., 2013; Diaz and Rosenberg, 2008). As the eutrophic state progresses, sediment mineralization becomes an increasingly important source of nutrients and can sustain eutrophication through the dry season as well as destabilize the trophic state of an estuary (Cowan and Boynton 1996; DiDonato et al., 2006; Seitzinger 1988; Kemp et al., 1990). Extended periods of eutrophication can lead to a shift from seagrass-dominated ecosystems to degraded, algae-dominated systems (DiDonato et al., 2006). During recent decades and associated with eutrophication, catastrophic losses of seagrass beds have been reported worldwide (Burkholder et al., 2007). Co-occurring with seagrass losses are more frequent harmful algal blooms (HABs) and occurrences of hypoxia and anoxia (Tetra Tech 2016). Even short hypoxic or anoxic events can decrease macrofaunal abundance and promote loss of ecosystem services, including bioturbation, that helps to maintain oxic surface sediments. Loss of ecosystem services can lead to an increasingly anoxic sedimentary environment with implications to mineralization of organic matter and nutrients and geochemical nutrient cycling (Pelegri et al., 1994; Foster and Fulweiler 2019; Seitzinger 1991; Kemp et al., 2009).

A distinct difference in the ability to cope with eutrophication has been observed among estuaries with varying geomorphologies and residence times or flushing times for water (Twilley et al., 1999; Defne and Ganju 2015). Poorly flushed estuaries with long residence times, like the Indian River Lagoon (IRL) system, more readily retain nutrients to promote algal blooms, loss of seagrass beds, hypoxia, and loss of ecosystem services (Defne and Ganju 2015; Kemp et al., 1992; Twilley et al., 1999). Conversely, well-flushed estuaries with shorter residence times have greater resilience to the impacts of eutrophication (Defne and Ganju 2015). Historically, estuarine flushing has been controlled by fluvial discharge, tides, wind mixing, and the geomorphology of the estuary, as well as other forcing over longer timescales (Defne and Ganju 2015; Csanady 1978; Jassby and Van Nieuwenhuyse 2005).

The processes responsible for exchanges of water in estuaries can influence stratification with implications to nutrient cycling and ultimately the degree to which circulation can mitigate the impacts of eutrophication (Defne and Ganju 2015). For example, freshwater discharges can promote stratification that circulates water; however, geochemical processes occurring at the sediment-water interface can promote continued eutrophication and hypoxia or anoxia in a layer of more stagnant bottom water (Jassby and Van Nieuwenhuyse 2005). In shallow estuaries, the impacts of stratification are often overcome by wave-induced circulation (Csanady 1978); however, as sediment health declines, enhanced utilization of oxygen by sediments can induce hypoxic or anoxic events over short timescales, including on daily cycles. Despite the potential for wind mixing, stratification that may result from additions of water can have important implications to nutrient cycling, especially in stabilizing diurnal fluctuations. In contrast to unidirectional fluvial discharges, bidirectional tidal forcing near inlets has been shown to mix water throughout the water column; nevertheless, despite mixing, tidal exchanges are typically limited in spatial extent (Defne and Ganju, 2015). To overcome spatial limitations of inlets whether natural or anthropogenic, ocean inflow may offer a viable option to promote mixing over large spatial scales, thereby enhancing circulation throughout the lagoon.

Enhanced circulation in the IRL could contribute towards lowering nutrient concentrations that support the onset and proliferation of algal blooms. Another potential benefit would likely be to increase and or stabilize the concentration of dissolved oxygen (DO), yielding enhanced resilience

to anoxia and fish kills. The main benefits of decreased nutrient concentrations and possibly increased DO would likely result from changes to geochemical cycling, with spatially limited impacts from direct dilution by seawater. Results from Phase 1 of this study were consistent with literature and suggest that enhanced circulation could lead to decreased concentrations of nutrients in areas of the IRL. Decreases would be associated with (1) direct dilution by mixing where nutrients would be transported to other areas and the coastal Atlantic Ocean and (2) sequestration in sediments, especially for phosphorus (P), and removal from the system via denitrification and or anammox that would likely be promoted in sediments with an oxic-anoxic boundary. The objectives of the Phase 2 effort built on results from Phase 1 and determined potential impacts to water quality that could result from (1) direct dilution by seawater, plus changes to the residence time for water in the lagoon and (2) changes in geochemical cycling that result from changes to temperature, salinity, and DO that could occur due to various levels of proposed pumping. Additional objectives were to (3) investigate temporal trends for nutrient fluxes from sandy sediments that occupy most of the lagoon and (4) investigate how geochemical cycling might favor certain types of algae based on change the nitrogen (N):P ratio or the speciation of N. Water quality sensors were used to determine the homogeneity of bottom water conditions, both temporally and spatially, over a variety of sediment types. In addition to contributing towards establishing a “baseline,” this study identified discrepancies between data from existing water quality sensors, mostly located near the middle of the water column, and bottom water conditions near proposed pumping locations. Data from this investigation are available to modelers to better predict changes to nutrient and DO concentrations and ratios under various pumping scenarios. Regardless of inflow, this new dataset will help modelers and managers to better predict how changes to temperature, salinity, and/or DO influence water quality in the IRL. These changes could result from a changing climate with impacts to temperature or precipitation (salinity) in the region.

1.2 Study Area

The IRL is a shallow (<5 meter [m]), bar-built, lagoon-type estuary that extends 250 kilometers (km) along the central east coast of subtropical Florida and ranges in width from <1 to ~9 km (Sigua et al., 2000; **Figure 1**). In the past decade, water quality in the IRL has declined with more severe and more frequent harmful algal blooms (IRL coalition; Tetra Tech 2016). The IRL is poorly flushed with 140 km between the Sebastian and Ponce de Leon inlets. The northern portion of the IRL is micro tidal and tidal flushing is negligible (Smith 1993) where tides are of only minor significance toward flushing (Smith 1993). Based on rainfall and low-frequency coastal water level variations, the 50% renewal time for water in the northern and central IRL sections ranges from ~100-300 days (Smith 1993).

This study was carried out to evaluate possible impacts of enhanced circulation in the Banana River Lagoon (BRL) with an emphasis at two primary locations: (1) North Banana River, considered as a likely inflow site (centered near 28.407, -80.638); and (2) Central Banana River, evaluated as a reference area where any impacts of inflow would be minimized due to geomorphological conditions that limit circulation (centered near 28.287, -80.6100). The North Banana River site was selected as a test location based on several factors. For example, the embayment provides a well-defined area for the test where the impacts of pumping could be tracked as inflow water mixed westward into the lagoon. A well-defined treatment area representing the lagoon for a scaled pilot-project minimizes risk that impacts are undetectable due to mixing. The control area was selected based on evaluation of models to identify candidate locations with limited circulation associated with proposed pumping volumes, followed by a comparison of water depth and bottom type at candidate sites versus the proposed inflow location (North Banana River) (**Figure 1** and **Figure 2**). Sampling sites inside the IRL and BRL were

selected using a stratified, random approach to ensure that data are scientifically and statistically sound and can be extrapolated to a larger area (e.g., White et al., 1992). Seawater samples were also collected from within Port Canaveral as this is the most likely source of sweater for the proposed inflow project based on logistical considerations identified during Phase 1 of this study.

Note: Red circles show a 1 km radii around the proposed pumping location and reference site for scale.

Figure 1. Map of the study area showing potential pumping location in the North Banana River and the reference site in the Central Banana River

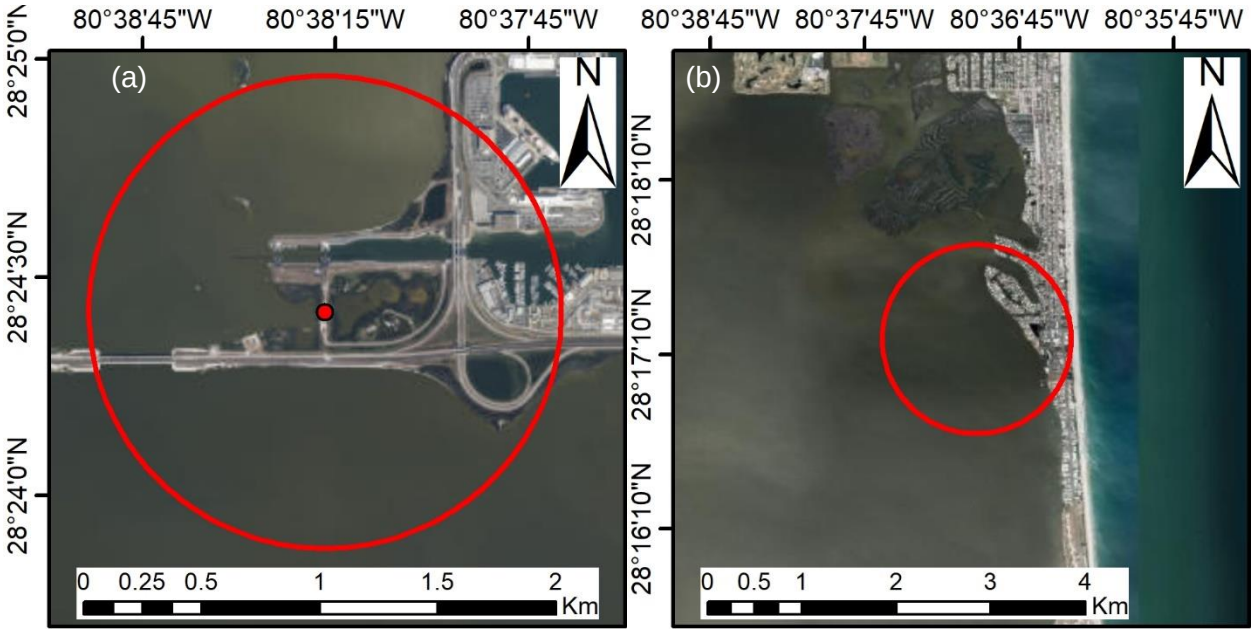

Note: Red circles show a 1-km radius around the potential pumping location and is shown for scale at the proposed reference site.

Figure 2. Proposed (a) inflow and (b) reference locations in BRL

1.3 Objectives

The objectives of this geochemical evaluation were as follows:

- Investigate temporal trends for geochemical processes (nutrient and oxygen cycling plus temperature and salinity regimes) in sediments and water near potential inflow locations. Resolve, temporally and spatially, the direct impacts of proposed inflow (seawater or Port water) on concentrations of nutrients in the lagoon, plus, calculate the quantity of nutrients that would be discharged into the coastal ocean using robust temporally resolved datasets.
- Determine how changes to temperature, salinity, and DO that could result from various levels of inflow would influence the geochemical cycling of N, P, and oxygen in lagoon water and sediments. Estimate/model the potential impacts of inflow towards indirect changes to nutrient concentrations in the lagoon.
- Temporally resolve datasets for DO and nutrients in surface and bottom water in areas pursued for permitting. Determine if data from existing water quality sensors (~0.5-1.0 m) can be extrapolated to determine conditions in the complete water column (e.g., bottom water) near proposed inflow locations. Increase spatial resolution for bottom water DO monitoring.
- Determine how inflow plus geochemical processes and changes to these processes may influence water quality conditions to favor specific groups or types of algae (nutrient stoichiometry plus temperature and salinity regimes).

2 Methods

2.1 Field Sampling

2.1.1 Water Sampling

Continuous vertical profiles for salinity, temperature, pH, oxidation reduction potential (ORP), and DO were obtained using a YSI ProDSS (Yellow Springs Instruments). The sonde was calibrated prior to each sampling event following the manufacturer's guidelines. Discrete water samples were collected using a 1.7 liter (L) horizontal Niskin water sampler (General Oceanics) that was tripped at targeted depths using a weighted messenger. Water samples were filtered immediately after collection using Whatman 0.45 micrometer (µm) polypropylene syringe filters. Additional unfiltered samples were collected for processing in the laboratory. All water samples were transported to the laboratory in a cooler on ice in the dark.

2.1.2 Sediment Sampling

Sediment samples were obtained using a 0.1 square meter (m^2) Ekman Grab that was lowered slowly from an anchored boat until it hit the bottom. This process has been observed by Self-Contained Underwater Breathing Apparatus (SCUBA) to verify collection of 10–15 centimeters (cm) of stratified sediment and overlying water (Figure 3). Any standing water was siphoned off prior to sample collection. A ~3 cm layer of surface sediments was subsampled from the grab using a clean spoon and placed in a ~55 milliliter (mL) polycarbonate vial that was then sealed with parafilm and stored on ice, in the dark for transport to the laboratory.

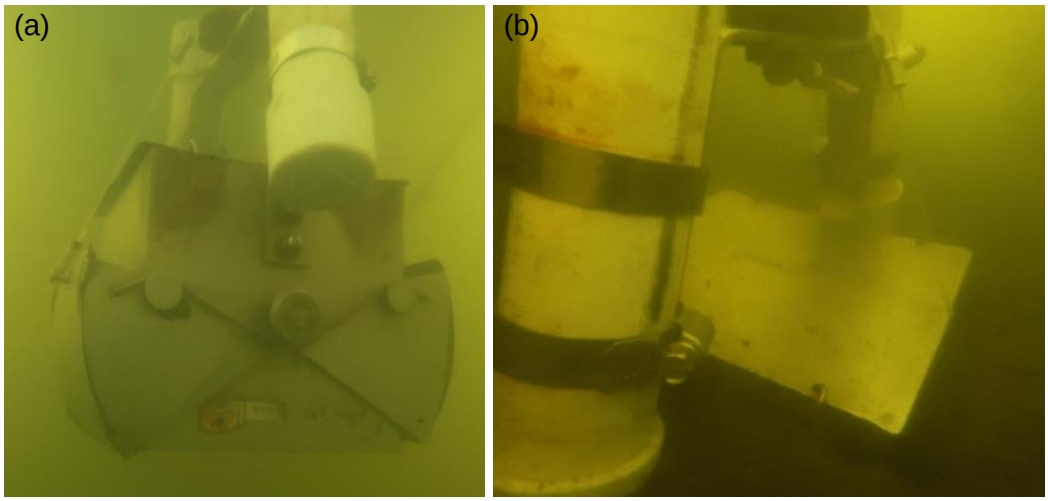

Figure 3. Ekman Grab photographed by scientist with SCUBA (a) descending through the water column and (b) settled in sediments with no visible disturbance to the sample

2.1.3 Water Column Respiration, SOD, and Nutrient Fluxes

Darkened, benthic (sediment) and "blank" chambers were used to determine fluxes of dissolved oxygen (sediment oxygen demand [SOD]) and nutrients from sediments and from suspended particles (water column respiration). Methods used in this study were developed following guidelines in a synthesis of techniques by Boynton et al. (2018). Blank chambers containing HOBO U26 Dissolved Oxygen data loggers and mechanical stirrers were rinsed and then completely filled with bottom water (**Figure 4a**). Water samples were obtained and immediately

filtered through Whatman 0.45 µm polypropylene syringe filters and stored on ice until return to the laboratory. The volume of water removed for samples was replaced with bottom water and chambers containing no air were sealed and incubated for 1.5 to 2 hours. Chambers were kept in the shade at a constant in-situ temperature for the duration of the incubation. Following the incubation period, chambers were opened, and a final water sample was extracted and immediately filtered and placed on ice for transport to the laboratory.

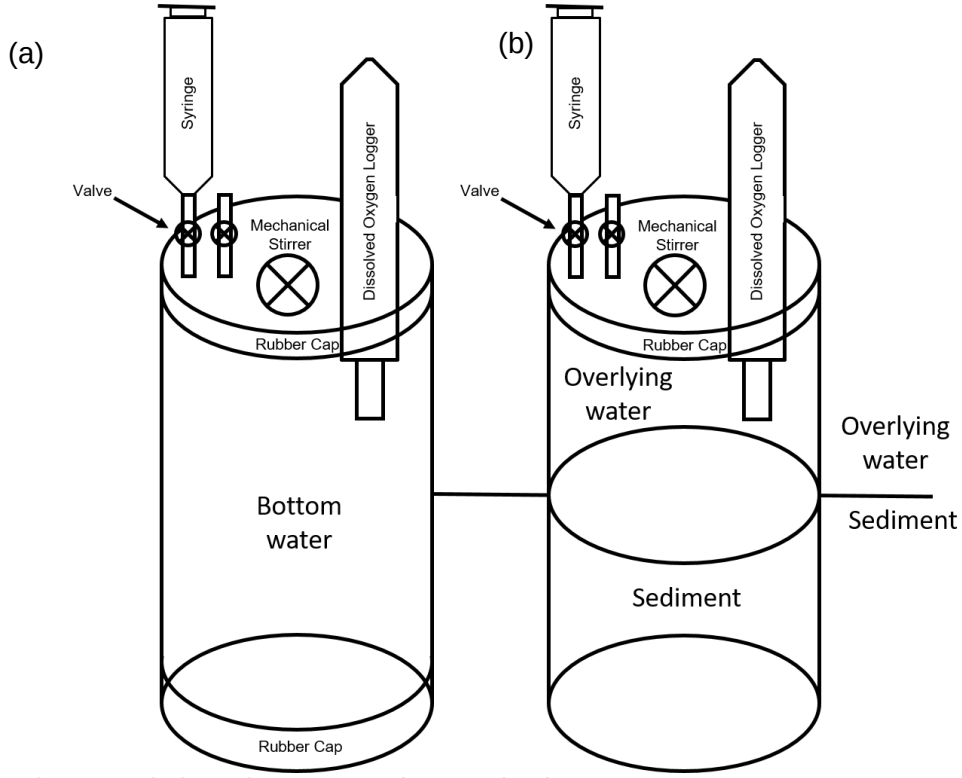

Note: Chambers are darkened to prevent photosynthesis.

Figure 4. Schematic diagram of the (a) blank and (b) benthic chambers used to determine water column respiration, SOD, and nutrient fluxes

Benthic chambers were pushed vertically into sediments without side-to-side movement to avoid creating channels that would allow water exchanges. Chambers were pushed at least 10 cm into the sediments to prevent burrowing organisms from creating channels that would allow exchange of water with the outside environment. The height of each chamber was recorded to calculate the total volume of water in each chamber (e.g., Boynton et al., 2018). Once inserted, chambers were left open to the water column for 2-5 minutes to allow particles and sediments to settle and allow water to be exchanged with undisturbed bottom water. Before sealing each chamber, water samples were obtained from inside the chamber and immediately filtered using Whatman 0.45 µm polypropylene syringe filters. Chambers were then sealed with lids containing mechanical stirrers to keep the water well-mixed and to prevent buildup of a concentration gradient in a boundary layer at the sediment-water interface. Stirrers were designed and deployed to mix the overlying water without causing sediment resuspension. HOBO U26 Dissolved Oxygen data loggers were mounted through an airtight seal in the lid of each chamber (**Figure 4b**). The rate of decline of the DO within the chamber was then measured over a 1.5 to 2-hour period for sand and for 20 to 45 minutes for mud. At the end of each deployment, a syringe was attached to a valve on the top of the chamber and a 60 mL water sample for nutrient analysis was extracted and immediately filtered and stored on ice (**Figure 5**). At the end of each deployment, a sediment

sample was obtained from inside the sediment chamber and placed in a polycarbonate vial (~55 mL) for sediment analysis.

Figure 5. Collecting water samples from a benthic chamber deployed in shallow water

Sediment cores for laboratory incubation experiments were obtained by carefully pushing core barrels vertically into the sediments to avoid creating channels or resuspending/disturbing sediments. Cores were then capped to create a vacuum, extracted from the sediment and a cork was immediately placed in the bottom of the core. Retrieved cores were then placed in a dark cooler and transported to the laboratory. If any disturbance was noted throughout the collection process, the core was discarded, and a new core was obtained. Large (at least 2 L) unfiltered water samples were collected for replacement of the overlying water at the beginning of laboratory incubation experiments and to be run as water blanks.

Continuous monitoring of bottom water DO was carried out using Onset HOBO U26 Dissolved Oxygen data loggers. Loggers deployed in polyvinyl chloride (PVC) housings equipped with copper based antifouling guards to promote reliable datasets collected over the targeted 14-30 day deployment periods. Sensor housings were designed to keep sensor faces within 10 cm of the bottom with development during Phase 1 of this project. Sensors were lab calibrated immediately before each deployment and field data was validated at the beginning and end of each deployment by comparison with data obtained using a calibrated YSI ProDSS (Yellow Springs Instruments) data sonde. Results are reported in mg/L and hypoxia has been defined as DO less than 2 mg/L.

2.2 Laboratory Analyses

2.2.1 Nutrient and Water Analyses

Concentrations of ammonium (NH_4), nitrate + nitrite (NOx), total dissolved nitrogen (TDN), orthophosphate (PO_4), total dissolved phosphorus (TDP), and silica (SiO_2) were determined using a SEAL AA3 HR Continuous Segmented Flow Autoanalyzer following manufacturer's methods. The NIST-traceable Dionex 5-Anion Standard was analyzed as a reference standard with each batch of samples to ensure accuracy; Values are consistently within the 95% confidence interval for the prepared standard. Analytical precision (relative standard deviation) for lab duplicates was <3% for nutrient analyses.

pH was determined using Hach Sension1 pH meter and an Oakton field probe. The apparatus was calibrated using a 3-point calibration immediately prior to use. Initial calibration verification was checked using a pH 7 buffer and was always better than 1%.

Turbidity was determined on unfiltered samples using a Hach 2100 turbidimeter. The turbidimeter was calibrated prior to each use and checked periodically throughout the analyses.

Concentrations of chlorophyll *a* were determined by vacuum filtering ~50 mL of homogenized water through pre-combusted Whatman 0.7 µm pore size glass fiber filters. Filters were folded and placed in polypropylene centrifuge tubes and frozen overnight to lyse cell walls. Chlorophyll *a* was extracted from filters by placing them in a 90% acetone solution at 4 degrees Celsius (°C) in the dark for at least 24 hours. Extracted chlorophyll *a* was analyzed using a Turner Designs 10-AU fluorometer (Turner Designs, San Jose, California) following methods by Welschmeyer (1994). The fluorometer was initially calibrated using a chlorophyll standard (Turner designs Part No. 10–850) and during sampling using a solid secondary standard (Turner Designs Part No. 10-AU-904).

Concentrations of chloride, sulfate and alkalinity were determined using a SEAL AQ400 discrete auto analyzer following manufacturer's methods.

2.2.2 Laboratory Incubation Experiments

Laboratory incubations were carried out in a manner consistent with previous studies (e.g., Cowan et al., 1996; Hammond et al., 2004; Boynton et al., 2018; Foster and Fulweiler 2019). Intact sediment cores were placed in temperature-controlled recirculating water baths set to approximate in-situ conditions (**Figure 6**). Incubations were set up by first removing caps used to transport cores and overlying water was siphoned off, leaving ~1 cm of overlying water to prevent disturbance of the sediment-water interface. Bottom water collected from the field site was then slowly pumped into the chamber using a floating diffuser to prevent disturbance of the sediment water interface. Water was replaced before each incubation to ensure that water quality conditions at the start of the incubation were as close to in-situ conditions as possible and to remove any nutrient accumulation that had occurred between collection of each core and the beginning of the incubation. At the beginning of each incubation, water samples (T_0) were collected from each core. Water samples were immediately filtered using Whatman 0.45 µm polypropylene syringe filters and stored in a refrigerator until analysis. The volume of water removed for the initial sample was displaced by the HOBO U26 Dissolved Oxygen data logger and the mechanical stirrer that was attached to the lid. For experiments where DO was maintained at 100%, cores were left open to the atmosphere and stirred using diffused bubbles. Cores were incubated for 18 hours with samples taken after 1.5 to 2 hours and at the end of the 18-hour incubation. For experiments were DO was manipulated, mixed gases, air and nitrogen, were bubbled into each chamber to maintain

constant DO concentrations. For experiments where salinity was manipulated, salinity was decreased by dilution using deionized water or increased using instant-ocean sea salt. For experiments where temperature was manipulated, temperatures were adjusted and controlled at ± 0.2°C using microcontroller-controlled heat baths. Following each incubation, a final water sample (T_f) was extracted, immediately filtered and stored in the refrigerator at 4˚C until analysis. With each batch of laboratory incubations, a blank chamber containing unfiltered site water was processed as described above for field incubations. Fluxes from the blank chambers were subtracted from values for chambers containing sediments in order to track water column and sediment processes independently.

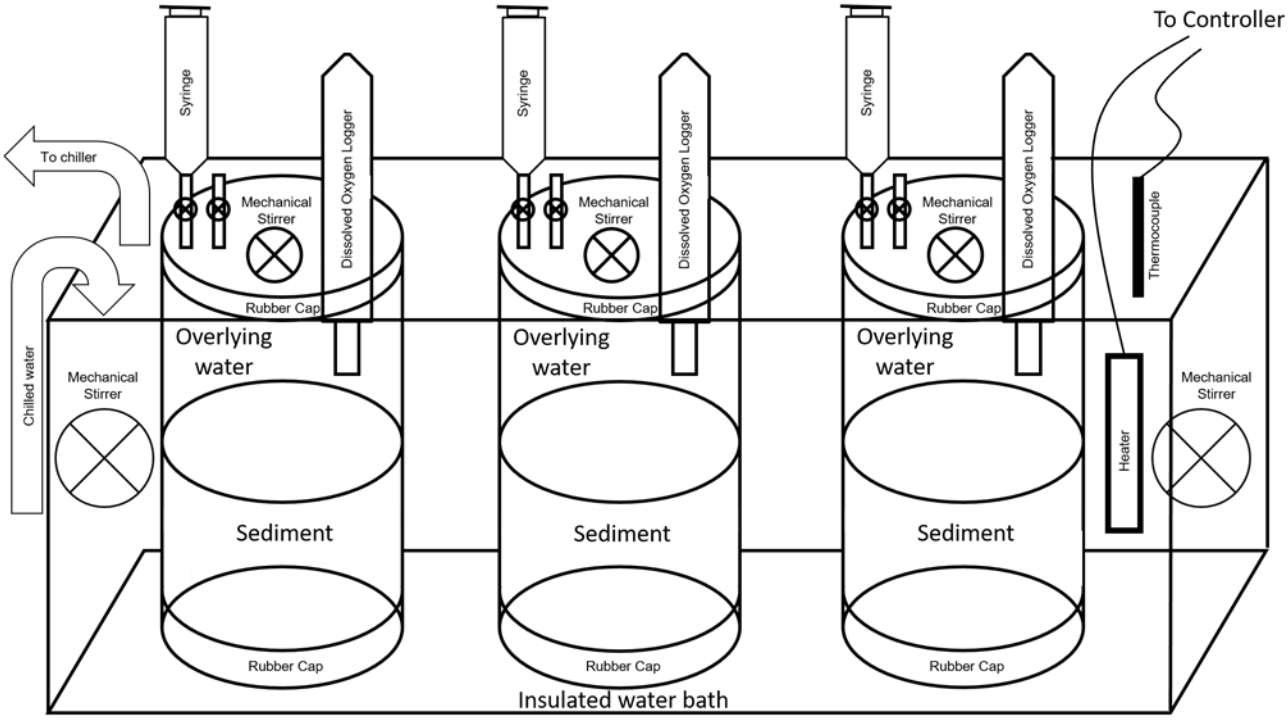

Figure 6. Schematic diagram of triplicate laboratory incubation chambers in an insulated, recirculating, temperature-controlled water bath

2.2.3 Sediment Analyses

All sediment samples were weighed, freeze dried using a Labconco FreeZone 6 system, and reweighed to determine water content. Freeze-dried samples were then powdered using a SPEX Model 8000 Mixer/Mill. Loss on Ignition (LOI) at 550˚C is determined following the method of Heiri et al. (2001). Values for LOI estimate the fraction of organic matter (OM) in the sample. Concentrations of calcium carbonate were determined by heating the sediment that had been treated for LOI at 550˚C to 950˚C following the method of Heiri et al. (2001). Average precisions for LOI and calcium carbonate (relative standard deviation) were to date, 2.0% and 1.0%, respectively.

2.3 Data and Statistical Analyses

2.3.1 Data Processing

Data and graphical analyses were carried out using Systat 12, SigmaPlot 10 (Systat Software, Inc.), Excel 2016 (Microsoft), ArcGIS (Version 10.2.2.3552, Esri, Redlands, CA), and HOBOware

Pro 3.7.17. An alpha value to define statistical significance was set at 0.05 for statistical tests and regressions. Least squares linear regressions were calculated to determine relationships between individual pairs of parameters. All correlation coefficients are presented with a corresponding *p* value. Comparisons of two independent groups of data were carried out using two-tailed t-tests assuming equal variance unless otherwise noted. Independent groups of data with *p*-values >0.05 were considered not significantly different from one another.

2.3.2 Power Analysis

Prior to the sampling effort, power analyses were carried out using G*Power 3.1 to determine minimum sample sizes required to obtain satisfactory power (0.8) for laboratory experiments showing linear regression between benthic fluxes and environmental parameters (t-test: linear regression size of slope, one group). A similar approach was used to determine the number of sites/samples required for comparison of the proposed treatment and reference areas using two-tailed tests (t-test: means, difference between two independent means). For all power analyses the α error probability was set to 0.05 and power was set at 0.8. Effects sizes were estimated from preliminary means and standard deviations.

2.3.3 Oxygen and Nutrient Flux Calculations

SOD was determined by subtracting the water column respiration (milligrams per liter per hour [mg/L/hr]) values for “blank” chambers from values obtained from benthic chambers (Ziegler and Benner 1999). The total rate of oxygen utilization by sediments, accounting for the volume in the benthic chamber [DO used by sediments (mg/L/hr) times the volume of the benthic chamber (L), calculated using the height of the chamber above the sediments] was divided by the surface area of sediment to yield values for SOD. Values for SOD are reported in micromoles per square meter per hour (µmoles/m^2/hr).

Benthic nutrient fluxes were determined from benthic and blank chambers by subtracting initial nutrient concentrations (micromolar [µM]) from final concentrations for both benthic and blank chambers. The changes in concentrations (µM) were then divided by the elapsed time (hours) of each incubation to yield rates in µM/hr. The rate of nutrient production/utilization in blank chambers was then subtracted from the rate calculated for benthic chambers, to determine the production/utilization by sediments and particles independently. The rate (µM per hour) for the benthic chamber was then multiplied by the volume of the chamber, calculated using the height of the chamber above the sediments, to yield the amount of nutrients produced/used by sediments in the chamber per hour (µmoles/hr). This value was divided by the surface area of sediments in the chamber to yield a flux in µmoles/m^2/hr consistent with units used in the literature (e.g., Boynton et al., 2018). A similar approach was used to determine nutrient fluxes from laboratory incubations. Nutrient fluxes were evaluated against the rate of oxygen utilization to ensure that linear nutrient production/utilization could be assumed. If the chamber went anaerobic during the deployment or oxygen utilization was non-linear, nutrient fluxes were flagged and not included in data interpretation.

3 Results and Discussion

3.1 Temperature, Salinity, and Density

Long-term datasets for temperature and salinity were obtained for 2015 through July 2021 from sources including St. Johns River Water Management District (SJRWMD), National Oceanic and Atmospheric Administration’s National Data Buoy Center (NDBC), Ocean Research and

Conservation Association's network of Kilroys, and a network of sensors deployed and maintained by Florida Institute of Technology (Florida Tech). Overall, the annual average lagoon temperature was ~25°C and followed seasonal patterns with a range of ~17°C, with a minimum at ~15°C typically reported during February to a maximum of ~32°C typically reported during August and September (e.g., **Table 1**).Temperatures of seawater in Port Canaveral followed similar seasonal patterns; however, minimum temperatures during winter were higher, typically at ~16°C and maximum temperatures during summer were lower, typically at ~31°C (e.g., **Figure 7**; data from multi-year analysis).

During winter 2020–2021 (Phase 2), the lowest temperature recorded near the proposed inflow location in the lagoon was 12.1°C (12/26/2020), compared to 17.1°C in Port Canaveral. Overall, average temperatures during January 2020 and February 2021 were 0.9°C and 0.6°C cooler in the lagoon relative to Port Canaveral. Based on these data plus long-term datasets, pumping during winter months could bring warmer water into the lagoon from the ocean. The lagoon also had a higher maximum temperature during summer 2020 (August) at 33.1°C, relative to 31.7°C in Port Canaveral. These data were consistent with results obtained during Phase 1 and with long-term datasets where typical spring-fall lagoon temperatures were 0.5-1.0°C warmer compared to water in Port Canaveral and adjacent coastal Atlantic Ocean.

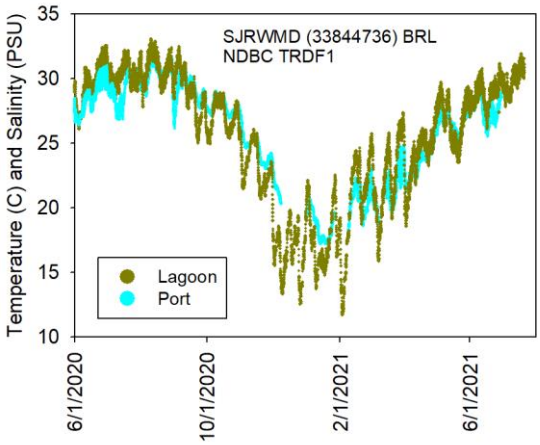

Note: Data obtained from SJRWMD site 33844736 and from NDBC site TRDF1.

Figure 7. Temperature in BRL in the area of inflow and in Port Canaveral, the proposed source of inflow water

Table 1. Average monthly temperature (°C) each month in Port Canaveral BRL in the area of inflow (2020-2021).

Location	Aug	Sep	Oct	Nov	Dec	Jan	Feb	Mar	Apr	May	June	July	Source
Trident Pier	30.3	29.1	27.8	24.6	20.0	18.5	20.5	21.3	23.5	26.6	27.6		Ndbc.noaa.gov
Banana River	30.7	28.8	26.9	23.2	16.6	17.6	19.9	22.3	23.8	26.8	28.89	30.0	sjrwmd.com/data/water-quality/

Salinity was lower in BRL compared to values for Port Canaveral. For example, during 2020–2021, salinity in BRL ranged from 16–23 practical salinity units (PSU) and, as expected, salinity in the lagoon was lower than the range of salinities obtained for seawater in Port Canaveral (27–34 PSU) (**Figure 11**). Vertical profiles for salinity in seawater from the proposed inflow location

(Port Canaveral) showed a salinity gradient with the lowest salinities in surface water at 27–32 PSU, increasing with depth to 30–34 PSU (**Figure 8**).

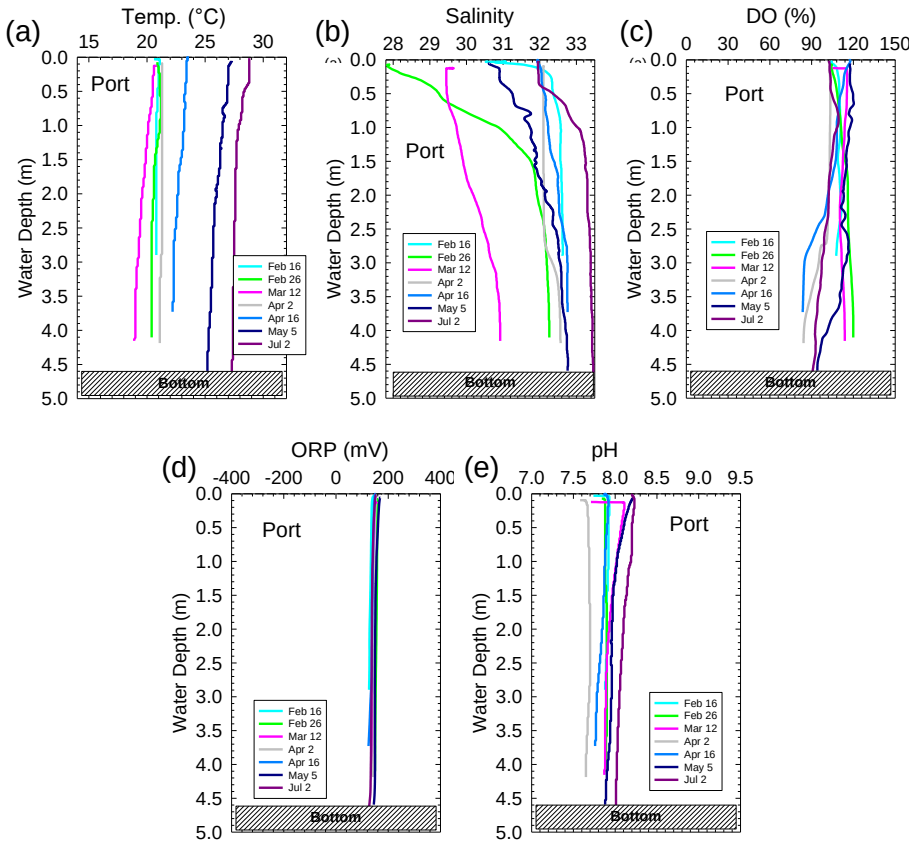

Figure 8. Vertical profiles for (a) temperature, (b) salinity, (c) DO, (d) ORP, and (e) pH in Port Canaveral during discrete sampling events

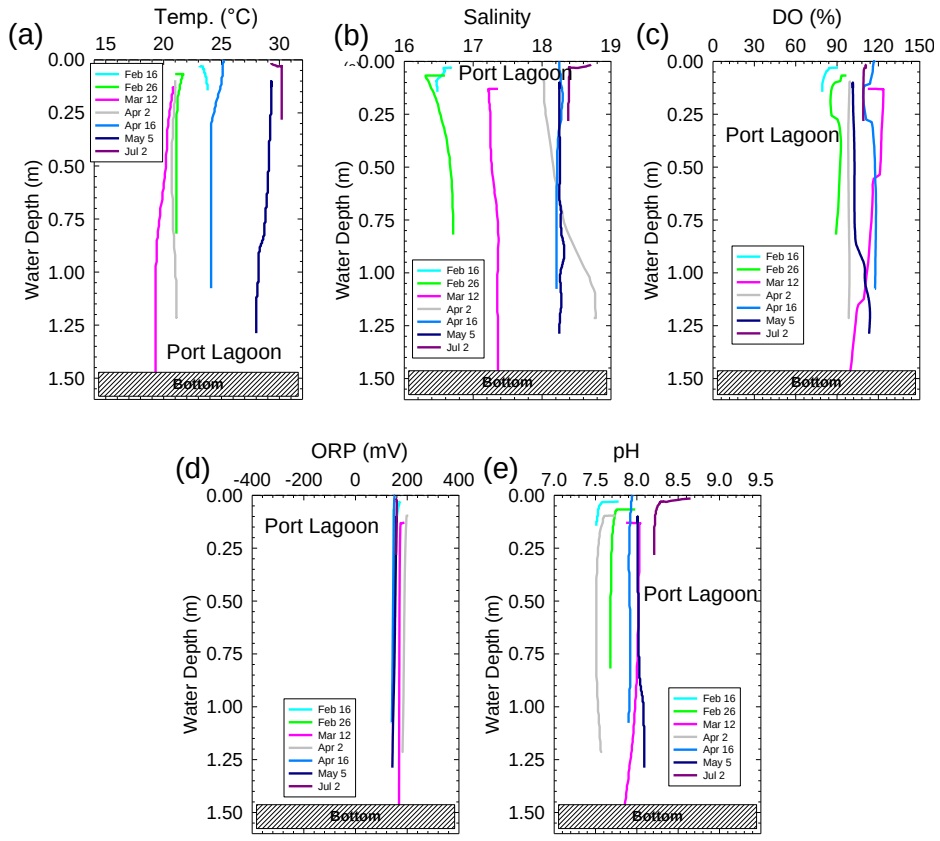

Figure 9. Vertical profiles for (a) temperature, (b) salinity, (c) DO, (d) ORP, and (e) pH in BRL at the proposed inflow location during discrete sampling events

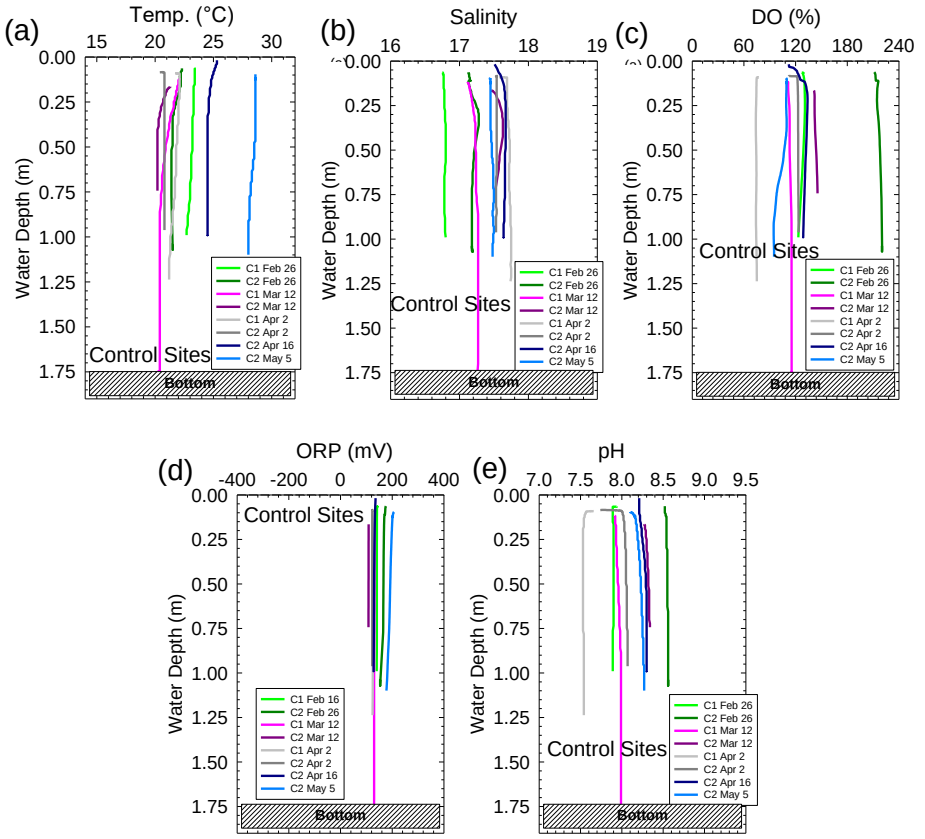

Figure 10. Vertical profiles for (a) temperature, (b) salinity, (c) DO, (d) ORP, and (e) pH in BRL in the reference/control area during discrete sampling events

Using data for temperature and salinity, the density of water was calculated as an indication of the likelihood of mixing or the degree of stratification that could occur if seawater were to be pumped into the system (**Figure 11** and **Figure 12**). Overall, consistent with lower salinity in the lagoon versus the Port, the density of water in BRL was 1,012 kilograms per cubic meter (kg/m^3) (average), 1.3% less dense than typical seawater at 1,025 kg/m^3. This seemingly small difference in density is enough to maintain discrete stratified layers and is greater than differences in density identified among existing layers observed during this study. For example, during Phase 1, discrete surface and bottom layers were identified at offshore sites based on temperature alone with densities of 1,022.9 kg/m^3 and 1,023.2 kg/m^3 for surface and bottom water respectively, a difference of only 0.03%.

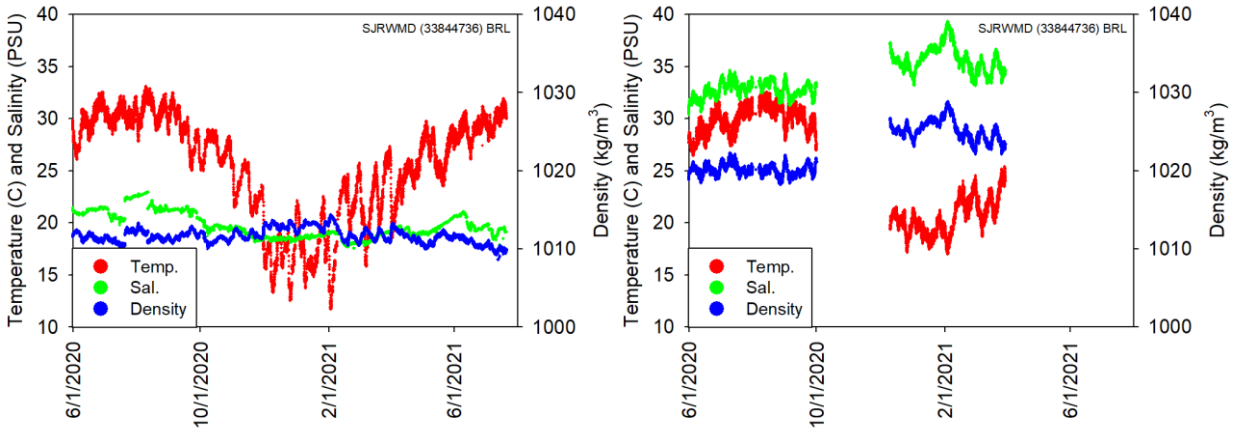

Figure 11. Temperature (red), salinity (green), and density (blue) in (a) BRL in the area of inflow and (b) in Port Canaveral

Collectively, data for temperature and salinity were used to determine the density of the two water masses (lagoon and seawater). Despite lower lagoon versus seawater temperatures during winter months, the higher salinity in the Port resulted in a higher density of seawater during the complete study (seawater density 1,018-1,028 kg/m^3 versus lagoon water density 1,008-1,016 kg/m^3, Figure 12). These data indicate that, regardless of mixing, inflow of seawater would preferentially support circulation in bottom water of the lagoon and at the sediment water interface either as a stratified layer of seawater or as a mixed water mass with a higher density than existing water in the BRL.

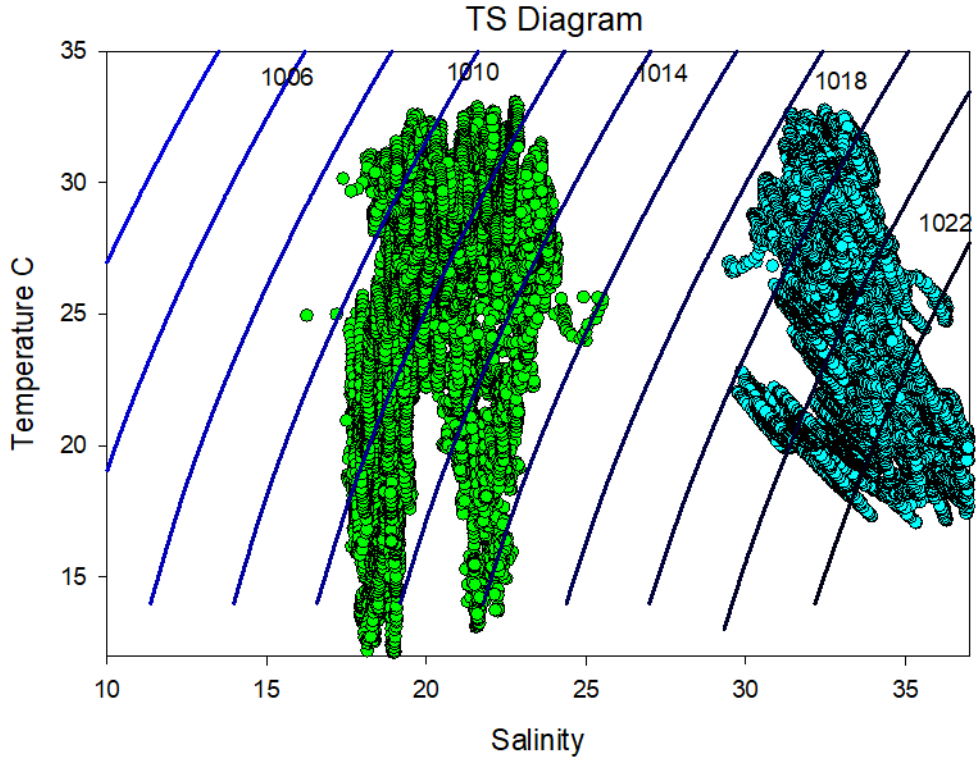

Figure 12. Temperature-salinity diagram showing data (2020–2021) from Port Canaveral (cyan on right) and the adjacent lagoon (light green on left)

Regardless the degree of mixing, inflow of seawater would stabilize temperature and salinity in the lagoon, producing slightly cooler (<<1°C) lagoon water during summer months and potentially, if inflow occurred, warmer water during winter months. Salinity would increase slightly in the area of inflow as discussed in the corresponding modeling section of the final report (**Task 1**) and concentrations of DO would likely be more stable over time.

Trends for salinity represent what can be expected based on the conservative properties of seawater. Although temperature is conservative, the shallow lagoon plus dark water and sediments are subject to more rapid heating relative to seawater, where changes to lagoon temperature may not behave conservatively. Other variables that, together with temperature and salinity, collectively describe water quality would likely experience less predictable variations as a result of inflow. For example, clearer and lower turbidity seawater typically has more stable DO. The following sections discuss how changes to the conservative properties of seawater could influence other variables. For example, a predictable quantity of nutrients (N and P) would be pumped into the lagoon via inflow and another quantity would be discharged through inlets into the coastal ocean. Simple calculations can describe a “conservative” approach to nutrients in the lagoon, and a simple estimate of the decrease in nutrient concentrations can be made. However, this approach fails to account for the non-conservative nature of nutrient geochemistry that this report addresses. For example, the standing stock of nutrients in the lagoon is based on an existing homeostasis between freshwater inputs including rainfall, tributaries, and groundwater, plus in-situ N fixation and denitrification, evaporation, point sources, legacy loads, algal and bacterial biomass and cycling, existing water quality, as well as other processes. This study addresses these non-conservative processes by studying in the field and in the laboratory how geochemical nutrient cycling responds to changes in temperature, salinity and DO, variables likely to change in response to inflow. The ability to model geochemical responses to these variables is essential not only to evaluating the impacts of enhanced ocean inflow, but these data can be used to assist in modeling how the lagoon will respond to changes in temperature and rainfall associated with climatic changes over time.

3.2 Dissolved Nutrients

3.2.1 Concentrations and Speciation

Data obtained during this study complement existing long-term datasets for nutrient concentrations in the IRL. Collectively, these data were used to further evaluate potential impacts of inflow on nutrient concentrations in the IRL by modeling the quantity of nutrients that would be removed through natural geochemical processes promoted by inflow relative to the quantity of nutrients that would likely be discharged through inlets to the coastal ocean.

To that end, nutrient concentrations (Phase 2) were monitored through discrete sampling in Port Canaveral, the proposed source of inflow water discussed in the accompanying engineering and modeling report (**Task 1**). Nutrients were also monitored (Phase 2) in BRL near the proposed inflow location (Lagoon Inflow) and at a reference/control site south of the Minutemen Causeway in an area where models showed little impact from the proposed inflow based on conservative tracers (numerical dye) (**Table 2**; locations shown in **Figure 2**).

Overall, concentrations of dissolved nutrients in Port Canaveral were relatively low, with average concentrations of TDN, TDP, and SiO_2 at 23 ± 10 µM, 0.37 ± 0.19 µM, and 11.9 ± 9.9 µM, respectively. Consistent with data from Phase 1, no significant vertical trends were observed for TDN, TDP, SiO_2, or speciation in Port Canaveral (**Figure 13**).

Concentrations of dissolved nutrients in the lagoon were more variable compared to values for seawater from Port Canaveral, as shown using both discrete sampling events during this study (Phases 1 and 2) and long-term datasets (**Table 2**). Despite variability, trends for increases and decreases in nutrient concentrations over time tracked one another at the lagoon inflow and lagoon reference sites, suggesting that without treatment, these sites follow the same regional trends and that these sites are reasonable for future comparisons during the proposed pilot study. Overall, during this study, TDN, TDP, and SiO_2 at lagoon inflow site averaged 127 ± 39 µM, 1.3 ± 0.76 µM, and 24 ± 50 µM, respectively, relative to 113 ± 29 µM, 1.2 ± 0.68 µM, and 42 ± 50 µM, respectively at the reference/control site. Collectively, concentrations of TDN, TDP, and SiO_2 in lagoon samples were (119 ± 35 µM TDN, 1.2 ± 0.71 µM TDP, and 34 ± 51 µM SiO_2) 5-fold, 3-fold, and 3-fold higher, respectively, than values for seawater from Port Canaveral; no significant difference was identified for concentrations at the proposed inflow versus control sites (**Table 1**). Reflecting on results from Phase 1, seawater at 10-m isobaths located 1-2 km offshore were 8 ± 2.4 µM TDN, 0.15 ± 0.05 µM TDP, and 3 ± 1 µM SiO_2, which are 15-fold, 8-fold and 1.4-fold lower than values for our lagoon samples.

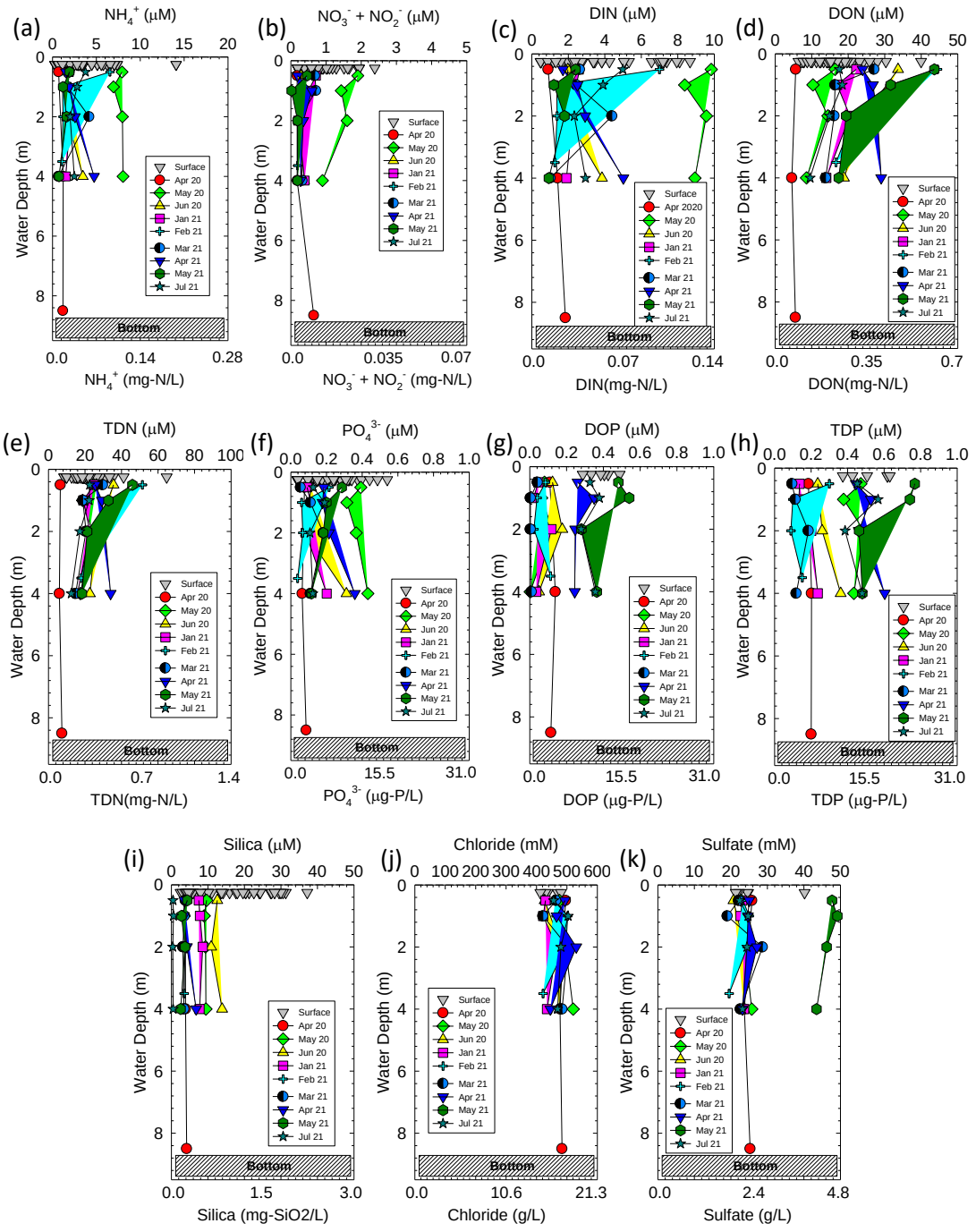

Note: Red dots from April 20 showing values from 1-2 km offshore at the 10-m isobath.

Figure 13. Vertical profiles for (a) dissolved NH_4, (b) dissolved NO_x, (c) dissolved inorganic nitrogen (DIN), (d) dissolved organic nitrogen (DON), (e) TDN, (f) dissolved PO_4, (g) dissolved organic phosphorus (DOP), (h) TDP, (i) dissolved SiO_2, (j) chloride, and (k) sulfate in Port Canaveral

Table 2. Average nutrient concentrations for samples from the (1) lagoon reference site (n=17), (2) lagoon inflow site (n = 11), and (3) in Port Canaveral (n = 77).

Site	NH_4 (µM)	NOx (µM)	TDN (µM)	DIN (µM)	DON (µM)	PO_4 (µM)	TDP (µM)	DOP (µM)	SiO_4 (µM)	Chloride (mM)	Sulfate (mM)	Alkalinity (mg/L)
Lagoon Reference	8.1 ± 11.7	1.1 ± 1.1	112 ± 21.2	9.2 ± 12.2	103 ± 10.4	0.25 ± 0.14	1.00 ± 0.34	0.8 ± 0.29	32 ± 31	238 ± 19	11.8 ± 0.8	74 ± 10.6
Lagoon Inflow	16 ± 24	0.5 ± 0.2	138 ± 47.9	17 ± 24	121 ± 42	0.35 ± 0.38	1.5 ± 0.9	1.2 ± 0.6	48 ± 86	251 ± 29	12.3 ± 1.6	79 ± 31
Port	3.0 ± 2.5	1.6 ± 5.1	23 ± 10	4.6 ± 5.5	18.5 ± 9.5	0.20 ± 0.11	0.37 ± 0.19	0.20 ± 0.16	11.9 ± 9.9	516 ± 137	26.3 ± 7.8	67.5 ± 6.7
Ocean (year1)	0.9 ± 0..2	0.3 ± 0.1	8 ± 2.4	1.2 ± 0.3	6.8 ± 2.4	0.06 ± 0.02	0.15 ± 0.05	0.09 ± 0.04	3 ± 1	466 ± 25	24 ± 2	69 ± 4

Differences in TDN and TDP between Port and lagoon samples were accompanied by variations in nutrient speciation. For example, in Port Canaveral, NH_4, NOx, and organic N accounted for, on average, 15%, 3%, and 82% of the TDN, respectively. Data from N speciation in Port Canaveral were consistent with data for the coastal Atlantic Ocean obtained during Phase 1 at 15% NH_4, less than 4% NOx, and 81% organic N. In the lagoon, a larger fraction of the TDN was present as organic N, with NH_4, NOx, and organic N accounting for, on average, 6%, less than 1%, and 93% of the TDN, respectively (8%, less than 1%, and 92% respectively, in the inflow area; and 5%, 1%, and 94%, respectively, in the reference area). These data were consistent with trends observed for long-term datasets in the IRL (e.g., SJRWMD). Higher concentrations of NH_4, especially relative to NOx, are known to stimulate blooms of *Aureoumbra lagunensis* and other harmful algal species and large fractions of the TDN present as organic N indicate rapid recycling (e.g., Liu et al., 2001).

Overall, PO_4 and organic P accounted for 55% and 45% of the TDP in Port Canaveral (38% and 62% of the TDP at offshore sites during Phase 1) relative to 19% and 81% in the open lagoon (14% and 86% at the inflow area and 22% and 78% in the reference/control area). Differences in speciation among locations influence bioavailability as discussed below.

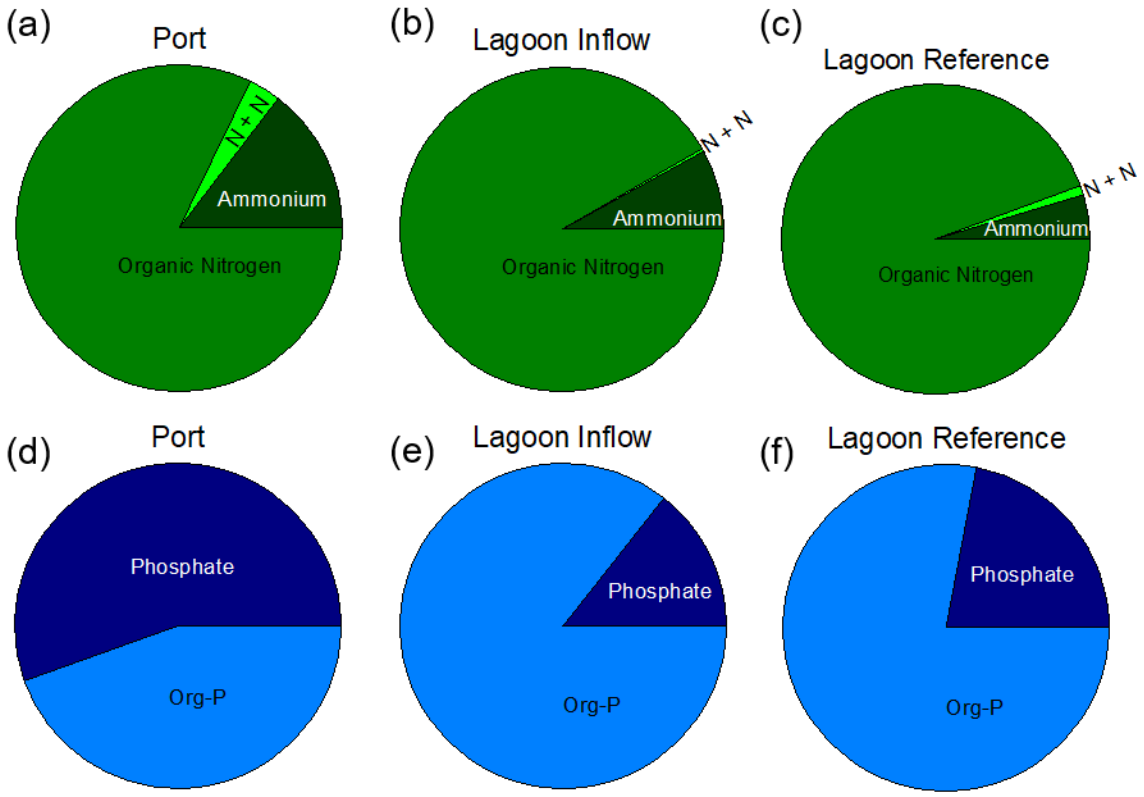

Figure 14. Pie diagrams showing the percent NH_4, percent NO_x, and percent organic N in (a) Port Canaveral, (b) BRL at the proposed inflow location, and (c) south of Minutemen Causeway in the proposed reference/control area and the percent PO_4 and percent organic P in the water column in (a) Port Canaveral, (b) BRL at the proposed inflow location and (c) south of Minutemen Causeway in the proposed reference/control area

3.2.2 DIN:DIP, TDN:TDP, N:P:SiO2 Ratios (Current/Historical)

Although total nutrient concentrations are frequently used as an indicator of the eutrophic state of an estuary, speciation and the relative abundance of bioavailable species of N:P:SiO_2 have consistently been shown to contribute to algal community composition, whereby at the same total concentrations, shifts in speciation, and the relative abundance of N:P:SiO_2 can favor shifts from beneficial or less harmful photosynthesizers (e.g., seagrasses) to harmful species (e.g., *Aureoumbra lagunensis*) or vice versa (e.g., Choudhury and Bhadury 2015). A basis for evaluating N:P ratios originated with Redfield in the 1930s (Redfield 1934) and this traditional N:P ratio at 16:1 has been utilized over decades and, in some cases, expanded to include other macro or micronutrients (e.g., Choudhury and Bhadury 2015). For example, many studies now include SiO_2 due to its importance for diatom growth. P is used as cellular energetic currency and in ribosomal ribonucleic acid N and SiO_2 are utilized as a structural components of hard parts (SiO_2 tests) and proteins whereby changes to N:P and N:SiO_2 ratios can promote one species versus another based on differences in metabolic and growth requirements (Harris 1986). Ratios have classically focused on nutrient species that are readily bioavailable, in other words: NH_4 + NOx (DIN) versus PO_4 (SRP). More recently, several species of harmful algae, including *Aureoumbra lagunensis,* the brown tide species in the IRL, have been identified to use organic N and organic P (Liu et al., 2001). In addition to the ability to use organic N and organic P, species such as *Aureoumbra lagunensis* are not able to use nitrate, complicating interpretations of water quality

based on N:P. To provide a more complete picture, data are presented here for both DIN:SRP and TDN:TDP.

Overall, DIN:SRP ratios varied among sample locations; for example, DIN:SRP in Port Canaveral averaged 20 ± 10 (median 22), consistent with ratios identified offshore during Phase 1 (offshore DIN:SRP = 20) and with ratios previously identified for the coastal Atlantic Ocean (Cavender-Bares et al., 2001; Martiny et al., 2014). The average ratio in seawater was more than 2-fold lower than the average DIN:SRP ratio of 45 ± 56 for lagoon water; however, it was consistent with the median at 19 for lagoon samples during this study. The ratio for lagoon water during Phase 2 was higher than the average ratio identified during Phase 1 sampling; this difference was at least partially explained by sampling at predominantly northern sites during Phase 2. Higher N:P ratios in the northern lagoon were consistent with a trend identified during Phase 1 and supported by results from Lapointe et al. (2020) showing a similar north-south pattern for the N:P ratios in seagrasses. Despite north-south trends that Lapointe et al. (2020) identified for seagrasses (beneficial photosynthesizers) each species in their study had a relatively narrow range of N:P (*S. filiforme*, *T. testudinum* and *H. wrightii* range) and large differences in N:P have been shown to drive change in the composition of photosynthesizers (e.g., seagrasses versus algae, Hillebrand et al., 2013).

Ratios of TDN:TDP were higher than values for DIN:SPR discussed above. In Port Canaveral, TDN:TDP averaged 97 ± 75 (median 62) relative to 113 ± 46 (median 110) in the lagoon (119 ± 47 inflow and 109 ± 44 control). These data reflect the larger fraction of TDN relative to P that is present in less bioavailable, organic forms. Traditionally these organic nutrients have not been considered bioavailable; however, many small bloom-forming algae can utilize the organic forms of both N and P (Liu et al., 2001). High ratios of TDN:TDP are known to enhance the risk for *Aureoumbra lagunensis* blooms (Liu et al., 2001; DeYoe et al., 2007) whereby, some cyanobacteria and HAB dinoflagellates can store P within their cells helping to promote their taxa when P is otherwise limiting (e.g., Hillebrand et al., 2013; Burford et al., 2014; Willis et al., 2015; Glibert et al., 2012; Accoroni et al., 2016).

In effort to understand functional reasons behind the Redfield ratio, other studies have identified optimal $N:P_{opt}$ (molar) ratios (where limitation switches from N to P) for different groups of algae. For example, Hillebrand et al. (2013) reported the lowest $N:P_{opt}$ for diatoms at 14.9 increasing to 15.1 for dinoflagellates, 25.8 for cyanobacteria, and 27.0 for chlorophytes. At high N:P ratios, diatoms which would generally be considered a fast-growing can be outcompeted by species, such as dinoflagellates, cyanobacteria, and chlorophytes, that have a higher optimal N:P ratios and are more frequently HAB-forming (Phlips et. al., 2010). In the lagoon, high N:P ratios are preferred by HAB species such as *Pyrodinium bahamense var. bahamense, Aureoumbra lagunensis* and *Akashiwo sanguinea*, which are commonly encountered in the northern IRL where muck and organic-rich sediments are prominent (e.g., Foster et al., 2018; **Figure 15**). Muck further promotes the dominance of HAB species by preferentially releasing ammonium, the preferred form of nitrogen of many harmful phytoplankton species, including *Pyrodinium bahamense var. bahamense* (e.g., Liu et al., 2001).

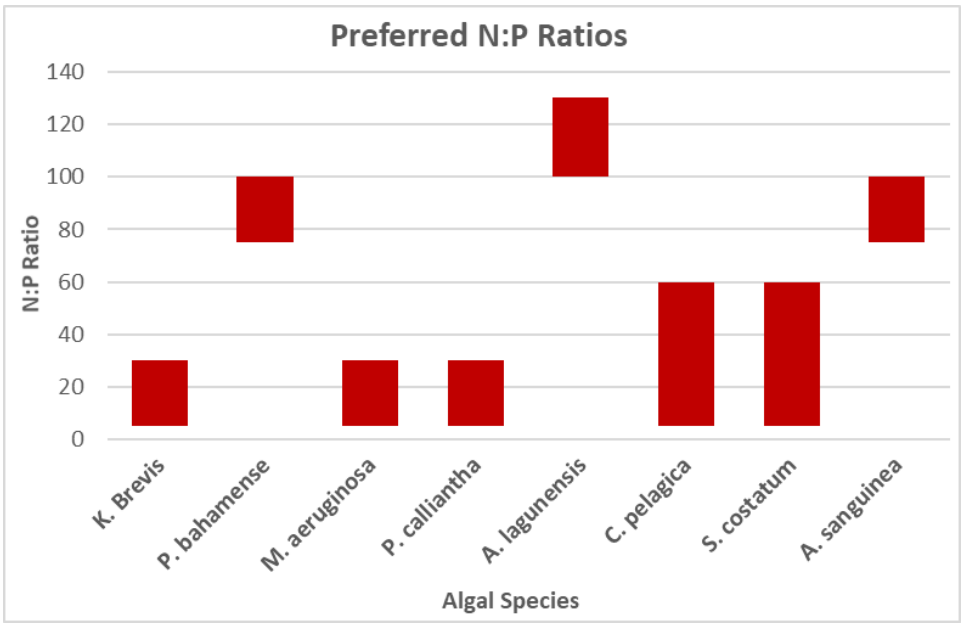

Figure 15. Preferred N:P ratios of selected algal species found in the IRL: *K. brevis* (Vargo et. al, 2008), *P. bahamense* (Azanza et. al., 2004), *M. aeruginosa* (Smith et. al., 1983), *P. calliantha* (Guo et. al., 2017), *A. lagunensis* (Liu et. al., 2001), *C. pelagica* (Hauss et. al., 2012), *S. constatum* (Maso and Garces, 2006), and *A. sanguinea* (Chen et. al., 2019)

Based on global trends plus data from this study and long term datasets, potential shifts in N:P ratios (DIN:SRP and TDN:TDP and perhaps other N:P ratios) should be considered a component of overall water quality and should be a consideration for modeling and predicting algae blooms and bloom composition (Hillebrand et al., 2013). Based on the importance of N:P ratios towards promoting certain algal groups, restoration efforts, including inflow, should be viewed not only as removing N or P but as regulating the ratio of these elements. Based on data for water in Port Canaveral or the coastal Atlantic Ocean, inflow water had both lower concentrations of nutrients and lower ratios of both DIN:SRP and TDN:TDP, relative to values in the lagoon.

3.2.3 Nutrients Exchanges Based on Standing Stocks Assuming Conservative Behavior (Direct Discharges)

Nutrient concentrations determined for the lagoon during this study were not significantly different from long-term averages using data from SJRWMD. Nevertheless, to use the most robust dataset available, 5-year averages (2016–2021) for nutrient concentrations at sites near Sebastian Inlet were used to calculate discharges (metric tons/year) to the coastal ocean based on various levels of inflow (**Table 3** and **Table 4**). These estimates do not account for nutrients that would be removed from the system via geochemical processes and therefore not discharged to the coastal ocean. A comparison of net discharges and geochemical removal is discussed in detail in **Section 3.3**. Based on a proposed pilot pumping rate of 0.5 cubic meters per section (m^3/sec) at the northern lagoon site (lagoon inflow), 4.3 x 10^8 L of lagoon water is expected to be discharged through inlets per day, or 1.6 x 10^{10} L per year (**Table 4**). Based on these data, an annual discharge of nutrients through inlets to the coastal Atlantic Ocean associated with the pilot project (0.5 m^3/sec) is calculated at approximately 6.5 metric tons of N and 0.6 metric tons of P per year (**Table 4**). The discharge (0.5 m^3/sec) of dissolved nutrients is equal to about 0.5% and 0.4% of the annual total estimated inputs of N (1,400 tons/year) and P (140 tons/year) to IRL/BRL system per year, respectively (Brevard County Save Our Indian River Lagoon Project Plan 2020 Update).

Using average nutrient concentrations from **Table 3,** plus an average lagoon depth of 1.5 m and a surface area for the BRL at 170 km^2 and 270 km^2 in the northern IRL, standing stocks of N and P are estimated at about 300 and about 30 metric tons, respectively. Overall, maximum annual discharges from the pilot study would be equal to about 2% of the standing stock of N and 2% of P currently in the lagoon. The relatively small direct removal of N and P of the pilot project is expected because the pilot study is intended to treat only a small area in the lagoon as a test of this technique and to validate data and models so impacts of a full-scale system could be more accurately modeled. Also, enhanced circulation is aimed at restoring natural ecosystem services (biogeochemical processes) that will remove/sequester nitrogen and phosphorus whereby direct discharges are ideally a secondary result.

Table 3. Nutrient concentrations (5-year running averages) at stations near Sebastian Inlet (IRLI28) and Fort Pierce Inlet (IRLIRJ08) plus data from this study.

Location	NH_4 (mg/L)	NOx (mg/L)	DIN (mg/L)	Organic N (mg/L)	TDN (mg/L)	PO_4 (mg/L)	TDP (mg/L)	DOP (mg/L)
Sebastian (IRLI28)	0.03 ± 0.03	0.01 ± 0.03	0.04 ± 0.06	0.37 ± 0.17	0.41 ± 0.23	0.01 ± 0.01	0.04 ± 0.02	0.025 ± 0.008
Banana River (IRLB04)	0.05 ± 0.1	0.02 ± 0.03	0.07 ± 0.14	1.01 ± 0.12	1.08 ± 0.26	0.01 ± 0.01	0.03 ± 0.02	0.015 ± 0.003
Open Lagoon (This Study)	0.12 ± 0.20	0.01 ± 0.01	0.13 ± 0.20	1.5 ± 0.4	1.7 ± 0.5	0.01 ± 0.01	0.04 ± 0.02	0.03 ± 0.01
Port (This Study)	0.04 ± 0.04	0.02 ± 0.07	0.06 ± 0.08	0.26 ± 0.13	0.32 ± 0.14	0.01 ± 0.00	0.01 ± 0.01	0.01 ± 0.00

Table 4. Maximum tons of N and P that would be discharged to the coastal ocean per year from Sebastian Inlet, associated with various levels of inflow if no geochemical removal occurred.

Pumping Rate	L/day	L/year	NH_4 (tons/ year)	NOx (tons/ year)	DIN (tons /year)	Organic N (tons/ year)	TDN (tons/ year)	PO_4 (tons/ year)	TDP (tons/ year)	DOP (tons/ year)
0.5 m^3/sec	$4.3*10^7$	$1.6*10^{10}$	0.5	0.2	0.63	5.8	6.5	0.2	0.6	0.39
2.5 m^3/sec	$2.2*10^8$	$7.9*10^{10}$	2.4	0.8	3.2	29	32	0.8	3.2	2.0
5 m^3/sec	$4.3*10^8$	$1.6*10^{11}$	4.8	1.6	6.4	59	66	1.6	6.4	4
10 m^3/sec	$8.6*10^8$	$3.2*10^{11}$	9.6	3.2	12.8	118	131	3.2	12.8	8
15 m^3/sec	$1.3*10^9$	$4.7*10^{11}$	14.1	4.7	18.8	174	193	4.7	18.8	11.8
20 m^3/sec	$1.7*10^9$	$6.3*10^{11}$	18.9	6.3	25.2	233	258	6.3	25.2	15.8

Table 5. Tons of N and P that would be brought into the lagoon associated with various levels of inflow.

Pumping Rate	L/day	L/year	NH4 (tons/ year)	NOx (tons/ year)	DIN (tons/ year)	Organic N (tons/ year)	TDN (tons/ year)	PO4 (tons/ year)	TDP (tons/ year)	DOP (tons/ year)
0.5 m^3/sec	$4.3*10^7$	$1.6*10^{10}$	0.69	0.14	0.82	4.18	5.00	0.10	0.18	0.00
2.5 m^3/sec	$2.2*10^8$	$7.9*10^{10}$	3.43	0.70	4.12	20.94	25.06	0.52	0.91	0.02
5 m^3/sec	$4.3*10^8$	$1.6*10^{11}$	6.96	1.42	8.34	42.41	50.75	1.06	1.84	0.03
10 m^3/sec	$8.6*10^8$	$3.2*10^{11}$	13.91	2.84	16.68	84.81	101.50	2.12	3.68	0.06
15 m^3/sec	$1.3*10^9$	$4.7*10^{11}$	20.43	4.18	24.51	124.57	149.08	3.11	5.40	0.09
20 m^3/sec	$1.7*10^9$	$6.3*10^{11}$	27.39	5.60	32.85	166.98	199.83	4.17	7.24	0.12

Because inflow would create an exchange of water, nutrients brought from the coastal ocean into the lagoon should be subtracted from discharge estimates to determine net removal from the lagoon and a net discharge into the ocean (not accounting for removal by decreased fluxes).

Using the proposed pilot pumping rate of 0.5 m^3/sec at the northern lagoon site (lagoon inflow), approximately 5.0 metric tons of N and 0.2 metric tons of P would be brought into the lagoon per year (**Table 5**). Based on these calculations, the net discharge (out minus in) of nutrients to the coastal ocean would be 1.5 metric tons of N and 0.4 metric tons of P per year during the pilot study. The direct discharge of nutrients would be greater if inflow water was obtained from offshore as reflected in data obtained during Phase 1 for sites both offshore and in Port Canaveral (**Table 2**). The comparison of standing stock (300 and 30 metric tons of N and P, respectively) relative to inputs (1,400 tons N/year and 140 tons P/year) illustrates the relative importance of geochemical nutrient cycling, where small changes to cycling can have large impacts on concentrations of bioavailable nutrients. Based on these data and calculations, the entire standing stock of nutrients in the lagoon is replaced ~5-times per year by inputs included in current models including point sources, atmospheric deposition, stormwater runoff, groundwater seepage (baseflow), and internal inputs from muck.

Table 6. Tons of N and P that would be pumped into the lagoon associated with pumping seawater from offshore at various pumping rates (based on data from Phase 1).

Pumping Rate	L/day	L/year	NH_4 (tons/ year)	NOx (tons/ year)	DIN (tons/ year)	Organic N (tons /year)	TDN (tons/ year)	PO_4 (tons/ year)	TDP (tons/ year)	DOP (tons/ year)
0.5 m^3/sec	$4.3*10^7$	$1.6*10^{10}$	0.2	0.1	0.3	1	2	0.02	0.08	0.04
2.5 m^3/sec	$2.2*10^8$	$7.9*10^{10}$	1.0	0.3	1.3	5	9	0.1	0.4	0.2
5 m^3/sec	$4.3*10^8$	$1.6*10^{11}$	2.1	0.6	2.7	11	18	0.3	0.7	0.4
10 m^3/sec	$8.6*10^8$	$3.2*10^{11}$	4.2	1.2	5.4	21	36	0.6	1.4	0.9
15 m^3/sec	$1.3*10^9$	$4.7*10^{11}$	6.2	1.7	7.9	31	52	0.8	2.1	1.3
20 m^3/sec	$1.7*10^9$	$6.3*10^{11}$	8.3	2.3	10.6	42	70	1.1	2.8	1.8

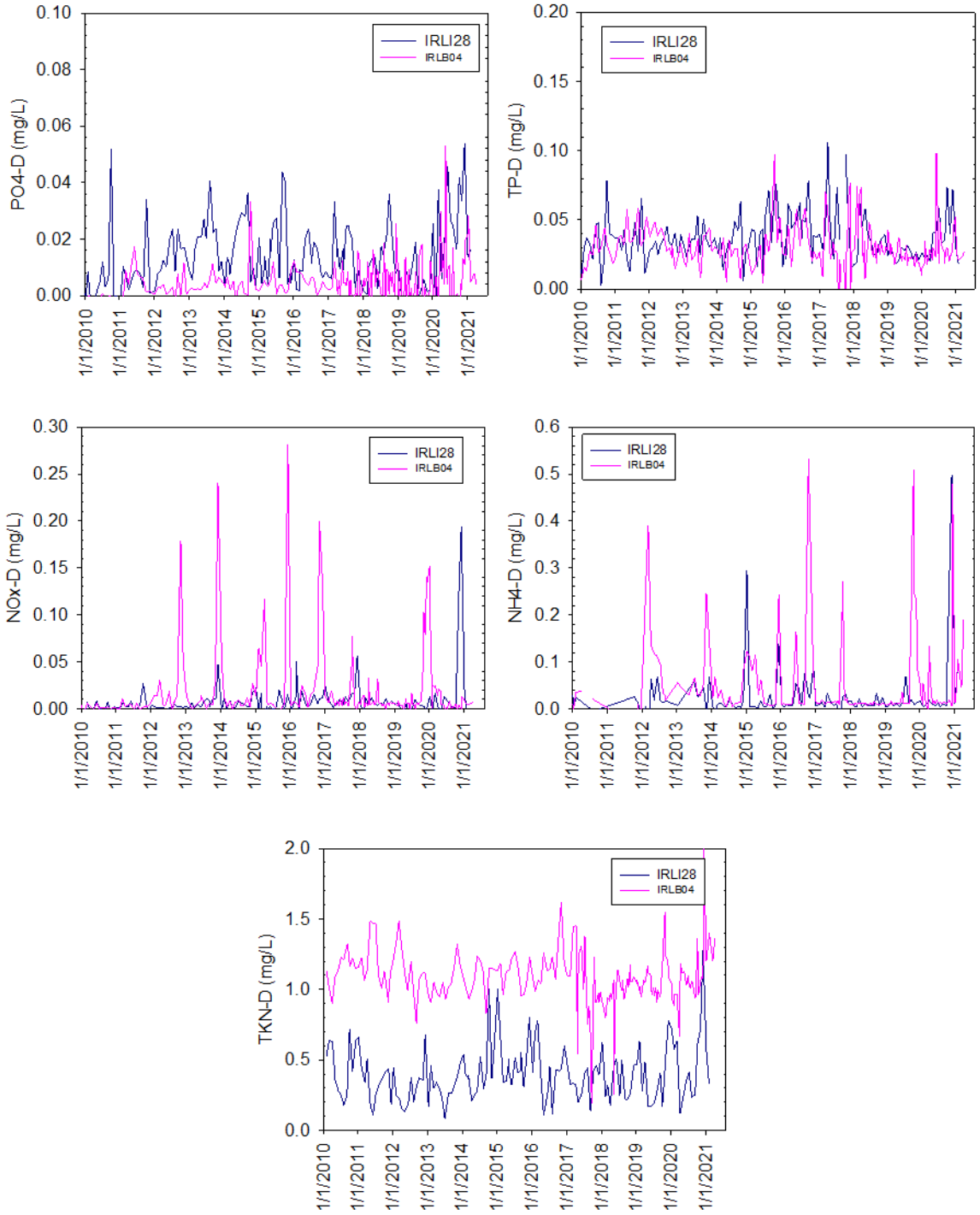

Note: Data obtained from SJRWMD.

Figure 16. Concentrations of (a) dissolved PO_4, (b) TDP, (c) NOx, (d) NH_4, and (e) total Kjeldahl nitrogen at sites near Sebastian Inlet (IRLI28) and the proposed inflow location (IRLIB04)

3.3 Geochemical Nutrient Cycling (In-situ)

Due to the non-conservative nature of nutrients and strong benthic-pelagic coupling in shallow estuarine systems, processes in sediments and on particles make it difficult to estimate how the combined inflow and discharges (net discharge) of nutrients from the lagoon associated with inflow would change concentrations and ratios of nutrients in lagoon water over time. To address these complex geochemical processes, nutrient and oxygen cycling were investigated in water from Port Canaveral and from the lagoon at the inflow and reference sites and in laboratory experiments to investigate how changes to temperature, salinity, and DO might influence geochemical nutrient cycling in the water column and sediments. Results from these investigations are presented here first in **Section 3.3.1** discussing water column cycling and then in **Section 3.4.1** discussing sediment processes and finally a synthesis is presented in **Section 3.5.**

3.3.1 In-situ Water Column Processes

Water column respiration (dark) in the IRL was highly variable and consumed oxygen at 0.19 ± 0.15 mg/L/hr. In Port Canaveral, water column respiration (dark) was ~30% lower at 0.12 ± 0.09 mg/L/hr (**Figure 17**). Overall, water column respiration (dark) in the lagoon accounted for 50->80% of the total respiration (sediments + water) and is a major contributor to hypoxia or anoxia, when it occurs (**Table 7**). The importance of water column processes are captured by our continuous dissolved oxygen data at the proposed inflow location and in Port Canaveral, where high rates of SOD and water column respiration lead to large diurnal fluctuations in DO concentrations in the lagoon, with lower magnitude diurnal cycles in seawater from Port Canaveral (e.g., **Figure 38**).

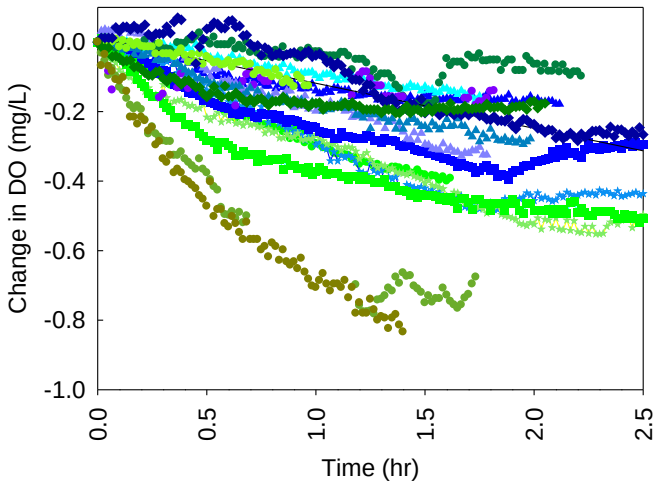

Note: Seawater samples are depicted as triangles in shades of blue, lagoon samples are depicted as circles in shades of green.

Figure 17. Change in DO over time for water incubated in the dark at in-situ conditions

Table 7. Rates of water column respiration and SOD and the relative importance of sediments towards total respiration for varying water depths (per 1m^2 of lagoon). Calculated using average rates of water column respiration (-0.19 mg/L/hr) and SOD (~3000 µmoles/m^2/hr = ~100 mg/m^2/hr) from sandy sediment.

Depth	DO consumed by sed (mg/m^2/hr)	Water volume / m^2 (L)	DO consumed by water (mg/hr)*	% consumed by sediments
0.5	100	500	95	51
1.0	100	1,000	190	34
1.5	100	1,500	285	26
2.0	100	2,000	380	21
2.5	100	2,500	475	17

Water column respiration (dark conditions) is accompanied by increased nutrient concentrations (particle fluxes). Incubations carried out under dark conditions show how respiration and decomposition of particles in the water column influence dissolved nutrient concentrations. Previous studies have shown that these dark processes are relatively well matched, but opposite during light experiments to maintain nutrient concentrations over time (Ziegler and Benner, 1999). In that context, results presented here should be viewed as an indication of recycling rates and how exchanges of particles during inflow may influence concentrations of dissolved nutrients over time. In the lagoon, NH_4, nitrate, DIN, organic N, and TDN (dark conditions) increased by (median ± standard error) 0.05 ± 0.43 µM/hr, 1.8 ± 7.1 µM/hr, 1.9 ± 6.9 µM/hr, 4.6 ± 3.8 µM/hr and 6.5 ± 10 µM/hr, respectively (**Table 8** and **Figure 18**). Releases of N associated with water column respiration in BRL were 2-4 times higher than particle fluxes from seawater in Port Canaveral with median values at 0.01 ± 0.9 µM/hr, 0.95 ± 1.9 µM/hr, 0.96 ± 2.0 µM/hr, 1.4 ± 6.0 µM/hr, and 2.4 ± 6.8 µM/hr for NH_4, nitrate, DIN, organic N, and TDN respectively (**Table 8**). Releases of P from water column respiration were similar in BRL and Port Canaveral (PO_4 0.03 ± 0.03 µM/hr in the lagoon relative to 0.03 ± 0.12 µM/hr in the Port; **Table 8** and **Figure 19**). Overall, water column fluxes (dark) were variable; however, ranges were more or less consistent or slightly higher than values reported in previous studies for similar systems (e.g., Ziegler and Benner 1999). Based on these data, turnover times for TDN and TDP were 2-fold and >6-fold higher in lagoon water relative to seawater from Port Canaveral (**Table 9**).

Table 8. Water column fluxes in Port Canaveral and in the adjacent lagoon (inflow and reference sites (µM/hr; dark conditions).

	NH_4 (µM/hr)	NOx (µM/hr)	DIN (µM/hr)	Organic N (µM/hr)	TDN (µM/hr)	PO_4 (µM/hr)	TDP (µM/hr)	DOP (µM/hr)
Port Canaveral	0.01 ± 0.90	0.95 ± 19	0.96 ± 2.0	1.4 ± 6.0	2.4 ± 6.8	0.03 ± 0.12	0.07 ± 0.17	0.04 ± 0.07
Lagoon	0.05 ± 0.43	1.8 ± 7.1	1.9 ± 6.9	4.6 ± 3.8	6.5 ± 10	0.03 ± 0.03	0.04 ± 0.06	0.004 ± 0.06

Table 9. Turnover time in hours for N and P in Port Canaveral and BRL

	NH_4	NOx	DIN	Organic N	TDN	PO_4	TDP	DOP
Port Canaveral	290	2	5	13	10	11	5	8
Lagoon	170	0.4	5	23	18	11	32	240

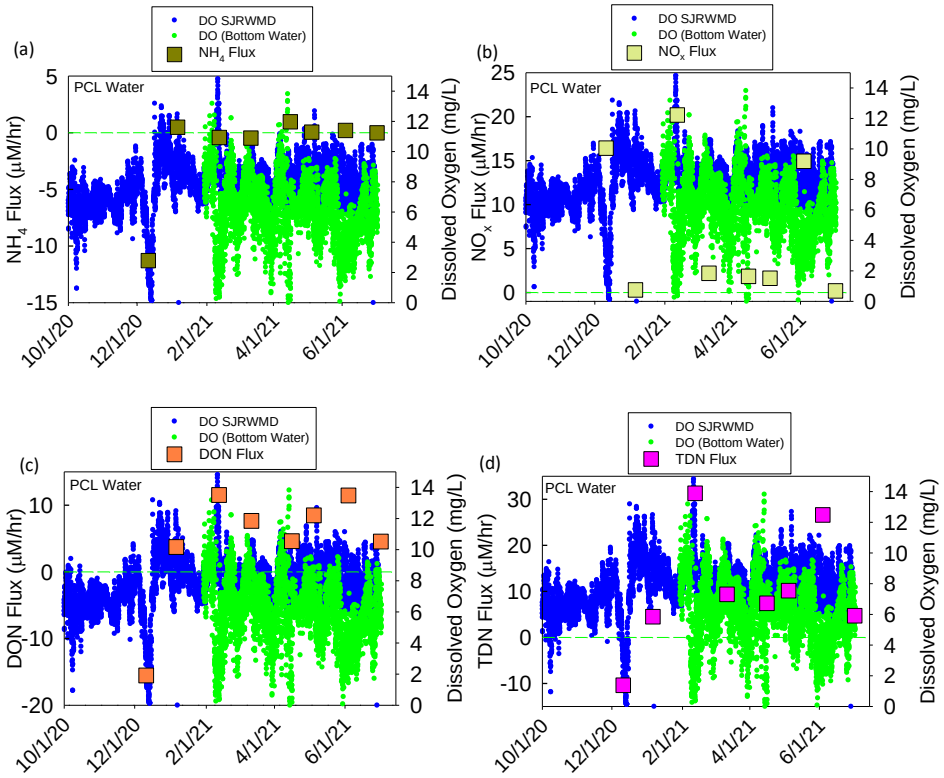

Note: Green and blue dotted lines show DO in the region at mid water depths (SJRWMD site IRLB04) and in bottom water at the inflow site.

Figure 18. Water column fluxes of (a) NH_4, (b) NO_x, (c) DON and (d) TDN

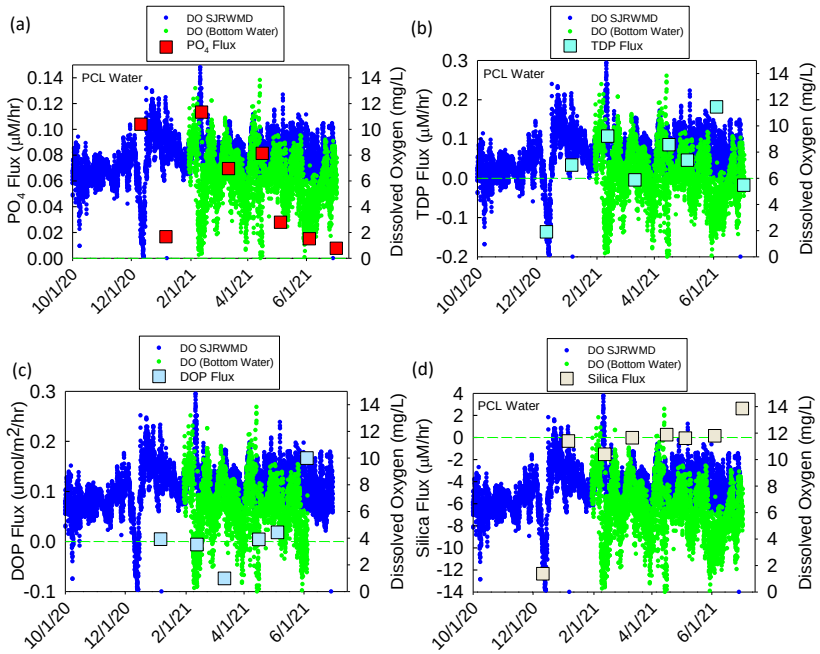

Note: Green and blue dotted lines show DO in the region at mid water depths (SJRWMD site IRLB04) and in bottom water at the inflow site.

Figure 19. Water column fluxes of (a) PO_4, (b) TDP, (c) DOP and (d) SiO_2

3.3.2 Water Column Ratios and Fluxes of Oxygen (O):N and N:P

Overall, data for water column recycling from this study indicate that inflow of seawater would bring water with lower rates of dark respiration (~30% lower O consumption) into the lagoon, thereby increasing resilience to hypoxia while also decreasing the rate of nutrient recycling in the water column. Because rates of nitrogen recycling were 2-4 times higher and rates of P recycling were similar in lagoon water compared to water from Port Canaveral, lower N:P ratios were identified for recycling in seawater from Port Canaveral. Based on data from this study, the water column recycling ratio of DIN:SRP for Port water was 10, relative to the DIN:SRP recycling ratio for lagoon water at 46. As expected, ratios for recycling of TDN:TDP were higher at 17 in the Port and 88 in lagoon water during this study. These rates were highly variable, responding to changes in water quality; nevertheless, these recycling ratios act to stabilize ratios of N to P in water over time and these recycling ratios followed patterns for ratios observed for the standing stock of nutrients observed in the Port and in the lagoon discussed in **Section 3.2.2**. Based on these data and consistent with global processes, water column recycling acts to buffer against changes to the relative abundance of N to P and helps to sustain algal communities over time. In addition to exchanging dissolved nutrients, restoration efforts such as ocean inflow would exchange particles, altering water column processes and respiration. In the case of inflow, inputs of seawater to the lagoon would decrease ratios of N:P recycling in the water column likely leading to a lower N:P ratio of the standing stock of nutrients in the lagoon over time.

3.3.3 Importance of Benthic-pelagic coupling (fluxes)

Benthic fluxes of N and P from muck are estimated to contribute more than 30% of the annual N and P loading to the IRL (Tetra Tech 2016, Fox and Trefry 2018). These estimates are based only on fluxes from fine-grained, organic-rich sediments locally referred to as “muck.” Because sand covers at least 90% of the lagoon bottom, non-trivial fluxes from sand need to be considered when evaluating the importance of internal nutrient sources and geochemical nutrient cycling within the lagoon. To evaluate the importance of these geochemical processes towards regulating nutrient concentrations in lagoon water, residence times for nutrients were calculated using benthic nutrient fluxes, long-term average nutrient concentrations in lagoon water (**Table 3**) and an average lagoon depth of 1.5 meters. Data from this study serve as a baseline from which the importance of sandy sediments as both a source and sink of nutrients can be evaluated. Although this study focused on sandy sediments, non-trivial fluxes from muck would be influenced by changes to temperature, salinity, and DO. For example, Fox and Trefry (2018) reported a 7-10% increase in benthic fluxes of N and P from fine-grained organic rich sediments “muck” per 1°C increase in lagoon temperature. Lagoon-wide, this equates to a decrease of ~40 tons of N per year if lagoon temperature decreased by 1°C.

3.3.4 Benthic Fluxes

During this study, including Phase 1, no significant trends for benthic nutrient fluxes versus the composition of sandy sediments (e.g., sediment OM content) were identified in the lagoon (**Figure 20**). This contrasts an established pattern where sediment water and OM content are strongly correlated with benthic fluxes from fine-grained, organic-rich sediments, “muck,” throughout the IRL (Fox and Trefry 2018). The absence of a trend for sandy sediments is likely at least partially related to groundwater seepage into the lagoon through water-permeable sandy sediments (Pandit, et al. 2017). Based on data from mini-seepage meters deployed during this study, it is likely that benthic chambers deployed along the west shoreline of the IRL were influenced to some extent by groundwater seepage with rates ranging from less than 1 up to about 30 cm/day (Bethel Creek) from sites within about 10 m of the western shoreline. Where groundwater seepage occurs, fluxes are more likely the result of advective versus diffusive processes. Nevertheless,

fluxes reported below represent either inputs (positive values) or removal (negative values) of nutrients and oxygen from the lagoon system. During Phase 2, benthic chambers were focused along the eastern shoreline of the BRL in the proposed area of inflow with chambers also deployed in the reference/control area (also along the eastern shoreline). This approach during Phase 2 provided a detailed temporal evaluation of fluxes at the proposed inflow site relative to the higher spatial coverage during Phase 1.

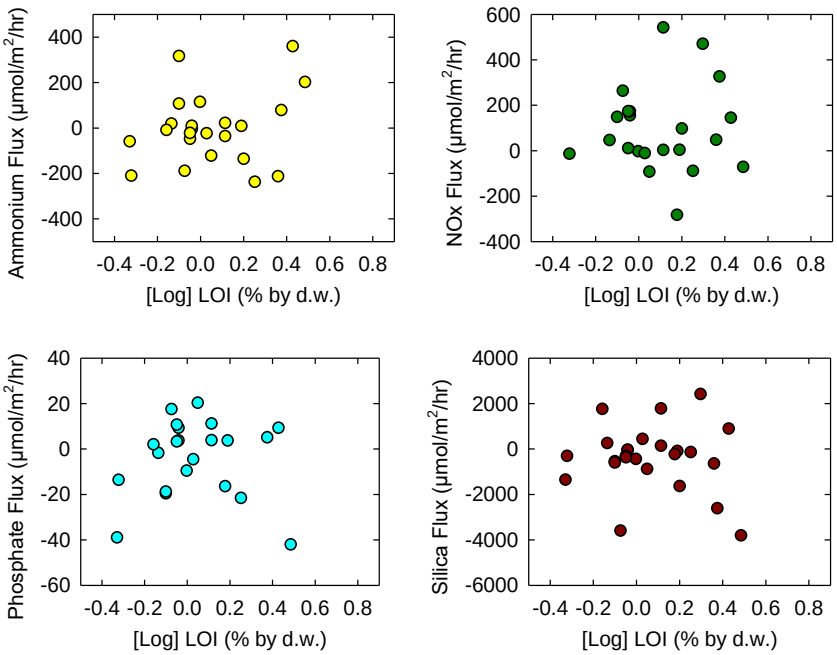

Figure 20. Benthic fluxes of (a) NH_4, (b), NO_x, (c) PO_4, and (d) SiO_2 versus OM content as log[LOI] for Phase 1 sampling

Collectively, median ± standard deviation SOD (oxygen flux into sediments) for sandy sediments during Phases 1 and 2 (including data from other projects) was -3,100 ± 2400 µmoles/m^2/hr (median 2,900 µmoles/m^2/hr, n = 53) for sediment collected throughout the IRL system. Values during Phase 2 at the proposed inflow and referenced sites agreed well with the lagoon-wide dataset at -2,500 ± 1,600 µmoles/m^2/hr (median 2,600 µmoles/m^2/hr, n = 22). Overall, concentrations of DO in bottom water and rates of oxygen consumption varied together with lower bottom water DO identified during periods with higher oxygen demand (more negative SOD), except when DO in bottom water approached zero and there was no oxygen to consume (i.e., December 2020, **Figure 21**). Overall, values for sandy sediment in the IRL and BRL fit nicely within a range of values previously reported for estuaries around the world, at -200 to -7,000 µmoles/m^2/hr (Boynton et al., 2018). Oxygen demand of muddy sediments were higher and more variable at -5,700 ± 4,600 µmoles/m^2/hr (n = 8); however, muddy sediments were investigated primarily during cooler months and the current average fluxes from muddy sediments almost certainly underestimate annual average values where SOD as high as -9,000 µmoles/m^2/hr were measured during summer months.

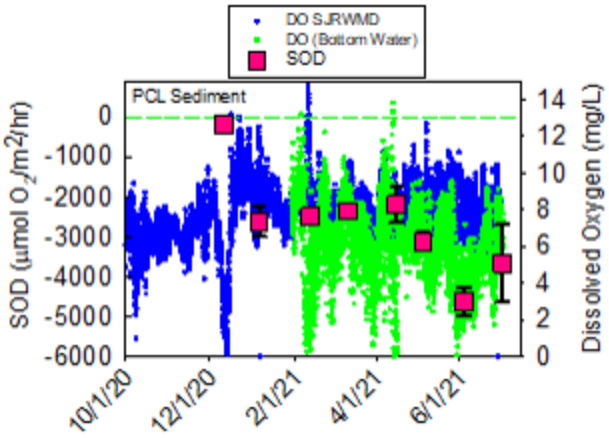

Note: Blue and green dotted lines show DO in mg/L at mid water depth (SJRWMD sensor IRLB04) and in bottom water, respectively.

Figure 21. SOD over time at the inflow site

During Phase 1, median ± standard deviation N fluxes varied among areas with sandy versus muddy sediments. Lagoon wide, DIN was released from sandy sediments (median ± SE = 260 ± 170 µmoles/m^2/hr, 32 tons/km^2/year) primarily as NO_x (63% of DIN, 150 ± 150 µmoles/m^2/hr, 20 tons N/km^2/year), and NH_4 accounted for 37% of the DIN efflux from sandy sediments at 90 ± 60 µmoles/m^2/hr (11 tons N/km^2/year). During Phase 2, similar values were identified from higher resolution sampling at the inflow and reference sites, with an efflux of DIN at 70 ± 52 µmoles/m^2/hr (8 tons/km^2/year). During Phase 2, 76% of the DIN flux was accounted for by NO_x at 53 ± 42 µmoles/m^2/hr (7 tons/km^2/year) and NH_4 accounted for 24% of the DIN flux at 17 ± 21 µmoles/m^2/hr (1 ton/km^2/year). In roughly one third of chambers, NH_4 fluxes were directed into sediments, likely due to nitrification in aerobic (oxic) surface sediments. In contrast, during and shortly following hypoxic events (December 20 and February 2021 on **Figure 22**Note: Green and blue dotted lines show DO in the region at mid water depths (SJRWMD site IRLB04) and in bottom water at the inflow site.
Figure 22**a**), the flux of reduced N (NH_4) was elevated as expected for anaerobic sediments.

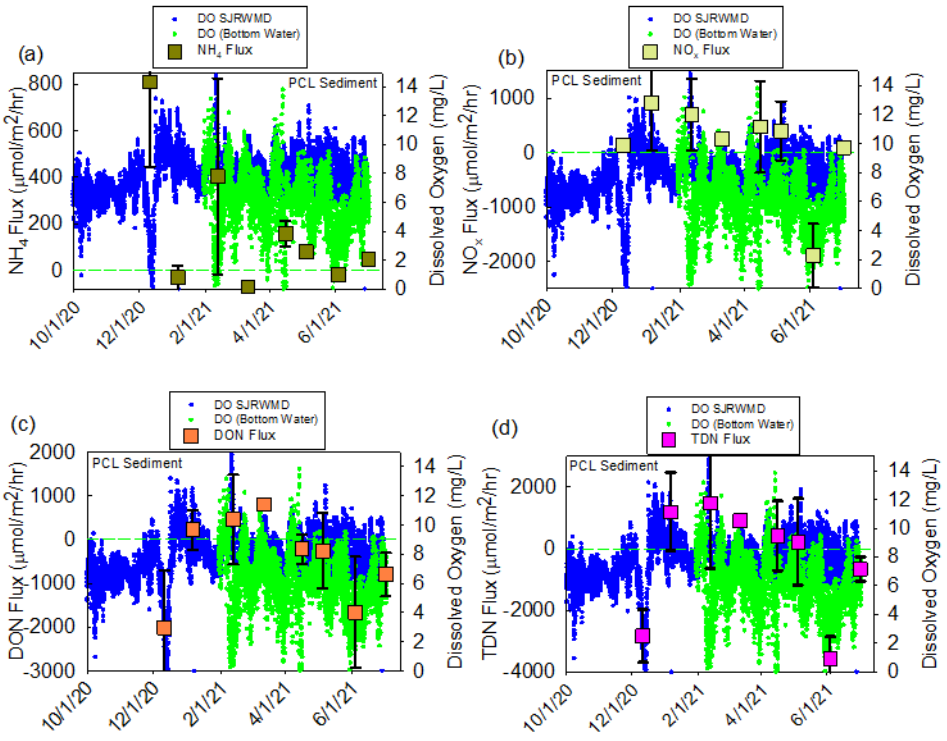

Note: Green and blue dotted lines show DO in the region at mid water depths (SJRWMD site IRLB04) and in bottom water at the inflow site.

Figure 22. Benthic fluxes of (a) NH_4, (b) NO_x, (c) DON and (d) TDN

During Phase 1, fluxes of DON were highly variable with median DON fluxes directed out of sediments for a median TDN flux from sandy sites at 290 ± 430 µmoles/m^2/hr (35 tons N/km^2/year). During Phase 2 at the inflow and reference site, DON fluxes were highly variable and typically directed into sediments from overlying water with a median at -480 ± 52 µmoles/m^2/hr (**Figure 22c**). Different outcomes from Phase 1 and Phase 2 demonstrate the susceptibility of sediment processes to changing conditions as well as variations among sites. For example, previous studies have identified moderate post-bloom organic enrichment of sediment to stimulate denitrification and thereby N removal; however, over enrichment and oxygen depletion can suppress nitrifying bacteria, favoring production of NH_4 over nitrate, helping to sustain eutrophic conditions (a positive feedback loop) (Bartoli et al., 2021). Overall, sandy sediments (this study) represented both a source and a sink for N where small changes to fluxes had a dramatic impact on nitrogen supply or removal from the lagoon. With this, first of its kind in the IRL, relatively limited dataset, we are not yet able to isolate event scale changes from seasonal patterns. With continued sampling will hope to resolve these differences that are critical to understanding nitrogen in this system.

At muddy sites (muck), fluxes of NO_x were directed from the water into sediments (-5 ± 19 µmoles/m^2/hr; -0.5 tons N/km^2/year), consistent with the use of nitrate as an oxidizing agent for the decomposition of OM in suboxic/anaerobic sediments. Releases of DIN from muddy sediments were virtually 100% NH_4 at a median of 580 ± 460 µmoles/m^2/hr (71 tons N/km^2/year), >2-fold higher than DIN fluxes from sandy sediments and positive relative to on average negative TDN fluxes identified for sandy sediments. Based on data presented here, muddy sediments represented a significant source of reduced N to overlying water (~70 tons/km^2/year). When applied to the surface area of muck discussed in **Section 3.5.2,** we get ~400-500 tons N entering

the lagoon per year from muck, consistent with data obtained using other methodologies from the Brevard County Save Our Indian River Lagoon Project Plan 2020 Update.

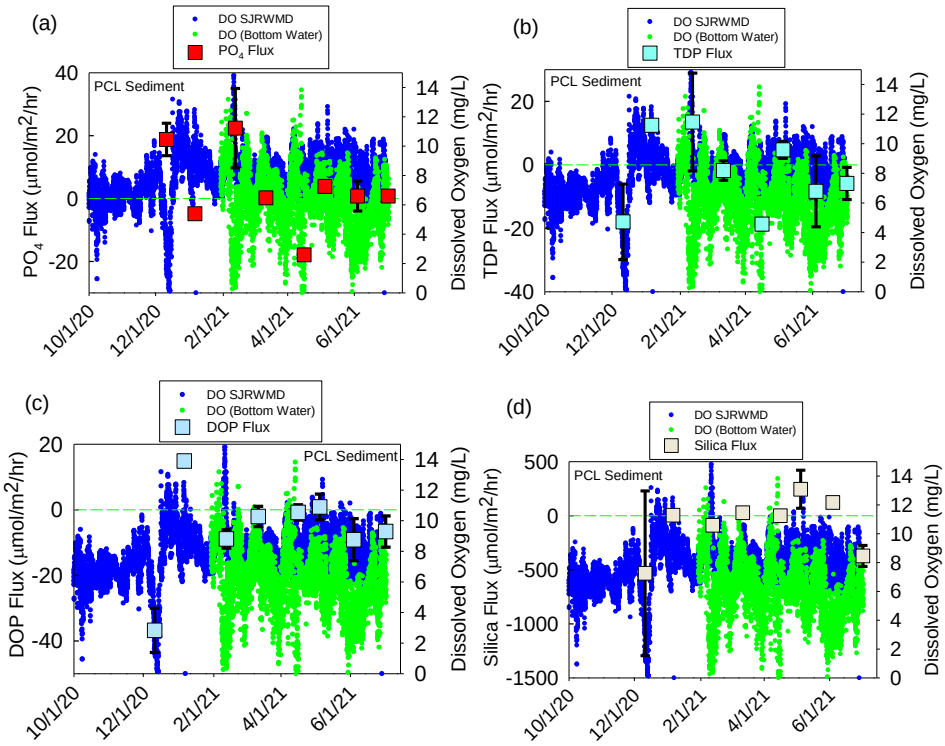

Note: Green and blue dotted lines show DO in the region at mid water depths (SJRWMD site IRLB04) and in bottom water at the inflow site.

Figure 23. Benthic fluxes of (a) PO_4, (b) TDP, (c) DOP and (d) SiO_2

During Phase 1, at sandy sites through the lagoon, the median ± standard error PO_4 flux was 4.1 ± 8.1 µmoles/m^2/hr (1.1 ton/km^2/year). During Phase 2 at the inflow and reference sites, PO_4 flux was lower at 1.8 ± 0.6 µmoles/m^2/hr (0.5 tons/km^2/year). Wide ranges of values for P fluxes are not unexpected because P fluxes vary as a result of bacterial decomposition and concentration gradients, but also due to changing redox conditions in sediments and overlying water. As sediments and water become aerobic (oxic), P is scavenged by oxidized iron and aluminum while simultaneously aerobic decomposition of sediment OM can promote releases of PO_4 from sediments. Under anaerobic conditions, bacterial metabolism of OM slows; however, PO_4 can be released from reduced sediments, temporarily increasing fluxes (Cowan and Boynton 1996; Boynton et al., 2018). Data presented here show this change where sediments switch from a sink to a source of PO_4 (e.g., **Figure 23a**). For example, during sampling in December 2020, bottom water DO at the inflow site was hypoxic at 1.3-1.5 mg/L and P fluxes were very high and directed out of sediments (18.8 ± 5.2 µmoles/m^2/hr, **Figure 23a**). A similar, high P flux was identified in February 2021 (22 ± 12 µmoles/m^2/hr) immediately following a hypoxic event the night before. During subsequent sampling events (excluding December 2020 and February 2021), DO was >5 mg/L at the time of sampling and P fluxes from the same location were lower at 0.38 ± 0.5 µmoles/m^2/hr (overall, 1.8 ± 0.5 µmoles/m^2/hr, **Figure 23a**).

Lagoon-wide DOP fluxes were directed into sandy sediments at -4.7 ± 4.9 µmoles/m^2/hr, consistent with mineralization of DOM and a concentration gradient driving fluxes into sediments. Fluxes from the inflow and reference sites agreed well with Phase 1 data at -4.2 ± 0.6 µmoles/m^2/hr. Based on these collective datasets, the net TDP flux was directed into sandy

sediments from overlying water at -0.6 µmoles/m^2/hr (-0.2 tons/km^2/year) for sites throughout the lagoon and -2.6 ± 0.7 µmoles/m^2/hr (-0.7 tons/km^2/year) at the inflow and reference sites.

At muddy sites, the median PO_4 flux was 12 ± 18 µmoles/m^2/hr (3.3 tons/km^2/year). Higher PO_4 fluxes in muddy/anaerobic sediments from the IRL are consistent with data previously reported for other estuaries (e.g., Cowan and Boynton 1996). Fluxes of DOP were also directed out of sediments at 8.8 ± 6.6 µmoles/m^2/hr (2.4 tons/km^2/year). Overall TDP fluxes were directed out of muddy sediments and the net flux of P was large and positive, compared to a flux directed into sandy sediments throughout the lagoon and at the inflow and reference sites (**Table 10**).

Table 10. Median ± standard error for benthic fluxes from sandy and muddy sediments in µmoles/m^2/hour for lagoon wide sampling of sandy sediments during Phase 1 (lagoon wide sand) and high resolution sampling at the proposed inflow and reference sites during Phase 2.

Sediment	Oxygen	NH_4	NOx	DIN	PO_4	TDP	DOP
Lagoon Wide Sand	-3,200 ± 900	90 ± 60	150 ± 150	260 ± 170	4.1 ± 8.1	-0.6	-4.7 ± 4.9
Inflow/ Reference	-2,500 ± 1,600	17 ± 21	53 ± 42	70 ± 52	1.8 ± 0.6	-2.6 ± 0.7	-4.2 ± 0.6
Muck	-4,300 ± 2,500	580 ± 460	-180 ± 200	400	12 ± 18	20 ± 23	8.8 ± 6.6

Collectively, these data yielded trends in nutrient fluxes that were at least partially explained by changes to temperature and DO of bottom water. For example, during oxic conditions, sandy sediments were a sink for P (e.g., **Figure 23a**); however, during or shortly following periods of hypoxia or anoxia, sandy sediments were a source of P to overlying water. At the same time, during oxic conditions, sandy sediments promoted fluxes of oxidized forms of N (NOx) and during periods of hypoxia, sandy sediments were more frequently a large source of reduced N (NH_4) (**Figure 22a**). Pulses of bioavailable P can support algal growth and fluxes of reduced N during periods of hypoxia, preferentially support small, fast-growing algae like picocyanobacteria including *Aureoumbra lagunensis* (Liu et al., 2001).

3.3.5 Benthic Flux O:N and N:P Ratios

Previous studies have used O:N (oxygen to NH_4) ratios to infer whether or not certain geochemical process are occurring in sediments (e.g., Cowan and Boynton 1996). For example, mineralization of phytoplankton derived OM yields stoichiometric ratios producing 16 atoms of N as nitrate (oxidized from NH_4), 1 atom of P as PO_4 for every 276 atoms of oxygen consumed (O:N = 17.25, O:P 276). If N is not oxidized and remains NH_4, the theoretical O:N ratio is 14.25. Certainly, other geochemical processes such as re-oxidation of reduced sediments can consume oxygen leading to higher ratios. It is also possible that the use of alternate oxidizing agents (e.g., NO_3, iron, manganese) under suboxic or anoxic conditions can lead to values lower than the Redfield ratio. Nevertheless, these ratios have been used to help describe sediment processes (e.g., Boynton et al. 2018). Based on data from this study, the median O:NH_4 for sandy sediments throughout the lagoon was 21.4 ± 34.2 versus 6.9 ± 6.8 for muddy sediments. These data combined with in many cases negative TDN fluxes suggest that coupled nitrification-denitrification likely occurred in sandy sediments throughout the lagoon (Nixon 1981) and also confirm the use of alternate oxidizing agents such as nitrate for decomposition in muddy sediments.

Due to highly variable fluxes of both N and P, into and out of sediments, it is difficult to identify a reliable consistent molar N:P ratio for sandy or muddy sediments. The wide range of N:P values identified during this study were consistent with ranges of values previously identified in the IRL,

likely related to seasonal and event scale variations in temperature and DO (Fox and Trefry, 2018).

3.3.6 Turnover Times

Benthic nutrient and oxygen fluxes plus existing nutrient concentrations in the IRL were used to estimate residence (turnover) times for nutrients in the IRL, based on water column processes and based on sediment fluxes individually and collectively. Residence times indicate the theoretical amount of time required for all of a nutrient in the water column to be either re-generated or consumed. If other nutrient sources were to be included (e.g., tributaries), residence times for nutrients would decrease. Relatively short residence times for nutrients (e.g., hours to weeks) relative to water (months to years) indicate that water column processes and benthic-pelagic coupling buffer nutrient concentrations against changes resulting from external sources. Although existing conditions discussed in this section act to buffer against changes to nutrient concentrations, sediment and water column process would respond to changes in water quality (e.g., temperature, salinity, and DO) as discussed in **Section 3.4.2**.

Residence times based on fluxes alone were calculated. Using an average lagoon depth of 1.5 m, each 1 m^2 section of lagoon contains 1.5 m^3 or 1,500 L of water (1 m_{Length} x 1 m_{width} x 1.5 m_{depth} = 1.5 m^3 = 1,500 L; **Figure 24**). Nutrient concentrations (µmoles/L, **Table 3**) times volume (1,500 L) yields the total quantity of nutrients (µmoles) in each 1 m^2 section of the lagoon. The total quantity of nutrients was then divided by fluxes (µmoles/m^2/hr) to yield residence times in hours.

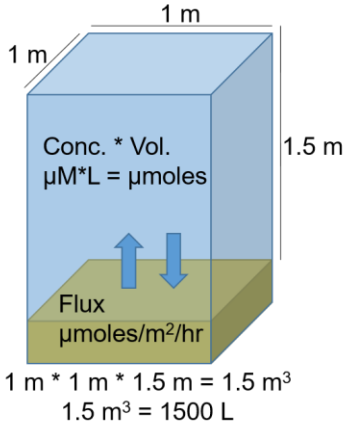

Figure 24. Conceptual diagram showing a 1 m^2 column of water and sediments from the IRL using an average depth of 1.5 m

Overall, turnover times for nutrients varied from hours to days. In sandy sediments, the residence time for NH_4 was ~140 hours based on average nutrient concentrations at lagoon sites during this study (**Table 3**) (e.g., 0.12 mg NH_4-N/L in the lagoon; **Table 3**) times 1,500 L/m^2 of lagoon (**Figure 24**) = 180 mg N/m^2 divided by 1.3 mg/m^2/hr (**Table 10,** lagoon wide sand, 90 µmoles/m^2/hr * 0.014 mg/µM = 1.3 mg/m^2/hr from) = 140 hours (~6 day). Using an average depth of 1.5 m, recycling in the water column could turn over the standing stock of NH_4 in 170 hours (180 mg N/m^2 / 0.05 µmol/hr * 0.014 mg/µmol = 170 hours; water column respiration from **Table 8**; **Table 11**). Based on these data, water column respiration accounted for ~50% of the NH_4 recycling in the lagoon (**Table 11**).

NOx fluxes from sandy sediments were higher than NH_4 fluxes and concentrations in lagoon water were lower yielding turnover times based on sediment fluxes ranging from ~10 to 20 hours (**Table**

11). Together, sediment DIN fluxes could replace all dissolved N in the water column (TDN) in about 100 days (2,600 hours). Rapid recycling of NOx in the water column coupled with low concentrations yielded a turnover time in water of less than one hour. Based on these data, water column processes accounted for 95% of NOx recycling in the lagoon (**Table 11**).

Turnover times for NH_4 and NO_x from muck were 20 hours and 10 hours, respectively, where muck acted as a major source of NH_4 (~70 tons/km^2/year) and a sink for NOx (~-22 tons/km^2/year; **Table 10**). Because NO_x fluxes into sediments are balanced by increased NH_4 fluxes from sediments, the NH_4 flux accounted for NO_x with regards to turnover of all the N in the water column. Based on these data, NH_4 could replace all the dissolved N in the water column overlying muck in approximately 13 days (300 hours); however, when water column processes are included, this decreases to less than 3 days.

Turnover times for PO_4 from sandy sediments varied from 10 to 270 hours, or <1 to 11 days, compared to only 14 hours for areas with muck sediments (**Table 11**). To cycle the complete pool of dissolved P, it would take 500–1,100 hours, or 20–50 days, for sandy sediments and 60 hours, or 2 to 3 days, for muck. Water column processes appeared to be much more important compared to sediments for P cycling and water column processes cycled the complete pool of TDP in just 32 hours and in the adjacent Port, TDP was recycled in only 5 hours (**Table 9**). Due to rapid recycling in the water column, in areas with sandy sediments, benthic fluxes accounted for only 0.1% of the total recycling; in muddy areas, sediments accounted for only 1% of the total phosphorus recycling.

Due to the large temporal and spatial variability in DO throughout the lagoon, turnover times for oxygen were highly variable. If the 5-year average DO concentration in the lagoon is used or 100% saturation at 20 PSU and 25˚C of 7.4 mg/L, turnover times based on SOD alone (not including water) ranged from 140 hours for sandy sites in the inflow area to 80 hours for mucky sites (e.g., 7.4 mg/L / 32 mg/mmol * 1,000 µmol/mmol = 231 µmoles/L * 1,500L/m^2 of lagoon = 347,000 µmoles/m^2 divided by 3,200 µmoles/m^2/hr at sandy sites (**Table 10**) = 110 hours). When water column respiration and SOD are considered together, turnover times based on a 1.5-m deep water column were ~30 hours for sandy sites and 26 hours for muddy sites. Overall, sediments accounted for 26% and 32% of the total oxygen demand for areas containing sand and muck, respectively (assuming 1.5 m average depth, sandy sediments shown in **Table 7**). These short turnover times are consistent with observed nighttime (dark) decreases in DO observed throughout the lagoon in continuous monitoring networks (e.g., **Figure 38**). The Florida Tech network of bottom water DO sensors (**Section 3.5.1**) captures the importance of sediments towards overall oxygen consumption and nutrient recycling.

Table 11. Turnover times calculated using nutrient recycling in the water column and benthic fluxes, nutrient concentration in the water column, and an average depth of 1.5 m based on conceptual diagram in Figure 24.

Sediment	Oxygen (hours)	NH_4 (hours)	NOx (hours)	DIN to replace TDN (hours)	PO_4 (hours)
Water Column	40	170	0.4	60	10
Inflow/ Reference	140	760	20	2600	270
Lagoon Wide Sand	110	140	10	700	120
Muck	80	20	10*	460	10
Water + Sand	30	80	0.4	60	9
Sediment/Total	26%	55%	5%	-	0.1%

*removal by sediments

Despite the importance of benthic-pelagic coupling and short residence times for nutrients in shallow coastal systems, improved water quality that could result from artificial inflow would likely modify geochemical processes, possibly increasing or decreasing benthic fluxes into overlying water and changing residence times for nutrients. To address some of these potential changes, laboratory incubation experiments were carried out for water and sediments to investigate how changes to temperature, salinity, and DO might influence nutrients in the lagoon. Nevertheless, the large fraction of total nutrient cycling that occurs in the water column suggest that direct exchanges of water and particles would likely have large impacts on nutrient cycling in the lagoon.

3.4 Laboratory Experiments

3.4.1 Water Column; Dark, Laboratory Conditions

Geochemical responses to changes in water quality that could result from enhanced ocean inflow were evaluated through a series of laboratory incubation experiments. These experiments were carried out to stimulate changes in lagoon temperature, salinity, and DO that could occur as a result of inflow. These data also provide insight into how nutrient cycling may respond to other processes including warming temperatures and enhanced rainfall. With respect to ocean inflow, the most likely results would be a small decrease in lagoon temperature, an increase in salinity, and more stable DO as discussed above. Consistent with data for temperature and DO, changes to water column salinity were used to isolate responses of sediments; however, intrinsic changes to particles during salinity adjustments confound interpretation of responses within the water column; as a result, no discussion for changes to water column salinity is included here.

No significant trends for N or P were identified for water column fluxes as a function of temperature, salinity, or DO (**Table 10, Table 12**, **Table 13**, **Table 14**, and **Table 15** plus **Figure 25** and **Figure 26**).

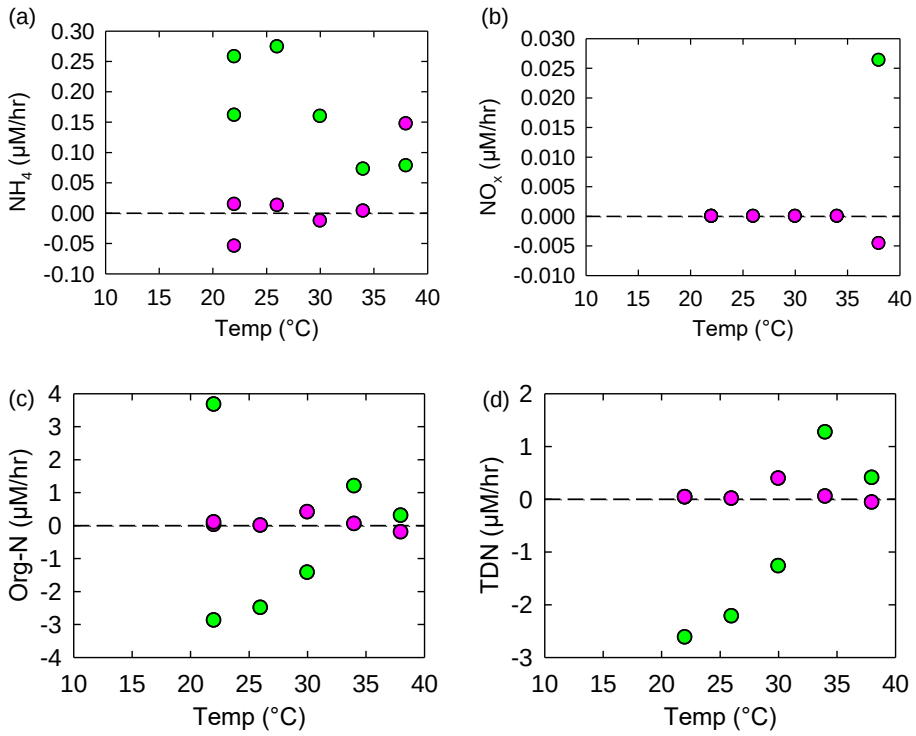

Figure 25. Water column fluxes from laboratory incubations in µM/hr versus temperature for (a) NH_4, (b) NO_x, (c) organic N and (d) TDN

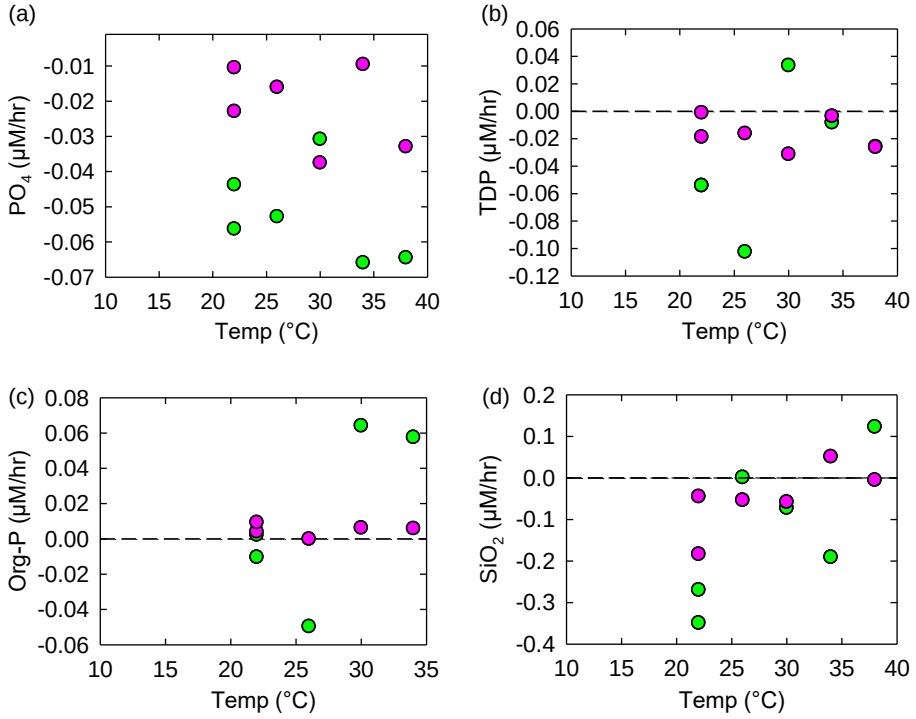

Figure 26. Laboratory incubation water column fluxes in µM/hr versus temperature (°C) for (a) PO_4, (b) TDP, (c) organic P, and (d) SiO_2

Table 12. Coefficient of determination (R^2), probability values (*p*) and equations for water column fluxes (dark) versus temperature (0–2 hours).

Plot	R^2*	P-value*	Equation
TDN and Temp	0.007	0.874	-
NH_4 and Temp	0.617	0.064	-
NO_x and Temp	0.490	0.122	-
DIN and Temp	0.548	0.093	-
DON and Temp	0.011	0.841	-
PO_4 and Temp	0.185	0.395	-
TDP and Temp	0.248	0.315	-
DOP and Temp	0.425	0.161	-
Silica and Temp	0.520	0.106	-
H^+ and Temp	0.001	0.944	-
DIN:SRP and Temp	0.490	0.122	-
TDN:TDP and Temp	0.154	0.442	-

Table 13. Coefficient of determination (R^2), probability values (*p*) and equations for water column fluxes (dark) versus temperature (2–18 hours).

Plot	R^2*	P-value*	Equation
TDN vs. Temp	0.004	0.908	-
NH_4 vs. Temp	0.524	0.104	-
NO_x vs. Temp	0.490	0.122	-
DIN vs. Temp	0.522	0.105	-
DON vs. Temp	0.085	0.575	-
PO_4 vs. Temp	0.140	0.464	-
TDP vs. Temp	0.110	0.521	-
DOP vs. Temp	0.017	0.807	-
Silica vs. Temp	0.510	0.111	-
H^+ vs. Temp	0.838	**0.010**	**H^+(nmol/hr) = -0.005[°C] + 0.17**
DIN:SRP vs. Temp	0.491	0.121	-
TDN:TDP vs. Temp	0.151	0.446	-

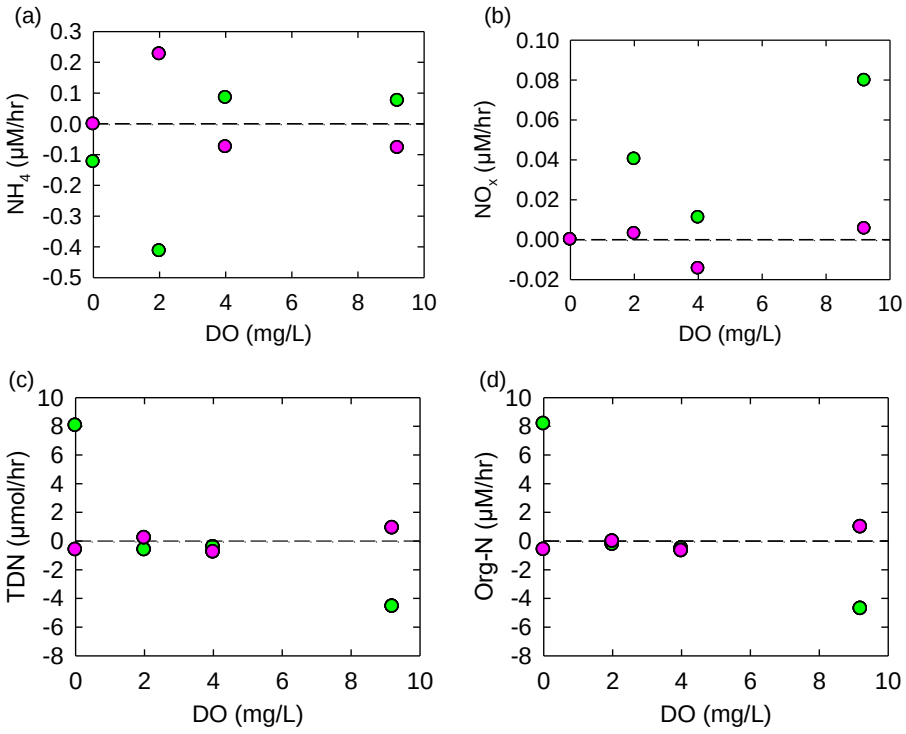

Figure 27. Water column fluxes from laboratory incubations in µM/hr versus DO for (a) NH_4, (b) NO_x, (c) TDN, and (d) organic N

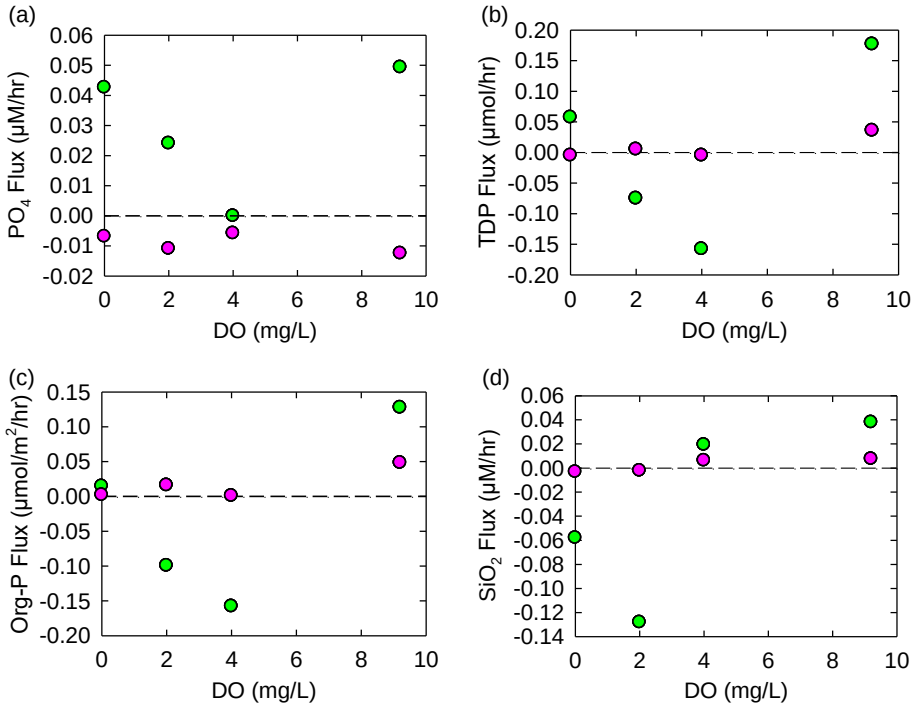

Figure 28. Laboratory incubation water column fluxes in µM/hr versus DO for (a) PO_4, (b) TDP, (c) organic P, and (d) SiO_2

Table 14. Coefficient of determination (R^2), probability values (*p*) and equations for water column fluxes (dark) versus DO (0–2 hours).

Plot	R^{2*}	P-value*	Equation
TDN vs. DO	0.741	0.139	-
NH_4 vs. DO	0.349	0.409	-
NO_x vs. DO	0.726	0.148	-
DIN vs. DO	0.493	0.298	-
DON vs. DO	0.770	0.123	-
PO_4 vs. DO	0.054	0.767	-
TDP vs. DO	0.232	0.519	-
DOP vs. DO	0.271	0.479	-
Silica vs. DO	0.533	0.270	-
H^+ vs. DO	0.873	0.066	-
DIN:SRP vs. DO	0.001	0.976	-
TDN:TDP vs. DO	0.610	0.219	-

Table 15. Coefficient of determination (R^2), probability values (*p*) and equations for water column fluxes (dark) versus DO (2–18 hours).

Plot	R^2	P-value	Equation
TDN vs. DO	0.526	0.274	-
NH_4 vs. DO	0.243	0.507	-
NO_x vs. DO	0.041	0.799	-
DIN vs. DO	0.219	0.532	-
DON vs. DO	0.680	0.175	-
PO_4 vs. DO	0.365	0.396	-
TDP vs. DO	0.778	0.118	-
DOP vs. DO	0.733	0.144	-
Silica vs. DO	0.774	0.120	-
H^+ vs. DO	0.120	0.653	-
DIN:SRP vs. DO	0.152	0.610	-
TDN:TDP vs. DO	0.245	0.505	-

3.4.2 Laboratory Experiments (Sandy Sediments)

To estimate how changes to temperature, salinity, and DO may influence geochemical processes within sediments, laboratory experiments with sandy sediments were carried out with temperatures ranging from 13˚C to 32˚C, salinities ranging from 0 to 34 PSU, and DO ranging from 0% (0 mg/L) to 100% (about 9 mg/L). Wide ranges of values for temperature, salinity and DO were investigated to resolve changes among large natural variability while also controlling other variables. Using equations from statistically significant trends, responses to small changes in temperature, salinity, or DO over large areas of the lagoon can be modeled as discussed below in **Section 3.5**. During Phase 2, incubations were carried out with multiple sampling intervals to investigate immediate responses to changes in temperature, salinity, or DO (0–2 hours) and responses after the initial change (2–18 hours). Water column processes were tracked separately (discussed above **Section 3.3.1**) and subtracted from sediment fluxes allowing for sediment and water column processes to be evaluated independently.

3.4.3 Temperature

Collectively, during Phases 1 and 2, temperature was adjusted between 13 and 38˚C (±0.2˚C) using recirculating water baths to simulate the maximum annual range of lagoon temperatures, including extreme heat and cold events. Sediments cores from the IRL were returned to the laboratory and slowly adjusted to the desired temperature within 2 hours of collection. After

reaching the desired temperature, cores were allowed to equilibrate for at least 1 hour before overlying water was drained and replaced with new water from the collection site. Once temperature was stable for at least 1 hour, start samples (time 0) were collected and cores were stirred using air diffusers to maintain DO at 100%. Diffusers were installed in such a way as to prevent the buildup of concentration gradients at the sediment-water interface without causing resuspension. Samples were then collected at 2 and 18 hours after starting incubations.

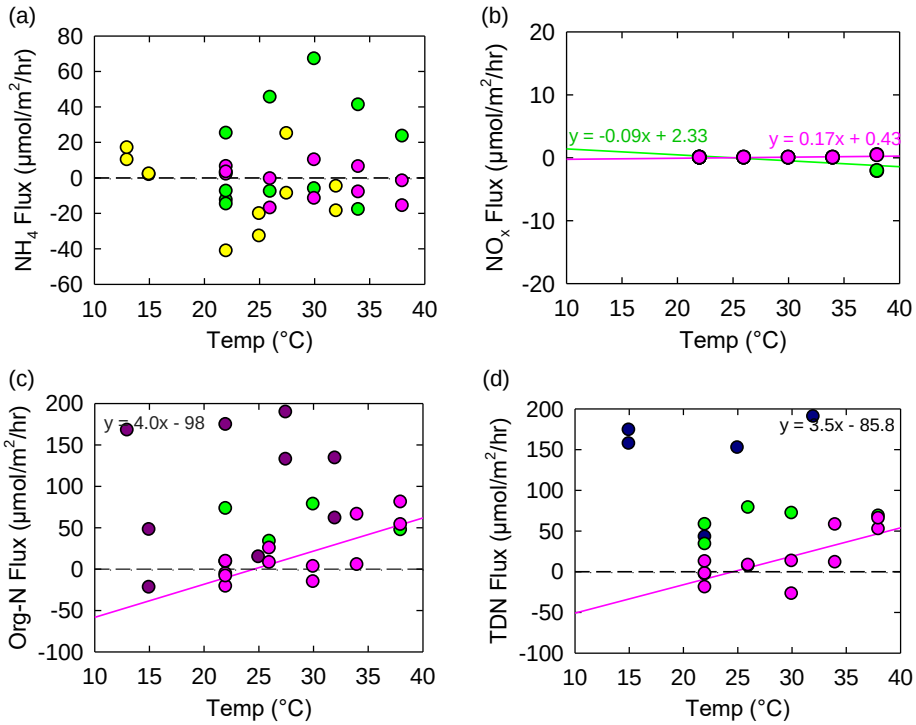

Figure 29. Fluxes from laboratory incubations (sandy sediment) in µmoles/m^2/hour versus sediment temperature for (a) NH_4, (b) NO_x, (c) organic N, and (d) TDN

Significant positive correlations were identified for TDN (TDN flux [µmoles/m^2/hr] = 3.5 * [˚C] – 85.8, *p* = 0.006, r = 0.55; **Figure 29d**; **Table 17**), NO_x (NO_x flux [µmoles/m^2/hr] = 0.17 * [˚C] – 0.43, *p* = 0.012, r = 0.49; **Figure 29b**; **Table 17**), and DON (DON flux [µmoles/m^2/hr] = 4.0 * [˚C] – 98, *p* = 0.005, r = 0.57; **Figure 29c**; **Table 17**) from sandy sediments versus sediment temperature. Overall, NO_x fluxes were positively correlated with temperature but accounted for only a small (<1%) fraction of the TDN. TDN increased by 3.5 µmoles/m^2/hr (0.4 tons/km^2/year) per °C, virtually all as organic N with sediments switching from a sink for N at temperatures below 25°C to a source of N into overlying water at temperatures above 25°C (**Figure 29**).

Table 16. Coefficient of determination (R^2), probability values (*p*) and equations for benthic fluxes versus temperature (0-2 hours).

Plot	R^{2*}	P-value*	Equation
TDN vs. Temp	0.008	0.778	-
NH_4 vs. Temp	0.275	0.080	-
NO_x vs. Temp	0.490	**0.025**	Y=-0.09x+2.33
DIN vs. Temp	0.267	0.086	-
DON vs. Temp	0.028	0.603	-
PO_4 vs. Temp	0.317	0.057	-
TDP vs. Temp	0.081	0.371	-

Plot	R^2*	P-value*	Equation
DOP vs. Temp	0.248	0.100	-
Silica vs. Temp	0.417	**0.023**	Y=27.0x-868
H^+ vs. Temp	0.096	0.328	-
DIN:SRP vs. Temp	0.058	0.452	-
TDN:TDP vs. Temp	0.142	0.227	-

Table 17. Coefficient of determination (R^2), probability values (*p*) and equations for benthic fluxes versus temperature (2-18 hours).

Plot	R^2*	P-value*	Equation
TDN vs. Temp	0.550	**0.006**	Y=3.5x-85.8
NH_4 vs. Temp	0.130	0.249	-
NO_x vs. Temp	0.488	**0.012**	Y=0.17x-0.43
DIN vs. Temp	0.123	0.264	-
DON vs. Temp	0.567	**0.005**	Y=4.0x-98
PO_4 vs. Temp	0.001	0.915	-
TDP vs. Temp	0.184	0.164	-
DOP vs. Temp	0.624	**0.002**	Y=0.12x-4.1
Silica vs. Temp	0.682	**0.001**	Y=14.9x-513
H^+ vs. Temp	0.022	0.647	-
DIN:SRP vs. Temp	0.0001	0.978	-
TDN:TDP vs. Temp	0.0767	0.384	-

Based on data from Phase 1, fluxes of dissolved PO_4 from sandy sediments were positively correlated with temperature (PO_4 flux [µmoles/m^2/hr] = 0.58 * [˚C] – 7.6, *p* = 0.04, r = 0.63) and increased from near 0 µmoles/m^2/hr at 13˚C to 5 to 10 µmoles/m^2/hr at 32˚C. During Phase 2, a significant positive correlation was identified for DOP versus temperature (DOP flux [µmoles/m^2/hr] = 0.12 * [˚C] – 4.1, *p* = 0.002, r = 0.62; **Figure 30c**, **Table 17**) and SiO_2 fluxes were positively correlated with sediment temperature increasing by 14.9 µM/m^2/hr per ˚C (SiO_2 flux [µmoles/m^2/hr] = 14.9 * [˚C] – 513, *p* = 0.01, r = 0.68; **Figure 30d**, **Table 17**).

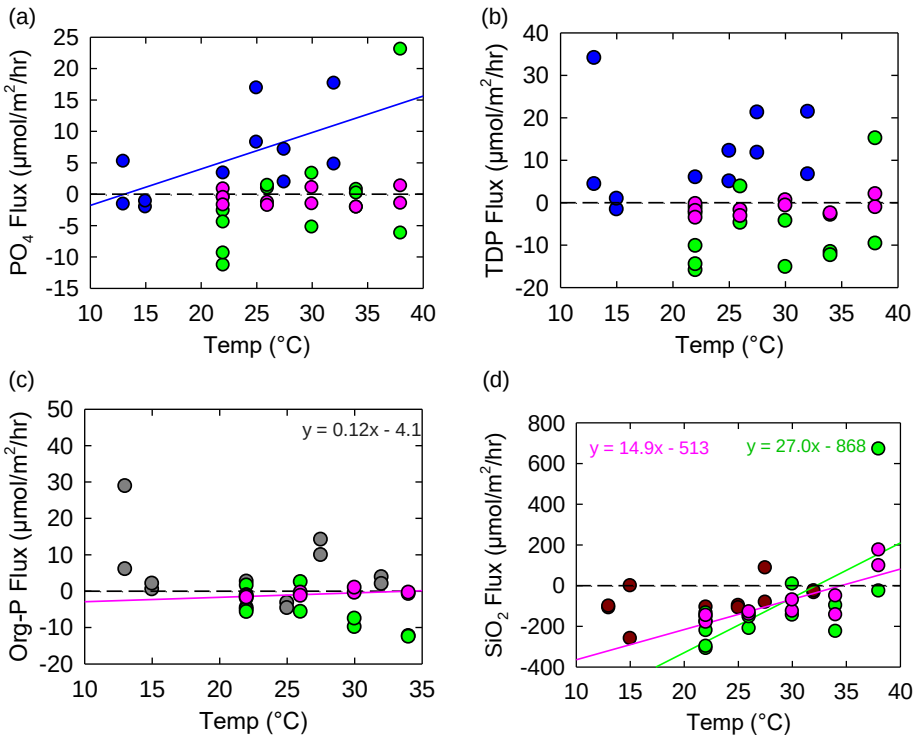

Figure 30. Laboratory incubation fluxes (sandy sediments) in µmoles/m²/hour versus sediment temperature for (a) PO_4, (b) TDP, (c) organic P, (d) SiO_2

Based on significant positive correlations between sediment temperature and NO_x, DON, TDN, PO_4, DOP, and SiO_2 fluxes, a decrease in water temperature that could result from inflow would decrease inputs of these nutrients into the lagoon. For example, a 1˚C decrease in lagoon temperature would decrease PO_4 fluxes from sandy sediments by about 0.16 tons/km²/year (0.58 µmoles/m²/hr per ˚C) or about 15% from the current median at 4.1 µmoles/m²/hr (1.1 ton/km²/year; **Table 10**). Although lagoon-wide changes to temperature are likely to be small, small changes applied to large areas of the lagoon could have significant impacts on nutrient loading. Decreased inputs of these nutrients due to restoration of ecosystem services could be of more significance than decreased concentrations due to dilution by seawater mitigating impacts of flushing on the coastal ocean as discussed in **Section 3.5**.

3.4.4 Salinity

Laboratory experiments were carried out to evaluate potential uptake or releases of nutrients associated with changes to salinity of overlying water. These experiments were carried out in water baths at 22˚C (laboratory temperature) and chambers were stirred using diffused air to maintain oxygen at 100% saturation. Before each experiment, overlying water was drained from cores and replaced with a mixture of either site water plus deionized water (decreased salinity) or with site water and added sea salt (higher salinity). Once overlying water was exchanged, cores were allowed to equilibrate for at least one hour before sampling.

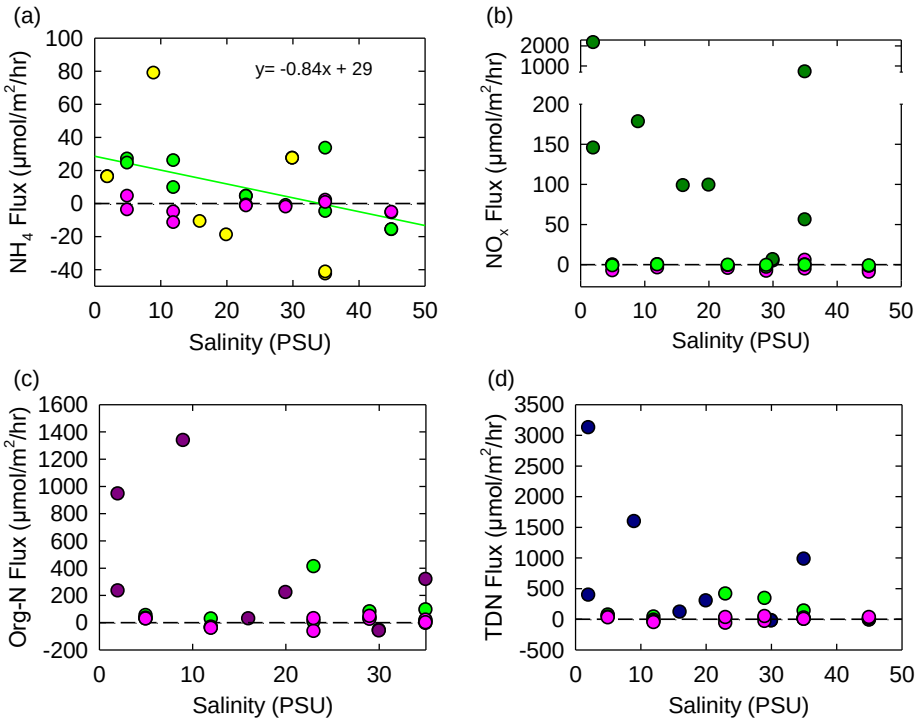

Note: Green dots show incubations from time 0–2 hours, pink dots show incubations from 2–18 hours. Other colors show data from Phase 1 experiments.

Figure 31. Laboratory incubation fluxes (sandy sediment) in µmoles/m^2/hour versus salinity for (a) NH_4, (b) NO_x, (c) organic N, and (d) TDN

During Phase 1, a significant correlation was identified for NO_x (flux (µmoles/m^2/hr) = -4.7 * [PSU] + 180) with a decrease in NO_x flux of 4.7 µmoles/m^2/hr (about 0.6 tons/km^2/hr) per PSU or about 3% per PSU from the median of 150 µmoles/m^2/hr (-20 tons N/km^2/year) for sandy sites throughout the lagoon (**Figure 31b**). This trend likely represented short-term equilibrium processes during the shorter duration experiments carried out during Phase 1. This same trend was not identified during Phase 2, likely because there was very little NO_x present in any of the cores. During Phase 2, a significant correlation was identified for NH_4 flux versus salinity (NH_4 flux (µmoles/m^2/hr) = -0.84 [PSU] + 29) during the initial incubation period where NH_4 flux decreased by 0.84 µmoles/m^2/hr per PSU) (**Figure 31a, Table 18**). This equates to a decrease of ~1% per PSU from the median of 90 µmoles/m^2/hr (11 tons N/km^2/year) for sandy sites throughout the lagoon. These trends for small changes to N fluxes observed shortly after changes to salinity likely reflect lower concentrations in overlying water for diluted (lower salinity) samples. The absence of tends over the longer incubation periods (2–18 hours) suggest that small changes to salinity alone are not likely to influence geochemical N cycling over the long-term.

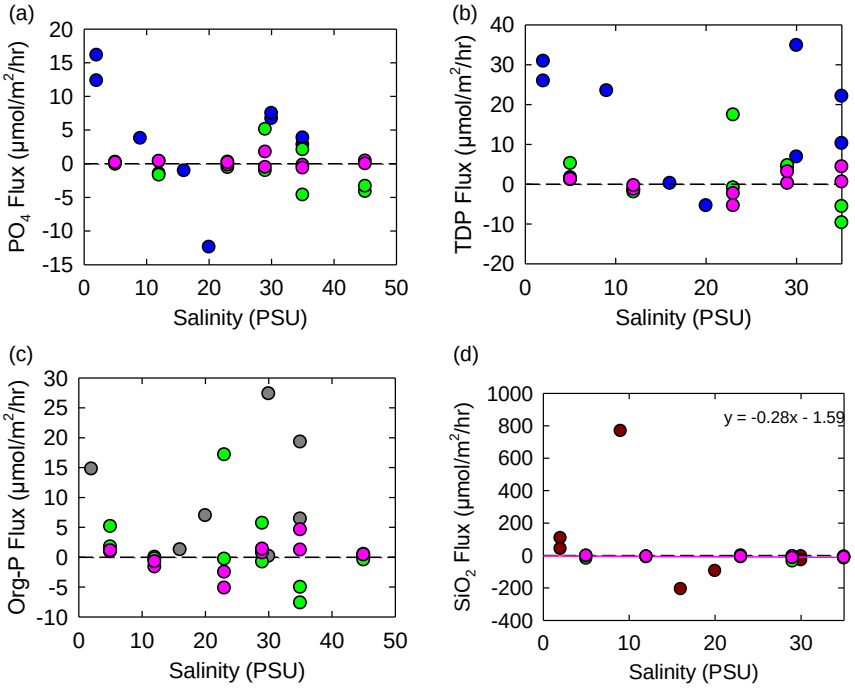

Note: Green dots show incubations from time 0–2 hours, pink dots show incubations from 2–18 hours. Other colors show data from Phase 1 experiments.

Figure 32. Results from laboratory incubation experiments showing fluxes in µmoles/m^2/hour versus the salinity of overlying water for (a) PO_4, (b) TDP, (c) organic P, and (d) SiO_2

Table 18. Coefficient of determination (R^2), probability values (*p*) and equations for benthic fluxes versus salinity (0-2 hours).

Plot	R^2*	P-value*	Equation
TDN vs. Salinity	0.002	0.886	-
NH_4 vs. Salinity	0.500	0.005	Y=-0.84x+29
NO_x vs. Salinity	0.036	0.553	-
DIN vs. Salinity	0.005	0.822	-
DON vs. Salinity	0.0001	0.978	-
PO_4 vs. Salinity	0.080	0.373	-
TDP vs. Salinity	0.137	0.237	-
DOP vs. Salinity	0.086	0.356	-
Silica vs. Salinity	0.092	0.339	-
H^+ vs. Salinity	0.201	0.144	-
DIN:SRP vs. Salinity	0.076	0.386	-
TDN:TDP vs. Salinity	0.022	0.649	-

Table 19. Coefficient of determination (R^2), probability values (*p*) and equations for benthic fluxes versus salinity (2-18 hours).

Plot	R^2*	P-value*	Equation
TDN vs. Salinity	0.032	0.576	-
NH_4 vs. Salinity	0.009	0.773	-
NO_x vs. Salinity	0.151	0.212	-
DIN vs. Salinity	0.012	0.733	-
DON vs. Salinity	0.061	0.437	-
PO_4 vs. Salinity	0.019	0.670	-

Plot	R^2*	P-value*	Equation
TDP vs. Salinity	0.040	0.532	-
DOP vs. Salinity	0.059	0.447	-
Silica vs. Salinity	0.657	**0.001**	Y=-0.28x-1.59
H^+ vs. Salinity	0.500	**0.010**	Y=2.65x-97
DIN:SRP vs. Salinity	0.236	0.120	-
TDN:TDP vs. Salinity	0.031	0.583	-

No significant trends were identified for fluxes of dissolved PO_4 versus salinity during any of the Phase 1 or Phase 2 experiments (**Figure 32; Table 18, Table 19**). These data suggest that no significant long-term changes to N or P cycling are expected based on changes to salinity. A similar study of N and P exchanges along a salinity gradient in the Florida Everglades found no correlation between fluxes of N or P and salinity while investigating how restored flow to the everglades may influence nutrient cycling (Owens et al., 2021).

3.4.5 DO

Even though DO is not a conservative property of seawater, it is one of the water quality variables likely to change if seawater were to flow into the lagoon and it is arguably one of the most important variables controlling nutrient cycling, infauna, epifauna, fish populations, and overall lagoon health. Changes to DO would likely result from (1) a change in the solubility of oxygen due to changing temperature and salinity, plus (2) inflow of lower turbidity seawater with lower respiration, and (3) higher density seawater and enhanced circulation that could mix deep areas currently prone to stagnation and low DO events. To manipulate DO concentrations in the laboratory, cores were place in temperature stable water baths (22°C laboratory temperature) and continuously bubbled using mixed gases (air and nitrogen) to maintain DO concentrations between 0% (0 mg/L) and 100% saturation (7-8 mg/L).

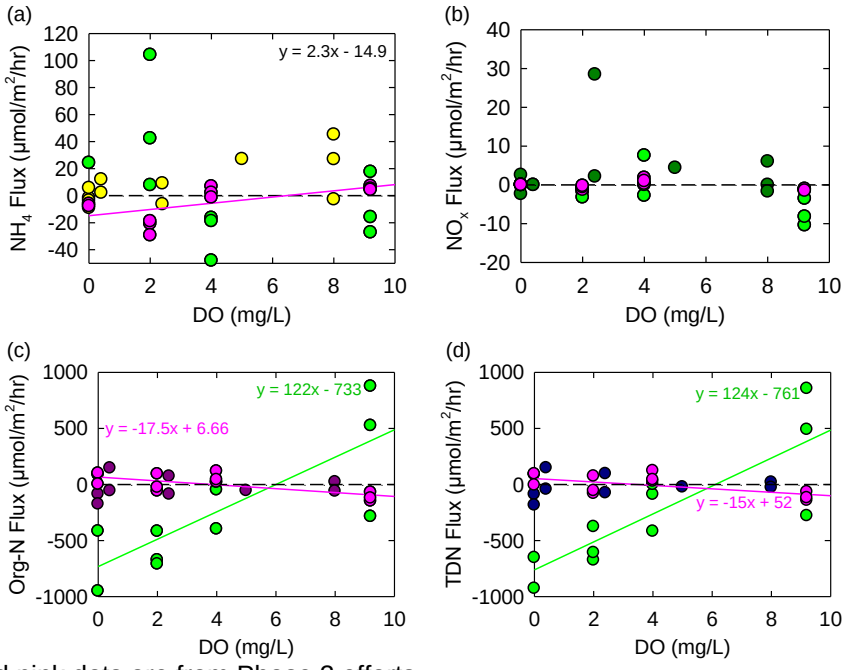

Note: Green and pink dots are from Phase 2 efforts.

Figure 33. Results from laboratory incubation experiments showing fluxes in µmoles/m²/hour versus bottom water DO concentrations (mg/L) for (a) NH_4, (b) NO_x, (c) organic N, and (d) TDN versus the salinity of overlying water

Consistent with trends observed for in-situ benthic chambers, significant positive correlations were identified for organic and total N versus concentrations of DO in bottom water (DON flux [µmoles/m^2/hr] = 122 * [mg/'] – 733, *p* = 0.003, r = 0.63; TDN flux (µmoles/m^2/hr) = 124 * [mg/L] – 761, *p* = 0.002, r = 0.69; **Table 20**, **Figure 33**). In both the field and in the laboratory, sediments switched from a sink of organic and total N to a source, as DO concentrations increased above ~6-8 mg/L. These data show an ~15 tons/km^2/year increase in TDN fluxes, almost all as organic N, per mg/L increase in DO. This result is likely tied to the relationship between SOD and bottom water DO, where greater oxygen consumption (respiration and nutrient cycling) by sediments yielded lower bottom water DO concentrations. In other words, higher rates of decomposition in sediments yielded higher fluxes of organic and total N. In the laboratory, following an initial pulse of organic N and TDN, aerobic sediments were a net sink for organic N and TDN (-82 ± 89 µmoles/m^2/hr) and anaerobic sediments were sometimes a source of organic N and TDN to overlying water (119 ± 240 µmoles/m^2/hr) (**Figure 33**), with a significant negative correlation (-15 µmoles/m^2/hr per mg/L) identified between TDN flux and DO over the 2-18 hour incubation (**Figure 33**; **Table 20**, **Table 21**).

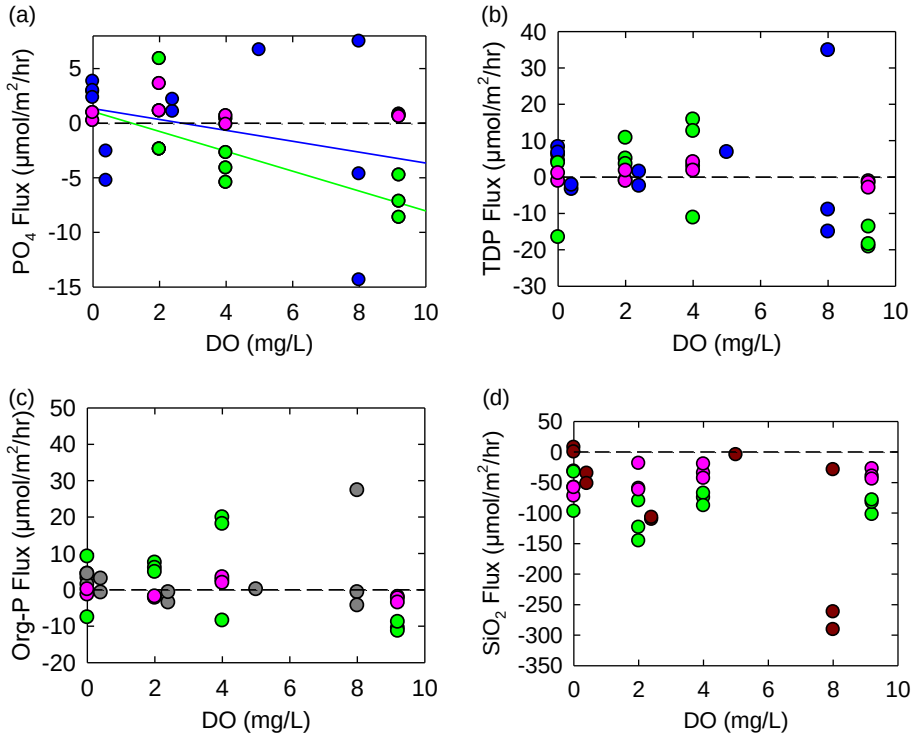

Note: Hashed box shows DIN:SRP values below zero where either DIN or SRP were directed into sediments.

Figure 34. Results from laboratory incubation experiments showing fluxes in µmoles/m^2/hour versus bottom water DO concentrations (mg/L) for (a) PO_4, (b) organic P, (c) TDP, and (d) SiO_2 plus (e) molar ratios of DIN to SRP versus sediment temperature

Fluxes of dissolved PO_4 decreased at higher concentrations of bottom water DO (PO_4 flux [µmoles/m^2/hr] = -0.9 * [mg/L] + 1.6, *p* = 0.03, r = 0.50; **Figure 34**, **Table 20**).These observations were consistent with data from the field study, where PO_4 fluxes from hypoxic sediments were typically higher and positive from anaerobic sediments (19 ± 11 µmoles/m^2/hr in December 2020 and February 2021), compared to a negative median flux (-4.4 ± 7.3 µmoles/m^2/hr) under aerobic

conditions during all other sampling events (**Figure 34a** and **Figure 23a**). Laboratory incubations with multiple sample intervals captured changes to nutrient cycling that resulted from the initial change and dump of P and longer-term sampling captured the more stable fluxes at new DO concentrations. Variable responses as identified during different experimental periods are consistently identified in the literature (e.g., Foster and Fulweiler 2019), mostly due to the complexities of the N and P cycles as discussed earlier.

Table 20. Coefficient of determination (R^2), probability values (*p*) and equations for benthic fluxes versus DO (0–2 hours).

Plot	R^{2}*	P-value*	Equation
TDN and DO	0.686	**0.002**	Y=124x-761
NH_4 and DO	0.021	0.673	-
NO_x and DO	0.368	0.048	
DIN and DO	0.014	0.730	-
DON and DO	0.633	**0.003**	Y=122x-733
PO_4 and DO	0.500	**0.033**	Y=-0.9x+1.06
TDP and DO	0.279	0.095	-
DOP and DO	0.252	0.116	-
Silica and DO	0.0001	0.978	-
H^+ and DO	0.007	0.802	-
DIN:SRP and DO	0.016	0.709	-
TDN:TDP and DO	0.165	0.215	-

Table 21. Coefficient of determination (R^2), probability values (*p*) and equations for benthic fluxes versus DO (2–18 hours).

Plot	R^2	P-value	Equation
TDN and DO	0.371	**0.047**	Y=-15x+52
NH_4 and DO	0.420	**0.031**	Y=2.3x-14.9
NO_x and DO	0.174	0.202	-
DIN and DO	0.370	**0.047**	-
DON and DO	0.474	**0.019**	Y=-17.5x+66.6
PO_4 and DO	0.042	0.545	-
TDP and DO	0.146	0.247	-
DOP and DO	0.077	0.409	-
Silica and DO	0.214	0.152	-
H^+ and DO	0.064	0.454	-
DIN:SRP and DO	0.453	**0.023**	Y=2.8x-15.0
TDN:TDP and DO	0.429	**0.029**	Y=11.4x-32.0

3.5 Summary of Experimental Results

Although water column processes play a major role in overall nutrient recycling, no significant correlations were identified between water column nutrient fluxes and changes to temperature, salinity, or DO (**Section 3.4.1**). Although no changes were observed in response to variations in temperature, salinity, or DO, mixing seawater with differing turnover times into lagoon water would, in and of itself, influence nutrient cycling in the area of inflow as discussed in **Section 3.3.1**. Significant positive correlations were identified for NO_x, TDN, PO_4, DOP, and SiO_2 versus sediment temperature (**Table 17**), indicating that lower temperature would decrease internal loading (inputs) of these nutrients into the IRL. Shortly after changing salinity, significant negative correlations were identified between NH_4 and nitrate fluxes and salinity; however, these gave way to no significant correlations beyond initial pulses of NH_4 and nitrate released following a decrease in salinity. Significant positive correlations were identified between DO and both DON

and TDN (**Table 20**); however, after initial releases, significant negative correlations were identified between DON and TDN and DO and a positive correlation between ammonium and DO (**Table 21**).

Overall, significant correlations were identified between N and P and temperature plus DO, but not salinity. Using equations from statistically significant relationships, quantities of nutrients that could be removed or prevented from entering the lagoon in response to changes in temperature or DO have been calculated using preliminary data from this study. Because these responses are scalable depending on the magnitude of change to temperature or DO and the area of lagoon that experiences various levels of change (km^2), results are presented per °C and per mg/L per km^2 (**Table 22**).

Table 22. Expected changes to fluxes of N and P resulting from an increase in temperature of 1°C and an increase in DO of 1 mg/L.

	Change in N flux / °C	**Change in P flux / °C**
Water	-	-
Sediment	0.4 tons/km^2/year/°C	0.16 tons/km^2/year/°C
	Change in N flux / mg*L^{-1}	**Change in P flux / mg*L^{-1}**
Water	-	-
Sediment	1.8 tons/km^2/year/mg*L^{-1}	-0.9 µmoles/m^2/hr (0.24 tons/km^2/year/mg*L^{-1})

Using a simple mixing model for temperature, a current residence time for water in the northern lagoon (~300 days, Smith 1993), inflow of seawater at 0.5 m^3/sec, and average difference in temperature in the lagoon and in Port Canaveral (~0.5°C), the average change in lagoon temperature over various spatial scales with inflow (new equilibrium temperatures) was calculated and used to estimate decreases in N and P loading from sandy sediments. Changes in temperature assume that heating is proportional to ratios of lagoon water and Port water with associated particles and color (i.e., clearer water absorbs less heat). Even though the change in temperature would be greater if mixing occurred over a smaller area, small changes over larger areas would have more impact on decreasing fluxes and internal nutrient loading. For example, if mixing from the pilot study (0.5 m^3/sec) occurred over 5 km^2, we calculated that 0.6 tons of N and 0.3 tons of P would be prevented from entering the lagoon each year based on a decrease in lagoon temperature of 0.23°C over 5 km^2 and decreased fluxes (e.g., 0.4 tons N/km^2/year/°C * 0.23°C * 5 km^2 = 0.6). If mixing occurred throughout the entire 170 km^2 of the BRL, we estimate that 1.6 tons of N and 0.7 tons of P would be prevented from entering the lagoon each year based on a 0.02°C decrease in lagoon temperature over 170 km^2. Based on modeling of inflow in the corresponding engineering and modeling report (Task 1), mixing after the startup period is expected with limited impacts throughout the BRL. Based on these data and calculations, the quantity of nutrients removed via changes to benthic fluxes is expected to be greater than the net quantity of nutrients that would be discharged to the coastal ocean (**Section 3.2.3**). Additional benefits are expected based on increased DO concentrations; however, these improvements are less easily modeled. Nevertheless, these data suggest that a pilot inflow project would yield net removal of N and P from the combined lagoon-ocean system, where decreased nutrient concentrations resulting from changes to internal cycling are expected to exceed changes to resulting from direct exchanges of water.

Although trends used here were statistically significant, varying responses over different time intervals and large natural variability resulted in low than expected statistical power. For this reason, we use caution when extrapolating these small changes over large areas as presented here and plan to focus future efforts in developing trends. Our recommendation is to carry out

additional focused sampling to better link field and laboratory results thereby improving power of these outcomes.

Overall, laboratory experiments carried out to estimate the potential impacts of pumping on geochemical nutrient cycling showed that lower lagoon temperature and higher DO led to significant decreases in benthic fluxes for N and P. These observations suggest that geochemical responses to inflow would contribute to decreasing nutrient concentrations within the IRL, mitigating discharges to the coastal ocean. Data obtained during this study illustrate the importance of DO in the IRL towards regulating fluxes and cycling of dissolved nutrients. Despite the relative importance of DO towards predicting nutrient fluxes, few data are available for bottom water DO near the sediment-water interface where DO influences benthic fluxes. To that end, Florida Tech established a network of DO sensors to aid in modeling efforts and to better understand benthic-pelagic coupling in this system. These observations are consistent with recent other studies showing that sediments play a key role in maintaining hypoxic conditions in bottom water (e.g., Rabouille et al., 2021).

3.5.1 Bottom Water DO

Due to the dependence of biogeochemical nutrient cycling on DO, it is not possible to accurately model nutrient fluxes, turnover times, or nutrient concentrations without a detailed picture of DO in the lagoon. To assist modeling efforts, long-term datasets for DO concentrations from the IRL and BRL were obtained for surface water from SJRWMD (**Figure 35**). Most existing sensors record DO at fixed depths, often in the middle of the water column, and can miss events that are restricted to the near bottom. For example, sensors referenced in this study had average depths during 2019 to 2021 of ~0.5-1.5 m (SJRWMD). Overall data for DO from these sensors showed annual trends relatively consistent with variations in DO solubility. For example, at a salinity of 25, a reasonable average for the IRL, DO solubility increases from 6.4 mg/L at 32°C to 8.7 mg/L at 15°C, an annual range of 2.3 mg/L (**Figure 36**). In addition to this expected range in DO (at 100%), values sometimes fell below saturation during summer with some instances of hypoxia (<2 mg/L) recorded by existing sensors located in the middle of the water column (e.g., cyan line, **Figure 35**). Consistent with the more limited dataset from Phase 1, during winter months, DO in bottom water at sandy sites typically tracked patters for DO at 0.5-1.5 m (**Figure 35**); however, during summer months, bottom water DO was often lower and less stable, especially following peaks in DO concentrations (pink line, **Figure 35**).

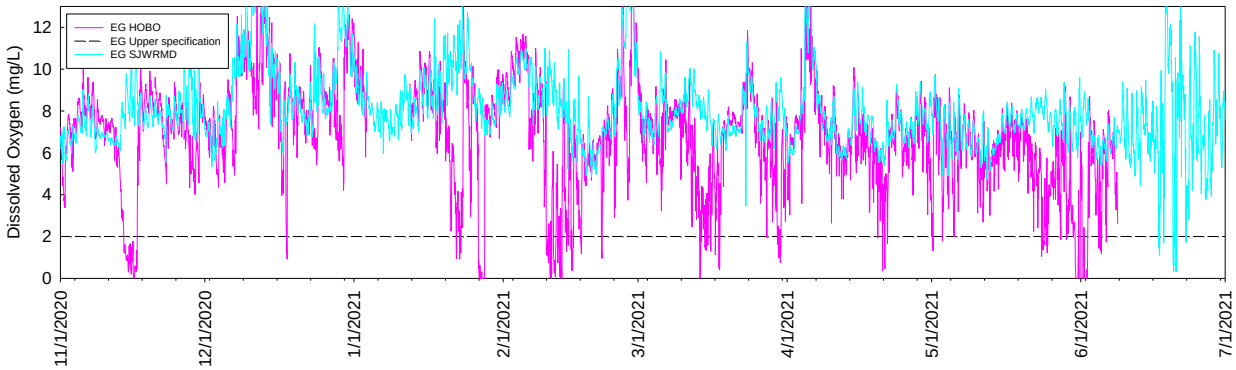

Figure 35. Concentrations of DO (mg/L) in the IRL near Eau Gallie in bottom water (<10 cm above the bottom; cyan line) and at mid-depths ~1-1.5m (pink line) with the dashed black line at 2 mg/L indicating hypoxic conditions

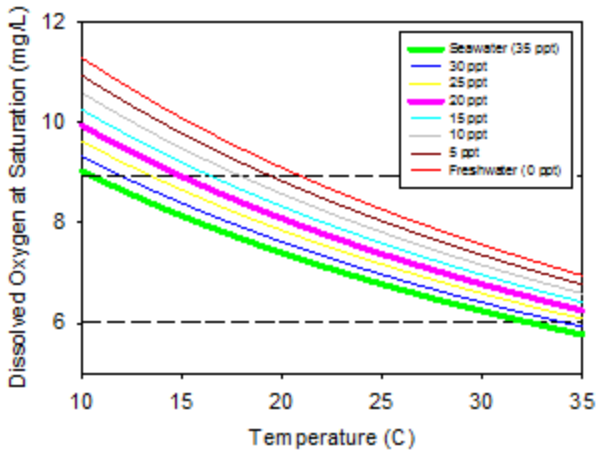

Figure 36. DO (mg/L) at saturation (100%) versus temperature for seawater at 35 PSU, freshwater at 0 PSU and at 5 PSU intervals

Sensors deployed in the BRL near the reference/control location showed stark differences for DO in bottom water overlying mud (muck) versus sand, although the sensors are only about 200-m apart (**Figure 37**). These data are consistent with SOD differences among substrates from -3,200 µmoles/m^2/hr for sandy sites (lagoon wide annual average) and -4,300 µmoles/m^2/hr for muddy sites (during winter months).

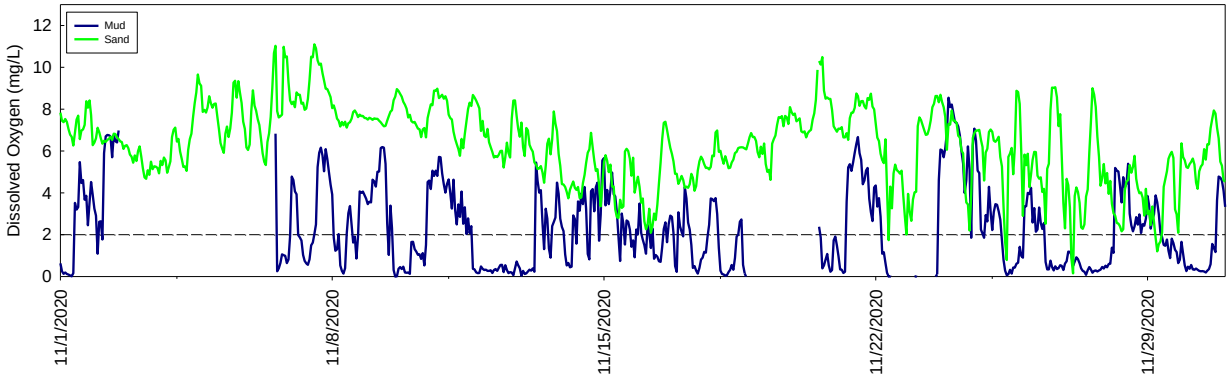

Figure 37. Bottom water DO at sites near the lagoon reference area at sites containing muck (blue line) and sand (green line) with the dashed black line at 2 mg/L indicating hypoxic conditions

In Port Canaveral, concentrations of DO followed patterns similar to those observed in the adjacent lagoon (**Figure 38**); however, diurnal fluctuation in the Port were much less than those observed in the lagoon. For example, DO in the lagoon varied by 4-6 mg/L on a daily basis (dark yellow line on **Figure 38**), relative to diurnal variations of only 1-2 mg/L in Port Canaveral (dark yellow line **Figure 38**).

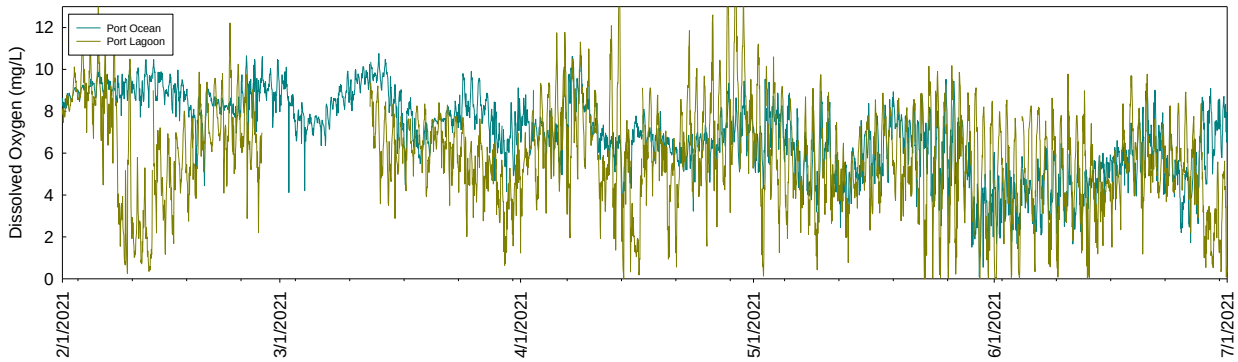

Figure 38. DO in the BRL in the area of inflow and in Port Canaveral

Temporal and spatial differences in bottom water DO, such as the examples shown above, can drive spatial and temporal changes, where sediments alternate between sinks and sources of nutrients (**Section 3.3** and **Section 3.4**). Changes to DO in bottom water lead to changes in concentrations and the relative abundance of bioavailable N and P with implications to algal community composition and density. As a result, data for bottom water DO are essential to improving lagoon modeling, not only for this project but for any generalized nutrient loading or HAB models (**Figure 39**).

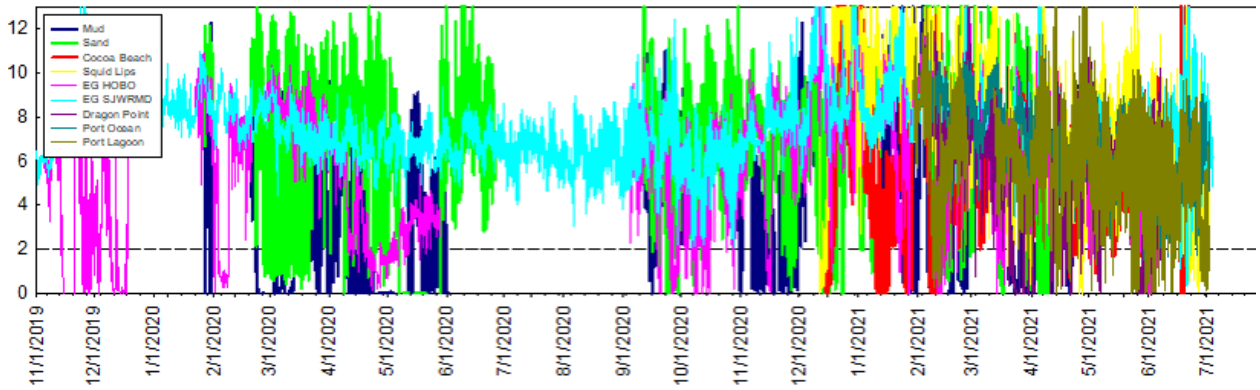

Figure 39. Plot showing all data for bottom water DO obtained during this study

3.5.2 Known Muck Distribution

N and P loading from muck deposits are calculated and modeled based on estimates for the current surface area of muck present in the lagoon at a given time. Despite coving only an estimated <10% of the lagoon bottom, muck is a significant source of N and P to overlying water while also acting as a large sink for dissolved oxygen (Fox and Trefry 2018). To assist in modeling efforts and to better resolve the relative importance of muck versus sand, data for known muck deposits in the IRL have been synthesized into a single map (e.g., **Figure 40**).

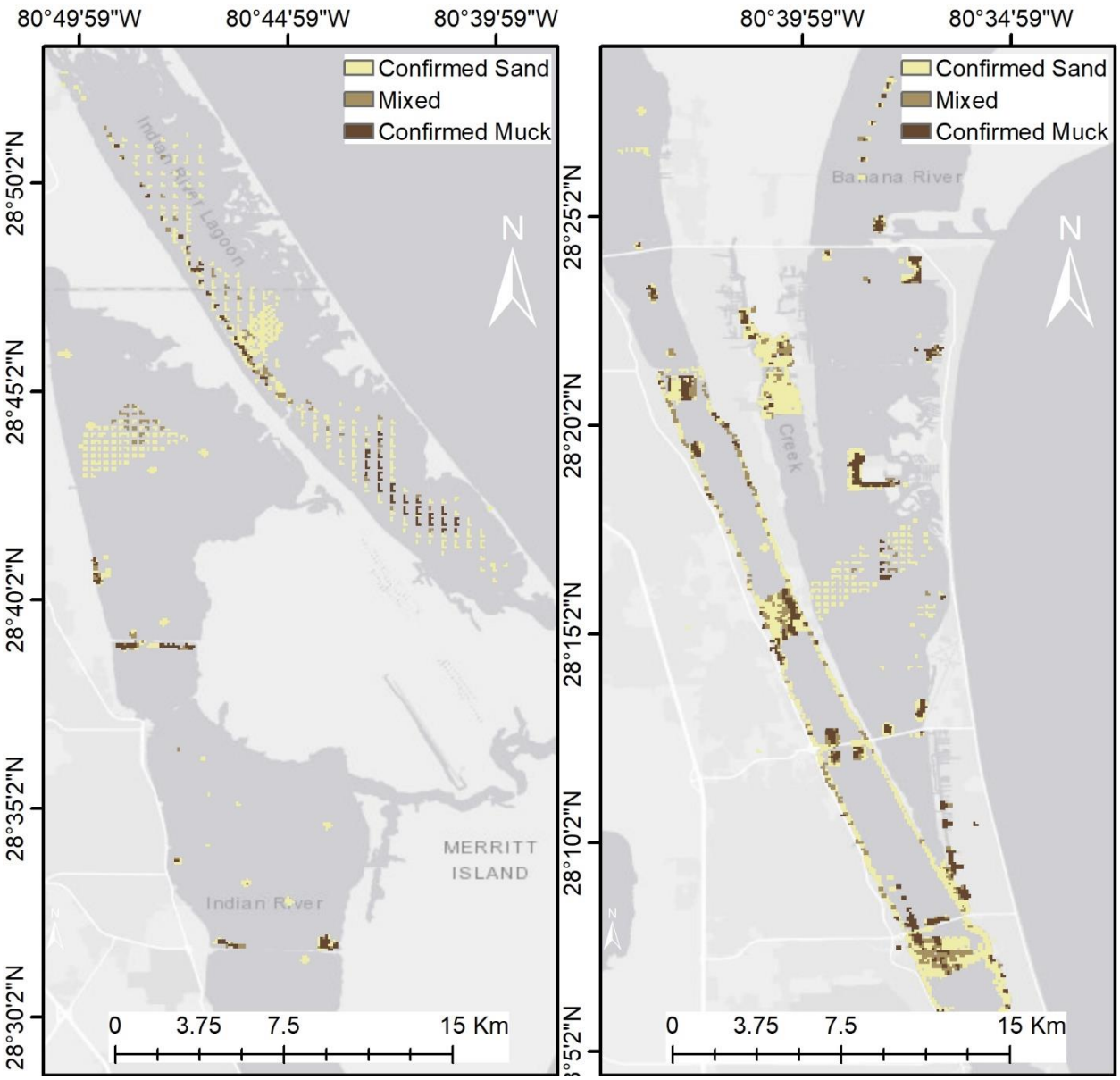

Figure 40. Map of the northern IRL, Mosquito Lagoon, and BRL showing locations of confirmed sand, mixed sand and muck, and confirmed muck with 100 m spatial resolution

This years-long effort has yielded numerous contoured plots showing detailed distributions of muck in discrete deposits; however, for a larger, lagoon-wide map, contouring often misrepresents areas where muck is present and changes in thickness have not been identified. In other words, contouring does not allow for unbiased inclusion of individual data points and can be misleading when conducted over large areas. With input from computer modelers, the lagoon-wide map was approached as a gridded raster where each cell contains a value signifying known sand, known muck (probe penetration), or something in-between only where data are available. Although the resolution could change from region to region based on the resolution of available data, this initial synthetic map uses a 100 m (~300 ft) grid pattern showing only areas where data is present (**Figure 40**).

4 Summary, Next Steps, and Timeline

Eutrophication of coastal marine ecosystems around the world has become increasingly common due to enhanced nutrient loading from adjacent watersheds (Brady et al., 2013; Diaz and Rosenberg 2008). As the eutrophic state progresses, sediment mineralization becomes increasingly important as a source of nutrients to overlying water as has been observed in the IRL (Cowan and Boynton 1996; DiDonato et al., 2006; Seitzinger 1988; Kemp et al., 1990; Fox and Trefry 2018). In eutrophic systems, HAB events contribute to occurrences of hypoxia and anoxia, where even short hypoxic or anoxic events can promote loss of ecosystem services including coupled nitrification-denitrification that removes N from the system as inert N gas and sequestration of P into sediments. Loss of these ecosystem services over time and space create positive feedback loops sustaining eutrophication. Distinct differences in the ability of poorly flushed versus well flushed estuaries to cope with eutrophication have been observed throughout the literature, where poorly flushed estuaries with long residence times, like the IRL, more readily retain nutrients to promote algal blooms, loss of seagrass beds, hypoxia, and loss of ecosystem services (Defne and Ganju 2015; Kemp et al., 1992; Twilley et al., 1999). Within this conceptual framework, impacts of enhanced inflow of seawater into the IRL were evaluated for its potential to (1) directly decrease nutrient concentrations and (2) promote water column and sediment processes that would help to restore ecosystem services to remove or prevent N and P from entering the lagoon.

Overall, temperatures in Port Canaveral and the coastal Atlantic Ocean were moderate relative to more variable and extreme temperatures in the lagoon, with roughly 0.5-1°C cooler temperatures in Port Canaveral during March to November and in some cases 4-5°C warmer temperatures during winter months. Salinity was, on all occasions, higher in Port Canaveral than in the lagoon, leading to distinct densities among the lagoon (1,008-1,016 kg/m^3) and Port (1,018-1,028 kg/m^3) water masses. These data indicate that inflow of seawater and a mixed water mass would favor circulation in bottom water, on average decreasing temperature, raising salinity (slightly) and helping to raise and stabilize concentrations of DO at the sediment-water interface.

Overall, concentrations of TDN and TDP were lowest at offshore sites (8 ± 2.4 µM TDN, 0.15 ± 0.05 µM TDP); nevertheless, concentrations in Port Canaveral (23 ± 10 µM TDN, 0.37 ± 0.19 µM TDP) were 5-fold and 3-fold lower than concentration in the IRL (119 ± 35 µM TDN, 1.2 ± 0.71 µM TDP). If the proposed pilot inflow project (0.5 m^3/sec) were to occur, 6.5 tons of N and 0.6 tons of P would be discharged from the lagoon, mostly through Sebastian Inlet to the coastal Atlantic Ocean. Conversely, seawater from Port Canaveral would bring with it 5 tons of N and 0.2 tons of P for a maximum net discharge, assuming no change to internal nutrient cycling, of 1.5 tons of N and 0.4 tons of P per year. In the context of nutrient loading, these values represent 0.1% and 0.3% of the annual inputs of N and P (1,400 tons N and 140 tons of P) from the lagoon each year, respectively. Consequently, this small pilot project would have little impact at the lagoon scale; however, changes at the inflow site would facilitate a scientifically sound scaled down study of inflow in a well-defined area while preserving reference/control sites and also mitigating risk of adverse impacts to the broader lagoon. Data from the pilot study could then be used to determine the scale of a full-sized project necessary to achieve desired improvement to water quality.

Biogeochemical responses of the water column and sediments to changes in temperature, salinity, and DO were investigated using a combination of field and laboratory experiments. Sediment and water column incubations in the field were used to establish current rates of nutrient fluxes and cycling from sandy sediments and water in the lagoon and to serve a baseline to evaluate changes over time. Overall, benthic fluxes from sandy sediments could cycle all of the

N in the water column in ~7 days relative to <1 day via recycling in the water column, and sediments accounted for only 10% of the total nitrogen cycling. The complete pool of dissolved P could be completely removed by oxic sandy sediments in ~18 days and recycling in the water column replaced all the dissolved P in less than 2 days. Similar to results for N, sediments accounted for only ~10% of the TDP cycling. Overall, at sandy sites, TDN fluxes were highly variable and on average directed into sediments; however, fluxes of NH_4 and nitrate were directed out of sediments at 90 ± 60 μmoles/m^2/hr (11 tons/km2/year) and 150 μmoles/m^2/hr (tons/km2/year), respectively. Similar to trends for N, TDP was directed into sandy sediments and inorganic P (PO_4) had a positive flux at 4.1 ± 8.1 μmoles/m^2/hr (1.1 ton/km2/year).

Despite the importance of water column processes on overall nutrient cycling, no significant correlations were identified between water column fluxes of N or P and changes to temperature, salinity, or DO. Despite no significant changes, lower rates of recycling in the proposed inflow water from Port Canaveral and lower N:P ratios (DIN:SRP 45 in the lagoon, 20 in Port Canaveral; TDN:TDP 113 in the lagoon, 97 in Port Canaveral) would, when mixed, help to slow recycling and promote lower N:P ratios in the new, mixed water mass. Lower concentrations and ratios of N:P would help to promote beneficial photosynthesizers. In laboratory incubation experiments, significant positive correlations were identified between benthic fluxes of NO_x, TDN, PO_4, DOP, and SiO_2 versus sediment temperature. Collectively, these data show that lowering lagoon temperatures, a likely result of inflow, would help to reduce inputs of both N and P to the lagoon. Based on a simple mixing model, the pilot project is expected to prevent 1.6 tons of N and 0.7 tons of P from entering the lagoon each year based on lower lagoon temperatures. Using average costs for removal of N and P from the Brevard County Save Our Indian River Lagoon Project Plan (Tetra Tech, 2021; $384 per pound of N and $4,650 per pound of P), estimated load reductions from sediments alone would be valued at greater than $9 million per year. Overall, based on laboratory experiments, no long-term changes in nutrient cycling are expected based on changes to salinity. Finally, in both field measurements and laboratory experiments, low DO promoted release of PO_4 and NH_4, both known to promote HABs. In contrast, higher, stable concentrations of DO promoted removal of PO_4 while also promoting fluxes of nitrate over NH_4, both changes that support beneficial photosynthesizers. Based on these data and trends, lower lagoon temperatures and higher and stabilized bottom water DO expected to result from inflow would support lower nutrient concentrations and ratios promoting species of nutrients that are more favorable to beneficial photosynthesizers.

Concentrations of DO in bottom water (<10 cm above the bottom) followed general seasonal patterns observed at mid-depths reported by other existing monitoring networks; however, bottom water experienced frequent periods of hypoxia or anoxia, likely due to proximity to sediments responsible for 20-50% of the total respiration. These new data are essential towards improving lagoon models used in this study and other generalized nutrient loading or HAB models. Other notable observations from our growing network of bottom water DO sensors was lower concentrations of DO overlying muck deposits relative to concentrations in bottom water overlying directly adjacent sand. On an annual scale, concentrations of DO in Port Canaveral tracked concentrations in lagoon water, both lagoon and seawater varying in response to changes in solubility over time. Despite similarities in long-term trends, diurnal fluctuations in Port Canaveral were much less that those in the lagoon, due mostly to 30% lower rates of dark respiration in Port Canaveral and almost monthly instances of hypoxia observed in lagoon were not observed in Port Canaveral.

To date, this project has greatly improved our understanding of nutrient cycling in the IRL system, especially in sandy sediment and in the water column. These data are useful not only to modeling possible impacts of inflow, but for HAB and for generalized nutrient load modeling, especially as

we look to addressing changes to temperature and rainfall associated with changing climatic patterns. Despite knowledge gained during this study, the lagoon is dynamic and with this temporally limited dataset, it is not possible to isolate natural, seasonal patterns from event scale occurrences, something that would be more feasible in the near future (1-2 years) if data collection were able to continue. Data to date have demonstrated the importance of processes in sandy sediments and on particles and have yielded wide ranges of values for these critical processes. Additional data collection is needed to explain seasonal versus event scale variability and improve statistical power of trends identified to date, improving confidence in extrapolated models. Due to the importance of bottom water DO towards cycling of both N and P and because this is the only continuous dataset for bottom water DO to date, we hope to find long-term support for this network of quality controlled bottom water sensors. We view these collective datasets as tools that will help managers select restoration projects based on potential to restore natural cycling of N or P to make efficient use of taxpayer dollars. To continue the specific study of inflow and in response to results to date, we plan to investigate changes in oxygen and nutrient cycling in direct mixtures of lagoon water and seawater over time. This next step (1 year) reflects the large fraction of the overall nutrient cycling that occurs in the water column and non-conservative changes when particles are mixed. We propose these next steps to take place before and alongside the proposed pilot inflow project that will move water from the coastal Atlantic Ocean into the lagoon. Overall, data to date support a limited test of inflow as part of a multifaceted approach to lagoon restoration.

5 References

Accoroni, S., Romagnoli, T., Pichierri, S., and Totti, C. 2016. Effects of the bloom of harmful benthic dinoflagellate Ostreopsis cf. ovata on the microphytobenthos community in the northern Adriatic Sea. Harmful Algae, 55, 179-190.

Azanza, R. V., Siringan, F. P., San Diego-Mcglone, M. L., Yniguez, A. T., Macalalad, N. H., Zamora, P. B., Agustin, M. B., Matsuoka, K. 2004. "Horizontal dinoflagellate cyst distribution, sediment characteristics and benthic flux in manila bay, philippines." Phycological Research 52(4):376-386.

Bartoli, M., Nizzoli, D., Zilius, M., Bresciani, M., Pusceddu, A., Bianchelli, S., Sundback, K., Razinkovas-Baziukas, A., and Viaroli, P. 2021. Denitrification, nitrogen uptake, and organic matter quality undergo different seasonality in sandy and muddy sediments of a turbid estuary. Frontiers in Microbiology. 11:612700. doi: 10.3389/fmicb.2020.612700.

Boynton, W.R., M.A.C. Ceballos, E.M. Bailey, C.L.S. Hodgkins, J.L. Humphrey, and J.M. Testa. 2018. "Oxygen and nutrient exchanges at the sediment-water interface: a global synthesis and critique of estuarine and coastal data." Estuaries and Coasts 41:301-333.

Brady, D.C., J.M. Testa, D.M. Di Toro, W.R. Boynton, and W.M. Kemp. 2013. "Sediment flux modeling: calibration and application for coastal systems." Estuarine, Coastal and Shelf Science 117:107-124.

Burford, M.A., Davis, T.W., Orr, P.T., Sinha, R., Willis, A., and Neilan, B.A. 2014. Nutrient-related changes in the toxicity of field blooms of the cyanobacterium Cylindrospermopsis raciborskii. FEMS Microbiology and Ecology 89:135–148, https://doi.org/10.1111/1574-6941.12341.

Burkholder, J.M., D.A. Tomasko, and B.W. Touchette. 2007. "Seagrasses and Eutrophication." Journal of Experimental Marine Biology and Ecology 350:46-72.

Cavender-Bares, K.K., Karl, D.M., Chisholm, S.W. 2001. "Nutrient gradients in the western North Atlantic Ocean: Relationsips to microbial community structure and comparison to patterns in the Pacific Ocean." Deep-Sea Research I 2373-2395.

Chen, B., Kang, W., and Hui, L. 2019. Akashiwo sanguinea blooms in Chinese waters in 1998–2017. Marine Pollution Bulletin, 149, 110652.

Choudhury, A.K., and P. Bhadury. 2015. "Relationship between N:P:Si ratio and phytoplankton community composition in a tropical estuarine mangrove ecosystem." Biogeosciences Discussions 12:2307-2355.

Cowan, J.L.W., and W.R. Boynton. 1996b. "Sediment-water oxygen and nutrient exchanges along the longitudinal axis of Chesapeake Bay: seasonal patterns, controlling factors and ecological significance." Estuaries 19:562-580.

Cowan, J.L.W., Pennock, J.R., and W.R. Boynton. 1996a. "Seasonal and interannual patterns of sediment-water nutrient and oxygen fluxes in Mobile Bay, Alabama (USA): regulating factors and ecological significance." Marine Ecology Progress Series 141:229-245.

Csanady, G.T. 1978. "The arrested topographic wave." Journal of Physical Oceanography 8:47-62.

Defne, Z, and Ganju, N.K. 2015. "Quantifying the residence time and flushing characteristics of a shallow, back-barrier estuary: application of hydrodynamic and particle tracking models." Estuaries and Coasts 38:1719-1734.

DeYoe, H.R., Buskey, E.J., and Jochem, F.J. 2007. Physiological responses of Aureoumbra lagunensis and Synechococcus sp. to nitrogen addition in a mesocosm experiment. Harmful Algae, 6(1), 48-55.

Diaz, R.J., and R. Rosenberg. 2008. "Spreading dead zones and consequences for marine ecosystems." Science 321:926-929.

DiDonato, G.T., E.M., Murrell, M.C. Lores, L.M. Smith, and J.M. Caffrey. 2006. "Benthic nutrient flux in a small estuary in northwest Florida (USA)." Gulf and Caribbean Research 18:15-26.

Foster, S.Q., and R.W. Fulweiler. 2019. "Estuarine sediments exhibit dynamic and variable biogeochemical responses to hypoxia." Journal of Geophysical Research: Biogeosciences 124:737-758.

Fox, A.L., and J.H. Trefry. 2018. "Environmental dredging to remove fine-grained, organic-rich sediments and reduce inputs of nitrogen and phosphorus to a subtropical estuary ." Marine Technology Society 52: 42-57.

Glibert, P.M., Burkholder, J.M., and Kana, T.M. 2012. Recent insights about relationships between nutrient availability, forms, and stoichiometry, and the distribution, ecophysiology, and food web effects of pelagic and benthic Prorocentrum species. Harmful Algae, 14, 231-259.

Guo, H., Guan, C., Yang, L., and Lu, D. 2017. Pseudo-nitzschia species. Conditions promoting extreme Pseudo-nitzschia events in the eastern Pacific but not the western Pacific, PICES Report No. 53:20-27.

Hammond, D.E., K.M. Cummins, J. McManus, W.M. Berelson, G. Smith, and F. Spagnoli. 2004. "Methods for measuring benthic nutrient flux on the California margin: comparing shipboard core incubations to in situ lander results." Limnology and Oceanography 2:146.

Harris, G. P. 1986. Phytoplankton ecology: Structure, function, and fluctuation. London; New York: Chapman and Hall.

Harris, L.A., C.L.S. Hodgkins, M.C. Day, D. Austin, J.M. Testa, W. Boynton, L. Van Der Tak, and N.W. Chen. 2015. "Optimizing recovery of eutrophic estuaries: impact of destratification and re-aeration on nutrient and dissolved oxygen dynamics." Ecological Engineering 75:470-483.

Hauss, H., Franz, J. M., and Sommer, U. 2012. Changes in N: P stoichiometry influence taxonomic composition and nutritional quality of phytoplankton in the Peruvian upwelling. Journal of sea Research, 73:74-85.

Heiri, O., A.F. Lotter, and G. Lemcke. 2001. "Loss on ignition as a method for estimating organic and carbonate content in sediments: reproducibility and comparability of results." Journal of Paleolimnology 25:101-110.

Hillebrand, H., Steinert, G., Boersma, M., Malzahn, A., Meunier, C.L., Plum, C., Ptacnik, R. 2013. Goldman revisited: Faster-growing phytoplankton has lower N:P and lower stoichiometric flexibility. Limnology and Oceanography 58:2076-2088.

J.B., Martin, J.E. Cable, C. Smith, M. Roy, and J. Cherrier. 2007. "Magnitudes of submarine groundwater discharge from marine and terrestrial sources: Indian River Lagoon, Florida." Water Resources Research 43:1-15.

Jassby, A.D., and E.E. Nieuwenhuyse. 2005. "Low dissolved oxygen in an estuarine channel (San Joaquin River, California): mechanisms and models based on long-term time series." San Francisco Estuary and Watershed Science 3(2).

Kemp, W.M., J.M. Testa, D.J. Conley, D. Gilbert, and J.D. Hagy. 2009. "Temporal responses of coastal hypoxia to nutrient loading and physical controls." Biogeosciences 6:2985-3008.

Kemp, W.M., Sampou, P.A., Garber, J., Tuttle, J., and Boynton, W.R. 1992. "Seasonal depletion of oxygen from bottom waters of Chesapeake Bay: relative roles of benthic and planktonic respiration and physical exchange processes." Marine Ecology Progress Series 85:137.

Kemp, W.M., P. Sampou, J. Caffrey, M. Mayer, K. Henriksen, and W.R. Boynton. 1990. "Ammonium recycling versus denitrification in Chesapeake Bay sediments." Limnology and Oceanography 35:1545-1563.

Klump, J.V., and C.S. Martens. 1981. "Biogeochemical cycling in an organic-rich coastal marine basin-2. Nutrient sediment-water exchange processes." Geochimica Cosmochimica Acta 45:101-121.

Lapointe, B.E., L.W. Herren, R.A. Brewton, and P.K. Alderman. 2020. "Nutrient over-enrichment and light limitation of seagrass communities in the Indian River Lagoon, an urbanized subtropical estuary." Science of the Total Environment 699:134068.

Li, H., and S. Gregory. 1974. "Diffusion of ions in sea water and in deep-sea sediments." Geochemica Cosmochemica Acta 88:703-714.

Liu, H., Laws, E. A., Villareal, T. A., Buskey, E. J. 2001. "(2001). nutrient-limited growth of aureoumbra lagunensis (pelagophyceae), with implications for its capability to outgrow other phytoplankton species in phosphate-limited environments." Journal of Phycology 37(4): 500-508.

Martiny, A,C., Vrugt, J.A., Lomas, M.W. 2014. "Concentrations and Ratios of Particulate organic carbon, nitrogen, and phosphorus in the Global Ocean." Scientific Data 140048(2014).

Maso, M. and Garces, E. 2006. Harmful microalgae blooms (HAB); problematic and conditions that include them. Marine pollution bulletin 53(10-12)620-630.

Nixon, S.W. 1981. "Remineralization and nutrient cycling in coastal marine ecosystems. ." In Estuaries and Nutrients, by B.J., Cronin, L.E.J. Ed. Nielson, 111-138. Clifton, New Jersey: Humana.

Pandit, A., H.H Heck, A. Berber, W. Al-Taliby, and K. Mamoua. 2017. Sediment Survey and Fluxes of Nutrients from Sediments and Groundwater in the Northern Indian River Lagoon, Florida (Part III). Annual report submitted to SJRWMD for Contract # 27815.

Pelegri, S.P., L.P. Nielsen, and T.H. Blackburn. 1994. "Denitrification in estuarine sediment stimulated by the irrigation activity of the amphipod Corophium volutator." Marine Ecology Progress Series 105:285-290.

Phlips, E.J., S. Badylak, M.C. Christman, and M.A. Lasi. 2010. Climatic trends and temporal patterns of phytoplankton composition, abun- dance and succession in the Indian River Lagoon, Florida, USA. Estuaries and Coasts, 33: 498-512.

Rabouille, C., Lansard, B., Owings, S.M., Rabalais, N.N., Bombled, B., Metzger, E., Richirt, J., Eitel, E.M., Boever, A.D., Beckler, J.S., Taillefert, M. 2021. Early Diagenesis in the Hypoxic and Acidified zone of the northern Gulf of Mexico: is organic matter recycling in sediments disconnected from the water column? Frontiers in Marine Science. 8:604330. doi: 10.3389/fmars.2021.604330.

Redfield, A. C. 1934. "On the proportions of organic derivations in sea water and their relation to the composition of plankton." In James Johnstone Memorial Volume, by Ed. R. J. Daniel, 177–192. Liverpool, UK: University Press of Liverpool.

Seitzinger, S.P. 1988. "Denitrification in freshwater and coastal marine ecosystems: ecological and geochemical significance." Limnology and Oceanography 33:702-724.

Seitzinger, S.P. 1991. "The effect of pH on the release of phosphorus from Potomac estuary sediments: implications for blue-green algal blooms." Estuarine, Coastal and Shelf Science 33:409-418.

Sigua, G.C., J.S. Steward, and W.A. Tweedale. 2000. "Water-Quality Monitoring and Biological Integrity Assessment in the Indian River Lagoon, Florida: Status, Trends, and Loadings (1988-1994)." Environmental Management 25:199-209.

Smith, N.P. 1993. "Tidal and nontidal flushing of Florida's Indian River Lagoon." Estuaries 16:739-746.

Smith, S.V. 1984. "Phosphorus versus nitrogen limitation in the marine environment." Limnology and Oceanography 29(6):1149-1160.

Sundby, B., C. Gobeil, and N. Silverberg. 1992. "The phosphorus cycle in coastal marine sediments." Limnology and Oceanography 37:1129-1145.

Tech, Tetra. 2016. Save our Indian River Lagoon Project Plan for Brevard County, Florida.

Tech, Tetra. 2021. 2021 Update to the Save our Indian River Lagoon Project Plan for Brevard County, Florida.

Tweilley, R.R., J. Cowan, T. Miller-Way, P.A. Montagna, and B. Mortazavi. 1999. "Benthic Nutrient Fluxes in Selected Estuaries in the Gulf of Mexico." In Biogeochemistry of Gulf of Mexico Estuaries, by J.R. Pennock, R.R. Twilley Eds. T.S. Bibnchi, 163-209. John Wiley & Sons.

Vargo, G.A., Heil, C.A., Fanning, K.A., Dixon, L.K., Neeley, M. B., Lester, K., Ault, D., Murasko, S., Havens, J., Walsh, J., and Steven, B. 2008. Nutrient availability in support of Karenia Brevis blooms on the central West Florida Shelf: What keeps Karenia blooming? Continental Shelf Research, 28:73-98.

Welschmeyer, N.A. 1994. "Fluorometric analysis of chlorophyll a in the presence of chlorophyll b and phaeopigments." Limnology and Oceanography 39:1985-1992.

Willis, A., Adams, M.P., Chuang, A.W., Orr, P.T., O'Brien, K.R., and Burford, M.A. 2015. Constitutive toxin production under various nitrogen and phosphorus regimes of three ecotypes of cylindrospermopsis raciborskii ((Woloszynska) Seenayya et Subba Raju). Harmful Algae, 47:27-34.

Ziegler, S.E. and Brenner, R. 1999. Dissolved organic carbon cycling in a subtropical seagrass-dominated lagoon. Marine Ecology Progress Series, 188:51-62.

Appendix C Task 3 – Biology Report

Restore Lagoon Inflow Research (Phase 2)

Task 3, Biological Monitoring

PREPARED FOR

Florida Department of Education
325 W Gaines Street
Tallahassee, FL 32399

PREPARED BY

Jesse Blanchard, Florida Ichthyological Services and Habitat Consulting L.L.C.
Jeff Eble, Kevin B. Johnson, Ralph Turingan, Ocean Engineering and Marine Sciences, Florida Institute of Technology
150 West University Boulevard
Melbourne, FL 32901

FLORIDA TECH

August 2021

Table of Contents

List of Tables

List of Figures

Acknowledgements

We would like to thank representatives in the Legislature and the public for support of lagoon science. We thank Robert Salonen, Frank Kinney, and John Windsor for making this opportunity possible and the external reviewers whose contributions helped improve the project. We would also like to thank the students and technicians who offered their dedication and passion, including Carly McCall, Kyle Heffner, Danielle Juzwick, Connor Wong, Sean Crowley, Liam Corcoran, Melissa Rivera, Sophia Byrd and Rachael Stark.

We would especially like to thank the following individuals and groups for their advice and support:

Drs. Douglas Adams (FWC Melbourne Fisheries Lab); Jeffrey Collins (NASA Kennedy Space Center); Duane De Freese (Indian River Lagoon National Estuary Program); Michelle Gaither (University of Central Florida); Charles Jacoby (St. Johns River Water Management District); Girish Kumar (University of Central Florida); Richard Paperno (FWC Melbourne Fisheries Lab); Ed Phlips (University of Florida); Paul Wills (Harbor Branch Oceanographic Institute); and the Herndon Solutions Group biologists (NASA Kennedy Space Center).

Photograph on cover: http://www.floridasportsman.com/2016/03/24/indian-river-fish-kill/.

List of Acronyms

ANOVA	Analysis of Variance
ANOSIM	Analysis of Similarity
ASV	Amplicon Sequence Variants
BACI	Before-After-Control-Impact
BRL	Banana River Lagoon
BRN	Banana River North
BRS	Banana River South
°C	Degrees Celsius
Chl-a	Chlorophyll-a
COI	Cytochrome Oxidase Subunit I
DNA	Deoxyribonucleic Acid
DO	Dissolved Oxygen
eDNA	Environmental DNA
FIM	Fisheries Independent Monitoring
Florida Tech	Florida Institute of Technology
FWC	Florida Fish and Wildlife Conservation Commission
FWRI	Florida Fish and Wildlife Research Institute
HAB	Harmful Algal Bloom
IRL	Indian River Lagoon
km	Kilometers
L	Liter
m	Meters
m^3/sec	Cubic meters per second
mL	Milliliters
MM	Michaelis-Menten

NASA	National Aeronautics and Space Administration
NCBI	National Center for Biotechnology Information
NMDS	Non-Metric Multidimensional Scaling
NOAA	National Oceanic and Atmospheric Administration
PCR	Polymerase Chain Reaction
PERMANOVA	Permutational Multivariate ANOVA
PSU	Practical Salinity Unit
RLI	Restore Lagoon Inflow
rRNA	Ribosomal Ribonucleic Acid
SJRWMD	St. Johns River Water Management District
SoI	Species of Interest
TL	Trophic Level
µg/L	Micrograms Per Liter
UGE	Ugland-Gray-Elligsen
µm	Micrometer
VB	Vero Beach

Task Summary

Biological research conducted during project Phases 1 and 2, and proposed for Phase 3, anticipate concerns by stakeholders and permitting agencies regarding the impact of proposals for enhanced ocean circulation on Indian River Lagoon (IRL) biological communities. This includes modeling and monitoring to assess the potential impacts of enhanced inflow on seagrasses, phytoplankton, benthic fauna, and fishes.

To predict potential changes in fish distribution and abundance in response to enhanced inflow, fish population models were developed using the 1996-2018 monitoring data of the Florida Fish and Wildlife Conservation Commission (FWC) Fisheries Independent Monitoring (FIM) program. These models were then used to build predictive models that enable simulation of fish population responses to preliminary estimates of projected water quality changes under a range of potential inflow scenarios. Investigations into the dynamic relationship between fish populations and harmful algal blooms (HABs) were also initiated.

To determine the status of IRL populations that may be impacted by proposed enhanced inflow and to enable direct tracking of biodiversity loss and recovery in response to inflow, we have developed baseline databases documenting IRL species distribution, recruitment, and biodiversity. While historically there has been considerable biological sampling within the IRL, studies are often restricted in spatial and temporal scale or limited to one or a few species. Because the conditions that determine species occurrence and community diversity vary significantly within the IRL over space and time, baseline sampling must be closely aligned with anticipated impacts. To address this, we investigated seasonal and spatial variation in IRL biological communities using a combination of traditional and emerging techniques, focusing on the location of proposed inflow.

Fish modeling: In the Phase 1 final report, we articulated that salinity, temperature, and dissolved oxygen, among all the physical parameters collected with fish abundance, consistently emerged as the key determinants of fish community structure in the IRL. In Phase 2, we built predictive models of fish abundance using those key parameters, and some spatial parameters, then applied those models to project changes in abundance of eight species of interest and four metrics of community structure. We then performed preliminary analyses of the interactions between fish abundances, algal blooms, and time, and a review of relevant literature on the movement ecology of fishes in the Banana River Lagoon. Model projections suggest a complex, species-specific response to increased oceanic inflow with several species increasing and several decreasing in abundance over a nine-month period. For Phase 3, we propose to investigate the ecophysiological and behavioral mechanisms underlying these models, and to collaborate with the Kennedy Space Center biology team on a telemetry study observing behavioral responses to the proposed pilot pumping project. Doing so will allow us to bolster the robustness of our Phase 2 models projections. While the existing Phase 2 models are powerful predictors of observed, historical data, they are limited to only being able to predict changes within the realm of what has been seen in the IRL in the past. The ultimate goal of the Restore Lagoon Inflow (RLI) Research team is to change those conditions, improve them. It is imperative, now that we have the ability to predict current conditions, we build on that to gain the ability to predict future conditions as well.

Environmental Deoxyribonucleic Acid (DNA): Environmental DNA (eDNA) sampling was coupled with next-generation DNA sequencing to provide complimentary information on species occurrence and community diversity across taxonomic groups. The resulting biodiversity data were leveraged to initiate three approaches to directly investigate system response to experimentally enhanced inflow proposed for Phase 3. Analyses completed in Phase 2 help to

improve understanding of biodiversity patterns in the lagoon and the utility of the experimental approach. This includes evidence highlighting the presence of regional drivers of fish diversity and the impact of frequent HABs on Banana River Lagoon fishes. For Phase 3 we propose enhancement of the existing eDNA baselines and post pumping eDNA sampling and data analysis to be completed concurrently in a period of one year ending six months after completion of experimental pumping.

Seagrass and benthic algae: At selected locations, transects 100 meters (m) long were surveyed perpendicular to the shoreline with the goal of documenting the presence of seagrasses, rooted algae, and drift algae. Quadrats were laid down every 10-m along the transect lines, and benthic/drift vegetation were scored according to standard methods (Virnstein and Morris 1996; Morris et al., 2001). Measurements included seagrass visual percent cover (estimated coverage upon imagining the seagrass crowded into corner of quadrat at a high density) and analogous measurements for the rooted alga *Caulerpa prolifera*. Drift algae presence was scored on a relative qualitative scale. Benthic/drift vegetation sampling was repeated quarterly (seasonally) for all sites. Key findings include confirmation of seagrass presence in the area, namely the shoal grass *Halodule wrightii* that dominates in the northern IRL, and all sampled transects. Coverage was most abundant in Phase 1 summer, ranging from 0-9% and 0-6% at Banana River South (BRS), the control site, and Banana River North (BRN), the proposed inflow site, respectively. Next steps should be to continue monitoring seagrasses for baseline data to reveal seasonal and annual patterns of variability. It is critical that seagrass monitoring continue throughout any inflow pilot study to document how seagrasses around the inflow respond to environmental and water quality changes contrasted with seagrass data at the control site.

Benthic fauna: Sediment grabs for infaunal analysis were collected at the 50-m mark along all seagrass transects described above via petite Ponar grab (n = 3 per transect). Triplicate samples were collected at each station. This sampling strategy was repeated quarterly (seasonally) for all sites. Benthic infaunal communities were tested for correlations with sediment and environmental parameters. At least 105 species are confirmed as part of the benthic infaunal community at the proposed inflow and control sites. Of these species, 7 polychaetes, 4 amphipods, 1 ostracod, 1 sipunculan, 1 phoronid, 2 gastropods, and 3 bivalves were nearly universally present at both locations throughout all seasons and years. Overall (cumulative community) infaunal densities ranged from 1.9-4.0 x 10^4 organisms m^{-2} in Phase 1, and approached 1.5 x 10^5 organisms m^{-2} in Phase 2 near the proposed inflow site. It is recommended that monitoring of benthic fauna be ongoing before, during, and after implementation of a pilot RLI project so that community changes due to inflow-driven environmental shifts can be documented and understood.

Phytoplankton: These drifting microscopic photosynthesizers create turbidity and attenuate light. This has caused the disappearance of tens-of-thousands of acres of seagrasses in the IRL. Such dense blooms of algae are considered HABs because they kill seagrasses and fish and can harm other lagoon life. HABs may also be a result of toxicity, which is present in some species. HABs are largely responsible for public alarm concerning the state of the lagoon. Phytoplankton were sampled via plankton tows for cell identification, and via whole water samples for flow cytometer analysis. Regarding plankton tows, four were conducted quarterly at the proposed inflow site (n=4). Tows utilized a 20 micrometer (µm) mesh plankton net. Whole water samples for flow cytometry were collected at every station (n=5) approximately 0.5 m below the surface of the water. This sampling strategy was repeated quarterly (seasonally) for all sites. A total of 62 diatom species, 16 dinoflagellate species, and a dozen other algal species are confirmed as part of the phytoplankton community at the proposed inflow and control sites. Of these species, 8 species of diatoms and 2 species of dinoflagellates were present at both locations during most seasons and years. One species of observed diatom and 3 species of observed dinoflagellates are known to

produce toxins and contribute to HABs in other estuaries. The most abundant phytoplankton were neither diatoms nor dinoflagellates, but non-cyanobacterial nanoplankton-sized flagellated cells reaching densities as high as $7x10^8$ cells per liter (L) (near the proposed inflow site at BRN, in fall 2020). Cyanobacteria reached peak densities as high as $5x10^7$ cells L^{-1} (also at BRN in fall 2020). It is recommended that monitoring of phytoplankton and potentially harmful algal species be ongoing before, during, and after the implementation of a pilot inflow project so that community changes due to inflow-driven environmental shifts can be documented and understood. Ongoing monitoring is critical for phytoplankton, because the community includes potential HAB species, which have been at the heart of problems plaguing the lagoon, such as shading of seagrasses, muck inundation, and fish kills.

Key Phase 1 and 2 Findings

Fish Modeling

- Strong models, capable of predicting real-world observations with over 90% accuracy were developed to enable quantification of fish responses to changes in Banana River Lagoon salinity, dissolved oxygen, and temperature in space and time.
- Current model projections suggest the abundances of five of the eight species of interest would increase, while three species abundances are projected to decrease in response to increased inflow of seawater. As more data become available in future phases, these projections can be updated accordingly.
- Significant positive and negative associations between fish abundances and chlorophyll a concentrations exist in the Banana River Lagoon.
- Significant influences of the time*chlorophyll a interaction on fish community structure in the Banana River Lagoon, suggesting a need to include the possibility of feedbacks with chlorophyll a concentrations over time to fully realize the implications of pumping.
- Site fidelity and habitat use vary significantly among sport fishes, including the valuable Red Drum and Spotted Seatrout. Inclusion of these metrics in future modelling efforts will improve final species response predications.

Environmental DNA

- Development of eDNA markers targeting bony fishes, sharks, and rays was completed in Phase 1.
- Development of eDNA markers targeting crustaceans and metazoans was initiated to improve marker specificity and limit detection of non-target taxa (e.g., phytoplankton).
- One full seasonal cycle of eDNA baseline data collection was completed in Phase 2.
- Three approaches were initiated to directly investigate inflow impacts using eDNA detection patterns.
- eDNA sampling at the designated Phase 3 experimental site demonstrates the sufficiency of the current sampling plan and the power of the proposed experimental design.
- Fish diversity based on eDNA detections increased from north to south, with the lowest diversity across all biodiversity measures occurring in the Banana River Lagoon.
- Of the three candidate experimental inflow sites examined in Phase 1, Bethel Creek and an adjacent site exhibited the highest seasonal diversity of eDNA fish detections.
- Similar fish communities were detected at the Phase 3 experimental and control sites setting the foundation for before-after-control-impact tests.
- Pairwise estimates of eDNA site similarity/dissimilarity highlight the presence of regional drivers of fish diversity, with higher similarity among sites within regional basins than between sites in different basins.

- Comparison of eDNA-based estimates of taxonomic distinctness measures against a fixed baseline highlight the impact of frequent harmful algal blooms on fish diversity in the Banana River Lagoon.
- eDNA sites closest to Sebastian Inlet standout as having fish communities that are both species rich and taxonomically diverse.

Seagrasses, Phytoplankton, and Benthic Fauna

- The seagrasses, macroalgae, benthic infauna, and phytoplankton that occur in the estuary in the area of proposed inflow withstand tremendous fluctuations of salinity, temperature, and other water quality measures. The organisms found here are euryhaline and eurythermal, meaning they can withstand relatively large fluctuations in salinity and temperature, in contrast to organisms found in offshore coastal environments, which may be restricted to a narrow range of salinities and temperatures.
- Key findings include documentation of seagrasses (the shoal grass *Halodule wrightii*) in the area. Seagrass coverage during Phase 1 summer was up to 9% (BRS) and 6% (BRN). Also present is the rooted macroalgae *Caulerpa prolifera*. However, historical data indicate that the area had far greater densities of seagrasses in the past, whereas in current surveys they are absent or nearly so.
- A total of 105 infaunal species were confirmed present at the study sites. Seven polychaetes, 4 amphipods, 1 ostracod, 1 sipunculan, 1 phoronid, 2 gastropods, and 3 bivalves were abundantly present at both locations throughout all seasons and years. Overall infaunal densities ranged from 1.9-4.0 x 10^4 organisms m^{-2} in Phase 1, and approached 1.5 x 10^5 organisms m^{-2} in Phase 2 near the proposed inflow site.
- A total of 62 diatom species, 16 dinoflagellate species, and a dozen other algal species are confirmed phytoplankton at both study sites. Of these, 8 species of diatoms and 2 species of dinoflagellates were present at both locations during most seasons and years. Some species (1 diatom and 3 dinoflagellates) produce toxins and contribute to HABs in other estuaries. The most abundant phytoplankton were non-cyanobacterial nanoplankton-sized flagellated cells reaching densities as high as $7x10^8$ cells L^{-1} (near the proposed inflow site at BRN, in fall 2020). Cyanobacteria reached peak densities as high as $5x10^7$ cells L^{-1} (also at BRN in fall 2020).
- Principle components analyses indicated that sediment conditions (percent organic content, percent silt-clay content, percent water content) and water column conditions (bottom water dissolved oxygen) determine species occurrence.

Completion of project Phases 1 and 2 biological resource assessments improves understanding of the IRL system and sets the foundation for the proposed Phase 3 investigation of experimental inflow impacts. Phase 3 biological assessment goals include validation of fish population models and direct assessment of experimentally enhanced ocean water exchange on seagrasses, plankton communities, benthic fauna, fishes, and manatees. Assessments will be completed using complimentary experimental approaches and sampling strategies including direct comparison of experimental and control sites before and after pumping, comparison of community response against model predictions, and tracking of system response against established baselines. For Phase 3, biological baselines will be further expanded with federal and university partners to directly track inflow impacts on both HAB community structure and manatee habitat use. Proposed Phase 3 fish modeling and follow-up eDNA assessment will be completed concurrently in a period of two years that would extend six months past completion of experimental pumping. Benthic and planktonic community monitoring during the permitting pilot

process is recommended, along with monitoring during pilot inflow and then for at least one year after inflow to better reveal treatment effects.

1 Fish Modeling

1.1 Introduction

The Indian River Lagoon (IRL) is home to one of the richest estuarine fish communities in the world, with over 400 described species (Gilmore, 1995) occupying different types of habitats from oyster reefs to mud flats, which are affected by inflows through oceanic inlets and freshwater river discharges (Dutka-Gianelli et al., 2011; Gilmore, 1995). Predicting how this complex ecosystem responds to any given perturbation is a challenge for ecologists and biologists. As poikilotherms, fish physiology is intricately linked to water chemistry. Any change in the level of dissolved oxygen (DO), salinity, pH, temperature, or any other abiotic factor has consequential effect on the flora and fauna of the IRL. The behavioral and physiological response of a resident population triggers a cascade of changes to the whole ecosystem (Blanchard et al., 2021; Bonte et al., 2012; Carere and Gherardi, 2013; Sih et al., 2012; Spiegel et al., 2017). At this stage of the study, the fish biology team has attempted to inform our understanding of the complex interactions between biotic and abiotic components of the IRL in the following manner. First, in Phase 1, using a series of multivariate statistical analyses using the 1996-2018 monitoring data of the Florida Fish and Wildlife Conservation Commission (FWC) Fisheries Independent Monitoring (FIM) program, the team concluded that salinity, DO, and temperature underlie the formation of community structure, abundance, and distribution of fishes in the IRL. In this report, we capitalize on the conclusion of the Phase 1 analyses to build predictive models that enable the quantification of fish population responses to these abiotic factors. In addition, the team initiated the examination of the same metrics of fish responses used in Phase 1 to the occurrence of harmful algal blooms (HABs), and the movement and habitat use of fishes in the IRL.

Understanding the movement of fish within an ecosystem is critical to our understanding of the impacts of change in the environmental conditions on the community dynamics within the ecosystem. Within estuaries such as the IRL, patterns of variation in fish community structure, species richness, abundance and distribution in estuaries are strongly influenced by environmental factors including DO, salinity, pH, and temperature (e.g., Bacheler et al., 2009; Moulton et al., 2017). Any change in the current, normal flow of seawater into the IRL is expected to cause changes in these metrics of fish responses to the environmental change. Knowledge of the patterns of movement and habitat use of resident fishes in the IRL provides valuable information about the extent to which the proposed inflow of fresh Atlantic Ocean seawater into the Banana River Lagoon (BRL) section of the IRL will impact these fishes. This component of the study aims to initiate conducting a meta-analysis of fish movement and habitat use in total and species-specific abundance of fishes in the IRL, with emphasis on the BRL proposed site for the inflow pilot study.

Here, we present the results of three concerted efforts to address the goals of Phase 2 of this project. First, we report on our primary goal of developing and using predictive models to quantify fish responses to changes in salinity, DO, and temperature. Second, we present preliminary investigations into the associations between HABs and fish populations in the IRL. Third, we present the results of an initial meta-analysis of the movement and habitat use of fishes within the IRL. Finally, we discuss how the results of this phase provide the foundation and rationale for the series of questions we will address in Phase 3 of this project.

1.2 Fish Methods

For this report, our primary goal was to provide preliminary projections of how increased inflow into the BR) region of the IRL would influence the fish community. This primary goal, goal 1,

represents the bulk of our effort. For the first goal we used the lessons learned in Phase 1 to develop predictive models and apply them to the data produced by the Restore Lagoon Inflow (RLI) Research Task 1 team. This collaborative effort projects changes in the IRL fish community structure in response to various inflow scenarios. We had two new goals added to our effort in quarter 4. Goal 2 was to begin investigating the influence of algal blooms on fish community structure in the BRL. The ultimate aim of this line of inquiry is to understand how the changes in algal blooms, as predicted by other RLI tasks, would influence the abundance of fishes. Finally, Goal 3 was to initiate investigating some of the mechanisms that may underlie the patterns of relationships and predictability of fish responses to the proposed inflow and HAB outbreaks addressed in goals 1 and 2 by looking at the patterns of fish movement and habitat use in BRL.

1.2.1 Fish Community Modeling

1.2.1.1 Fish Community Modeling Methods Summary

To accomplish our first goal, we built models predicting the effects of salinity, temperature, DO, latitude, and longitude (i.e., predictive variables) on four key metrics of community structure and the relative abundance of eight key Species of Interest (SoI). The BRL region is the sole focus of this report because it was identified by the RLI team as the most feasible location for the pilot study, slated for future phases. The predictive variables chosen were the three which contributed the most to explaining variation in community structure of fishes in IRL and are each likely to be influenced by increased inflow, as discussed in our Phase 1 reports (Florida Insititute of Technology [Florida Tech], 2020; Johnson et al., 2020). Using the most recent FWC Fish and Wildlife Research Institute (FWRI) FIM program fish community data available, we used multiple linear regressions to investigate the individual and combined effects of each predictive variable on key metrics of fish community structure for the entire available data range, 1996-2018. These models were ‘trained’ with a randomly drawn subset of half of the available data, and their performance was evaluated by comparing their predictions to the remaining half of the data, the ‘validation data.’ Once built and validated, in collaboration with the RLI Task 1 team, the models were then applied to Dr. Zarillo’s model projections of how these variables would change under different inflow scenarios.

1.2.1.2 Fish Community Modeling Methods Details

Using the most recent FWC FWRI FIM fish community data available (see FWRI, 2009; Paperno, 2002 for methodological details on fish collections), we built models predicting the effects of environmental change associated with enhanced inflow into the BRL using a series of multiple linear regressions. These models were designed to project changes of eight SoI’s abundances and four metrics of community structure as a result of changing abiotic conditions in the BRL. The abiotic predictive variables used (i.e. salinity, temperature, and DO) were indicated by our Phase 1 work as the strongest determinants of fish community structure in the IRL (see Johnson et al., 2020). This previous work (Johnson et al., 2020), consultations with experts in the region, and personal observations indicated a strong influence of spatial heterogeneity of fish community structure in the BRL, so we also included the spatial variables of latitude and longitude as descriptors in our candidate models. These models were built to project changes in α-diversity (i.e., species richness), Shannon diversity index (H, a combined measure of relative abundance and evenness), Pielou’s evenness index (J, a combined measure of richness and evenness), and mean community trophic level (TL, a representation of the trophic ecology of the system). Both H and J were calculated following Troast et al. (2020), and TL was calculated for each sample as the relative abundance weighted mean trophic level of the constituent community following Blanchard (2018). Each species’ individual trophic levels were retrieved from FishBase (Froese

et al., 1992; Froese and Pauly, 2020) where possible. Species complexes, such as Saratherodon/Oreochromis spp., tend to lack documented TL. In such instances, the TL was calculated as the mean TL for every member of encompassed genera that have been noted in the upper IRL. The SoI themselves were selected based on discussions with the FWC laboratory in Melbourne, Florida, and as recommended by the external reviewers of the RLI project's Phase 1 report (Florida Tech, 2020). These were the Bay Anchovy, *Anchoa mitchilli*; Sheepshead, *Archosargus probatocephalus*; Spotted Seatrout, *Cynoscion nebulosus*; Mangrove Snapper, *Lutjanus griseus*; Pinfish, *Lagodon rhomboides*; Black Drum, *Pogonias cromis*; Red Drum, *Sciaenops ocellatus*; and Gulf Pipefish, *Syngnathus scovelli*. For species abundance models, we performed analyses in tandem both including and excluding outliers in the source data to determine which approach may be more useful. Outliers were defined as any abundance more than two standard deviations above the mean. Candidate models targeting SoI abundance and community structure metrics, which involved all possible combinations of the available descriptive factors, were evaluated and the 'best models' were selected using Akaike's Information Criterion (Aho et al., 2014). Models were trained using a randomly drawn half of the available FWC data for each gear type deployed within the BRL. We then evaluated the performance of each model by using them to blindly predict the other half of the available data. While our past work focused on four FWC gear types (FWC gear codes 20, 160, 300, and 301), our current focus on BRL precludes involving gears 300 and 301, as they are no longer deployed in that area. This report focuses on gear 20, a small seine which catches primarily small fishes (i.e., anchovies and other small species, or juveniles of larger species), and gear 160, a much larger seine which is inefficient at capturing small fish but is adept at catching larger animals (i.e., adult sportfish). See the FWRI-FIM procedural manual for methodological details (FWRI, 2009), or Paperno (2002) for a more succinct summary. As they have different biases and efficiencies, each gear was analyzed separately resulting in a target of 8 Soi*2 gears*2 (with or without outliers) = 32 abundance models and 4 community structure metrics * 2 gears = 8 community structure models. All analyses were inclusive of the entire time span of available data, 1996-2018.

Once selected and tested, each model was then used to project changes in the dependent variable (i.e., SoI abundance or community metric) as a result of changing mean conditions due to various inflow scenarios as projected by Dr. Zarillo's team (Task 1; base conditions or no change, 10, 5, 2.5, 1, and 0.05 cubic meters per second [m^3/sec]), where such abiotic projections were available. All increased inflow scenarios were plotted with reference to the base over the span of nine months, the entirety of available abiotic projections, to determine the temporally explicit and net impacts of each scenario on the SoI or community metric being projected. Changing abiotic conditions are to be projected by the Task 1 portion of the RLI team and provided to the Task 3 team in a collaborative RLI team effort.

1.2.2 Fish and Chlorophyll-a (Chl-a)

1.2.2.1 Fish and Chl-a Methods Summary

To address our second goal, we capitalized on two long-term data sets, St. Johns River Water Management District's (SJRWMD) Chl-a concentration and dominant phytoplankton species data from 2002–2018, and FWC FWRI FIM fish community data inclusive of the same time span, to perform preliminary investigations on the associations of BRL fishes and algal blooms. Specifically, we used Spearman Rank Correlations (Zar, 1999) to look for associations of Chl-a with the time series mean relative abundances of all eight SoI and four metrics of community structure (see Section 1.2.1), and Analyses of Variance (ANOVA) (Zar, 1999) to look at the influence of the interaction of Chl-a and time on the four metrics of community structure. These

preliminary analyses were aimed at refining future works to enhance efficiency and efficacy of future phases.

1.2.2.2 Fish and Algae Methods Details

To begin investigating potential associations between algal blooms and the BRL fish community, we used data from the SJRWMD monitoring program. The data provided include monthly measurements of Chl-a concentrations, in micrograms per liter (µg/L) in the BRL from 2002–2018, using Chl-a concentrations as a proxy measurement for microalgal density and primary productivity in the water column (see Huot et al., 2007 for an analysis of this type of proxy data) as indicators of algal density. Where possible, the dominant phytoplankton taxa present was also noted for each month in the SJRWMD data. These Chl-a records were matched with the fish data provided by FWC over the same time period. Where multiple fish samples were available for a single month, we used the mean abundance among the samples for that month. We then performed a series of Spearman Rank correlations (Zar, 1999) to test for associations between median Chl-a concentrations and the relative abundances of each of the eight SoI and four community structure metrics, described in the fish community modeling methods section. These data were also plotted over time to allow for visual inspection of the associations for signals which could only be described in detail with the more comprehensive analyses planned for Phase 3 (i.e., time lagged responses, state shifts, break points, etc.).

To begin laying the groundwork for the Phase 3 analyses, we also used a series of ANOVA (Zar, 1999) to examine the importance of the interaction of time and Chl-a concentrations on the metrics of community structure. We know that the IRL has been substantially different since 2011 (Kamerosky et al., 2015) and BRL is likely no exception. We expected a strong influence of time in these analyses and would hypothesize that the 2011 superbloom marks a state shift, after which the community likely behaves differently. Details are still limited regarding the specifics of how the BRL fish community is being affected. This effort is aimed at determining which SoI and metrics of community structure show the strongest association with Chl-a concentrations in the BRL, and which metrics of community structure are most heavily influenced by the interaction of time and Chl-a. With that information, we will be able to refine and focus future efforts on the most salient and impactful analyses (i.e., temporal breakpoint analyses, habitat suitability modeling, species distribution modeling, etc.). The enhanced focus afforded by this preliminary investigation will permit more efficient expenditures of time and funding in Phase 3.

1.2.3 Fish Movement

A short period of an extensive literature survey was conducted to gather information on the patterns of fish movement and habitat use in the IRL, particularly in the vicinity of the BRL site of the proposed RLI pumping station. The results of this meta-analysis focusing on two commercially and recreationally important species of fish (Red Drum, *Sciaenops ocellatus*; and seatrout *Cynoscion nebulosus*) are summarized. We also examined the association between patterns of variation in fish abundance and environmental parameters including oxygen, salinity, temperature, and pH in BRL (**Figure 1**) at the proposed pilot pumping site and the Patrick Air Force Base area of the IRL during the 1996–2018 monitoring period of the FWC-FIM program to infer intra-IRL variation in habitat utilization of these SoI.

Figure 1. Map of the study area showing the proposed pumping location in the northern BRL (top-most circle) and adjacent site in the Patrick Air Force Base area (middle circle)

1.3 Results

1.3.1 Fish Community Modeling

Phase 2 fish community modeling efforts were focused on developing predictive models capable of using the abiotic projection data (see Dr. Zarillo's Task 1 report) to project changes in the abundances of eight SoI and four key metrics of community structure. Four of the targeted models (gear 160: *Anchoa mitchilli* and *Syngnathus scovelli*; gear 20: *Pogonias cromis* and *Lutjanus griseus*) could not be generated as there were not enough occurrences in the source data to support the effort. All other models were successfully produced and tested. See **Table 1** for the full list of model equations and performance values for all models. All available Task 1 abiotic data were successfully applied to these data to generate the targeted projections with 100% completion of anticipated deliverables.

Table 1. Model equations and assessments for all eight SoI and four metrics of community structure across both gear types

Note: P values presented are for the selected model. The n value represents the number of samples included in the training and validation data. The model R^2 is the amount of variation explained in the training data explained by the initial model. The validation R^2 is a measure of model performance, derived by regressing projected data with observed. All models shown here exclude outliers, except for the metrics of community structure which included all available data. Sal.=Salinity, Temp.=Temperature, Lon.=Longitude, Lat.=Latitude, N=population abundance.

Modeled parameter	Gear	Model equation	P	n	Model R^2	Validation R^2
Anchoa mitchilli	20	N=169023.43+(DO*-13192.15)+(Sal.*-1687.43)	0.01	209	3.14%	98.00%
Anchoa mitchilli	160	Insufficient occurrences in source data				
Archosargus probatocephalus	20	N=−1363.94+(Temp.*10.28)+(DO*102.35)+(Sal.*22.34)	0.02	9	75.21%	53.66%
Archosargus probatocephalus	160	N=-689.56+(Temp.*41.38)+(DO*-122.91)+(Sal.*57.29)	<0.001	171	9.83%	95.63%
Cynoscion nebulosus	20	N=610.65+(Sal.*−22.25)	0.55	94	0.69%	99.88%
Cynoscion nebulosus	160	N=33.52+(Sal.*30.76)	0.05	161	1.70%	95.96%
Lagodon rhomboides	20	N=1181.59+(Temp.*8.10)+(Sal.*−0.31)+(DO*−11)+(Lon.*−39.59)	0.68	21	8.99%	96.62%
Lagodon rhomboides	160	N=-5655.76+(Temp.*176.14)+(DO*-2044.63)+(Sal.*1640.06)	<0.001	280	4.09%	6.79%
Lutjanus griseus	20	Insufficient occurrences in source data				
Lutjanus griseus	160	N=-1963.70+(Sal.*-16.80)+(Lat.*94.75)	0.33	25	1.29%	97.34%
Pogonias cromis	20	Insufficient occurrences in source data				
Pogonias cromis	160	N=-186559.43+(DO*-428.85)+(Lat.*6731.00)	0.01	41	16.70%	59.73%
Sciaenops ocellatus	20	N=-242768.50+(DO*105.95)+(Lat*8553.75)	0.08	22	15.79%	16.40%
Sciaenops ocellatus	160	N=-1566.01+(Temp.*14.33)+(Sal.*39.56)+(DO*98.21)	<0.001	210	11.51%	86.38%
Syngnathus scovelli	20	N=−165.48+(Temp.*23.94)	0.09	14	1.61%	98.98%
Syngnathus scovelli	160	Insufficient occurrences in source data				
H diversity	20	$H=-328.30+(Lon.*-4.09)+(Temp*(-1.09*10^{-2}))$	0.03	227	0.02%	<0.01%
H diversity	160	H=1.00+(Sal.*-0.01)+(Temp.*0.02)	<0.001	515	3.51%	0.03%
α diversity	20	α=-184.33+(Lat.*6.93)+(Sal.*-0.11)+(DO*-0.23)	<0.001	223	0.05%	4.16%
α diversity	160	α=3.96+(Temp.*0.28)+(DO*-0.23)	<0.001	515	13.85%	13.28%
J evenness	20	$J=-138.80+(Lon.*-1.73)+(Sal.*(4.74*10^{-3}))+(Temp*(-1.11*10^{-2}))$	0.01	223	0.04	2.59
J evenness	160	J=5.85+(Sal.*-0.004)+(Lat.*-0.18)+(Temp.*-0.004)	0.00	514	2.10	2.73
Mean trophic level	20	TL=1.27+(Sal.*0.01)+(Temp.*-0.02)	0.02	224	0.03	8.80
Mean trophic level	160	TL=1.15+(Temp.*-0.02)+(DO*0.03)	<0.001	515	4.99	9.14

1.3.1.1 Outlier Assessment

Overall, models of species abundance excluding outliers were better able to predict validation data than those including outliers and, therefore, we will be presenting the outlier-excluded projects here. No metrics of community structure were subjected to outlier-excluded analyses as it would not be ecologically meaningful to do so.

1.3.1.2 Model Projection Results

Model projections were produced for 0.5, 1, 2.5, 5, and 10 m^3/sec enhanced inflow scenarios, as well as the no inflow change, base, scenario for all models where sufficient abiotic project data were available. The Task 1 team provided salinity projections for all scenarios, temperature projections for all but the 10 m^3/sec scenario, and DO projections for the base and 5 m^3/sec scenarios. As there was not a full suite of abiotic projections available, we could not produce a full suite of model projections for all species or metrics of community structure. With the data provided, we projected changes in abundance for 26 different species*gear*pumping scenario combinations and 23 community structure metric*gear*pumping scenario combinations. Subtracting the projected base scenario value from each increased inflow scenario's projections for the entire projected timeline, we calculated a total projected net effect for each scenario (**Figure 2**). The majority of abundance projections, 20 of the 26, suggest net positive increases in abundance over a 9-month period, while a notable few do suggest net decreases. For the community structure projections, the model projections were more varied with 11 projecting increases in the metric modeled and 12 projecting decreases. These results will be discussed for each species individually.

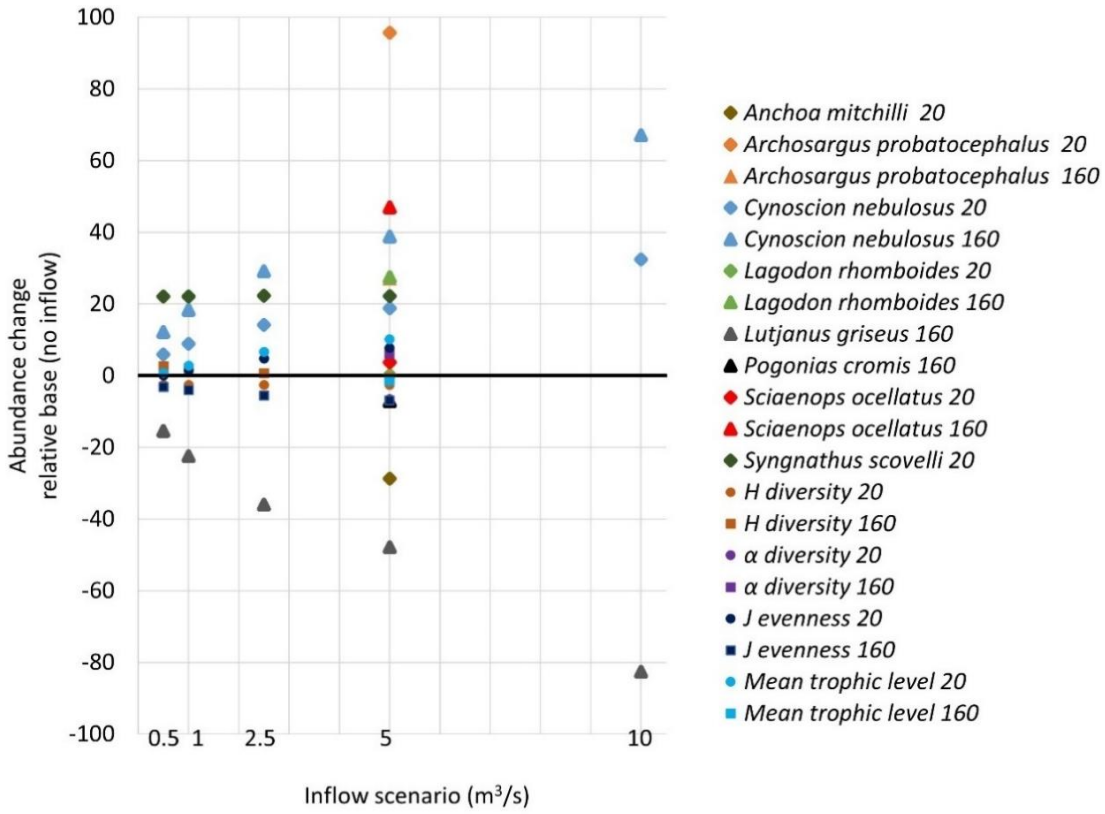

Note: Positive values represent increases in the modeled parameter relative to the base scenario, negatives represent decreases. For abundance projections, gear type 20 is shown by diamonds, and gear type 160 is shown by triangles. For community structure projections, gear type 20 is represented by circles while 160 is shown as squares. The reader is cautioned against making comparisons between species here. The relative magnitude of change can be inferred, but exact changes in abundance between species is not accurately reflected here.

Figure 2. Net effect of nine months for each pumping scenario on all fish populations and community structure metrics for which sufficient source data and abiotic projection data were available to produce projections

Table 2. Net effects of enhanced inflow projected by each model

Note: Gray cells represent models which were generated but we were unable to provide projections due to a lack of input data. Red cells represent net reductions, and green cells represent net increases.

Modeled parameter	Gear	Enhanced inflow scenario (m^3/sec)				
		0.5	1	2.5	5	10
Anchoa mitchilli	20				-28.68	
Anchoa mitchilli	160	Insufficient occurrences in source data				
Archosargus probatocephalus	20				95.70	
Archosargus probatocephalus	160				27.15	
Cynoscion nebulosus	20	5.89	8.89	14.12	18.80	32.46
Cynoscion nebulosus	160	12.17	18.36	29.18	38.84	67.06
Lagodon rhomboides	20				0.21	
Lagodon rhomboides	160				27.45	
Lutjanus griseus	20	Insufficient occurrences in source data				
Lutjanus griseus	160	-15.41	-22.49	-35.98	-47.83	-82.60
Pogonias cromis	20	Insufficient occurrences in source data				
Pogonias cromis	160				-7.20	
Sciaenops ocellatus	20				3.71	

Modeled parameter	Gear	Enhanced inflow scenario (m^3/sec)				
		0.5	1	2.5	5	10
Sciaenops ocellatus	160				46.95	
Syngnathus scovelli	20	22.05	22.13	22.32	22.25	
Syngnathus scovelli	160	Insufficient occurrences in source data				
H diversity	20	-2.56	-2.59	-2.63	-2.60	
H diversity	160	2.68	1.99	0.67	-0.56	
α diversity	20				-6.62	
α diversity	160				6.08	
J evenness	20	-0.01	1.62	4.76	7.69	
J evenness	160	-3.17	-4.00	-5.57	-6.92	
Mean trophic level	20	0.78	2.80	6.64	10.20	
Mean trophic level	160				-1.34	

1.3.1.2.1 *Anchoa mitchilli* – Bay Anchovy

This species is not efficiently collected by gear type 160. As a result, the gear 160 model was data deficient for this species and could not be generated. The gear type 20 model was a significant, but weak, predictor of the training data ($P = 0.014$, $R^2 = 3.138\%$). When used to blindly predict the validation data, the model performed well with $R^2 = 98\%$ and $P < 0.001$. As this model relied on a combination of salinity and DO, only the 5 m^3/sec scenario could be projected at this time. With the changes projected by the Task 1 team, assuming no substantive behavioral or physiological responses, influences on local recruitment not captured in the FWC data, and lacking details on ecological feedbacks loops, the projected inflow scenario suggests a decrease in the abundance of *Anchoa mitchilli* over a 9-month period can be expected (**Figure 2** and **Figure 3**).

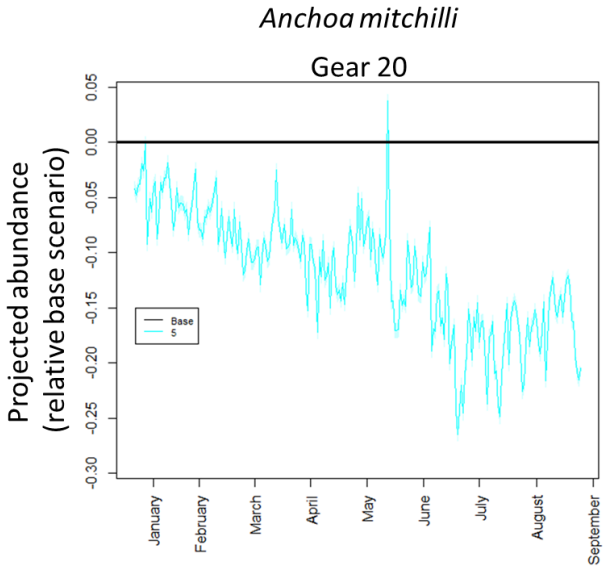

Note: Numbers in the legend refer to the volume pumping scenario, in the unit of m^3/sec. Base refers to the baseline, no change, scenario. The shaded region around each line represents the 95% confidence interval of the model.

Figure 3. Projected changes in *Archosargus probatocephalus* abundance in BRL over a 9-month period for all available scenarios using data from gear type 20, excluding outliers

1.3.1.2.2 *Archosargus probatocephalus* – Sheepshead

This species occurs in multiple ontogenetic stages within the IRL and is a regular occurrence in both gear types observed. The models describing this species were significant predictors of both the training (gear 20: P = 0.018, R^2 = 75.21%; gear 160: P < 0.001, R^2 = 9.83%) and validation data (gear 20: P < 0.001, R^2 = 53.66%; gear 160: P < 0.001, R^2 = 95.63%). As these models rely on salinity, temperature, and DO, our projections are limited to inflow scenario where all three abiotic factors were available, 5 m^3/sec. With the changes projected by the Task 1 team, assuming no substantive behavioral or physiological responses, influences on local recruitment not captured in the FWC data, and lacking details on ecological feedbacks loops, all inflow scenarios are projected to increase the abundance of *Archosargus probatocephalus* over a 9-month period, for both gear types (**Figure 2** and **Figure 4**).

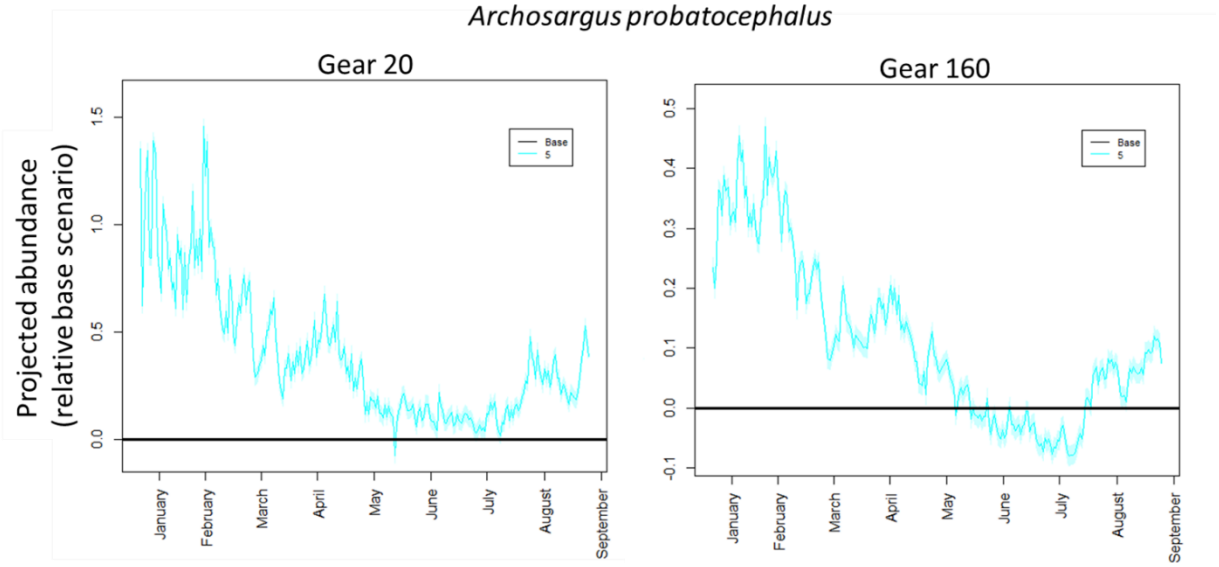

Note: Numbers in the legend refer to the volume pumping scenario, in the unit of m^3/sec. Base refers to the baseline, no change, scenario. The shaded region around each line represents the 95% confidence interval of the model.

Figure 4. Projected changes in *Archosargus probatocephalus* abundance in BRL over a 9-month period for all available scenarios using data from gear types 20 (left) and 160 (right) excluding outliers

1.3.1.2.3 *Cynoscion nebulosus* – Spotted Seatrout

This species occurs in multiple ontogenetic stages within the IRL and is a regular occurrence in both gear types observed. Additionally, the best models describing this species rely exclusively on salinity, for which a full suite of projection data were available. Therefore, projections are available for all inflow scenarios for both gear types. With the changes projected by the Task 1 team, assuming no substantive behavioral or physiological responses, or influences on local recruitment not captured in the FWC data and lacking details on ecological feedbacks loops, all inflow scenarios are projected to increase the abundance of *Cynoscion nebulosus* over a 9-month period, with increasing levels of inflow increasing the effect, for both gear types (**Figure 2** and **Figure 5**). While neither model was a significant predictor of the source data (gear 20: P = 0.549, R^2 = 0.69%; gear 160: P = 0.054, R^2 = 1.703%), both performed well at blind predictions of the validation data with gear 20 and 160 models explaining 99.88% and 95.95%, with P < 0.001, of the variation, respectively.

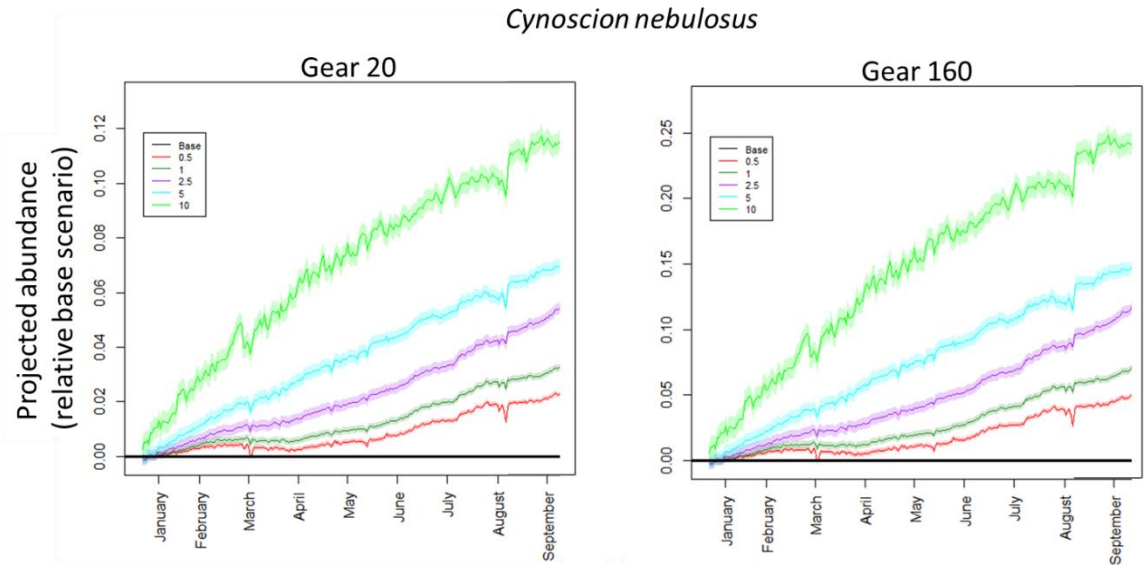

Note: Numbers in the legend refer to the volume pumping scenario, in the unit of m^3/sec. Base refers to the baseline, no change, scenario. The shaded region around each line represents the 95% confidence interval of the model.

Figure 5 Projected changes in *Cynoscion nebulosus* abundance in BRL over a 9-month period for all available scenarios using data from gear types 20 (left) and 160 (right) excluding outliers

1.3.1.2.4 *Lagodon rhomboides* – Pinfish

This is a fairly ubiquitous forage fish in the IRL and is a regular occurrence in both gear types observed, although their abundance does seem to have declined substantially over the past decade. While still frequent enough in these data to generate the targeted models, this decline, and the as of yet undescribed mechanism behind it, likely significantly skews the final model form. The gear type 20 model describing this species was not a significant predictor of the training data ($P = 0.667$, $R^2 = 8.99\%$), but was effective at blindly capturing the majority of the variation in the validation data ($P < 0.001$, $R^2 = 96.62\%$). The gear type 160 model describing this species was a significant predictor of the training data ($P = 0.002$, $R^2 = 4.085\%$), but was not effective at blindly capturing the majority of the variation in the validation data ($P < 0.001$, $R^2 = 6.79\%$). As these models rely on salinity, temperature, and DO, as well as longitude for gear type 20, our projections are limited to inflow scenarios where all three abiotic factors were available, 5 m^3/sec. With the changes projected by the Task 1 team, assuming no substantive behavioral or physiological responses, or influences on local recruitment not captured in the FWC data and lacking details on ecological feedbacks loops, the projections suggest an increase the abundance of *Lagodon rhomboides* over a 9-month period, for both gear types (**Figure 2** and **Figure 6**).

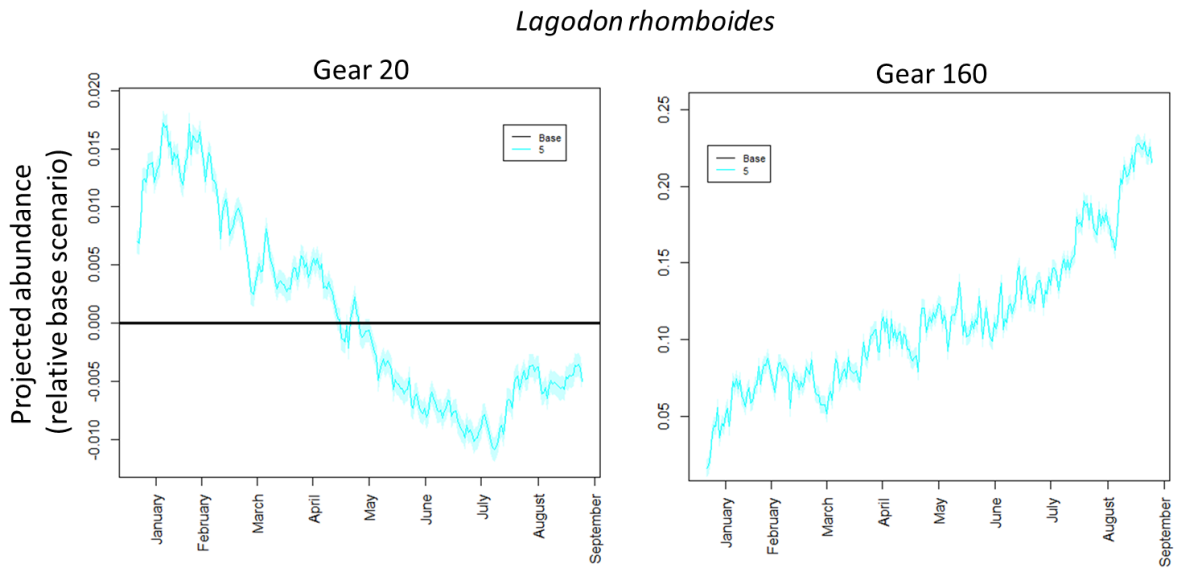

Note: Numbers in the legend refer to the volume pumping scenario, in the unit of m^3/sec. Base, y axis= 0, refers to the baseline, no change, scenario. The shaded region around each line represents the 95% confidence interval of the model.

Figure 6. Projected changes in *Lagodon rhomboides* abundance in BRL over a 9-month period for all available scenarios using data from gear types 20 (left) and 160 (right) excluding outliers

1.3.1.2.5 *Lutjanus griseus* – Gray Snapper

This is a relatively common Snapper species, which uses the IRL for several of its ontogenetic stages. Their presence was fairly common in the gear 160 data; however, they were not observed by gear 20 within the target. The gear type 160 model describing this species was not a significant predictor of the training data ($P = 0.333$, $R^2 = 1.293\%$), but was effective at blindly capturing the majority of the variation in the validation data ($P < 0.001$, $R^2 = 97.34\%$). As this model relies on salinity and latitude, we were able to generate a full suite of projections for gear 160. With the changes projected by the Task 1 team, assuming no substantive behavioral or physiological responses, or influences on local recruitment not captured in the FWC data and lacking details on ecological feedbacks loops, we project a decrease in *Lutjanus griseus* over a 9-month period, with higher levels of inflow exacerbating the effect (**Figure 2** and **Figure 7**).

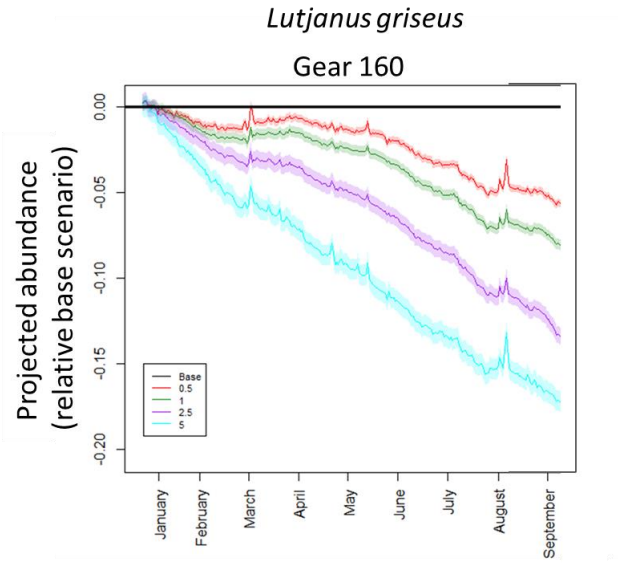

Note: Numbers in the legend refer to the volume pumping scenario, in the unit of m^3/sec. Base refers to the baseline, no change, scenario. The shaded region around each line represents the 95% confidence interval of the model.

Figure 7. Projected changes in *Lutjanus griseus* abundance in BRL over a 9-month period for all available scenarios using data from gear type 160, excluding outliers

1.3.1.2.6 *Pogonias cromis* – Black Drum

While this species is not rare in the IRL, it is commonly associated with strata over which the FWC gear types observed are not as effective (i.e., oyster bars or submerged riprap), resulting in a data deficiency for the gear 20 model. With gear 160, the model was a significant predictor models describing this species were significant predictors of both the training ($P = 0.012$, $R^2 = 16.70\%$) and validation data ($P < 0.001$, $R^2 = 59.73\%$). As this model relies on DO and latitude, our projections are limited to the 5 m^3/sec scenario for which sufficient abiotic projection data are available. With the changes projected by the Task 1 team, assuming no substantive behavioral or physiological responses, or influences on local recruitment not captured in the FWC data and lacking details on ecological feedbacks loops, this model projects a decrease in the abundance of *Pogonias cromis* 9-month period (**Figure 2** and **Figure 8)**.

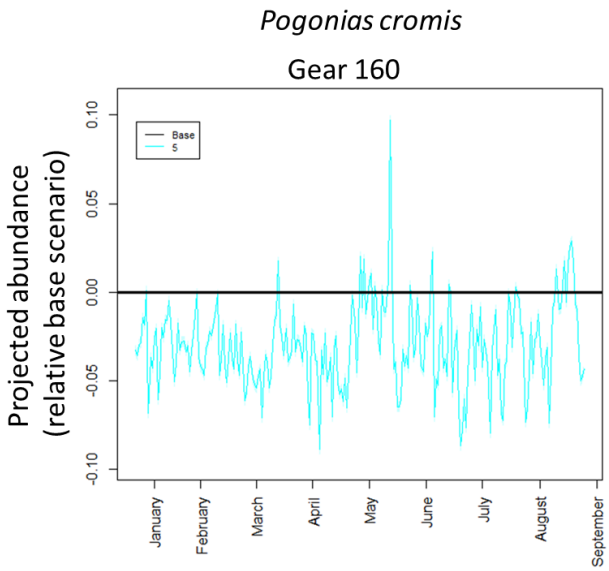

Note: Numbers in the legend refer to the volume pumping scenario, in the unit of m^3/sec. Base refers to the baseline, no change, scenario. The shaded region around each line represents the 95% confidence interval of the model.

Figure 8. Projected changes in *Pogonias cromis* abundance in BRL over a 9-month period for all available scenarios using data from gear type 160, excluding outliers

1.3.1.2.7 *Sciaenops ocellatus* – Red Drum

Among the most valuable fishes in the IRL, this species is well known in the target area for world record catches, as well as for using the area throughout multiple ontogenetic stages. They were more common in gear 160 data but occurred enough in both gear types to generate both models. The gear type 20 model was not a significant predictor of either the training ($P = 0.868$, $R^2 = 4.852\%$) or validation data ($P > 0.05$, $R^2 = 16.40\%$), likely due to the low amount of training data, $n = 22$. With substantially more samples to train the model with, $n = 210$, the gear type 160 model was a more powerful significant predictor of variation in the training ($P<0.001$, $R^2=11.51\%$) and validation ($P < 0.001$, $R^2 = 86.38\%$) data. As both models rely, in part, on DO, our projections for this species are limited to the 5 m^3/sec and base, no change, inflow scenarios. With the changes projected by the Task 1 team, assuming no substantive behavioral or physiological responses, or influences on local recruitment not captured in the FWC data and lacking details on ecological feedbacks loops, this model projects an increase in the abundance of *Sciaenops ocellatus* over a 9-month period (**Figure 2** and **Figure 9**).

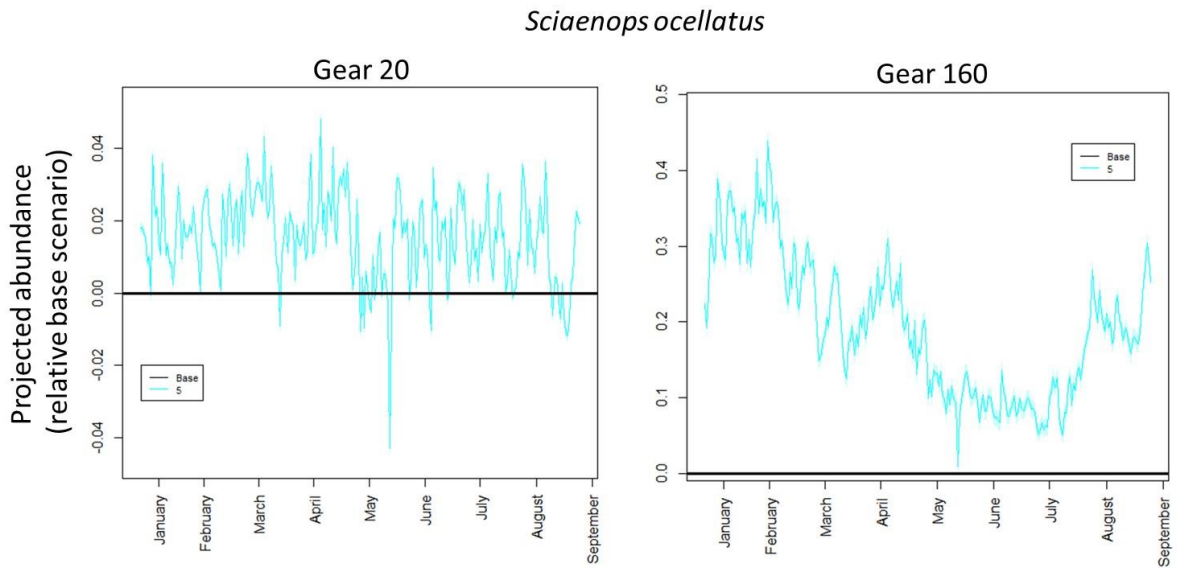

Note: Numbers in the legend refer to the volume pumping scenario, in the unit of m^3/sec. Base, y axis= 0, refers to the baseline, no change, scenario. The shaded region around each line represents the 95% confidence interval of the model.

Figure 9. Projected changes in *Sciaenops ocellatus* abundance in BRL over a 9-month period for all available scenarios using data from gear types 20 (left) and 160 (right) excluding outliers

1.3.1.2.8 *Syngnathus scovelli* – Gulf Pipefish

In general, Pipefish are not efficiently sampled using gear type 160, presumably as their body shape allows them easy escape from the net, resulting in a data deficiency for gear 160 model generation. The gear 20 model, which was dependent only on temperature data, was produced for all but the 10 m^3/sec scenario. This model was not a significant predictor of the training data ($P = 0.094$, $R^2 = 1.61\%$), but was successfully able to blindly predict variation in the validation data ($P < 0.001$, $R^2 = 98.98\%$). With the changes projected by the Task 1 team, assuming no substantive behavioral or physiological responses, or influences on local recruitment not captured in the FWC data and lacking details on ecological feedbacks loops, this model projects an increase in the abundance of *Syngnathus scovelli* over a 9-month period, with no notable difference between scenarios (**Figure 2** and **Figure 10**).

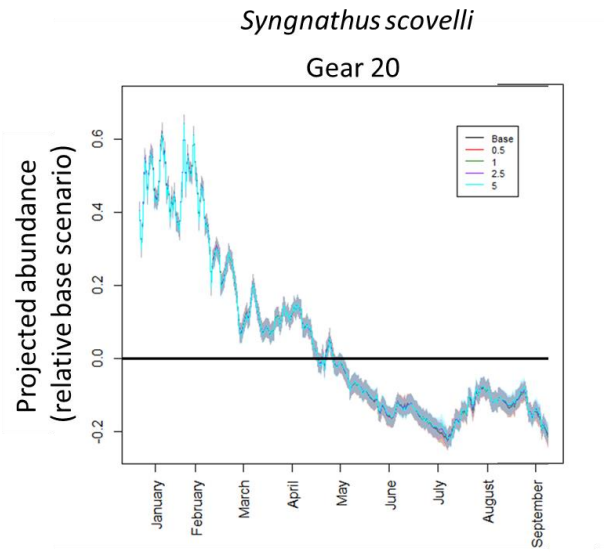

Note: Numbers in the legend refer to the volume pumping scenario, in the unit of m^3/sec. Base refers to the baseline, no change, scenario. The shaded region around each line represents the 95% confidence interval of the model.

Figure 10. Projected changes in *Syngnathus scovelli* abundance in BRL over a 9-month period for all available scenarios using data from gear type 20, excluding outliers

1.3.1.2.9 Alpha Diversity

Referenced here as total fish species diversity, the models produced for alpha diversity of the BRL were significant predictors of the training data (gear 20: $P = 0.002$, $R^2 = 0.05\%$; gear 160: $P < 0.001$, $R^2 = 13.85\%$), but were not able to accurately predict the validation data (gear 20: $P > 0.05$, $R^2 = 4.16\%$; gear 160: $P > 0.05$, $R^2 = 13.28\%$). As these models performed poorly in predicting the observed validation data and were not significant predictors of alpha diversity in the BRL training data, it would not be appropriate to use these models in any decision-making processes. Net results are presented in **Figure 2** and **Figure 11** for the sake of thoroughness and completeness of the Task 3 team deliverables but will not be discussed.

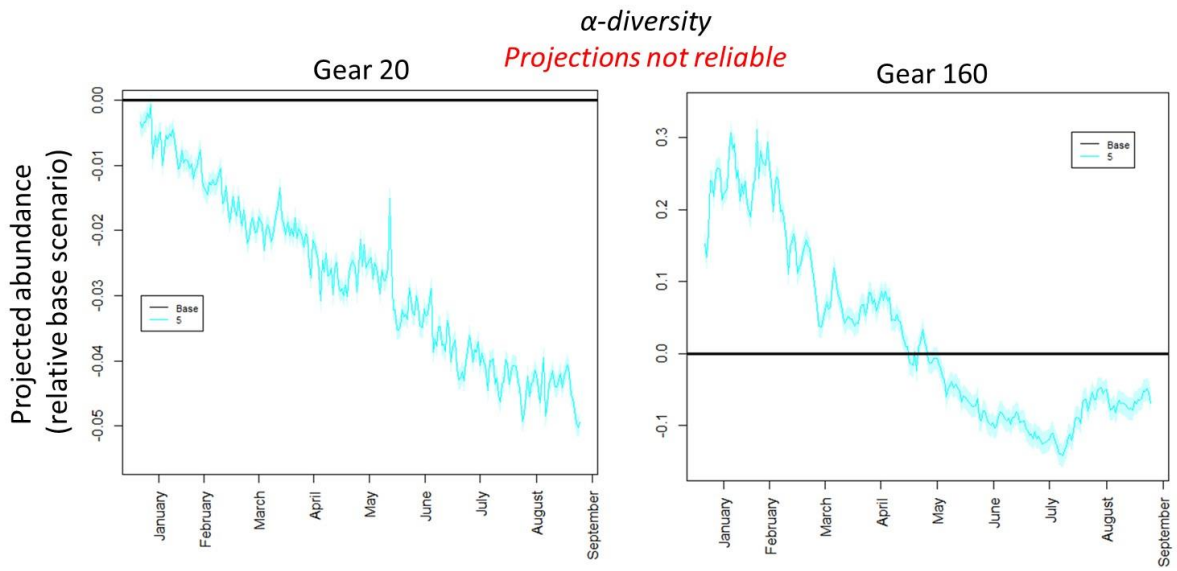

Note: Numbers in the legend refer to the volume pumping scenario, in the unit of m^3/sec. Base refers to the baseline, no change, scenario. The shaded region around each line represents the 95% confidence interval of the model. As these models were not significant predictors of the training data nor were they able to accurately represent the validation data, they should not be used in decision-making processes and are only included here to provide the requisite deliverable.

Figure 11. Projected changes in fish alpha diversity in BRL over a 9-month period for all available scenarios using data from gear type 20 (left) and gear type 160 (right)

1.3.1.2.10 Shannon's H

The models produced for Shannon's diversity of the BRL were significant predictors of the training data (gear 20: $P = 0.028$, $R^2 = 0.023\%$; gear 160: $P < 0.001$, $R^2 = 3.51\%$), but were not able to accurately predict the validation data (gear 20: $P > 0.05$, $R^2 = 0.004\%$; gear 160: $P > 0.05$, $R^2 = 0.029\%$). As these models performed poorly in predicting the observed validation data and were not significant predictors of Shannon diversity in the BRL training data, it would not be appropriate to use these models in any decision-making processes. Net results are presented in **Figure 2** and **Figure 12** for the sake of thoroughness and completeness of Task 3 team deliverables but will not be discussed.

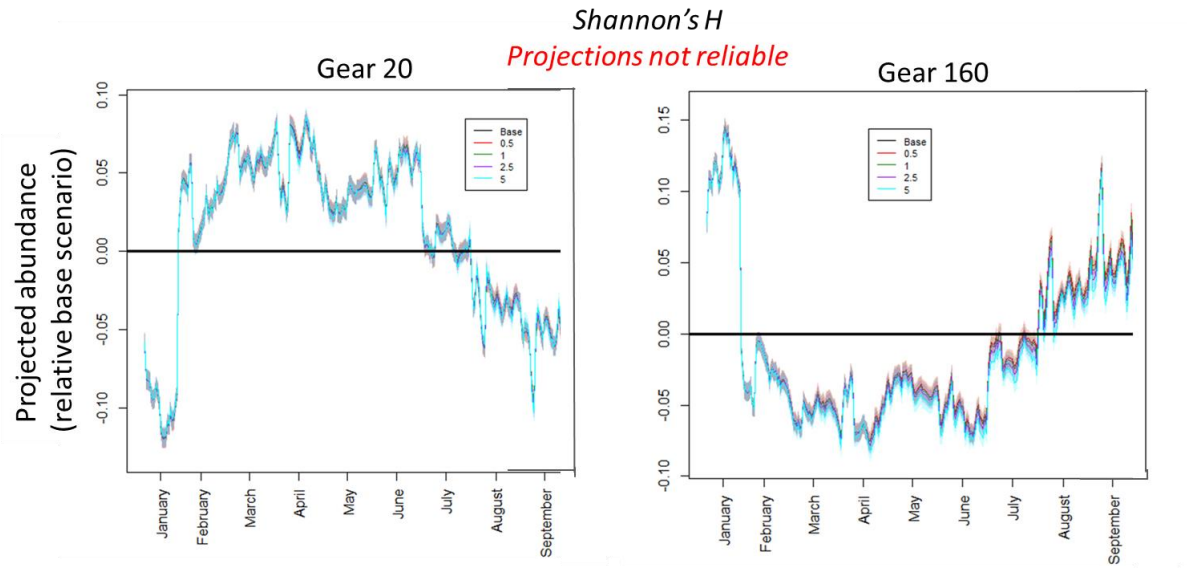

Note: Numbers in the legend refer to the volume pumping scenario, in the unit of m^3/sec. Base refers to the baseline, no change, scenario. The shaded region around each line represents the 95% confidence interval of the model. As these models were not significant predictors of the training data nor were they able to accurately represent the validation data, they should not be used in decision-making processes and are only included here to provide the requisite deliverable.

Figure 12. Projected changes in fish Shannon diversity in BRL over a 9-month period for all available scenarios using data from gear type 20 (left) and gear type 160 (right)

1.3.1.2.11 Pielou's Evenness

The models produced for Pielou's evenness of the BRL were significant predictors of the training data (gear 20: P = 0.010, R^2 = 0.036%; gear 160: P = 0.003, R^2 = 2.098%), but were not able to accurately predict the validation data (gear 20: P > 0.05, R^2 = 2.588%; gear 160: P > 0.05, R^2 = 2.732%). As these models performed poorly in predicting the observed validation data and were not significant predictors of Pielou's evenness in the BRL training data, it would not be appropriate to use these models in any decision-making processes. Net results are presented in **Figure 2** and **Figure 13** for the sake of thoroughness and completeness of Task 3 team deliverables but will not be discussed.

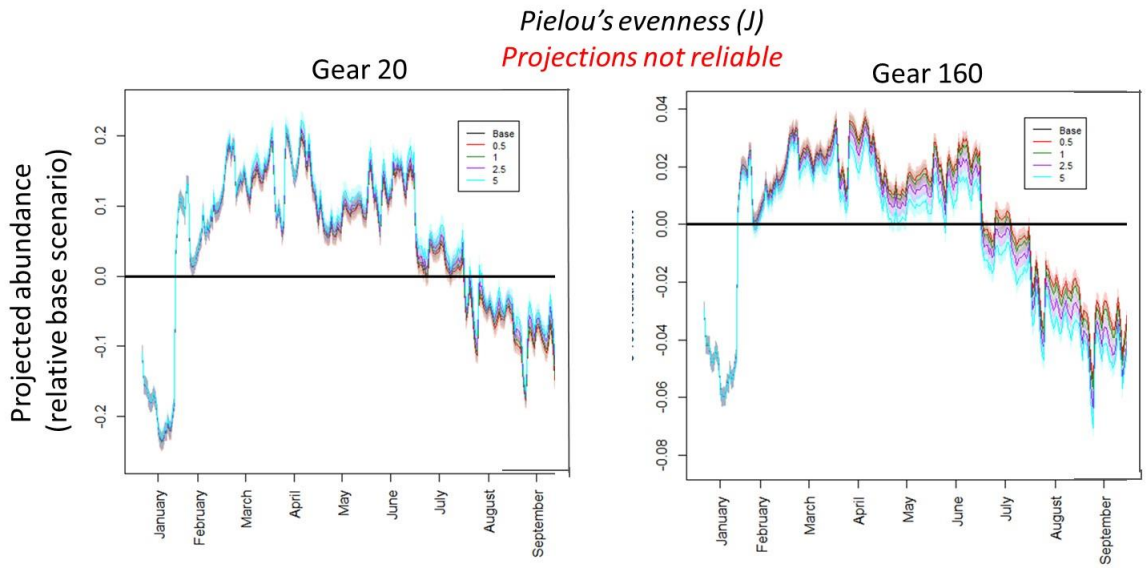

Note: Numbers in the legend refer to the volume pumping scenario, in the unit of m^3/sec. Base refers to the baseline, no change, scenario. The shaded region around each line represents the 95% confidence interval of the model. As these models were not significant predictors of the training data nor were they able to accurately represent the validation data, they should not be used in decision-making processes and are only included here to provide the requisite deliverable.

Figure 13. Projected changes in fish Pielou's evenness in BRL over a 9-month period for all available scenarios using data from gear type 20 (left) and gear type 160 (right)

1.3.1.2.12 Mean Trophic Level

The models produced for mean trophic level of the BRL fish community were significant predictors of the training data (gear 20: $P = 0.021$, $R^2 = 0.025\%$; gear 160: $P < 0.001$, $R^2 = 4.993\%$), but were not able to accurately predict the validation data (gear 20: $P > 0.05$, $R^2 = 8.80\%$; gear 160: $P > 0.05$, $R^2 = 9.138\%$). As these models performed poorly in predicting the observed validation data and were not significant predictors of mean fish community trophic level in the BRL training data, it would not be appropriate to use these models in any decision-making processes. Net results are presented in **Figure 2** and **Figure 14** for the sake of thoroughness and completeness of Task 3 team deliverables but will not be discussed.

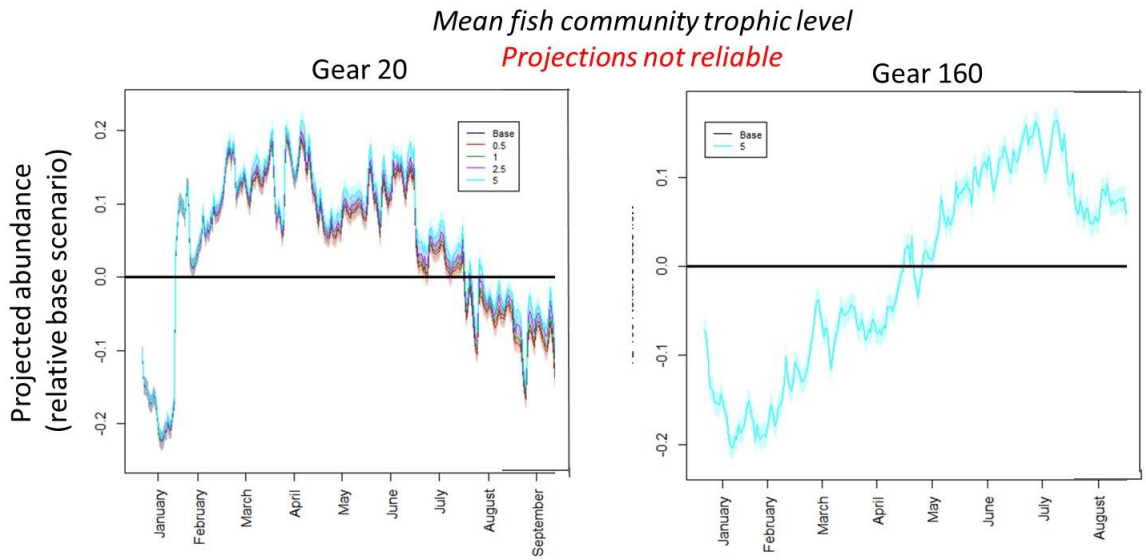

Note: Numbers in the legend refer to the volume pumping scenario, in the unit of m^3/sec. Base refers to the baseline, no change, scenario. The shaded region around each line represents the 95% confidence interval of the model. As these models were not significant predictors of the training data nor were they able to accurately represent the validation data, they should not be used in decision-making processes and are only included here to provide the requisite deliverable.

Figure 14. Projected changes in fish community's mean trophic level in BRL over a 9-month period for all available scenarios using data from gear type 20 (left) and gear type 160 (right)

1.3.2 Fish and Chl-a

The BRL Chl-a concentrations range from 0.350–135.250 µg/L between 2002 and 2018. However, from 2002–2010 Chl-a never exceeded 19.45 µg/L with a mean value of 6.68 µg/L. From 2011–2018, the mean Chl-a concentration was 24.36 µg/L, exceeding the maximum value of all preceding years. This pattern is demonstrated by a moderately strong association between Chl-a concentration and time ($P < 0.001$, $S = 618503$, $rho = 0.563$). Spikes in Chl-a concentrations, exclusively in 2011 and after, co-occur with a prevalence of cyanobacteria during the known HABs in 2011, 2016, and 2018. When looking at the influence of this interaction between time and Chl-a concentrations on the metrics of community structure discussed in **Section 1.2.1.1**, it is unsurprising to see all metrics of community structure were significantly affected. The one exception to this statement being no significant influence detected on mean trophic level of the community sampled by gear type 160 (**Table 3**).

Table 3. Statistics for two-way ANOVAs

Note: Dependent: fish community structure metrics. Independents: time (month and year) and Chl-a concentrations.

Gear type	Descriptor	Factor	F	P
160	α	Time	30.464	<0.001
		Chl-a	75.483	<0.001
		Time*Chl-a	3.969	0.046
160	H	Time	31.680	<0.001
		Chl-a	0	0.985
		Time*Chl-a	102.220	<0.001
160	J	Time	5.268	0.022
		Chl-a	50.209	<0.001

Gear type	Descriptor	Factor	F	P
		Time*Chl-a	87.369	<0.001
160	TL	Time	9.459	0.002
		Chl-a	85.495	<0.001
		Time*Chl-a	1.231	0.267
20	α	Time	193.92	<0.001
		Chl-a	27.610	<0.001
		Time*Chl-a	31.150	<0.001
20	H	Time	14.830	<0.001
		Chl-a	9.560	0.002
		Time*Chl-a	18.010	<0.001
20	J	Time	9.406	0.002
		Chl-a	1.777	0.183
		Time*Chl-a	6.660	0.010
20	TL	Time	140.192	<0.001
		Chl-a	1.962	0.162
		Time*Chl-a	5.190	0.023

All metrics of community structure were also significantly associated with Chl-a concentrations, save Pielou's evenness for the gear type 20 fish community, with the associations being primarily negative and relatively weak (**Table 4**). The only positive associations were found with mean trophic level of the fish community from gear type 20, and the alpha diversity of the fish community from gear type 160. All associations were relatively weak, possibly due to the strong influence of time which could not be captured in these preliminary analyses. Such an interaction would be visible in **Figure 15**, yet we find no indication of such a pattern.

Table 4. Associations between metrics of fish community structure and Chl-a concentrations

Note: Rho with an absolute value less than 0.3 is considered weak, and the sign in front of Rho denotes the direction of the association.

Metric	Gear	S	rho	P
α	20	121985294	-0.289	<0.001
α	160	2030138219	0.17	<0.001
H	20	109932910	-0.162	<0.001
H	160	2645081446	-0.082	<0.001
J	20	47651932	-0.051	0.197
J	160	2563346190	-0.219	<0.001
TL	20	76706078	0.189	<0.001
TL	160	3049733054	-0.247	<0.001

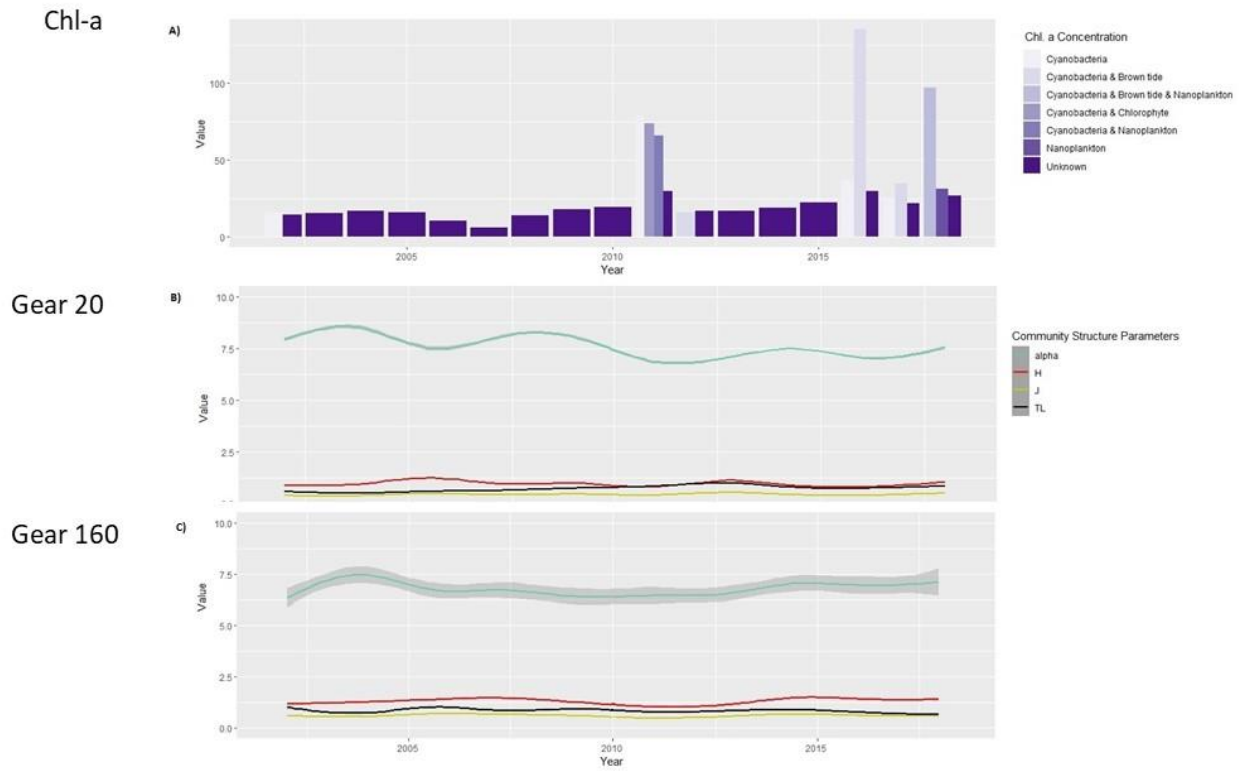

Note: Colors in plot A represent the dominant phytoplankton species present, when known. Shaded regions around the lines in the bottom two plots represent the standard error of the mean.

Figure 15. Plots of Chl-a concentrations (A) and fish community structure metrics for gears type 20 (B) and 160 (C) from 2002–2018

Nearly all fish populations showed significant associations with Chl-a concentrations in the BRL (**Table 5**). Only *Anchoa mitchilli* and *Lagodon rhomboides,* from gear type 20, showed no association. Most of the associations were, however, very weak. *Pogonias cromis* and *Syngnathus scovelli* abundances, being the only exceptions, both had moderately strong associations to Chl-a concentrations, but in different directions, positively and negatively, respectively.

Table 5. Spearman Rank correlations between each SoI and Chl-a concentrations in BRL

Species	Gear	S	rho	P
Anchoa mitchilli	20	90595843	0.042	0.223
Anchoa mitchilli	160	Insufficient data		
Archosargus probatocephalus	20	88201793	0.068	0.051
Archosargus probatocephalus	160	2025176393	0.172	<0.001
Cynoscion nebulosus	20	103448862	-0.09	0.007
Cynoscion nebulosus	160	2123212110	0.132	<0.001
Lagodon rhomboides	20	98570020	-0.04	0.229
Lagodon rhomboides	160	2210494529	0.096	<0.001
Lutjanus griseus	20	76737404	0.189	<0.001
Lutjanus griseus	160	2789936992	-0.14	<0.001
Pogonias cromis	20	82853763	0.124	<0.001
Pogonias cromis	160	1534390098	0.372	<0.001
Sciaenops ocellatus	20	87560645	0.074	0.032
Sciaenops ocellatus	160	2341575504	0.042	0.036

Species	Gear	S	rho	P
Syngnathus scovelli	20	129120010	-0.36	<0.001
Syngnathus scovelli	160	Insufficient data		

Visual inspection of these patterns (**Figure 16**) suggests that 2011 indeed may have marked a state shift for the fish community in the BRL. A strong decline in nearly all SoI followed the 2011 superbloom event. Notably *Syngnathus scovelli*, currently being evaluated as a potential indicator species for IRL health (personal communication – Dr. Richard Paperno, FWC), and *Lagodon rhomboides,* an important forage fish throughout the IRL, have both experienced a steady decline since the 2011 event. All SoI show patterns with typical time-lagged responses to algal blooms, as well, suggesting individual species time series break-point-analyses would be useful to understand the interplay between the BRL's abiotic and biotic stressors on these SoI to more accurately predict how increased inflow may influence them.

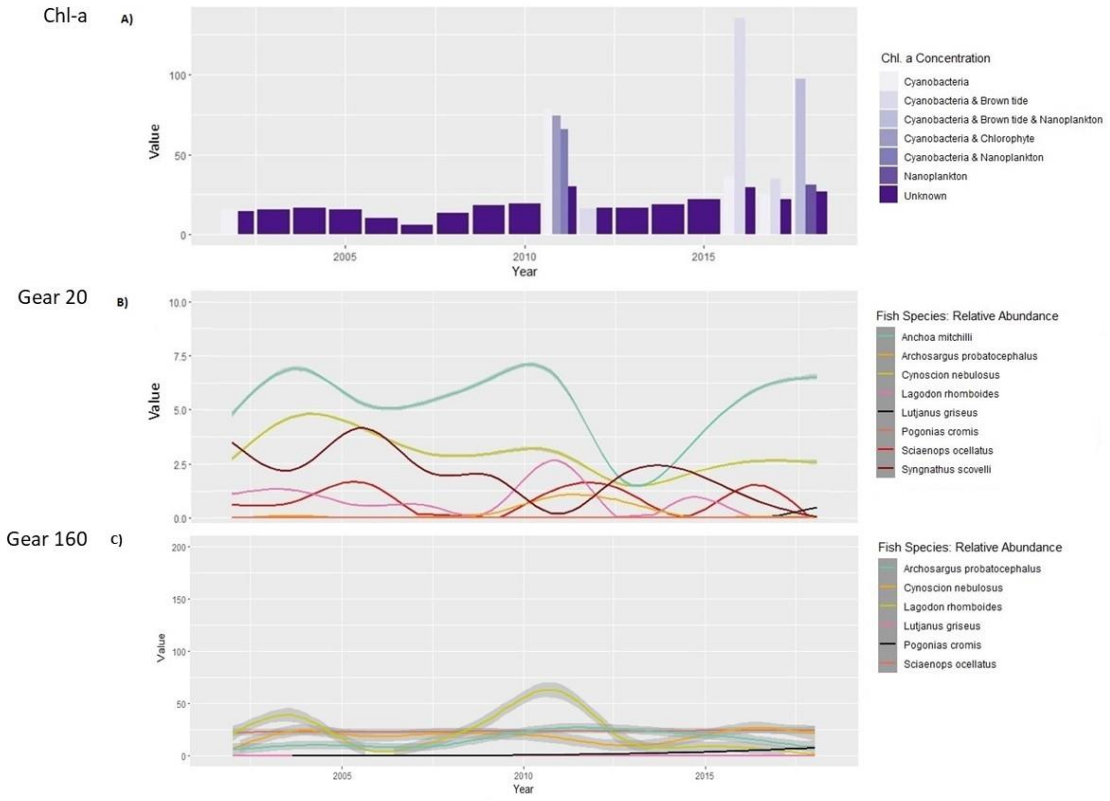

Note: Colors in plot A represent the dominant phytoplankton species present, when known. Shaded regions around the lines in the bottom two plots represent the standard error of the mean.

Figure 16. Plots of Chl-a concentrations (A), and relative fish abundances for gears type 20 (B) and 160 (C) from 2002–2018

1.3.3 Fish Movement

Among the studies examined, three are worthy of summarizing in this report: (1) Tremain, Harnden, and Adams (2003) Multidirectional movements of sportfish species between an estuarine no-take zone and surrounding waters of the Indian River Lagoon, Florida; (2) Reyier, Lowers, Scheidt, and Adams (2011) Movement patterns of adult Red Drum, *Sciaenops ocellatus*, in shallow Florida lagoons as inferred through autonomous acoustic telemetry; and (3) Reyier, Scheidt, Stolen, Lowers, Halloway-Adkins, and Ahr (2020) Residency and dispersal of three

species from a coastal marine reserve: Insights from a regional-scale acoustic telemetry network. These studies make three compelling conclusions that are relevant to this report. First, Red Drum and seatrout exhibit very strong site fidelity, meaning their movement within their post-settlement habitat is very limited, an average of less than 0.10 km per day. Second, long distance movement, ranging from 150 to 650 km are associated with known species-specific spawning period. And third, life-history stage specific movement within the IRL are apparent.

An examination of the 1996–2018 FWC-FIM monitoring data indicate that the pattern of variation in the mean total fish abundance and the species-specific mean abundance of Red Drum and seatrout and the pattern of variation in DO, salinity, temperature, and pH are correlated. This covariation also differs between the BRL site of the proposed pilot pumping station and the Patrick Air Force Base site within the IRL (see **Figure 17** and **Figure 18**). It is interesting to note that a decrease in temperature and salinity, and an increase in pH between 2015 and 2018 are associated with the decrease in abundance of Red Drum and seatrout in the BRL (**Figure 17**). This pattern differs from that of the Patrick Air Force Base site **(Figure 18**).

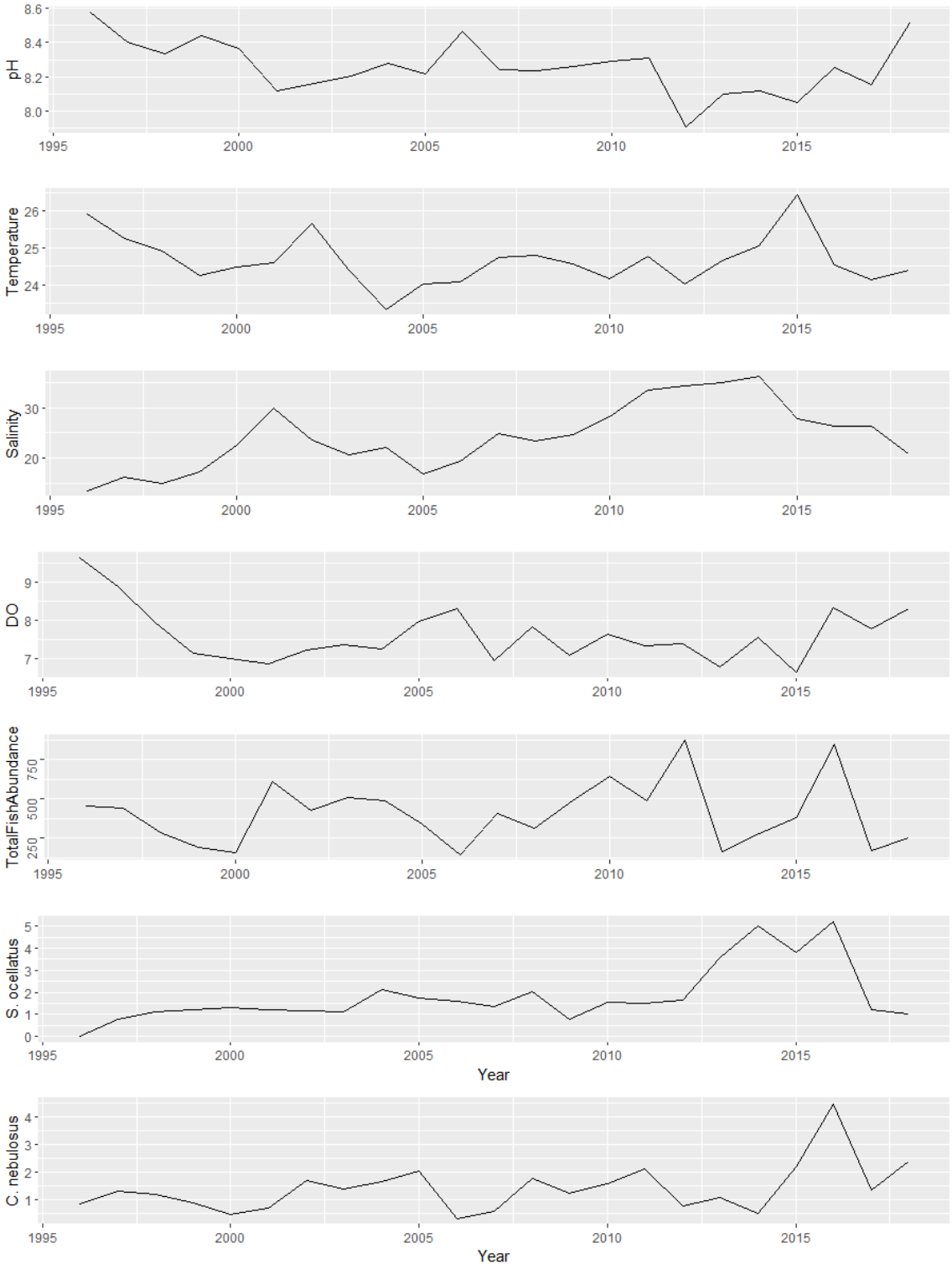

Figure 17. Patterns of variation in mean fish abundance and environmental factors in BRL between 1996 and 2018

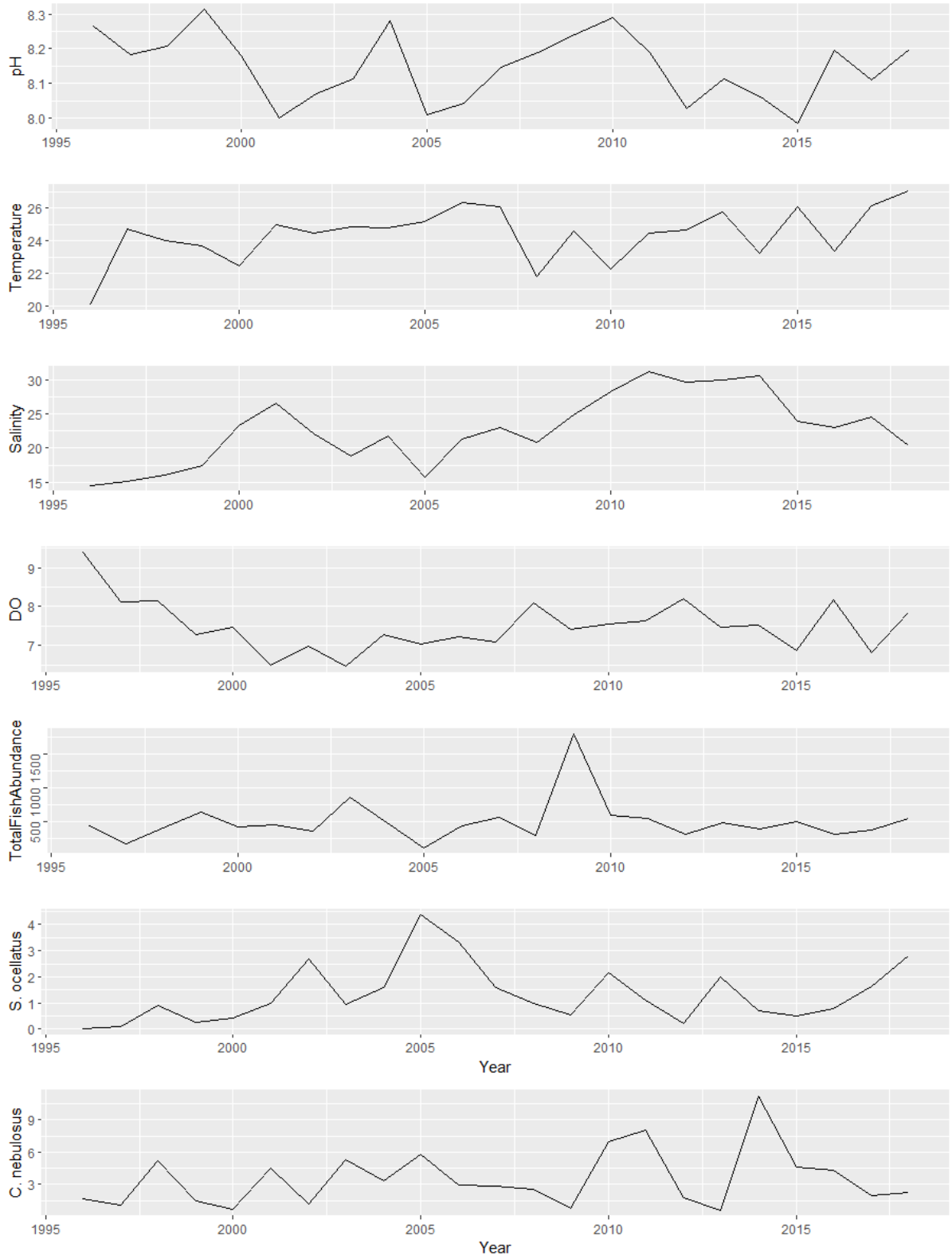

Figure 18. Patterns of variation in mean fish abundance and environmental factors in the Patrick Air Force Base area of the IRL between 1996 and 2018

1.4 Conclusions

1.4.1 Fish Community Modeling

In Phase 1, the fish biology team concluded that among the abiotic factors that are known to affect fishes, the variation in fish community structure, abundance, and distribution of fishes in the IRL are associated with variation in salinity, temperature, and DO and identified species of interest for further study (Florida Tech, 2020; Johnson et al., 2020). Based on this foundational knowledge, in this phase (Phase 2) of the project, the team built predictive models to quantify the strength of the relationships between these environmental factors and the metrics of fish responses mentioned above. We then used these models to provide preliminary projections of nine months of change in abundance and fish community structure resulting from preliminary projected changes in the abiotic environment generated by the Task 1 team. Phase 2 fish response models will be updated in the proposed Phase 3 with validated and revised water quality projections.

Most of the Phase 2 abundance models performed exceedingly well at predicting fish responses to changes in environmental conditions. Seven of the models were able to predict the fish responses with more than 95% accuracy (**Table 1**), and only two, Red Drum from gear type 20 and Pinfish from gear type 160, had accuracy less than 50%. The poor performance of the Red Drum model likely stems from the noise generated from lumping all age groups into one abundance estimate. Typically, only juveniles and subadults Red Drum are captured by that gear; however, the model uses the entire population. It is known that Red Drum undergo several ontogenetic habitat shifts, preferring structured seagrass beds and mangroves early in life and then shifting toward more open areas as they grow (Bacheler et al., 2009; Moulton et al., 2017; Reyier et al., 2011; Stunz et al., 2001), with complex movement patterns increasing the complexity further (Adams and Tremain, 2000). With changing habitat preferences likely comes different driving factors of abundance and capture probability. Accurately modeling this species will likely require a more intensive spatiotemporally mediated age-structured population modeling approach, which was beyond the scope of this phase but is proposed for Phase 3. Until such an effort is completed, however, the gear 160 model Red Drum model is reasonably useful. The Pinfish model showed poor predictive performance, with less than 10% accuracy. Perhaps this rooted in the complex relationship this species has with its environment. Most age classes of Pinfish are captured in gear 160, with 460 records in the BRL data used in this study. They are known to be a hardy fish that capitalizes on many different structured habitats and can frequently be found moving through ‘open-water.’ Given this result, habitat and age-structured species distribution models are likely needed to accurately model the dynamic relationship between this species, and many other fish populations, and changes in the abiotic and biotic conditions in IRL.

These results support a logical, and very important conclusion that each species is expected to respond to increased inflow differently (**Figure 1**), and without a mechanistic modeling effort (e.g., to include species specific behavior, physiology, and age-structured data), it will be difficult to accurately project the responses of fishes on environmental changes in the IRL. The valuable recreational sportfish Sheepshead, Spotted Seatrout, and Red Drum; ecologically and economically valuable Pinfish; and ecologically important Gulf Pipefish are all projected to increase in abundance (**Table 2**). Alternatively, the valuable recreational sportfish Gray Snapper and Black Drum, as well as one of the most abundant low trophic-level fishes, the Bay Anchovy, are projected to decrease in abundance (**Table 2**). With the available data, we cannot generalize the way the fish community will respond to increasing inflow in the BRL area. This sentiment is bolstered by lack of predictive power held in any of the models predicting metrics of whole fish community structure (see **Section 1.3.1.2.9** through **Section 1.3.1.2.12** and **Table 1**). Moreover, details of the mechanisms behind these relationships are severely lacking and need to be understood to begin to appreciate the rippling implications of these patterns. Will a decline in Bay

Anchovy result in a decline of large sportfish that feed on them, or perhaps result in an increase in comb jellyfish, another pelagic filter feeder in the region? Will an increase in Sheepshead put top-down pressure on the invertebrate population, resulting in a feedback declining Pinfish leading to an ultimate decline in Spotted Seatrout? Several world record breaking catches of Red Drum have come from the BRL area, how will this impact the fishing industry? If seagrass are restored in the BRL by these actions, it may improve recruitment of many sportfish, such as Red Drum.

For Phase 1 we took the 62 mile 'view from space' asking the broad question "what is important to look at?" In Phase 2, we dug deeper into the patterns and developed quantified models to start projecting impacts. Now, we need to understand the mechanisms behind those patterns and extrapolate them out in both space and time to understand how increasing inflow will impact the invaluable fish community of the IRL.

1.4.1.1 Model Caveats

Here, we have shown significant responses to increased inflow by some of Florida's most economically, ecologically, and recreationally valuable fishes. It is important, however, to put this in the context of the limits of this statement. These models were produced using the best fish community data available for the IRL. The FWC FWRI FIM database is an invaluable resource, hence it deserves to be fully supported continuously. However, all sampling techniques have their inherent biases. These fish data exclusively rely on net collections. Each net is known to have its own set of biases, strengths and weaknesses (FWRI, 2009). To overcome these limitations, the FIM program deploys a large number of different types of nets (FWRI, 2009). No single type of net can offer a full picture of the fish community. Unfortunately, with the different biases of the nets, the data are not comparable and we are limited here to discussing them independently. As a result, each model offers only a piece of the picture so they must be interpreted with caution. For example, a projected decrease in the abundance of Black Drum from gear 160 may not represent a population wide decrease. Rather it suggests a likely decrease in the age groups susceptible to capture by gear 160 but may not directly reflect changes in individuals too small to be captured by that gear type or transient populations. The environmental deoxyribonucleic acid (eDNA) work presented in this report can provide a complimentary snapshot of community structure, as well. While the genetic technology has its own strengths (i.e. highly sensitive, capable of recording cryptic species, not size selective, fast and comparably inexpensive) and weaknesses (i.e. strongly density dependent, difficult interpretation of a positive/negative presence, more subject to dynamic biochemical processes), using the two methods in tandem, as we have done in this report, can offer a more thorough assessment of the community structure of the IRL. The reader is referred to the eDNA portion of the report (**Section 2**), prepared by Dr. Eble's team, for more information on this.

It is also important to note that these initial abundance projections are based on projected data themselves, which are still preliminary. Our models were trained and tested using real world data, but the only way to predict responses to a given scenario (i.e., new oceanic inflow into the BRL) is to predict what the environment will look like during that scenario. The reader is referred to the Task 1 team's Phase 2 report to fully understand the limitations inherent in those model projections and the proposed Phase 3 efforts to calibrate and validate water quality models. As the Task 1 team continues their invaluable work and updates their water quality projections, these fish abundance and community structure models will also be updated.

Finally, we have shown here a series of linear single population models. Those models were trained using 28 years of real-world data, and most are quite powerful predictors of population abundances under those conditions. What we lack is a mechanistic understanding of why we are

seeing the patterns we see. Wanting for that understanding, we lose the ability to confidently project what patterns we will see if and when conditions change. We have shown here, as have our colleagues from other tasks, that increased oceanic inflow will result in change. If that change represents a change in 'the drivers of the system' (i.e., disruptions to the trophic ecology, primary productivity, flow rates, flow directions, bathymetry, human use patterns, changes in the species pool itself, etc.), then our models will quickly lose their predictive power. Similarly, these models do not account for ecological feedback loops, interactions between species, ontogenetic changes, density dependent factors, recruitment, or behavior; all of which are known to be important. This Phase 2 study represents an important and necessary next step toward evaluating the potential impacts of increased oceanic inflow into the IRL, or any other proposed changes to the ecosystem. It was a necessary step, but not the final necessary step.

1.4.2 Fish and Chl-a

These preliminary analyses of algal associations with fish abundances and community structure suggest significant influences of algae (**Table 5**). We expected negative associations to be the norm in this study, as algal blooms are known to cause physiological stress to fishes (Altieri and Gedan, 2015; Cochrane et al., 2009; Feyrer et al., 2015; Glibert et al., 2014; Macusi et al., 2015), and indeed this work does suggest significant negative associations. However, some positive associations were noted, such as significant positive associations for both Black Drum and Gray Snapper with Chl-a concentrations. As both of these species are associated with structured benthos, it is possible that the low oxygen conditions typical late in algal blooms (Altieri and Gedan, 2015) push them out making them more readily captured by nets, or perhaps there is some undescribed mechanism at work which somehow benefits this species. Along with the abiotic stress algal blooms cause in fishes, particularly when they result in anoxic events, we can also expect that they influence fish behavior as well. Recent works have demonstrated that individual behavior can have significant, landscape scale impacts on several aspects of a population's ecology (Blanchard et al., 2021). Physiological stress is often accompanied by such behavioral manifestations (McEwen, 2007). Abandonment of a patch, increased aggression, 'hunkering down,' and increased passivity are all typical responses to physiological stress (Love et al., 2013; McEwen, 2007, 1998; Teller et al., 2014). If fishes are exhibiting any of these responses, it could significantly skew their susceptibility to capture and therefore skew their probability of occurring in the FIM data. Further investigations into the mechanisms behind the associations between fish and algal blooms are needed to understand what role they play in altering projections made by the models presented above. Quantifying these mechanisms will be necessary to fully understand the implications of changing the frequency of algal blooms, as seems a likely result of this effort given the Task 1 and Task 2 teams' work.

1.4.3 Fish Movement

The initial meta-analysis of the movement and habitat use of fishes in the IRL suggests very strong site fidelity in these fishes and movement of fishes within the IRL are associated with spawning episodes and ontogenetic change in habitat and food requirements (Reyier et al., 2020, 2011; Tremain et al., 2004). These findings suggest that changes in the water and habitat quality in the IRL influence the recruitment and subsequent survivorship of fishes the IRL. The association in patterns of variation between fish abundance and water/habitat quality is not unique to the IRL; it appears to be ubiquitous in estuarine ecosystems, for example in Tampa Bay (Lowerre-Barbieri et al., 2013), North Carolina (Bacheler et al., 2009), and Texas (Moulton et al., 2017). These studies further suggest that maintenance of optimal environmental conditions and preventing large fluctuations in environmental parameters though mitigating mechanisms such as the proposed pumping project may promote the sustainability of estuarine-fish communities.

1.5 Next Steps

Capitalizing on the successes of our Phase 1 and Phase 2 efforts, we propose to address two major goals for Phase 3 of the project. First, we need to update the projections here using empirical values for salinity, DO, and temperature provided by the physical oceanography team. The timeline for this first goal is relatively short, less than three months would be needed once updated water quality data are available. The second goal would be to build mechanistic models to quantify the "cause-effect" responses of fish abundance, movement, and habitat use to specific change in salinity, DO, and temperature in the IRL. For this second goal, it will be necessary to continue our budding relationship with the National Aeronautics and Space Administration (NASA) Kennedy Space Center and Herndon Solutions Group biologists to study fish movement both in time and space via acoustic telemetry. This work would ideally begin a few months before, continue during, and extend for at least six months after any pilot pumping takes place. Our partnership with Kennedy Space Center biologists will help maximize our efficiency and capitalize on previous state funding expenditures by using the equipment already deployed in the area (the IRL Florida Atlantic Coast Telemetry array) while minimizing our needs of extra purchasing and improving the return on investment. For Phase 3 we will also need to provide support for FWRI's FIM team to increase sampling frequency and the speed of data availability in the BRL area with support for one OPS Biologist I and extra sampling. Data collection for this effort would need to begin in Phase 3, continue through the pilot pumping, and ideally would extend for a minimum of six months after the pumping finishes so that we can observe the effects of the pumping and collect sufficient data to support creation of the mechanistic models. Building the mechanistic models themselves will be fairly time and resource intensive, but the infrastructure for the models can be built while field data are being collected by partners and would be a deliverable for Phase 3. Running the mechanistic models and producing final species and community response projections would then be possible.

2 Environmental DNA

2.1 Introduction

eDNA sampling was coupled with next-generation deoxyribonucleic acid (DNA) sequencing to provide information on species occurrence and community diversity across taxonomic groups (Ruppert et al. 2019). This research, initiated in Phase 1 and continued in Phase 2, is intended to improve understanding and management of the IRL system by filling data gaps and by establishing an eDNA biodiversity baseline to directly test the impacts of the proposed Phase 3 experimental inflow project on lagoon biodiversity.

eDNA is emerging as a powerful assessment and monitoring tool and eDNA detections are now regularly used to determine species occurrence (presence/absence; Eble et al., 2020). The approach relies on the capture and analysis of trace genetic material in environmental samples, enabling species detection without the need to directly observe or capture organisms in the field (Bohmann et al., 2014). eDNA detections have been found to directly compliment traditional survey strategies by helping to increase sampling effort and species detection (Hansen et al., 2018).

To investigate community response to enhanced inflow using eDNA sampling, three approaches were initiated in Phase 1 and continued in Phase 2. These efforts were designed to directly compliment fish population modeling and baseline biological monitoring being conducted by other members of the team. Our first eDNA approach leverages the power of sampling before and after enhanced inflow at pre-determined experimental and control sites. This before-after-control-

impact (BACI) experimental design is commonly used in ecological studies when experimental sites cannot be randomly assigned and when the timing and location of the impact are known (Smokorowski and Randall, 2017). To improve detection of environmental impacts we have amended the traditional BACI design to include supplemental control sites (Underwood, 1994). Our second approach investigates regional biodiversity patterns using complimentary diversity metrics to track changes in community diversity that may result from the proposed pilot project. Under this framework, biodiversity was characterized at site, basin, and regional scales to determine how communities are structured across the central IRL and BRL. This baseline can then be used track any changes in community similarity/dissimilarity that may result from the proposed Phase 3 experimental inflow, or other perturbations. Our third approach uses randomization tests to detect differences in site-specific measures of taxonomic distinctness from a fixed baseline derived from a master species list for the IRL. The particular value of this approach is both its insensitivity to sample size and ability to track improvements or declines in site diversity against a fixed baseline (Clarke and Warwick, 2001).

All three eDNA approaches have been initiated and our methods, preliminary findings, and next steps are described below.

2.2 Methods

To ensure data quality, sample collection, processing, and analysis followed developing best practices, including strict procedures to minimize both false positives and false negatives detections (Eble et al., 2020). False positives are a significant concern in eDNA sampling because of the potential for contamination with exogenous DNA and cross-contamination between samples during field sampling or laboratory analyses. To minimize cross-contamination, we followed established contamination management guidelines that included thorough decontamination of equipment and laboratory work surfaces with bleach and ultraviolet light, and the addition of negative controls at each step in the workflow to ensure detection and removal of contaminated samples (Ficetola et al., 2016). The occurrence of false negatives is not unique to eDNA and any well-developed ecological sampling must account for a failure to detect species present in the system as the result of environmental or experimental factors. To minimize false negatives, we followed established sampling guidelines to minimize DNA degradation and undertook extensive primer testing to ensure sufficient detection of target taxa.

2.2.1 Field Collections

For Phase 2, eDNA field collections were coordinated with project team members to support collection of 101 water samples from the IRL. To continue assessment of seasonal variation in species composition initiated during Phase 1, three replicate 500 milliliter (mL) water samples were collected at sites 1–12 and sites 24–26 (**Figure 19**) in April and July 2021. An additional twenty 500 mL samples were collected at site 2 in January 2021 to allow estimation of sample sufficiency and power. Together with Phase 1 sampling, a total of 185 IRL water samples have been collected and preserved to support assessment of pumping impacts. In each case, water samples were collected 3 inches below the surface using bleach sterilized Nalgene bottles. To limit DNA degradation, samples were held on ice and filtered within 6 hours of collection using 0.45 µm pore size mixed cellulose ester filters (Kumar et al., 2020). Filter membranes containing eDNA were then stored at -20 degrees Celsius (°C) in Longmire's buffer solution until DNA extraction.

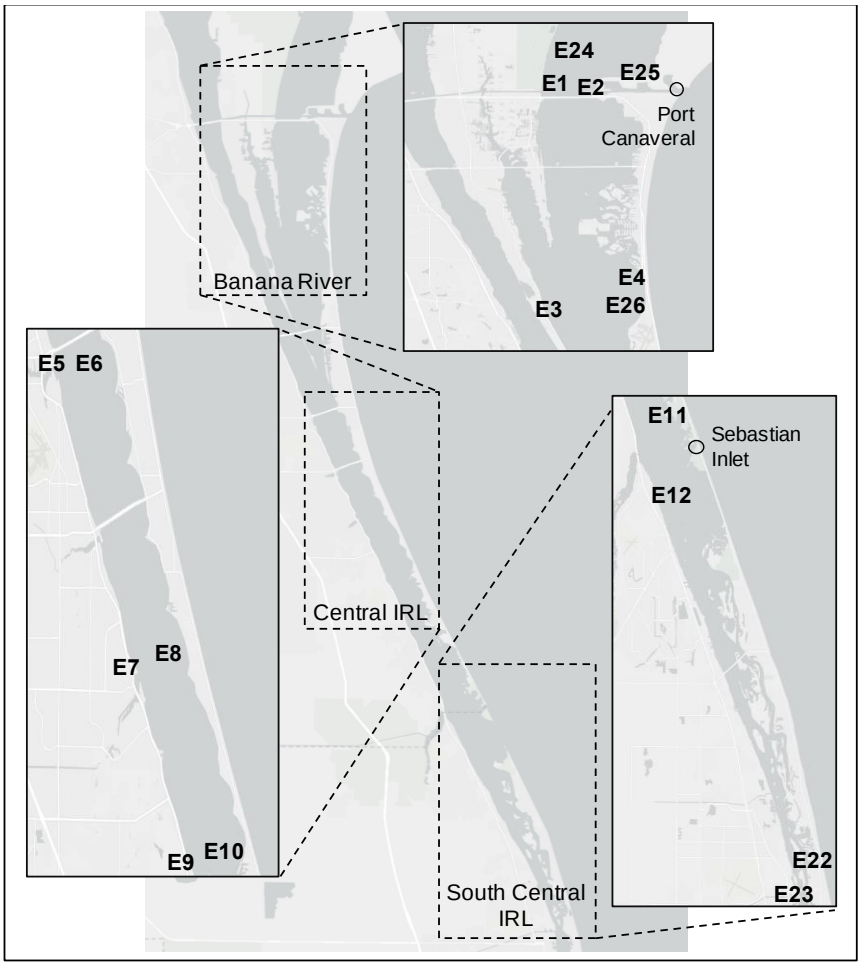

Note: Phase 3 experimental sites (E1 and E2) and control sites (E4 and E26) are highlighted. Sites E22 and E24 were sampled in Phase 1 to determine the location of the proposed pilot pumping system and were not sampled in Phase 2. Sites E24–E26 were established in Phase 2 to improve resolution of regional biodiversity patterns and direct testing of inflow impacts.

Figure 19. Map of the central IRL and BRL with insets depicting Phases 1 and 2 eDNA study sites in BRL, central IRL, and south central IRL

2.2.2 Miseq Library Preparation and Sequencing

Marker development and sequencing focused on fishes using mitochondrial primers for 16S ribosomal ribonucleic acid (rRNA; Deagle et al., 2007; Berry et al., 2017). To investigate the feasibility of increasing the taxonomic breadth of proposed future sampling, a subset of filtered samples were analyzed using taxa specific mitochondrial primers for 16S rRNA (Berry et al., 2017) and cytochrome oxidase subunit I (COI; Leray et al., 2013) targeting crustaceans and metazoans, respectively (**Table 6**).

To prepare samples for paired-end sequencing on the Miseq sequencing platform (Illumina, San Diego), eDNA was extracted from half of each mixed cellulose ester filter using the Dneasy Blood and Tissue extraction kits (Qiagen Inc., Germantown, MD), followed by polymerase chain reaction (PCR) inhibitor removal using the OneStep PCR Inhibitor Removal kit (Zymo Research, Inc., Irvine, CA). The remaining half of each filter was archived for future analyses. Once the DNA was extracted, sequencing libraries were prepared by amplifying eDNA using a two-step PCR process (sensu Cruaud et al., 2017). In brief, the first PCR step utilized quantitative PCR and tailed taxa

specific primers (**Table 6**) to amplify target eDNA against a backdrop of mixed DNA from all species present at the survey site. During the second PCR step, samples were prepared for multiplexing with the addition of Illumina adaptors and a unique index sequence (**Table 7**) added to both forward and reverse reads to reduce sequence misidentification (Kircher et al., 2012). Following each PCR, samples were quantified using a Qubit 4 Fluorometer (Invitrogen, Carlsbad, CA) and cleaned using the EZNA Cycle Pure Kit (Omega Bio-Tek, Norcross, GA). Resulting tagged amplicons were pooled in equimolar concentrations, size-selected using a PippinHT (Sage Science, Beverly, MA), and bi-directionally sequenced (paired-end sequencing) on the University of Central Florida Illumina MiSeq system using both V2 and V3 reagent kits. Sequencing data were then demultiplexed using the Illumina MiSeq software and downloaded for processing and analysis.

Table 6. Step 1 tailed quantitative PCR primers with primer name, target gene, target taxa, and nucleotide sequence

Note: Taxa specific sequences are shown in bold.

Name	Gene	Taxa	Sequence
meta-16SF-deg	16s rRNA	Class Actinopterygii and Chondrichthyes	TCGTCGGCAGCGTCAGATGTGTATAAGAGACAG**GACCCTATGGAGCTTTARAC**
meta-16S2R-deg	16s rRNA	Class Actinopterygii and Chondrichthyes	GTCTCGTGGGCTCGGAGATGTGTATAAGAGACAG**CGCTGTTATCCCTADRGTAACT**
meta-mlCOIintF	COI	Subkingdon Metazoa	TCGTCGGCAGCGTCAGATGTGTATAAGAGACAG**GGWACWGGWTGAACWGTWTAYCCYCC**
meta-jgHCO2198	COI	Subkingdon Metazoa	GTCTCGTGGGCTCGGAGATGTGTATAAGAGACAG**TAIACYTCIGGRTGICCRAARAAYCA**
Crust16s-F	16s rRNA	Subphylum Crustacea	TCGTCGGCAGCGTCAGATGTGTATAAGAGACAG**GGGACGATAAGACCCTATA**
Crust16s-R	16s rRNA	Subphylum Crustacea	GTCTCGTGGGCTCGGAGATGTGTATAAGAGACAG**ATTACGCTGTTATCCCTAAAG**

Table 7. Step 2 example dual indexed PCR primer pair with primer name, index (bold), and sequence

Note: All samples were dual indexed to ensure the accuracy of paired-end sample identification.

Name	i5 or i7 Index	Sequence
S502-P5	CTCTCTAT	AATGATACGGCGACCACCGAGATCTACAC**CTCTCTAT**TCGTCGGCAGCGTC
N701-P7	TCGCCTTA	CAAGCAGAAGACGGCATACGAGAT**TCGCCTTA**GTCTCGTGGGCTCGG

2.2.3 Sequence Quality Control and Taxonomic Assignment

Annotation of sequences generated by eDNA metabarcoding has customarily relied on the construction of operational molecular taxonomic units that merge sequence reads that differ by a fixed dissimilarity threshold. This approach reduces the computational complexity of downstream analyses at a cost to sequence resolution and data transferability among projects (Callahan et al., 2017). Here we apply recent advances in sequence analysis to resolve exact amplicon sequence variants (ASVs) down to the level of single-nucleotide differences. This approach improves resolution of biodiversity patterns and allows for direct comparison or merging of independently processed datasets within and between studies.

2.2.3.1 Sequence Quality Control

To ensure accurate taxonomic assignment, paired-end sequence reads were filtered and trimmed in Rstudio (Rstudio Team, version 1.3.959) using the DADA2 pipeline (Callahan et al., 2016). Gene-specific, demultiplexed sequences were trimmed to remove amplicon primers and low-quality bases (median quality score < 30) at the beginning and end of the sequence, filtered to remove sequences with ambiguous base calls (max N = 0; max E = 2) and Phix control reads, and dereplicated and denoised based on read identify and quality. Forward and reverse reads

with ≥20 base pairs overlap were then merged to obtain full denoised sequences, after which chimeras were removed and an exact amplicon ASV table was constructed to provide a summary of the unique DNA sequences detected in each sample.

2.2.3.2 Taxonomic Assignment

ASVs were blasted against the National Center for Biotechnology Information's (NCBI) GenBank nucleotide database using the Basic Local Alignment Search Tool (BLAST) with the default parameters on the University of Central Florida COOMBS computer cluster. To retrieve the full taxonomic identity, each of the "taxids" from the Basic Local Alignment Search Tool results was quired against the NCBI database using the "taxonkit lineage" command of taxonkit (Shen & Xiong, 2019). To reduce uncertainty in taxonomic assignment, ASVs with a bitscore below 250 and/or query coverage below 100% were discarded. Only ASVs meeting the threshold criteria for species level assignment ≥ 99% similarity were retained (sensu West et al., 2020). Species level assignments were collapsed to genus level if the assigned taxa were not known to occur in the IRL or Florida Atlantic coast, or if more than one match exceeded the assignment threshold (e.g., 99% species level assignment). ASVs with ≥ 99% match to a taxa that was not listed in the IRL species inventory maintained by the Smithsonian Fort Pierce Marine Station but that had been recorded elsewhere along the Florida Atlantic coast (FishBase; www.fishbase.org) were considered to be new records. Taxon name, rank, and NCBI taxon identifier were then output for biodiversity assessment.

2.2.4 Sample Sufficiency and Power

Successful resolution of biodiversity patterns is determined by both the sufficiency and power of the sampling strategy (Li et al., 2020). With low sample sufficiency many species present at a site may go undetected, potentially increasing variability among samples and decreasing the power to resolve differences in species occurrence between sites and within sites over time, when significant differences exist. To address this issue, we estimated how much sampling effort (i.e., samples collected) is needed to reliably resolve site diversity by analyzing the diversity of fish detected in 20 replicate water samples collected in January 2021 from the experimental site just south of Port Canaveral locks (E2). Because sample power is also determined by sample variance, which decreases with increasing sample sizes, we conducted a separate power analysis of the proposed BACI experimental design using estimates of species richness and group standard deviation derived from the Port Canaveral samples.

2.2.4.1 Sample Sufficiency

Sample processing and quality control was conducted as described above and species accumulation curves were developed in Primer 7 (Quest Research Limited, Auckland, NZ) using the Ugland-Gray-Elligsen (UGE) index and Michaelis-Menten (MM) model with 999 permutations. UGE is backward looking and estimates the behavior of species richness estimates with increasing number of samples up to the maximum number collected (20; Ugland et al., 2003)). The MM estimator is forward looking and estimates the total number of species that would be observed at each step as the number of samples increases to infinity (Colwell and Coddington, 1994).

2.2.4.2 Sample Power

A 2-way ANOVA was implemented to analyze BACI design power using estimates of species richness and group standard deviation derived from the Port Canaveral samples across sample size ranging from 1 to 20. Because these data were derived from samples collected in the winter,

a separate power analysis was conducted using projected species richness and standard deviation for samples collected across all four seasons.

2.2.5 Biodiversity Assessment

We have initiated three approaches to investigate community response to enhanced inflow using eDNA sampling:

1. BACI experimental design to investigate differences in species occurrence both before and after enhanced inflow at the pre-determined experimental and control sites.
2. Assessment of regional biodiversity patterns at site, basin, and regional scales to track changes in community similarity/dissimilarity that may result from enhanced inflow, or other perturbations.
3. Monitoring changes in community taxonomic structure over time relative to a fixed baseline to track biodiversity recovery or loss.

All analyses and summary biodiversity data were generated in Primer 7 with number of sequence reads transformed to strict presence/absence.

2.2.5.1 Site Diversity (Alpha Diversity)

Four measures of site-specific diversity were estimated for each site across seasonal samples analyzed to date (fall, winter, and spring). Samples collected in July 2021 are being processed and will be analyzed as part of the proposed Phase 3 pilot experiment. The four site-specific diversity metrics examined were the total number of species (species richness), Shannon diversity index (log base *e*; Shannon, 2001), and two estimates of sample taxonomic distinctness (average distinctness and variation in distinctness; Warwick and Clarke, 1995). Taxonomic distinctness measures the relatedness of species within a sample as defined by traditional Linnaean taxonomy. Estimates of both average and variation in taxonomic distinctness have been shown to be useful alternative measures of diversity that are insensitive to sample size (Clarke and Warwick, 2001), sensitive to environmental disturbance (Warwick and Clarke, 1995), and a direct compliment to standard richness-related like the Shannon diversity index (Gallardo et al., 2011). Sample taxonomy was assessed for assigned species across the taxonomic levels of genus, family, order, and class with an unlimited number of lineage paths and equal path weights (Clarke and Warwick, 2001).

2.2.5.2 BACI

Analysis of the BACI design experimental and control sites with permutational multivariate ANOVA (PERMANOVA) will be conducted upon completion of the proposed pilot inflow experiment (project Phase 3). To provide additional information on the power of the BACI design, community composition between designated experimental and control sites was assessed with a non-parametric Analysis of Similarity (ANOSIM) which compares the mean of ranked similarities between sample groups to ranked similarities within groups. The significance of the ANOSIM was determined by 999 group membership permutations.

2.2.5.3 Regional Diversity Structure

Assessment of the impact on enhanced inflow will be conducted upon completion of the proposed pilot inflow experiment (project Phase 3). A preliminary evaluation of biodiversity patterns across sites, basins, and regions was conducted to better understand how eDNA-based estimates of biodiversity were structured across the study area in response to both abiotic factors and

anthropogenic impacts. These analyses provide an important baseline from which changes in the similarity/dissimilarity of the proposed experimental sites to other sites within the survey area can be tracked over time in response to experimental inflow or other perturbations. To meet these goals, pairwise similarity among sampled sites were evaluated using both the Sørenson similarity index and estimates of taxonomic similarity derived from site-based estimates of taxonomic distinctness. The Sørenson index is an extension of the commonly used Bray-Curtis similarity index for presence/absence data. Among group taxonomic similarity is a further extension of Sørenson that leverages taxonomic information to inform understanding of biodiversity patterns (Clarke et al. 2006). As with estimates of within site taxonomic distinctness, taxonomic similarity of communities detected at individual sites was assessed from genus to class with an unlimited number of lineage paths and equal path weights. Statistical assessment and visualization of pairwise Sørenson similarity estimates were assessed using a combination of cluster plots and similarity profile permutation tests (e.g., Clarke et al., 2008) to depict statistically significant similarities/dissimilarities among sites and regions without any prior determination of site groupings. This approach differs from and is complimentary to the BACI model with PERMANOVA analysis described above, which specifically tests differences among previously defined site groups (i.e., control and experimental sites).

2.2.5.4 Tracking Eutrophication Impacts and Recovery Against a Fixed Baseline

Because site specific estimates of taxonomic distinctness have repeatedly been shown to reflect the extent of anthropogenic impacts, including eutrophication (Mouillot et al., 2005; Gallardo et al., 2011; Tweedley et al., 2017), a randomization test was initiated to detect differences in taxonomic distinctness from the expected value derived from a master species list for the IRL. The complete species list of IRL fishes maintained by the Smithsonian Fort Pierce Field Station was used to establish a fixed baseline to assess the relative taxonomic distinctness of sites and to track changes in biodiversity over time in response to the proposed inflow or other impacts. Estimates of taxonomic distinctness derived from all IRL fishes was used to produce a 95% 'confidence funnel' against which site-specific estimates distinctness measures could be compared. The power of this approach lies in both the insensitivity of taxonomic distinctness measures to sample size and the ability to track change in community taxonomic structure over time relative to a fixed baseline (Clark and Warwick 2001).

2.3 Results

2.3.1 Miseq Sequencing and Quality Control

Paired-end sequencing on the Miseq platform was initiated in Phase 1 with an analysis of samples collected at IRL sites E1–E12 and E22 and E23 during fall 2019 and winter 2020. Phase 1 sequencing libraries were developed using the fish specific 16s rRNA primer set. Phase 2 sequencing was directed towards samples collected at sites E1–E12 and E24–E26 during spring 2021 using the fish specific 16s rRNA primer set. An additional 20 samples collected just south of the Port Canaveral Lock in winter 2021 were sequenced during Phase 2 using both fish and crustacean specific 16s rRNA primer sets along with the COI primer set targeting metazoan diversity. Samples collected in July from sites E1–E12 and E24–E26 were archived for analysis during the proposed project Phase 3.

Optimization of Miseq operating parameters and sequence quality control was required to ensure sufficient species detection. Two sequencing runs failed due to Miseq platform issues and were rerun at no cost to the project. Four sequencing runs have been completed to date using a combination of the V2 NANO reagent kit (2 runs), V2 150-cycle reagent kit (1 run), and the V3 300-cycle reagent kit (1 run). A combined 22.4 million sequences were generated during Phases

1 and 2 (**Table 8**). Following optimization of sequence quality control parameters, a combined 13.9 million sequences passing sequence filtering and processing were used to identify unique exact ASVs present in the sequence libraries (**Table 9**).

Table 8. Summary of Miseq run quality control and filtering with run name, number of reads generated (input), and number of reads passing quality control

Run	Input	Filtered	DenoisedF	DenoisedR	Merged	No chimera
Marker test: 16s-fish, 16s-crustacean, & COI	361,033	315,798	317,201	317,170	314,774	313,437
Pilot study baseline: 16s-fish	745,379	617,860	617,201	616,630	607,085	596,888
Fall & winter IRL samples: 16s-fish	8,625,029	3,833,754	3,827,848	3,823,693	3,589,083	3,555,313
Spring IRL samples: 16s-fish	12,659,527	10,334,864	10,276,005	10,274,805	10,259,505	9,471,121

2.3.2 Taxonomic Assignment and Detections

A combined 4,439 unique ASVs were identified across all sequencing runs resulting in 107 unique species level identifications (**Table 9**). Most unique taxa detected (89) were generated from libraries prepared using the fish specific 16s rRNA primers. Test libraries developed for crustaceans and metazoans were overwhelmed by sequencing of both non-target and highly abundant target taxa. The COI test libraries produced no informative species level identifications. The crustacean libraries predominately generated sequences from uncultured bacteria and an unidentified marine copepod (family *Canuellidae*). Seven fishes and 9 crustaceans were identified to species level in the crustacean libraries. Additional optimization of both the metazoan and crustacean marker sets is required to support inclusion in Phase 3.

Table 9. Number of sequence reads, ASVs, and number of unique species detected for target taxa

Target taxa	Reads	ASVs	Species
Elasmobranchii & Actinopterygii	13,874,072	3,939	89
Crustaceans	62,687	500	17

Of the 89 species detected in the fish specific 16s rRNA libraries, 77 were confirmed to occur in the IRL. An additional 12 species not known to occur in the IRL or Florida's Atlantic coast were reassigned to genus level, as they likely represent misassignment due to deficiencies in the NCBI reference sequence database. Of the 77 confirmed IRL species, 28 were unique to sites in south central IRL (including 13 species unique to sites E22 and E23 in Vero Beach), while 25 species detected at one or more sites in the central or south central IRL were not detected in BRL.

Taken together, 16s rRNA sequencing of 185 IRL samples identified a diverse community of 77 species representing 63 genera, 39 families, 23 orders, and 3 classes of fish (**Table 10**). Teleosts were the dominant class of fish detected (67 species). Nine Chondrichthyes species were detected, including 2 that are not known to occur in the IRL or Atlantic coast and likely reflect species level misassignment. One species from Class Actinopteri was detected (Longnose gar; *Lepisosteus osseus*).

Table 10. Taxonomic summary of fish species detected in 185 eDNA samples collected from the IRL (2019 – 2021)

Genera	Families	Orders	Classes
Achirus	Achiridae	Pleuronectiformes	Teleostei
Aetobatus	Myliobatinae	Myliobatiformes	Chondrichthyes
Anchoa	Engraulidae	Clupeiformes	Actinopteri
Archosargus	Sparidae	Eupercaria incertae sedis	
Ariopsis	Ariidae	Siluriformes	
Bairdiella	Sciaenidae	Perciformes	
Brevoortia	Clupeidae	Carangiformes	
Caranx	Carangidae	Carcharhiniformes	
Carcharhinus	Carcharhinidae	Tetraodontiformes	
Centropomus	Centropomidae	Gobiiformes	
Chaetodipterus	Ephippidae	Elopiformes	
Chilomycterus	Diodontidae	Cyprinodontiformes	
Chloroscombrus	Gobiidae	Blenniiformes	
Ctenogobius	Dasyatidae	Atheriniformes	
Cynoscion	Gerreidae	Lepisosteiformes	
Dasyatis	Eleotridae	Centrarchiformes	
Diapterus	Elopidae	Cichliformes	
Diplodus	Serranidae	Mugiliformes	
Dormitator	Cyprinodontidae	Scorpaeniformes	
Elops	Poeciliidae	Scombriformes	
Epinephelus	Gobiesocidae	Beloniformes	
Eucinostomus	Gymnuridae	Gasterosteiformes	
Eugerres	Blenniidae	Aulopiformes	
Floridichthys	Atherinopsidae		
Gambusia	Lepisosteidae		
Gerres	Centrarchidae		
Gobiesox	Lutjanidae		
Gobiomorus	Cichlidae		
Gobiosoma	Mugilidae		
Gymnura	Haemulidae		
Harengula	Pomatomidae		
Hypleurochilus	Triglidae		
Labidesthes	Rhinopterinae		
Lagodon	Scombridae		
Leiostomus	Tetraodontidae		
Lepisosteus	Sphyrnidae		
Lepomis	Belonidae		
Lophogobius	Syngnathidae		
Lutjanus	Synodontidae		
Mayaheros			
Membras			
Microgobius			
Micropogonias			
Mugil			
Oligoplites			
Opisthonema			
Oreochromis			
Orthopristis			
Poecilia			
Pogonias			
Pomatomus			
Prionotus			
Rhinoptera			
Sarotherodon			

Genera	Families	Orders	Classes
Sciaenops			
Scomberomorus			
Selene			
Sphoeroides			
Sphyrna			
Strongylura			
Syngnathus			
Synodus			
Trachinotus			

2.3.3 Sample Sufficiency and Power

Species accumulation curves generated from 20 samples collected at site E2 indicate the current replication of three samples per site each season is sufficient to resolve a majority (57%) of the fish diversity detected in the full dataset (**Figure 20**). An average of 12 species were detected in each set of three samples, out of a combined total of 21 species. For the same samples, species richness projections (MM) are well resolved with three replicates. Sample sufficiency is further improved with regional within basin replication, which varies from 6–12 sample replicates per season (see **Figure 19**). This same pattern can be seen in power analyses, with the power of the BACI design to detect differences among experimental and control sites each season (n = 6–12) near or exceeding the accepted 80% power threshold (**Figure 20**). Estimated power based of the BACI design to detect differences among experimental and control sites across all four seasons is lower (57%; n = 24). However, for simplicity, power analyses assumed a 2-way ANOVA, which inflated within the sample residual variance by combining seasonal samples into a single group. The statistical approach currently planned for the BACI design is to apply a mixed model using a PERMANOVA framework to accommodate seasonal effects (Anderson, 2005). This approach is commonly used to test the simultaneous response of multiple variables to one or more factors and is expected to significantly increase power by diminishing residuals (Anderson, 2014).

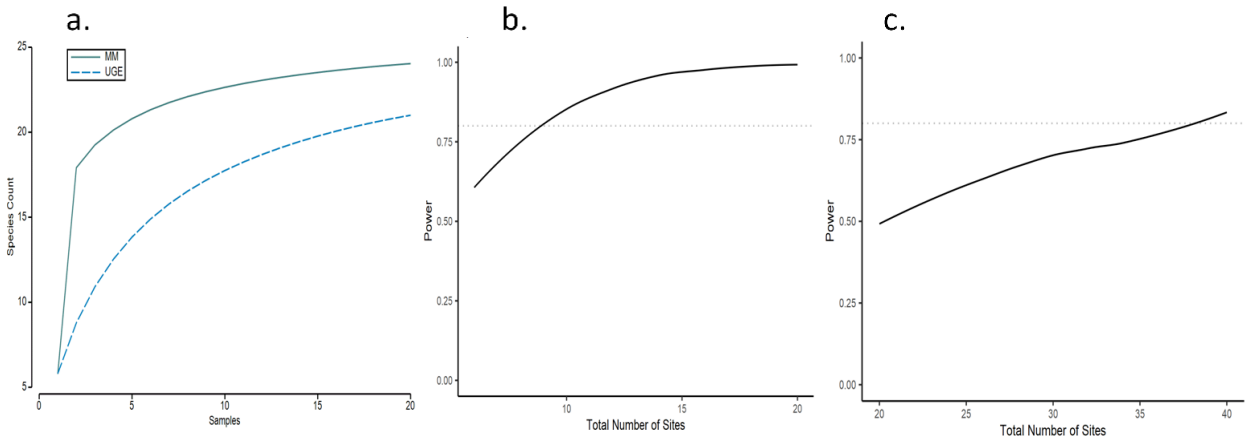

Note: Analysis of the BACI design with PERMANOVA to control seasonal effects is proposed for Phase 3.

Figure 20. Estimates of sample sufficiency and power derived from 20 samples collected at site E2 with (a) UGE and MM estimates of species richness derived and estimated power of the BACI design with 2-way ANOVA for (b) estimated seasonal species richness and (c) projected, combined annual species richness

2.3.4 Site Diversity (Alpha Diversity)

Each of the four selected measures of within site diversity (richness, Shannon diversity, average taxonomic distinctness, and variation in taxonomic distinctness) for combined fall, winter, and spring collections show a general trend of increasing diversity from north to south (**Figure 21**). In each case, average diversity was lowest in BRL and highest in the south central IRL. Sites E22–E26 were not included in cumulative analyses but within season comparisons show a similar trend of declining diversity with increasing latitude (data not shown). Richness and Shannon diversity measures were highly correlated ($R^2 = 0.98$, $p < 0.001$) indicating they provide similar information about site diversity. The correlation between richness or Shannon diversity and taxonomic distinctness was also significant but less pronounced ($R^2 = 0.41$, $p = 0.02$), with site-specific differences revealing additional information for monitoring impacts during Phase 3 experimental pumping. Variation in taxonomic distinctness was uncorrelated with, and therefore complimentary to, each of the other measures ($R^2 > 0.6$, p = NS).

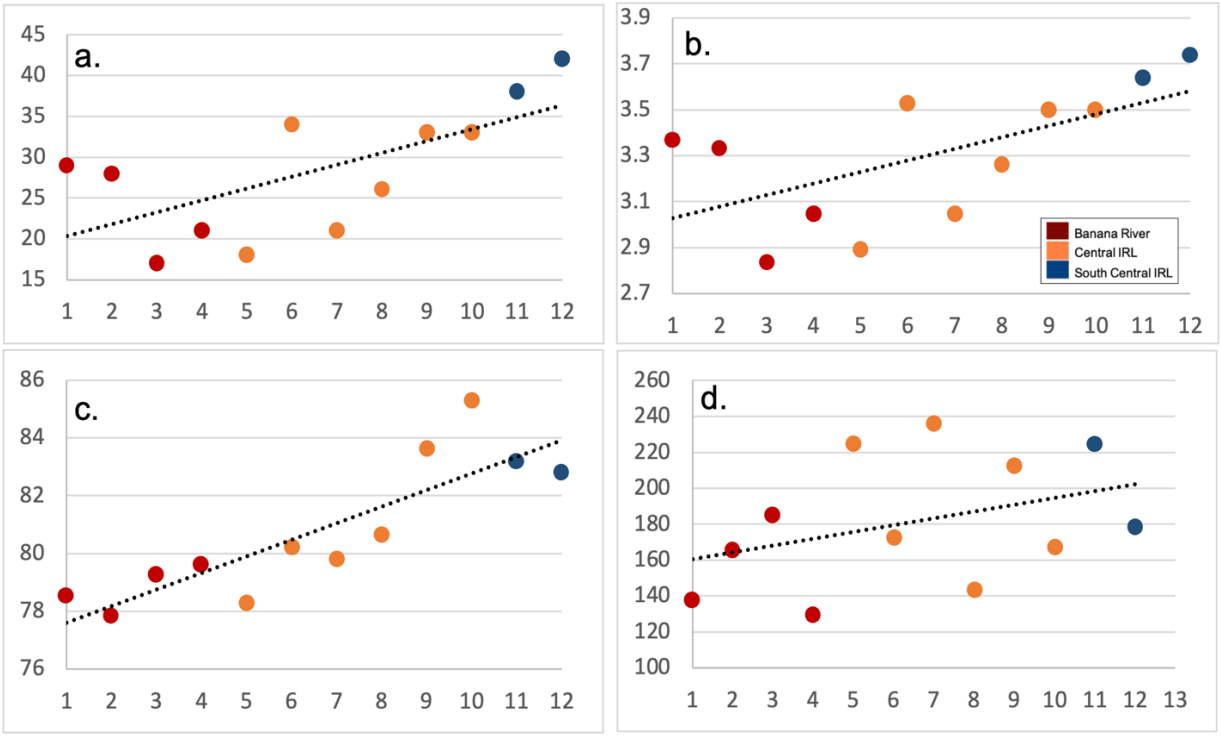

Figure 21. Estimates of fish diversity for sites E1–E12 for combined fall, winter, and spring collections with (a) species richness, (b) Shannon diversity, (c) average taxonomic distinctness, and (d) variation in taxonomic distinctness

2.3.5 BACI

Comparison of biodiversity patterns before and after inflow at experimental and control sites will be completed upon completion of Phase 3 pumping using the BACI design and PERMANOVA framework to control for seasonal effects. A comparison of ranked dissimilarities in species occurrence between designated experimental (E1 and E2) and control sites (E4 and E26) before inflow revealed no significant dissimilarity between sites ($R = -0.33$ to -0.11, $p = 0.60$ to 0.99). An ANOSIM R value close to or below zero indicates an evenness in ranked species occurrence between groups, demonstrating the efficacy of the selected sites for investigating Phase 3 pumping induced changes in species occurrence and site diversity.

2.3.6 Regional Diversity Structure

A complimentary assessment of community response to enhanced inflow based on patterns of site, basin, and regional similarity/dissimilarity will be conducted following completion of the proposed Phase 3 pilot pumping project.

To inform on the appropriateness of the designated approach and to provide additional information on how fish biodiversity is structured across the survey area, pairwise similarity/dissimilarity among sampled sites were evaluated using both the Sørenson similarity index and estimates of taxonomic similarity derived from site-based estimates of taxonomic distinctness (**Table 11**). With the exception of site E6, there was a consistent pattern of higher similarity among sites within regional basins than between sites in different basins. Within basin similarity estimates ranged between 59.0–72.5 for the Sørenson index and 80.0–87.0 for taxonomic similarity, while estimates of similarity for comparisons between sites in different basins ranged between 49.0–55.0 and 75.4–77.2 for Sørenson and taxonomic similarity respectively.

Table 11. Pairwise estimates of fish community similarity based on (a) Sørenson similarity index and (b) taxonomic similarity

Note: BRL sites are shown in red, central IRL sites in yellow, and south central IRL sites in blue.

a.	E1	E2	E3	E4	E5	E6	E7	E8	E9	E10	E11	E12
E1	-											
E2	73.7	-										
E3	60.9	62.2	-									
E4	64.0	69.4	68.4	-								
E5	55.3	69.6	57.1	66.7	-							
E6	57.1	51.6	43.1	47.3	46.2	-						
E7	60.0	57.1	68.4	57.1	56.4	61.8	-					
E8	61.8	63.0	60.5	59.6	68.2	66.7	68.1	-				
E9	54.8	65.6	56.0	51.9	58.8	50.7	51.9	67.8	-			
E10	51.6	55.7	52.0	51.9	47.1	59.7	51.9	57.6	72.7	-		
E11	50.7	48.5	40.0	44.1	32.1	41.7	37.3	46.9	62.0	50.7	-	
E12	53.5	51.4	47.5	50.8	46.7	44.7	44.4	58.8	69.3	61.3	72.5	-

b.	E1	E2	E3	E4	E5	E6	E7	E8	E9	E10	E11	E12
E1	-											
E2	84.6	-										
E3	77.4	76.9	-									
E4	81.6	85.3	83.2	-								
E5	76.6	85.2	81.1	83.1	-							
E6	76.2	69.4	65.5	71.3	68.8	-						
E7	80.0	77.6	84.2	81.0	81.0	80.4	-					
E8	81.5	80.0	76.3	80.9	84.5	83.3	86.8	-				
E9	76.5	83.3	73.6	76.7	82.4	73.1	77.0	84.7	-			
E10	74.8	74.4	69.6	75.6	72.5	80.3	76.3	80.7	87.9	-		
E11	74.6	73.0	67.3	74.2	67.5	72.8	74.9	76.9	82.3	79.4	-	
E12	75.2	75.1	68.8	75.9	72.3	73.4	74.6	82.1	85.1	83.2	87.0	-

To further explore the relationship between sites within and among regional basins a combination of cluster plots and similarity profile permutation tests were used to depict statistically significant similarities/dissimilarities among sites and regions. Statistically significant patterns of site similarity/dissimilarity were examined for each season for which data were currently available (fall, winter, and spring) and on the combined three season dataset. Seasonal analyses of site groupings are not shown here but they support the general pattern of greater within site than between site similarity, highlighting significant regional differences in fish eDNA detections across seasons, including in all comparisons with samples collected in the fall and winter at sites E22

and E23 (Vero Beach; data available upon request). The relationship between individual sites varies somewhat among seasons; however, both the Sørenson index and estimates of taxonomic similarity show BRL sites consistently clustering together and most different from the south central IRL sites. This same pattern can be seen in the combined three season datasets (**Figure 22**), with significant differences in fish community structure generally aligning with basin boundaries and greatest dissimilarity occurring between BRL and south central IRL sites.

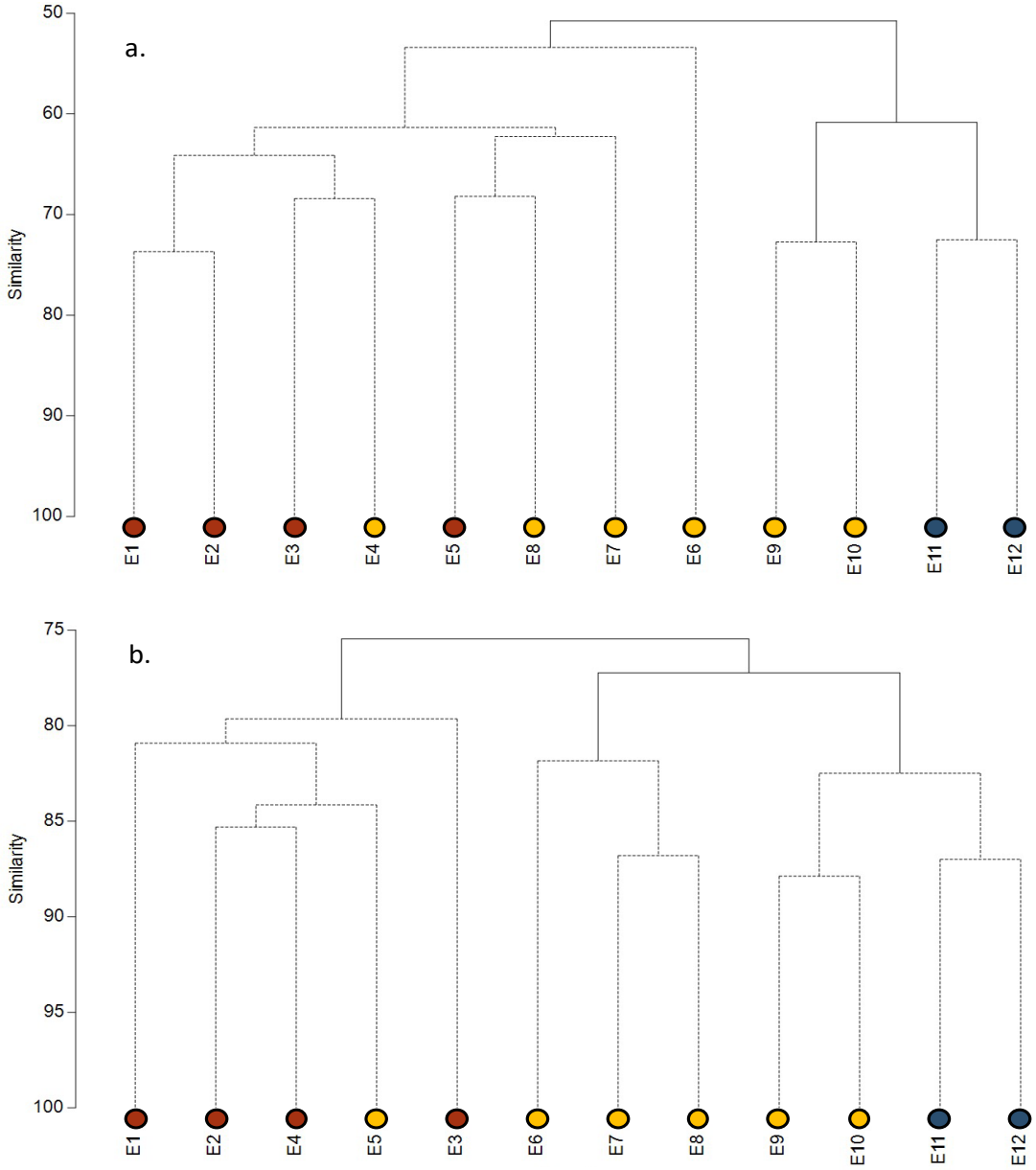

Note: BRL sites shown in red, central IRL sites in yellow, and south central IRL sites in blue. Overlying colored squares depict statistically significant site groupings as determined by Simprof permutation tests.

Figure 22. Cluster analysis of fish community similarity for (a) Sørenson similarity index and (b) taxonomic similarity

Site groupings highlight fish communities shaped by regional differences in both abiotic factors (e.g., temperature and salinity) and perturbation history, including eutrophication (e.g., Mouillot et

al., 2005; Gallardo et al., 2011; Tweedley et al., 2017). The relatively high similarity of sites within BRL provides further support for the value of the BACI design to directly test pumping impacts against within basin control sites. The pronounced dissimilarity of BRL sites from sites in the central and south central IRL demonstrate the opportunity regional sampling provides to track community response to proposed inflow as a compliment to the BACI design. Measures of taxonomic distinctness may be particularly useful for tracking biodiversity loss or gain resulting from the proposed pilot pumping experiment as they have repeatedly been shown to be more sensitive to perturbations than more commonly used diversity measures that rely on species richness (Gallardo et al., 2011).

2.3.7 Tracking Eutrophication Impacts and Recovery Against a Fixed Baseline

The demonstrated sensitivity of taxonomic distinctness measures to anthropogenic impacts provides an opportunity to track biodiversity loss or recovery over time in response to the proposed Phase 3 pilot study or other anthropogenic impacts.

The list of IRL fishes maintained by the Smithsonian Fort Pierce Field Station was used to develop funnel plots depicting the average taxonomic distinctness and variation in taxonomic distinctness of all IRL fishes with 95% confidence intervals reflecting sampling effort (i.e., number of species detected). With a few exceptions, site distinctness measures mapped onto the respective confidence funnel reinforce the general pattern of increasing similarity among sites within basins compared to sites in different basins (**Figure 23**). Exceptions highlight the unique taxonomic diversity of individual sites (e.g., E9–E12; **Figure 23a**) and the relatively low taxonomic diversity of BRL sites. Sites E9–E12 in the south central IRL standout as having fish communities that are both species rich and taxonomically diverse.

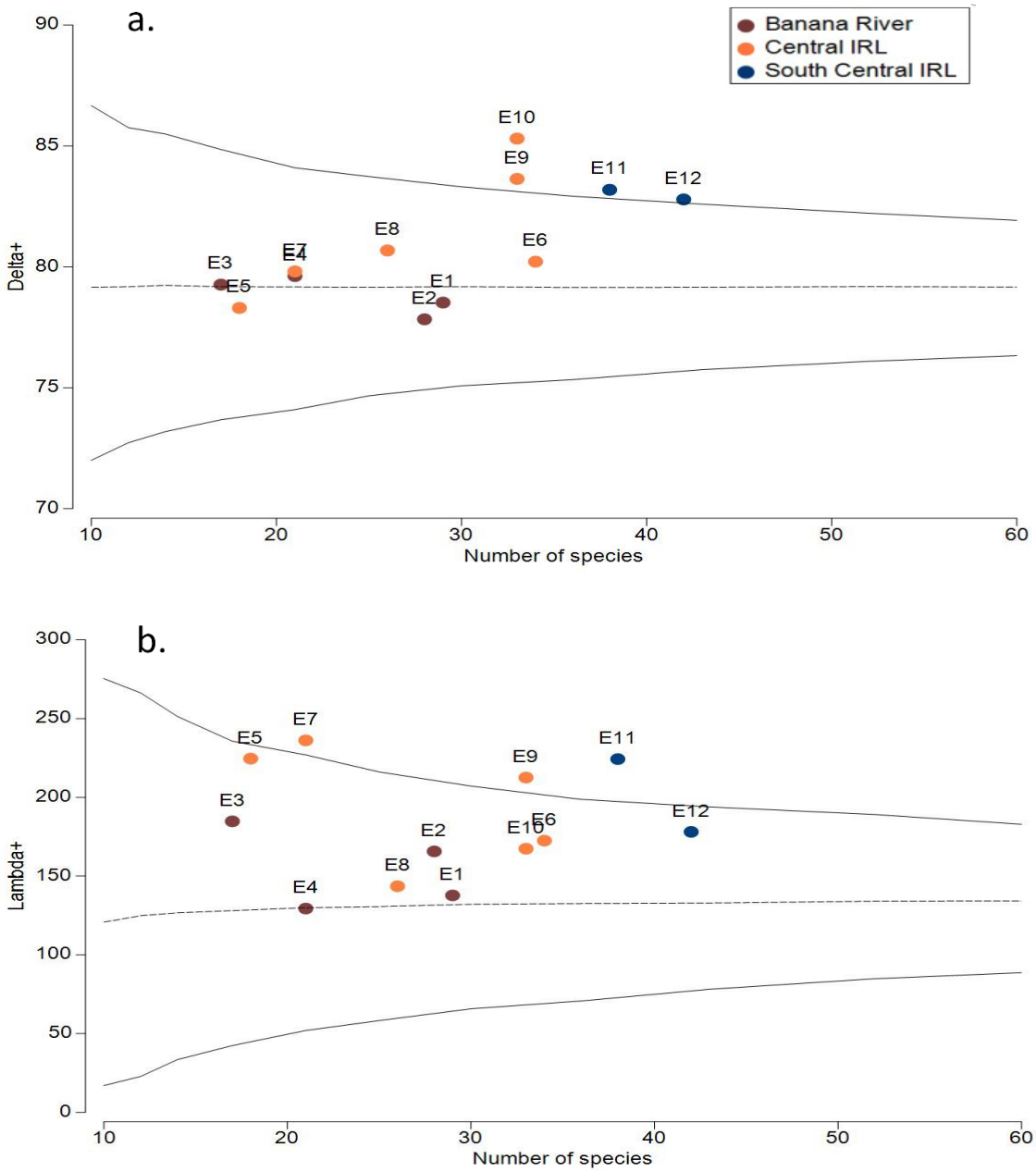

Note: Site specific taxonomic distinctness estimates derived from eDNA detections are color coded by lagoon region.

Figure 23. Fixed reference funnel plots with 95% confidence interval for (a) average taxonomic distinctness and (b) variation in taxonomic distinctness of all fishes known to occur in the IRL

2.4 Discussion

As a compliment to team biological modeling and monitoring, three eDNA-based approaches were initiated during project Phase 1 and continued through Phase 2 to support testing of potential impacts to biodiversity that may result from proposals to improve lagoon water quality with enhanced ocean water exchange. These are: (1) comparison of control and experimental sites

before and after experimental inflow; (2) assessment and monitoring of site, basin, and regional biodiversity patterns; and (3) direct tracking of taxonomic distinctness metrics against a fixed baseline. Complete assessment of the impacts of enhanced inflow using eDNA sampling requires completion of the proposed Phase 3 pilot pumping project. However, a variety of analyses have been completed to improve understanding of how diversity is organized in the IRL and to investigate the strengths of the selected experimental approaches.

eDNA sampling and community level sequencing required significant optimization to overcome technical challenges, including high phytoplankton abundance and resulting impacts to both sample processing and target species detection. Genetic marker development to enable detection of a taxonomically diverse set of Metazoans and detailed information on Crustaceans will require additional optimization. Development of genetic markers to support the detection of fishes (taxonomic Class Actinopterygii and Chondrichthyes) was completed in Phase 1. Samples collected in Phase 1 (fall and winter) and Phase 2 (spring) have been sequenced using the fish genetic marker set. A one-month project extension awarded in spring 2021 enabled a final round of baseline sampling in July to complete a full seasonal sample cycle. July samples have been preserved for analysis in Phase 3.

Extensive sampling at the designated experimental site just south of Canaveral Lock demonstrated both the sufficiency of the current sampling plan and power of the proposed experimental design (**Figure 20**). Sampling is not intended to provide a census, rather the goal is to reliably identify sufficient species to allow detection of differences in species composition both among sites and over time, should they exist. The resolution of regional biodiversity patterns demonstrated by a combination of complimentary analyses and diversity metrics further highlights the value of the designated approach.

Using a combination of samples collected during Phases 1 and 2, we evaluated detection patterns for fishes across the south central IRL, central IRL, and BRL. Sampling during Phase 1 allowed initiation of seasonal sampling and a direct examination of diversity at three candidate sites for placement of the temporary pilot inflow experiment (i.e., Bethel Creek in Vero Beach and two sites in BRL). This work was conducted concurrently with team modeling efforts to identify key abiotic determinants of fish diversity and habitat use (**Section 1**). Of the three candidate experimental inflow sites, Bethel Creek and an adjacent site in the IRL exhibited the highest seasonal diversity of fishes, including 13 species not detected elsewhere. Seasonal sampling was completed in Phase 2 with the addition of three sites in BRL to improve resolution of local diversity patterns.

Comparison of species occurrence at the designated Phase 2 experimental (E1 and E2) and control sites (E4 and E26) highlighted the similarity of the fish community prior to initiation of the proposed pilot experiment and demonstrate the strength of the BACI design.

Within site diversity (alpha diversity) measured by species richness, Shannon diversity, average taxonomic distinctness, and variation in taxonomic distinctness demonstrated a significant decline in diversity from south to north, with the lowest diversity across all measures occurring in BRL (**Figure 21**). A comparison of diversity measures shows that while species richness and Shannon diversity provide similar information about site diversity, and are therefore redundant, both measures of taxonomic distinctness provide complimentary data that when considered in combination with either of the richness measures can provide a more detailed understanding of biodiversity structure and response to impacts.

Pairwise estimates of site similarity/dissimilarity highlight the presence of regional drivers of fish diversity, with sites within basins more similar to each other than to sites in either of the other

basins (**Table 11**). Comparisons with the highest dissimilarity were between sites in BRL and southern end of the survey area (south central IRL). This is in line with previous studies of IRL fishes and ongoing team fish modeling that show regional differences in fish diversity and community structure, and a general pattern of decreasing diversity with increasing latitude (Gilmore, 1981; Snelson, 1983; Tremain and Adam, 1995; Paperno et al., 2001; **Section 1**).

Similarity patterns based on eDNA detections varied somewhat with seasons (data not shown), likely reflecting seasonal variation in species abundance patterns and habitat in response to changes in temperature and salinity and ontogenic habitat shifts (Virnstein, 1990; Paperno et al., 2001; **Section 1**). However, a clear pattern was seen across all seasons and within the combined dataset (**Figure 22**) confirming patterns indicated in the pairwise tests. Specifically, relatively high similarity was seen among sites within each region, with a few informative exceptions. In the central IRL, fishes detected at sites E9 and E10 were more similar to sites E11 and E12 near Sebastian Inlet than to sites further north, which were comparatively less diverse and more distinct. Similarity among adjacent sites may in part be explained by the high site fidelity IRL fishes exhibit (**Section 1**). Gilmore (1981) and others have noted the unique diversity of fish communities within or adjacent to IRL inlets, and declining diversity with increasing distance from the inlet. This pattern is thought to reflect both the complexity of habitats found around inlets and the opportunity inlets provide for marine species to directly access the lagoon (Gilmore, 1981; Snelson, 1983). These trends are now overlayed with impacts from nearly 50 years of increasing nutrient loading that is driving a shift from a system dominated by macrophytes to a phytoplankton dominated system with related impacts to habitat builders, benthic fauna, and fishes (Virnstein and Morris, 1996; Sigua et al., 2000; Sigua and Tweedale, 2003; Morris et al., 2021; Sweat et al., 2021; Wassick et al., 2021; **Section 1**). Impacts from declining water quality and increasingly frequent HABs are not evenly distributed across the IRL, and the northern IRL and BRL appear to be particularly vulnerable (Badylak & Phlips, 2004; Phlips et al., 2011; Task 1 Hydrological Modeling).

In line with expectations based on the high frequency of HAB outbreaks in BRL (Gallardo et al., 2011; Phlips et al., 2011), site-specific estimates of taxonomic distinctness compared against a fixed baseline highlight the low taxonomic diversity of fish detected in BRL and comparatively higher taxonomic diversity of fishes in the central and south central IRL (**Figure 23**). A significant negative bias in measures of taxonomic distinctness has been seen in response to increasing eutrophication levels in freshwater invertebrates (Gallardo et al., 2011), marine plants (Mouillot et al., 2005), and estuarine fishes (Tweedley et al., 2017). In each of these cases, more commonly employed diversity measures provided useful data on the status and drivers of biodiversity; however, taxonomic distinctness measures were the only diversity measures to show a direct relationship with water quality condition (e.g., Chl-a; Gallardo et al., 2011). This is thought to be because as impacts increase, higher taxonomic groups that are only represented by one or a few species are lost. The chance loss of one or a few species will have little effect on richness-based diversity measures. Yet, the loss of less specious taxonomic groups and maintenance of taxa containing a high number of closely related species will drive down estimates of both average taxonomic distinctness and variation in taxonomic distinctness (Clarke and Warwick, 2001). This pattern can be seen in the **Figure 23** funnel plot with eDNA detections from BRL revealing a low diversity fish community, even when species richness is relatively high. Conversely, sites E9–E12 near Sebastian Inlet standout as having fish communities that are both species rich and taxonomically diverse, as expected for sites that are buffered against eutrophication impacts (Gallardo et al., 2011; Phlips et al., 2011).

2.5 Next Steps

Baseline eDNA sample analyses initiated in Phase 1 and completed in Phase 2 improve understanding of biodiversity patterns in the lagoon and confirm the utility of the three approaches we have initiated to compliment the team's multidisciplinary efforts to investigate system response to enhanced inflow. However, completion of the proposed Phase 3 temporary pilot pumping experiment is required to provide the data needed to determine the feasibility and impacts of using enhanced inflow to restore lagoon water quality.

Specifically, to fully leverage eDNA data to investigate impacts of enhanced inflow on lagoon diversity, we propose the following goals for Phase 3 as a compliment to proposed finalization of fish models (**Section 1**) and direct assessment of experimental inflow impacts on key groups (**Section 3**):

1. Enhancement of existing eDNA baselines
2. Post pumping eDNA sampling and data analysis

Phase 3 eDNA goals have been broken down into core deliverables listed below. For planning, we have provided an estimate of the time required for completion of each deliverable. It is currently assumed that eDNA deliverables can be completed concurrently in a period of one year that would extend six months past completion of experimental pumping.

- Continue metazoan and crustacean marker testing and application to newly collected and archived samples (1 year)
- Process and analyze samples collected in July during Phase 2 (2 months)
- Post pumping sampling, sample processing, and analysis (6 months)
- Final analyses and write-up (2 months)

3 Benthic Fauna, Seagrasses, and Phytoplankton Monitoring

3.1 Introduction

3.1.1 Background

> "Ecosystem monitoring is critical to ecosystem health and answers important questions about the effectiveness of programs to maintain ecosystem health"
> - U.S. Geological Survey
> https://www.usgs.gov/centers/oki-water/science/ecological-monitoring?qt-science_center_objects=0#qt-science_center_objects

This statement on ecological monitoring is even more relevant when the strategy for maintaining ecosystem health is a dramatic intervention intended to reverse the decline of a degraded system. A large-scale engineering project intended to mitigate poor water quality and improve habitats, such as the proposed enhancement of circulation of the IRL, requires an accurate understanding of the current status of water quality and biological resources to determine impacts and assess project success. In the IRL system, possible changes or improvements are best measured by their impacts on water quality (e.g., salinity, temperature, and nutrients) and biological responses (plankton, fishes, seagrasses, and benthic fauna).

For monitoring to authoritatively demonstrate an after-effect, it is necessary to have baseline measurements "before" for comparison. It is especially important to monitor well in advance of anticipated changes to a system to provide an understanding of expected population fluctuations

unrelated to the mitigation effort. Natural changes due to seasonal or annual shifts in water quality, geochemical cycling, reproductive cycles, and other sources of variability can be accounted for in evaluating project impacts if baseline ecosystem monitoring is of sufficient duration.

Seagrasses, benthic infauna, and phytoplankton are key communities to be monitored in the event of a restored inflow project, both because their responses may be generally ecologically important and because they are at the heart of detrimental impacts that pollution is having on the lagoon. Some of the first outward evidence of a declining lagoon ecosystem included a large percentage of seagrass meadows dying due to shading from dense HABs. If the lagoon is to be rehabilitated through restored inflow, seagrass recovery will be one of the long-term measures of the success of restoration efforts. Seagrasses importance is greater for the fact that it serves as food for manatees and food and shelter for many invertebrates and juvenile fishes. Phytoplankton are another key community to monitor because harmful algae causing seagrass deaths and degrading the estuary in other ways are themselves phytoplankton. It is self-evident HAB monitoring will be critical during an inflow restoration project. Finally, infauna are an important monitoring community for a project such as this because they are fairly permanent residents of the benthic sediments that are polluted due to muck, and they are an ecologically important group, serving as food for fishes and other estuarine organisms.

There are some historical and publicly available records for seagrasses and fishes in the IRL that can inform on the status and trends of these communities. However, the sites of historical data collection are not tailored to the site being considered as a possible ocean inflow pumping location. It is critical that pumping and ecological sampling sites be tightly aligned to reliably investigate the extent of pumped water impacts, both in severity and area influenced. This is particularly true for benthic sessile organisms that will be unable to flee the region of greatest impact and will therefore be subjected to the most extreme environmental changes.

3.1.2 Objectives

To document baseline biological characteristics of the IRL. The proposed location was provided by the engineering team working in tandem with this project (see Task 1, Modeling and Engineering). The goal is to understand the current biology of the proposed site, including natural seasonal or other fluctuations, as much as is feasible given the sampling duration. Categories of biological characteristics to be monitored include:

- Seagrasses and drift algae
- Benthic fauna
- Phytoplankton/harmful algae

This objective will be met by making comparisons over space and time, including abundances, species richness, community associations, and critical abiotic environmental variables. Where appropriate, statistical analyses will be conducted, including ANOVAs, T-tests, and non-metric multidimensional scaling (NMDS). Abundances will be presented in the way most appropriate for the particular taxonomic group and data collection technique.

Data on species densities and distributions, and environmental and community associations, were collected as part of the baseline study. These baseline biological data will become even more valuable if a pilot pumping project moves forward. In that event, post-inflow restoration data will be compared to earlier baselines to reveal the impacts of the project.

3.2 Methods

3.2.1 Seagrasses, Rooted Algae, and Drift Algae Methods

At selected locations (**Figure 24**), transects 100-m long were surveyed perpendicular to the shoreline with the goal of documenting the presence of seagrasses and drift algae. Quadrats were laid down every 10-m along the transect lines, and seagrasses and drift algae were scored according to standard methods (Virnstein and Morris, 1996; Morris et al., 2001). Measurements included seagrass visual estimate percent cover (estimated coverage upon imagining the seagrass crowded into corner of quadrat at a high density), seagrass percent coverage or occurrence (proportion of 100 quadrat sub-squares having at least 1 blade of seagrass), seagrass density (number of shoots per area), seagrass canopy height (length of blade from sediment to tip), drift algae percent occurrence (proportion of 100 quadrat sub-squares having any drift algae), drift algae biomass estimate (estimated coverage upon imagining drift algae crowded into corner of quadrat), and drift algae canopy height (Virnstein and Morris, 1996; Morris et al., 2001). This sampling strategy was repeated quarterly for all sites.

Power analysis was conducted on seagrass, rooted algae, and drift algae data to confirm the viability of sampling for making statistical determinations of benthic/drift vegetation impacts. The plan for future analysis is a BACI design. BACI designs can be analyzed as a 2-way ANOVA model:

$$Response = Intercept + \beta 1 * Period + \beta 2 * Treatment + \beta 3 * Period{:}Treatment$$

where Period is before or after, Treatment is control or impact, and Period:Treatment denotes an interaction term. A power analysis was run on various response variables. Power is the probability of detecting a significant difference, given that a significant difference truly exists. Mathematically, power can be expressed as:

$$Power = 1 - \beta$$

$$\beta = Probability(Reject\ Ho\ |Ha\ is\ True)$$

where Ho is the null hypothesis (no difference among groups), Ha is the alternative hypothesis (differences exists among groups), and beta is the probability of rejecting the null hypothesis, given that a significant difference truly does exist. Power analysis inputs typically include estimates of means and standard deviations, and the significance level. Power is then predicted for a range of sample sizes. For the BACI studies, estimates of the mean and standard deviation for the four groups was provided. A significance level of 0.05 was used. The "emon" package (Barry and Maxwell, 2017) for R software (R Core Team, 2021) was used to estimate the power.

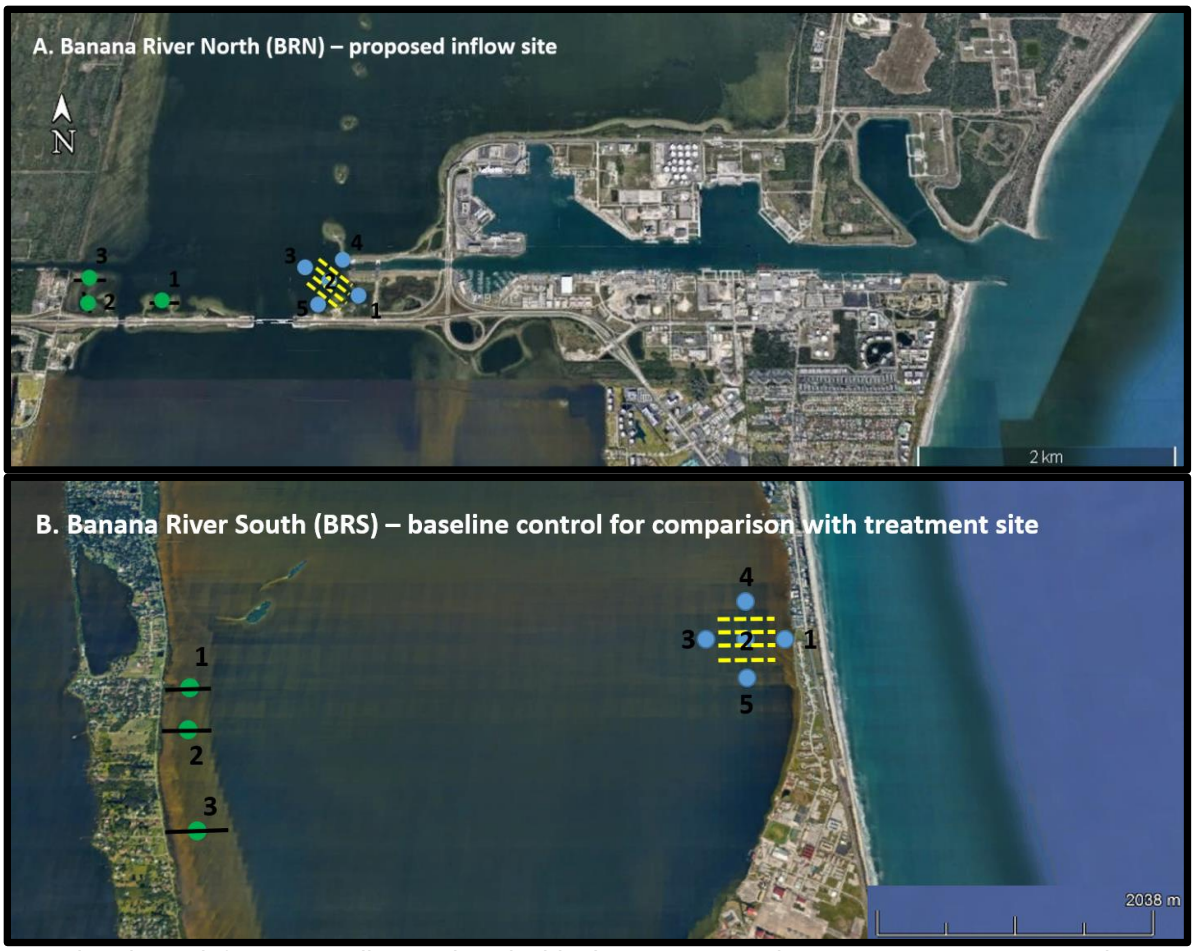

Note: Blue dots = infauna sampling stations inside the IRL. Green dots = seagrass transect and associated infauna stations. All dots, infauna sample n = 3. Yellow dashed line = plankton tow location. Whole water flow cytometer samples were collected at all infauna sampling stations (blue and green dots, n = 4 per station).

Figure 24. Samples collected and station locations for the proposed pilot inflow site: A) Banana River North (BRN) near Port Canaveral and B) control site for treatment comparisons Banana River South (BRS) near Patrick Air Force Base

3.2.2 Benthic Fauna Methods

Sediment grabs for infaunal analysis were collected at the 50-m mark along all seagrass transects described above (**Figure 24**) via petite Ponar grab (n = 3 per transect). Triplicate samples were collected at each station. This sampling strategy was repeated quarterly for all sites. Sampling and identification of infauna were conducted consistent with the methods of benthic studies of the IRL (Mason, 1998; Cooksey, 2007) and were be tested for correlations with sediment parameters, including percent organic content (dry weight), percent water content by weight, and percent silt/clay content (dry weight), and also environmental parameters. Biological communities are summarized as biodiversity (Shannon-Wiener Diversity Index), species richness, and overall abundances. Where appropriate, statistical analyses included 2-way ANOVAs (factors of site and year), Principle Components Analysis (comparing biological parameters between years as a multivariate function of multiples sediment and water column environmental conditions), and NMDS (community analyses with the basic summary biological parameters) with post hoc ANOSIM.

Power analysis was conducted on some infauna data to confirm the viability of sampling for making statistical determinations of infauna impacts of restored inflow. As with seagrasses, the plan for future analysis is a BACI design (see seagrass methods above for details).

3.2.3 Phytoplankton/Harmful Algae Methods

Phytoplankton were sampled via plankton tows for cell identification, and via whole water samples for flow cytometer analysis. Both types of samples were collected in conjunction with the infauna sampling schedule and locations shown in **Figure 24** and discussed above. Regarding plankton tows, 4 were conducted quarterly at the proposed inflow site (n = 4). Tows utilized a 20-µm mesh plankton net towed for approximately 2 minutes. Flow rate and submersion time were recorded and used to estimate volume processed for each plankton sample. Samples were preserved in 4% buffered formaldehyde to await enumeration and identification via microscopy. Whole water samples for flow cytometry were collected at every station (n = 5) using a bottle to collect unfiltered water approximately 0.5 m below the surface of the water. These samples were set on ice and processed in the flow cytometer immediately upon returning from the field. This sampling strategy was repeated quarterly for all sites.

NMDS graphs were used to group the phytoplankton communities based upon similarity and as a function of year, season, and location/site. ANOSIM and PERMANOVA analysis were used to evaluate the strength and significance of NMDS outcomes.

3.3 Results

3.3.1 Seagrasses, Rooted Algae, and Drift Algae Results

Seagrasses are present in the IRL and an attempt was made to seek out the nearest beds to the proposed inflow crossover site. Within the IRL, seagrasses are patchy and, when present, vary from sparse to abundant at the selected seagrass locations examined for this study. The primary species of seagrass observed at all locations has been the seagrass *Halodule wrightii* (**Figure 25**).

Figure 25. Transect and quadrat sampling of the shoal grass *Halodule wrightii*, the dominant seagrass in the northern IRL and the only seagrass sampled in the IRL estuary at the site proposed for potential restored inflow

Abundances of seagrass in terms of percent cover are presented in **Figure 26**. Seagrass percent cover was greatest in Phase 1 summer, ranging from 0–9% and 0–6% at BRS and BRN, respectively. Canopy heights were highest in the summer (Quarter 3, **Figure 28**), as high as 5.7 centimeters at BRS.

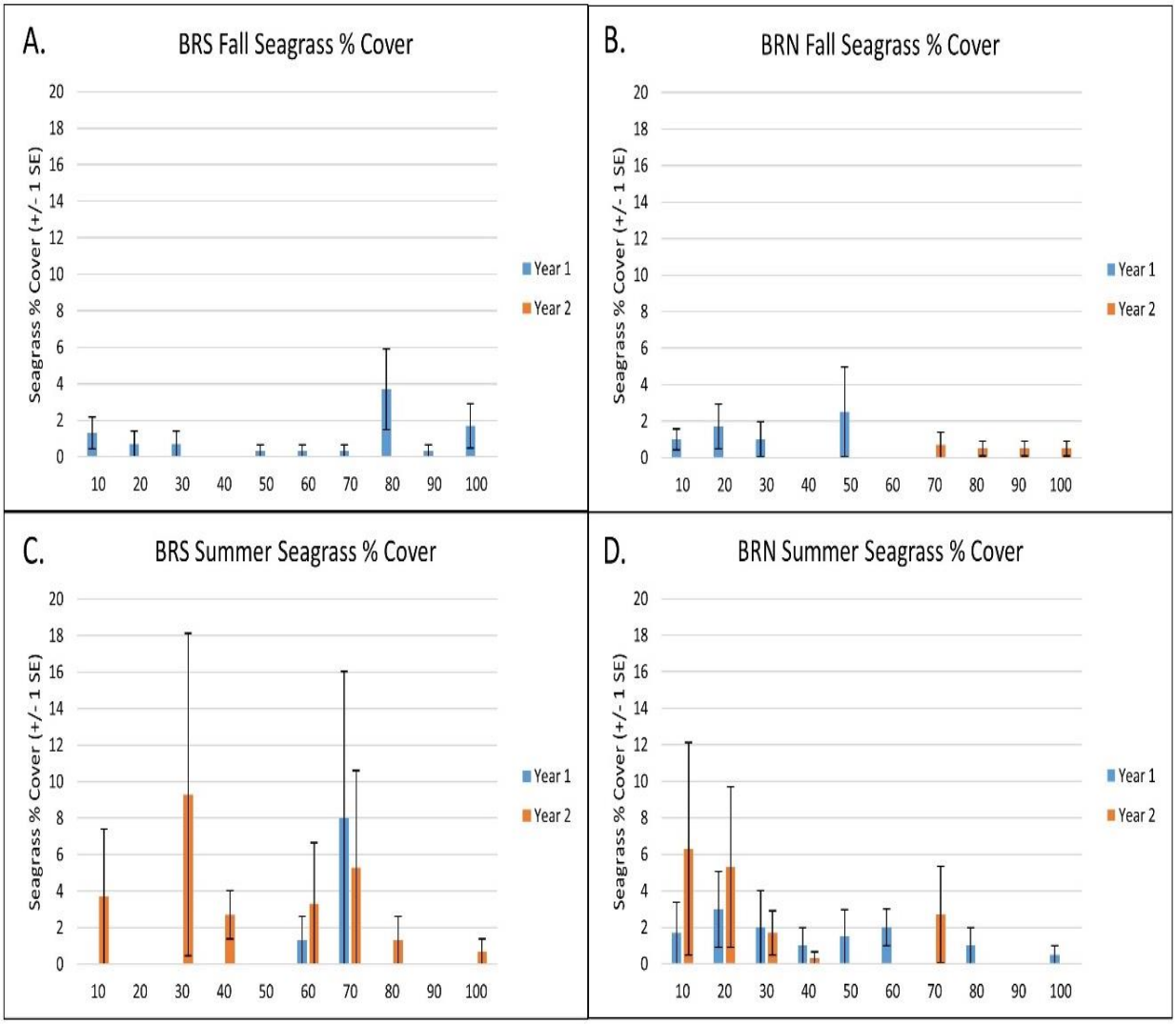

Note: Blue bars = Phase 1 of baseline sampling (RLI1); orange bars = Phase 2 of baseline sampling (RLI2).

Figure 26. Seagrass mean percent cover in fall (A and B) and summer (C and D), comparing Phases 1 and 2 for transects nearest the proposed inflow crossover point at A) BRS in the fall, B) BRN in the fall, C) BRS in the summer, and D) BRN in the summer

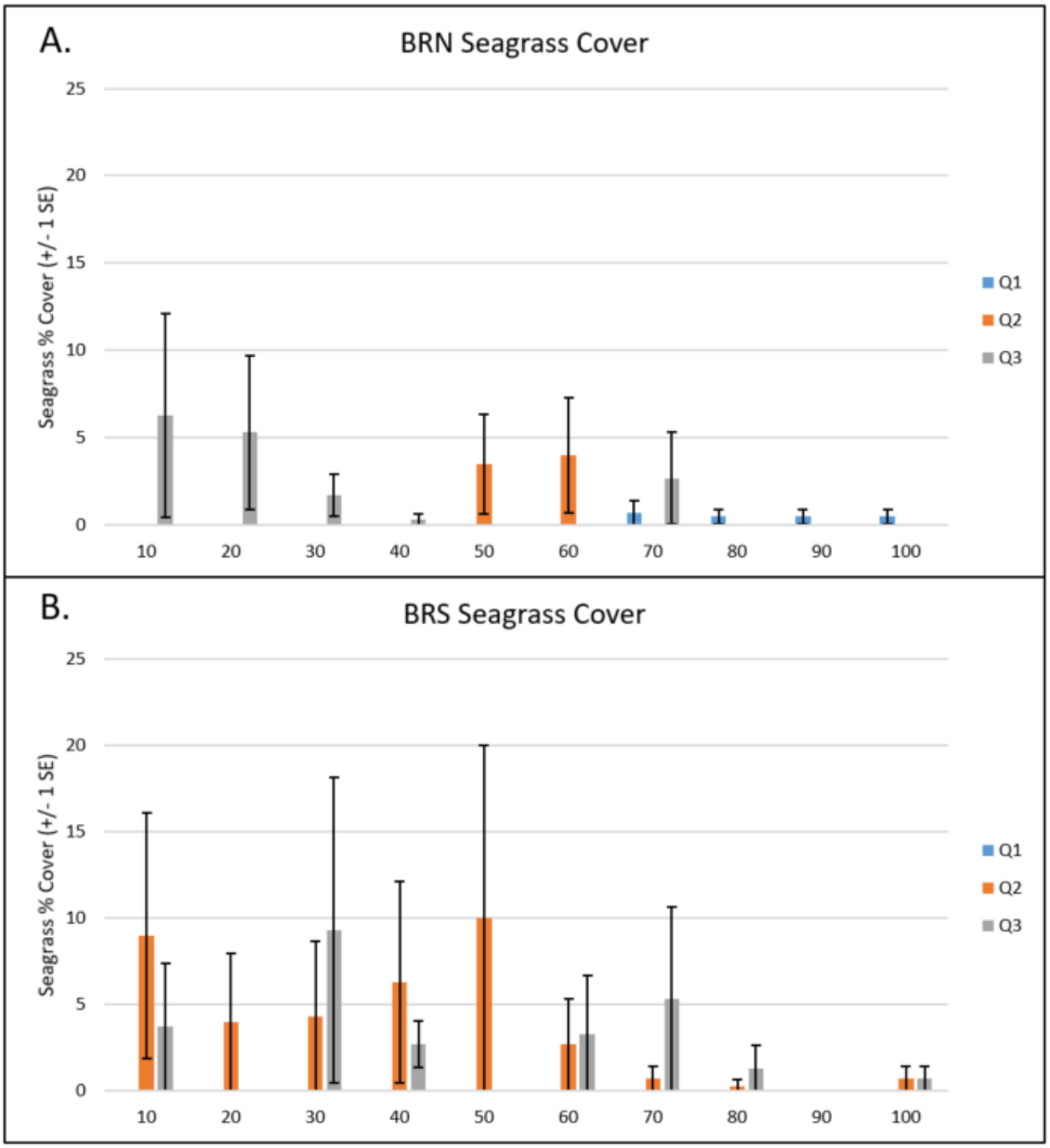

Note: Q1 is winter, Q2 is spring, and Q3 is summer.

Figure 27. Seagrass mean seasonal percent cover during Phase 2 (2021) for A) BRN (proposed crossover location) and B) BRS (control site)

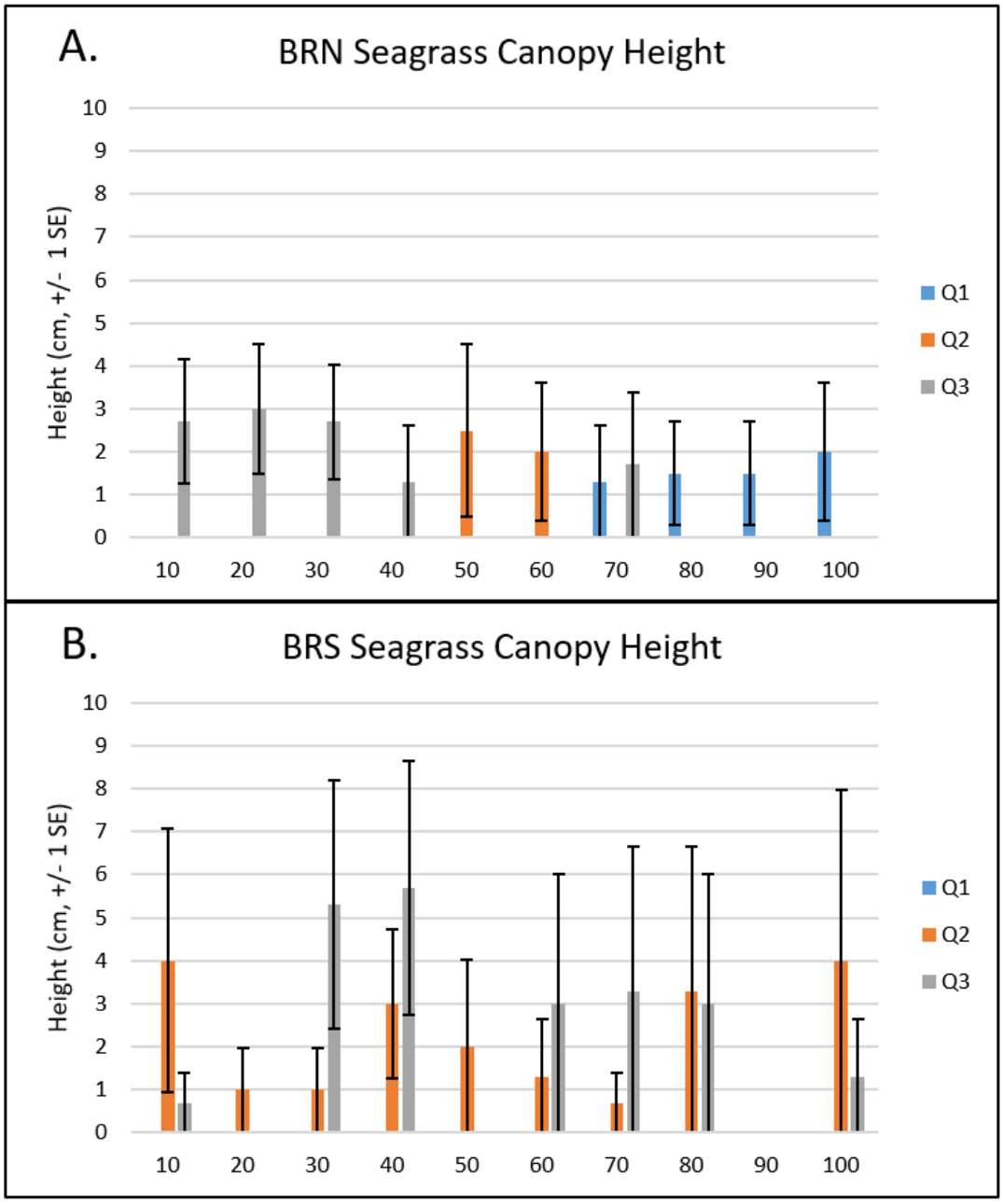

Note: Q1 is winter, Q2 is spring, and Q3 is summer.

Figure 28. Seagrass mean seasonal canopy height during Phase 2 (2021) for A) BRN (proposed crossover location) and B) BRS (control site)

Epiphytes growing on shoal grass blades showed different seasonal patterns based on site and were most abundant at BRN in the spring and summer (**Figure 29**).

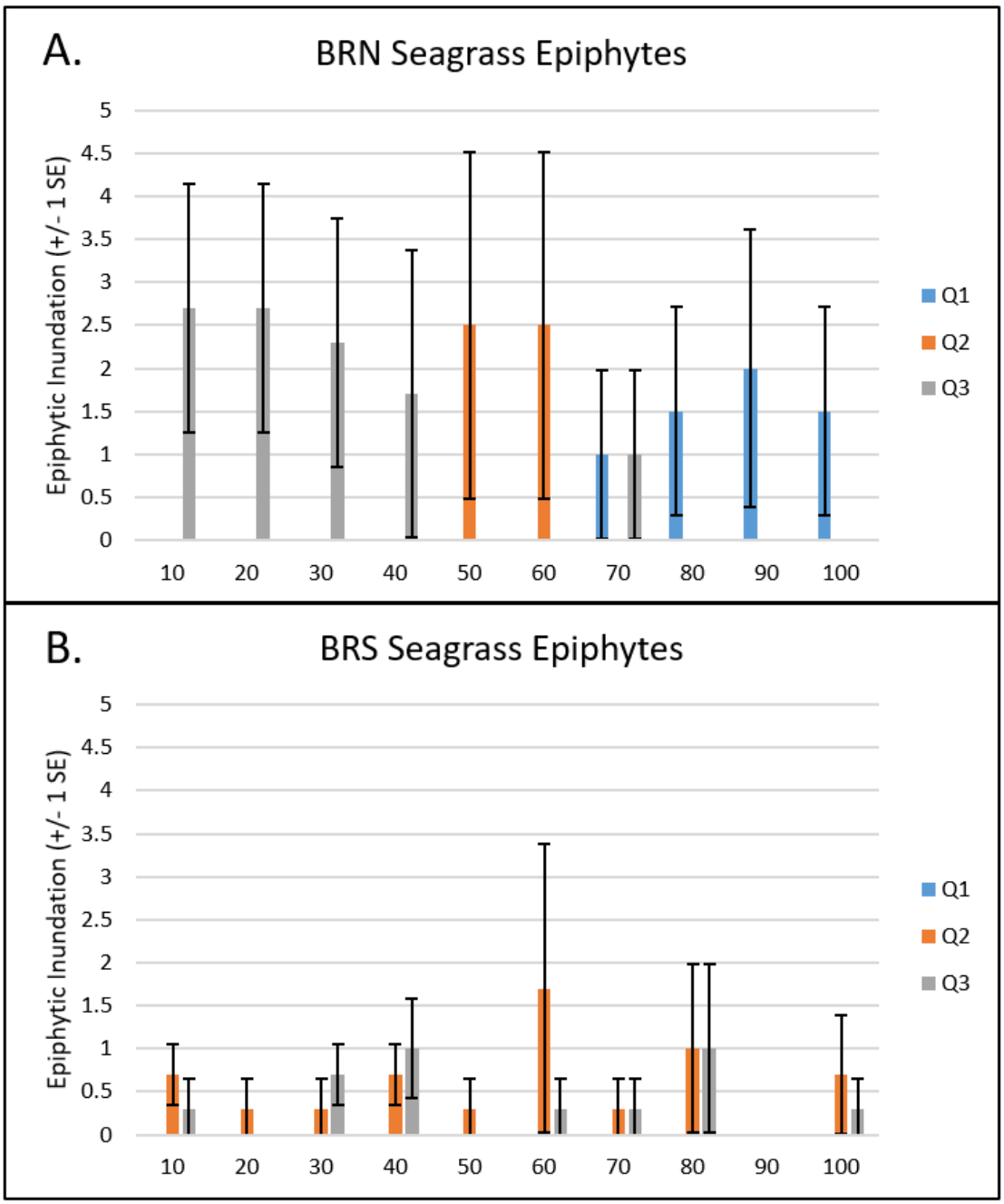

Note: Q1 is winter, Q2 is spring, and Q3 is summer. "Inundation" is a subjective determination of the relative abundance of epiphytes on a scale of 0-5.

Figure 29. Epiphyte mean seasonal inundation during Phase 2 (2021) for A) BRN (proposed crossover location) and B) BRS (control site)

Rooted alga of the genus *Caulerpa* had the greatest coverage in the summer, particularly at the proposed crossover site BRN (2–68% in Phase 1, 4–52% in Phase 2) (**Figure 30**).

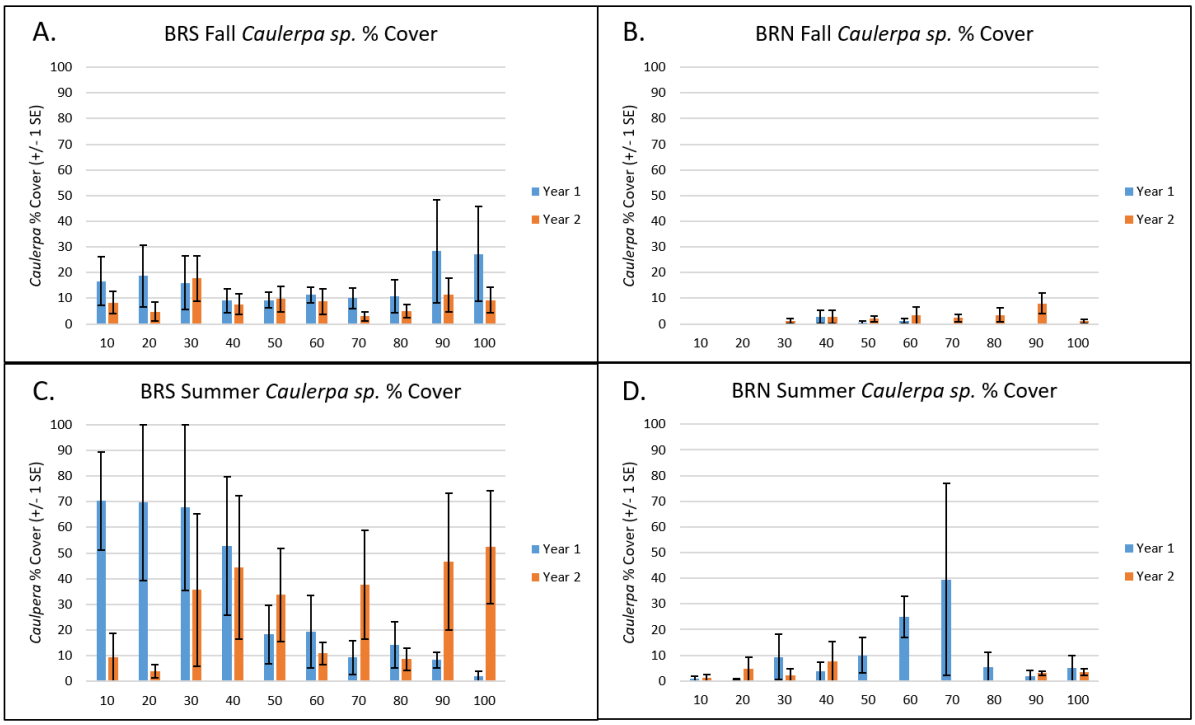

Figure 30. Rooted algae (Caulerpa sp.) mean percent cover during Phases 1 and 2 for the proposed crossover location (BRN – B and D) and the control site (BRS – A and C), comparing fall (A and B) and summer (C and D)

Drift algae was virtually absent in the fall of both years, but had a strong presence in the summer both at BRN and BRS, particularly in Phase 2 (0–33%) (**Figure 31**).

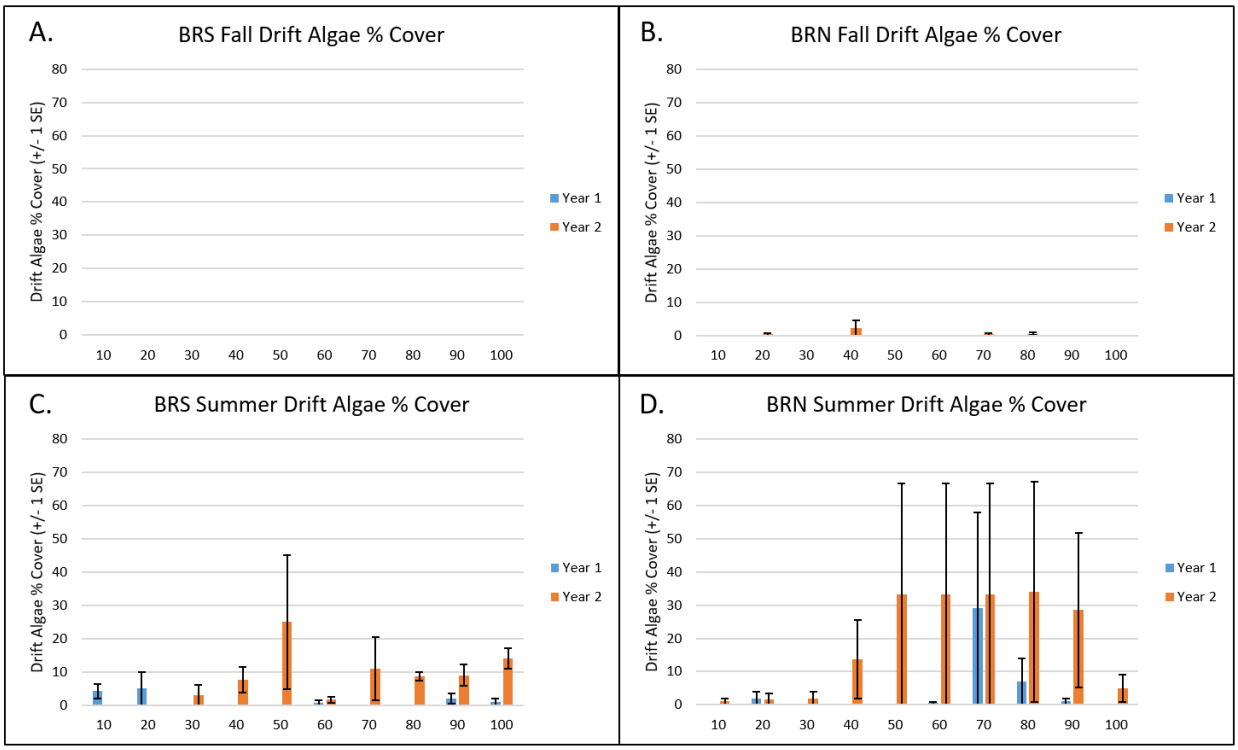

Figure 31. Drift algae mean percent cover during Phases 1 and 2 for the proposed crossover location (BRN – B and D) and the control site (BRS – A and C), comparing fall (A and B) and summer (C and D)

Results of the power analysis on benthic/drift vegetation ranged from 0.04 to 0.83, with the highest power being for drift algae percent cover in the winter.

3.3.2 Benthic Fauna Results

Error! Reference source not found. reports the infauna species found in terms of presence or absence throughout the seasons at the treatment versus control site. Species universally present, or almost universally present, at both locations and throughout all seasons and years are the polychaetes *Alitta succinea*, *Capitella capitata*, *Ctenodrilus serratus*, *Glycera americana*, *Hypereteone heteropoda*, *Paradiopatra hispanica*, and *Pectinaria gouldii*; amphipod crustaceans *Ampelisca abdita*, *Cerapus tubularis*, *Cymadusa compta*, and *Eusirus cuspidatus*; ostracod crustacean *Eusarsiella zostericola*; peanut worm *Phascolion cryptus*; phoronid *Phoronis* sp.; gastropods *Acteocina canaliculata* and *Phrontis vibex*; and bivalves *Anomalocardia cuneimeris*, *Mulinia lateralis*, and *Parastarte triquetra* (Error! Reference source not found.). Other species in Error! Reference source not found. are more uncommon and may be limited to certain seasons or locations.

Table 12. Occurrence of infauna at the proposed inflow (BRN = N) and control (BRS = S) sites

Note: Infauna are associated with bare sediments (left) or amongst seagrasses (right). Sampling was seasonal (F = Fall, W = Winter, Sp = Spring, Su = Summer) for approximately 2 years (19 = 2019, 20 = 2020, 21 = 2021).

	BARE SEDIMENTS														SEAGRASS-ASSOCIATED SEDIMENTS											
	N	S	N	S	S	N	S	N	S	N	S	N	S		N	S	N	S	S	N	S	N	S	N	S	N	S
	F	F	W	W	Sp	Su	Su	F	F	Sp	Sp	Su	Su		F	F	W	W	Sp	Su	Su	F	F	Sp	Sp	Su	Su
	19	19	20	20	20	20	20	20	20	21	21	21	21		19	19	20	20	20	20	20	20	20	21	21	21	21
Annelids																											
Alitta succinea	x	x	x	x	x	x	x	x	x	x	x	x			x	x	x	x	x	x	x	x	x	x	x		x
Annelid I																				x				x			
Annelid J								x		x		x						x				x	x	x		x	x
Armandia maculate			x																				x			x	
Capitella capitata		x		x			x	x	x	x	x	x	x		x	x				x	x	x	x	x		x	x
Ctenodrilus serratus	x	x	x	x	x	x	x	x	x	x	x	x	x		x	x	x	x	x	x	x	x	x	x	x	x	x
Diopatra cuprea								x		x		x				x	x					x	x				
Eulalia viridis						x		x			x		x							x			x				
Glycera americana	x	x	x	x	x	x				x	x				x	x	x	x	x	x			x	x			x
Hypereteone heteropoda	x	x	x	x	x					x	x				x	x		x	x	x		x	x	x	x		x
Ophryotrocha A																										x	
Paradiopatra hispanica	x	x	x	x	x	x	x	x		x	x	x	x		x	x	x	x	x	x			x	x		x	x
Pectinaria gouldii	x	x	x	x	x	x	x	x	x	x	x		x		x	x	x	x	x	x	x		x	x	x	x	x
Polychaete BB								x									x	x									
Polychaete GG			x																								
Polychaete HH								x																			
Polychaete JJ																	x										
Polychaete LL																	x										
Polychaete OO								x																			
Polychaete P																										x	
Polychaete PP								x																			
Polychaete S															x												
Polychaete Y																x		x			x					x	x
Saggita A								x									x	x									
Scolecida																							x	x	x		x
Arthropods																											
Acartia clausi																						x					
Acartia tonsa			x												x									x			
Americhelidium americanum			x										x											x			
Ampelisca abdita (Amph D)	x	x	x	x	x	x	x	x		x	x		x		x	x	x	x	x		x		x		x	x	
Cerapus tubularis	x	x	x		x	x	x	x							x		x	x	x	x	x						
Corophium sp.			x			x											x				x						
Crab B		x			x		x										x		x			x		x			x
Crab Zoea A																								x			
Cumacean B				x			x	x														x					
Cymadusa compta (Amph C)	x	x		x	x	x	x						x		x	x	x	x	x	x			x	x	x	x	x
Erichthonius brasiliensis (Amph H)																	x										
Eurypanopeus depressus	x				x								x						x		x		x				x
Eusarsiella zostericola	x	x	x	x	x	x	x	x		x							x		x	x							
Eusirus cuspidatus	x	x	x	x	x	x		x		x	x	x					x	x	x	x	x				x		
Gammarus mucronatus (Amph I)		x	x	x	x	x		x	x	x	x		x			x	x	x	x	x	x	x	x	x	x	x	
Gammerid Amphipod J																x											
Grandidierella bonnieroides(Amp	x	x	x	x	x	x	x	x					x			x	x	x	x	x	x	x	x	x	x		x
Hargeria rapax	x	x	x	x	x	x	x									x	x	x	x	x	x						
Harpacticoid Copepod A					x														x								x
Isopod A				x													x			x					x		x

	BARE SEDIMENTS														SEAGRASS-ASSOCIATED SEDIMENTS													
	N F	S F	N W	S W	S Sp	N Su	S Su	N F	S F	N Sp	S Sp	N Su	S Su		N F	S F	N W	S W	S Sp	N Su	S Su	N F	S F	N Sp	S Sp	N Su	S Su	
Arthropods, continued	19	19	20	20	20	20	20	20	20	21	21	21	21		19	19	20	20	20	20	20	20	20	21	21	21	21	
Isopod B						x											x	x				x	x		x		x	
Isopod C	x				x	x							x			x	x		x								x	
Isopod D	x	x	x		x	x	x			x									x									
Juvenile Ocean Crab A					x	x	x														x							
Leptochelia dubia	x	x	x	x	x	x	x	x							x	x	x	x	x	x	x		x	x	x	x		
Lysomata zoea																										x		
Megalops A		x																										
Metacaprella sp A																										x		
Nannastacidae A	x	x	x	x	x	x		x	x	x					x	x		x	x			x	x	x	x			
Oithona sp A	x				x					x								x	x					x				
Oxyurostylis smithi	x	x	x	x	x		x	x		x	x		x		x	x	x	x	x	x	x	x	x	x	x	x	x	
Palaemonetes vulgaris		x	x		x										x	x		x	x	x	x		x	x	x	x	
Peratocytheridea setipunctata	x	x	x	x	x	x	x	x		x		x			x		x	x	x	x	x	x	x	x	x		x	
Shrimp C																								x				
Shrimp H													x															
Tanaid A		x		x									x			x		x			x			x		x	
Tanaid C																		x										
Chordata																												
Fish A		x																										
Tunicate A						x											x			x								
Tunicate B															x													
Echinodermata																												
Ophiophragmus filograneus			x														x						x		x		x	
Ocean Brittle Star A						x																						
Platyhelminthes																												
Turbellaria A	x	x		x	x	x		x	x	x		x			x	x	x	x	x	x		x	x	x	x	x	x	
Foraminiferea																												
Ammonia parkinsoniana	x	x	x	x	x	x	x	x	x	x		x	x		x	x	x	x	x	x	x	x	x	x	x	x	x	
Ocean Foram A						x						x					x											
Ocean Foram B			x			x		x		x		x					x					x		x				
Ocean Foram C																						x						
Nematoda																												
Nematode A	x	x	x	x	x	x	x			x		x			x	x	x		x	x	x	x	x	x		x		
Nemertea																												
Nemertia A	x		x	x			x			x		x	x		x		x	x	x	x		x	x	x				

Sipuncula																										
Phascolion cryptus	x	x	x	x		x		x		x	x			x	x	x	x		x		x	x	x		x	
Sipuncula B																x										
Sipuncula C																x										
Phoronida																										
Phoronis A	x					x		x		x		x			x	x	x		x			x				
Mollusca																										
Acteocina atrata														x	x	x	x					x		x		
Acteocina canaliculata	x	x	x	x	x	x	x	x		x	x	x		x	x	x	x	x	x	x	x	x		x		x
Ameritella versicolor			x												x	x	x									
Amygdalum papyrium	x	x	x	x	x	x							x	x	x	x		x	x			x			x	
Anomalocardia cuneimeris		x	x	x	x	x	x	x	x	x	x	x	x	x	x	x		x	x	x		x	x	x	x	x
Astyris lunata	x			x				x								x									x	
Caecum pulchellum					x													x								
Clam DD																				x						
Crepidula atrasolea					x			x														x				
Cyrtopleura costata							x									x	x		x	x						
Haminoea elegans (Snail Q)	x		x											x	x	x	x		x	x	x		x			x
Haminoea succinea						x			x													x		x		x
Japonactaeon punctostriatus								x		x									x		x					
Limpet B				x	x	x	x				x						x	x	x			x		x		x
Limpet C																								x		x
Mercenaria mercenaria (Clam H)		x						x													x	x		x	x	
Mulinia lateralis	x	x	x	x	x	x	x	x	x	x	x	x		x	x	x	x	x	x	x	x	x	x	x	x	
Odostomia laevigata														x					x	x						
Parastarte triquetra	x	x	x	x	x	x	x	x	x	x	x	x	x	x	x	x	x	x	x	x	x	x	x	x	x	x
Phrontis vibex		x	x	x	x	x		x		x					x		x	x	x	x		x	x			x
Prunum apicinum														x	x	x			x				x			
Snail BB								x																		
Snail J																	x									
Snail O					x										x			x								
Snail P		x						x																		
Snail R																x			x		x		x			

Overall infaunal densities in bare sediments ranged from 1.9-4.0 x 10^4 organisms m^{-2} in Phase 1. In Phase 2, there was evidence of a large recruitment event near the proposed inflow site, with densities approaching 1.5 x 10^5 organisms m^{-2}. In contrast, infauna living amongst seagrasses ranged from 4.3-4.7 x 10^4 m^{-2} in Phase 1 (BRN and BRS, respectively), and densities dropped to 1.0 x 10^4 and 1.2 x 10^4 m^{-2} in Phase 2 (BRS and BRN, respectively). Two-way ANOVA results are reported in infauna in **Figure 32** through **Figure 40** with letters indicating significance at the alpha = 0.05 level.

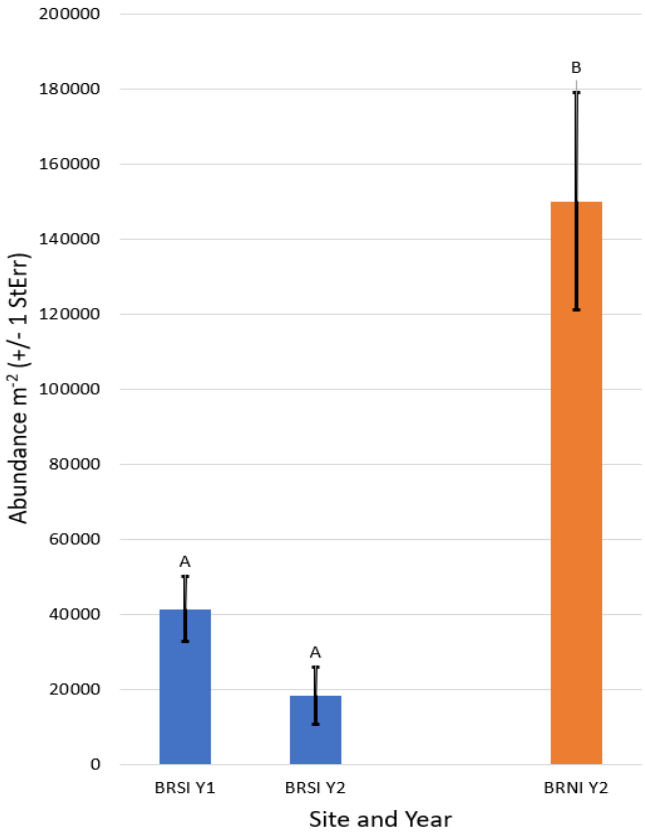

Note: Samples were not collected in Phase 1 spring because of the global pandemic and a COVID-19 outbreak in the lab.

Figure 32. Mean spring general infauna abundances at the proposed restored inflow site (BRN – orange) and the control site (BRS – blue) during the first and second phases of baseline monitoring ($p < 0.001$)

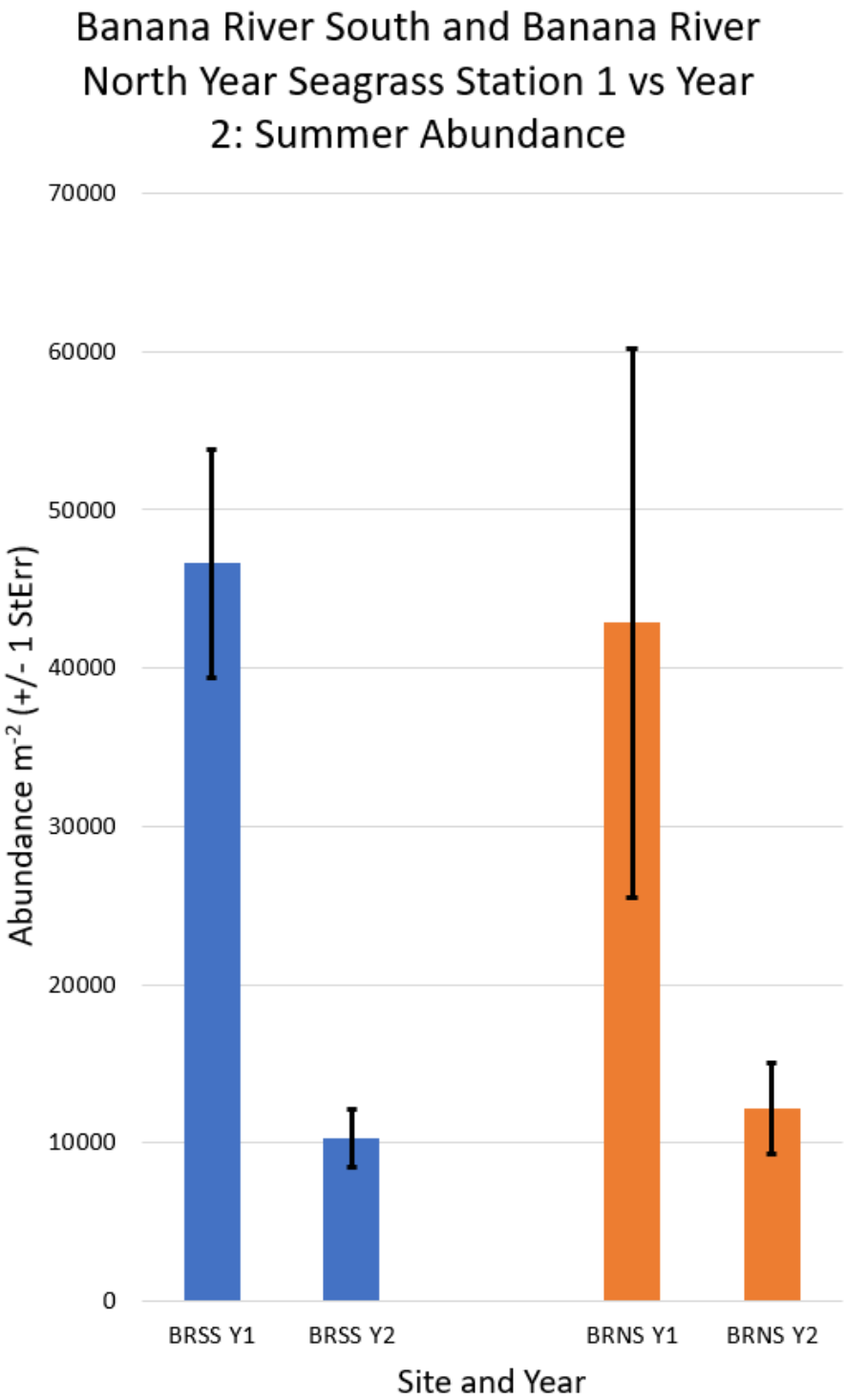

Figure 33. Mean summer general infauna abundances in seagrass sediments at the proposed restored inflow site (BRN – orange) and the control site (BRS – blue) during the first and second phase of baseline monitoring ($p < 0.002$)

The polychaete annelid *Alitta succinea* and the bivalve *Parastarte triquetra* have been selected as focal species for this report due to their high densities and consistent presence. In bare sediments, *A. succinea* densities ranged from 2 x 10^2 worms m^{-2} (BRS inside lagoon, Phase 2)

to 1.6 x 10^3 m^{-2} (BRN inside lagoon, Phase 2) (**Figure 34**). When amongst seagrass sediments, *A. succinea* densities ranged from near zero to as high as 1.1 x 10^3 animals m^{-2} (**Figure 35**). *P. triquetra* were most abundant in the fall, and especially abundant at the BRS inside lagoon control site during Phase 1 (5.7 x 10^3 clams m^{-2}, **Figure 36**).

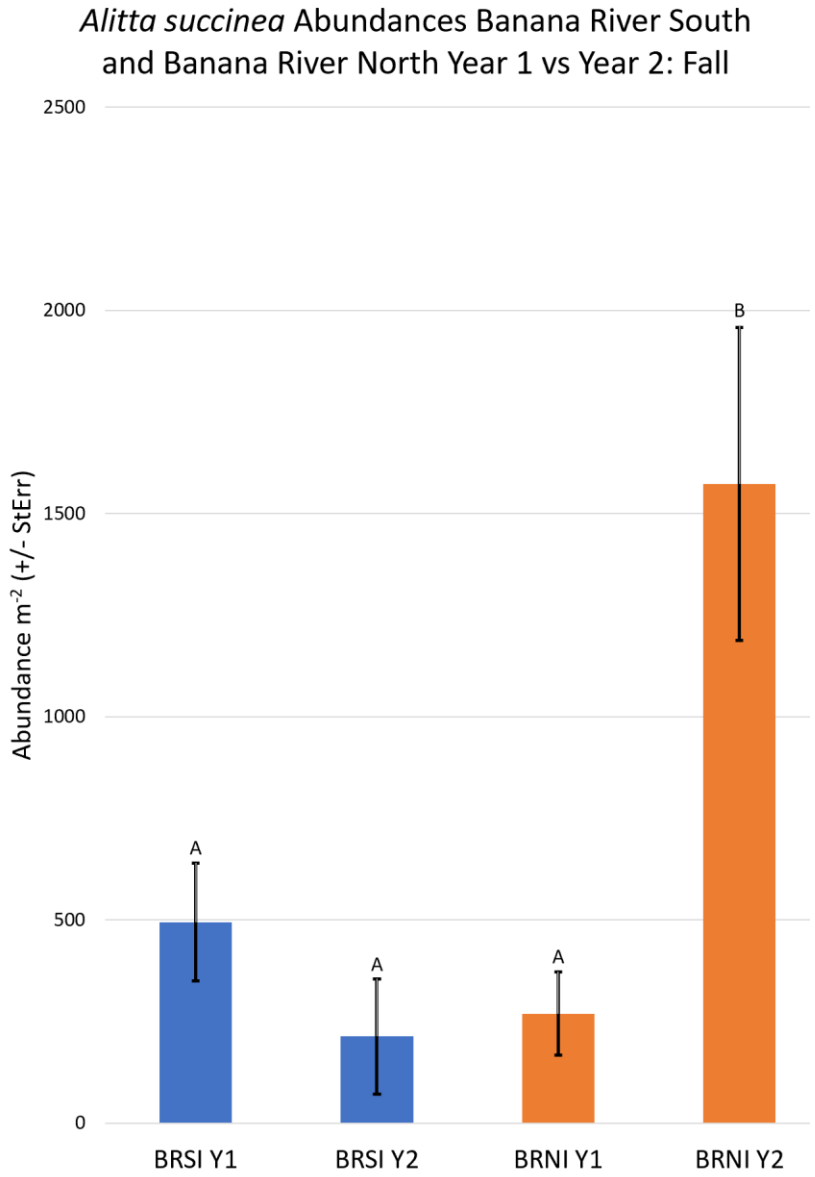

Figure 34. Mean abundance of the infaunal polychaete *Alitta succinea* at the proposed restored inflow site (BRN – orange) and the control site (BRS – blue) during the first and second phase of baseline monitoring (p = 0.006)

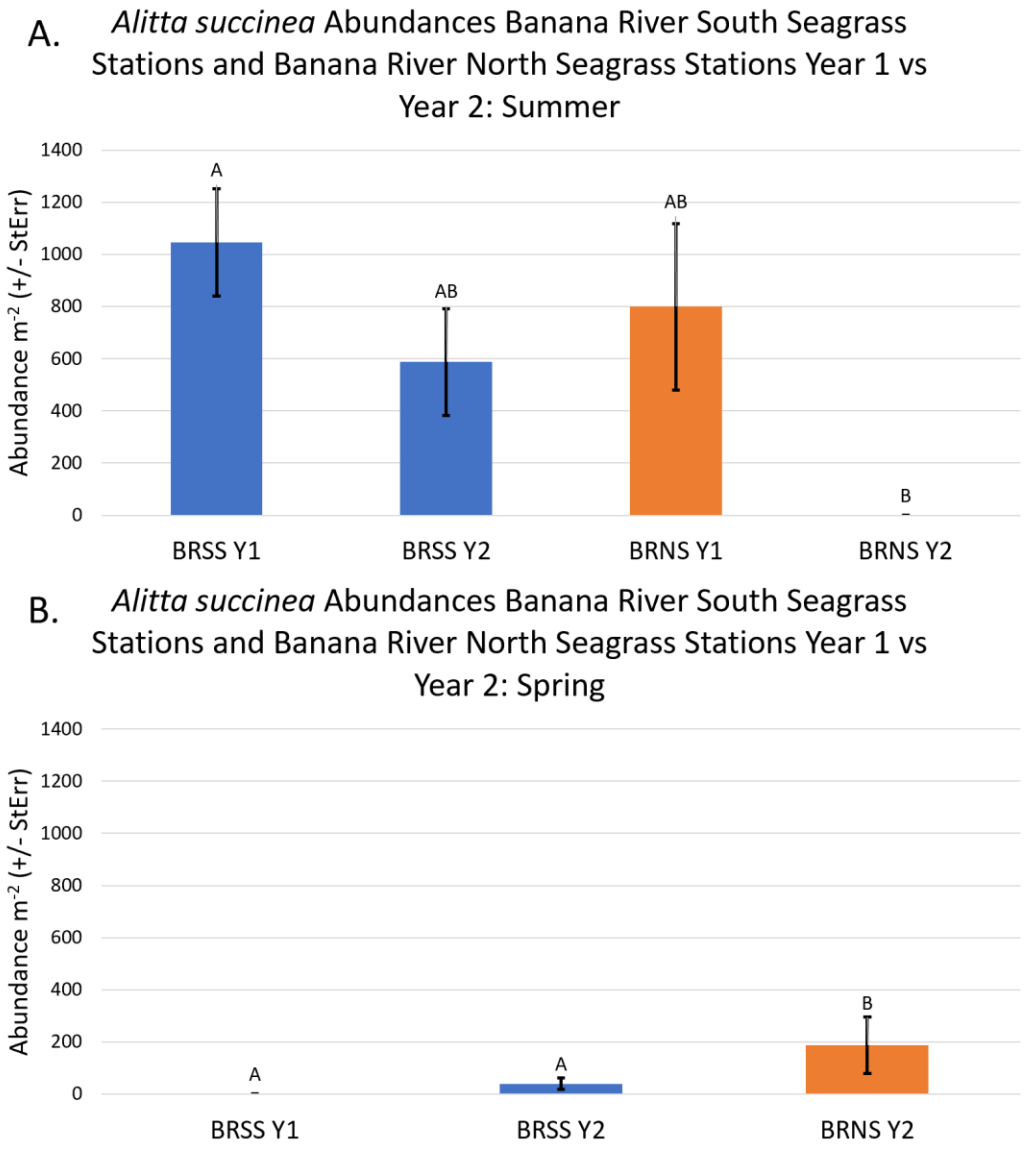

Figure 35. Mean abundance of the infaunal polychaete *Alitta succinea* in seagrass-associated sediments at the proposed restored inflow site (BRN – orange) and the control site (BRS – blue) during the first and second phase of baseline monitoring in the A) summer (p = 0.044) and B) spring (p = 0.006)

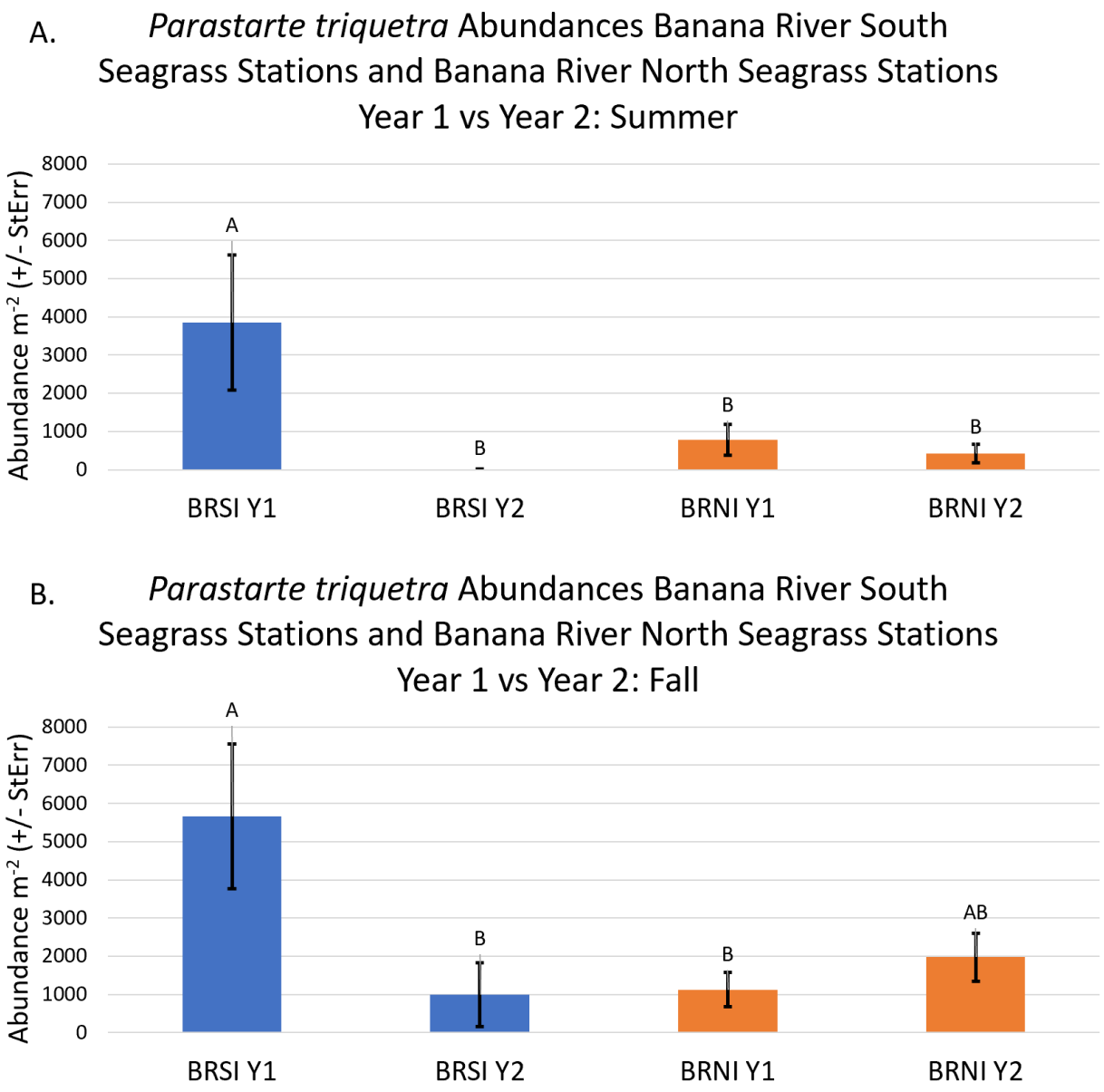

Figure 36. Mean abundance of the infaunal brown gem clam *Parastarte triquetra* in seagrass-associated sediments at the proposed restored inflow site (BRN – orange) and control site (BRS – blue) during Phases 1 and 2 of baseline monitoring in A) summer (p = 0.01) and B) fall (p = 0.02)

Infaunal species richness was 4–13.7, with the highest being at BRS inside lagoon during the fall of Phase 1 (**Figure 37** and **Figure 38**). Biodiversity ranged from 0.5–1.8, no matter the site, year, season, or whether they were found in bare sediments or seagrass sediments (**Figure 39** and **Figure 40**).

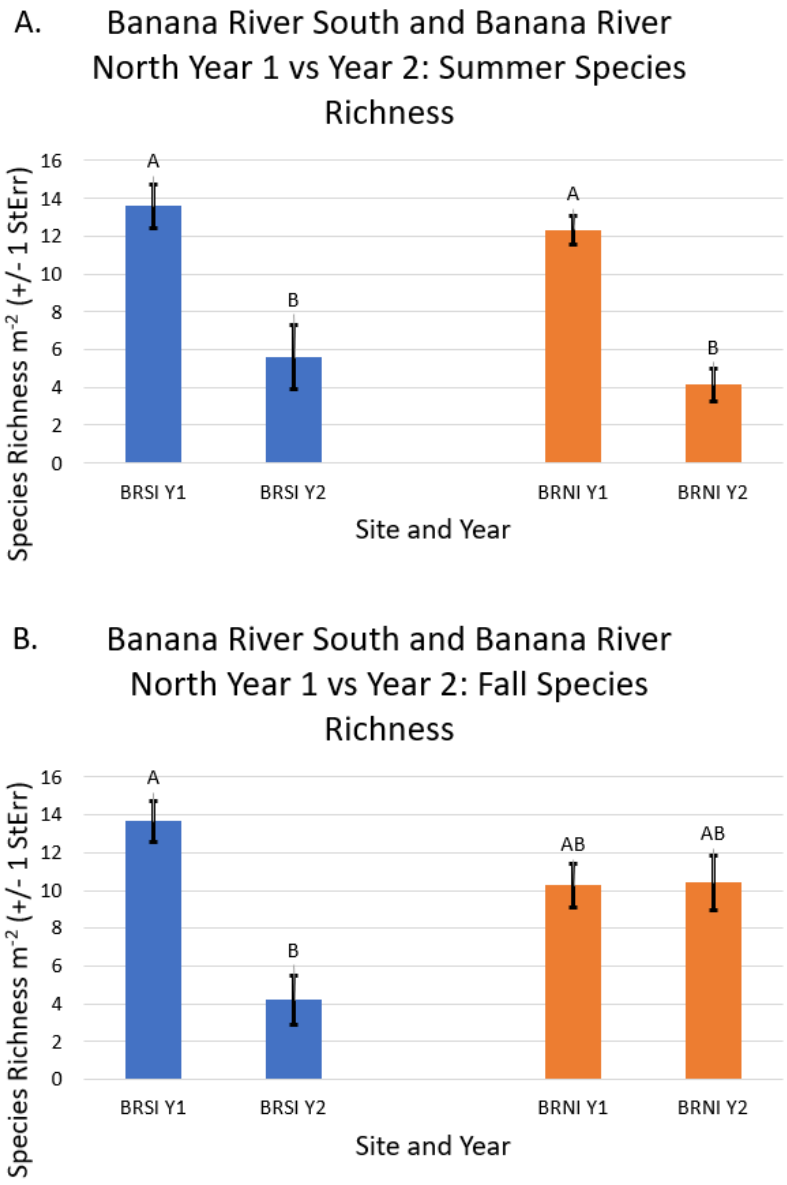

Figure 37. Mean benthic fauna species richness for bare sediments at the proposed restored inflow site (BRN – orange) and control site (BRS – blue) during Phases 1 and 2 of baseline monitoring during A) summer ($p < 0.001$) and B) fall ($p = 0.03$) seasons

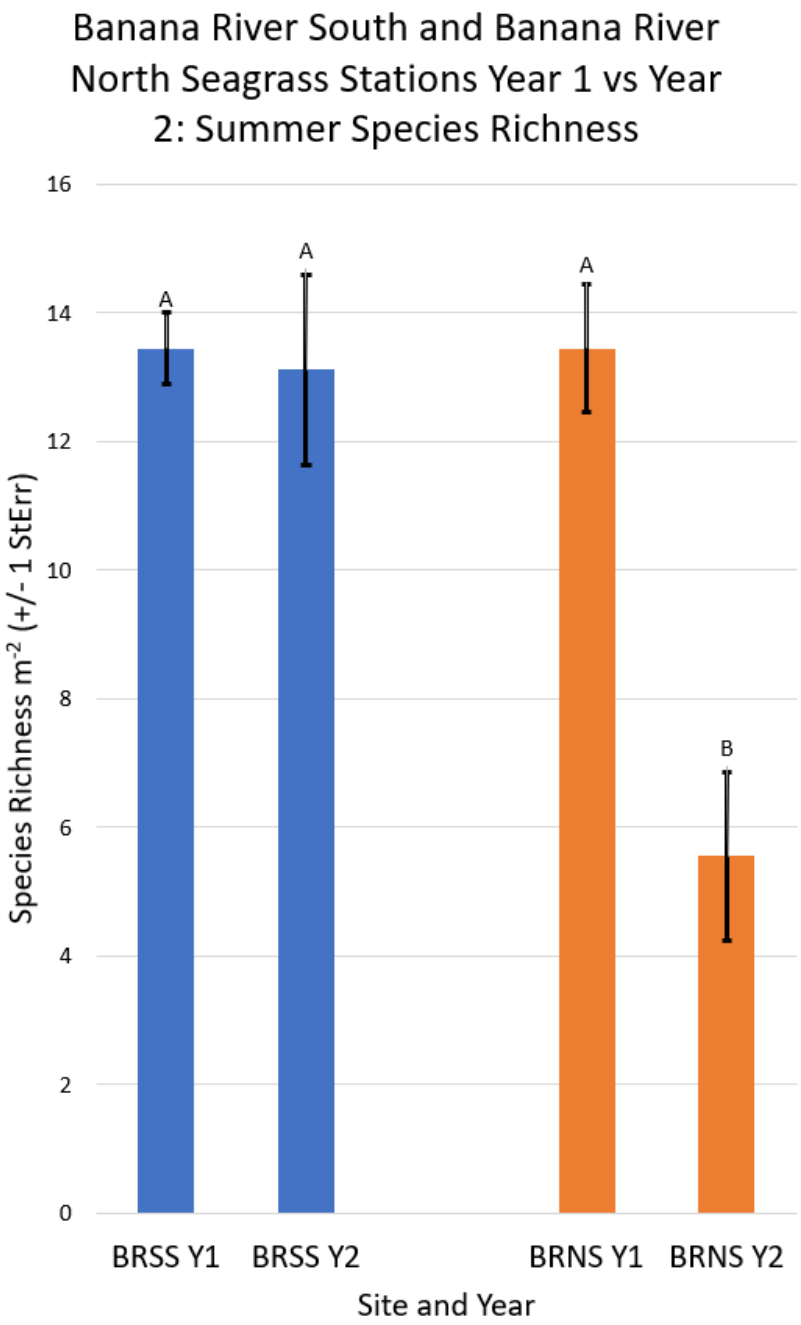

Figure 38. Mean benthic fauna species richness for seagrass-associated sediments at the proposed restored inflow site (BRN – orange) and control site (BRS – blue) during Phases 1 and 2 of baseline monitoring during the summer season (p = 0.002)

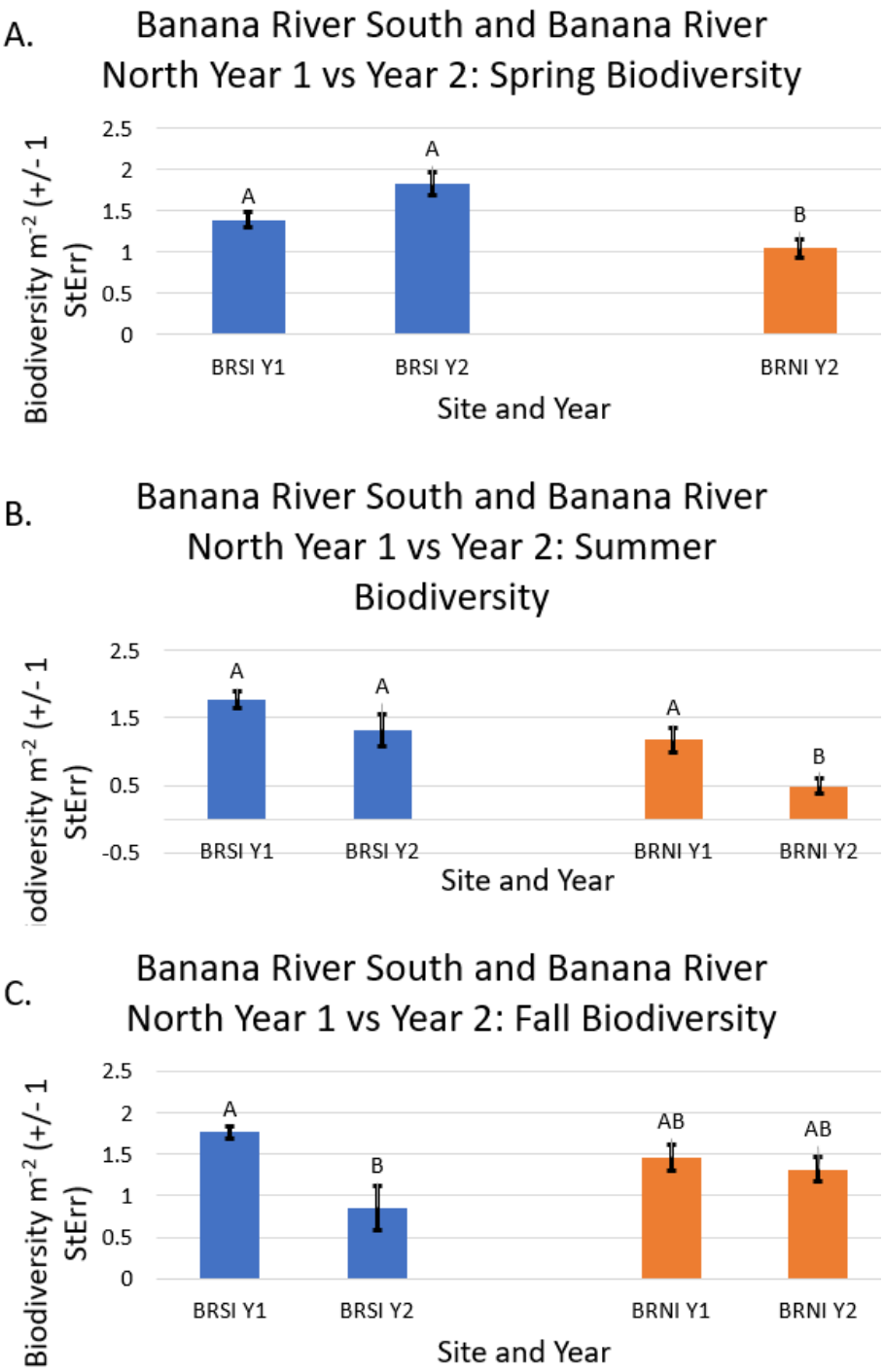

Figure 39. Mean benthic fauna biodiversity for bare sediments at the proposed restored inflow site (BRN – orange) and control site (BRS – blue) during Phases 1 and 2 of baseline monitoring during A) spring (p = 0.002), B) summer (p = 0.001), and C) fall (p = 0.012) seasons

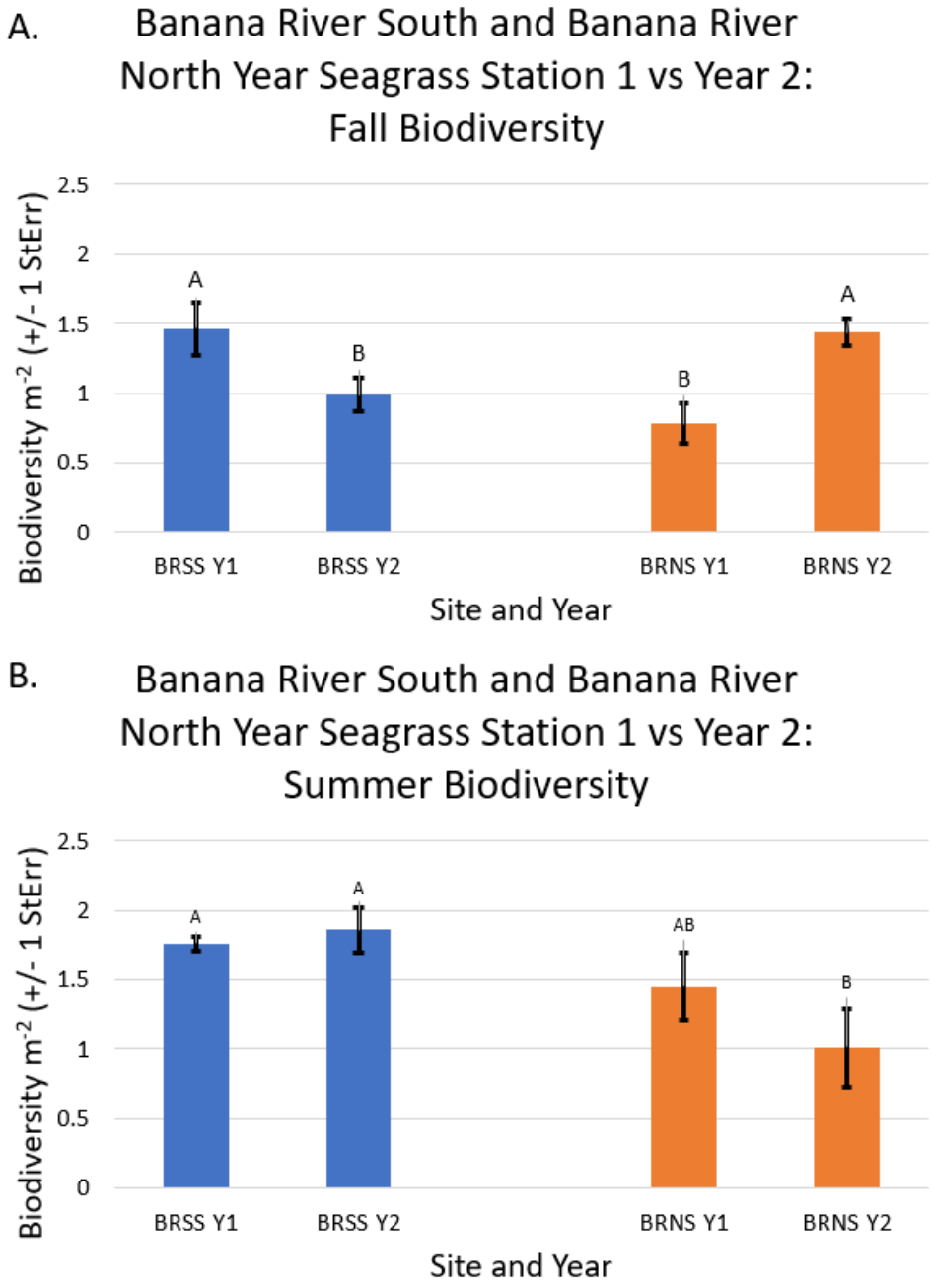

Figure 40. Mean benthic fauna biodiversity for seagrass-associated sediments at the proposed restored inflow site (BRN – orange) and control site (BRS – blue) during Phases 1 and 2 of baseline monitoring during A) fall ($p < 0.001$) and B) summer ($p = 0.006$) seasons

Principle components analysis revealed that sediment conditions (percent organic content, percent silt-clay content, and percent water content) were the most influential environmental factors impacting the site, followed by bottom water DO (**Figure 41**).

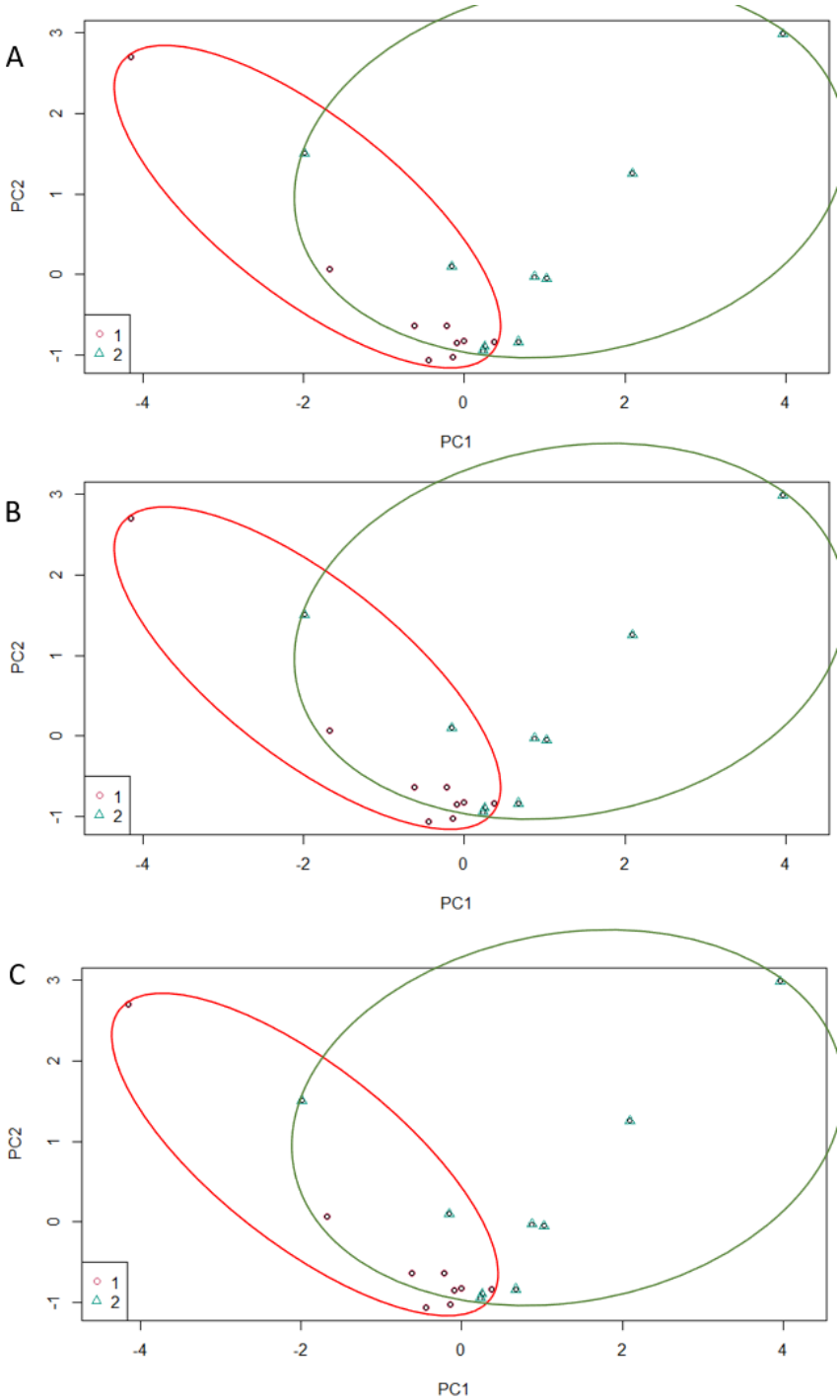

Note: PC1 = sediment percent organic content combined with sediment silt-clay and water contents. PC2 = percent DO in bottom water. Ellipses represent distinct groups based on similarity of principle components.

Figure 41. Principle components analysis of benthic infauna at BRN seagrass stations in Phases 1 and 2, analyzing the principle components driving A) biodiversity, B) species richness and C) abundance

NMDS plots show considerable overlap from one year to the next in community data, whether looking at biodiversity, species richness or abundance (**Figure 42**). Results of power analysis on

species diversity was as high as 0.83 and indicated that power should be sufficient for analysis with the current sample design.

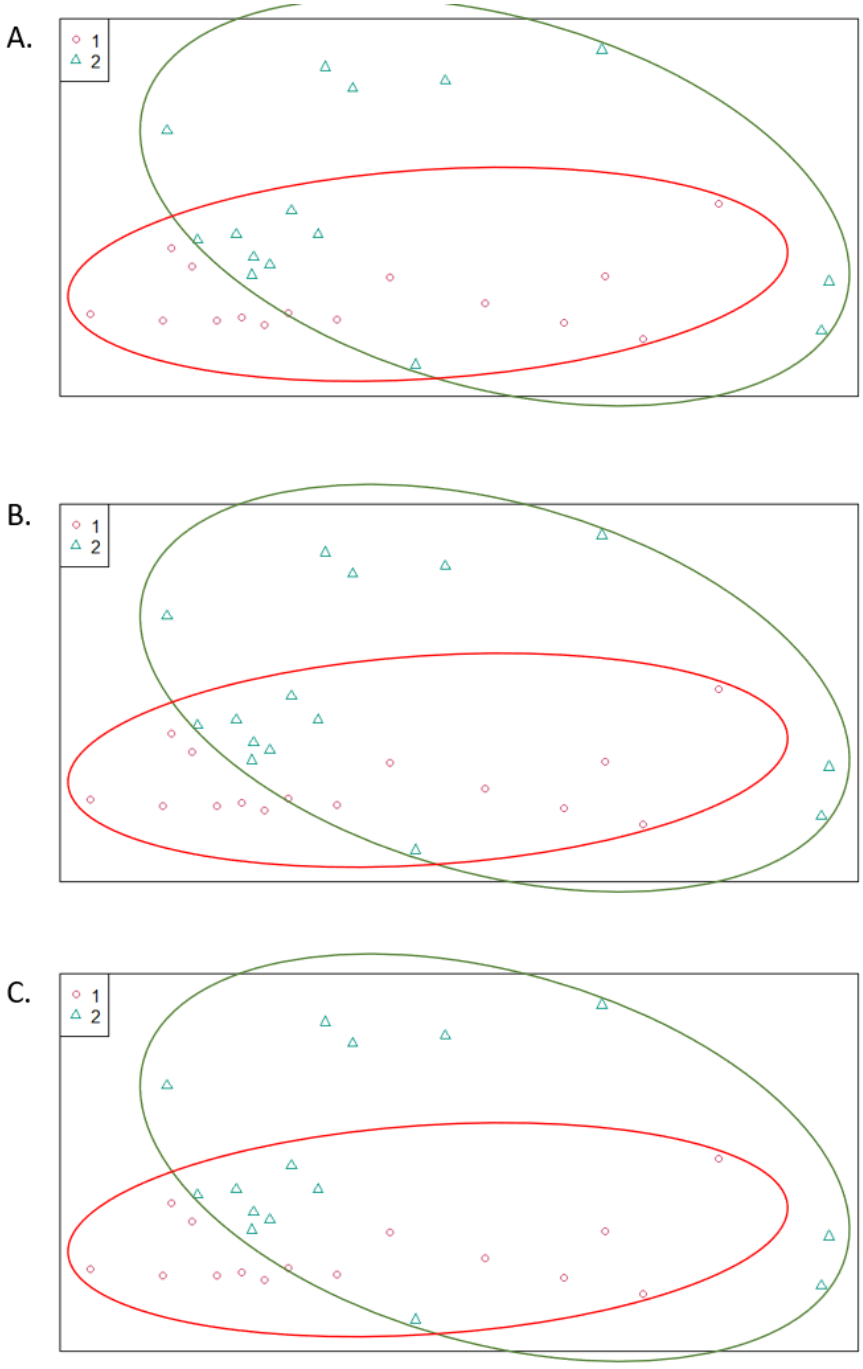

Note: Ellipses represent distinct groups based on similarity of the community.

Figure 42. NMDS of the benthic infauna community data at BRN seagrass stations in Phases 1 and 2, namely A) biodiversity, B) species richness, and C) abundance

NMDS was also used to examine patterns of seagrass coverage, and there were some significant differences based on year, season, and site (**Figure 43**).

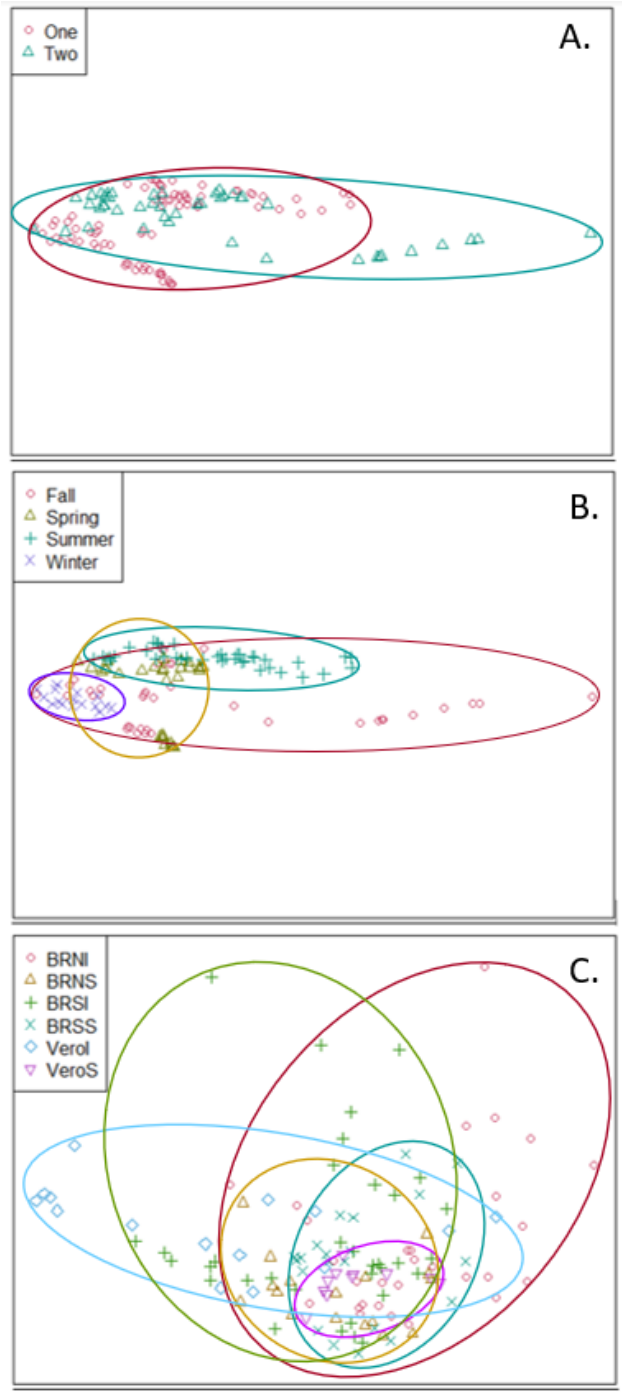

Site legend: BRNI = BRN in lagoon; BRNS = BRN seagrass; BRSI = BRS in lagoon; BRSS = BRS seagrass; VeroI = Vero Beach in Bethel Creek; VeroS = Vero Beach seagrass.

Figure 43. NMDS plots of seagrass percent cover as a function of environmental and other biological factors with aggregation of seagrasses according to A) year (p = 0.001), B) season (p = 0.001), and C) site (p = 0.001)

3.3.3 Phytoplankton/Harmful Algae Results

The IRL and corresponding outer coast stations share many phytoplankton species in common, but some are unique to one environmental or the other. For a list of the distributions and relative abundances of diatoms and a similar list of dinoflagellates and other plankton see **Table 13**.

Diatom species that were dominant during the majority of seasons and locations included *Chaetoceros* spp., *Coscinodiscus* spp., *Cylindrotheca closterium*, *Navicula* spp., *Nitzschia* spp., *Odontella* spp., *Pleurosigma* spp., and *Rhizosolenia* spp.. Diatoms of the genus *Pseudo-nitzschia* are known to cause HABs in other estuaries via the production of domoic acid (**Table 13**).

Dinoflagellates that were frequently present, often in high numbers, included *Ceratium* spp. And *Prorocentrum* sp. The following dinoflagellates were also present in the estuary, sometimes in high numbers, and are known to produce toxins and create harmful conditions: *Gonyaulax* spp., *Gymnodinium* spp., and *Pyrodinium bahamense* (**Table 13**).

Table 13. Seasonal presence/absence of planktonic diatoms at the proposed inflow (BRN) and control site (BRS)

Note: Samples were collected from estuarine stations I. In Phase 1, samples were also collected from complimentary coastal sites I or within Port Canaveral (P). Species presence (L,M or H for low, medium, and high) or absence (blank) are indicated. “L” is present in 1 station, “M” is 2-3, and “H” is 4.

	Banana River North										Banana River South									
Season >>	Fall			Win			Sum	Fall	Spr	Sum	Fall		Win		Spr	Sum	Fall	Spr	Sum	
Estuarine vs. Coastal Location >>	E	P	C	E	P	C	E	E	E	E	E	C	E	C	E	E	E	E	E	
Keys species:																				
Actinoptychus senarius			L			L	L					L			M				L	
Actinoptychus splendens												L								
Asterionellopsis glacialis		H	H		M	M						H								
Amphiprora sp.						M	L							L					M	
Amphitetras sp.												L								
Amphora proteoides																				
Amphora sp.			M	M	H	L	L			L			L	L	L				M	
Bacillaria paxillifera			M		L	L						L								
Bacteriastrum spp.			M			H						M		L						
Bellerochea horologicalis			L																	
Bellerochea malleus		L										M								
Biddulphia alternans					H	M														
Biddulphia rhombus						M						L								
Biddulphia sp.					L															
Chaetoceros spp.	H	H	H	H	H	H	H	H	L	H	H	H	M	H	M	L	M	H	M	
Climacodium frauenfeldianum																				
Corethron spp.		L	M		L	H						M								
Coscinodiscus spp.	M	H	H	L	H	H	H	H	M		M	H		L	M	L	M	L	M	
Cyclotella sp.	L		L		L	L	M								L					
Cylindrotheca closterium		H	H	M	M	M		M		M		H	L	M			H	M	M	
Cymatosira belgica		L	H		M	H						M								
Delphineis surirella		L																		
Diploneis sp.												L								
Dactyliosolen fragilissimus					M	L	H						M							
Detonula pumila					L															
Epithemia sorex																		M		
Eucampia sp.					M	H														
Eunotogramma sp.				L			L													
Grammatophora marina			L																	
Grammatophora spp.		L					L												L	
Guinardia flaccida		M	M			M						M								
Guinardia striata			M		L	M						M		M						

Gyrosigma fasciola					L					L										
Haslea wawrickae			L																	
Hemiaulus hauckii		M	M			H														
Hemiaulus membranaceus						H						M								
Hemiaulus sinensis					L	L														
Hemiaulus spp.			L			L						M								
Leptocylindrus danicus	H	H	L	L	L	M	H			H		H		M	M					H
Licmophora sp.						H														L
Lioloma pacificum						L														
Lithodesmium undulatum												M								
Melosira moniliformis					L															
Meuniera membranacea												L								
Navicula spp.			H	H	M	H				L		M		L	M		L	L	M	
Nitzschia longissima			L		L		L													
Nitzschia spp.		M	M	L	H	H	M					L	M		H		L		L		M
Odontella spp.		M	H		H	H			M	L			M		M					
Paralia sulcata		M	H	L	H	H							H		L					
Pleurosigma spp.		M	H	M	H	H	M		M	M			M		M	L	M				H
Pseudofalcula hyalina																				
Pseudo-nitzschia spp.		M	H		L	M							M			L				
Rhizosolenia spp.	H	M	H			H	H	M	H	H		L	H		H	H	L		H	H	M
Skeletonema costatum		L	H		L	H							H			L				
Stephanopyxis sp.		H	M		L	M														
Surirella sp.					M												L			
Thalassionema frauenfeldii		M	H			L							H			L				
Thalassionema nitzschoides		H	H	L	H	H							H		L	M				
Thalassiosira sp.					L	M	L													
Triceratium brightwellii					M	H														
Triceratium sp.		L	L		L	M							M							
Trigonium sp.						L														

Table 14. Seasonal presence/absence of planktonic dinoflagellates and other groups at the proposed inflow (BRN) and control site (BRS)

Note: Samples were collected from estuarine stations I. In Phase 1, samples were also collected from complimentary coastal sites (C) or within Port Canaveral (P). Species presence (L,M, or H for low, medium, and high) or absence (blank) is indicated. "L" is present in 1 station, "M" is 2-3, and "H" is 4.

		Banana River North										Banana River South								
	Season >>	Fall			Win			Sum	Fall	Spr	Sum	Fall		Win		Spr	Sum	Fall	Spr	Sum
	Estuarine vs. Coastal Location >>	E	P	C	E	P	C	E	E	E	E	E	C	E	C	E	E	E	E	E
	Keys species:																			
Dinoflagellates	*Actiniscus pentasterias*																			
	Ceratium spp.	L	L	H				M	H	H				L	M		H	H	H	H	H	H
	Ceratocorys armata																L					
	Dinophysis argus								L									L					
	Dinophysis sp.							M														
	Gonyaulax spp.	M							H									H		M		M
	Gymnodinium spp.															H		L				
	Oxyphysis sp.							L														
	Oxytoxum sp.																	M				
	Peridinium sp.							M	M								M	H				
	Podolampas sp.							L									M					
	Prorocentrum sp.						L	M	H	L					M	L		H	H	M	M	H
	Protoperidinium spp.	L							M							L		L	M		H	M
	Pyrocystis fusiformis																	L				
	Pyrocystis lanceolata																					
	Pyrodinium bahamense		L						L									L	H			H
Cyanobacteria	*Anabaena sp.*							L														
	Lyngbya sp.																				L	
	Oscillatoria sp.						L															
Tintinnids	*Amphorellopsis sp.*																	L				
	Eutintinnus sp.								H									M	L			L
	Helicostomella sp.	H						H	L										M			H
	Tintinnopsis sp.							M										L	L			L
Silicoflagellate	*Dictyocha fibula*			M			M	M	H						M				H			
Raphidophycea	Cryptophycean																	L				
	Raphidophycean	L							H					L	M	M		H	L			
Misc.	Peridinial Dinoflagellate	L																				
	Raphid Bacillariophyceaen Diatom			L																		
	Sponge Tylostyle Spicules					L	M		L					L		L		M		L		L
	Unidentified Protist						H	M														

The most abundant phytoplankton were non-cyanobacterial cells <40-µm, and these tended to be more abundant in the estuary near the region of the proposed for restored inflow, especially in Phase 2 of sampling (**Figure 44**). Cyanobacteria densities measured by phycocyanin pigment presence range from nearly absent to 4 x 10^7 cells L^{-1}, and were especially abundant in the estuary during 2021. Cyanobacteria detected by the presence of phycoerythrin pigment were more consistently present and peaked at about the same order-of-magnitude as phycocyanin-bearing cells.

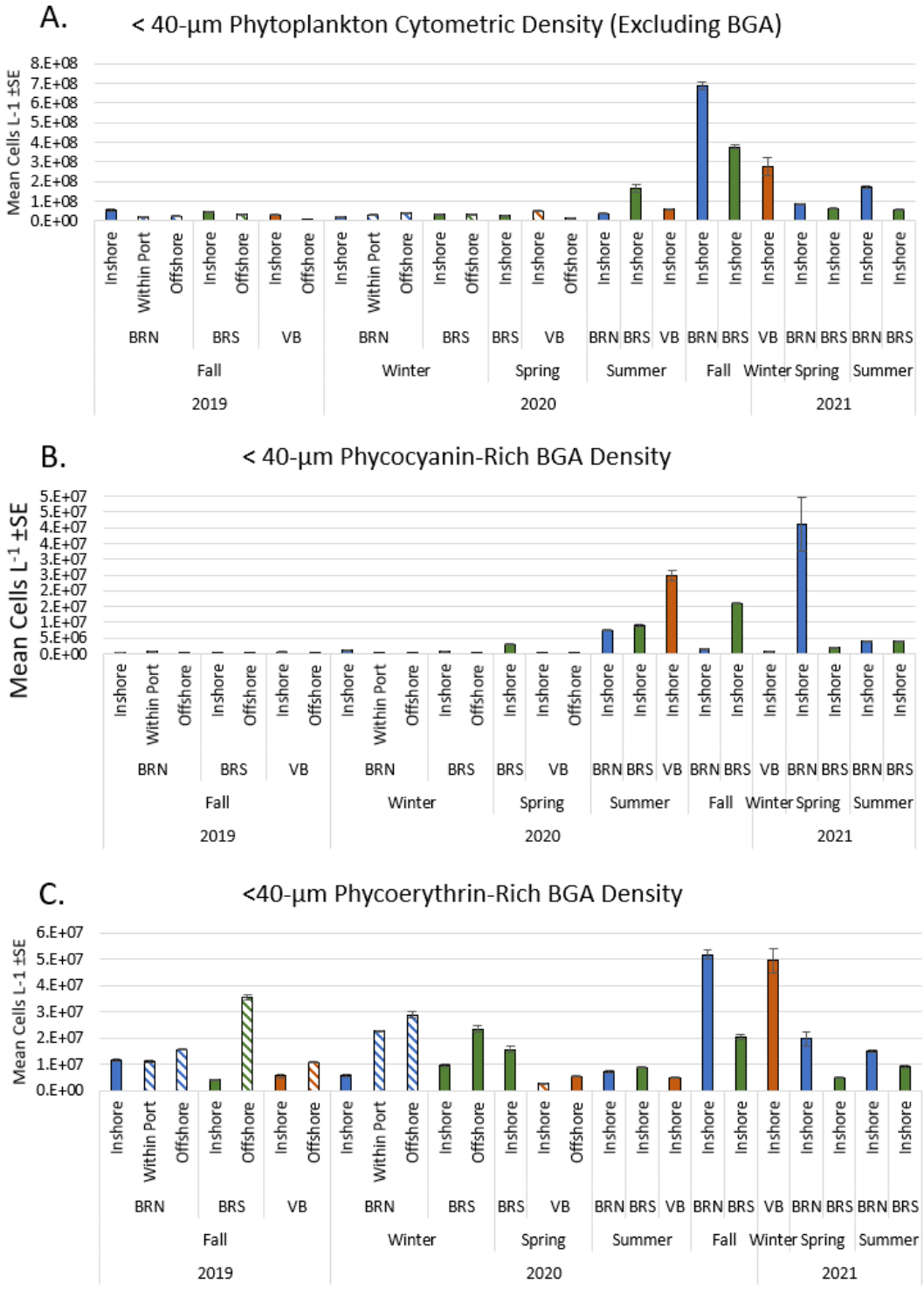

Note: Sites are BRN, BRS, and Vero Beach (VB). "Inshore" is within the estuary. "Offshore" is coastal.

Figure 44. <40-µm phytoplankton densities for A) non-cyanobacteria, B) cyanobacteria as indicated by phycocyanin presence, and C) cyanobacteria as indicated by phycoerythrin presence

Larger phytoplankton (>25-µm due to tow net mesh size) were mostly diatoms and dinoflagellates (**Table 13**,

Table 14). The greatest abundances of >25-µm cells was $4.5x10^3$ – $5.9x10^3$ cells L^{-1} in the estuary at BRS (**Figure 45**).

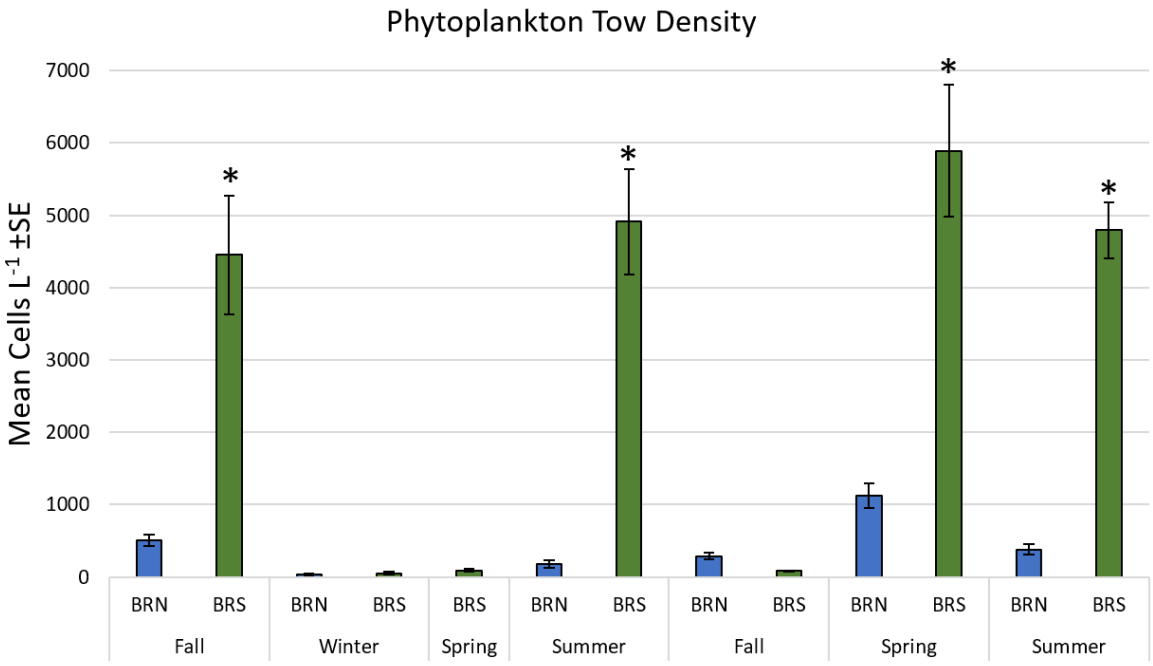

Figure 45. >25-µm phytoplankton mean densities inside and outside of the proposed inflow site (BRN) and control (BRS), seasonally from fall 2019 to summer 2021

Phytoplankton biodiversity, species richness, and evenness were calculated for tow plankton >25-µm and reported in **Figure 46**.

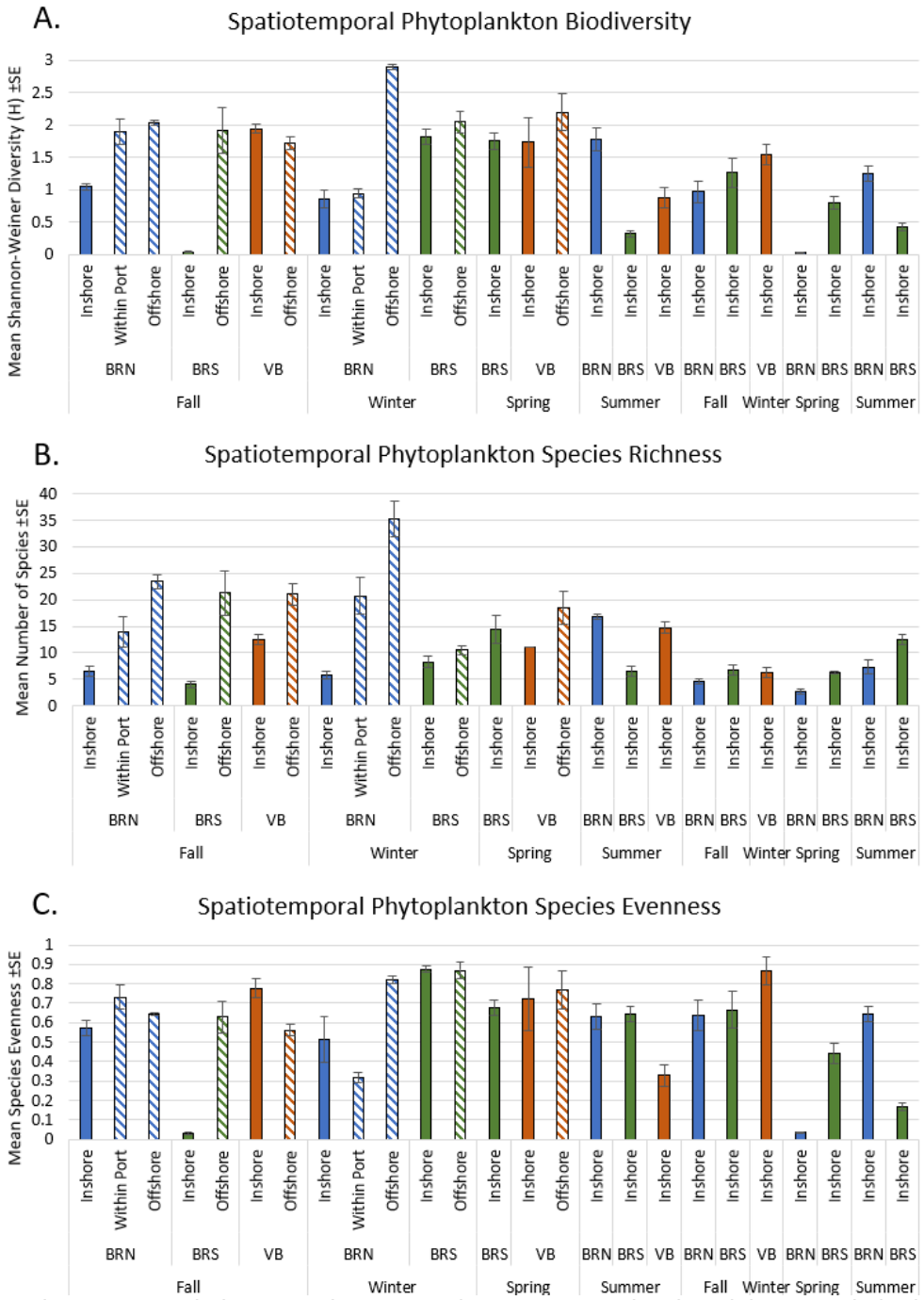

Note: Comparisons are made between the estuary (BRN, BRS, and VB) and the same latitude in the coastal ocean at each of the potential inflow sites ("offshore"), the latter during the first year of sampling only.

Figure 46. Phytoplankton mean Shannon-Weiner Diversity Index (A), mean species richness (B), and mean community evenness (C)

Using NMDS plots to group communities based on relative species abundances shows communities fall out based on season and location (**Figure 47**, stress 0.15–0.24, ANOSIM R=

0.23-0.99, p < 0.05). Estuarine plankton communities were most distinct from one another when compared via pooled seasons per site (**Figure 47**, panel B).

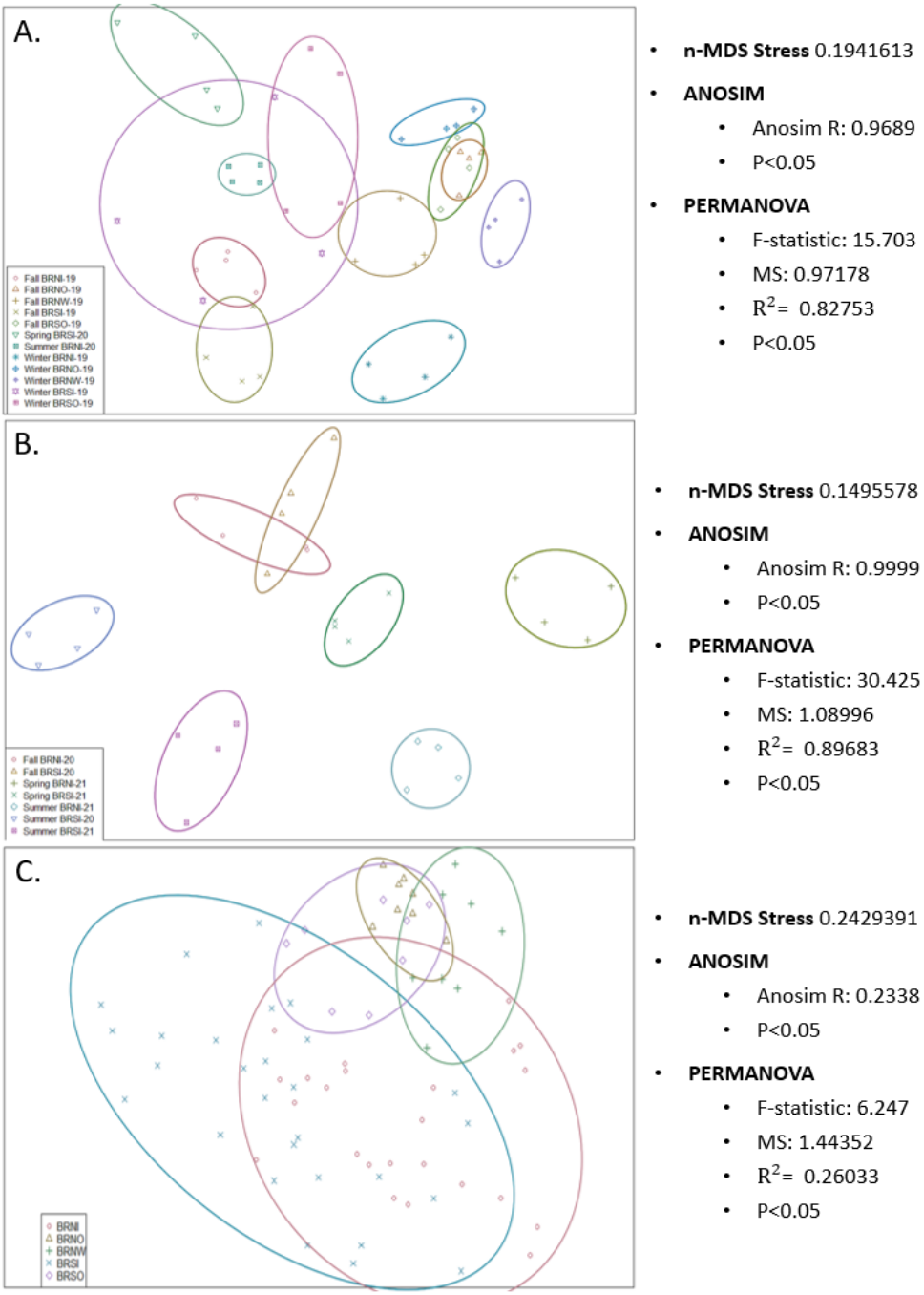

Note: Symbols represent BRN (inside estuary, within port, and outside coastal – BRNI, BRNW, and BRNO, respectively) and BRS (inside estuary and outside coastal – BRSI and BRSO, respectively). Outer coastal and port sites (BRNO, BRNW, and BRSO) were sampled only in Phase 1.

Figure 47. NMDS associations of >25-µm phytoplankton communities based on species and abundances, comparing A) seasons and locations for Phase 1 (2019–2020); B) seasons and locations for Phase 2 (2020–2021); and C) locations only with seasons and years pooled

3.4 Discussion

This report describes the spatial and temporal variation in species occurrence within the IRL estuarine environment over almost two years starting in fall 2019.

Objective: The primary objective of this project is to document baseline biological characteristics of the IRL in the vicinity of proposed inflow. Baseline data will be used to compare with conditions following restored inflow.

Abundance and distribution data presented herein form the foundation of a baseline dataset collected in the IRL estuary near the proposed inflow site, and at a control site for comparison. Should a restoration of inflow be initiated at, or near, any of the sites, these data can be used to track and evaluate the condition of the system and identify ecological risk, with a focus on determining responses in seagrasses, benthic fauna, phytoplankton, ichthyoplankton, and fishes.

Estuaries are semi-enclosed coastal bodies where interaction between freshwater from rivers and streams, and tidally forced salt water from the sea, produce a highly dynamic system subject to changes occurring over short spatial and temporal scales. Estuarine species are therefore commonly euryhaline and eurythermal, meaning they can withstand relatively large fluctuations in salinity and temperature, while organisms found in offshore coastal environments are typically restricted to a narrow range of salinities and temperatures.

The moderate salinity and temperature ranges maintained within a few kilometers of ocean inlets (e.g. Sebastian Inlet) allow many offshore species to use estuaries for foraging and nursery habitat. Upstream of inlets, environmental conditions vary considerably, favoring species with broad physiological tolerances. The pattern of estuarine species having wider ranges of tolerances for abiotic environmental conditions is found throughout disparate taxonomic groups.

The main biological concerns when restoring inflow are how changes in water and sediment quality will impact the species composition and abundances of the estuarine community.

3.4.1 Seagrass, Rooted Algae, and Drift Algae Discussion

Seagrasses provide habitat for other organisms, and a protective nursery environmental for vulnerable developmental stages. They are a food source for numerous animals, and serve to stabilize sediments (Zieman, 1982; Dawes et al., 1995).

There are seven species of seagrasses known to occur in various parts of the IRL estuary. However, in the northern IRL, the shoal grass *Halodule wrightii* dominates and was the only seagrass species documented in the surveys conducted for this study. *H. wrightii* has a wide range of habitats and lives in salt marshes, estuaries and, under some circumstances, coastal areas. It occurs both intertidally and in shallow subtidal habitats. In the northern IRL, *H. wrightii* is thought to occur no deeper than about 2 m, and optimally <1 m (Phillips, 1960), due to turbidity and lack of water clarity severely limiting light penetration. However, in the clearer water of the Florida Keys and the Caribbean, it can be found as deep as 12 m (Bulthuis, 1987). Coastal surveys in this study were too deep (>10 m) to conduct via snorkeling, but hundreds of sediment grab samples have not yielded incidental seagrass capture. Additionally, anecdotal video evidence by tethered remotely operated vehicle shows no *H. wrightii* on the coastal side of proposed inflow locations. Further south in coastal waters, however, there are almost certainly beds of *H. wrightii* living subtidally at depths not possible in the turbid northern IRL. Propagules or vegetative fragments would be carried northward by longshore currents. *H. wrightii* would likely inhabit the coastal sites in this study were it not for unhospitable depths and water clarity.

The environmental tolerances of *H. wrightii* are broad. Shoal grass is considered a weed-like pioneer species. It is eurythermal and euryhaline, with likely optimal temperature tolerance range of 20–30 °C (McMillan, 1982) and reported in Florida to withstand salinities of at least 12–38.5 parts per thousand (Phillips, 1960). *H. wrightii* is also flexible with regard to nutrient and organic sediment levels and can be found in sediments ranging from silty mud to sand with limited organic material (Phillips, 1960). With these impressive ranges of tolerances, and with the knowledge that *H. wrightii* occurs in deeper coastal ocean water in the tropics where water clarity is better, it seems unlikely that *H. wrightii* would be directly harmed by the abiotic environmental changes that will come with restored lagoon inflow. If water clarity improves, *H. wrightii* may even be able to recruit into deeper parts of the IRL previously inaccessible due to depth and photosynthesis limitations. If the water column becomes less eutrophic, or if sediments have less silt and organic material, shoal grass could benefit from a less polluted and stressful environment. On the other hand, shoal grass is considered a tolerant pioneer species (Gutierrez, 2010) and, if there is dramatic water quality and sediment improvement, shoal grasses could experience competition for space with other seagrass species which are not present under current conditions. It should be noted that we currently lack sufficient information to predict how *H. wrightii* might be impacted by changes in herbivory or competition due to a shifting ecosystem driven by restored inflow. If a pilot RLI project is undertaken, continued ecosystem and biological monitoring will allow comparisons with the data reported herein, and it should be possible to say something about the impacts, or lack thereof, of complex ecosystem dynamics due to restored inflow.

Notorious herbivorous fish known to graze on *H. wrightii* include Pinfish (*Lagodon rhomboides*), surgeonfish (*Acanthurus bahianus* and *A. coeruleus*), and parrotfish (*Scarus taeniopterus*, *S. iseri*, and *Sparisoma aurofrenatum*). Increases in these fish in the IRL due to restored inflow would likely increase grazing pressure on *H. wrightii*. The West Indian Manatee is a voracious grazer on *H. wrightii*, but it is not anticipated that restored inflow will greatly change manatee presence directly due to water quality conditions, since they are found regularly both in the estuary and on the outer coast. Monitoring of seagrasses and these grazers during a pilot study would provide data on how inflow impacts seagrasses through water quality changes and, possibly, a shifting guild of grazers.

Results of power analysis on benthic/drift vegetation generally ranged from 0.05–0.35. To differentiate treatments with statistical significance, it is likely that sample sizes would need to be dramatically increased. This is due to the extreme variability of benthic/drift vegetation, which can vary from virtually absent to high percentages of coverage. Nevertheless, continued monitoring of seagrasses (and other vegetation) is essential to document and detect any dramatic crashes or improvements in response to a restored inflow pilot study.

3.4.2 Benthic Fauna Discussion

> ***"Benthic infauna are increasingly employed as a bioindicator of environmental quality"***
>
> - *Kuk-Dzul et al. 2012*

Benthic fauna are key indicators of local environmental conditions due to their unique life histories and, therefore, an important component of monitoring. Their benthic and sessile nature (relative to fishes, for example) renders them unable to easily escape when sediment or water column conditions shift. For this reason, discussion here will focus on some benthic infauna species whose abundance and presence has been confirmed in baseline sampling. The discussion will include their life history, environmental tolerances, and ecological niches to better understand

how they may respond to restored lagoon inflow and how that may impact the ecosystem as a whole.

Infaunal species from prominent taxa dominating the IRL benthic community include six benthic fauna that are abundantly present in the estuarine sediments near the proposed inflow site, and also at the control site. They are considered to hold special ecological importance and their life histories and environmental tolerances are reviewed here based on published literature.

The gammarid amphipod *Cymadusa compta* is a ubiquitous amphipod found in throughout the IRL in almost all benthic habitats (Zimmerman, 1971; Stoner, 1983). Its latitudinal distribution ranges from the coast of Maine and southward to Florida and the Gulf of Mexico (Bousfield, 1973; Morgan and Kitting, 1984; Hauxwell et al., 1998), and is therefore considered eurythermal. It has been collected at salinities ranging from 5-44 practical salinity units (PSU) (Boesch and Diaz, 1974; National Oceanic and Atmospheric Administration(NOAA) National Benthic Inventory). *C. compta* feeds on drift algae, epiphytes, and phyto-detritus (Zimmerman et al., 1979; Luczkovich et al., 2002). These food sources are abundantly available in the IRL estuary, and this may explain why *C. compta* tends to be found there, but not on the outer coast. Temperature and salinity changes in the IRL due to inflow are unlikely to directly force the displacement of *C. compta* given its broad physical and chemical tolerances, although if water quality changes were to successfully reduce drift algae, epiphytes, and detritus, *C. compta* might be impacted by reduced food availability. Live healthy seagrasses are not a primary food source for *C. compta* (Kelly et al., 1990). Pinfish and other benthic foraging fish are important predators on *C. compta* (Stoner, 1979 and 1983; Nelson, 1995), and environmental shifts that impact those fish populations could well have an indirect impact on benthic prey like *C. compta*.

The gammarid amphipod *Cerapus tubularis*' distribution, tolerances, and life history are not well-described in the literature, especially for Florida and IRL (NOAA National Benthic Inventory; Felder and Camp, 2009). However, it is consistently present in the IRL estuary in medium abundances. Because it is absent from coastal samples, this is a species that should be monitored for impacts due to inflow if a pilot project is undertaken. As many gammarid amphipods, this species may be an important food source for benthic foraging fish (Stoner, 1979), and there is the potential for indirect trophic web impacts if inflow changes the guild or ratio of predators.

The gammarid amphipod *Gammarus mucronatus* is thought to occur in both brackish estuaries and out coastal sediments from the Gulf of St. Lawrence (Nova Scotia) to Florida and the Gulf of Mexico (Bousfield, 1969 and 1973). *G. mucronatus* is likely also found in outside coastal sediments based on published preferred habitats and regional distributions (Watling and Maurer, 1972; Bousfield, 1973; van Maren, 1978; Nelson, 1980). *G. mucronatus* is recognized as strongly eurythermal (Fredette and Diaz, 1986) and euryhaline (Bousfield, 1973), and those in the estuary are not likely to be displaced directly by seawater influx. They are, like the gammarids above, an important part of the diet of benthic foraging fish, such as the Pinfish *Lagodon rhomboids* (Nelson, 1979 and 1980), surgeonfish, and parrotfish. Seawater impact on those fish populations may indirectly impact gammarid amphipods, including *G. mucronatus*.

The ostracod crustacean *Eusarsiella zostericola* is eurythermal, occurring from Maine to the Gulf of Mexico, and can tolerate salinities from 22–36 PSU (Kornicker, 1967 and 1986). *E. zostericola* was observed within all the IRL estuary sites (BRN in lagoon, BRS in lagoon, and VB in lagoon) in low, medium, and high abundances in all seasons. In contrast, they are not commonly found in coastal sediments. Given their persistence in the IRL through fall, winter, and spring, it seems likely they can withstand salinities below 22 PSU. *E. zostericola* has been an invasive species in some parts of the world, but is has not been documented to displace species,

nor does it have recognizable trophic impacts through grazing on prey or serving as food for predators (Ruiz et al., 2011).

The bivalve mollusc *Parastarte triquetra* is subtropical to tropical, found from Florida through most of the Caribbean (Abbott and Morris, 1995), and is considered a characteristic species of IRL, where it can occur in densities exceeding 2 x 104 m^{-2} (Mikkelsen et al., 1995). *P. triquetra* was found within the IRL estuary at all sites (BRN in lagoon, BRS in lagoon, and VB in lagoon) in low, medium, and high abundances in all seasons. Relatively little is known about the detailed tolerances, life history, and ecological interactions of this bivalve, and it should be monitored before, during, and after any inflow project is undertaken.

The gastropod mollusc *Acteocina canaliculata* is eurythermal, occurring in Maine, the mid-Atlantic, Florida, throughout the Caribbean, and at least as far south as Suriname (Brunel et al., 1998,; Rosenberg et al., 2009). They are found in sediments with >38% silt-clay content (Kennish et al., 2004; Flanagan et al., 2018). In the IRL, this level of silt-clay tends to accompany polluted organic sediments. Coastal sediments rarely have this level of silt-clay, and this may explain why *A. canaliculata* is not found at BRN outside, BRS outside, and VB outside. Franz (1971) collected individuals for spawning that were in water that varied 28-–31 PSU in salinity, but their occurrence throughout the IRL makes it almost certain they can withstand much lower salinities.

It is recommended that monitoring of benthic fauna be ongoing before, during, and after the implementation of a pilot RLI project. Continued baseline monitoring ahead of pilot pumping is advisable from the perspective of having a better understanding of the biology and ecology of the system. Biological populations are notoriously variable, and that variation increases with seasonal changes. The more pre-pilot monitoring data that we have, the better we will be able to differentiate differences due to inflow treatment (Giovannoni and Vergin, 2012; Kroodsma et al., 2018).

Results of power analysis on benthic infaunal species richness and biodiversity generally ranged from 0.5–0.99. The higher outcomes suggest that there will be cases where it will be possible to distinguish treatments statistically with regard to biological community parameters using the sampling regime that has been in place for the first two years of sampling.

3.4.3 Phytoplankton/Harmful Algae Discussion

“Algal blooms are indicators of marine ecosystem health; thus, their monitoring is a key component of effective management of coastal and oceanic resources.”
- Blondeau-Patissier et al. 2014

Phytoplankton are drifting microalgae of various taxa (e.g., dinoflagellates, diatoms, nanoflagellates), and can sometimes be responsible for harmful or toxic algal blooms. Phytoplankton, by definition, drift with currents, and will travel wherever the flow directs. Monitoring their distributions is challenging, because they are extremely variable and patchy in time and space (e.g., Bengfort et al., 2006; Trudnowsky et al., 2016; Breier et al., 2018). Phytoplankton data were collected using two different methods for this evaluation. Larger phytoplankton (>25-µm) were collected via plankton net tow, and visually identified and counted via light microscopy. Smaller phytoplankton (<40-µm) are difficult, often impossible, to identify the taxon visually. These small cells were counted via whole water samples using a flow cell cytometer. The cytometer cannot differentiate species. It does, however, reveal different size groups of the small cells, which have a greater chance of being a coherent bloom. The cytometer

also analyzes the photosynthetic pigments, which reveals to which major phytoplankton groups the small cells likely belong.

There are at least 82 species of diatoms comprising the dynamic phytoplankton community in the proposed IRL inflow and control sites. At least one of these genera (Pseudo-nitzschia) is a known toxin (domoic acid) producer and a HAB species in other systems. Pseudo-nitzschia has not, however, contributed substantially to the HABs of concern in the IRL in the last decade. There are least 16 species of dinoflagellates confirmed to occur near the proposed inflow site. Of these, at least 4 genera or species (*Gymnodinium*, *Dinophysis*, *Gonyaulax*, and *Pyrodinium bahamense*) are known toxin producers and form HABs in other systems. Only *P. bahamense*, however, has bloomed and created trophic web toxicity in the IRL in the last decade. Most of the HABs in the IRL have been smaller cells that are difficult to identify without genetic confirmation. These blooms are quantified by our cytometer cell counts. There have been substantial HABs of these smaller-celled bloom species measured in this study, including non-cyanobacterial cells, cyanobacteria with phycocyanin pigments, and cyanobacteria with phycoerythrin pigments. These species play a role in the planktonic ecosystem within the IRL, and they could be directly or indirectly impacted by changes in estuarine water quality. Plankton monitoring in the estuary should continue in order to describe responses in these species or groups.

HABs caused by phytoplankton create turbidity and attenuate light and have caused the death of tens-of-thousands-of-acres of seagrasses in the IRL (Tetra Tech, 2016), and HABs are largely responsible for public alarm concerning the state of the lagoon. Should an inflow project be implemented, one of the most positive potential outcomes would be a reduction in frequency and severity of IRL HABs. For the toxic and otherwise harmful dinoflagellates, diatoms, and cyanobacteria, we now have baseline lists and concentrations at inflow sites to compare if an inflow restoration project is undertaken by the state. It will be critical to continue monitoring these populations to document the successes and shortcomings of the project. Regarding pre-pilot monitoring, it is recommended that this continue until such time as a pilot is implemented, giving the best possible understanding of the natural variation of the system (Giovannoni and Vergin, 2012; Kroodsma et al., 2018). With continued monitoring of phytoplankton and HABs, seasonal variation will be better understood and treatment impacts more certain.

3.5 Key Findings for Benthic/Drift Vegetation, Benthic Infauna, and Phytoplankton Monitoring

Types of organisms present in the vicinity of proposed lagoon inflow and the control site: The seagrasses, macroalgae, benthic infauna, and phytoplankton that occur in the estuary in the area of proposed inflow withstand tremendous fluctuations of salinity, temperature, and other water quality measures. The organisms found here are euryhaline and eurythermal, meaning they can withstand relatively large fluctuations in salinity and temperature, in contrast to organisms found in offshore coastal environments, which may be restricted to a narrow range of salinities and temperatures.

Seagrasses, rooted algae, and drift algae: Key findings include confirmation of seagrass presence in the area, namely the shoal grass *Halodule wrightii* dominates in the northern IRL and all sampled transects. Coverage was most abundant in Phase 1 summer, ranging from 0–9% and 0–6% at BRS (control site) and BRN (proposed inflow site), respectively. Also present is the rooted macroalgae *Caulerpa prolifera*.

Benthic Fauna: At least 105 species are confirmed as part of the benthic infaunal community at the proposed inflow and control sites. Of these species, 7 polychaetes, 4 amphipods, 1 ostracod,

1 sipunculan, 1 phoronid, 2 gastropods, and 3 bivalves were nearly universally present at both locations throughout all seasons and years. Overall infaunal densities ranged from 1.9-4.0 x 10^4 organisms m^{-2} in Phase 1, and were approached 1.5 x 10^5 organisms m^{-2} Phase 2 near the proposed inflow site.

Phytoplankton: A total of 62 diatom species, 16 dinoflagellate species, and a dozen other algal species are confirmed as part of the phytoplankton community at the proposed inflow and control sites. Of these species, 8 species of diatoms and 2 species of dinoflagellates were present at both locations during most seasons and years. One species of observed diatom and 3 species of observed dinoflagellates are known to produce toxins and contribute to HABs in other estuaries. The most abundant phytoplankton were neither diatoms nor dinoflagellates, but non-cyanobacterial nanoplankton-sized flagellated cells reaching densities as high as $7x10^8$ cells L^{-1} (near the proposed inflow site at BRN, in fall 2020). Cyanobacteria reached peak densities as high as $5x10^7$ cells L^{-1} (also at BRN in fall 2020).

Environmental Factors Dominating the Ecosystem: Principle components analyses have suggested that sediment conditions (percent organic content, percent silt-clay content, percent water content) and water column conditions (bottom water DO).

3.6 Conclusions and Recommended Next Steps

Most estuarine animals tolerate fluctuations and relative extremes in temperatures, salinities, turbidity, nutrients, and pollutants. By comparison, coastal ocean conditions are relatively constant and fall well within the ranges of estuarine organism tolerances. It seems unlikely, therefore, that enhanced inflow will shape the abiotic environment in such a way as to directly harm or displace estuarine organisms. However, indirect impacts on the estuarine community due to biotic factors, such as predation by, or competition with, organisms from the coastal ecosystem, are harder to predict. Reliable evaluation of the biological impacts of restored inflow will be best accomplished through a pilot project of modest scope where biological responses are carefully monitored. This might be an ecologically risky undertaking if the two ecosystems (IRL estuary and coastal ocean) were isolated hydrodynamically and migration between populations on either side of the barrier island was not possible. However, given that (1) the northern IRL estuary has been connected to the coastal ocean via inlets in the past, (2) the Port Canaveral shipping locks already provide a limited hydrodynamic connection and migration opportunity, and (3) the proposed pumping project is projected to change water quality only minimally in the immediate region of inflow, it would seem a reasonable proposition to conduct a cautious inflow pilot project to document small-scale ecosystem changes. This would allow a more confident projection of the likely effects of a full-scale inflow restoration.

Inflow initiation or restoration projects for mitigating impaired estuaries have been carried out in other locations, and some have been successful from the perspective of enhanced fisheries or reduced HABs. The Maketu Estuary of New Zealand was restored to a century-old riparian flow pattern in 2019 to restore collapsing fisheries for indigenous Māori tribes. This restoration is ongoing but is showing success in clearing sediments and increasing fishery populations (K.B. Johnson, *unpublished*). A restored tidal exchange in western Australia reduced eutrophication and drift algae and increased larger pelagic fish (Potter et al., 2016). Multiple projects have had success in reducing HABs in estuaries through hydrological ecosystem engineering (summarized in Elliott et al., 2016). In other cases, storms may create accidental inlets with positive water quality impacts, and such was the outcome with Hurricane Sandy, where clam growth showed improvement after the breach (Gobler et al., 2019).

Literature suggests that IRL species in the area of inflow may have minimal direct impacts from an influx of coastal water. First, species present in estuaries are frequently euryhaline and eurythermal, meaning they can withstand relatively large fluctuations in salinity and temperature compared to ocean species. For instance, fish are among the most motile of estuarine populations, yet, even if they have tidal migration, an enhanced ability to osmoregulate in changing conditions is required (Allen et al., 2006). The pattern of estuarine species having wider ranges of tolerances for abiotic environmental conditions is found throughout disparate taxonomic groups. Additional examples include estuarine molluscs, which must be adapted to extreme fluctuations of salinity and pollutants (Levinton et al., 2011). Estuarine phytoplankton have a wider salinity tolerance than oceanic phytoplankton, and, as one might predict, coastal phytoplankton are intermediate in their tolerance (Brand, 1984). Additional information easing some concerns about inflow impacts on estuarine species includes the existing ocean connection through the Port Canaveral Lock and subtlety of projected changes due to restoring IRL inflow (based on Dr. Gary Zarillo's hydrodynamic model, Task 1, Modeling and Engineering). The lock, located in the northern BRL, opens to vessel passage an average of 48 times daily, and water levels can change by 3 to 4 feet as water moves from the ocean/port to the estuary (Berman, 2019). Thus, there is already some degree of coastal influence in the northern BRL. With the open lock comes the opportunity for migration, larval transport, and gene flow between coastal and estuarine populations. Diatoms may be transported with water, or on the boats themselves (Sweat et al., 2017). However, indirect impacts of modest inflow may impact the estuarine ecosystem. These potentially include the possibility of new predators and competitors being introduced into the system, or a shift in existing community balance. Continued biological monitoring throughout a pilot inflow project is critical for documenting both predicted and unanticipated changes.

It is critically important that impacts on the ecosystem and numerous key species be documented through a small-scale pilot project before implementing anything larger. However, extensive ecosystem and biological measurements during and after a pilot project will reveal little without baseline data for comparison. The data presented herein about IRL populations and ecosystem are a good start on the essential baseline for successful project monitoring. Monitoring thus far encompasses nearly two years of population dynamics in seagrasses, benthic infauna, phytoplankton, fishes, and eDNA surveys. As we mark time waiting for the possible start of a pilot inflow study, continued baseline monitoring will help eliminate the uncertainty created by poorly understood seasonal and annual changes. Then it may be possible to identify major responses of pilot inflow without confusion over other sources of change.

Recommended Next Steps:

1. Obtain ecological permits for an inflow pilot study, identify a state agency to manage the pilot study, and implement the pilot study. Timeline: permits may take approximately 1 year, and then a pilot inflow study of 1–2 years can be undertaken.
2. In the meantime, continue monitoring seagrasses for baseline data to reveal seasonal and annual patterns of variability. It is critical that seagrass monitoring continue throughout any inflow pilot study to document how seagrasses around the inflow respond to environmental and water quality changes contrasted with seagrass data at the control site. Ongoing monitoring is critical for seagrasses because their disappearance is at the heart of the estuary's decline. An additional year of pre-inflow monitoring during the permitting process is recommended, along with monitoring during pilot inflow and then for at least one year after inflow. This will allow for data collected in the year after completion of the pilot project to be compared to three years of pre-inflow data, where much of the seasonal variation can be accounted for to better reveal treatment effects.

3. Continue monitoring benthic fauna before, during, and after the implementation of a pilot RLI project so that community changes due to inflow-driven environmental shifts can be documented and understood. An additional year of pre-inflow monitoring during the permitting process is recommended, along with monitoring during pilot inflow and then for at least one year after inflow. This will allow for data collected in the year after pilot project completion to be compared to three years of pre-inflow data, with much seasonal variation accounted for to better reveal treatment effects.
4. Continue monitoring phytoplankton and potentially harmful algal species before, during, and after the implementation of a pilot RLI project so that community changes due to inflow-driven environmental shifts can be documented and understood. Ongoing monitoring is critical for phytoplankton, because the community includes potential HAB species, which have been at the heart of problems plaguing the lagoon, such as shading of seagrasses, muck inundation, and fish kills. An additional year of pre-inflow monitoring during the permitting process is recommended, along with monitoring during pilot inflow and then for at least one year after inflow. This will allow for data collected in the year after pilot project completion to be compared to three years of pre-inflow data, with much seasonal variation accounted for to better reveal treatment effects.

4 References

Abbott, R.T. and Morris, P.A. 1995. A Field Guide to Shells: Atlantic and Gulf Coasts and the West Indies. New York: Houghton Mifflin, 73.

Adams, D.H. and Tremain, D.M. 2000. Association of large juvenile red drum, Sciaenops ocellatus, with an estuarine creek on the Atlantic coast of Florida. Environ. Biol. Fishes 58, 183–194. https://doi.org/10.1023/A:1007614930445.

Aho, K., Derryberry, D., and Peterson, T. 2014. Model selection for ecologists: the worldviews of AIC and BIC. Ecology 95, 631–636.

Allen, L., Lokyavich, M., Cailliet, G., and M. Horn. 2006. Ch.5 Bays and Estuaries, In: The Ecolog of Marine Fishes: California and Adjacent Waters (eds: Allen, L, Pondella, D., and M. Horn). University of California Press, Berkeley. 659 pp.

Altieri, A.H. and Gedan, K.B. 2015. Climate change and dead zones. Glob. Chang. Biol. 21, 1395–1406. https://doi.org/10.1111/gcb.12754.

Anderson, M.J. 2005. Permutational multivariate analysis of variance. Department of Statistics, University of Auckland, Auckland, 26, 32-46.

Anderson, M.J. 2014. Permutational multivariate analysis of variance (PERMANOVA). Wiley statsref: statistics reference online, 1-15.

Bacheler, N.M., Paramore, L.M., Burdick, S.M., Buckel, J.A., and Hightower, J.E. 2009. Variation in movement patterns of red drum (Sciaenops ocellatus) inferred from conventional tagging and ultrasonic telemetry. Fish. Bull. 107, 405–419.

Badylak, S. and Phlips, E. J. 2004. Spatial and temporal patterns of phytoplankton composition in subtropical coastal lagoon, the Indian River Lagoon, Florida, USA. Journal of plankton research, 26(10), 1229-1247.

Bengfort, M., Feudel, U., Hilker, F.M., and Malchow, H. 2014. "Plankton blooms and patchiness generated by heterogeneous physical environments." Ecological complexity 20 (2014): 185-194.

Berman, D. 2019. Canaveral Lock at Port Canaveral to close to boaters for four months for repairs. Florida Today, 30 July 2019. https://www.floridatoday.com/story/news/2019/07/30/canaveral-lock-port-canaveral-close-four-months-repairs/1864684001/.

Berry, D. and Gutierrez, T. 2017. Evaluating the detection of hydrocarbon-degrading bacteria in 16S rRNA gene sequencing surveys. Frontiers in microbiology, 8, 896.

Blanchard, J.R. 2018. A confluence of invasion, behavioral, and theoretical ecology: what drives ephemeral metacommunity re-assembly? Florida International University. https://doi.org/10.25148/etd.FIDC006532.

Blanchard, J.R., Santos, R.O., and Rehage, J.S. 2021. Sociability interacts with temporal environmental variation to spatially structure metapopulations: A fish dispersal simulation in an ephemeral landscape. Ecol. Modell. 443. https://doi.org/https://doi.org/10.1016/j.ecolmodel.2021.109458.

Blondeau-Patissier, D., Gower, J.F.R., Dekker, A.G., Phinn, S.R., and Brando, V.E. 2014. "A review of ocean color remote sensing methods and statistical techniques for the detection, mapping and analysis of phytoplankton blooms in coastal and open oceans." Progress in oceanography 123 (2014): 123-144.

Boesch, D.F. and Diaz, R.J. 1974. New records of peracarid crustaceans from oligohaline waters of the Chesapeake Bay. Chesapeake Science 15:56-59.

Bohmann, K., Evans, A., Gilbert, M. T. P., Carvalho, G. R., Creer, S., Knapp, M., ... and De Bruyn, M. 2014. Environmental DNA for wildlife biology and biodiversity monitoring. Trends in ecology & evolution, 29(6), 358-367.

Bonte, D., Van Dyck, H., Bullock, J.M., Coulon, A., Delgado, M., Gibbs, M., Lehouck, V., Matthysen, E., Mustin, K., Saastamoinen, M., Schtickzelle, N., Stevens, V.M., Vandewoestijne, S., Baguette, M., Barton, K., Benton, T.G., Chaput-Bardy, A., Clobert, J., Dytham, C., Hovestadt, T., Meier, C.M., Palmer, S.C.F., Turlure, C., and Travis, J.M.J., 2012. Costs of dispersal. Biol. Rev. 87, 290–312. https://doi.org/10.1111/j.1469-185X.2011.00201.x.

Bousfield, E.L. 1969. New records of Gammarus (Crustacea: Amphipoda) from the Middle Atlantic Region. Chesapeake Science 10:1-17.

Bousfield, E.L. 1973. Shallow-water gammaridean Amphipoda of New England. Cornell University Press, Ithaca, New York. 312p.

Brand, L. 1984. The salinity tolerance of forty-six marine phytoplankton isolates. Estuarine, Coastal and Shelf Science, 1984, Volume 18, Issue 5.

Breier, R.E., Lalescu, C.C., Waas, D., Wilczek, M., and Mazza, M.G. 2018. "Emergence of phytoplankton patchiness at small scales in mild turbulence." Proceedings of the national academy of sciences 115, no. 48 (2018): 12112-12117.

Brunel, P., Bosse, L., and Lamarche, G. 1998. Catalogue of the marine invertebrates of the estuary and Gulf of St. Lawrence. Canadian Special Publication of Fisheries and Aquatic Sciences, 126. 405 p.

Bulthuis, D. 1987. Effects of temperature on photosynthesis and growth of seagrasses. Aquatic Botany. 27: 27–40. doi:10.1016/0304-3770(87)90084-2.

Callahan, B.J., McMurdie, P. J., and Holmes, S. P. 2017. Exact sequence variants should replace operational taxonomic units in marker-gene data analysis. The ISME journal, 11(12), 2639-2643.

Camp, D.K. 1998. "Checklist of shallow-water marine malacostracan Crustacea of Florida." Checklists of selected shallow-water marine invertebrates of Florida. Florida Marine Research Institute Technical Report TR-3 (1998): 123-189.

Carere, C. and Gherardi, F. 2013. Animal personalities matter for biological invasions. Trends Ecol. Evol. 28, 5–6. https://doi.org/10.1016/j.tree.2012.10.006.

Clarke, K.R. and Warwick, R.M. 2001. A further biodiversity index applicable to species lists: variation in taxonomic distinctness. Marine ecology Progress series, 216, 265-278.

Clarke, K.R., Somerfield, P.J., and Chapman, M.G. 2006. On resemblance measures for ecological studies, including taxonomic dissimilarities and a zero-adjusted Bray–Curtis coefficient for denuded assemblages. Journal of experimental marine biology and ecology, 330(1), 55-80.

Clarke, K.R., Somerfield, P.J., and Gorley, R.N. 2008. Testing of null hypotheses in exploratory community analyses: similarity profiles and biota-environment linkage. Journal of experimental marine biology and ecology, 366(1-2), 56-69.

Cochrane, K., De Young, C., Soto, D., and Bahri, T. 2009. Climate change implications for fisheries and aquaculture: Overview of current scientific knowledge.

Colwell, R.K. and Coddington, J.A. 1994. Estimating terrestrial biodiversity through extrapolation. Philos Trans R Soc London B-Biol Sci 345: 101-118.

Cooksey, C. and Hyland, J. 2007. Sediment quality of the Lower St. Johns River, Florida: An integrative assessment of benthic fauna and general characteristics. Marine Pollution Bulletin 54:9–21.

Cruaud, P., Rasplus, J.Y., Rodriguez, L.J., and Cruaud, A. 2017. High-throughput sequencing of multiple amplicons for barcoding and integrative taxonomy. Scientific reports, 7(1), 1-12.

Dawes C.J., Hanisak D., and Kenworthy, J.W. 1995. Seagrass biodiversity in the Indian River Lagoon. Bull Mar Sci 57: 59-66.

Deagle, B.E., Gales, N.J., Evans, K., Jarman, S.N., Robinson, S., Trebilco, R., and Hindell, M.A. 2007. Studying seabird diet through genetic analysis of faeces: a case study on macaroni penguins (Eudyptes chrysolophus). PLoS One, 2(9), e831.

Dutka-Gianelli, J., Taylor, R., Nagid, E., Whittington, J., and Johnson, K., 2011. Habitat Utilization and Resource Partitioning of Apex Predators in Coastal Rivers of Southeast Florida, Library. https://doi.org/FWRI Library No. F2771-07-11-F.

Eble, J.A., Daly-Engel, T.S., DiBattista, J.D., Koziol, A., and Gaither, M.R. 2020. Marine environmental DNA: Approaches, applications, and opportunities. Advances in Marine Biology, 86(1), 141-169.

Elliott, M., Mander, L., Mazik, K., Simenstad, C., Valesini, F., Whitfield, A., and Wolanski, E. 2016. Ecoengineering with ecohydrology: successes and failures in estuarine restoration. Estuarine, Coastal and Shelf Science, 176, 12-35.

Felder, D.L., and Camp, D.K. 2009. eds. Gulf of Mexico origin, waters, and biota: Biodiversity. Texas A&M University Press.

Feyrer, F., Cloern, J.E., Brown, L.R., Fish, M.A., Hieb, K.A., and Baxter, R.D. 2015. Estuarine fish communities respond to climate variability over both river and ocean basins. Glob. Chang. Biol. 21, 3608–3619. https://doi.org/10.1111/gcb.12969.

Ficetola, G.F., Taberlet, P., and Coissac, E. 2016. How to limit false positives in environmental DNA and metabarcoding?

Florida Tech. 2020. Restore Lagoon Inflow Research (Phase 1) Summary Report.

Flanagan, A.M., Flood, R.D., Frisk, M.G., Garza, C.D., Lopez, G.R., et al. 2018. The relationship between observational scale and explained variance in benthic communities. PLoS One; San Francisco Vol. 13, Iss. 1, (Jan 2018): e0189313. DOI:10.1371/journal.pone.0189313.

Franz, D.R. "Development and metamorphosis of the gastropod Acteocina canaliculata (Say)." Transactions of the American Microscopical Society (1971): 174-182.

Fredette, T.J. and Diaz, R.J. 1986. Life history of Gammarus mucronatus Say (Amphipoda: Gammaridae) in warm temperate estuarine habitats, York River, Virginia. Journal of Crustacean Biology 6:57-78.

Froese, R., Palomares, M.L.D., and Pauly, D. 1992. Draft user's manual of FishBase, a biological database on fish. ICLARM Softw.

Froese, R. and Pauly, D., 2020. FishBase [WWW Document]. World Wide Web Electron. Publ. URL www.fishbase.org.

FWRI. 2009. Fisheries-Independent Monitoring Program Procedure Manual.

Gallardo, B., Gascón, S., Quintana, X., and Comín, F. A. 2011. How to choose a biodiversity indicator–Redundancy and complementarity of biodiversity metrics in a freshwater ecosystem. Ecological indicators, 11(5), 1177-1184.

Gianuca, A. T., S. A. J. Declerck, M. W. Cadotte, C. Souffreau, T. De Bie, and L. De Meester. 2016. Integrating trait and phylogenetic distances to assess scale-dependent community assembly processes. Ecography:1–11.

Gilmore, R.G., Donohoe, C.J., Cooke, D.W., and Herrema, D.J. 1981. Fishes of the Indian River Lagoon and adjacent waters, Florida. Harbor Branch Foundation. Inc., Tech. Rpt, (41), 1-36.

Gilmore, R.G. 1995. Environmental and Biogeographic Factors Influencing Ichthyofaunal Diversity: Indian River Lagoon. Bull. Mar. Sci. 57, 153–170.

Giovannoni, S.J. and Vergin, K.L. 2012. "Seasonality in ocean microbial communities." Science 335, no. 6069 (2012): 671-676.

Glibert, P.M., Dugdale, R.C., Wilkerson, F., Parker, A.E., Alexander, J., Antell, E., Blaser, S., Johnson, A., Lee, J., Lee, T., Murasko, S., and Strong, S. 2014. Major - but rare - spring blooms in 2014 in San Francisco Bay Delta, California, a result of the long-term drought, increased residence time, and altered nutrient loads and forms. J. Exp. Mar. Bio. Ecol. 460, 8–18. https://doi.org/10.1016/j.jembe.2014.06.001.

Gobler, J.C. et al. 2019. Accidental ecosystem restoration? Assessing the estuary-wide impacts of a new ocean inlet created by Hurricane Sandy. Estuarine, Coastal and Shelf Science. Volume 221, 31 May 2019, Pages 132-146.

Gutierrez, M. A., Cardona, A. A., and Smee, D. L. 2010. Growth patterns of shoal grass Halodule wrightii and manatee grass Syringodium filiforme in the western Gulf of Mexico. Gulf and Caribbean Research, 22(1), 71-75.

Hansen, B.K., Bekkevold, D., Clausen, L.W., and Nielsen, E.E. 2018. The sceptical optimist: challenges and perspectives for the application of environmental DNA in marine fisheries. Fish and Fisheries, 19(5), 751-768.

Hauxwell, J., McClelland, J., Behr, P.J., and Valiela, I. 1998. Relative importance of grazing and nutrient controls of macroalgal biomass in three temperate shallow estuaries. Estuaries 21:347-360.

Henry, R.P., Garrelts, E.E., McCarty, M.M., and Towle, D.W. 2002. Differential induction of branchial carbonic anhydrase and Na+/K+ ATPase activity in the euryhaline crab, Carcinus maenas, in response to low salinity exposure. Journal of Experimental Zoology, 292(7), 595-603.

Huot, Y., Babin, M., Bruyant, F., Grob, C., Twardowski, M.S., and Claustre, H. 2007. Does chlorophyll a provide the best index of phytoplankton biomass for primary productivity studies? Biogeosciences Discuss. 4, 707–745.

Johnson, K.B., Turingan, R.G., Eble, J., Shenker, J., and Blanchard, J.R. 2020. Restore Lagoon Inflow Research Project (Phase 1) Task 2, Biological Monitoring.

Johnson, K.B. and Soltis, K. 2017. Larval supply and recruitment of the ivory barnacle Balanus eburneus on oyster cultch used in oyster-reef restoration. The Journal of Crustacean Biology 37(3), 243–248.

Kamerosky, A., Cho, H.J., and Morris, L. 2015. Monitoring of the 2011 super algal bloom in Indian River Lagoon, FL, USA, Using MERIS. Remote Sens. 7, 1441–1460. https://doi.org/10.3390/rs70201441.

Kelly, J.R., Levine, S.N., Buttelm L.A., Carr, K.A., Rudnick, D.T., and Morton, R.D. 1990. The effects of tributyltin within a Thalassia seagrass ecosystem. Estuaries 13:301-310.

Kennish, M.J., Haag, S.M, Sakowicz, G.P., and Durand, J.B. 2004. Benthic Macrofaunal Community Structure along a Well-Defined Salinity Gradient in the Mullica River-Great Bay Estuary. Journal of Coastal Research, suppl. Special Issue; Fort Lauderdale Vol. SI, Iss. 45: 209-226.

Kircher, M., Sawyer, S., and Meyer, M. 2012. Double indexing overcomes inaccuracies in multiplex sequencing on the Illumina platform. Nucleic acids research, 40(1), e3-e3.

Kornicker, L.S. 1967. A study of three species of Sarsiella (Ostracoda: Myodocopina). Proceedings of the United States National Museum 122(3594): 1–46, 4 pls.

Kornicker, L.S. 1986. Sarsiellidae of the Western Atlantic and Northern Gulf of Mexico, and revision of the Sarsiellinae (Ostracoda: Myodocopina).

Kroodsma, D.A., Mayorga, J., Hochberg, T., Miller, N.A., Boerder, K., Ferretti, F., Wilson, A., Bergman, B., White, T.D., Block, B.A., Woods, P., Sullivan, B., Costello, C., and Worm, B. 2018. Tracking the global footprint of fisheries. Science 359, no. 6378 (2018): 904-908.

Kuk-Dzul, J., Gold-Bouchot, G.G., and Ardisson, P-L. 2012. "Benthic infauna variability in relation to environmental factors and organic pollutants in tropical coastal lagoons from the northern Yucatan Peninsula." Marine Pollution Bulletin 64, no. 12 (2012): 2725-2733.

Kumar, G., Eble, J.E., and Gaither, M.R. 2020. A practical guide to sample preservation and pre-PCR processing of aquatic environmental DNA. Molecular ecology resources, 20(1), 29-39.

Leray, M., Yang, J.Y., Meyer, C.P., Mills, S.C., Agudelo, N., Ranwez, V., ... and Machida, R.J. 2013. A new versatile primer set targeting a short fragment of the mitochondrial COI region for metabarcoding metazoan diversity: application for characterizing coral reef fish gut contents. Frontiers in zoology, 10(1), 1-14.

Levinton, M.D., Ralston, D., Starke, A., and Allam, B. 2011. Climate change, precipitation and impacts on an estuarine refuge from disease. PLoS One, 6 (2011), p. e18849.

Li, F., Zhou, Y., Zhang, X., Tang, J., Yang, Q., Zhang, Y., ... and Zhu, F. 2020. SSizer: determining the sample sufficiency for comparative biological study. Journal of molecular biology, 432(11), 3411-3421.

Love, O.P., McGowan, P.O., and Sheriff, M.J. 2013. Maternal adversity and ecological stressors in natural populations: the role of stress axis programming in individuals, with implications for populations and communities. Funct. Ecol. 27, 81–92. https://doi.org/10.1111/j.1365-2435.2012.02040.x.

Lowerre-Barbieri, S.K., Walters, S., Bickford, J., Cooper, W., and Muller, R. 2013. Site fidelity and reproductive timing at a spotted seatrout spawning aggregation site: Individual versus population scale behavior. Mar. Ecol. Prog. Ser. 481, 181–197. https://doi.org/10.3354/meps10224.

Macusi, E.D., Abreo, N.A.S., Cuenca, G.C., Ranara, C.T.M., and Deepananda, A. 2015. The Potential Impacts of Climate Change on Freshwater Fish, Fish Culture and Fishing Communities. J. Nat. Stud. 14, 1689–1699. https://doi.org/10.1017/CBO9781107415324.004.

Mason, W.T., Jr. 1998. Macrobenthic monitoring in the lower St. Johns River, Florida. Environmental Monitoring and Assessment 50:101-130.

McEwen, B.S. 1998. Stress, adaptation, and disease: Allostasis and allostatic load. Ann. New York Acad. Sciences 840, 33–44.

McEwen, B.S. 2007. Physiology and neurobiology of stress and adaptation: central role of the brain. Physiol. Rev. 87, 873–904. https://doi.org/10.1152/physrev.00041.2006.

McMillan, C. 1982. Reproductive physiology of tropical seagrasses. Aquatic Botany 14 (1982): 245-258.

Mikkelsen, P.M., Mikkelsen, P.S., and Karlen, D.J. 1995. "Molluscan biodiversity in the Indian River lagoon, Florida." Bulletin of Marine Science 57, no. 1 (1995): 94-127.

Morgan, M.D. and Kitting, C.L. 1984. Productivity and utilization of the seagrass Halodule wrightii and its attached epiphytes. Limnology 29:1066-1076.

Morris, L. J., Hall, L. M., Miller, J. D., Lasi, M. A., Virnstein, R., and Jacoby, C. 2021. Diversity and distribution of seagrasses as related to salinity, temperature, and availability of light in the Indian River Lagoon, Florida. Florida Scientist, 84, 119-137.

Morris, L.J., Hall, L.M., and Virnstein, R.W. 2001. Field guide for fixed seagrass transect monitoring in the Indian River Lagoon. St. Johns River Water Management District, Palatka, Florida.

Mouillot, D., Gaillard, S., Aliaume, C., Verlaque, M., Belsher, T., Troussellier, M., and Do Chi, T. 2005. Ability of taxonomic diversity indices to discriminate coastal lagoon environments based on macrophyte communities. Ecological Indicators, 5(1), 1-17.

Moulton, D.L., Dance, M.A., Williams, J.A., Sluis, M.Z., Stunz, G.W., and Rooker, J.R. 2017. Habitat Partitioning and Seasonal Movement of Red Drum and Spotted Seatrout. Estuaries and Coasts 40, 905–916. https://doi.org/10.1007/s12237-016-0189-7.

Nelson, W.G. 1979. Experimental studies of selective predation on amphipods: Consequences for amphipod distribution and abundance. Journal of Experimental Marine Biology and Ecology 38:225-245.

Nelson, W.G. 1980. The biology of eelgrass (Zostera marina L.) amphipods. Crustaceana 39:59-89.

Nelson, W.G. 1995. Amphipod crustaceans of the Indian River Lagoon: current status and threats to biodiversity. Bulletin of Marine Science 57:143-152.

NOAA National Benthic Inventory: https://products.coastalscience.noaa.gov/nbi/.

Paperno, R. 2002. Age-0 Spot (Leiostomus xanthurus) from Two Estuaries Along Central Florida's East Coast: Comparisons of the Timing of Recruitment, Seasonal Changes in Abundance, and Rates of Growth and Mortality. Florida Scientist 65:85–99.

Paperno, R., Mille, K. J., and Kadison, E. 2001. Patterns in species composition of fish and selected invertebrate assemblages in estuarine subregions near Ponce de Leon Inlet, Florida. Estuarine, Coastal and Shelf Science, 52(1), 117-130.

Phillips, R.C. 1960. Observations on the ecology and distribution of the Florida seagrasses. Professional Paper Series No. 2. Florida State Board Conserv Mar Lab, St. Petersburg, FL.

Phlips, E. J., Badylak, S., Christman, M., Wolny, J., Brame, J., Garland, J., ... and Steidinger, K. 2011. Scales of temporal and spatial variability in the distribution of harmful algae species in the Indian River Lagoon, Florida, USA. Harmful Algae, 10(3), 277-290.

R Core, T. 2012. R: A language and environment for statistical computing. R Foundation for Statistical Computing, Vienna, Austria.

Reyier, E.A., Lowers, R.H., Scheidt, D.M., and Adams, D.H. 2011. Movement patterns of adult red drum, Sciaenops ocellatus, in shallow Florida lagoons as inferred through autonomous acoustic telemetry. Environ. Biol. Fishes 90, 343–360. https://doi.org/10.1007/s10641-010-9745-3.

Reyier, E.A., Scheidt, D.M., Stolen, E.D., Lowers, R.H., Holloway-Adkins, K.G., and Ahr, B.J. 2020. Residency and dispersal of three sportfish species from a coastal marine reserve: Insights from a regional-scale acoustic telemetry network. Glob. Ecol. Conserv. 23, e01057. https://doi.org/10.1016/j.gecco.2020.e01057.

Rosenberg, G., Moretzsohn, F., García, E. F. 2009. Gastropoda (Mollusca) of the Gulf of Mexico, Pp. 579–699 in: Felder, D.L. and D.K. Camp (eds.), Gulf of Mexico–Origins, Waters, and Biota. Texas A&M Press, College Station, Texas.

Ruiz, G., Fofonoff, P., Steves, B., and Dahlstrom, A. 2011. "Marine crustacean invasions in North America: a synthesis of historical records and documented impacts." In in the Wrong Place-Alien Marine Crustaceans: Distribution, Biology and Impacts, pp. 215-250. Springer, Dordrecht.

Ruppert, K.M., Kline, R.J., and Rahman, M. S. 2019. Past, present, and future perspectives of environmental DNA (eDNA) metabarcoding: A systematic review in methods, monitoring, and applications of global eDNA. Global Ecology and Conservation, 17, e00547.

Shannon, C.E. 2001. A mathematical theory of communication. ACM SIGMOBILE mobile computing and communications review, 5(1), 3-55.

Shen, W. and Xiong, J. 2019. TaxonKit: a cross-platform and efficient NCBI taxonomy toolkit. Biorxiv, 513523.

Sigua, G.C., Steward, J.S., and Tweedale, W.A. 2000. Water-quality monitoring and biological integrity assessment in the Indian River Lagoon, Florida: Status, trends, and loadings (1988–1994). Environmental Management, 25(2), 199-209.

Sih, A., Cote, J., Evans, M., Fogarty, S., and Pruitt, J. 2012. Ecological implications of behavioural syndromes. Ecol. Lett. 15, 278–89. https://doi.org/10.1111/j.1461-0248.2011.01731.x.

Smokorowski, K.E. and Randall, R.G. 2017. Cautions on using the Before-After-Control-Impact design in environmental effects monitoring programs. Facets, 2(1), 212-232.

Snelson Jr, F.F. 1983. Ichthyofauna of the northern part of the Indian River Lagoon System, Florida. Florida Scientist, 187-206.

Spiegel, O., Leu, S.T., Bull, C.M., and Sih, A. 2017. What's your move? Movement as a link between personality and spatial dynamics in animal populations. Ecol. Lett. 20, 3–18. https://doi.org/10.1111/ele.12708.

Stoner, A.W. 1979. Species-specific predation on amphipod Crustacea by the pinfish Lagodon rhomboides: Mediation by macrophyte standing crop. Marine Biology 55:201-207.

Stoner, A.W. 1983. Distributional ecology of amphipods and tanaidaceans associated with three sea grass species. Journal of Crustacean Biology 3:505-518.

Stunz, G.W., Levin, P.S., and Minello, T.J. 2001. Selection of estuarine nursery habitats by wild-caught and hatchery-reared juvenile red drum in laboratory mesocosms. Environ. Biol. Fishes 61, 305–313.

Sweat, L.H., Stephens, M., and Reed, S.A. 2021. Insights from 15 years of benthic infaunal monitoring in a coastal lagoon system. Florida Scientist, 84, 147-161.

Sweat, L.H., Swain, G., Hunsucker, K., and Johnson, K.B. 2017. Transported biofilms and their influence on subsequent macrofouling colonization. Biofouling 33(5):433-449.

Teller, B.J., Campbell, C., and Shea, K. 2014. Dispersal under duress : Can stress enhance the performance of a passively dispersed species? Ecology 95, 2694–2698.

Tetra Tech. 2016. Save Our Lagoon Project Plan for Brevard County, Florida. Contract #: 260070-14-009. Prepared by Tetra Tech, Inc. and Closewaters, LLC. 82 pp.

Tremain, D.M. and Adams, D.H. 1995. Seasonal variations in species diversity, abundance, and composition of fish communities in the northern Indian River Lagoon, Florida. Bulletin of Marine Science, 57(1), 171-192.

Tremain, D.M., Harnden, C.W., and Adams, D.H., 2004. Multidirectional movements of sportfish species between an estuarine no-take zone and surrounding waters of the Indian River Lagoon, Florida. Fish. Bull. 102, 533–544.

Troast, B., Paperno, R., and Cook, G.S., 2020. Multidecadal shifts in fish community diversity across a dynamic biogeographic transition zone. Divers. Distrib. 26, 93–107. https://doi.org/10.1111/ddi.13000.

Trudnowska, E., Gluchowska, M., Beszczynska-Möller, A., Blachowiak-Samolyk, K., and Kwasniewski, S. 2016. "Plankton patchiness in the Polar Front region of the West Spitsbergen Shelf." Marine Ecology Progress Series 560 (2016): 1-18.

Tweedley, J.R., Warwick, R.M., Hallett, C.S., and Potter, I.C. 2017. Fish-based indicators of estuarine condition that do not require reference data. Estuarine, Coastal and Shelf Science, 191, 209-220.

Ugland, K.I., Gray, J.S., and Ellingsen, K.E. 2003. The species–accumulation curve and estimation of species richness. Journal of Animal Ecology, 72(5), 888-897.

Underwood, A.J. 1994. On beyond BACI: sampling designs that might reliably detect environmental disturbances. Ecological applications, 4(1), 3-15.

van Maren, M.J. 1978. Distribution and ecology of Gammarus tigrinus Sexton, 1939 and some other amphipod Crustacea near Beaufort (NC, USA). Bijdragen tot de Dierkunde 48:46-56.

Virnstein, R.W. 1990. The large spatial and temporal biological variability of Indian River Lagoon. Florida Scientist, 249-256.

Virnstein, R.W. and Morris, L.J. 1996. Seagrass preservation and restoration: a diagnostic plan for the Indian River Lagoon. St. Johns River Water Management District.

Warwick, R.M. and Clarke, K.R. 1995. New\'biodiversity\'measures reveal a decrease in taxonomic distinctness with increasing stress. Marine ecology progress series, 129, 301-305.

Wassick, A., Hunsucker, K., and Swain, G. 2021. Does the benthic invertebrate community reflect disturbances in the central Indian River Lagoon?. Florida Scientist, 84, 162-172.

Watling, L. and Maurer, D. 1972. Marine shallow water amphipods of the Delaware Bay area, USA. Crustaceana, Suppl. 3:251-266.

West, K.M., Stat, M., Harvey, E.S., Skepper, C.L., DiBattista, J.D., Richards, Z.T., ... and Bunce, M. 2020. eDNA metabarcoding survey reveals fine-scale coral reef community variation across a remote, tropical island ecosystem. Molecular ecology, 29(6), 1069-1086.

Zar, J.H. 1999. Biostatistical Analysis, fourth. ed, Prentice Hall New Jersey. Pearson education.

Zieman, J.C. 1982. Ecology of the seagrasses of south Florida: a community profile. No. FWS/OBS-82/25. Virginia Univ: Charlottesville, VA (USA). Dept Environ Sci.

Zimmerman, R., Gibson, R., and Harrington, J. 1979. Herbivory among gammaridean amphipods from a Florida seagrass community. Marine Biology 54:41-47.

Appendix D Permitting Information

Restore Lagoon Inflow Research (Phase 2)
Permitting Narrative

PREPARED FOR

Florida Institute of Technology
150 West University Boulevard
Melbourne, FL 32901

PREPARED BY

Tetra Tech, Inc.
11 Riverside Drive, Suite 204
Cocoa, FL 32922

September 2021

Table of Contents

List of Figures

List of Acronyms

BRL	Banana River Lagoon
FEMA	Federal Emergency Management Administration
IRL	Indian River Lagoon
USACE	United States Army Corps of Engineers

1 Introduction

This is a research project designed to evaluate the effects of providing ocean inflow to the Indian River Lagoon (IRL) on water quality, biology, and geochemistry. The project site is located at the Canaveral Lock, in Cape Canaveral, Florida, and will be constructed on United States Army Corps of Engineers (USACE) and Canaveral Port Authority land located in Sections 9, Township 24, Range 37 at 1000 Mullet Road Unit Locks in Cape Canaveral, Brevard County, Florida. The proposed project area is the approximately 5-acre portion of the 92-acre locks facility. The proposed project area will be referred to as the proposed Restore Lagoon Inflow Research Project Area. See Attachment 1 Site Plan Sheets 1 and 4. The project will pump ocean water from the east side of the Canaveral Lock to a cove on the IRL side and to the south of the Lock.

Permit applications will be required for the installation of a pump and the associated intake and discharge line that will bypass the existing locks bringing seawater water from the east side of the Canaveral Lock to a cove on the IRL side and to the south of the Lock. Site Plans are provided in Attachment 1. An Environmental Resources Permit using forms A, C, and E will be required. No wetlands impacts are proposed as a part of this project, and waters of the U.S. or State Assumed Waters are affected by this project; therefore, it is assumed that USACE or Florida State 404 authorization is required. Due to the proximity of the project to the federal channel and the use of USACE land, it is assumed that USACE Section 408 authorization is also required. The contributed funds agreement template to be used to fund the USACE 408 process is provided in Attachment 2.

1.1 Current Site Conditions

The current land use in the site is undeveloped with exception of the nearby Canaveral Locks and associated operation facilities. Natural soil characteristics in the vicinity of the site are described as Canaveral-Urban Land Complex (50% Canaveral soils, 40% Urban Land, 10% soils of minor extent).

1.2 Preapplication Meetings

Preapplication meetings were held with state and federal permitting agencies and presented the conceptual project plans for the project. Meetings were held with St. Johns River Water Management District on January 8, 2021, Florida Department of Environmental Protection on March 5, 2021, and USACE on October 15, 2020 and July 1, 2021.

2 Proposed Site Development

The purpose of this application is for the design of the pump system to convey ocean water to the Banana River Lagoon (BRL) of the IRL system. The site plans located in Attachment 1 show the locations and sizes of the proposed pump and the associated system components including power supply, screen, pipe network and support, discharge revetment, and proposed site elevations.

3 Wetlands and Marine Resources

No wetlands impacts are proposed as a part of this project, and waters of the U.S. or State Assumed Waters are affected by this project; therefore, it is assumed that USACE or Florida State

404 authorization is required. A marine resources survey was completed on June 1, 2021, and the complete Marine Resource Survey Field Observation Report is provided as Attachment 3.

4 Floodplain

The proposed Restore Lagoon Inflow Research Project Area is located in Flood Zone X and AE (EL 3 or 7). The Federal Emergency Management Administration (FEMA) Flood Map in the vicinity of the site is provided as **Figure 1**.

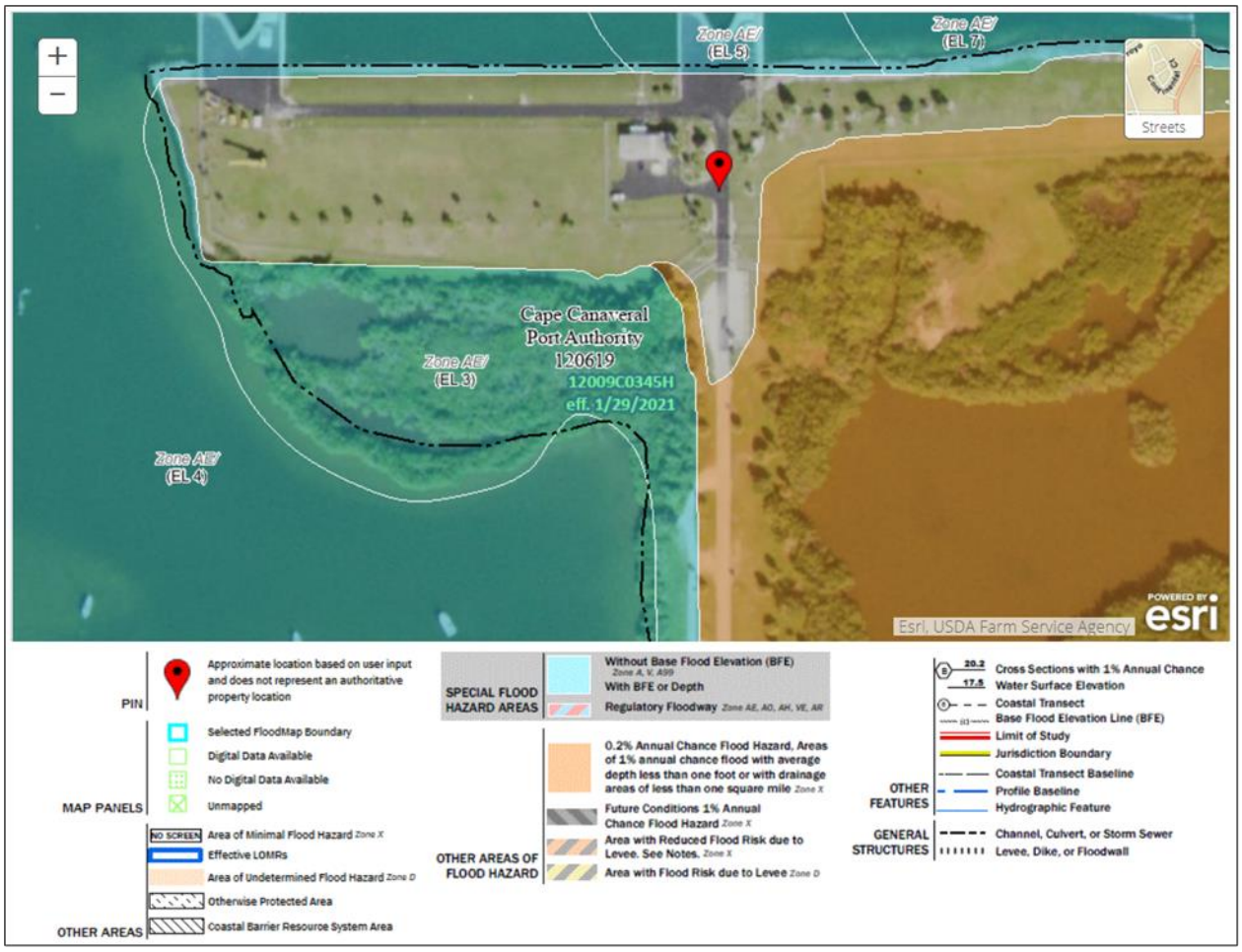

Figure 1. FEMA Flood Map

5 Construction Techniques

The contractor shall utilize best management practices during construction to prevent erosion, turbidity, and sedimentation in offsite swales or waterbodies. The contractor shall also provide a silt fence in accordance with St. Johns River Water Management District standards and specifications. An erosion and sediment control plan will be provided in the final plan set.

After construction is complete, all disturbed areas shall be neatly graded, seeded, and mulched or sodded as noted on the plans. Limited surface disturbance is anticipated from the construction.

6 System Operation and Maintenance

System operation and maintenance procedures will be established in later phases of the project. This is a research project so monitoring of biological and geochemical parameters should exceed any permitting requirements. A robust baseline dataset has been established in the vicinity of the project and reference site, which has been identified to the south, as shown on **Figure 2**. Monitoring within both the inflow and reference site will be completed to assist in determining changes are a result of inflow compared to normal fluctuations within the IRL system.

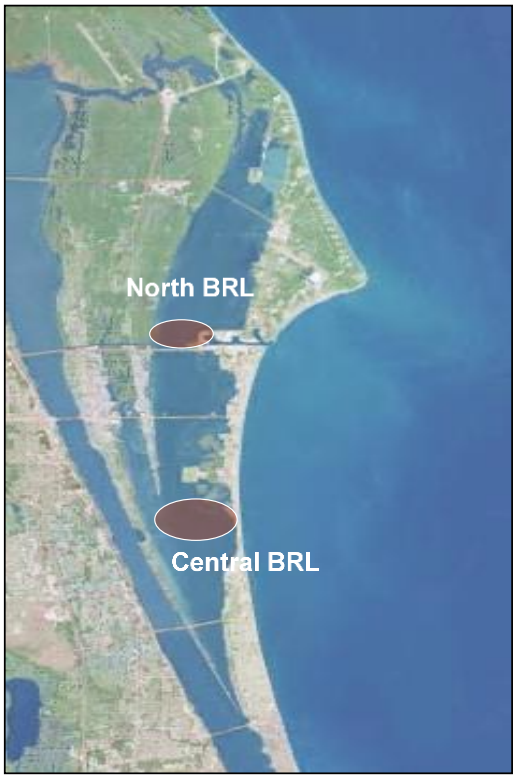

Figure 2. Proposed pilot inflow site in north BRL and reference site in central BRL

Attachment 1. 60% Design Drawings

FLORIDA INSTITUTE OF TECHNOLOGY
150 WEST UNIVERSITY BLVD.
MELBOURNE, FL
32901

TETRA TECH, INC.
11 RIVERSIDE DRIVE
SUITE 204
COCOA, FL 32940
TEL: (321) 636-6470
EXT. 6378099

RESTORE LAGOON INFLOW RESEARCH PILOT PROJECT INDIAN RIVER, FLORIDA

PROJECT NO.

VICINITY MAP

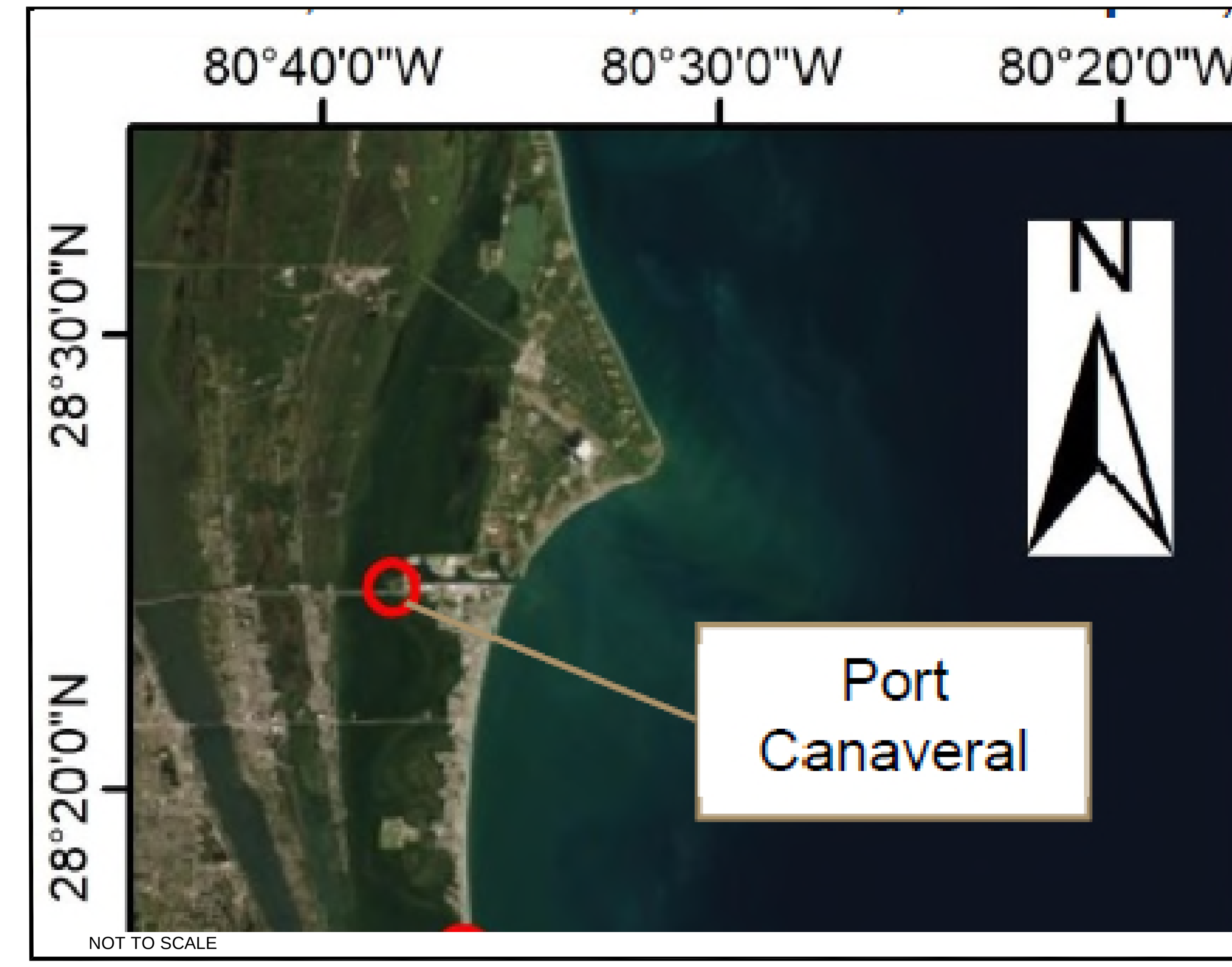

SHEET INDEX:

SHEET #	TITLE	LATEST UPDATE	REV.
1	COVER SHEET AND VICINITY MAP	09-SEPT-21	1
2	BATHYMETRY AND TOPOGRAPHY	09-SEPT-21	1
3	TIDAL DATUMS	09-SEPT-21	1
4	SITE PLAN	09-SEPT-21	1
5	DETAIL A - INTAKE PLANS	09-SEPT-21	1
6	DETAIL A1 - INTAKE ELEVATION VIEW	09-SEPT-21	1
7	DETAIL A2 - PUMP POWER UNIT	09-SEPT-21	1
8	DETAIL A3 - INTAKE SCREEN DETAILS	09-SEPT-21	1
9	DETAIL B - PIPELINE ROAD CROSSING	09-SEPT-21	1
10	DETAIL C - OUTFLOW	09-SEPT-21	1
11	BIOLOGICAL SURVEYS	09-SEPT-21	1

NOT FOR CONSTRUCTION

REV	DESCRIPTION	CHK	APP	DATE
0	FOR REVIEW ONLY	ETE	RC	06/17/21

Designed By: R. CZLAPINSKI
Drawn By: E. ERTON
Checked By: R. CZLAPINSKI
Reviewed By: R. CZLAPINSKI
Design File No. IRL_COVER SHEET 2021.DWG
Scale: As Shown

TETRA TECH
11 RIVERSIDE DRIVE
SUITE 204
COCOA, FL 32940
TEL: 321.636.6470 EXT. 6378099

RESTORE LAGOON INFLOW RESEARCH PILOT PROJECT
COVER SHEET & VICINITY MAP
CAPE CANAVERAL, FL

Sheet Reference:

Sheet 1 of 11

PLAN VIEW (NAVD 88)

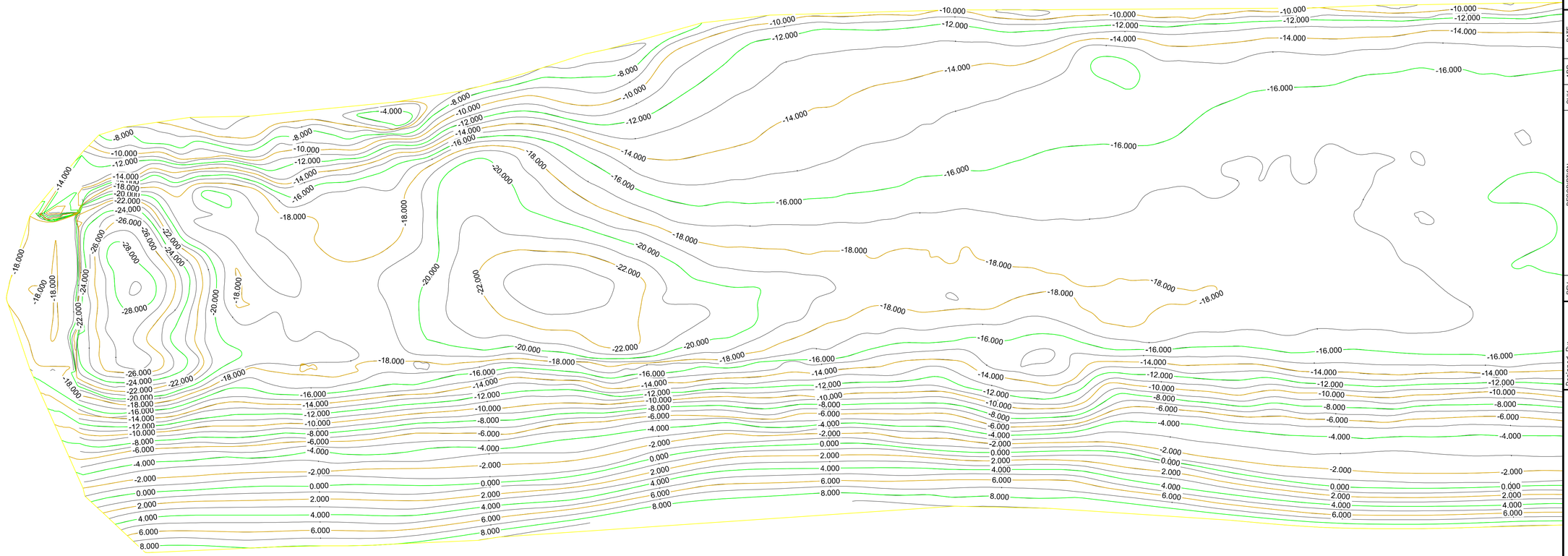

NOTE: SURVEY COMPLETED BY OCEANSIDE SOLOUTIONS ON MARCH 31, 2021

REV	DESCRIPTION	CHK	APP	DATE
0	FOR REVIEW ONLY	ETE	RC	09/09/21

Designed By: R. CZLAPINSKI
Drawn By: E. ESTEBAN
Checked By: R. CZLAPINSKI
Reviewed By: R. CZLAPINSKI
Design File No. 210331 RL INFLOW PHASE II CANAVERAL CONTOURS 1FT NAVD.DWG
Scale: As Shown

TETRA TECH
11 RIVERSIDE DRIVE
SUITE 204
COCOA, FL 32940
TEL: 321.636.6470 EXT. 6378099

RESTORE LAGOON INFLOW RESEARCH PILOT PROJECT

CAPE CANAVERAL, FL

Sheet Reference:

Sheet 2 of 11

Datums for 8721604, Trident Pier, Port Canaveral, FL

All figures in feet relative to NAVD88

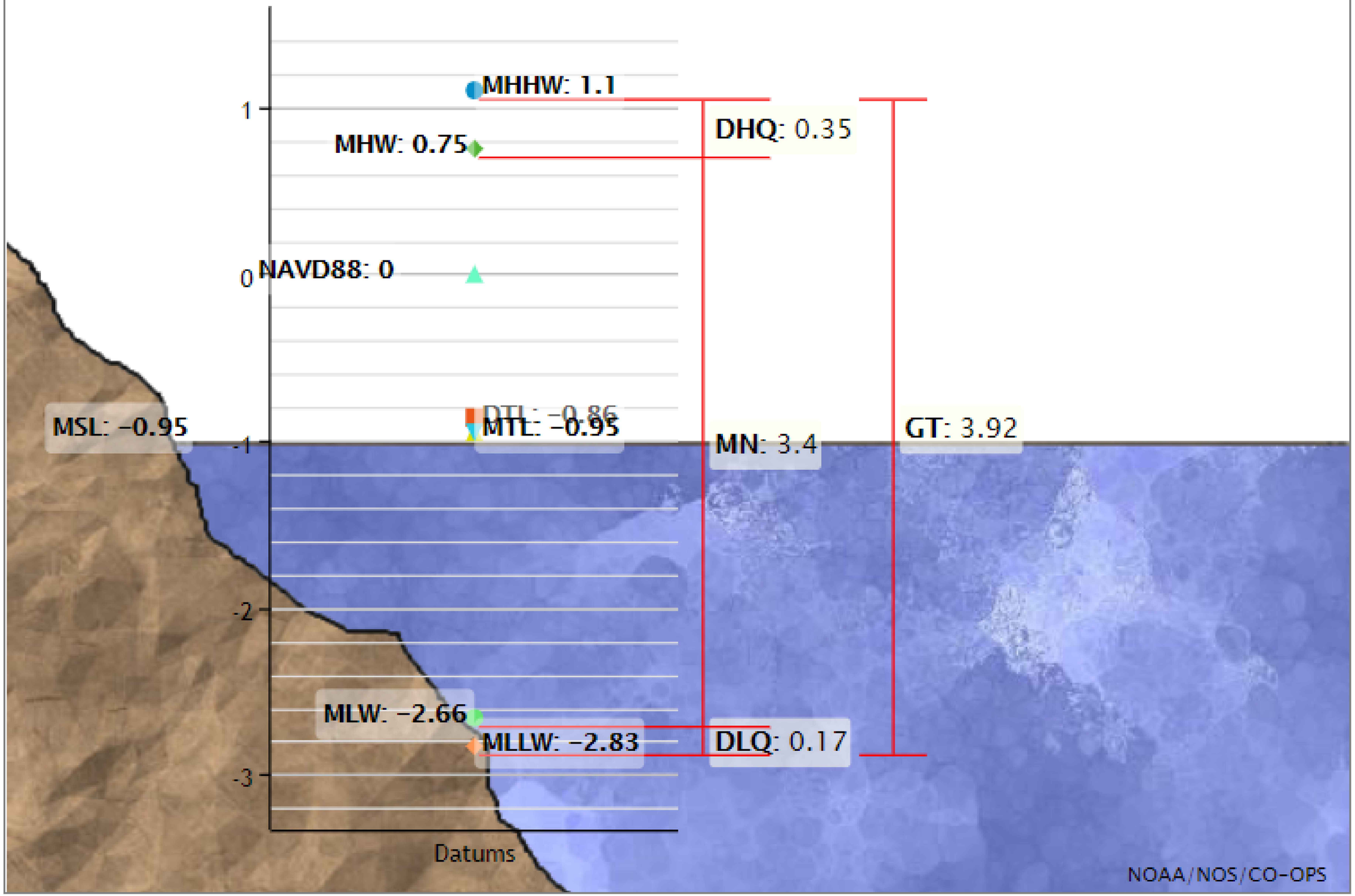

REV	DESCRIPTION	CHK	APP	DATE
0	FOR REVIEW ONLY	ETE	RC	09/09/21

Designed By: R. CZLAPINSKI
Drawn By: E. ETOYO
Checked By: R. CZLAPINSKI
Reviewed By: R. CZLAPINSKI
Design File No. INFLOW STRUCTURE SIZE HAC16.DWG
Scale: As Shown

TETRA TECH
11 RIVERSIDE DRIVE
SUITE 204
COCOA, FL 32940
TEL: 321.636.6470 EXT. 6378099

RESTORE LAGOON INFLOW RESEARCH PILOT PROJECT

CAPE CANAVERAL, FL

Sheet Reference:

Sheet 3 of 11

SITE PLAN

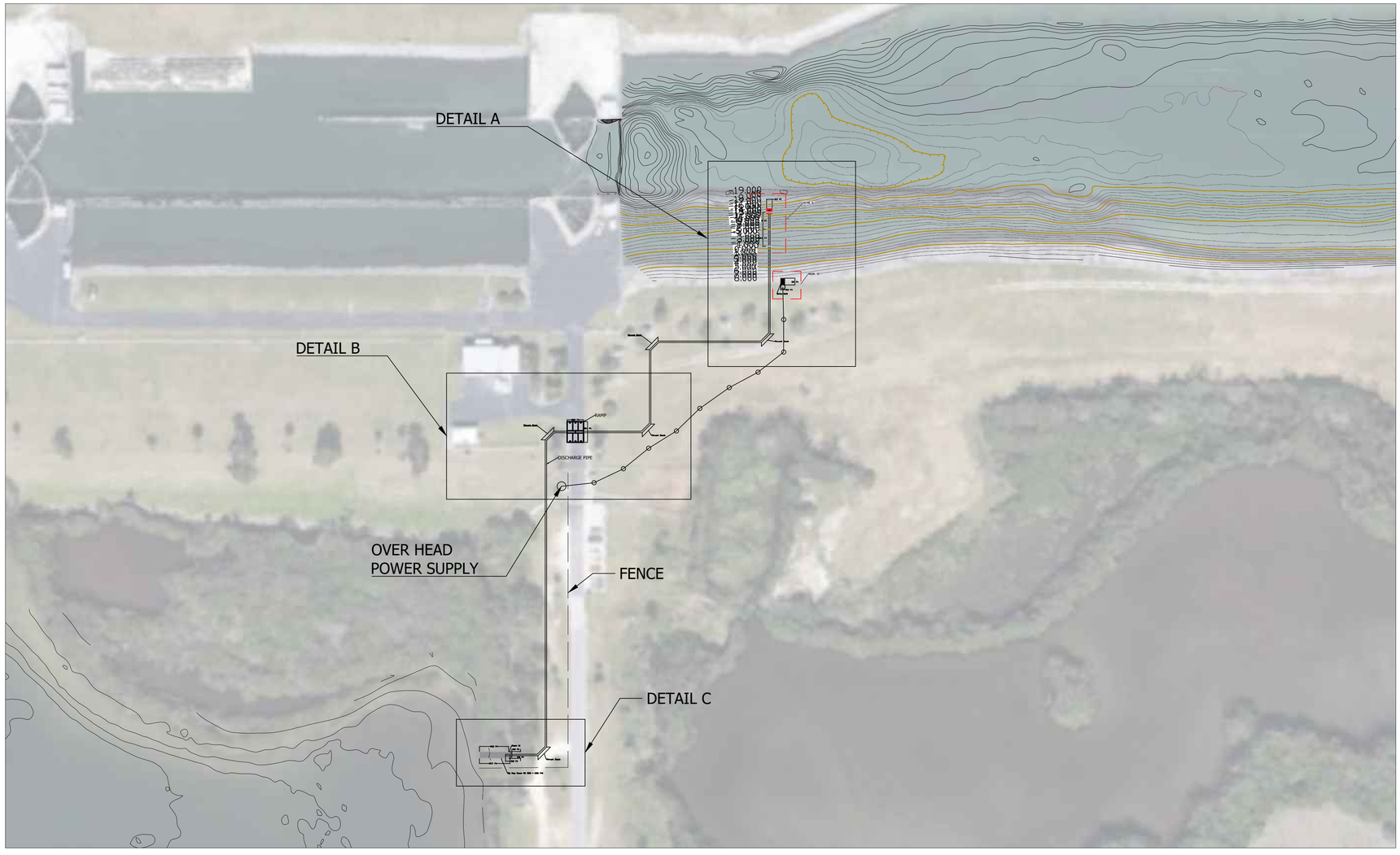

REV	DESCRIPTION	CHK	APP	DATE
0	FOR REVIEW ONLY	ETE	RC	09/09/21

Designed By: R. CZLAPINSKI
Drawn By: E. ETTON
Checked By: R. CZLAPINSKI
Reviewed By: R. CZLAPINSKI
Design File No. BLUFF MANUFACTURING RAMP.DWG
Scale: As Shown

TETRA TECH
11 RIVERSIDE DRIVE
SUITE 204
COCOA, FL 32940
TEL: 321.636.6470 EXT. 6378099

RESTORE LAGOON INFLOW RESEARCH PILOT PROJECT

CAPE CANAVERAL, FL

Sheet Reference:

DETAIL A INTAKE PLAN
(NAVD 88)

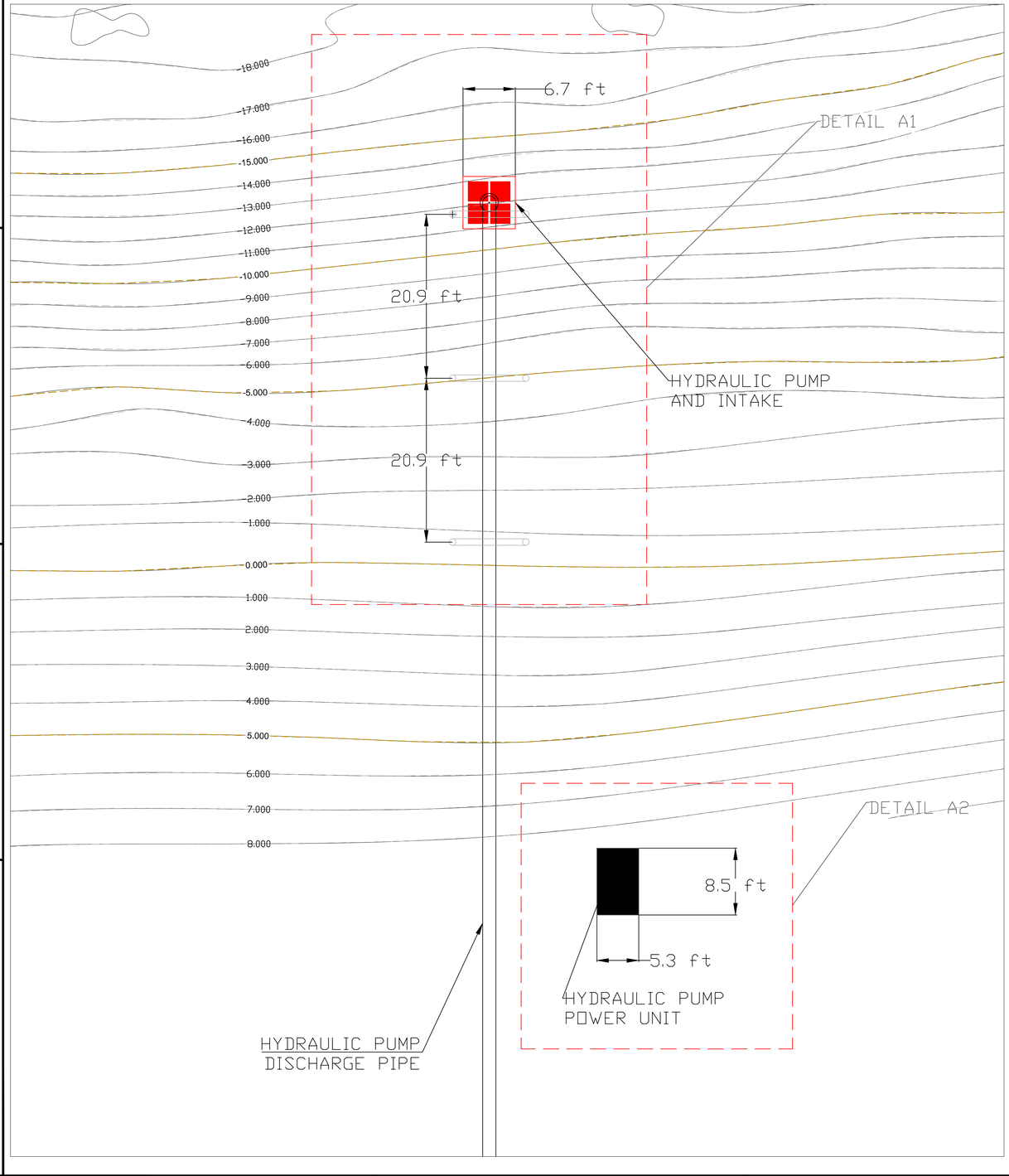

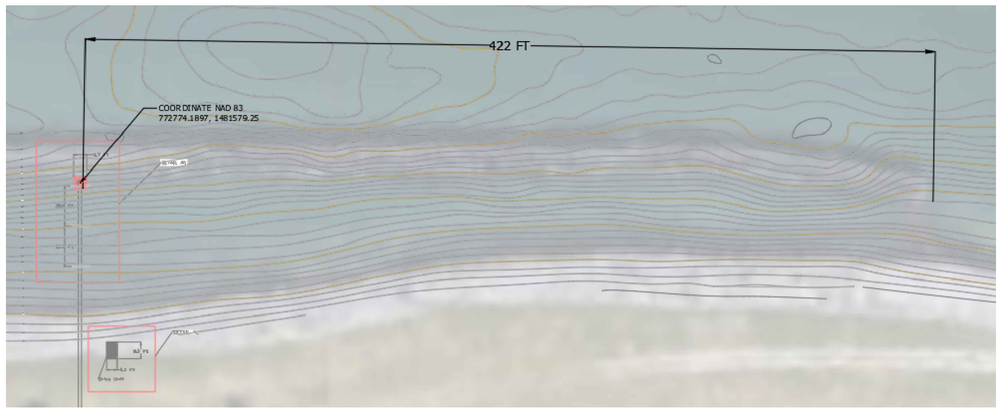

NOTE: POWERLINES NOT REPRESENTED
IN DRAWING FOR CLARITY

REV	DESCRIPTION	CHK	APP	DATE
0	FOR REVIEW ONLY	ETE	RC	09/09/21

Designed By: R. CZLAPINSKI
Drawn By: E. ERTON
Checked By: R. CZLAPINSKI
Reviewed By: R. CZLAPINSKI
Design File No. RL INFLOW PHASE II CONTOURS 1FT NAVD TOP VIEW.DWG
Scale: As Shown

TETRA TECH
11 RIVERSIDE DRIVE
SUITE 204
COCOA, FL 32940
TEL: 321.636.6470 EXT. 6378099

RESTORE LAGOON INFLOW RESEARCH PILOT PROJECT

CAPE CANAVERAL, FL

Sheet Reference:

DETAIL A1 – INTAKE ELEVATION VIEW

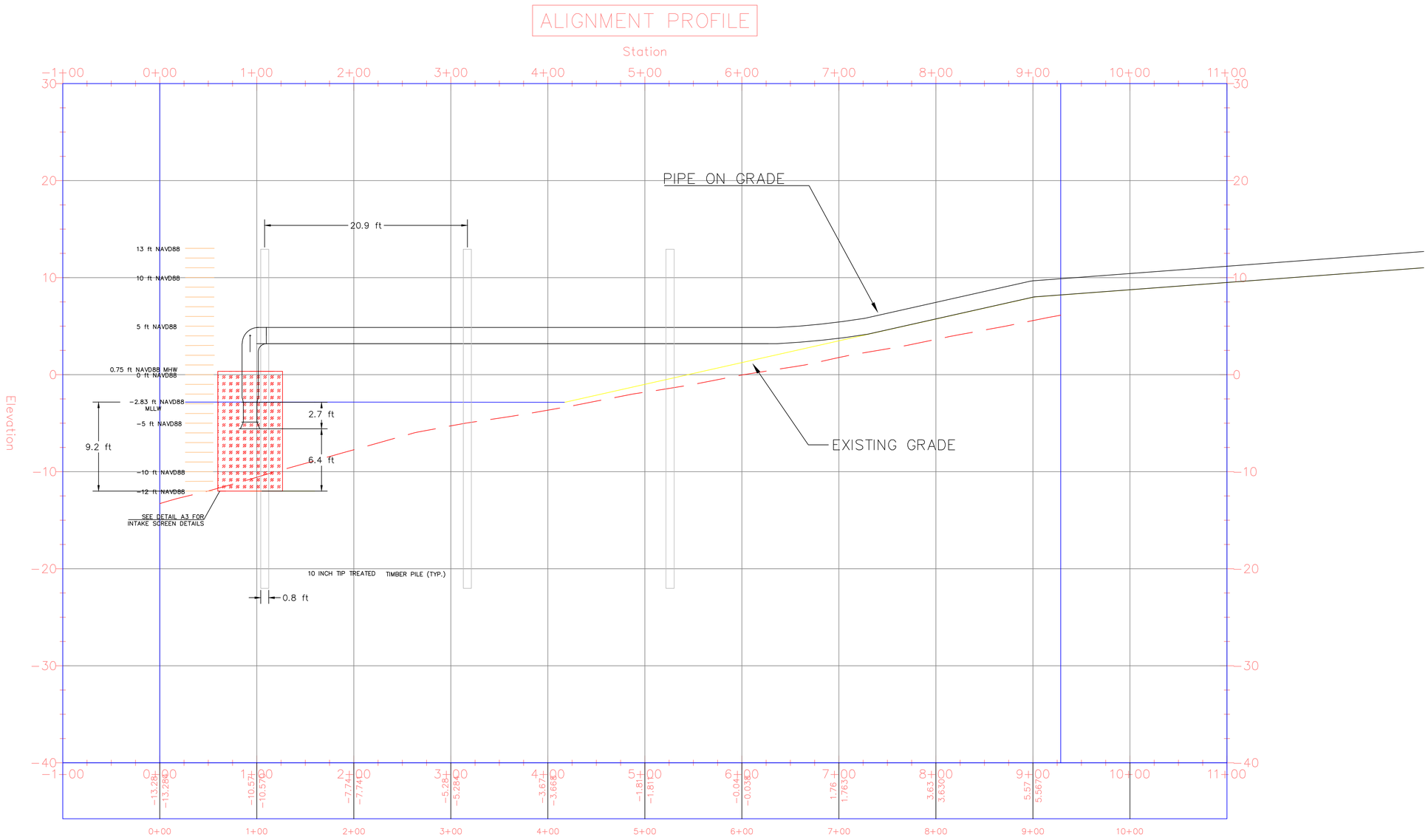

NOTE: DETAIL NOT TO SCALE

REV	DESCRIPTION	CHK	APP	DATE
0	FOR REVIEW ONLY	ETE	RC	09/09/21

Designed By: R. CZLAPINSKI
Drawn By: E. ERTOP
Checked By: R. CZLAPINSKI
Reviewed By: R. CZLAPINSKI
Design File No. INFLOW STRUCTURE SIZE HAC316.DWG
Scale: As Shown

TETRA TECH
11 RIVERSIDE DRIVE
SUITE 204
COCOA, FL 32940
TEL: 321.636.6470 EXT. 6378099

RESTORE LAGOON INFLOW RESEARCH PILOT PROJECT

CAPE CANAVERAL, FL

Sheet Reference:

DETAIL A2 – PUMP POWER UNIT

PUMP DETAILS

- MWI HYDRAFLO PUMP MODEL HAC 316
- SINGLE STAGE HYDRAULICALLY DRIVEN PUMP
- ELECTRIC POWER UNIT USING 3 PHASE 460–VOLT POWER
- 20 IN ID DISCHARGE PIPE
- DESIGN FLOW 0.5 CUBIC METERS PER SECOND
- SKID–MOUNTED, SELF CONTAINED UNIT

REV	DESCRIPTION	CHK	APP	DATE
0	FOR REVIEW ONLY	ETE	RC	09/09/21

Designed By: R. CZLAPINSKI
Drawn By: E. ENTOV
Checked By: R. CZLAPINSKI
Reviewed By: R. CZLAPINSKI
Design File No. INFLOW STRUCTURE SIDE HAC316.DWG
Scale: As Shown

TETRA TECH
11 RIVERSIDE DRIVE
SUITE 204
COCOA, FL 32940
TEL: 321.636.6470 EXT. 6378099

RESTORE LAGOON INFLOW RESEARCH PILOT PROJECT

CAPE CANAVERAL, FL

Sheet Reference:

DETAIL A3– INTAKE SCREEN DETAILS

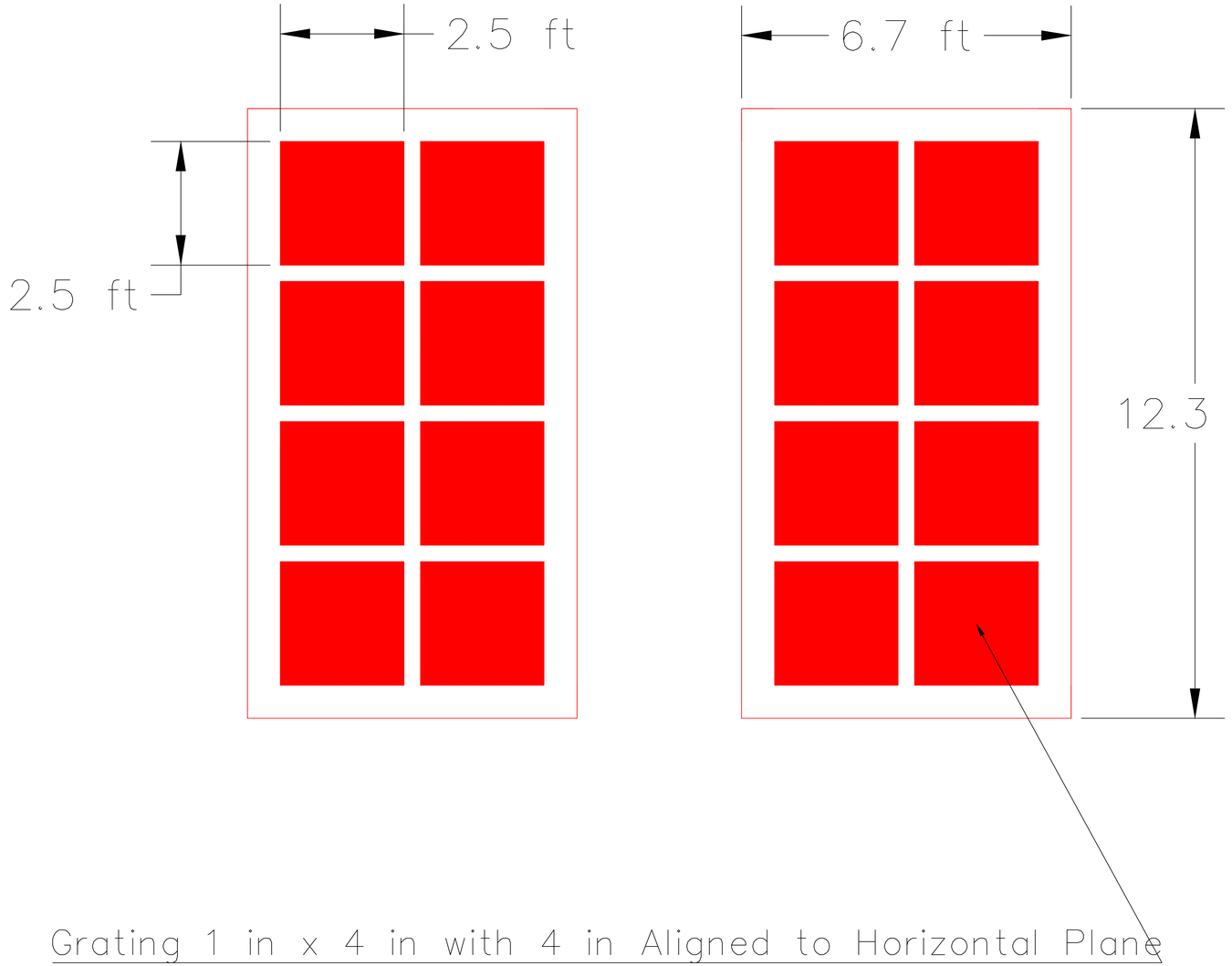

REV	DESCRIPTION	CHK	APP	DATE
0	FOR REVIEW ONLY	ETE	RC	09/09/21

Designed By: R. CZLAPINSKI
Drawn By: E. ERTON
Checked By: R. CZLAPINSKI
Reviewed By: R. CZLAPINSKI
Design File No. CAGE STRUCTURE SIDE.DWG
Scale: As Shown

TETRA TECH
11 RIVERSIDE DRIVE
SUITE 204
COCOA, FL 32940
TEL: 321.636.6470 EXT. 6378099

RESTORE LAGOON INFLOW RESEARCH PILOT PROJECT

CAPE CANAVERAL, FL

Sheet Reference:

DETAIL B - PIPELINE ROAD CROSSING

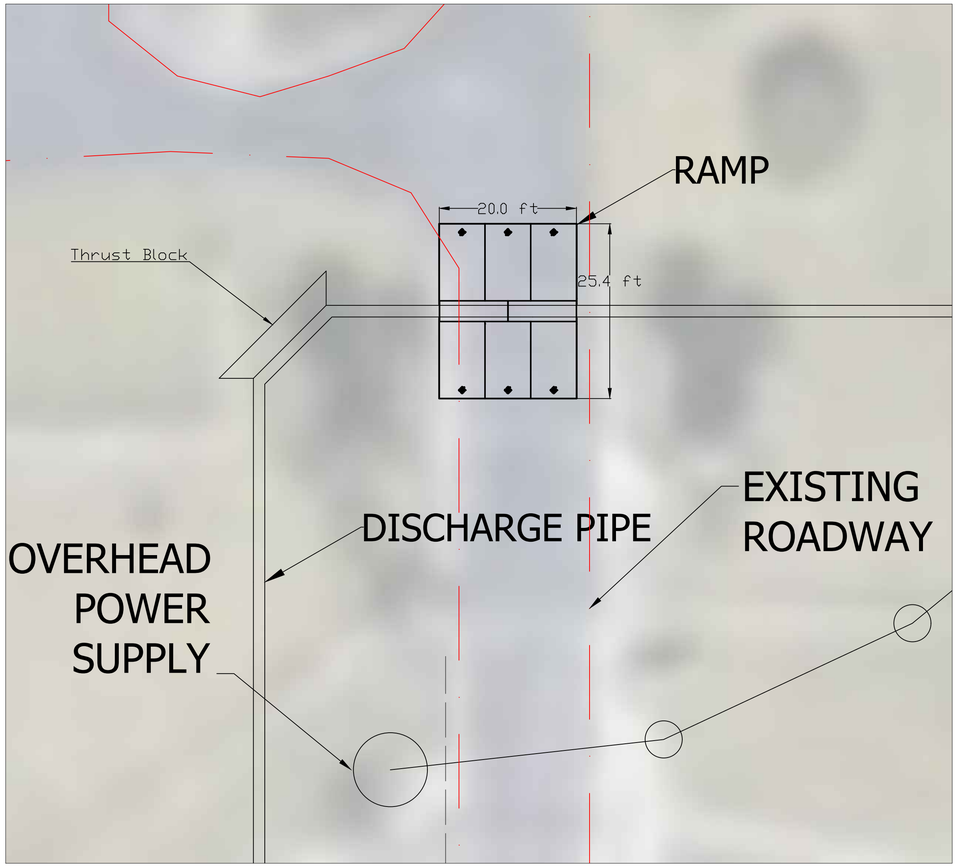

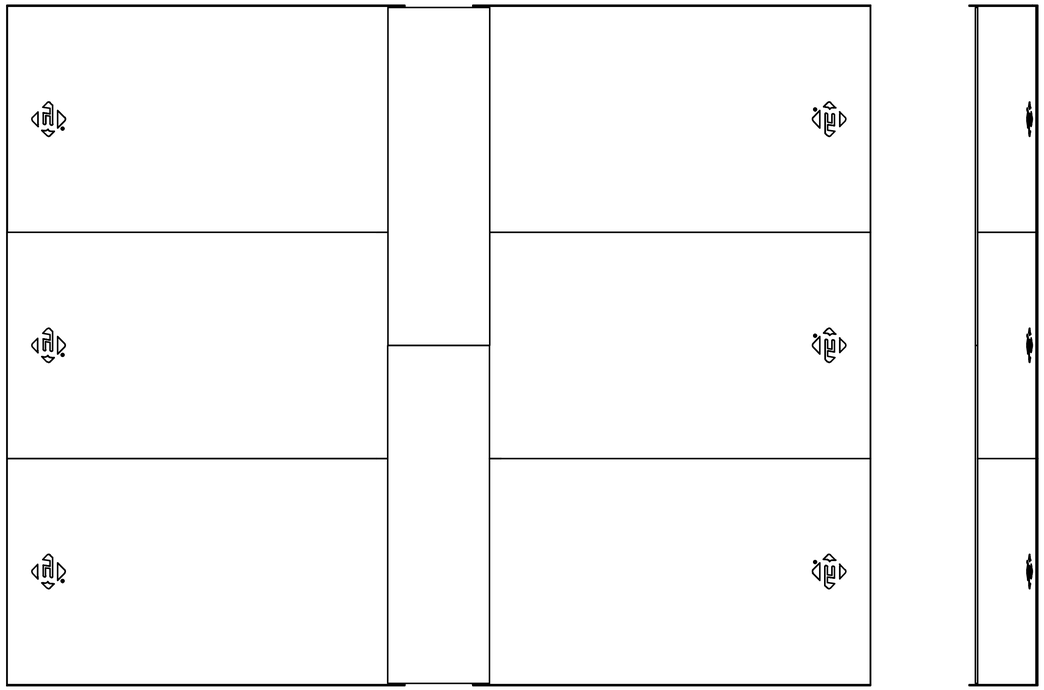

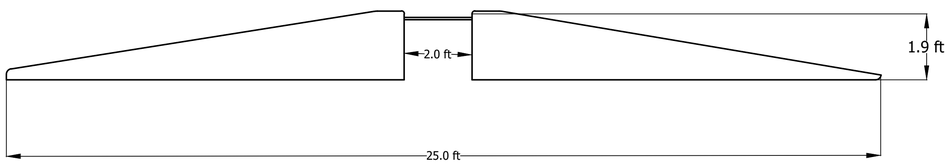

NOTES:
1. CAPACITY IS 32,000 LB PER AXLE (HS-20 LOADING)

2. DESIGNED AND MANUFACTURED BY BLUFF MANUFACTURING

REV	DESCRIPTION	CHK	APP	DATE
0	FOR REVIEW ONLY	ETE	RC	09/09/21

Designed By: R. CZLAPINSKI
Drawn By: E. ETHOMPSON
Checked By: R. CZLAPINSKI
Reviewed By: R. CZLAPINSKI
Design File No. BLUFF MANUFACTURING RAMP.DWG
Scale: As Shown

TETRA TECH
11 RIVERSIDE DRIVE
SUITE 204
SOCOLA, FL 32940
TEL: 321.636.6470 EXT. 6378099

RESTORE LAGOON INFLOW RESEARCH PILOT PROJECT

CAPE CANAVERAL, FL

Sheet Reference:

DETIAL C – OUTFLOW

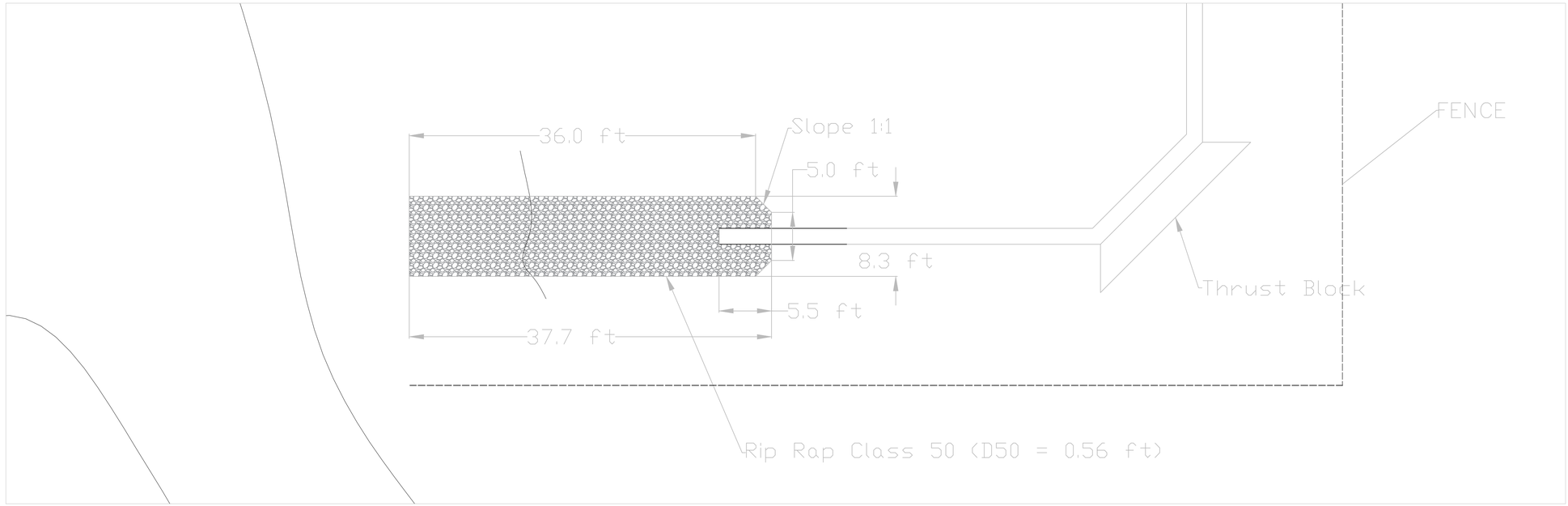

PLAN VIEW

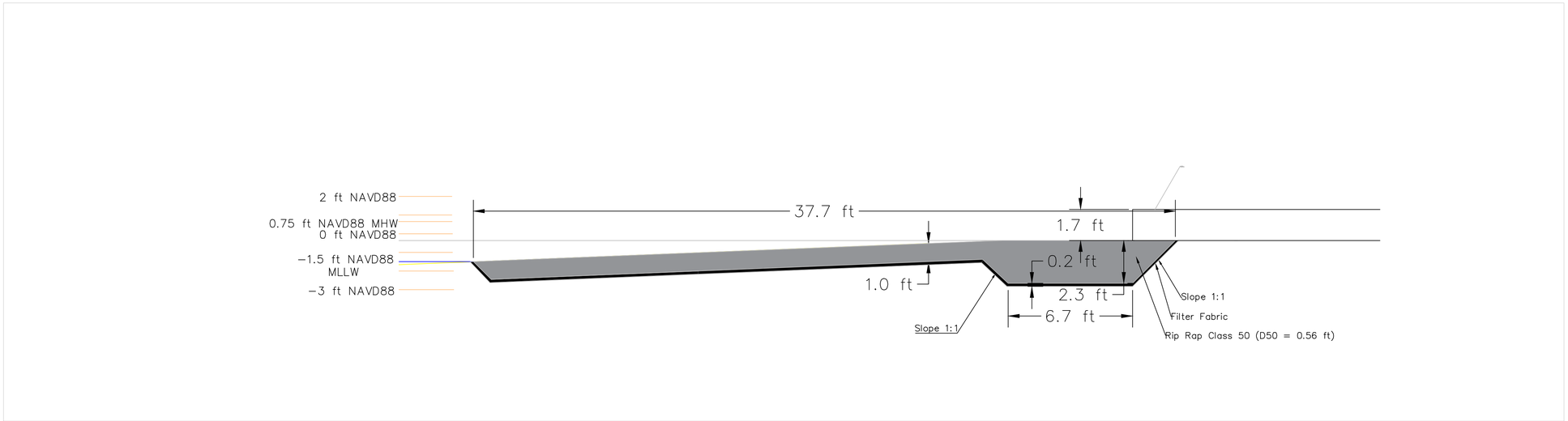

SIDE VIEW

REV	DESCRIPTION	CHK	APP	DATE
0	FOR REVIEW ONLY	ETE	RC	09/09/21

Designed By: R. CZLAPINSKI
Drawn By: E. PENA
Checked By: R. CZLAPINSKI
Reviewed By: R. CZLAPINSKI
Design File No. OUTFLOW STRUCTURE SIDE.DWG
Scale: As Shown

TETRA TECH
11 RIVERSIDE DRIVE
SUITE 204
COCOA, FL 32940
TEL: 321.636.6470 EXT. 6378099

RESTORE LAGOON INFLOW RESEARCH PILOT PROJECT

CAPE CANAVERAL, FL

Sheet Reference:

BIOLOGICAL SURVEYS

LEGEND

- SHOAL GRASS
- VEGETATION
- BLACK MANGROVE

NOTE: MARINE BIOLOGICAL RESOURCE SURVEY COMPLETED JUNE 2021

REV	DESCRIPTION	CHK	APP	DATE
0	FOR REVIEW ONLY	ETE	RC	09/09/21

Designed By: R. CZLAPINSKI
Drawn By: E. ETOW
Checked By: R. CZLAPINSKI
Reviewed By: R. CZLAPINSKI
Design File No. BLUFF MANUFACTURING RAMP.DWG
Scale: As Shown

TETRA TECH
11 RIVERSIDE DRIVE
SUITE 204
COCOA, FL 32940
TEL: 321.638.8470 EXT. 6378099

RESTORE LAGOON INFLOW RESEARCH PILOT PROJECT

CAPE CANAVERAL, FL

Sheet Reference:

Sheet 11 of 11

Attachment 2. USACE Contributed Funds Agreement Template

AGREEMENT FOR ACCEPTANCE OF CONTRIBUTED FUNDS FOR A SECTION 408 EVALUATION

Applicability and Instructions:

1. The attached agreement is provided as a template to be used in the development of an agreement for accepting funds from non-federal public or private entities to evaluate requests under 33 U.S.C. 408. The template agreement may be modified as appropriate to address case-specific circumstances. Guidance on the acceptance and expenditure of such funds is provided in the Implementation Guidance for Section 1156(a)(2) of WRDA 2016.

2. Make all required insertions; remove this cover page; remove the open and close brackets and any instructional text; and ensure the spacing and page breaks throughout the agreement are appropriate.

3. Following review and concurrence by the District Counsel or Division Counsel, as applicable, that the negotiated agreement is acceptable, the District Commander or Division Commander, respectively, may approve and sign the agreement.

AGREEMENT BETWEEN
THE DEPARTMENT OF THE ARMY
AND
[FULL NAME OF CONTRIBUTOR]

THIS AGREEMENT is entered into this ____ day of _____, 20__, by and between the Department of the Army (hereinafter the "Government"), represented by the U.S. Army Engineer, **[Insert either _____ Division, or _____District, as applicable and insert "(hereinafter "Division Engineer" or the "District Engineer", as applicable)]** and the **[FULL NAME OF THE CONTRIBUTOR]** (hereinafter the "Contributor"), together ("the Parties").

WITNESSETH, THAT:

WHEREAS, the Contributor considers it to be in its own interest to contribute funds voluntarily to be used by the Government to evaluate a request under 33 U.S.C 408 (hereinafter "Section 408") to alter **[DESCRIBE FEDERAL PROJECT(S) AFFECTED]** ("hereinafter the "Project(s)");

WHEREAS, the Government is authorized pursuant to Section 408 to accept and expend funds to evaluate such requests;

NOW, THEREFORE, the Government and Contributor agree as follows:

1. The Contributor plans to contribute funds to the Government to pay costs associated with evaluation of engineering plans and other information prepared by Contributor related to a request under Section 408. The Contributor shall provide funds in accordance with the provisions of this paragraph:

a. The Government and Contributor shall develop a scope of work for activities that will be undertaken with funds provided by the Contributor. The scope of work shall provide a detailed description of activities to be undertaken, including a detailed estimate of cost for each activity and schedules, and identification of travel by Government personnel that may be necessary to the activities covered under this Agreement, with such travel to be undertaken in accordance with the Federal Travel Regulations and estimated separately. The Government and Contributor shall review and update, as necessary, the scope of work.

b. Prior to the Government initiating any activities identified in the scope of work, the Contributor shall provide to the Government funds to cover the estimated cost of activities under the scope of work through the current and next fiscal year quarter of the Government. No later than fifteen calendar days before the beginning of each subsequent fiscal year quarter, the Contributor shall provide to the Government funds for all estimated costs of activities to be accomplished during that quarter.

c. If at any time the Government determines that additional funds are needed, the Government shall notify the Contributor in writing and no later than fifteen calendar days from receipt of such notice, the Contributor shall provide to the Government the full amount of such additional funds.

d. The Contributor shall provide funds to the Government by delivering a check payable to "FAO, USAED _____" to the **[insert District Engineer or Division Engineer, as applicable]** or by providing an Electronic Funds Transfer of such funds in accordance with procedures established by the Government.

2. The Government shall provide the Contributor with quarterly reports of obligations for the activities under this Agreement. The Government shall provide the first report within thirty calendar days after the final day of the first full fiscal year quarter following initial receipt of funds pursuant to this Agreement. The Government shall provide subsequent reports within thirty calendar days after the final day of each succeeding quarter until the Government concludes work under this Agreement.

3. Upon conclusion of all work under this Agreement, the Government shall complete a final accounting and furnish the Contributor with written notice of the results of such final accounting. If the costs of the activities under this Agreement exceed the amount of funds provided by the Contributor, the Contributor shall provide the required additional funds within thirty calendar days of such written notice. If any funds provided by the Contributor were not obligated for activities under this Agreement, the Government shall refund those funds to the Contributor within thirty calendar days of completion of the final accounting.

4. No credit or repayment is authorized, nor shall be provided, for any funds provided by the Contributor and obligated by the Government for activities under this Agreement

5. Nothing herein shall constitute, represent, or imply any commitment regarding the Government's consideration of the Section 408 request. The acceptance and expenditure of funds will not impact impartial decision making at any level of the Government with respect to the review and any final decision, either substantively or procedurally. The review must comply with all applicable laws, regulations and procedures. None of the funds provided under this Agreement will be used by the decision maker in his or her review, recommendations, or decision concerning a Section 408 request.

6. The Parties agree to use their best efforts to resolve any dispute in an informal fashion through consultation and communication. If the Parties cannot resolve the dispute through negotiation, they may agree to a mutually acceptable method of non-binding alternative dispute resolution with a qualified third party acceptable to the Parties. Each party shall pay an equal share of any costs for the services provided by such a third party as such costs are incurred. The existence of a dispute shall not excuse the parties from performance pursuant to this Agreement.

7. This Agreement may be modified only by a written amendment to this Agreement signed by both Parties. Either party may terminate further performance under this Agreement by providing 60 calendar days advance written notice to the other party. In the event of termination, the

Contributor remains responsible for all costs incurred by the Government pursuant to this Agreement.

8. Any notice, request, demand, or other communication required or permitted to be given under this Agreement shall be deemed to have been duly given if in writing and delivered personally or mailed by registered or certified mail, with return receipt, as follows:

If to the Contributor:
[TITLE]
[ADDRESS]

If to the Government:
[Title: District Engineer or Division Engineer, as applicable]
[ADDRESS]

A party may change the recipient or address to which such communications are to be directed by giving written notice to the other party in the manner provided in this paragraph.

9. In the exercise of their respective rights and obligations under this Agreement, the Government and the Contributor each act in an independent capacity, and neither is to be considered the officer, agent, or employee of the other.

10. To the extent permitted by the laws governing each party, the parties agree to maintain the confidentiality of exchanged information when requested to do so by the providing party.

IN WITNESS WHEREOF, the parties hereto have executed this Agreement, which shall become effective upon the date it is signed by the **[Insert Division Engineer or District Engineer, as applicable]**.

DEPARTMENT OF THE ARMY	CONTRIBUTOR
BY: _____	BY: _____
[TYPED NAME]	**[TYPED NAME]**
[TITLE]	**[TITLE]**
DATE: _____	DATE: _____

Attachment 3. Marine Resources Survey Field Observation Report

Florida Tech Indian River Lagoon Inflow Phase II
Canaveral Lock, Cape Canaveral, Florida

Marine Resource Survey Field Observation Report

June 2021


Marine Resource Survey Field Observation Report

June 2021

PRESENTED TO

Florida Institute of Technology
Oceanography and Environmental Science
Ocean Engineering and Marine Sciences
Melbourne, Florida, USA 32901

PRESENTED BY

Tetra Tech, Inc.
Center for Coastal Services
1901 S. Congress Avenue
Suite 200
Boynton Beach, FL 33426

Tetra Tech Staff:

MATT SHELTON	PROJECT MANAGER
ROBERT M. BARON	PRINCIPAL SCIENTIST
MATTHEW LYBOLT	CONSULTING SCIENTIST
MIKE MENDOZA	BOAT OPERATOR
ANDREA RINNE	GIS SPECIALIST

TABLE OF CONTENTS

LIST OF FIGURES

LIST OF TABLES

LIST OF PHOTOGRAPHS

1.0 INTRODUCTION

Under contract with Florida Institute of Technology, as a preliminary investigation to delineate the marine resources within and adjacent to the proposed intake and outfall locations for the proposed inflow pilot system, Tetra Tech's marine scientists performed a marine resource survey on June 1, 2021 (Figure 1). The survey area included two sub-survey areas:

- Intake Location, approximately 4.5 acres (1.8 hectares)
- Outfall Location, approximately 4.6 acres (1.9 hectares)

The results of the survey will be used to determine the location and design of the inflow and outfall structures for the proposed Inflow pilot system.

The survey was completed during the peak growing season to capture the maximum spatial extent and cover of submerged aquatic vegetation (SAV). Per regulatory agency guidance, this is particularly important in portions of the state where seagrasses senesce during the winter. To remain consistent with federal requirements, the Florida Department of Environmental Protection (FDEP) recommends SAV surveys be completed between June 1st and September 30th.

A Health and Safety Plan (HASP) was prepared by Tetra Tech to evaluate site-specific field conditions, local medical facilities, potential risks, and mitigation measures associated with underwater activities in the Project area. The HASP was reviewed and approved by Tetra Tech's Director of Health and Safety prior to conducting field activities. A one-day permit level marine resource investigation of the area was conducted.

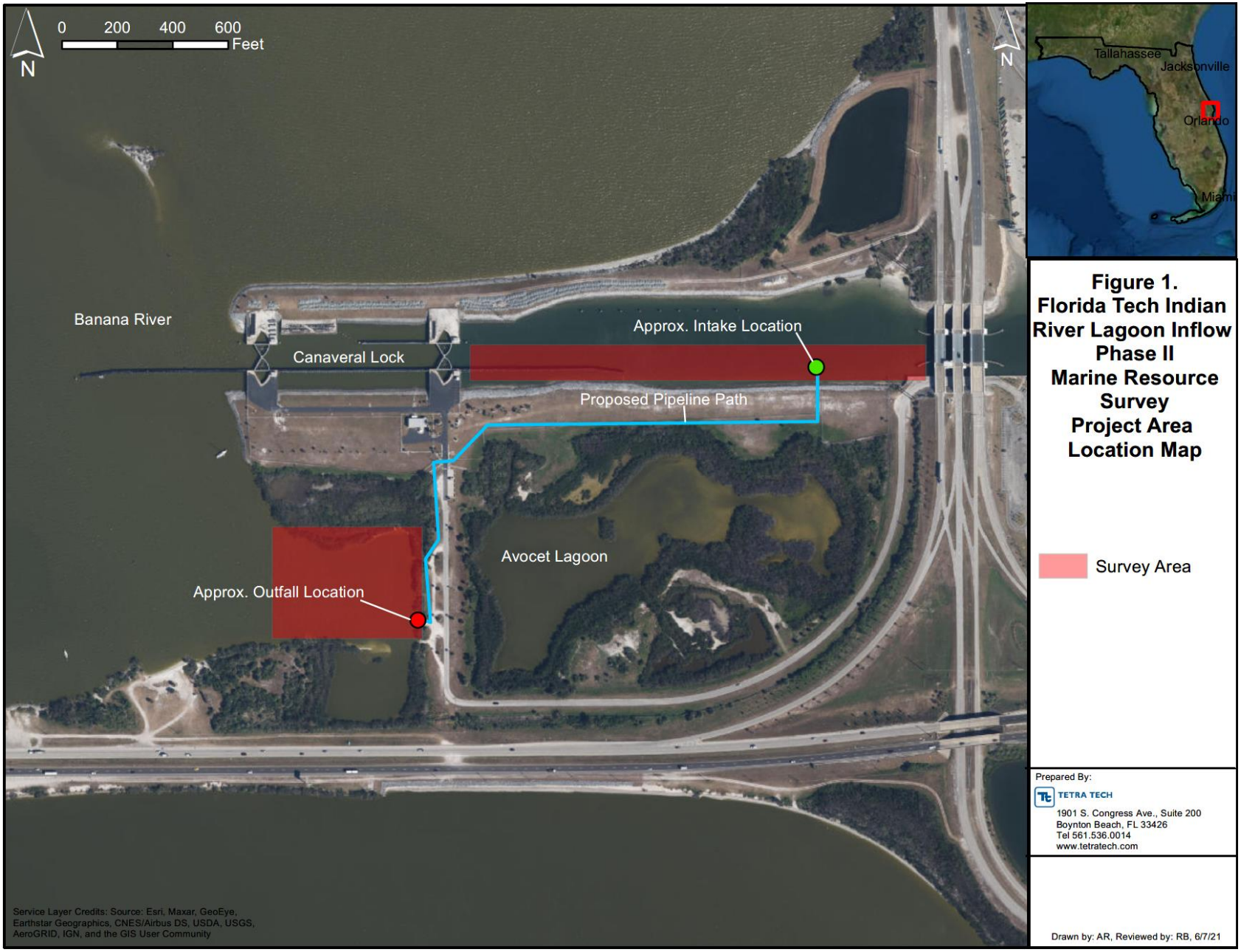

Figure 1. Marine Resource Survey Area.

2.0 METHODOLOGY

Upon arrival on site, a visual reconnaissance survey was first performed within each survey area to determine SAV presence/absence. The visual reconnaissance survey was accomplished by two Tetra Tech marine scientists snorkeling throughout the survey areas. The visual swath width for each observer within the intake survey area was typically 4 ft (1.2 m) and approximately 2 ft (0.6 m) within the outfall survey area. To ensure adequate survey coverage in the outfall survey area, due to the limited under water visibility, the observers swam in a zig-zagged pattern along the perimeter twice and crossed the center of the survey area in three equally spaced transects. When seagrass was observed during the initial reconnaissance survey, the location of each seagrass occurrence was documented and assessed (Photo 1). Differential Global Positioning System (DGPS) positions were also recorded at each occurrence of SAV.

Mapping of the mangrove/vegetation edge along the eastern shoreline at the outfall location was accomplished by walking around the vegetation perimeter while recording DGPS position.

Documentation included an assessment of SAV, mangroves, and other vegetation, which is intended to satisfy environmental permit requirements. Representative photographs were also taken using a Nikon Coolpix W300 underwater camera.

Photograph 1. Tetra Tech scientist snorkeling along the mangrove edge at the proposed outfall survey area.

3.0 RESULTS

3.1 HYDROMETEOROLOGICAL CHARACTERISTICS

The underwater current was negligible at both survey areas during the one-day survey. Low tide was at 0752 and high tide was at 1353. High air temperature was approximately 85º F with winds originating out of the northeast at 10-15 mph. Water temperature was in the low 80's during the survey and sea state was flat. Within the survey area, water depth ranged from 1 ft (30 cm) to 10 ft (3.0 m) and underwater visibility was approximately 2 ft (0.6 m) to 3 ft (0.9 m). The moderate underwater visibility in conjunction with shallow water depths, permitted for the use of snorkel to conduct the survey.

3.2 INTAKE LOCATION

The survey area east of the Canaveral Lock included rip rap along the shoreline (Photograph 2) that transitioned to a sand-shell mixture (Photograph 3) from the intertidal zone out to approximately 6 ft (2 m) deep. A mud component was noted within the sediment at approximately 6 ft (2 m) deep and increased with depth towards the channel where mud (Photograph 4) was the dominant sediment type. The slope was gradual in the majority of the survey area but became increasingly steeper towards the western end of the area south of the Canaveral Lock Arrival Point (Photograph 5).

Sparse black mangroves (*Avicennia germinans*), interspersed among the riprap shoreline (Photograph 6), were mapped in the eastern portion of the survey area (Figure 2). While not mapped due to the increased distance from the propose intake location, black mangroves were also present among the riprap along the western end of the survey area south of the Canaveral Lock Arrival Point.

While seagrass was absent from the survey area, very sparse patches of macroalgae (fine filamentous green algae and *Dasya* sp.) and filamentous turf algae/cyanobacteria were noted. Mature and juvenile oysters (*Crassostrea virginica*) (Photograph 7) were also present within the intertidal to shallow subtidal area but only approximately 25% were alive. Other sessile benthos observed included barnacles, bryozoans, hydroids, tunicates (Photograph 8), and anemones. Three colonies of the octocoral *Leptogorgia virgulata* (Photograph 9) were observed on submerged riprap along the western end of the survey area south of the Canaveral Lock Arrival Point.

Photograph 2. Riprap shoreline along the Intake Location Survey Area.

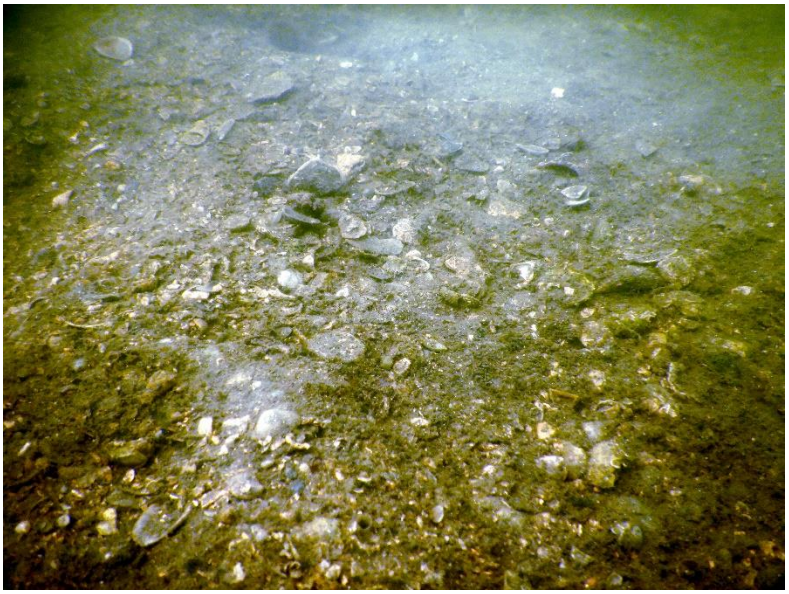

Photograph 3. Sand-shell substrate along the Intake Location Survey Area.

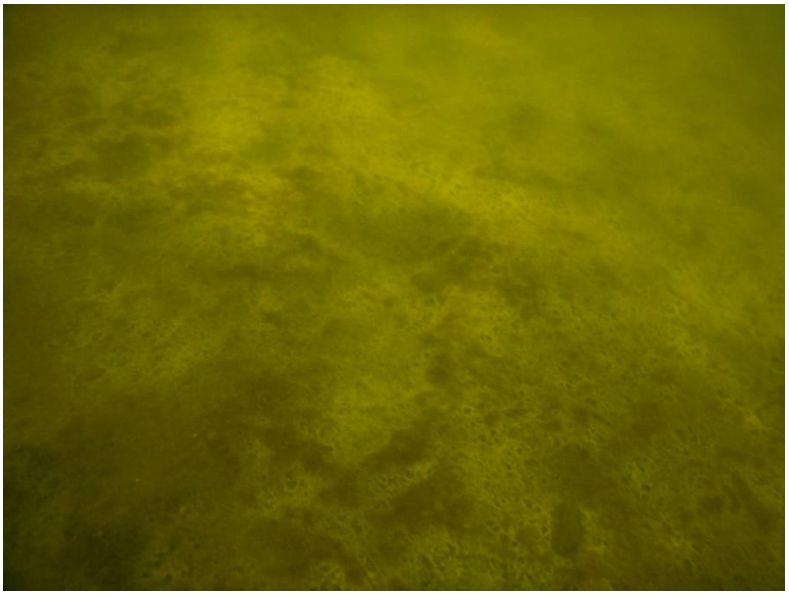

Photograph 4. Mud substrate was the dominant sediment type towards the channel.

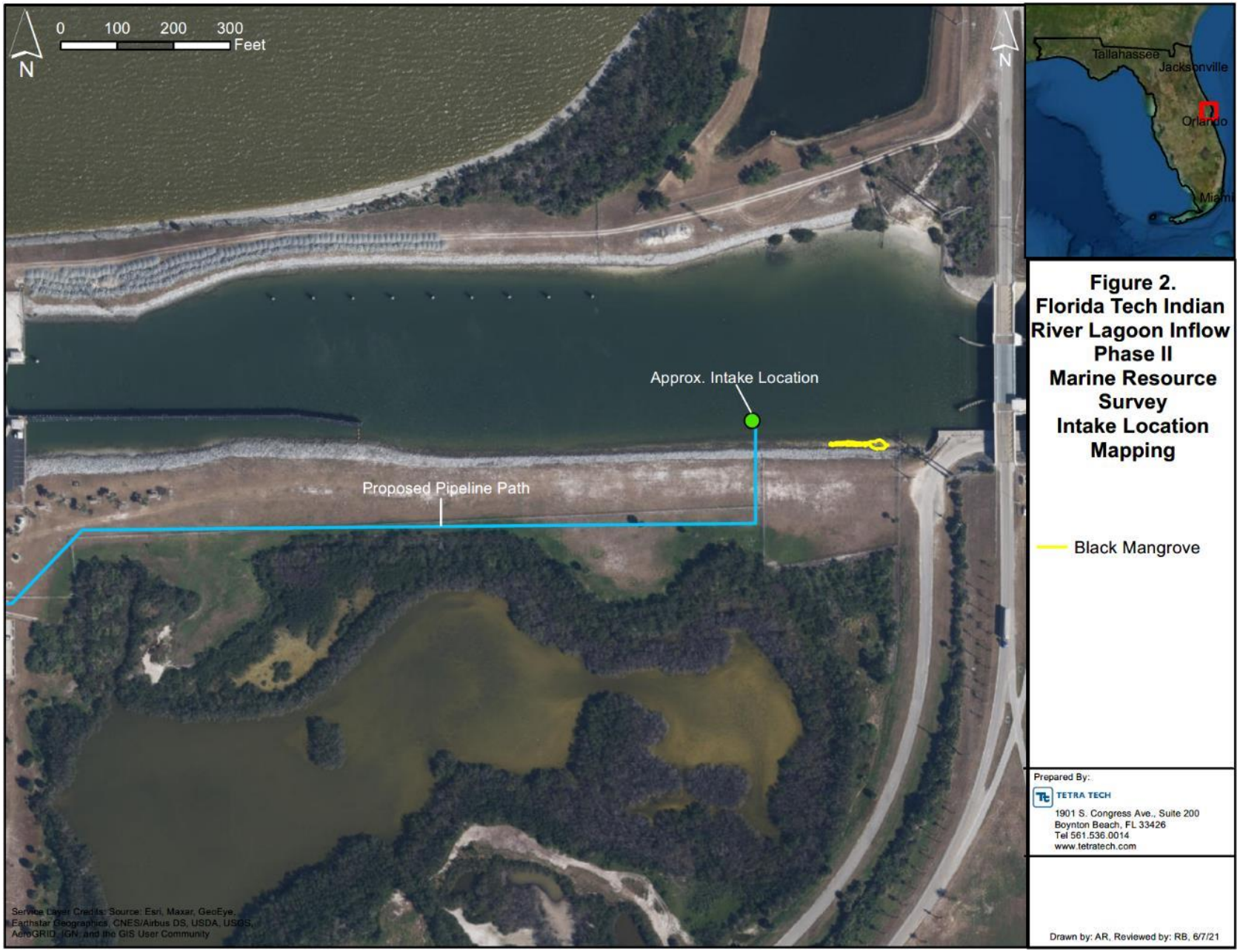

Figure 2. Marine Resource Survey: Intake Location Survey Area.

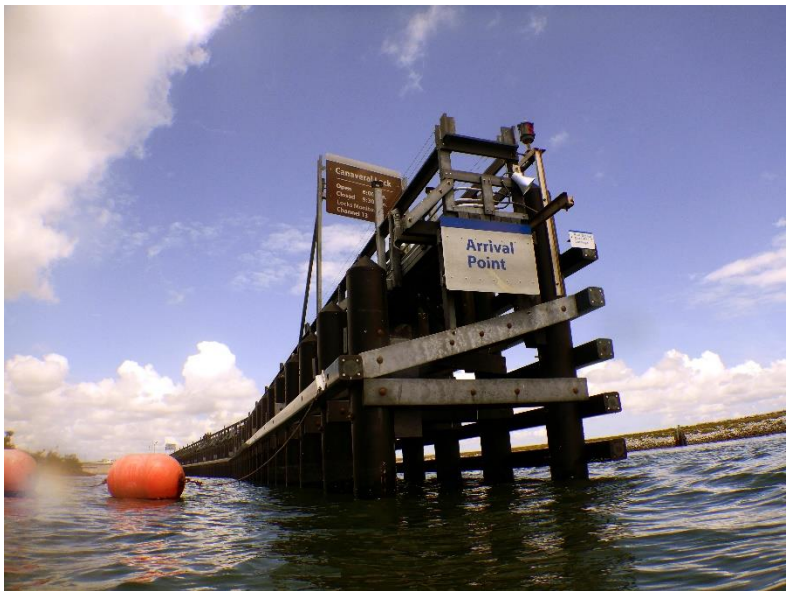

Photograph 5. Canaveral Lock Arrival Point at the western end of the survey area.

Photograph 6. Sparse black mangroves (*Avicennia germinans*) interspersed among the riprap shoreline.

Photograph 7. Oysters (*Crassostrea virginica*) present within the intertidal to shallow subtidal habitat.

Photograph 8. Pleated tunicate (*Styela plicata*) noted within the shallow subtidal habitat.

Photograph 9. Octocoral (*Leptogorgia virgulata*) observed on submerged riprap at the western end of the survey area

3.3 OUTFALL LOCATION

The submerged habitat within the outfall survey area included very sparse patches of shoal grass (*Halodule wrightii*) (Photograph 10) (Figure 3). The shoal grass was generally documented along the transition zone from shallow sand-shell to deeper sand-mud. The majority of shoal grass patches were less than six inches (15 cm) in diameter and were composed of 12 shoots or fewer. Due to the sparse nature of seagrass coverage, where seagrass was present, it was estimated that fewer than one out of 100 random quadrat samples would have included seagrass; therefore, quantitative quadrat sampling was not conducted. Within the total area surveyed, 17 shoal grass patches were observed (Figure 3). No seagrass was observed along the northwest margin and across the center of the survey area.

Other observations within the outfall location survey area included green algae (*Caulerpa prolifera*) (Photograph 11) which was common throughout the deeper, muddy portions. Similar to the intake survey area, other sessile invertebrates were uncommon. A thick layer of red dinoflagellate slime atop organic/calcareous mud (Photograph 12) was documented through the center of the outfall survey area. The mud through the center was greater than 6 inches (15 cm) thick.

Wetland/emergent vegetation documented along the eastern shoreline (Photograph 13), at the outfall location, is graphically depicted in Figure 3 and presented in Table 1.

Figure 3. Marine Resource Survey: Outfall Location Survey Area.

Photograph 10. Sparse patch of shoal grass (*Halodule wrightii*) located within the outfall survey area.

Photograph 11. Green algae (*Caulerpa prolifera*) observed inhabiting the deeper, muddy substrate.

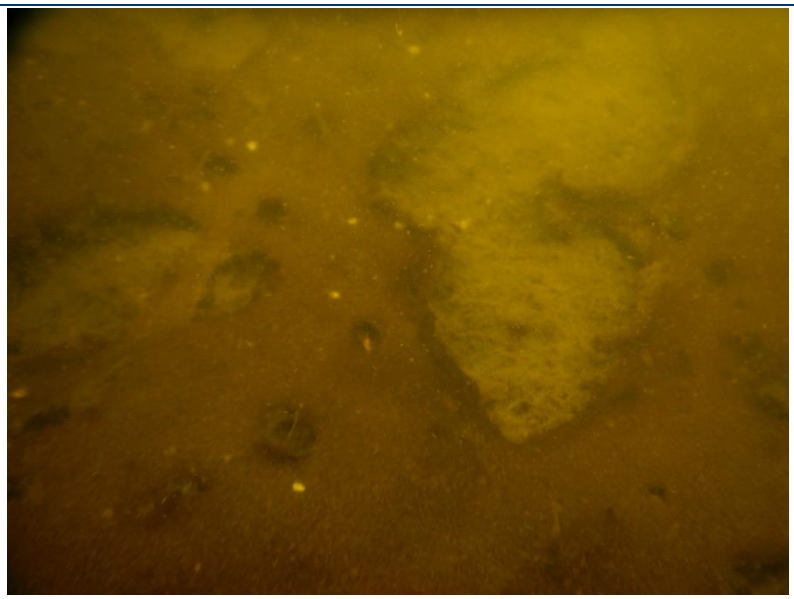

Photograph 12. Organic/calcareous mud documented through the center of the outfall survey area.

Photograph 13. Wetland/emergent vegetation documented along the eastern shoreline within the outfall survey area.

Table 1. Vegetation documented along the eastern shoreline of the outfall survey area.

Common Name	Scientific Name
Sabal palm	*Sabal palmetto*
Buttonwood	*Conocarpus erectus*
Red mangrove	*Rhizophora mangle*
Black mangrove	*Avicennia germinans*
Dahoon holly	*Ilex cassine*
Sea grape	*Coccoloba uvifera*
Saltbrush	*Baccharis halimifolia*
Scrub oak	*Quercus* sp.
Gray nickerbean	*Caesalpinia bonduc*
Unidentified herbs	N/A

4.0 CONCLUSIONS

The following observations highlight the results from the marine resource survey.

- Seagrass was not observed within the intake survey area.
- Within the outfall survey area, one seagrass species was sparsely present, primarily along the northeastern shoreline.
- Wetland/emergent vegetation included a variety of species that were documented and mapped along the eastern shoreline within the outfall survey area.

4.1 RECOMMENDATIONS

- As oysters are typically grouped with fouling organisms, no specific protections are in place for impacts to oysters in Class III waters within the state of Florida.
- Should construction of the outfall occur from the water, construction practices should plan to avoid direct impacts to the existing seagrass, including sedimentation.
- The new outfall should be sited as close to the southeastern portion of the outfall survey area as feasible to avoid potential impacts to the existing seagrass located along the northeastern survey area boundary.